University of Southampton

Faculty of Environmental and Life Science

School of Ocean and Earth Science

Development of Molecular Analytical Methods for *in situ* Detection of Marine Organisms using Microfluidic Biological Sensor Technologies

by

Ahmed Ibrahim Ibrahim Alrefaey

https://orcid.org/0009-0001-3191-3545

Thesis for the degree of Doctor of Philosophy

October 2023

University of Southampton

Abstract

Faculty of Environmental and Earth Science

School of Ocean and Earth Science

Doctor of Philosophy

Development of Molecular Analytical Methods for *in situ* Detection of Marine Organisms using Microfluidic Biological Sensor Technologies

by

Ahmed Ibrahim Ibrahim Alrefaey

Healthy seas are crucial for the protection of public health and to maximise the economic benefit from the use of the ocean for food production (including from aquaculture), resources, pharmaceuticals, and tourism. Sporadic occurrences of marine harmful algal blooms (HABs), however, can bring calamity to both the health and economic well-being of communities and businesses. In particular, toxigenic blooms can lead to significant harm to marine species and ecosystems, as well as human health and maritime industries. *Pseudo-nitzschia* is a genus of marine microalgae, belonging to the diatom group, which have been identified as a significant risk to human health and a contributor to ecological degradation from HABs. This is due to the production of domoic acid, a potent neurotoxin that is toxic to marine organisms and mammals. Early detection of domoic acid-producing blooms is necessary to minimise exposure. However, existing methods for discerning *Pseudo-nitzschia* abundance and the associated risks are long and protracted, labour-intensive and expensive. Implementing an early warning system using the state of the art in analytical methods will improve response times, improve accuracy and reduce cost; ultimately this will mitigate risk.

Molecular analytical techniques, particularly those based on nucleic acid (DNA or RNA) sequence amplification, are widely adopted in food and water quality assessment, public health protection, and environmental monitoring. These methods can be coupled with portable or deployable instrumentation to provide high integrity, laboratory-quality or better metrology in resource-limited settings. In particular, microfluidic 'lab-on-a-chip' (LOC) technology is at the forefront of de-centralised nucleic acid testing and offers advantages such as reduced reagent and energy consumption, ease of use, rapidity, and stability, all while maintaining high levels of specificity, sensitivity, and precision. Automation of these systems makes analysis possible for non-specialist end-users, increasing their scope of application.

This study was undertaken to explore new methods and technology for nucleic acid-based detection of *Pseudo-nitzschia* towards the provision of an integrated early warning system. It began with the design and testing of novel qPCR-based assay for *Pseudo-nitzschia* spp. detection and quantification. Then, the assay was combined with a reverse transcription step to investigate RNA-based (gene expression) responses in nutrient-depleted *P. multistriata* cells to the addition of essential nutrients phosphate, nitrate, and silicate. Nutrient availability was found to significantly influence domoic acid production, highlighting the relationship between nutrient availability and the toxic threat posed by

Pseudo-nitzschia blooms. Subsequently, a suite of novel isothermal assays targeting the *dabD* gene of *Pseudo-nitzschia* spp., which is linked to toxin biosynthesis, were designed utilising the LAMP and RPA chemistries. The LAMP assay outperformed the RPA assay in sensitivity and specificity, and its potential use for statutory algal surveillance was demonstrated by measuring *Pseudo-nitzschia* DNA in seawater samples collected over six months from a known HAB hotspot. To support the potential integration of the novel assays with fieldable instrumentation, a novel 'Vitrification' technique was developed for the simple and fast preservation and dry storage of complete reaction mixtures. The 'shelf-life' of the preserved reactions was at least six months at room temperature and represents a host of improvements upon existing methods. There were no significant differences in quantification performance between the dry-preserved reagents and freshly prepared reactions that relied on cold-chain-dependent, wet reagents. Finally, a new LOC system referred to as "LAMPTRON" was designed and fabricated from scratch, and developed for real-time detection and quantification of *P. multistriata* cells in a semi-autonomous fashion. LAMPTRON demonstrates a proof-of-concept for integrating automated DNA extraction with fully preserved DNA analysis, enabling the sensitive detection of toxigenic *P. multistriata* in a comparable timeframe to the leading commercial systems. These advances offer a faster, more sensitive, and simplified molecular analysis compared to existing statutory surveillance methods, which rely on costly reagents, sophisticated equipment, highly skilled personnel, and centralised laboratories. The ability to detect and quantify *Pseudo-nitzschia* cells using LOC technology could be modified towards a plethora of microbiological and eDNA targets for the surveillance and early warning of biohazards in aquatic environments.

Table of Contents

Table of Tables

Table of Figures

Research Thesis: Declaration of Authorship

Print name: Ahmed Ibrahim Ibrahim Alrefaey

Title of thesis: Development of Molecular Analytical Methods for *in situ* Detection of Marine Organisms using Microfluidic Biological Sensor Technologies

I declare that this thesis and the work presented in it are my own and has been generated by me as the result of my own original research.

I confirm that:

1. This work was done wholly or mainly while in candidature for a research degree at this University;
2. Where any part of this thesis has previously been submitted for a degree or any other qualification at this University or any other institution, this has been clearly stated;
3. Where I have consulted the published work of others, this is always clearly attributed;
4. Where I have quoted from the work of others, the source is always given. With the exception of such quotations, this thesis is entirely my own work;
5. I have acknowledged all main sources of help;
6. Where the thesis is based on work done by myself jointly with others, I have made clear exactly what was done by others and what I have contributed myself;
7. Parts of this work have been published as:-

McQuillan, J. S., A. Alrefaey, A. D. Turner, N. Morrell, O. Stoner, R. Brown, S. Kay, S. Cooke, and T. Bage. 2023. Quantitative Polymerase Chain Reaction for the estimation of toxigenic microalgae abundance in shellfish production waters. Harmful Algae 128:102497.

Ahmed Alrefaey, Jonathan S. McQuillan, Patricia López-García and Julie C. Robidart. Induction of toxin biosynthesis by nutrient depletion and addition in *Pseudo-nitzschia multistriata*. Submitted to the Harmful Algae Journal (Under peer review).

Ahmed Alrefaey, Jonathan S. McQuillan, Julie C. Robidart and Matthew C. Mowlem. Pre-storage of vitrified reagents for simple, precise and rapid molecular detection. For submission to the Journal of Microbiological Methods. (In prep).

Ahmed Alrefaey, Jonathan S. McQuillan, Fabrizio Siracusa, Allison Schaap, Christopher L. Cardwell, John Walk, Robert Euan Wilson, Daniel Rogers, Julie C. Robidart and Matthew C. Mowlem. LAMPTRON: a lab-on-a-chip system integrating DNA purification and loop-mediated isothermal amplified quantification of the toxic diatom *Pseudo-nitzschia multistriata*. For submission to Sensors & Diagnostics Journal (In prep).

Poster at the Marine Autonomy and Technology Conference 2022 titled ‘‘A novel method for simple and rapid isothermal molecular detection of a marine biohazard towards Lab on Chip applications’’ (https://techoceans.eu/resources/).

Signature: ..... Date: .....

Acknowledgements

I would like to express my greatest thanks to my primary supervisors Dr. Jonathan S. McQuillan and Dr. Julie C. Robidart for their guidance, encouragement, and outstanding support during my PhD. I am also very grateful to my secondary supervisors, Prof. Matthew C. Mowlem, Prof. Duncan Purdie and Dr. Phyllis Lam for sharing their knowledge and providing guidance through the project. I extend my appreciation to my unofficial supervisor, Dr. Allison Schaap, for her feedback and assistance during the sensor development process. I would like to extend my sincerest appreciation to Dr. Annika Simpson for all her support. I would like to express my gratitude to Dr. Susan Evans for sharing her expertise and providing assistance in editing this thesis. I would like to thank Dr. Sebastian Steigenberger for securing the necessary reagents and consumables essential for conducting this research. I would like to express my gratitude to Dr. Fabrizio Siracusa for his assistance in fabricating the sensor prototypes. I extend my thanks to Dr. Hachem Kasem for his encouragement throughout my PhD journey. Special thanks to Dr. Samuel Monk for his meticulous proofreading. I want to express my gratitude to all current and former members of the Ocean Technology and Engineering Group at the National Oceanography Centre Southampton (NOCS). The collaborative efforts of the group and their prior work on advancing Lab on Chip platforms have been instrumental in achieving this work. This research was supported by the EU TechOceanS project (101000858), the Natural Environment Research Council CLASS project Grant (NE/R015953/1), AtlantECO (H2020 Grant Agreement ID 862923), and the PhD scholarship from the Egyptian Cultural and Educational Bureau London, UK. Lastly, my deepest thanks to my family and friends for their love and support throughout the numerous challenges encountered during this study.

Definitions and Abbreviations

APTES ..... Aminopropyltriethoxysilane

AST ..... Amnesic Shellfish Toxins

BHQ ..... Black Hole Quencher

BIP ..... Backward inner primer

BLAST ..... Basic local alignment search tool

BSA ..... Bovine serum albumin

CCAP ..... Culture Collection of Algae and Protozoa

cDNA ..... Complimentary Deoxyribonucleic Acid

CO_2 ..... Carbon dioxide

COC ..... Cyclic-olefin copolymer

COI ..... Cytochrome c-oxidase subunit

C_t ..... Threshold cycle

CYP450 ..... Cytochrome protein 450

DA ..... Domoic acid

DMA ..... Dimethyl adipimidate

DNA ..... Deoxyribonucleic acid

DNase ..... Deoxyribonuclease

dNTPs ..... Deoxynucleotides

dsDNA ..... Double-Stranded Deoxyribonucleic Acid

EDTA ..... Ethylenediaminetetraacetic acid

ELISA ..... Enzyme-linked immunosorbent assay

EPT ..... end-product testing

ESP ..... Environmental Sample Processor

FAM ..... Fluorescein

FIP ..... Forward inner primer

FISH ..... Fluorescent in situ Hybridisation

FPP ..... Farnesyl pyrophosphate synthase

FW ..... Forward primer

gDNA ..... Genomic deoxyribonucleic acid

GPP ..... Geranyl pyrophosphate synthase

GuSCN ..... Guanidinum thiocyanate

HAB ..... Harmful Algal Blooms

HAD ..... Helicase Dependant Amplification

HEX ..... Hexachloro-fluorescein

HNLC ..... High-nutrient, low-chlorophyll

HPLC ..... High-performance liquid chromatography

ITS ..... Internal Transcribed Spacer

LAMP ..... Loop Mediated Isothermal Amplification

LB ..... Loop backward primer

LC-MS ..... Liquid-chromatography - Mass Spectrometry

LED ..... Light Emitting Diode

LF ..... Loop forward primer and

LOC ..... Lab On Chip

LOD ..... Limit of detection

LOQ ..... Limit of quantification

LT ..... Lipophilic Toxins

MEP ..... Methylerythritol Phosphate metabolic pathways

MEV ..... Mevalonate metabolic pathway

MGB ..... Minor Groove Binder

MPL ..... Maximum Permitted Limit or

N ..... Nitrate

NASBA ..... Nucleic Acid Sequence Based Amplification

NAT ..... Nucleic Acid Testing

NCBI ..... National Center for Biotechnology Information

NCTC ..... National Collection of Type Cultures

NRC-ARL ..... National Research Council Atlantic Regional Laboratory

OTE ..... Ocean Technology and Engineering Group, National Oceanography Centre

P ..... Phosphate

PBS ..... Phosphate Buffered Saline

pCO_2 ..... Partial pressure of carbon dioxide

PCR ..... Polymerase chain reaction

pDA ..... Particulate domoic acid

PDMS ..... Polydimethylsiloxane

PEG ..... Polyethylene glycol

PMMA ..... Polymethylmethacrylate

PST ..... Paralytic Shellfish Toxins

rbcL ..... Ribulose-biphosphate carboxylase large subunit

RPA ..... Recombinase Polymerase Amplification

rRNA ..... Ribosomal RNA

RT-LAMP ..... Reverse Transcription Loop Mediated Isothermal Amplification

RT-PCR ..... Reverse transcriptase polymerase chain reaction

SDA ..... Strand Displacement Amplification

SEM ..... Scanning Electron Microscopy

Si ..... Silicate

SPE ..... Solid Phase Extraction

SPR ..... Surface Plasmon Resonance

ssDNA ..... Single-Stranded DNA

Tg ..... Glass Transition Temperature

THF ..... Tetrahydrofuran

Tm ..... Theoretical Melting Temperature

TOD ..... Threshold of Detection

T_t ..... Threshold Time

UV ..... Ultraviolet

Chapter 1 Introduction

1.1 Harmful Algal Blooms (HABs)

Harmful Algal Blooms (HABs) are naturally occurring events caused by the expansion of algal cell numbers in aquatic environments. They occur all around the world, impacting coastlines, the open ocean, freshwater lakes, rivers, and estuaries. They represent a serious threat to the environment, ecosystems, human health and water-associated industries (including aquaculture, tourism and leisure) (Anderson et al. 2012). These increases in algal populations deplete key nutrients and dissolved gases, causing harm to wildlife, and may alter the colour and appearance (tubidity) of water bodies, making them unattractive for recreational use. However, perhaps the greatest impact of HABs is due to the ability of some species to biosynthesise potent toxins. Herbivorous fin fish and shellfish ingest algal cells, leading to the bioaccumulation of algal toxins in their tissues. The ill effects are transmitted to humans from the consumption of seafood, and to a lesser extent from direct exposure to contaminated water and the inhalation of aerosolised toxins (e.g., from breaking waves) (Anderson et al. 2021). Algal toxin exposure causes a range of debilitating health issues, including gastrointestinal, neurological, and respiratory problems (Kouakou and Poder 2019). This combined with the aforementioned effect of HABs on nutrients and dissolved gases can lead to collapses in aquatic populations, impacting the food web structure and overall biodiversity (Kazmi et al. 2022). Recently, a HAB toxin has been responsible for mass poisoning and mortalities of marine mammals on the Californian coastline (Ramirez 2023). After a bloom has subsided, the dying algal cells contribute to the sudden and massive release of organic matter, which in turn is decomposed by oxygen-consuming bacteria, further depleting dissolved oxygen levels. The expansion of oxygen-depleted zones inhibits the respiration of various marine organisms, resulting in substantial mortality among marine life (Joyce 2000). Globally, there is a perceived increase in the frequency and severity of HABs, albeit the contribution of increased surveillance and media attention to this assumption remains unclear. Nonetheless, as aquatic environments are increasingly used for the production of food, as well as leisure, there will ultimately be greater exposure of humans to the risks posed by HABs, making the issue of the upmost importance.

1.2 *Pseudo-nitzschia* Diatoms

Diatoms are one of the most abundant groups of phytoplankton, found in every aquatic environment. They are a major contributor to biological productivity and nutrient utilisation within the oceanic ecosystem (Benoiston et al. 2017). Diatoms can survive in diverse environments, indicating that they may

possess unique capabilities to adapt to rapid and severe environmental changes including those caused by the activity of human beings (Armbrust 2009). Within the diatom group, certain species of the genus *Pseudo-nitzschia* are able to synthesise a potent neurotoxin, known as domoic acid (DA) (Lelong et al. 2012). These species are consumed by a variety of marine fauna, which ultimately serve as vectors for trophic transfer (Bargu et al. 2002, Costa et al. 2005, Bates and Trainer 2006a, Mafra et al. 2010). Human exposure to DA is predominately through the consumption of contaminated seafood including herbivorous fin fish, bi-valve shellfish and gastropods; the most commonly contaminated food stocks in the UK are oysters, mussels and clams (Kvitek et al. 2008, Alves et al. 2019). DA can persist in the marine food web for days after biosynthesis (Sekula-Wood et al. 2009). In severe cases, the trophic transfer of algal toxins results in mass mortalities to diverse marine organisms including invertebrates, fish, birds and marine mammals (Trainer et al. 2012). In addition, human consumption of contaminated food can lead to a severe and sometimes fatal poisoning syndrome known as Amnesic Shellfish Poisoning (ASP), a condition that impacts the brain, leading to potential heart failure and permanent brain damage (Bates et al. 1989, Panlilio et al. 2023).

1.3 Global Distribution of *Pseudo-nitzschia* Species

The frequency of harmful algal blooms caused by *Pseudo-nitzschia* has increased in recent years (Bates et al. 2019). These events have been documented along coastlines and in open oceans, and within diverse environments ranging from the arctic circle to tropical waters, warm-temperate waters of both the Pacific and Atlantic Oceans, as well as the Mediterranean Sea (Quijano-Scheggia et al. 2008, Sahraoui et al. 2009, Hansen et al. 2011, Lim et al. 2012, Shuler et al. 2012, Downes-Tettmar et al. 2013, Husson et al. 2016, Lefebvre et al. 2016, Smith et al. 2018, Costa et al. 2019, Huang et al. 2019, Stonik et al. 2019, Arapov et al. 2020, Ajani et al. 2021, Kelchner et al. 2021, Anderson et al. 2022, Cook et al. 2022, Dzhembekova et al. 2022, Ramirez et al. 2022, Tankovic et al. 2022, Zheng et al. 2022). The documented global distribution of known *Pseudo-nitzschia* species *is* shown in Figure 1.1

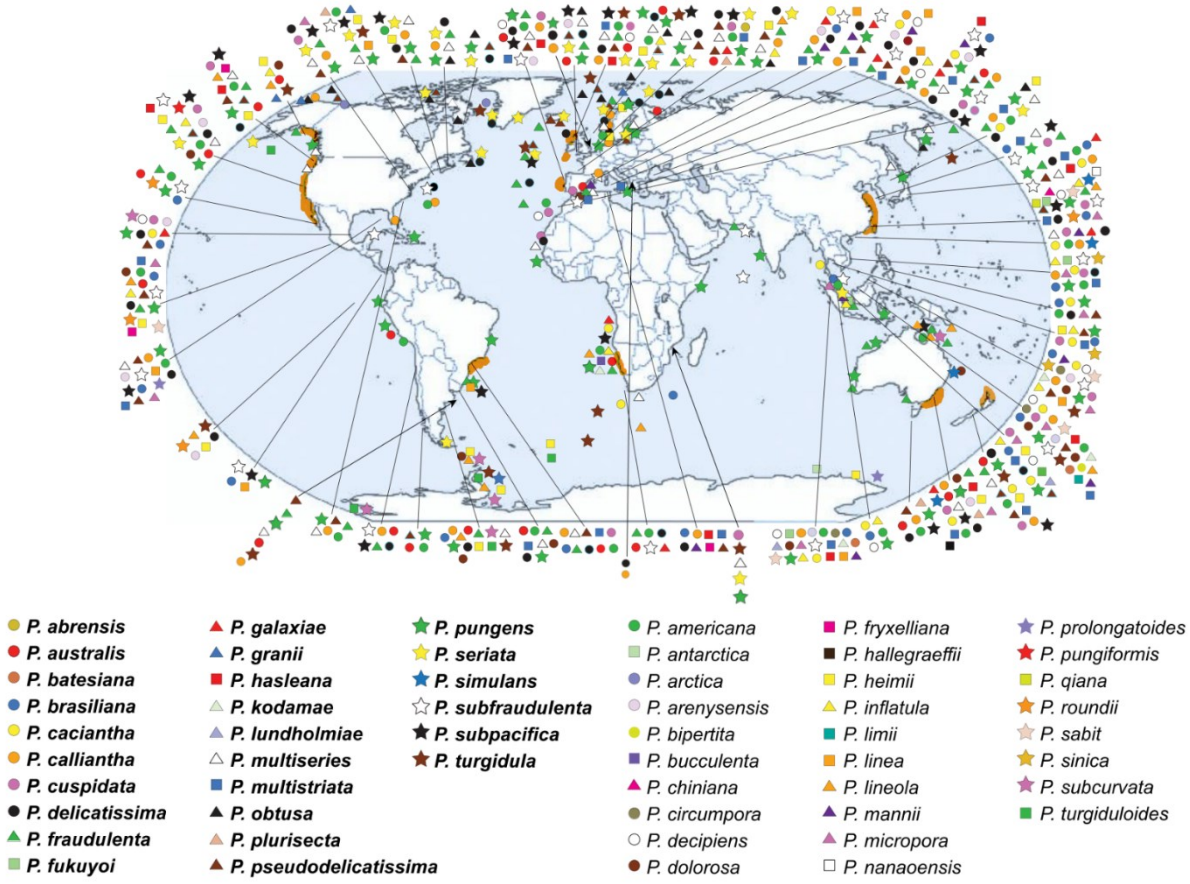

Figure 1.1 The global distribution of blooms caused by *Pseudo-nitzschia*. Strains known to produce DA are indicated in bold text, and non-toxic strains are presented in plain text. Coastal regions marked in orange indicate locations where shellfish and finfish harvesting have been historically closed due to elevated levels of DA (greater than 20 mg DA per g of the wet weight of shellfish tissue). The depicted *Pseudo-nitzschia* locations in this figure were derived from various studies including (Trainer et al. 2012, Bates et al. 2018, Bates et al. 2019, Huang et al. 2019, Arapov et al. 2020, Ajani et al. 2021, Kelchner et al. 2021, Anderson et al. 2022, Cook et al. 2022, Dzhembekova et al. 2022, Ramirez et al. 2022, Tankovic et al. 2022, Zheng et al. 2022).

1.4 Toxicity of *Pseudo-nitzschia* Species

Pseudo-nitzschia spp. were historically considered to be non-toxic. This was revised following the first reported case of amnesic shellfish poisoning, which was documented in Canada, in 1987 (Wright et al. 1989, Perl et al. 1990). It was caused by the consumption of shellfish contaminated with DA (Bates et al. 1991). A team of scientists at the National Research Council Atlantic Regional Laboratory (NRC-ARL) identified the pennate diatom *Pseudo-nitzschia multiseries* (referred to as *Nitzschia pungens f. multiseries* at the time) as the source of the toxin. Their findings included high levels of DA (790 µg DA g^{-1}) in blue mussels (*Mytilus edulis*) with lower levels (38 µg DA g^{-1}) in soft-shell clams (*Mya arenaria*) (Bates et al. 1989). In 2005, another amnesic shellfish poisoning incident was reported in France linked to the

consumption of clams (*Donax trunculus*) (Thebaud et al. 2005). The severity of DA poisoning is dependent on both the dose of the toxin and the health status of the affected individual. In the 1987 incident in Canada, elderly individuals were involved, resulting in fatalities (Teitelbaum et al. 1990).

1.5 Impacts of Domoic acid Exposure

1.5.1 Humans

DA structurally resembles the neurotransmitter glutamic acid (Kumar et al. 2009). It has a strong affinity for glutamate receptors in the central nervous system and can drive the uncontrolled influx of sodium and calcium ions into neural cells (La Barre et al. 2014). This leads to 'depolarisation', swelling and dysfunction, along with the production of reactive oxygen species, DNA damage, lipid peroxidation, energy depletion, mitochondrial damage, and ultimately, cell death (Berman and Murray 1997, Ramsdell 2007, Pulido 2008, Costa et al. 2010, Jia et al. 2016). As a result, DA poisoning often causes a range of debilitating syndromes including both neurological and gastrointestinal disorders. Typical symptoms include headache, loss of short-term memory, seizures, coma, vomiting, abdominal cramps and diarrhoea (Quilliam and Wright 1989, Teitelbaum et al. 1990). A study by (Petroff et al. 2019) showed that repetitive exposure to low levels of DA can cause chronic damage to the neurochemistry of the primate brain. Additionally, poisoning can affect various tissues and organs, leading to instability in blood pressure and arrhythmia (Pulido 2014) as well as kidney distress (Suzuki and Hierlihy 1993, Funk et al. 2014). (Alves et al. 2019) found that DA is highly bioavailable in the gut, favouring absorption by human intestinal epithelia after ingestion.

1.5.2 Ecosystems

DA has the potential to cause substantial ecological harm through the death or illness of various marine species, including fish, seabirds, sea otters, sea lions, and whales (Fritz et al. 1992, Work et al. 1993, Van Dolah 2000, Lefebvre et al. 2002b). *Pseudo-nitzschia* is an important and abundant primary producer that establishes the foundation of marine food webs and is readily available for consumption by a range of marine organisms (Bates and Trainer 2006a). They serve as vectors that transfer the toxins up the food chain (Figure 1.2) Filter-feeders, such as mussels and shellfish, actively accumulate toxic *Pseudo-nitzschia* cells, concentrating the DA in their digestive gland and other tissues (Mafra et al. 2010). Zooplankton can also accumulate DA and serve as vectors to higher trophic levels (Tester et al. 2000, Leandro et al. 2010).

The main source of DA exposure for humans is the consumption of contaminated seafood products (Kvitek et al. 2008).

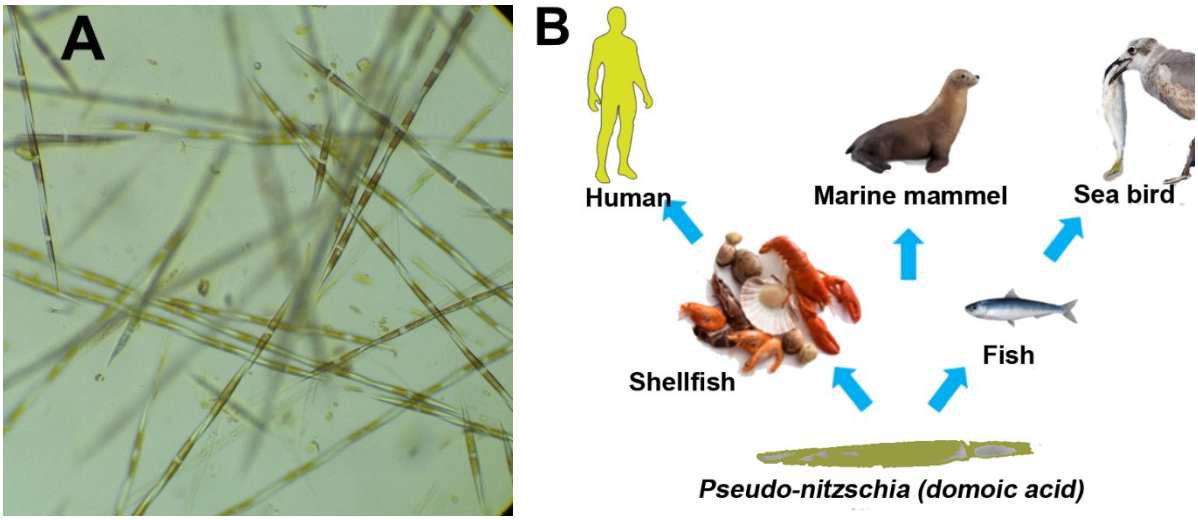

Figure 1.2 A) Microscopic image of *Pseudo-nitzschia* cells, credit: Alyssa Gellene, University of California. B) The impact of DA neurotoxin in the food web.

Wave action and turbulence enhance DA release from *Pseudo-nitzschia* cells (Sekula-Wood et al. 2009). However, it is a hydrophilic compound and this facilitates its rapid mixing (and therefore dilution) within the mass expanse of the ocean (Silver et al. 2010). Accordingly, more enclosed water bodies including coastal inlets, bays and estuaries are more likely to harbour dangerous levels of the toxin. It is also subject to photodegradation (Bouillon et al. 2006) and biodegradation processes (Hagstrom et al. 2007) that limit its longevity in the environment.

1.5.3 Industry

The occurrence of DA in water bodies has historically led to significant economic losses from the closure of fishing and tourism areas (Berdalet et al. 2016). For instance, the Dungeness crab industry on the West Coast of the United States suffered a significant financial loss in 2015 due to a *Pseudo-nitzschia* bloom, estimated at US$48 million (Brown 2016). Additionally, during 1998-1999 and 2002-2003, the long closure of the recreational razor clam fishery in WA, US resulted in an estimated direct loss of US$24 million (Moore et al. 2020). Currently, there are key factors that contribute to the challenges associated with monitoring DA levels in the environment. Firstly, the vastness of the oceans, which cover approximately 71% of the Earth's surface, facilitates the ubiquitous expansion of HABs, including the DA-producing blooms which can span remote areas from coastal regions to open waters. This expansive growth poses a logistical challenge for conducting routine monitoring and standard analysis. Additionally, the collection of samples from the rough seas, where rapid changes in weather, tides, and temperature are common, can introduce another challenge. To address these challenges, sustainable resources are

required to be allocated for conducting routine environmental monitoring at changing seas, through the deployment of specialised analytical equipment, research vessels, ongoing ocean sensors, autonomous vehicles, and trained operators. However, the existing constraints related to the availability of these monitoring technologies, expertise, and financial and logistical resources in regions affected by harmful algal blooms currently present a long-standing barrier to enabling effective monitoring to protect aquatic-based industries.

1.6 Domoic Acid Chemical Properties

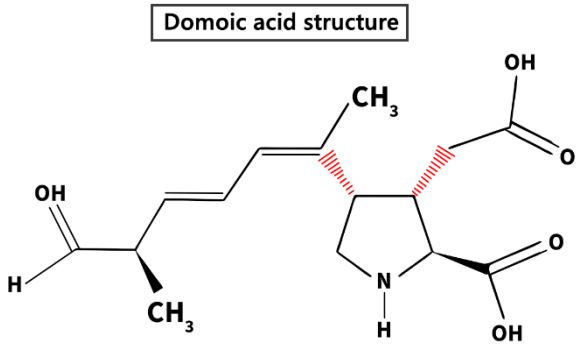

Figure 1.3 Chemical structure of domoic acid.

DA is a water-soluble amino acid with a molecular weight of 311 Daltons (Da). It contains a proline ring, one amino group, and three carboxyl groups (Figure 1.3). This structure has high hydrophilicity and polarity (Walter et al. 1992), which enables DA to persist in various marine organisms such as zooplankton (Leandro et al. 2010), crustaceans (Costa et al. 2003), and sediment (Burns and Ferry 2007, Sekula-Wood et al. 2009), and transfer stably through the food web. DA contains several polar functional groups, including carboxyl (COOH) and amino (NH_2) groups, as shown in Figure 1.3. These polar groups make the DA molecule highly hydrophilic, allowing a strong affinity for water molecules, and enabling rapid dissolution in aqueous medium such as seawater. Additionally, the planar and rigid arrangement of DA atoms minimises nonpolar interactions with any hydrophobic medium including soft tissues and sediment. This prevents DA from partitioning into these non-aqueous phases, supporting its long-term persistence in viscera of many marine animals. This unique configuration enables DA to be readily absorbed in various media like seawater, tissue, and sediment (Costa et al. 2010, Blanco et al. 2021).

DA has eight derivatives, known as isodomoic acid A-H (de La Iglesia et al. 2008). These are isomers and have been identified in various species including the red macroalga (a seaweed) *Chondria armata* (Maeda et al. 1986) and marine microalgae (diatoms) including *Nitzschia navisvaringica* (Romero et al. 2011), *Pseudo-nitzschia seriata* (Hansen et al. 2011), *Pseudo-nitzschia australis* (Rhodes et al. 2003), *Pseudo-nitzschia multiseries* and *Pseudo-nitzschia delicatissima* (Kotaki et al. 2008). Structural

differences between the DA analogues may alter their toxicity; isodomoic acids may have lower toxicity than DA (Hampson et al. 1992, Munday et al. 2008). The degree of toxicity varies among different isomers of isodomoic acid, with some being less toxic than others (Kotaki et al. 2005). Due to different structural arrangements, isodomoic acids have a lower binding affinity for the same neural receptors compared to the DA (Saeed et al. 2017a). This causes weaker and less effective binding of DA analogues with the receptors in the nervous system, leading to lower toxicity. However, isodomoic acids can still be toxic, albeit at a lower level than DA (Munday et al. 2008).

1.7 Domoic Acid Biosynthesis.

Recent work by (Brunson et al. 2018) identified a cluster of four genes: *dabA, dabB, dabC, and dabD* that are involved in DA biosynthesis in *P. multiseries.* Subsequent studies have shown that this gene cluster is regulated in response to various stressors including consumption of *Pseudo-nitzschia* by zooplankton (Hardardottir et al. 2019), phosphate and nitrate limitation (Lema et al. 2019), phosphate depletion and increased pCO_2 levels (Brunson et al. 2018). The biosynthesis of DA is initiated by the condensation of an L-glutamate starter unit, catalysed by the enzyme N-prenyltransferase encoded by the *dabA* gene to deliver the intermediate N-geranyl-l-glutamic acid (Brunson et al. 2018). N-prenylation conversion of glutamic acid into N-geranyl-l-glutamic acid requires a prenyl diphosphate donor such as geranyl pyrophosphate synthase (GPP) and farnesyl pyrophosphate synthase (FPP) to initiate the biosynthesis of DA (Chekan et al. 2020) (Figure 1.4). A cascade of biosynthetic reactions is regulated via Mevalonate (MEV) and Methylerythritol Phosphate metabolic (MEP) pathways. The current understanding of how this pathway is structured is illustrated in Figure 1.4. The *dab* gene cluster encodes four of the proteins involved in this pathway, including a predicted terpene cyclase (DabA), an α-ketoglutarate-dependent dioxygenase (DabC), a cytochrome P450 (DabD), and a protein of unknown function (hypothetical protein) (DabB). It has been shown that DabA generates N-geranyl-l-glutamic acid, which is converted by DabD cytochrome CYP450 enzyme into 7'-carboxy-l-NGG and cyclised by DabC into isodomoic acid (Brunson et al. 2018, Hardardottir et al. 2019). Interestingly, despite the genetic divergence between red algae and diatoms, DabA proteins found in *Pseudo-nitzschia spp.* (diatoms) are closely related to the KabA proteins from red algae (Chekan et al. 2020). The discovery of the DA biosynthetic genes may provide insight into the conditions that lead to toxin production and cessation and may prove to be valuable 'biomarkers' for monitoring the risks posed by *Pseudo-nitzschia spp.* blooms.

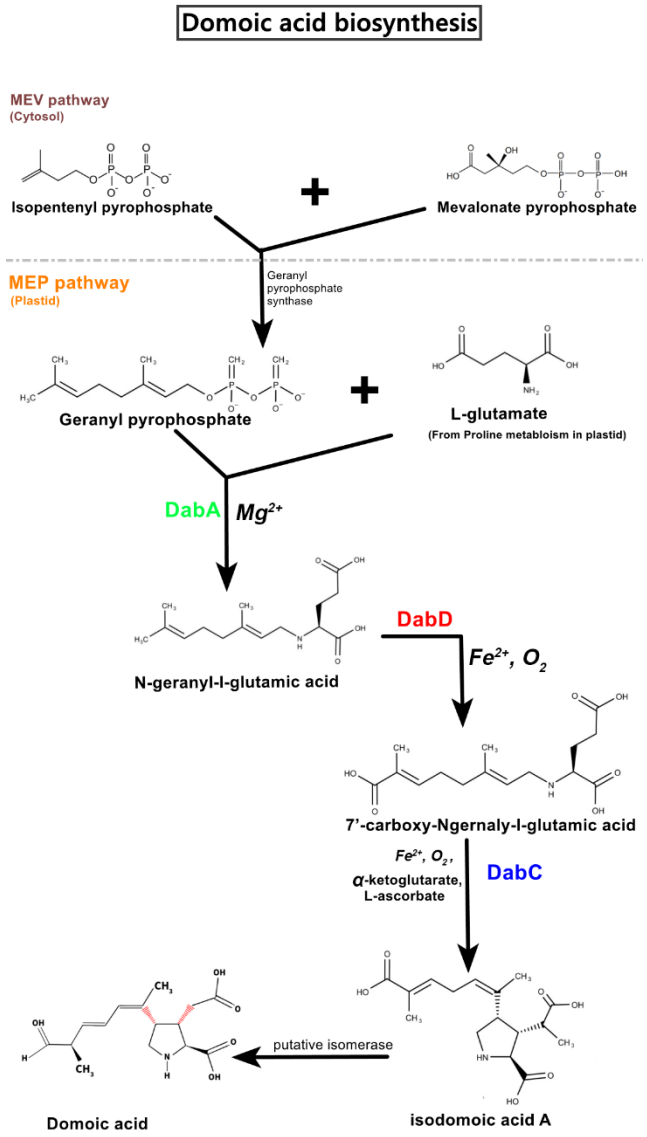

Figure 1.4 Biosynthetic pathway of DA in *Pseudo-nitzschia*. DA production is dependent on the availability of two precursor molecules, which are sourced through the mevalonate (MEV) pathway in the cytosol and the methylerythritol phosphate metabolic (MEP) pathway in the plastid. The transcription of the dab gene cluster is responsible for the encoding of DA biosynthetic steps. Redrawn from (Brunson et al. 2018, Hardardottir et al. 2019).

1.8 Factors Influencing Domoic Acid Production

DA production showed significant variability, extending not only across the *Pseudo-nitzschia* genus but also within strains of the same species. This variability has limited our understanding of the underlying factors that govern DA production. For example, both toxin and non-toxic strains of *P. multistriata* have been found in the same region of the Mediterranean sea (Quijano-Scheggia et al. 2010, Moschandreou et al. 2012, Pistocchi et al. 2012). In strains that do produce DA, the rate of production can also vary, for example with changing photoperiod. The influence of light:dark period on DA production was first

observed in *P. multiseries* under laboratory conditions (Bates et al. 1991). Interestingly, DA production can also vary between cells of the same genetic lineage and it has been reported that toxic cells can reproduce to form non-toxic 'offspring' in laboratory cultures (Bates et al. 1999). Overall, it is postulated that DA production is influenced by changes in a broad array of factors including nutrients, physical parameters, biological factors, and interspecies/strain variability within blooms (Mos 2001, Holtermann et al. 2010, Lelong et al. 2012). Coastal nutrients have been the focus of many studies due to the tendency of *Pseudo-nitzschia* blooms to form within coastal zones and the likely role of nutrient availability on bloom persistence and toxin production (Bates et al. 1998, Bates and Trainer 2006b, Schnetzer et al. 2007). Overall, the subject requires substantial further research. What is known about the factors that regulate DA production is summarised in the following sections.

1.8.1 Nitrogen

Nitrogen is an essential nutrient, and its availability is central to primary production (photosynthesis) (Kwon et al. 2022). The influence of nitrogen on DA production has been investigated in both environmental and laboratory studies. From these, it is known that low nitrate levels limit both growth rate and DA production in *P. multiseries*, probably due to the importance of N for photosynthesis and the biosynthesis of amino acids as precursors to DA (Bates et al. 1991). A two- to four-fold increase in DA production was observed in *P. multiseries* cells grown in elevated N concentration (as ammonium) (Bates et al. 1993). Members of the genus including *P. multiseries, P. fraudulenta, and P. calliantha* can utilise various nitrogen sources including nitrate, ammonium, urea, and glutamine (Thessen et al. 2009). Nitrogen sources may influence DA production (Kelly et al. 2021). For instance, *P. australis* showed a preference for using urea, leading to an increase in DA production, over other sources such as nitrate, ammonium, and glutamine (Howard et al. 2007, Cochlan et al. 2008). In contrast, *P. multiseries* demonstrates a preference for using arginine and glutamine (Martin-Jezequel et al. 2015), whilst, *P. cuspidata* and *P. fryxelliana* favour nitrate (Auro and Cochlan 2013).

1.8.2 Silicon and Phosphorus

Silicon and phosphorus are also essential nutrients and influence phytoplankton productivity, physiology and behaviour (including toxin production) (Sandoval-Belmar et al. 2023). A decline in silicate and phosphate concentration was found to elevate DA concentration in laboratory cultures of *Pseudo-nitzschia spp.* (Fehling et al. 2004, Thorel et al. 2017). In *P. multiseries*, there was an increase in DA production when phosphorous was limited, which coincided with a reduction in chlorophyll (and therefore also photosynthesis rate and ATP production) (Pan et al. 1996a). Silicate limitation also

stimulates toxin production, however, also leads to an increase in chlorophyll content (Pan et al. 1996c). High DA levels have been measured in *Pseudo-nitzschia spp.* cultures deficient in phosphorus, compared to those replete in phosphorus (Sun et al. 2011). Conversely, high DA levels seem to correlate with relatively high phosphate concentrations in coastal waters affected by upwelling events (Palenzuela et al. 2019). Upwelling events refer to the process where cold, nutrient-rich water from the deep ocean rises to the surface waters. This process transfers nutrients to the surface water, which benefits phytoplankton (Abrahams et al. 2021). Overall, further research is necessary to determine the influence of phosphorus and silicate concentration on DA production.

1.8.3 Iron

Iron serves as a key trace metal to modulate a range of cellular functions, including photosynthesis, respiration, enzyme composition, electron transport and energy conversion (Schoffman et al. 2016). The function of iron in phytoplankton physiology has been studied in both environmental samples and laboratory cultures, revealing conflicting effects on DA production. Over the past 15 years, outbreaks of DA poisoning along the California coast have been linked with iron enrichment from upwelling events (Smith et al. 2018). This finding is in contrast to earlier reports of iron deficiency and toxic blooms during upwelling (Trainer et al. 2009). In high-nutrient, low-chlorophyll waters, where iron is limiting, the *Pseudo-nitzschia* species showed the highest DA levels upon the addition of iron in experiments (Boyd et al. 2007, de Baar et al. 2008). These experiments, known as SOFeX, IronEx II, and PAPA station experiments, were conducted in the Southern Ocean to study the effects of iron addition to the seawater. These experiments enabled researchers to understand how adding iron might change the phytoplankton population and the marine ecosystem (de Baar et al. 2005). These experiments indicated the production of 220, 45 and 200 pg DA L^{-1}, respectively, through a sporicidal pulse of iron into the seawater (Silver et al. 2010, Trick et al. 2010). DA levels increased in *P. delicatissima* cells grown under iron-replete conditions (Prince et al. 2013). High iron concentrations were found to enhance DA production by *P. multiseries* (Sobrinho et al. 2017). These findings are supported by (Lelong et al. 2013), who observed no DA production by *P. delicatissima* under the limitation of iron.

Pseudo-nitzschia species have been found to employ two physiological strategies in response to severe iron (Fe) limitation in the open ocean and HNLC waters, as reported by (Martin and Fitzwater 1988, Pfaffen et al. 2013). *Pseudo-nitzschia* cells produce iron-acquisition proteins, such as ferritin, plastocyanin and flavodoxin, which enable the cells to sequester and store large amounts of Fe. *P. multiseries*, *P. australis*, and *P. granii* use stored iron in their cells as a backup to maintain growth in an environment of limited iron availability (Marchetti et al. 2009, Groussman et al. 2015, Marchetti et al.

2015). There is some evidence that DA itself may serve an important role in the acquisition of Iron. (Maldonado et al. 2002) demonstrated that *P. multiseries* cells increased the amount of particulate DA by 95% to enhance their activity of iron acquisition in iron-depleted conditions. This suggests that iron availability governs the physiology of *Pseudo-nitzschia* cells, altering their tendency to produce DA. This observation aligns with the known mechanism of DA biosynthesis, in which metals like iron play a regulating role in activating the metabolic processes leading to the production of DA, as shown in Figure 1.4 and discussed in section 1.7.

1.8.4 Irradiance

As photosynthetic organisms, *Pseudo-nitzschia* are particularly influenced by light intensity and photoperiod. Although *Pseudo-nitzschia* cells can survive for up to 6 weeks in darkness, a significant acclimatisation period is necessary for the cells to resume growth under normal light conditions (Mengelt 2002). Changes in light exposure are known to influence DA production (Bates et al. 1991, Pan et al. 1998). (Cusack et al. 2002) found that *P. australis* increased the DA production rate up to 24-130 times when these cultures were exposed to 115 µmol photons m^{-2} s^{-1} compared to those exposed to 12 µmol photons m^{-2} s^{-1}. (Thorel et al. 2014) found that DA biosynthesis in a different strain of *P. australis* was 18 times higher at 400 µmol photons m^{-2} s^{-1} than those *P. australis* cultures maintained at 35 µmol photons m^{-2} s^{-1}. (Fehling et al. 2005) studied the effect of spring (9:15 h light: dark) and summer (18:6 h light: dark) photoperiods on the toxicity of *P. delicatissima* and *P. seriata*, in laboratory cultures, finding that long photoperiods increased DA level, compared to replicates experienced shorter photoperiods. In summary, light serves as a fundamental energy source for photosynthetic reactions, and both insufficient and excessive light can stress the growth and photosynthesis of *Pseudo-nitzschia* spp. These stressors have the potential to impact the overall integrity and performance of the *Pseudo-nitzschia* cell, including its capacity for DA production, albeit the underlying mechanism remains unclear.

1.8.5 Temperature

Pseudo-nitzschia spp. can survive and grow over a wide range of temperatures. The ability of *Pseudo-nitzschia* cells to tolerate a wide range of temperatures allows them to thrive in diverse aquatic environments distributed across various regions (Ardyna et al. 2020, Roche et al. 2022). As with light exposure, the direct interplay between temperature and growth rate makes it difficult to determine if temperature has a direct influence on DA production, or if any link is predicated on the obvious correlation between temperature and cell growth rate. Temperature change is known to alter DA production (Lundholm et al. 1994). Increasing the temperature in *P. multiseries* cultures from 5°C to 25°C

led to a reduction in the growth rate of their cells and a simultaneous increase in the measured concentration of DA in the culture.

P. multiseries was found to increase DA production when the temperature increases from 5°C to 25°C, coinciding with a reduction in growth rate (Lewis et al. 1993). This temperature-dependent increase in DA production was observed in controlled conditions within a time series study, demonstrating how *P. multiseries* responds to temperature variations over time and its impact on DA production and growth rate. More recently, *P. multiseries* showed maximum toxin levels of 8.8 pg DA cell^{-1} at 20°C (Lewis et al. 2018). However, the toxin concentrations in *P. multiseries* were lower at 27°C than at 18°C (Amato et al. 2010). Despite these observations, most studies have demonstrated the stimulating impact of warming on DA production in *Pseudo-nitzschia* species (Zhu et al. 2017, Trainer et al. 2020, Clark et al. 2022). These results suggest that *Pseudo-nitzschia* bloom and DA elevations may be indirectly related to global warming. These findings suggest that DA elevation during *Pseudo-nitzschia* bloom could potentially serve as an indirect indicator of global warming.

1.8.6 pH

pH value quantifies the concentration of hydrogen ions (H^+) to measure the acidity or alkalinity of an aqueous solution. The pH values range from 0 to 14. pH of 7 indicates a neutral solution, while values below 7 demonstrate acidity and value above 7 indicates alkalinity (Nicolas et al. 2017). Changes in pH levels can significantly impact the growth of *Pseudo-nitzschia* spp., which, in turn, affects the production of DA (Wingert and Cochlan 2021b). For instance, a minor increase in alkalinity (from 8.8 to 9.1) was found to trigger an increase in DA production in *P. multiseries*, albeit a decline in its growth rate (Lundholm et al. 2004). Similar findings by (Trimborn et al. 2008) indicate that the highest DA concentrations (140 pg DA cell^{-1} in this case) were produced at pH 8.9. Conversely, lowering the pH from 8.38 to 7.95 increased DA content (Sun et al. 2011). Additionally, *P. fraudulenta* and *P. australis* produced their highest levels of particulate DA at pH 8.07 (Ayache et al. 2021). These findings suggest the significant role of pH in regulating DA biosynthesis, as even minimal pH changes can induce DA production. However, since pH also substantially influences growth rate, the precise underlying mechanism remains to be elucidated.

1.8.7 Carbon

Carbon dioxide (CO_2) is fixed into organic compounds through photosynthesis (Smith et al. 1983). The amount of carbon significantly impacts the carbon fixation rate and therefore the availability of energy sources and the organic compounds required for growth and cellular functions in all living organisms,

including phytoplankton (Moreno et al. 2022). Among the vital functions of toxigenic *Pseudo-nitzschia* cells is the production of DA. When the growth rate of *Pseudo-nitzschia* cells decelerated, and the cells entered the stationary phase, their consumption of carbon also reduced (Lundholm et al. 2004). This reduction in carbon utilisation leads to an elevation of both total inorganic carbon (TIC) and the partial pressure (P_a) of CO_2 (pCO_2) in the surrounding medium, leading to acidification. *Pseudo-nitzschia* cells may have evolved a mitigation strategy to cope with acidic environments by consuming excess carbon species in the process of DA biosynthesis (Trimborn et al. 2008, Sun et al. 2011). High levels of DA (at 5.5 pg DA $cell^{-1}$) were observed in *P. fraudulenta* cultures exposed to elevated pCO_2 concentrations of 765 ppm (Tatters et al. 2012b). Additionally, (Wohlrab et al. 2020, Wingert and Cochlan 2021b) demonstrated a significant increase in DA production as pCO_2 levels rise, by simulating scenarios of ocean acidification in laboratory settings. Thus, DA production could potentially serve as an indicator of ocean acidification.

1.8.8 Copepods

Copepods are a diverse group of aquatic crustaceans that belong to the subclass Copepoda. Copepods are primary consumers that feed on phytoplankton and detritus, providing a food source for higher trophic levels within the food web (Pierce and Turner 1992). Within a stable marine food web, copepod zooplankton can actively consume phytoplankton, including *Pseudo-nitzschia spp*., thereby regulating a normal primary production process in the marine ecosystem. But when copepod predation on *Pseudo-nitzschia* spp. is reduced, the abundance and dominance of *Pseudo-nitzschia* spp. is increased, leading to a disturbance in overall ecosystem balance. Conversely, increased copepod grazing activity lowers the competitive advantage of *Pseudo-nitzschia* spp., and indirectly influences the production of DA (Leandro et al. 2010, Tammilehto et al. 2015, Miesner et al. 2016, Hoffmeyer et al. 2020, Cook et al. 2022). This dynamic interplay between copepods and *Pseudo-nitzschia* constitutes a significant factor in regulating *Pseudo-nitzschia* dominance, and subsequently the patterns of DA production. (Haroardottir et al. 2015) reported an approximately 3300-fold increase in toxin production due to copepod grazing. In the presence of mixed diets, the ingestion rates of copepods varied depending on the diets, leading to a shift in copepod selection towards non-diatom prey that does not produce DA (Olson et al. 2006). The induction of DA production in response to grazers is linearly related to the presence of copepodamides, which are polar lipids excreted by copepods during predation (Lundholm et al. 2018). Overall, increased toxin production is suggested to be a defence mechanism for population survival that compensates for reduced growth and reproduction rates (Karban 2011, Selander et al. 2019). In summary, the presence of DA can indicate disruptions within the phytoplankton community, imbalances in primary production, and the subsequent potential for cascading effects throughout the marine ecosystem.

1.9 Removal and Inactivation of Domoic Acid

Several physical, chemical and biological parameters influence *Pseudo-nitzschia* growth and DA production. Given the challenges in controlling and mitigating some of these factors, for example, rising sea temperature or sporadic nutrient release from anthropogenic sources, current management authorities and policymakers have struggled to establish effective strategies to reduce *Pseudo-nitzschia* blooms and their widespread ecological disruption, economic loss, and public health consequences. One approach might be to decontaminate seafood products prior to consumption either by cooking or freezing. However, heating (including autoclaving) has limited effectiveness in reducing DA concentration in contaminated mussels (McCarron and Hess 2006) and, similarly, boiling *Pseudo-nitzschia* cultures has no impact on toxin concentration (Bajarias et al. 2006). This toxin compound cannot be destroyed even by strong solvents such as acetonitrile. DA remained stable in acetonitrile solution at 20°C for 9 months and in an aqueous solution (pH 5-7) at 4°C for a year (Quilliam 2003, Thomas et al. 2008). Freezing does not destroy the DA but ruptures harvested algal cells due to freezing and thawing, leading to the release of more toxin into the surrounding environment (Hatfield et al. 1995, Leira et al. 1998). Other potential approaches include the use of magnetic separation for clearing algal cells from the water column (Liu et al. 2013). This technique can also be employed to clear algal toxins like DA from seawater. To achieve this, a magnetic adsorbent is mixed with contaminated seawater, selectively binding to the DA toxin. A magnetic field is then applied to this mixture, directing the magnetic adsorbent nanoparticles, along with the bound DA, towards the magnet. After separating DA from the surrounding seawater, the DA is eluted and removed from the magnetic adsorbent by changing the pH of the solution (Lin et al. 2020). In practical applications for the removal of DA from large volumes of seawater, other methods such as adsorption onto activated carbon, membrane filtration, or chemical precipitation are more commonly employed (Pinto et al. 2023).

Alternatively, approaches that utilise other microorganisms including bacteria, fungi and protozoa may offer a cost-effective and eco-friendly solution (Sun et al. 2018). Bacteria produce bioflocculants, such as polysaccharides, proteins, and lipids, which inhibit algal growth by blocking photosynthesis and destroying cell membranes (Sun et al. 2018). Bacteria also facilitate the decomposition of DA in seawater using photochemical reactions (Wright et al. 1990, Bates et al. 2003, Bouillon et al. 2006, Bouillon et al. 2008, Gagez et al. 2017). The microbial degradation of DA decreases with salinity, leading to a longer residence time in the water column (Van Meerssche and Pinckney 2017). These findings suggest field solutions to directly remove the DA from seawater before it reaches human or their seafood (Djaoueda et al. 2008, Bandala et al. 2009, Caron et al. 2010, Robertson et al. 2012). As an example, bioreactors were used to physically separate and filtrate nutrients from seawater (Mao et al. 2020). Perhaps this can

be leveraged for large-scale field applications to be employed in tandem with existing water treatment facilities to ensure early removal of DA. Implementing these detoxification technologies will depend on their cost, efficiency, and capacity for DA removal.

1.10 Challenges with the Detection of *Harmful Algal Blooms*

Various strategies have been suggested and explored for detecting HABs, enabling local authorities to mitigate the associated hazards. The current statutory monitoring of HAB cells and toxins primarily involves the analysis of contaminated seafood and seawater samples. In response to HAB events, local authorities routinely collect samples of both water and shellfish and transport them to centralised laboratories for mandatory analysis, which typically includes: (i) the identification of HAB species and enumeration of HAB cells using microscopy. Typically, water samples are fixed on-site with Lugol's solution to settle HAB cells for several hours to enable specialist taxonomists to identify and count the cells of HAB species by light microscopy (Hasle G 1978). In certain cases, electron microscopy is necessary for identification purposes, particularly when HAB species have similarities in their ultra-small morphometric cellular components, among different strains of the same species as *Pseudo-nitzschia*. Sample processing for electron microscopy-based identification is more complex compared to the procedures used in light microscopy (Accoroni et al. 2020).

Alternatively, (ii) HAB toxins are measured in harvested shellfish extracts using liquid chromatography linked to fluorescence detection (LC-FLD), ultraviolet detection (LC-UV) or tandem mass spectrometry (LC-MS/MS), for Paralytic Shellfish Toxins (PST), Amnesic Shellfish Toxins (AST) and Lipophilic Toxins (LT), respectively (Turner et al. 2019). These methods require a centralised facility equipped with expensive instruments operated by highly trained personnel. Furthermore, these methods are not cost-effective since they rely on sophisticated equipment that must be operated by specialist personnel. Another disadvantage of these reference methods includes a long delay between sampling and results that can be extended up to 48 hours. When the toxin levels exceed a regulatory threshold group (also known as the Maximum Permitted Limit or MPL), the harvesting areas are temporarily closed. These closures remain in effect until toxin levels have consistently fallen below the MPL, in two consecutive analyses conducted at least 48 hours apart. In cases where food business operators have harvested shellfish from these closed sites without waiting for official control test results or without conducting their end-product testing (EPT), it becomes necessary to investigate the quantity of shellfish harvested since the last sample was taken. Depending on the findings, this may lead to further closure of shellfish harvesting sites and a recall of contaminated products across the food chains.

In certain cases, these food products may have already been consumed (Young et al. 2019). This is a risk for shellfish harvesters, public health and consumer confidence and creates challenges for businesses. These official regulatory techniques encounter challenges in accurately quantifying low algal cell counts per litre using microscopy and low toxin levels via HPLC technology. This limitation makes it challenging to identify early indicators of HAB, hindering proactive measures to mitigate their impacts. The following sections will explore potential improvements to existing analytical methods and practices to achieve early, rapid, and sensitive monitoring of HAB events, enabling authorities to effectively manage the collection and preparation of samples for laboratory analysis.

1.11 Detection of *Pseudo-nitzschia* species and Domoic Acid

The detection of *Pseudo-nitzschia* and domoic acid remains a significant challenge (Zabaglo et al. 2016, Bates et al. 2018, Smith et al. 2022). Remote sensing technology has been used to identify and track *Pseudo-nitzschia* through space and time. This is done using high-resolution satellite imagery to measure ocean colour and photosynthetic pigments associated with phytoplankton (Shen et al. 2012). This enables a wide-scale observation of the ocean and the dynamics and scale of phytoplankton blooms. However, there are a range of limitations such as difficulties in obtaining clear and accurate images over areas obscured by cloud cover, limited data access, and the necessity for proficient data analysts (Avtar et al. 2020). However, perhaps the greatest limitation is the poor resolution at a small spatial scale and a lack of specificity. To obtain high-resolution data for specific HAB species there are several methods which are predicated on the collection and analysis of samples.

1.11.1 Microscopy-based Identification of *Pseudo-nitzschia* species

Microscopic identification of *Pseudo-nitzschia* relies on a detailed examination of cell samples that require taxonomic expertise in distinguishing morphometric features. The cells are first settled in specialised chambers and then observed using light and electron microscopy (Kaczmarska et al. 2005). The cell wall of *Pseudo-nitzschia* includes structures known as frustules, which have a species-specific ultrastructural pattern that can only be distinguished at high magnification, as depicted in Figure 1.5, (Lundholm et al. 2002, Orlova and Shevchenko 2002). Preparing samples for electron microscopy involves a series of complicated and time-consuming steps (Arapov et al. 2023). Another challenge arises when the morphometric characteristics of frustules such as the number, dimensions, and geometry of fibulae, striae, and poroids, change due to environmental conditions, and may overlap among different species and strains (Cerino et al. 2005, Lundholm et al. 2006a, Amato et al. 2007, Hansen et al. 2011). Due to misidentification, toxic and non-toxic species can be identified as a single species, leading to both

false negative and false identifications. Accordingly, the taxonomic classifications of *Pseudo-nitzschia* species have significantly changed in recent years (Trainer et al. 2012). Despite current technological advances, taxonomic assessment using electron microscopy still presents challenges as it demands extra sample processing time, resources, and continuous training for taxonomists to accurately distinguish emerging cellular characteristics of *Pseudo-nitzschia* cells. Thus, electron microscopy should be complemented with other identification methods to ensure reliable and efficient characterisation.

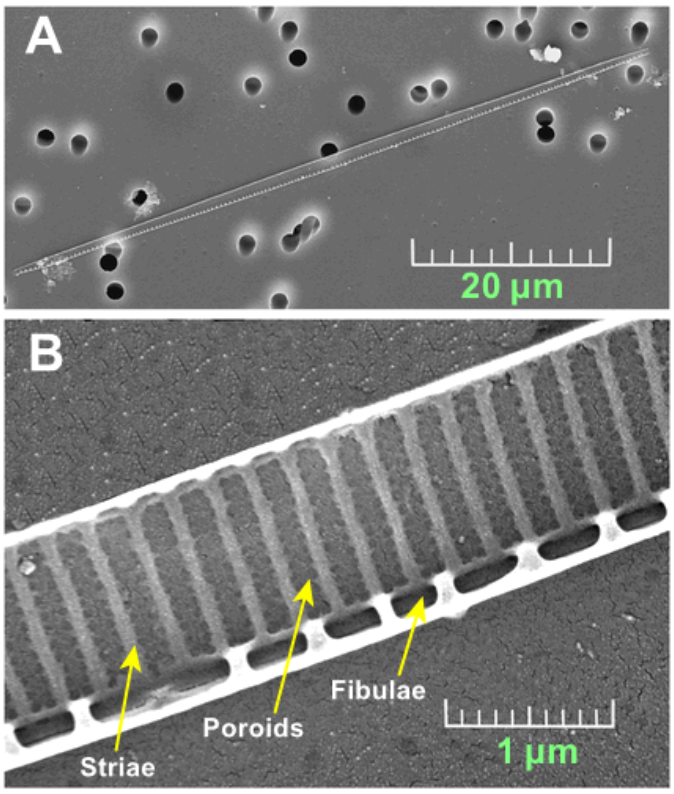

Figure 1.5 Scanning electron microscopy (SEM) images of DA-producing diatom, *Pseudo-nitzschia delicatissima*. A) View of whole cell B) Detail of the central part of the cell of (a), showing fibulae, striae and poroids. Scale bars: (a) 20 µm, (b) 1 µm. Updated from (Arapov et al. 2017).

1.11.2 High-Performance Liquid Chromatography (HPLC)

High-performance liquid chromatography (HPLC) has been routinely employed as a reliable, reproducible, sensitive and selective method for the detection of various marine toxins (Quijano-Scheggia et al. 2008, Zapata et al. 2011, Brunet et al. 2014). HPLC involves a multistep process to separate and quantify marine toxins of HABs. Initially, the toxins are extracted by a continuous flow of a given sample through a column (Santana-Viera and Lara-Martin 2023). Each toxin interacts with the column material at varying degrees, based on their unique chemical signatures, which include size, formula, charge, and polarity. These properties influence how tightly the toxins adhere to the column material and how fast they move via the mobile phase (Li et al. 2014). For example, larger toxins may be temporarily trapped in the column's pores, leading to slower movement, while smaller toxins pass

through rapidly. Similarly, toxins with charges opposite to the column material may bind strongly, resulting in slower elution, whereas those with matching charges elute faster (Coskun 2016). As the sample exits the column, a detector records its presence, creating a unique chromatogram for each toxin. By comparing the elution or exit times and patterns to known standards, the toxins present in a given sample can be identified and quantified (Kang 2012). HPLC technique has enabled the quantification of DA extracted from various samples including seawater, cultures, and contaminated shellfish and fish homogenates (Quilliam et al. 1989, Lefebvre et al. 1999).

Despite the HPLC utility in quantifying marine toxins, yet it has certain limitations. HPLC relies on reference standards for toxin identification, which may not cover all HAB toxins, potentially missing novel or less-studied compounds that are not covered by these standards (Etheridge 2010). Furthermore, HPLC was found not to be efficient in separating structurally similar toxins that can elute at similar times, leading to misidentification (Costa et al. 2009). To address this, a set of correction procedures becomes imperative to ensure the validity of spectral detection using HPLC. Variability in HPLC column performance and detector sensitivity can further impact the accuracy of toxin quantification among laboratories and regulation authorities (DeGrasse et al. 2011). Additionally, the sample preparation is a time-consuming process which prevents real-time monitoring of toxin levels, a crucial aspect for early warning systems (Vilarino et al. 2010). Moreover, the need for specialised equipment and trained personnel presents a challenge that restricts the readily accessibility of HPLC in resource-constrained settings.

1.11.3 Antibody-based Assays

Alternatively, ELISA (enzyme-linked immunosorbent assays) has been developed for rapid and simple detection of DA and other algal toxins (Briggs et al. 2004, Yu et al. 2004, Campas et al. 2008, Dubois et al. 2010). ELISA employs fluorescently labelled antibodies that exclusively target the specific structure of toxin protein known as epitope (Koivunen and Krogsrud 2006). The epitope is a specific region on the surface of an antigen, which serves as a unique identification tag, enabling immune system components, like T cells, to identify, distinguish and respond to foreign proteins, such as pathogens or harmful molecules (Suurmond and Diamond 2015). In the ELISA method, the binding event of the epitope triggers a series of enzymatic reactions, leading to the generation of a measurable signal, often visualised as a colour change (Wild 2013). DA ELISA assay relies on immobilising a DA-protein conjugate on plastic wells, exposing the sample to anti-DA-antibody-HRP conjugate, and measuring the binding reaction by incubating this sample with a substrate that produces a blue product upon reaction with the HRP enzyme (Figure 1.6). The colour intensity is measured spectrophotometrically and is proportional to the

concentration of DA in the sample (Kleivdal et al. 2007b, Tsao et al. 2007). This assay can be calibrated using standard solutions, offering low limits of quantification for DA in seawater and mussel homogenates, down to 10 µg l^{-1} and 0.003 µg g^{-1}, respectively (Kania and Hock 2002, Kleivdal et al. 2007a). The detection limits achieved by this method are lower than the regulatory threshold of 20 µg DA g^{-1}, which is typically used to determine the need for routine flesh and water sampling (Wekell et al. 2004). The sensitive quantification provided by the ELISA assay can significantly assist to minimise and prevent human exposure to DA.

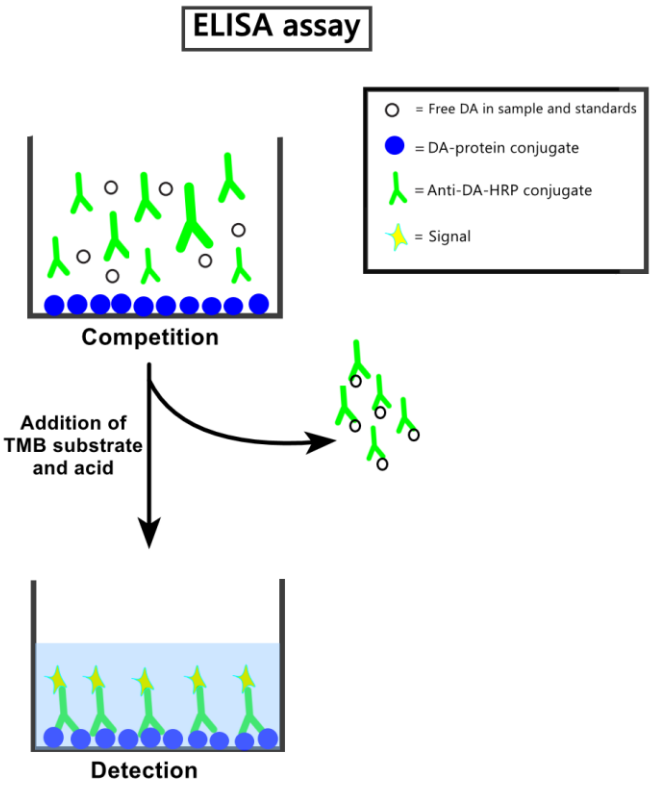

Figure 1.6 DA quantification by enzyme-linked immunosorbent (ELISA) assay. The ELISA kit is provided in strips of 12 microwells, each coated with DA protein conjugate. The anti-DA-HRP competes with the free DA in the sample to bind the conjugates. The unbound conjugates are removed during the rinsing steps, and the bound ones are quantified after the addition of substrate and acid to stop the reaction. This illustration was adapted from the user manual of the ELISA kit (ASP ELISA protocol-Biosense Laboratories).

Immunoassays have the potential to enable the multiplexed detection of marine toxins, including DA, even in the presence of compounds that share a similar chemical structure (Campbell et al. 2011). A multiplex lateral flow immunoassay has been developed for the sensitive and specific detection of DA, okadaic acid, and saxitoxin. The assay has working ranges of 0.2–1.5 ng ml^{-1} for okadaic acid, 2.5–65.0 ng ml^{-1} for saxitoxin, and 8.2–140.3 ng ml^{-1} for domoic acid (Mills et al. 2022). Combining the ELISA assay with multi-channel surface plasmon resonance (SPA) technology allowed for highly sensitive quantification of DA levels with no cross-reactivity with structurally related compounds such as

tetrodotoxin, saxitoxin, and okadaic acid (Yakes et al. 2016). A multiplex SPR analyser achieved low detection limits ranging between 1.0 and 1.7 ng ml^{-1} for the simultaneous immuno-based analysis of four phycotoxins, including DA, okadaic acid, neosaxitoxin, and saxitoxin (Campbell et al. 2011). This coupling of technologies has also enabled the multiplex detection of DA, saxitoxin, and okadaic acid in seawater, achieving a limit of detection for DA of 1.7 ng DA ml^{-1} within 7 hours for 24 samples (McNamee et al. 2013). However, ELISA has some limitations as it relies on the availability of specific antibodies that can selectively recognise the target molecule like toxins from its variants. If these antibodies are not readily available, performing ELISA testing of any particular target can be challenging (Li and Persson 2021). Additionally, cross-reactivity with structurally similar compounds can lead to false positives and difficulty in distinguishing between toxin analogues (Li and Persson 2021). Furthermore, the sensitivity of ELISA analysis can also be reduced by the sample matrix, particularly in environmental samples containing various non-target components (Gross et al. 2022). To address this, extensive sample preparation must be performed by skilled operators, which in turn, extending the analysis duration.

Alternatively, the lateral flow immunoassay format offers the potential for rapid and simple toxin testing in the field. Lateral flow-based ELISA kits allow the observation of the results by the naked eye or using electronic scanners (Dillon and Campbell 2023). Two commercially available kits were manufactured by Neogen and Scotia Rapid Testing Ltd, and provided a simple and accurate qualitative detection of DA in shellfish within 10-60 minutes, with limits of detection of 20 and 10 mg/kg, respectively (Johnson et al. 2016). A lateral flow immunoassay achieved 100% accuracy in quantifying DA levels from shellfish extracts at concentrations as low as 17.5 ppm, which is below the regulatory threshold levels of 20 mg DA/kg shellfish tissue (20 ppm) (Jawaid et al. 2013). This high level of accuracy highlights the potential of immunoassays for rapid and simplified on-site screening of shellfish harvesting sites.

For on-site testing, the ELISA assay was integrated into the Environmental Sample Processor (ESP), an autonomous robotic system with electromechanical and fluidic components (Moore et al. 2021). This system has enabled near real-time surveillance of DA levels and *Pseudo-nitzschia* abundance during five deployments over three years. These data were then compared to parameters associated with bloom initiation parameters, such as nutrient loading, in order to better understand the mechanisms underlying bloom dynamics (Moore et al. 2021). The ELISA assay has previously conducted using the same system, enabled automated extraction and detection of DA in 2-3 hours with a limit of detection of 40 ng DA l^{-1} (Doucette et al. 2009). The results compared well to standard bench-top ELISA procedures for detecting harmful algal toxins but experienced significant inefficiency during deployments in 2006 and 2007 in Monterey Bay, CA, USA, due to instability of the IgG antibody of DA under field conditions (Doucette et al. 2009). Furthermore, bench-top ELISA tests were found to slightly overestimate DA levels when compared to liquid chromatography methods (Kleivdal et al. 2007b). This may be due to the antibodies

of the ELISA reaction having an affinity for DA isomers that are also present in the sample and share similar structures and geometries with the DA (Saeed et al. 2017b). When the ELISA assay relies on a single epitope for antibody binding, there is a risk of cross-reactivity with structurally similar molecules, resulting false positives, reducing assay specificity (Mills and Campbell 2022). However, targeting multiple epitopes can significantly improve specificity by increasing the chances of selective and accurate target recognition (Mills and Campbell 2022). In summary, ELISA immuno-based assay can offer a rapid, sensitive, robust and promising tool for quantifying harmful algal toxins (HATs) in both laboratory and field settings.

1.11.4 Nucleic acid Sequence Amplification Methods

Molecular techniques have become a fundamental tool across various applications such as genetic testing, pathogen detection, gene expression analysis, forensic investigations, and environmental monitoring. These techniques rely on replicating genetic markers of nucleic acid sequence into a larger and detectable quantity of target genetic material at the end of the molecular reaction (Turner et al. 2023). The replication of specific DNA or RNA sequence components involves the employment of a purified DNA, RNA or cDNA template, specific primers to bind to the target sequence, DNA or RNA polymerase enzymes, as well as a mixture of nucleotides (A, C, G, T; U for RNA) for synthesising new DNA or RNA strands (Lefferts and Lefferts 2017). The temperature of the amplification reaction is a key parameter to enable the near-exponential increase of the target sequence in each step (Ochman et al. 1993). Therefore, precise management of reaction conditions such as temperature is required to ensure accurate and reliable amplification results.

Molecular genetic amplification methods can offer several advantages, one of which is the ability to identify HAB cells based on genetic information rather than relying on their morphology (Penna and Galluzzi 2013a, Pearson et al. 2021). Molecular-based techniques ensure the specific identification by employing oligonucleotides including primers and fluorescent reporters which are identical or closely matched to the target sequences of algal cells. Through careful assay design, the analysis can be customised to target potentially any species or taxonomic group with a high degree of selectivity. Incorporating a fluorescent reporter into the analysis enhances this selectivity and allows for real-time detection of the genetic targets. To accurately quantify algal cells, a comparison between the number of amplification cycles required to achieve a threshold level of fluorescence with a range of DNA standards that contain known quantities of target sequence copies. The outcome of this comparison us to calculate the abundance of the target sequence within the original sample and estimate the cell number present. These molecular techniques are sensitivity enough to identify and amplify low abundance of target DNA or RNA target sequence, allowing rapid results by duplicating a large number of copies of the target

sequence in a short time (Bej et al. 1991). Highly sensitive quantification offers significant advantages, allowing the detection of a small number of cells per litre of the sample. This level of sensitivity is crucial, especially in scenarios where algal toxins in seafood can reach harmful levels even when the surrounding water has very low cell densities (Dyhrman et al. 2010).

Molecular analysis techniques for detecting HAB taxa now allow for multiplexed or parallel quantification of multiple taxonomic marker sequences in a single reaction. Multiplexed assays offer several advantages, including a reduction in the time, reagents, and resources needed for individual tests. They also decrease the risk of cross-contamination and human error since all genetic markers are processed within a single reaction tube. Multiplexing allows for the rapid detection of a wider range of HAB taxa in a single test, enabling comprehensive monitoring of the algal community in each given sample and a better understanding of overall ecosystem health. These advantages make molecular genetic methods versatile and applicable across a wide range of genetic quantification, including HAB monitoring, gene expression analysis, genetic variation analysis, DNA sequencing, and forensic analysis (DeYoung and Honeycutt 2005).

While molecular techniques offer advantageous characteristics, certain limitations have been identified. Firstly, to achieve molecular-based identification, a series of extensive and time-consuming procedures is required before these identifications can be conducted. These procedures involve the sample processing and purification of genomic DNA from algal cell samples. Fortunately, these procedures can now be completed in a shorter time by utilising commercially available user kits, modern instrumentation, and reagents, as discussed in section 1.13. Nevertheless, the quality of DNA or RNA templates, and rigorous sterile techniques are essential for successful amplification. Since the amplification reaction is highly sensitive to contamination and inhibitors, low-quality RNA or DNA templates can inhibit enzymatic activity during the amplification reaction, leading to false negative results.

Secondly, factors like assay design, primer efficiency, assay specificity, and reproducibility can be challenging. In some cases, the target sequences may have challenging characteristics, such as palindromic (repetitive) regions or low GC content regions, which can prevent the design of highly efficient assays (van Pelt-Verkuil et al. 2008b). Thirdly, molecular amplification methods greatly depend on the availability of costly reagents, consumables, and technical expertise to operate specialised equipment, such as thermal cyclers (Oliver et al. 2014). Modern analysis workflows can now be carried out using automated processing equipment and commercially available user kits, reducing the level of molecular-biological training required and lowering costs for routine measurements. Considering both limitations and advantages, molecular techniques can still provide sensitive, specific and rapid detection

of harmful microorganisms including pathogenic bacteria and toxic microalgae (Medlin and Orozco 2017). Nucleic acid-based amplification methodologies have been extensively used for the identification of various harmful algal bloom (HAB) species, including *Pseudo-nitzschia*, as illustrated in Table 1.1.

1.11.4.1 RNA versus DNA

Detecting RNA molecules can offer an assessment of cell viability and metabolic activity, as RNA degrades rapidly upon cell death, in contrast to DNA, which remains relatively stable. This presents challenges and opportunities in monitoring cellular activity, including responses to environmental conditions or stressors, through tracking changes in RNA levels (Cenciarini-Borde et al. 2009). DNA molecules can persist for extended periods after cell death. They are naturally stable, reflecting their purpose which is to carry the genetic information required for all cell functions (Sontag 2005). The decoding of genetic information starts with the transcription process, where protein complexes containing RNA polymerases and transcription factors synthesise RNA from a DNA template (Feklistov 2013). The transcription of genomic DNA leads to the formation of messenger RNA (mRNA), which carries the genetic information throughout the cell for the manufacture of proteins. Other forms of RNA such as transfer RNA (tRNA), ribosomal RNA (rRNA), and other small regulatory RNAs also have important functions in metabolism (Moore 1999). Ribosomes and tRNA in the cytoplasm translate messenger RNA into polypeptides, consisting of amino acids, ultimately forming protein structures that drive gene expression and coordinate functional processes in cells (R. Harwood and Wipat 2002, Kozak 2005, Laursen et al. 2005).

Quantifying mRNA transcripts allows for studying gene expression profiling and determining which genes are active or inactive under different physiological or environmental conditions (Padovan-Merhar and Raj 2013, Tang and Amon 2013). However, mRNA molecules are prone to degradation by RNase enzymes, leading to a shorter lifespan compared to longer-lived, DNA, rRNAs and proteins (Hui et al. 2014). RNA, instead of DNA and proteins, provides a more accurate assessment of cell viability and physiology due to the higher number of RNA copies compared to DNA, even in cells with low expression levels (Lockhart and Winzeler 2000, Bustin and Mueller 2005). The molecular techniques developed for the detection of *Pseudo-nitzschia* using both RNA and DNA targets are summarised in Table 1.1.

Table 1.1 List of molecular assays targeting marker genes in species of *Pseudo-nitzschia*. (= "Yes") indicates the ability to produce domoic acid in the given strain. (= "Not tested") indicates that DA quantification was not performed. ("Yes/No") indicates that the given species in the same study are toxic, whereas DA was not detected in other species.

Species	Toxicity	Target gene	Sample	Location	Assay	Detection chemistry	Detection limit	References
P. pungens	not tested	*ITS*	culture, bloom	various	qPCR	EvaGreen intercalating dye	≤350 cells l^{-1}	(Kim et al. 2017)
P. pungens, P. mannii, P. delicatissima, P. calliantha	yes/no	*ITS*	culture, bloom	Mediterranean Sea, Italy	RT-qPCR	SYBR Green intercalating dye	1.2– 8.9 × 10^8 cells l^{-1}	(Penna et al. 2013)
P. calliantha	not tested	*ITS*	culture, bloom	Mediterranean Sea, Italy, Spain.	PCR	Gel electrophoresis	<10 cells l^{-1}	(Penna et al. 2007)
P. calliantha, P. delicatissima, P. multistriata, P. arenysensis, P. fraudulenta P.pungens, P. galaxiae, P. brasiliana	not tested	*ITS-1, 5.8S, ITS-2*	culture, bloom	Mediterranean Sea, Spain.	qPCR	SYBR Green intercalating dye	<200 cells l^{-1} - <480 cells l^{-1}	(Andree et al. 2011)
P. cuspidate, P. australis, P. pseudodelicatissima, P. delicatissima, P. seriata, P. multiseries, P. granii, P. pungens, P. fraudulenta	not tested	*18S rDNA*	culture, bloom	San Pedro Channel, USA	qPCR	SYBR Green intercalating dye	52 cells l^{-1} - 445 cells l^{-1}	(Fitzpatrick et al. 2010)
Pseudo-nitzschia sp.	not tested	*rbcL,18S rRNA, ITS, COI*	bloom	Shilaoren Bay, China	PCR	Gel electrophoresis	Not determined	(Guo et al. 2015)
P. calliantha, P. delicatissima, P. arenysensis, P. pungens	not tested	*LSU rDNA*	culture, bloom	Mediterranean Sea, Italy	qPCR	MeltDoctor™ HRM intercalating Dye	Not determined	(Pugliese et al. 2017)
P. pseudodelicatissima, P. delicatissima	not tested	*LSU*	culture, bloom	Mediterranean Sea, Italy	PCR	Gel electrophoresis	3.3 x 10^3 cells l^{-1}	(McDonald et al. 2007)

P. delicatissima, P. multistriata, P. galaxiae, P. mannii, P. subfraudulenta, P. calliantha	yes/no	*Prenyltransferase*	culture	Various culture collection	PCR	Gel electrophoresis	Not determined	(Dermastia et al. 2022)
P. australis, P. fraudulenta, P. pungens, P. multiseries	not tested	*LSU*	culture, bloom	Monterey Bay, USA	Whole-cell fluorescent *in situ* hybridisation (FISH)	Scanning electron microscopy (SEM) analysis	500 cells l^{-1}	(Miller and Scholin 1998)
P. australis, P. pungens, P. multiseries, P. heimii, P. fradulenta, P. pseudo-delicatissima, P. delicatissima	yes/no	*rRNA*	culture, bloom	Monterey Bay, USA	Sandwich hybridisation assay	DNA probe	6 x 10^3 cells l^{-1}	(Scholin et al. 1999)
P. pseudodelicatissima, P. cuspidata, P. cf. cuspidata, P. calliantha, P. delicatissima, P. fraudulenta P. hallegraeffii, P. hasleana, P. multiseries and P. multistriata, P. plurisecta, P. pungens var. pungens and P. simulans	yes/no	*ITS,5.8S, ITS2, LSU*	culture, bloom	Wagonga Estuary, Australia	qPCR	SYBR Green intercalating dye	4 - 8 cells l^{-1}	(Ajani et al. 2021)
P. calliantha, P. multistriata, P. pungens	no	*rRNA*	culture	Various culture collection	qPCR	Hydrolysis probe	10^6 cells l^{-1}	(Yarimizu et al. 2021)
P. multiseries, P. calliantha, P. americana, P. calliantha, P. subpacifica, P. plurisecta, P. delicatissima, P. delicatissima,	yes/no	*ITS1*	bloom	Narragansett estuary, USA	PCR	Gel electrophoresis	Not determined	(Sterling et al. 2022)

P. fraudulenta P. hallegraeffii, P. hasleana, P. galaxiae,								
P. australis, P. pungens, P. delicatissima P. fraudulenta, and P. multiseries	yes/no	*LSU*	culture, bloom	West Coast of Scotland, UK	Whole-cell fluorescent *in situ* hybridisation (FISH)	Scanning electron microscopy (SEM) analysis	600 cells l^{-1}	(Turrell et al. 2008)
P. granii	no	*FTN, ISIP2a, ACT*	culture, bloom	Northeast Pacific Ocean, USA	RT-qPCR	SYBR Green intercalating dye	Not determined	(Marchetti et al. 2017)
P. multiseries Hasle	no	*cyclophilin, SLC6, PFK, Aldo-keto reductase, GDH, PEPCK, SHSP*	culture, bloom	Prince Edward Island, Canada	RT-qPCR	SYBR Green intercalating dye	Not determined	(Boissonneault et al. 2013)
P. calliantha, P. pungens, P. delicatissima and P. fraudulenta, P. multiseries, P. seriata, P. cf. cuspidata	yes	*SSU*	bloom	Oslofjorden, Norway	RT-qPCR	SYBR Green intercalating dye	Not determined	(Dittami et al. 2013)
Isothermal amplification methods:								
P. pungens, P. multiseries, P. delicatissima, P. cuspidate, P. hasleana	not tested	*rbcS*	culture	Various culture collections	NASBA	Molecular beacon	10^3 cells l^{-1}	(Delaney et al. 2011)

1.11.4.2 Polymerase Chain Amplification (PCR)

The use of PCR has revolutionised the analysis of nucleic acids, making it a common method for monitoring microorganisms in water such as pathogens, biotoxins, and viruses (Su et al. 2011). PCR amplifies a specific fragment of nucleic acid by using a thermostable Taq polymerase enzyme and cyclic heating and cooling. This results in the production of several million DNA copies within a few hours, which can then be easily detected through electrophoresis or fluorescence methods (Livak et al. 1995, Green et al. 2015).

The PCR reaction starts with a denaturation step, where the hydrogen bonds holding the double-stranded DNA template together are broken by high-temperature exposure, leading to a separation of the secondary structure of the complex double-stranded DNA (dsDNA) into two complementary single strands of DNA (ssDNA). The length of this phase should be sufficient for the strands to be separated for priming, but not so long that the DNA is damaged. Since incomplete degradation of dsDNA molecules leads to decreased sensitivity in detection (Douglas and Atchison 1993). Oligonucleotides or primers are short stretches of DNA consisting of about 20 bases and are used to bind with the complementary sequences of the target region to be amplified on the DNA template. The reaction is then cooled to the primer annealing temperature, which is primer-dependent and usually falls between 50°C and 65°C, allowing the primers to hybridise with the complementary sequence on every single strand of DNA. The annealing temperature can be estimated to be 5°C lower than the melting temperature of the primer-template DNA duplex (van Pelt-Verkuil 2008).

The next step in the PCR reaction involves an extension, where the temperature is raised to 72°C for 20 seconds to one minute to enable replication of the template with the help of a thermostable DNA polymerase. The optimal extension temperature is determined based on the balance between the DNA polymerase activity and the primers' hybridisation specificity. With a 1-minute extension time, PCR amplicons up to 2 kilobases can be synthesised efficiently (Morrison and Gannon 1994). For amplifying larger amplicons, the extension step may be prolonged by an additional minute per kilobase (van Pelt-Verkuil 2008). Before the second cycle begins, two forms of the template are present in the reaction: fragments of original DNA strands and newly synthesised DNA strands that consist of the primer sequence followed by varying lengths of amplicon extended at the 3’ end (Green et al. 2015). Original DNA strands that were not primed and extended in the first cycle may be incorporated in the second cycle, resulting in molecules made up of primer and extension

products. On the other hand, the molecules from the first cycle that were primed and extended serve as the template for primers that are complementary to the newly synthesised material. By the third cycle, the newly generated target region DNA that resulted from the second cycle only comprises the amplicon and thus becomes the specific template (Green et al. 2015). The denaturation-annealing-extension cycle is repeated continuously, commonly between 25 and 40 times, leading to exponential amplification of the copied sequences, as shown in Figure 1.7.

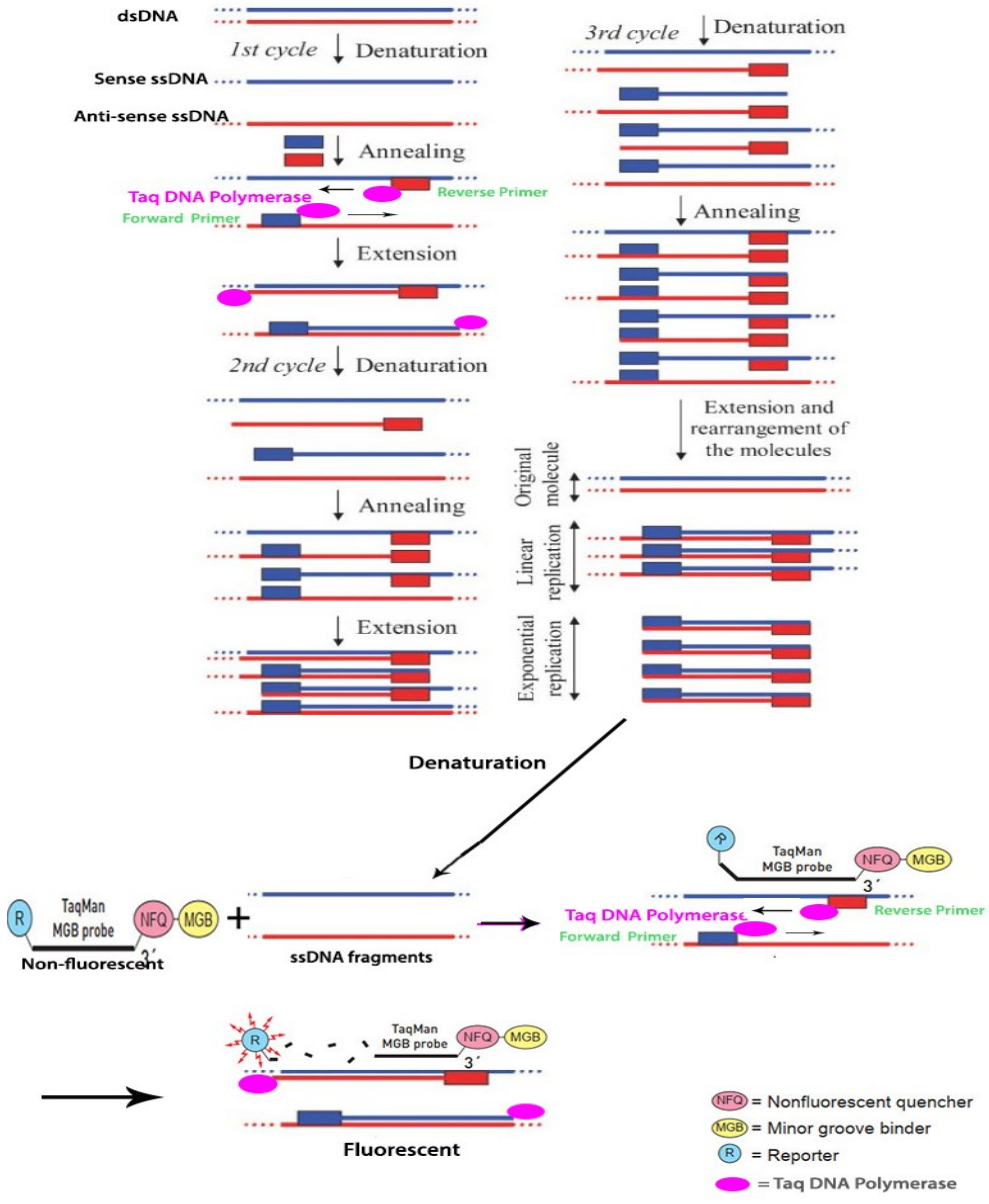

Figure 1.7 Mechanism of the PCR reaction and hydrolysis probe. The DNA template undergoes cycles of three steps: denaturation at 95°C, annealing at 50-65°C, and extension at 72°C, leading to the amplification of the PCR amplicons. The Taq DNA polymerase extends the primer located on

the same strand as the probe until it reaches the position of the probe. The inherent exonuclease activity of the polymerase breaks down the probe from 5' to 3', freeing the reporter dye into the solution and resulting in an increase in fluorescence. The fluorescence signal, proportional to the amount of target DNA in the sample, is then measured. The schematic illustration was redrawn from (Auroux et al. 2004).

The number of cycles required depends on the desired yield of the PCR product and is influenced by the initial starting copy number and amplification efficiency (Cha and Thilly 1993). This results in both linear amplification of the amplicons from the first cycle and exponential amplification of the amplicons from the second cycle. The linear amplification step may impact the total exponential amplification, although it produces smaller amounts of DNA. As the PCR reaction progresses, it continues to show exponential amplification until reaching a plateau phase caused by the nonspecific binding of the DNA polymerase to the DNA products (Kainz 2000, Mackay 2004).

The use of SYBR Green dye in PCR reactions can negatively impact accuracy due to its indiscriminate binding to all double-stranded DNA in the reaction pool (Dragan et al. 2012a). A better approach is to analyse PCR products through the melting curve analysis. This technique involves gradually raising the temperature to denature double-stranded PCR products, producing a unique melting temperature for each product that corresponds to its length and GC content (Druml and Cichna-Markl 2014). The melting curve can also detect nonspecific products that melt at different temperatures (Al-Robaiy et al. 2001). For real-time measurement, a fluorescent reporter probe is used, which is an indirect measure of the amount of nucleic acid present during each amplification cycle (Lee et al. 1993). The hydrolysis probe (also known as the TaqMan probe) is currently used for this purpose and is designed to hybridise to the internal region of the DNA template during the annealing phase. The hydrolysis probe is a single-stranded oligonucleotide labelled with a reporter dye and a quencher that is in close proximity. Upon specific hybridisation between the hydrolysis probe and DNA target, the probe becomes susceptible to the nuclease activity of DNA polymerase. The hydrolysis of the probe releases the reporter dye into the solution during subsequent cycles of the reaction, leading to an increase in fluorescent signal intensity that enables real-time fluorescence detection of the target (Livak et al. 1995), as shown in Figure 1.7.

The quantification cycle (C_q), also known as the threshold cycle (C_t-value), is a defining characteristic of a PCR run and is determined by the cycle at which the real-time fluorescent signal first rises above a set threshold. The threshold is used to differentiate between low initial concentrations of the template and background noise, which are too low to be detected (Gibson et al. 1996). The amount of target present at the beginning of the PCR amplification affects the C_t value: higher initial target

amounts lead to amplification in earlier cycles and a lower C_t value, while lower initial amounts result in later amplification and a higher C_t value (Gibson et al. 1996). This correlation between fluorescence, C_t, and the amount of amplified product allows for accurate quantification of the template over a broad dynamic range.

Microfluidic technology has enabled the miniaturisation of nucleic acid amplification via PCR methodology, despite the stringent operating conditions required such as stable thermal polymerase enzymes and precise thermal cycles (Zanoli and Spoto 2013, Ahrberg et al. 2016). The first PCR devices were developed by (Northrup et al. 1999) and (Wilding et al. 1994), with thermal cycling achieved by Peltier heater-coolers. Real-time detection of PCR products was achieved using TaqMan probes, followed by gel electrophoresis visual verification (Northrup et al. 1999). A handheld PCR device performing a faster reaction in less than 7 minutes was reported by (Belgrader et al. 1999). PCR in microstructures with real-time detection was demonstrated by detecting *Erwinia herbicola* and *Bacillus subtilis* in 16 minutes with detection limits of 10^2–10^4 cells ml^{-1} using thin-film resistive heaters in 10 silicon reaction chambers and solid-state optics (Belgrader et al. 1998). (Neuzil et al., 2006) fabricated another silicon-based PCR device that performed 50 amplification cycles within a few minutes. A microfluidic PCR system with rapid amplification in 1.3 minutes was achieved by optimising primers, and reagents, and reducing cycles to 0.4 to 2.0 seconds (Trauba and Wittwer 2017). Integrating microfluidic technologies with PCR analysis has demonstrated the potential for enabling sensitive detection.

1.11.4.3 Isothermal Amplification Methods

Isothermal amplification methods have become a popular alternative to the traditional PCR technique as they allow the detection of genetic target while avoiding thermal cycling (Zhao et al. 2015). Furthermore, performing amplification reactions at a constant temperature eliminates the need for rapid heating and cooling mechanisms, reducing reaction time and energy consumption, and making it more suitable for use in portable, battery-powered systems. The amplification rate is determined here by the activity of the enzymes and suitability of primer sequences in the reaction, rather than being limited by heating and cooling steps as in PCR practice (Craw and Balachandran 2012). The detection of DNA and RNA has been achieved through various isothermal amplification methods, including recombinase polymerase amplification (RPA) (Piepenburg et al. 2006), nucleic acid sequence-based amplification (NASBA) (Compton 1991), loop-mediated amplification (LAMP) (Notomi et al. 2000), helicase-dependent amplification (HDA) (Vincent et al. 2004), rolling circle

amplification (RCA) (Lizardi et al. 1998), and strand displacement amplification (SDA) (Shuler et al. 2012); (Walker et al. 1992).

1.11.4.3.1 Recombinase Polymerase Amplification (RPA)

The recombinase polymerase amplification (RPA) method is a well-established and widely used isothermal amplification technique that operates at a single temperature of 37°C (Piepenburg et al. 2006). It has been employed in the detection of various pathogens, including bacteria (Santiago-Felipe et al. 2015, Liu et al. 2017), viruses (Zaghloul and El-shahat 2014, Moore and Jaykus 2017), fungi (Lau et al. 2016) and parasites (Crannell et al. 2016, Subbotin 2019). The RPA method is capable of amplifying low numbers of copies of DNA and RNA targets from both crude samples and in the presence of background DNA and inhibitors (Piepenburg et al. 2006, Ahmed et al. 2014, Silva et al. 2015, Yang et al. 2016). Furthermore, RPA can be performed without a dedicated heating device, so long as the ambient temperature is above a minimum of 10 ^{o}C (Lillis et al. 2014). As a result, the mobile RPA assay is becoming a popular tool for enabling more portable genetic testing in point-of-care (POC) applications.

The RPA reaction starts with the binding of the recombinase enzyme to primers through the help of loading factors, forming a recombinase filament. This filament initiates the amplification cycle by searching for homologous sequences in the duplex template and opening the double strands to allow for hybridisation with the primer and target sequence, leading to strand exchange and insertion of the primer onto the target (Harris and Griffith 1989). The non-template strand is displaced and forms a d-loop structure, where one side is double-stranded and the other remains single-stranded stabilised by ssDNA binding proteins (gp32) to prevent re-annealing (Yonesaki and Minagawa 1985, Harris and Griffith 1987). The recombinase disassembles from the recombinase–primer complexes after strand exchange, allowing for the next pair of primers. The DNA polymerase extends primers from the 3’ end, causing the exponential accumulation of amplified duplex DNA through repetitive cycles (20-40 min) (Figure 1.8).

The RPA products can be detected using gel electrophoresis, and SYBR Green dye (Piepenburg et al. 2008). TwistAmp® commercially provides fluorophore/quencher probes including exo probe, fpg probe, and nfo probe for real-time RPA analysis (TwistDx 2009) (Lobato and O'Sullivan 2018). The biochemistry of RPA is incompatible with hydrolysis-based probes such as TaqMan and molecular beacons due to the endonuclease activity of the RPA enzymes (Kaiser et al. 1999). The use of TaqMan probe or Taq polymerase in RPA reactions is not possible due to their 5’→3’ exonuclease

activity, which prevents DNA amplification by digesting the displaced strand during the RPA strand displacement process. Thus, the use of strand displacement polymerases like *Bacillus subtilis* DNA polymerase I (Bsu) or *Staphylococcus aureus* polymerase (Sau), which lack the 5'→3' exonuclease activity is necessary for RPA-based detection (Lobato and O'Sullivan 2018).

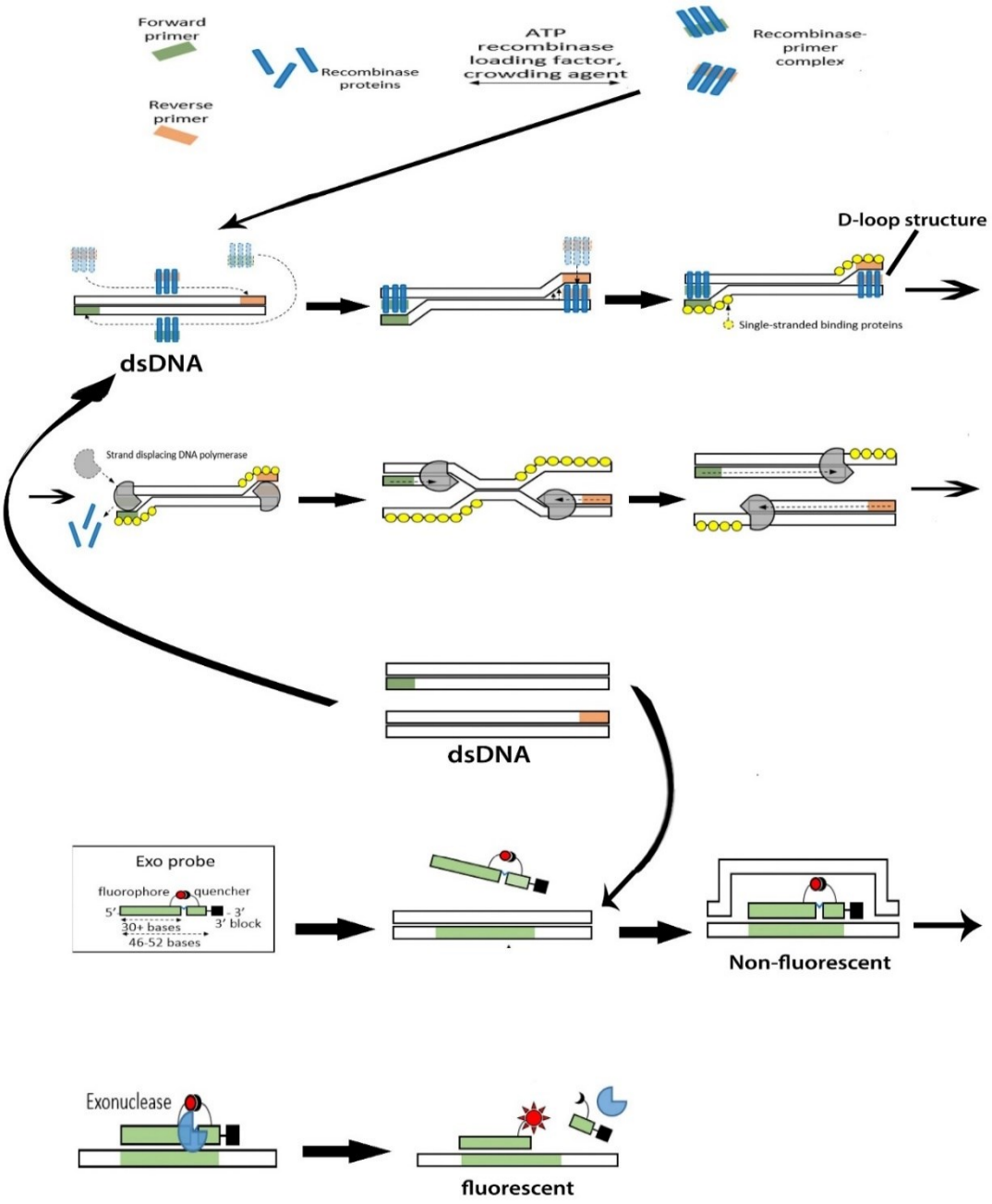

Figure 1.8 RPA reaction and the fluorescence generated by the exo probe for real-time detection. This process involves the formation of complexes between recombinase proteins and primers. These complexes cooperatively bind to primers in the presence of ATP, loading factors (such as UvsY) and crowding agents (such as Carbowax 20M). The recombinase/primer complex scans the DNA template for homologous sequences and inserts primers at the homologous site using strand-

displacement activity, creating a D-loop structure. Single-stranded binding proteins (gp32) stabilise the displaced DNA chain in a D-loop structure. Then, the recombinase disassembles, leaving the 3'-end of the primers accessible to a strand-displacing DNA polymerase, which elongates the primer. This process produces one complete copy of the amplicon in addition to the original template. The exponential amplification is achieved by the cyclic repetition of this process. Real-time fluorescence generation is enabled by the exo-probe, which anneals to the complementary sequence on the template DNA. When the probe binds, exonuclease III digests the THF spacer, leading to the generation of a fluorescence signal. Redrawn from (Li et al. 2019a).

The RPA assay can be performed in either a liquid or solid phase format, each with its advantages. In the solid-phase approach, primers and other reaction components are bound to a substrate surface, facilitating bridge amplification (Shin et al. 2013). This solid-phase RPA approach eliminates the need for post-amplification treatments (Khan et al. 2008, del Rio et al. 2015), and also offers multiplexing potential (Chao et al. 2015) and the flexibility to combine RPA amplification with diverse detection techniques, such as electrochemical and colourimetric detection (Liu et al. 2016, Yamanaka et al. 2017). In contrast, liquid-phase RPA allows for faster template and primer extension using RPA enzymes, leading to quicker amplification and lower detection limits compared to solid-phase RPA. This is due to the free diffusion of primers and reaction reagents that enables rapid and efficient mixing of reaction components including primers, DNA template, nucleotides, and enzymes, promoting efficient DNA amplification (Daher et al. 2016).

The RPA reaction has been adapted to allow the detection of multiple DNA/RNA targets in a single tube, a format known as multiplexing. Successful examples of multiplexing RPA assays include the detection of Staphylococcal *mec* junction targets and internal control using fluorescent detection by exo probes (Hill-Cawthorne et al. 2014). Another multiplex assay demonstrated the simultaneous amplification of five genes in two bacterial pathogens in food products using RPA, with the optical signal measurement using a DVD detector (Santiago-Felipe et al. 2016, Kim and Lee 2017). The highest level of multiplexity achieved with RPA was demonstrated by (Song et al. 2017), who developed a 16-plex assay for pathogen detection. However, multiplex RPA amplification assays tend to be less sensitive compared to equivalent single-target assays due to the consumption and compromise of enzymes and reagents during the reaction (Polz and Cavanaugh 1998). This reduced sensitivity can be further exacerbated by the sequestration of reaction components by high-abundance targets, resulting in the masking of low-abundance targets in samples (Kanagawa 2003, Okino et al. 2015). Therefore, further optimisation and validation are required to ensure the sensitivity and reliability of multiplex RPA amplification assays (Johnson and Loehr 2015).

The RPA reaction has demonstrated its ability to amplify target sequences in the presence of inhibitors and background DNA, making it a promising tool for in-field applications (Chao et al. 2015, Ng et al. 2015, Rohrman and Richards-Kortum 2015). Microfluidic RPA sensors have been developed by (Lutz et al. 2010) capable of detecting the *mecA* gene from *Staphylococcus aureus* with a limit of detection of 10 copies in less than 20 minutes. (Dao et al. 2018) also developed a microfluidic RPA sensor for the detection of *Salmonella* and *Brucella* pathogens, which indicated greater sensitivity than bench-top RT-qPCR assay. In addition, fully integrated RPA systems employed a 3D printed cartridge to perform the detection of specific genes in *Chlamydia Trachomatis* pathogenic bacteria. These systems can deliver results in as little as 10 minutes using a TwistAmp fpg probe (Ereku et al. 2018). These advancements in microfluidic and integrated RPA technologies offer advantages for rapid and sensitive on-site detection.

1.11.4.3.2 Loop-Mediated Isothermal Amplification (LAMP)

LAMP was initially described by (Notomi et al. 2000) and offers specific nucleic-acid-based detection compared to other isothermal methods. LAMP achieve this specificity by employing three sets of primers that target six distinct sites within the DNA target sequence (Soroka et al. 2021). The method involves the use of a strand-displacing DNA polymerase and six primers; two outer primers (F3 and B3), two inner primers (FIP and BIP), and two loop primers (Loop F and Loop B) (Salamin et al. 2017).

The LAMP reaction is conducted at a constant temperature typically between 60-65°C. It initiates with the hybridization of the inner primer (F2) to the target DNA, followed by an extension facilitated by a DNA polymerase enzyme. This is followed by the binding of the outer primer F3 to the same target strand and undergoes polymerase-mediated extension, leading to the displacement of the newly synthesised strand. The displaced strand forms a stem-loop structure at its 5' end due to the hybridisation of the F1c and F1 regions. At the 3’ end, the reverse primer set can then hybridise to this strand, generating a new strand with a stem-loop structure at both ends through polymerase extension. This continuous process creates a double-loop stem structure (dumbbell structure) which drives an exponential amplification where the target DNA is repeatedly extended and displaced. The amplified products consist of stem-loop DNAs with different inverted target repeats and complex cauliflower-like structures with multiple loops (Becherer et al. 2020). A detailed schematic of the LAMP amplification scheme is shown in (Figure 1.9).

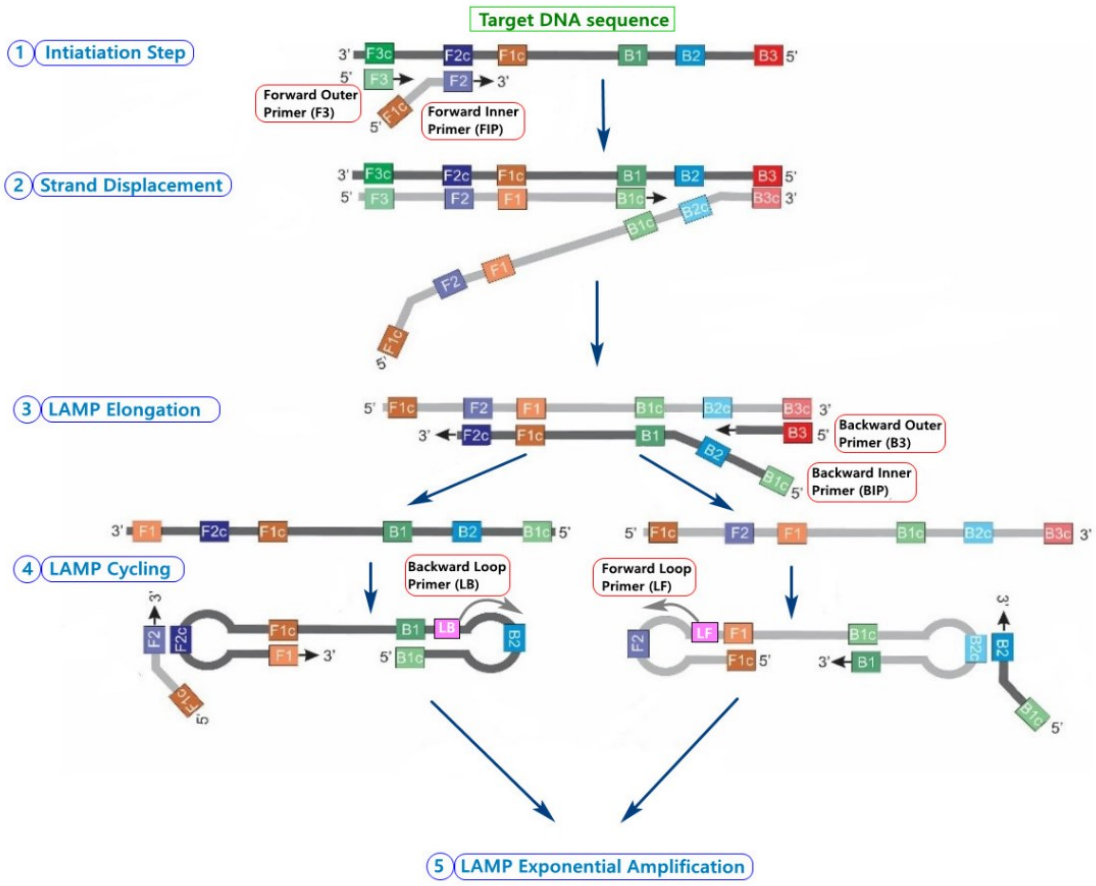

Figure 1.9 Amplification reaction of loop-mediated isothermal amplification (LAMP).

LAMP amplicons can be measured by a variety of techniques, including turbidity caused by magnesium pyrophosphate precipitate as a by-product (Huang et al. 2017b, Wachiralurpan et al. 2017), gel electrophoresis (Liu et al. 2022, Warmt et al. 2022), melting curve analysis (Rolando et al. 2020, Shen et al. 2022), electrochemiluminescence (Yuan et al. 2014, Martinez-Perinan et al. 2020), visually evaluating the solution colour change by naked-eye (Tanner et al. 2015, Lee et al. 2017, Zhang et al. 2022b), fluorgenic probes (Gadkar et al. 2018, Bhadra et al. 2021), intercalating fluorescent dyes (Tian et al. 2012, Lai et al. 2021), bioluminescence (Hardinge et al. 2018, Mirasoli et al. 2018), colourimetric detection (Roumani et al. 2022), metal calcium indicators (Wang et al. 2017), and magnetic beads (Roy et al. 2016, Chen et al. 2018).

The LAMP amplification reaction is characterised by the Time to Threshold (T_t) values, which indicate the moment when the real-time fluorescent signal first rises above the baseline background level (Diego et al. 2019). At the onset of the LAMP process, the fluorescence intensity is initially very low, falling below the detection threshold and within the system's "background

noise", due to the low initial concentration of the template. However, as the amplification reaction develops, a shorter T_t value is observed particularly in the earlier cycles when an abundant target sequence is present. In contrast, when the target sequence is present in fewer initial copies, the amplification occurs in later cycles, resulting in a longer T_t value (Yu et al. 2022).

The LAMP method is a simple and versatile technique capable of amplifying a few copies of the target DNA to over 10^9 copies in less than an hour, without the need for thermocycling. The reaction occurs in a single step at a constant temperature, typically maintained between two high temperatures 60°C and 65°C, making it highly suitable for the detection of microorganisms, even in the presence of substantial amounts of non-target DNA (Moehling et al. 2021). At elevated temperatures, it denatures secondary structures between non-specific DNA sequences and primers, and reduces non-specific binding, ensuring specific extension by DNA polymerase during LAMP reaction. However, the major challenge of LAMP is the design of its primer sets, which require coverage of six distinct regions in the target DNA. To simplify this task, web-based software has been developed to aid in the design of LAMP primers and loop primers (Eiken 2023). The LAMP method is an effective tool for identifying single-nucleotide mutations in target sequences, due to the utilisation of six LAMP primers that recognise six unique sites within the target sequence (Varona and Anderson 2021). This results in a high level of specificity for target detection, outperforming conventional PCR (Hardinge and Murray 2019, Kamra et al. 2022), and RPA methods (Zou et al. 2020).

The LAMP method demonstrated significant analytical sensitivity in quantifying HAB taxa, including *Karenia mikimotoi* (Wang et al. 2020c), *Karlodinium veneficum* (Huang et al. 2017a), *Alexandrium catenella* and *Alexandrium minutum* (Zhang et al. 2012), and *Prorocentrum minimum* (Zhang et al. 2014a). The reverse transcription loop-mediated isothermal amplification (RT-LAMP) method has been applied successfully in the detection of RNA sequences from various microorganisms, including the influenza virus (Nakauchi et al. 2014), zika virus (Wang et al. 2016), coronavirus (Huang et al. 2020, Tang et al. 2022), bacteria (Wu et al. 2018, Zhan et al. 2019), algae (Chen et al. 2013).

The multiplexing capability of LAMP enables the quantitative amplification of multiple targets simultaneously within a single reaction. A multiplex LAMP detection system was developed by combining hybridisation probes of different colours and LAMP primers for identifying the *Schistosoma* target (Crego-Vicente et al. 2023). In under 60 minutes, a multiplex LAMP format was employed for quantifying three antibiotic-resistant genes, *mcr-1*, *mcr-3*, and *mcr-4* (Zhong et al. 2019). A multiplex digital LAMP assay was developed for the simultaneous detection of five targets

in a single reaction within a single fluorescent range (Malpartida-Cardenas et al. 2022). (Oscorbin et al. 2021) demonstrated the sensitivity of multiplexed RT-LAMP amplification for detecting as low as 20 copies of SARS-CoV-2 RNA per reaction in just 40 minutes. These examples highlight the multiplexing capabilities of LAMP that enhance its efficiency and utility in various applications.

The versatility of the LAMP method extends to various applications in environmental monitoring, offering rapid, specific, and cost-effective genetic monitoring tools. For example, a colourimetric LAMP assay conducted on a handheld device enabled the direct detection of 5 copies of SARS-CoV-2 per reaction from crude samples (Papadakis et al. 2022). Simultaneous detection of two HIV RNA targets in plasma samples was achieved using a microcapillary LAMP (cLAMP) system (Zhang et al. 2014b). Another colourimetric LAMP assay, developed by (Song et al. 2022a), used a smartphone camera to monitor the colour change of LAMP amplicons, facilitating the classification of SARS-CoV-2 results as positive, negative, or false positive based on concentration levels. Additionally, (Wang et al. 2020d) demonstrated LAMP-on-a-chip for real-time detection of pathogenic bacteria *Salmonella* at a concentration of 14 CFU ml^{-1} within 1.5 hours, using preloaded lyophilized LAMP reagents in a heated polydimethylsiloxane (PDMS) microchamber at 65°C. Furthermore, a portable LAMP device was employed to rapidly detect a single cell of the toxic microalgae *Alexandrium catenella* per ml within 2 hours (Fujiyoshi et al. 2021). In summary, the LAMP method provides a rapid, specific, and cost-effective tool for genetic monitoring with a wide range of applications in environmental monitoring.

1.12 Automation of Molecular Methods for *in situ* Nucleic Acid Sensing

The demand for rapid analysis of small biological samples has led to significant advancements in miniaturisation and automation of nucleic acid detection technologies. The introduction of Micro Total Analysis Systems (µTAS), also known as "lab on a chip," has enabled the integration of sample preparation, nucleic acid amplification, and detection within microfluidic devices or at a microscale level (Dittrich et al. 2006, Chen et al. 2007a). Microfluidic lab-on-a-chip (LOC) devices mimic laboratory processes in a compact chip-sized format, with the aim of delivering high precision, portability, and reduced detection times by manipulating small volumes of samples and reagents, ranging from nano to picolitres within microchannels (Chang et al. 2013).

Lab-on-a-chip (LOC) is becoming an important tool for executing biological assays at a microscale, offering several advantages such as reduced reagent consumption, minimised contamination risk,

quicker analysis times, and simplified sample handling. In response to these advantages, molecular detection systems have been developed to integrate with microfluidic systems, facilitating rapid and precise identification of harmful microorganisms, including pathogenic bacteria and toxic microalgae (McQuillan and Robidart 2017). The application of these systems is considered a key to improving healthcare and environmental monitoring, especially in the domains of Point-of-Care (POC) and Point-of-Harvest (POH) testing, respectively. Miniaturising genetic testing offers a range of benefits, including faster results, reduced risk of contamination, low reagent consumption, as well as cost and time savings (Asiello and Baeumner 2011, Foudeh et al. 2012). One of the key advantages of microfluidic genetic testing is the elimination of the need for sample transportation and labour-intensive sample preparation, leading to complete automation and a streamlined biosensing workflow (sample in - answer out), as illustrated in Figure 1.10.

Ensuring the user-friendly operation of microfluidic systems is a paramount goal for any genetic analysis for both POC and POH applications. The adoption of the ASSURED standards is a widely accepted approach for evaluating the performance and operational adaptability of in-vitro molecular systems for end-users (Land et al. 2019). Furthermore, the United States Clinical Laboratory Improvement Amendment (CLIA) classifies molecular tests into three categories: high complexity, medium complexity, and waived (Ehrmeyer and Laessig 2007).

Ideally, a molecular device is classified as 'CLIA waived' as it operates the detection steps in a highly simple manner, minimising the likelihood of user-introduced errors (Niemz et al. 2011). Currently, a few commercial nucleic-acid detection systems have received the CLIA-waived status, such as Piccolo Xpress (Abbott), Cobas® Liat® System (Roche diagnostics), and GeneXpert System (Cepheid). Most of these platforms support fully automated workflow that provides ‘DNA sample-in/answer-out genetic testing. Therefore, the development of microfluidic systems has the potential to reduce operational complexity and minimise user intervention. However, the implementation of microfluidic systems faces challenges in incorporating multiple critical elements, including external actuators, valves, pumps, mixers, electromechanical interfaces, and detection modules (Farré et al. 2012). These challenges can compromise the advantages of simplicity, speed, low cost, scalability, and portability. Therefore, careful design considerations are crucial to fully realise the benefits of Lab-on-a-Chip (LOC) technology, as discussed in section 1.15.

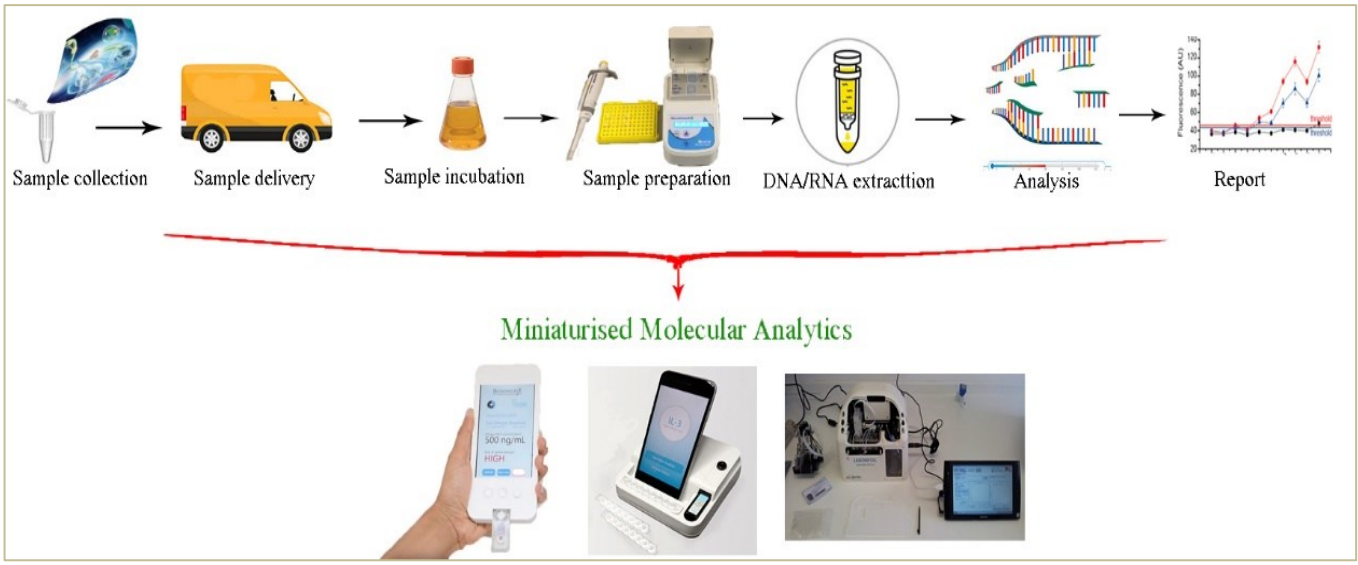

Figure 1.10 Miniaturised molecular devices simplify the operational procedures of genetic analysis.

1.13 Sample Preparation and Nucleic Acid Extraction

In recent years, various extraction procedures have been developed to obtain pure nucleic acids, including DNA and RNA, using either solution-based or column-based protocols. Achieving accurate molecular analysis depends on extracting high-quality nucleic acid samples. Complete disruption of target cells is important to efficiently recover their genetic material (Brown and Audet 2008). The proper preparation of a pure nucleic acid sample allows the success of downstream analyses, as the presence of other cellular components such as proteins and lipids can inhibit nucleic acid detection (McKiernan and Danielson 2017, Lee et al. 2019a).

Typically, the genomic DNA extraction process starts with the homogenisation of cell samples in a lysis solution containing a chaotropic salt such as guanidinium thiocyanate and phenol/chloroform, followed by centrifugation to separate the lysate into three phases (Tan and Yiap 2009). To aid in cell lysis and the solubilisation of proteins and lipids, a lysis buffer consisting of phosphate-buffered saline (PBS) and a detergent such as sodium dodecyl sulfate (SDS), Triton X-100, or deoxycholic acid may be added (McKiernan and Danielson 2017). To achieve enzymatic digestion of cellular proteins and associated polysaccharides, Proteinase K is commonly used (Yuan et al. 2017). However, magnesium ions (Mg^{2+}) can inhibit the activity of Proteinase enzymes and reduce protein degradation (Gueroult et al. 2010). To address this, the addition of a chelator agent such as Ethylenediaminetetraacetic acid (EDTA) sequesters the magnesium ions within the lysate,

improving enzymatic digestion. In the extraction process, RNase enzymes are introduced to facilitate RNA degradation in the lysate, while DNase enzymes are used to recover RNA selectively (Rezadoost et al. 2016). Following these steps, DNA/RNA is adsorbed onto silica columns, facilitating the removal of contaminants such as proteins, lipids, and polysaccharides. This purification protocol involves a series of sequential washing and elution steps (McKiernan and Danielson 2017). During the elution step, a hypotonic buffer (i.e., detergent-free solution, such as Tris-EDTA), is employed to solubilise DNA/RNA molecules, protecting them from degradation.

1.13.1 Conventional Nucleic Acid Extraction Methods

Traditional nucleic acids isolation protocols mostly consist of multi-step procedures involving the use of corrosive, and toxic chaotropic solutions such as phenol/chloroform, cetyltrimethylammonium bromide (CTAB), guanidinium thiocyanate (Mahalanabis et al. 2009). Chaotropic agents induce structural disruption of the cellular membrane by denaturing its proteins and other non-target cellular components (Salvi et al. 2005). These chaotropic agents precipitate nucleic acids by supporting the intra-molecular immobilisation of nucleic acids through hydrophobic linkages, hydrogen bonds, noncovalent bonds and van der Waals forces (Ali et al. 2017b). The cell lysate is then resuspended in an organic solvent or detergent buffer such as CTAB or phenol/chloroform mixture which leads to emulsion (Tan and Yiap 2009). A series of centrifugation steps are then conducted to separate the aqueous from the organic phase. The cellular denatured materials remain in the organic phase, whilst DNA persist in the aqueous phase at an alkaline pH value (Tan and Yiap 2009). The aqueous phase containing DNA is purified through a new clean tube via multiple steps till the interface is transparent rather than thick and opaque in appearance. Crude DNA samples can be directly recovered from the aqueous part after ethanol or isopropanol precipitation (Moore and Dowhan 2002).

These traditional purification methods are often combined with multiple buffer exchanges and washes to extract DNA/RNA (Chen et al. 2007b). However, the carryover of chaotropic agents like phenol can inhibit amplification reactions (e.g. PCR, RPA, HDA), reducing the sensitivity of those assays (Ye et al. 2018). Furthermore, buffer exchanges and multiple manual reloads of solutions between wash and elution steps affect the rapidity of extraction protocols and increase the risk of sample contamination (Marshall et al. 2012). Additionally, these labour-intensive procedures often require expensive and clean automated workstations as well as a high level of expertise to safely handle these hazardous chemical solutions. Integrating conventional DNA purification methods

with microfluidic platforms requires external actuation equipment (e.g. valves, actuators, pumps) to maintain an *in-situ* steady operation (Chin et al. 2007). This introduces further complications in the fabrication process due to the requirement for multiple materials, multi-level structures, bulky equipment and complicated assembly steps (Lim et al. 2019).

1.13.2 Bead-Based Nucleic Acid Extraction Methods

These purification techniques rely on a silica exchange system, which forms salt bridges between the negatively charged phosphorus groups of DNA and RNA and the positively charged silica membrane. Changing salt concentration within this system breaks the salt bridge and releases DNA or RNA molecules into an elution buffer, Figure 1.11 (Esser et al. 2006). This mechanism is known as the Boom principle, which employs silica magnetic beads for the extraction of RNA or DNA (Boom et al. 1990). Boom-based techniques are widely used in nucleic acid extraction from various biological mediums due to their ability to selectively bind and separate nucleic acids from other cellular components. Boom-based methods for nucleic acid extraction can be categorised as follows:

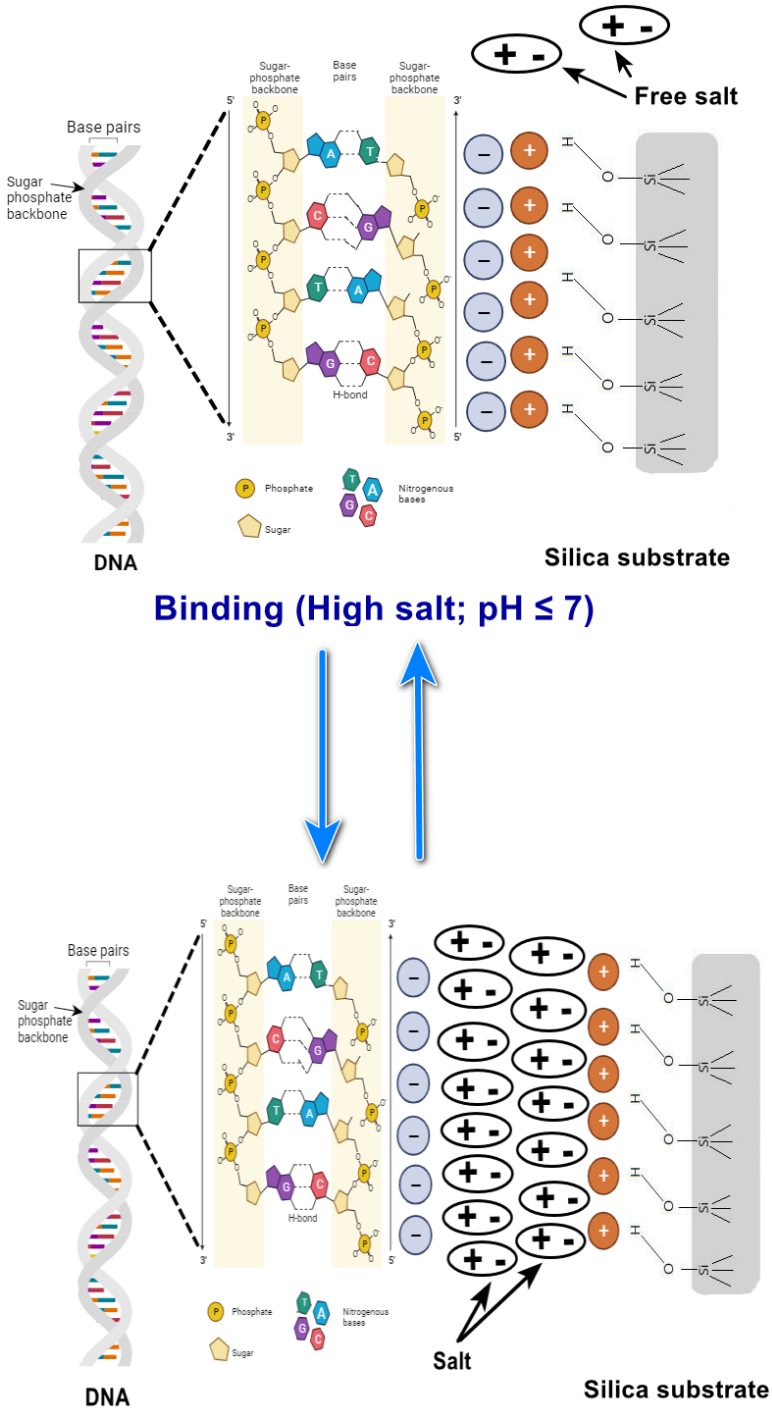

Figure 1.11 Binding of nucleic acid to a silica substrate. The purification process relies on the strong affinity between the negatively charged DNA molecule and the positively charged silica substrate (orange). In high salt conditions, the DNA binds tightly to the substrate, and thorough washing removes all non-target cellular components, purified DNA molecules can be eluted under low ionic strength conditions.

1.13.3 Solid-Phase Nucleic Acids Extraction

Solid-phase extraction (SPE) is the most commonly used technique for nucleic acid purification. In this method, a solid material such as a filtration membrane with special properties is used to selectively capture the nucleic acids including DNA or RNA, from a complex mixture (Reedy et al. 2010). By carefully controlling conditions such as pH and salt concentration, the nucleic acids bind to this solid material, while other cellular components like cell debris, lipids, and proteins are washed away. Following this process, the nucleic acids can be easily eluted from the solid phase in a solution, ensuring the integrity of the extracted DNA/RNA samples (Katevatis et al. 2017). Many commercial kits based on solid-phase silica extraction are available for extracting both DNA and RNA from various sources, including algal cells. These kits include DNeasy Plant Pro, DNeasy Plant Kits, RNeasy PowerWater (Qiagen), NucleoSpin Plant II, NucleoSpin TriPrep (Macherey-Nagel), easyMAG® (Biomérieux), Wizard® Genomic DNA Purification Kit, Maxwell® RSC simplyRNA kit (Promega), GenElute™ Water RNA/DNA (Sigma Adrich, UK), among others.

However, SPE-based extraction comes with certain limitations. Firstly, SPE columns and membranes have limited capacities, which may not be sufficient for extracting DNA/RNA traces from large sample volumes, thus requiring sample concentration or dilution (Schlappi et al. 2016). Additionally, the efficiency of SPE-based extractions can be affected by the composition of the sample matrix, as highly complex samples comprising salts, and other contaminants can lead to column clogging (Chiu et al. 2010). Moreover, multiple centrifugation steps are necessary for executing SPE-based extractions, which can limit their speed and integration with microfluidic structures (Han et al. 2009).

1.13.4 Magnetic Nucleic Acids Extraction

Magnetic bead extraction method has emerged as a versatile and efficient alternative method for isolating nucleic acids. These magnetic beads are usually coated with molecules that have a specific attraction to DNA or RNA, allowing them to selectively bind to genetic material through chemical interactions within the sample. A magnetic field is then applied to attract and immobilise the beads, along with the attached nucleic acids (Pezzi et al. 2018). By separating bead-bound nucleic acids from the rest of the sample using a magnet, the genetic material can be washed and eluted for further analysis, such as PCR, sequencing, or genetic testing.

However, the performance of magnetic-based extraction can be influenced by bead carryover and contaminants or impurities present in the sample matrix, which may interfere with nucleic acid binding with magnetic beads (Kovacevic 2016). Additionally, the yield of DNA/RNA depends on selecting magnetic beads of appropriate size and surface chemistry (Magnani et al. 2006). Furthermore, high-quality magnetic beads can be expensive, making them less accessible for some laboratories (Plouffe et al. 2015). While automation of magnetic bead extraction is possible and can increase throughput (Berensmeier 2006), it often requires specialised beards-trapping structures, magnetic-field control unit, and robotic parts, making it more complex for high-throughput testing applications (Ebrahimi et al. 2021).

1.13.5 Microfluidic-based Nucleic Acids Extraction

Recent microfluidic research has focused on miniaturising various extraction techniques, including solid-phase extraction (Kebede et al. 2022), magnetic beads extractions (Lee and Tripathi 2022) and paper-based extractions (Tang et al. 2017). To enable on-chip nucleic acid extraction, many microfluidic systems have been precisely designed to comprise fluid manipulations and automated control into a single system (Li et al. 2023). For example, the ProMagBot device enabled programmable magnetic-based procedures for extracting HIV RNA from pretreated blood samples (Politza et al. 2023). Similarly, (Bahi et al. 2011) utilised an on-chip technique that combined dielectrophoresis with magnetic beads for sample processing of dinoflagellates, *K. brevis*. The electroporated cells discharged their genetic material, including RNA which was later subjected to purification protocol using a commercial kit off-chip. (Easley et al. 2006) reported an integrated microfluidic device capable of conducting on-chip DNA-based purification of pretreated blood samples, followed by PCR amplification and enabled the electrophoretic detection of the amplified products in 30 min. Nevertheless, improving the tolerance of microfluidic systems towards crude samples remains a major challenge for achieving a fully automated sample-in-answer-out assay (Pattanayak et al. 2021, Wang et al. 2023).

Alternatively, state-of-the-art extraction technologies have been investigated for integration into microfluidic systems in recent years. For example, a method based on dimethyl adipimidate (DMA) has been used to capture nucleic acids (DNA and RNA) from a variety of sources, including mammalian, bacterial, and plant samples (Yin et al. 2019). (Shin et al. 2014) used DMA as a capturing reagent to perform one-step DNA extraction on a microfluidic device. DMA-microfluidic extractions employed a non-chaotropic technique, resulting in significantly high-quality DNA

recovery within less time compared to conventional DNA purification kits (Shin et al. 2015). An alternative approach relies on the use of chitosan-coated metrics to achieve one-step purification with concentration procedures (Gan et al. 2017). Other porous chitosan membranes were fluorescently labelled to monitor changes in fluorescence resulting from captured DNA samples. The eluted DNA from this system was amplified via PCR off-strip (Byrnes et al. 2015). In summary, new technologies including lateral-flow and DMA-based extractions offer *in-situ* compatible systems, providing instrumentation-free settings for nucleic-acid-based sensing systems.

1.13.6 Challenges with Nucleic Acid Extraction from *Pseudo-nitzschia*

Pseudo-nitzschia cells are commonly sampled from the environment through two primary routes: directly from crude seawater, filtering seawater, and shellfish tissue homogenates (Lelong et al. 2012). Ineffective processing of these samples can profoundly impact the performance of downstream molecular analysis (Ali et al. 2017a). To alleviate this, full disruption of cell membranes and walls is required to effectively collect the genetic material. The presence of other cellular components like proteins and lipids, however, can reduce the purity and integrity of extracted genetic material, which in turn, potentially interfere with downstream analysis.

Pseudo-nitzschia cell has a rigid cell wall reinforced by numerous frustules composed of amorphous silica (hydrated silicon dioxide) (La Barre et al. 2014). Thereby, the thickness of this silica cell wall in *Pseudo-nitzschia* increases within a range of 3-8 µm, making it thicker than the cell walls of many other microorganisms (Ajani et al. 2018). By comparison, the cell wall of *E. coli* consists of a single layer of peptidoglycan, typically measuring around 2 to 3 nanometers (nm) in thickness (Norris and Manners 1993). In the case of dinoflagellate phytoplankton like *K. brevis*, their cell wall thickness is in a range of hundreds of nanometers (Chan et al. 2019), generally thinner than the silica wall found in *Pseudo-nitzschia*. The thick cell wall of *Pseudo-nitzschia spp*. hinders the penetration of extraction buffers, making it difficult to recover nucleic acids from their cellular contents. Thus, commercial extraction procedures, such as the DNeasy Plant and DNeasy Pro kits (Qiagen), involve a mechanical disruption of *Pseudo-nitzschia* cells using stainless steel beads and tungsten carbide beads (Panova et al. 2016). This grinding process ensures the complete breakdown of the silica cell wall of *Pseudo-nitzschia*, allowing for the recovery of their genetic samples. Moreover, these protocols require the use of additional expensive equipment, such as the "TissueLyser," to ensure efficient extraction of nucleic acids from rigid-walled cells. Due to these requirements along with

the complexity of the cell wall structure, conducting the on-chip extractions for *in situ* sampling of *Pseudo-nitzschia* cells becomes more challenging.

There are additional limitations associated with sample processing of *Pseudo-nitzschia*, including challenges in handling, storing, and processing samples. These difficulties can lead to contamination by inhibitors, degradation of genetic samples, and the introduction of non-target genetic material (Hazen et al. 2013). On the other hand, the limited availability of representative sample sizes can also restrict the amount of genetic material for analysis and impact the sensitivity and reliability of the molecular assay (Demeke and Jenkins 2010). Moreover, the complexity of environmental samples, such as mixed microbial communities with a non-target genetic pool, can prevent the specific identification and sensitive quantification of target genetic markers (Theron and Cloete 2000). Additionally, the choice of suitable sampling methodologies and tools is vital to guarantee that the collected samples accurately reflect the desired environmental target (Clarke and Ainsworth 1993). To mitigate those limitations, careful and standardised environmental sampling protocols should be optimised for the specific characteristics of cells, coupled with appropriate controls and quality control measures, to enable accurate and reliable molecular analysis of environmental *Pseudo-nitzschia* samples.

1.14 Preservation of Analytical Reagents

The preservation techniques have emerged to support easy-to-use molecular analysis, by pre-loading necessary reagents onto portable and disposable devices, enabling cost-effective and simple testing in field applications (Primiceri et al. 2018). These easy-to-use, portable, affordable tools are convenient for non-skilled operators and have the potential to be used in environmental monitoring (Abbasi et al. 2019). Pre-loading reagents in microfluidic devices can extend the storage of primers, probes, and samples, and also eliminate the risk of contamination during the preparation of molecular testing (Von Lode et al. 2007, Stevens et al. 2008, Lutz et al. 2010, Liu et al. 2011). The integration of preserved reagents with state-of-the-art molecular assays can increase their utility and versatility on portable sensing devices. This allows for automated sample-to-answer molecular testing in remote areas, reducing the need for centralised laboratory equipment and saving time and cost for end-users (Yager et al. 2006). Many preservation techniques have been developed in the recent years. These are described below.

1.14.1.1 Freeze-drying

Freeze-drying is a widely used method for storing reagents of several amplification methods including PCR, RPA and LAMP (Heeroma and Gwenin 2020, Wan et al. 2020, Yang and Wen 2021). However, freezing procedures have been found to have limitations in re-activating downstream amplification reactions. Due to the low moisture content in freeze-dried enzymes, makes them susceptible to interference from ambient humidity, leading to the loss of their enzymatic activity to re-activate amplification reactions (Wang et al. 2012, Malik et al. 2017, Xu et al. 2020). Therefore, introducing stabilising additives is preferable to ensure stable storage of reagents in a solid state. For example, common stabilisers including paraffin, trehalose, polyethylene glycol (PEG), mannitol, and dextran, were employed in the freeze-drying process to ensure stable storage of amplification reagents (Schaikhaev 2005, Ahlford et al. 2010). For additional protection, PCR reagents were encapsulated in a paraffin film following freeze-drying procedures, as demonstrated by (Kim et al. 2009). When the amplicons were analysed through gel electrophoresis, their band intensities were found to be similar to those obtained from a PCR reactor without the paraffin layer. This efficient amplification performance was maintained for one to five months at room temperature without humidity control (Kim et al. 2009). The set-up of freeze-drying typically requires bulky equipment to operate the pressurising process at extremely low temperatures, which can lead to reduced stability and shorter shelf life of the dried reagents (Oddone et al. 2020). These findings indicate that freeze-drying procedures require precise control of temperature and pressure conditions and involve the use of additional substances and refrigeration to maintain the integrity of preserved reagents in cool conditions. These requirements increase costs and time for preservation procedures, ultimately limiting accessibility for many research facilities.

1.14.1.2 Gelification

Gelification is another preservation technique for the storage of amplification reagents (Rosado et al. 2011, Franco De Sarabia Rosado Pedro et al. 2016). (Sun et al. 2013) found that gelified PCR reagents had a shelf life of at least three months, compared to freeze-dried reagents, and did not negatively impact the enzymatic performance or fluorescence intensity of PCR products. However, the gelified reagents required a stable refrigeration at 4°C to enable an efficient downstream molecular analysis (Tsaloglou et al. 2013). Nevertheless, the gelification process can be challenging to implement in various molecular laboratories due to its reliance on expensive equipment and proprietary gelifying agents (Høgberg et al. 2011).

1.14.1.3 Vitrification

The vitrification technology has emerged as a promising alternative for preserving sensitive molecules in nucleic acid-based sensing systems. In comparison, the current lyophilisation technologies, require specialised technicians, and expensive lab equipment, and often result in process variability among laboratories (Roy and Gupta 2004, Emami et al. 2018). Furthermore, high pressure and temperature required for drying and removal of water during these methods can reduce the activity of pre-stored reagents (Champagne et al. 1996, Karlsson et al. 2019, Oyinloye and Yoon 2020, Wang et al. 2020a). Thankfully, vitrification technology can address most of the limitations of current preservation methods. Unlike traditional preservation methods like freeze-drying or gelification, the vitrification method eliminates the need for bulky equipment or vacuum incubators for stabilisation procedures and can be performed at room temperature with air exposure as the desiccant environment (Ahlford et al. 2010, Sun et al. 2013). This can enable a simple, cost-effective and energy-efficient preserving protocol, making it user-friendly for those without access to bulky vacuums and frozen storage facilities. The lack of a container in the closed-system vitrification process also eliminates the risk of contamination (Rombach et al. 2014a, Hayashida et al. 2015, Hayashida et al. 2019).

Vitrification technology has demonstrated broad compatibility in stabilising reaction mixtures of various nucleic acid-based amplification assays, including qPCR (Rombach et al. 2014a, Yu et al. 2015), RT-qPCR (Hayashida et al. 2015), PSR (Liu et al. 2018), RPA (Udugama et al. 2017), LAMP and RT-LAMP (Hayashida et al. 2019, Phillips et al. 2019), and SDA (Lafleur et al. 2016). This technology offers several advantages for a point-of-need analysis, including reduced time and complexity of fabrication, low cost, and the ability to mass-produce miniaturised instruments for *in-situ* genetic testing. The fast and affordable manufacturing meets the current growing demand for mass production of genetic testing devices.

During the vitrification process, liquid reagents are transformed into a glass-like state without forming ice crystals (Demirci and Montesano 2007). This strategy provides long-term preservation of enzyme and reagent function at ambient temperatures (Fox 1995). The process can also involve incubating the reagents with a vitrifying agent at a temperature equal to or lower than its glass transition temperature (Tg) (Figure 1.12). The Tg is the key parameter to solidify liquids without undergoing crystalline transformation (Roos and Karel 1991). At a temperature below Tg, the reagents experience a high viscosity that reduces their mobility and solidifies them into an

amorphous structure. While preventing any crystallisation of reagents but retaining them in a sticky, supercooled matrix, leading to stable and robust dry preservation of enzyme functions (Rossi et al. 1997).

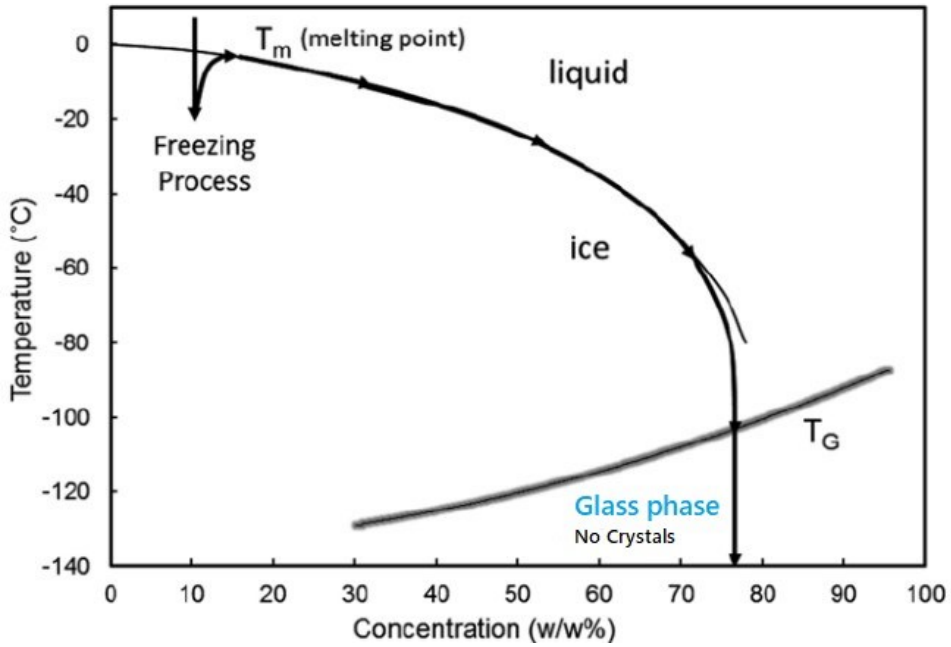

Figure 1.12 Schematic illustration of the temperature transitions during the vitrification process of glycerol. The thin line labelled Tm is the melting temperature of the solution, while the thick shaded line labelled Tg represents the glass transition temperature. The thick arrowed line shows the concentration of glycerol in the remaining unfrozen solution during slow cooling (approximately 1°C per minute) and tracks the melting temperature until viscosity hinders further ice growth and equilibrium cannot be reached. Below the Tg line, the sample consists of a mixture of ice and glass. Adapted from (Fahy and Wowk 2015).

The dehydration process allows mixing in vitrifying enzymes with stabilising agents to maintain the viscosity to further maintain the resulting glass structures (Colaco et al. 1992). For instance, trehalose (α-d-glucopyranosyl α-d-glucopyranoside), is a widely used non-reducing disaccharide for its preserving properties (Ohtake and Wang 2011). Trehalose has a high glass transition temperature (Tg = 106°C) compared to other disaccharides and remains in its glassy state even above room temperature (Roser 1991). Additionally, the end of the glucosyl residues in the trehalose structure prevents the Maillard reaction, which can damage proteins (Lins et al. 2004). Introducing trehalose during vitrification forms a highly viscous glass, which limits molecular mobility and protects the preserved reagents from processes such as crystallisation and degradation. The stabilising mechanism of trehalose is also reinforced due to its ability to replace

surrounding water molecules during hydration and drying, thereby preserving the native state of the enzyme molecule (Schebor et al. 1996).

The vitrification process also can involve the use of a mixture of protectants and surfactant agents to induce water replacement and hydrogen bonding (Crowe et al. 1998, Mensink et al. 2017). Protectants form hydrogen and hydrophobic bonds to counteract the denaturing effect of water removal during dehydration (Emami et al. 2018). For instance, glycerol is a reliable protectant due to its carbohydrate-based head groups that protect the hydrophobic surfaces of proteins and its low glass transition temperature Tg of -92°C (Bell and Hageman 1996). The composite temperature of the vitrifying mixture is developed from the Tg values of individual components, with a mixture of trehalose and glycerol requiring a low Tg for vacuum desiccation and storage at 25°C (Cicerone and Soles 2004). Polyethylene glycol (PEG) is often used as an excipient to prevent denaturation by kinetic mechanisms, but its high molecular weight may increase the Tg temperature of the glass composite above the desired storage temperature (Chang and Pikal 2009, Zadeh et al. 2017). Additionally, the use of surfactants like bovine serum albumin (BSA) is required to maintain the tertiary structure of enzymes and proteins in the glassy state. BSA reduces the interfacial tension between the liquid and glassy matrix which can cause folding and distortion of protein structures (Guell et al. 2017).

Many studies have explored special formulations comprising some of aforementioned stabilising substances, protectants and surfactants to enable the vitrified transformation of liquid reagents of nucleic acid amplification into a solid, glass-like state (Hayashida et al. 2015, Liu et al. 2018, Hayashida et al. 2019, Phillips et al. 2019). This process achieves reagent preservation without the need for extreme freezing conditions typically associated with conventional vitrification techniques. Instead of relying on low temperatures, it focuses on careful optimisation of ingredient combinations and a rapid air-cooling process that solidifies the reagents without the formation of traditional ice crystals. This method also offers the advantage of long-term storage for nucleic acid amplification reagents without the need for costly lyophilisation equipment and eliminates the risk of freezing-related damage (Lafleur et al. 2016). Furthermore, the vitrification technique ensures the stability of reagents at moderate temperatures without the constraints of cold storage, making them more convenient for transportation, and immediate use (Liu et al. 2018).

The reconstitution of vitrified reagents can be achieved by mixing them with an elution sample before initiating the amplification reaction (Garcia et al. 2004). Multiple studies have shown that the activity of vitrified reagents can be recovered even after long-term storage of several months

(Cardona et al. 1997, Rossi et al. 1997, Less et al. 2013). This is due to the amorphous format of the vitrified reagents, which maintains their functionality in a glassy state without the need for lyophilisation or freezing (Green and Angell 1989). Vitrification offers simpler chemical formulations over comparable preservation methods such as lyophilisation, (Roy and Gupta 2004, Kasper et al. 2013) and gelification, which requires complex and tedious protocol (Sun et al. 2013). Additionally, vitrified proteins were proved to be active and stable at ambient temperatures, with a shelf life ranging from 6 months to 2-5 years of functionality (Sun and Leopold 1994).

On the other hand, a simple vitrification protocol can enable a more rapid and simpler preservation process compared to traditional methods. The simplified preserving procedures by vitrification also promise to simplify the routine application of molecular tests and the mass production of microfluidic devices. The combination of vitrification with microfluidic technology offers cost-effective molecular tests with reduced handling steps, allowing the operation of nucleic-acid testing for unskilled users. The efficiency of vitrification on the stability and reactivity of enzymatic reagents for different amplification reactions was explored, as demonstrated in Chapter 5.

1.15 Microfluidic Parameters

We used a set of everyday forces involving capillary force, gravity, and suction for handling multiple reagents to perform routine bioassays in the laboratory. The concept of a microfluidic system is to implement and automate such routine laboratory procedures at the microscopic scale (Stone et al. 2004). Thus, microfluidics can provide tools to miniaturise molecular methods, and improve response times by simplifying analysis steps (Anderson et al. 2000, Verpoorte 2002, Sia and Whitesides 2003, Whitesides 2006). Yet, microfluidic systems require careful developmental steps, including integrating multidisciplinary components such as external actuators, valves, pumps, mixers, and electromechanical interfaces, enabling scaling down and portability of biological assays (Dittrich et al. 2006). Therefore, certain considerations need to be taken into account when designing microfluidic detection systems.

1.15.1 Microchip Substrate

The properties of the polymer substrate play a crucial role in the reliability of the microfluidic system for conducting molecular detection assays. The hydrophilic or hydrophobic nature of the microchip material can affect nucleic acid-based analysis, as demonstrated in Table 1.2. PDMS

(polydimethylsiloxane) is a cost-effective option for the rapid prototyping of microfluidic chips, while poly-methylmethacrylate (PMMA) is more suitable for production versions of microfluidic chips due to its superior strength, optical, thermal, and chemical properties (Liang et al. 2018). Oxygen plasma treatment can change the surface properties of PDMS and PMMA from hydrophobic to hydrophilic (Tan et al. 2010), but these surfaces can quickly return to their hydrophobic state if exposed to air for long duration (Bhattacharya et al. 2005). Therefore, special treatment may be required to enable an efficient nucleic acid analysis through the microchannel, as listed in Table 1.2.

It is advisable to avoid substrates that rely on thermal and solvent bonding techniques, to prevent the deformation of attached components on the microchip, which can inhibit on-chip molecular analysis (Ogilvie et al. 2010). To address this challenge, the adhesive-coated polypropylene film is currently available to provide a strong sealing, to maintain microfluidic structures (Temiz et al. 2015). For example, ThermalSeal RTS™ (Sigma-Aldrich, UK) is compatible with nucleic acids and can be used to bond microchannels and microchambers by lamination before performing amplification reactions. Adhesive bonding, which involves applying glue to a flexible plastic film on a rigid substrate, is also an alternative to preserve the integrity of microfluidic substrate during molecular analysis (Becker and Gartner 2000, Rotting et al. 2002, Miserere et al. 2012). These commercially available polypropylene films, offer a simple and rapid bonding method due to their good adhesion and easy-to-use roll-based laminators (Miserere et al. 2012, Liang et al. 2018). The reversible adhesive bonding enhances the versality and robustness of the design for mass production of nucleic-acid-based microfluidic devices.

Table 1.2 A summary of microfluidic materials affinity to nucleic acid-based analysis.

Material	Tolerated molecules	Coating/Treatment	Bio-assay	Detection	Reference
Poly-methyl methacrylate (PMMA)	RNA	Incubated in BSA overnight at 4°C	NASBA	Fluorescence	(Tsaloglou et al. 2011)
Cyclic-olefin copolymer (COC)	RNA	No treatment, but the microchannels are sealed by polypropylene film.	NASBA	Fluorescence	(Tsaloglou et al. 2013)
Cyclic-olefin copolymer (COC)	DNA	No treatment, but the microchannels are sealed by polypropylene film.	PCR	Fluorescence	(Sun et al. 2013)
Poly-methyl methacrylate (PMMA)	RNA	No treatment	Eectroporation Extraction	N/A	(Bahi et al. 2011)
Polydimethylsiloxane (PDMS)	DNA	No treatment	PCR	Fluorescence	(Fukuba et al. 2011)
Poly-methyl methacrylate (PMMA)	Protein	No treatment, but the chip was sealed with transparent plastic film	ELISA	Chemiluminescence	(Zirath et al. 2016)
Poly-methyl methacrylate (PMMA)	RNA	No treatment	LAMP	Fluorescence	(Chang et al. 2013)
Poly-methyl methacrylate (PMMA)	DNA	No treatment	SPE extractions	Fluorescence	(Reedy et al. 2010)

Borofloat glass	DNA	No treatment	SPE extractions/silica beads & PCR	Fluorescence	(Hagan et al. 2009)
Poly-methyl methacrylate (PMMA)	DNA	No treatment	DMA extraction & PCR	Fluorescence	(Han et al. 2016)
Silicon	DNA	No treatment	DMA Extraction & PCR	Fluorescence	(Shin et al. 2014)
Thin-film	DNA /RNA	No treatment	DPA extraction & PCRs	Fluorescence	(Jin et al. 2017)
Hydrophilic polyester films	DNA /Protein	No treatment	DMA extractions	Fluorescence	(Jang et al. 2019)
Poly-methyl methacrylate (PMMA)	RNA	No treatment	DMA extraction & PCRs	Fluorescence	(Yoon et al. 2018)
Poly-methyl methacrylate (PMMA)	RNA	No treatment	Magnetic beads extraction & RT-qPCRs	Fluorescence	(Zhang et al. 2019)

1.15.2 Fluid Manipulation

Fluid manipulation in microfluidics can be either active or passive (Beebe et al. 2002). Active fluid manipulation relies on external power sources such as electrostatic, electromagnetic, pneumatic, hydraulic, or thermal energy to deliver reagents (Terray et al. 2002, Vestad et al. 2004, Bengtsson et al. 2018). However, the main limitations of active microfluidics are the high energy demand, movable parts, wiring connections, and complex and expensive fabrication processes (Gervais et al. 2011). For instance, actuated valves require intricate chip fabrication and a bulky external instrument for operation (Unger et al. 2000). On the other hand, passive fluid manipulation is based on natural forces such as capillary force, surface tension, gravity, and air pressure (Narayanamurthy et al. 2020). Passive microfluidics enables autonomous, continuous, and steady fluid control without external power or fields (Haeberle and Zengerle 2007). However, the challenge remains to integrate nucleic acid purification and amplification into a simple detection platform that requires the timed delivery of reagents for extraction, to enable a robust amplification reaction at optimal temperatures while ensuring reproducible detection capabilities.

Various techniques can effectively manage fluidic reagents for molecular analysis. To ensure accurate and consistent injection/withdrawal of different reagents on a microfluidic chip, it is important to coordinate the application of pressure and time delays. Additionally, the mixing of fluids is a fundamental operation in molecular-based microfluidics. Homogenisation of co-flowing streams in a single microfluidic chip requires the use of micromixers. There are two types of mixing schemes commonly used in microfluidic systems, active and passive (Bayareh et al. 2020). Active micromixers employ external energy sources, such as electrostatic, electromagnetic, or thermal power, to mix the fluids (Liu et al. 2002, Rida and Gijs 2004, Harnett et al. 2008). However, their reliance on external power sources and complex fabrication processes makes them unsuitable for disposable microfluidic platforms (Nguyen and Wu 2005). In contrast, passive micromixers eliminate any need for external energy and can be easily achieved through normal diffusion mechanisms, such as laminar flow (Bhagat et al. 2007), splitting-and-recombination (Chen and Shen 2017), segmenting (Gunther et al. 2005) and chaotic advection (Nguyen et al. 2008). This layout can be produced by simple, low-cost fabrication techniques without the need for additional power or complex control units (Hessel et al. 2005). Passive micromixers are therefore more for integration with disposable microsystems due to their low-cost fabrication and stable operation (Bayareh et al. 2020).

1.16 Temperature Control

Maintaining temperature control for deployable molecular systems is currently a challenging goal due to the vast heat-absorbing capacity of the ocean. Therefore, isothermal amplification methods that operate at a constant temperature offer suitable options for in vitro molecular devices. In contrast, the deployable execution of the gold standard PCR method is challenging because it relies on cyclic temperature changes (Gao et al. 2022). The operational information on PCR and other isothermal techniques can be found in sections 1.11.4.2 and 1.11.4.3. Management of temperature on microfluidic devices can be achieved by using micro heater and temperature sensor (Chon and Li 2008). Either Peltier or resistive heaters can control heating and cooling profiles in microfluidic-based platforms (Dos-Reis-Delgado et al. 2023). Peltier operates by passing DC current through two dissimilar semiconductors, and by switching the direction of the electric current, heating and cooling can be achieved. When current is generated in one direction, heat is transferred from the bottom side to the top side of the Peltier to activate the amplification reaction. Conversely, cooling is achieved by reversing the current and thus the heat flow (Amasia et al. 2012). On the other hand, resistive heating provides faster heating with lower energy consumption than Peltier elements but requires the ambient temperature to be below 40°C to initiate an effective cooling process (Neuzil et al. 2006). In comparison, Peltier heaters provide faster heating and cooling rates, small thermal mass, and low thermal inertia, making them a suitable choice for PCR thermal cycling while resistive heaters are more suitable for high performance with isothermal methods (Zhong et al. 2009). Therefore, a microcontroller on the circuit board is a key heating component for regulating the input current to the microheater, adjusting it according to the temperature disparity between the measured value and the predetermined setpoint, which is determined by both the sensor and the microheater (Tseng et al. 2014). To ensure precise thermal control, it is recommended to incorporate a temperature sensor that provides feedback on thermal profiling during the amplification reaction (Jeroish et al. 2021). Therefore, optimising the performance of both the temperature sensor and the heater is important before conducting molecular analysis. To calibrate the Peltier heater with a temperature sensor, a calibration apparatus such as Fluke, Everett, WA or TSic™ or IST-AG, Switzerland can be used, and the temperature can be measured on the top of the coverslip in the amplification chamber. A precision threshold of ±0.5°C is considered suitable for thermal regulation (Miralles et al. 2013).

1.17 Detection Chemistries

Fluorescence chemistry is the most frequent detection technology employed to monitor the amplification of target nucleic acids in real-time. Fluorometric measurement allows low-cost, specific and highly sensitive detection technology (Myers and Lee 2008). There are two main categories of fluorescence chemistries involving fluorogenic probes and double-stranded DNA (dsDNA) intercalating binding dyes such as SYBR Green and EvaGreen dyes. Using these dyes provides a simple and cost-effective method, eliminating the necessity for meticulous design considerations required for fluorogenic probes.

However, there are disadvantages to using detection dyes as they have the potential to interact with various types of double-stranded molecules during amplification, leading to non-specific binding and false positive results. These limitations can be overcome by carefully optimising reaction conditions to minimise the non-specific binding associated with the use of dsDNA dyes. The reduced reaction efficiency caused by dsDNA dyes can be detected through post-amplification analyses such as gel electrophoresis and melting curve analysis (Yang and Rothman 2004). In comparison, fluorogenic probes provide highly specific and sensitive detection of genetic targets without any need for post-amplification analysis (Navarro et al. 2015). Fluorogenic probes are fluorogenic-labelled oligonucleotides such as TaqMan probes, Molecular Beacons, exo probes, and Scorpion probes (Ryu 2017).

In PCR reaction, the fluorescence signal is measured at the end of the extension phase at 72°C after thermal cycling (van Pelt-Verkuil 2008). In isothermal-based reactions, the signal is produced by the amplified nucleic acid following a single temperature incubation with reaction enzymes and other reagents (Ozay and McCalla 2021). During the isothermal reaction, a fluorescent signal is generated in proportion to the number of target sequences present, and this signal is continuously monitored as the amplification reaction progresses over time (Chang et al. 2012). Hence, the development of the fluorescence signal is dependent on the enzymatic kinetics during the isothermal reaction compared to PCR, where the signal accumulates over multiple cycles (Jiang et al. 2023). Inefficient enzymatic kinetics can lead to a lag in the development of the fluorescence signal during isothermal reaction, reducing its sensitivity to detect low concentrations of the target. To address this, isothermal reactions may require longer incubation times to achieve detectable fluorescence signals, however, this usually delays the assay turnaround time.

Alternatively, electrical detection monitors molecular interactions during the amplification reaction by measuring changes in electrical properties, such as impedance and current, (Wang 2002). Both

label-free and fluorescent-labelled detections are discussed in the following sections. This thesis focused on fluorescence-based detection as it provides reliable, robust, cost-effective and specific detection. In this research work, molecular detection was carried out using various detection chemistries including intercalating fluorescent dyes, hydrolysis probes, and exo-probes.

1.17.1 Label-Free Detection

Label-free detection strategy includes diverse techniques that offer versatile molecular analysis. For example, amperometric-based detection measures the electric current generated during a chemical reaction. By using an electrode to monitor variations in electrical current resulting during molecular binding between a target sequence and an amperometric surface (Chadha et al. 2022). When specific hybridisation occurs between the target sequence and the electrode surface, the electron transfer is increased, leading to a detectable electrochemical signal (Shanbhag et al. 2023). However, amperometric-based detection is susceptible to non-specific binding from other molecules present in the reaction, leading to signal interference, and a reduction in quantification performance due to an increased signal-to-noise ratio (Shanbhag et al. 2023). Additionally, calibrating non-specific amperometric assays can often be a complex and time-consuming process (Monosik et al. 2012). Addressing these limitations is required to ensure the successful application of electrical-based detection for molecular analysis.

Another example of label-free detection is surface plasmon resonance (SPR), which relies on the functionalisation of a sensing surface to measure changes in physical properties resulting from molecular interactions (Ibrahim et al. 2019). This technique typically requires coating the glass substrate with a metal surface with specific chemical properties to facilitate its binding to the target nucleic acid sequence (Nguyen et al. 2015). Several SPR sensing platforms have emerged to enable molecular-based quantification of DNA sequence targets (Park et al. 2022). While SPR technology is highly sensitive and specific, incorporating labelling techniques to SPR, such as the use of antibody binders for marine toxins analysis, can further enhance its selectivity, sensitivity and multiplexing capabilities (Campbell 2014).

However, biological samples that contain various components including proteins, lipids, and sugars, influence the SPR binding interactions, reducing the accuracy of results. Moreover, high temperatures can lead to the evaporation of the SPR reaction mixture, leading to a change in refractive index, and introducing noise into the SPR measurements (Nguyen et al. 2015). Additionally, performing SPR measurements at high temperatures can cause evaporation of the SPR reaction mixture including the sample. This evaporation can cause a change in the refractive index

of the sample, which in turn introduces noise into the SPR signal (Chen et al. 2023). Another disadvantage of using SPR is that it relies on expensive instruments, and extensive expertise is required to maintain the capture surface and operate the SPR measurement effectively (Ribeiro et al. 2022). Yet, SPR technology enables real-time detection with high specificity and sensitivity for nucleic acid targets and marine toxins.

On the other hand, pH-based assays provide a sensitive detection to changes in pH value, indicating the acidity or alkalinity of the amplification reaction, reflecting molecular binding interactions between the amplified products from the target sequence with the pH electrode (Choi et al. 2023). This methodology presents a simple and affordable tool to monitor the real-time amplification process occurring throughout the reaction without the need for labels (Aoki et al. 2021). However, the specificity of pH-based detection methods can be influenced by inhibiting factors such as temperature changes, and interference from other ions present in the amplification reaction (Miao et al. 2020). Therefore, procedures for reaction calibration and electrode maintenance are required to ensure accurate and reproducible genetic measurements.

Label-free detection offers attractive advantages for molecular analysis, providing accurate and dependable results. However, achieving these benefits depends on precise signal measurement optimisation, careful management of experimental variables, and the proficient use of specialised, often costly equipment, demanding a high level of expertise to effectively address the associated limitations.

1.17.2 Intercalating Fluorescent Dye

A fluorescent Intercalating dye is used to indirectly measure the quantity of nucleic acid amplifying during each PCR reaction cycle. SYBR Green provides a simple detection tool by binding to resulting dsDNA molecules during amplification. SYBR Green dye is a versatile fluorescent dye commonly used in various amplification reactions, including qPCR, RT-qPCR, NASBA, LAMP, and RCA amplification techniques for both DNA and RNA targets (Dragan et al. 2012b). It can emit fluorescence at low signal intensity which increases as more dye binds to the dsDNA amplicons during the PCR cycles, as shown in Figure 1.13. However, selectivity limitations associated with SYBR Green can bind to any double-strand DNA molecule present in the amplification reaction, leading to non-specific binding and false positives or overestimation of the target concentration. SYPR-based detection is even more challenging in achieving specific and accurate quantification, when amplifying low DNA template concentrations, particularly from environmental complex samples (Andersen et al. 2006). Unlike sequence-specific probes like hydrolysis probes, SYBR Green is less

suitable for detecting specific variants and multiplex detection. In addition, the fluorescence signal of SYBR Green tends to reach saturation at high DNA concentrations, preventing accurate measurements of differences in DNA concentration among samples containing higher DNA levels (Farrar et al. 2010). Since SYBR Green fluoresces upon binding to the higher DNA concentration, any further increases in DNA content will inhibit the amplification reaction and will prevent the proportional increase in fluorescence signal, limiting the quantification range of the assay.

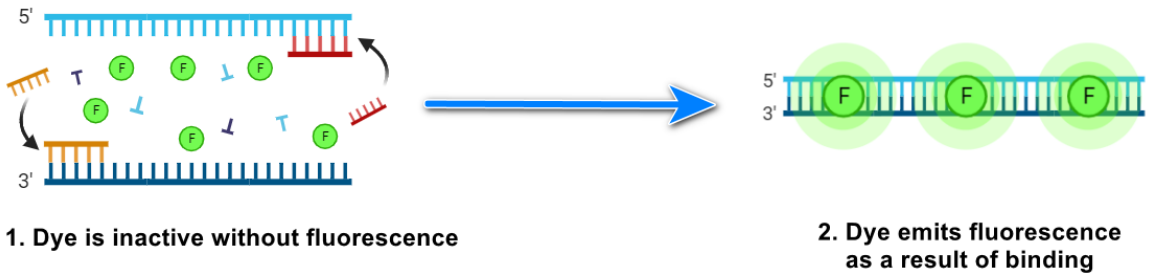

Figure 1.13 Mechanism of fluorescent intercalating dye

To address these limitations, post-amplification analysis is required to validate the specificity of the amplified product using SYBR Green. Melting curve analysis offers a robust validation method by gradually increasing the temperature, to dissociate the double-stranded DNA amplicon into single-stranded DNA. The resulting fluorescence data are collected at each temperature increment during the dissociation process (Lunn et al. 2008). The reduction in fluorescence intensity at the melting temperature provides a qualitative indicator proportional to the size of the specific PCR product. Using fluorogenic dyes in amplification reactions offers several advantages due to readily availability and compatibility with the majority of fluorescence detectors equipped with filters in the 520 nm range (Njage and Buys 2020). An additional benefit of using intercalating dyes is eliminating the need for costly detection probes, which can otherwise lead to the risk of secondary structures forming between primers and probes, inhibiting amplification reaction (Yang and Rothman 2004).

1.17.3 Hydrolysis Probe

On the other hand, probe-based assays require careful design considerations and several optimisation procedures of reaction conditions to ensure successful amplification. Factors like bioinformatic requirements, secondary structures and annealing temperature are important parameters to enable the specificity and activity of the hydrolysis probe, improving the overall efficiency of the amplification reaction (van Pelt-Verkuil 2008). The hydrolysis probe or (TaqMan) is a linear oligonucleotide that contains a complementary region to the target sequence being amplified. The probe is designed to bind between the upstream and downstream primer binding

sites, incorporating a 5’ reporter fluorophore and a 3’ quencher. Prior to the amplification reaction, the quencher is close to the fluorophore, preventing fluorescence. As the DNA polymerase extends the upstream primer, it encounters the bound probe to the target sequence, separating the fluorophore from the quencher, and enabling fluorescence generation (Marras et al. 2002). The 5' to 3' exonuclease activity of the polymerase cleaves the probe and releases the fluorophore into the reaction solution. The resulting fluorescent signal is proportional to the amplicon yield, providing specific and accurate quantification of low-copy number targets, as depicted in Figure 1.14. The release of the fluorophore is repeated in each subsequent amplification step, allowing real-time measurement of target levels at each cycle (Kalinina et al. 1997). Hydrolysis probes provide a high degree of specificity and precision for quantifying targets with low copy numbers, with the ability to identify specific genetic variations such as single nucleotide polymorphisms (SNPs) (Kim et al. 2016). Additionally, different probes can be multiplexed in a single reaction to detect multiple targets simultaneously, making them valuable in high-throughput genetic testing (Eckford-Soper and Daugbjerg 2015). Due to these analytical advantages, hydrolysis probes are commonly used in various nucleic acid amplification reactions including qPCR (Nagy et al. 2017), RT-qPCR (Wei et al. 2017) and (LAMP) (Bhat et al. 2019), facilitating real-time quantitative analysis.

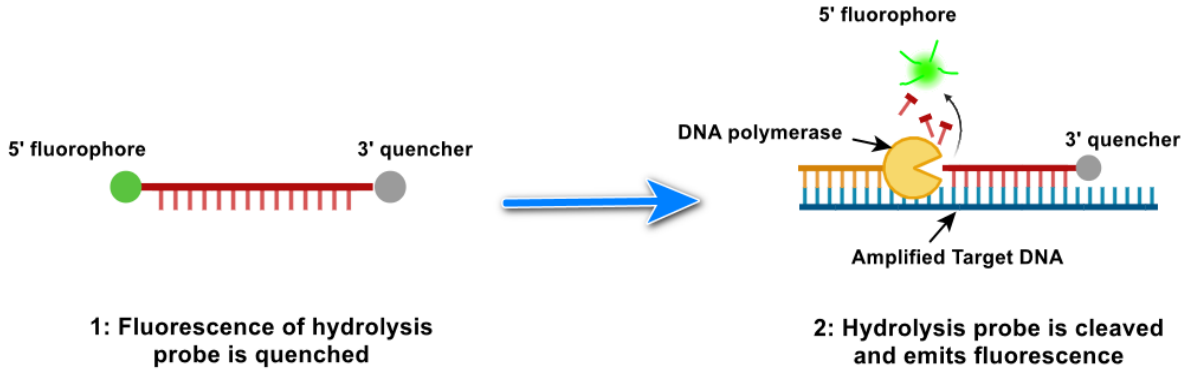

Figure 1.14 Mechanism of hydrolysis probe.

1.17.4 Molecular Beacon

A molecular beacon is a single-stranded probe that consists of a hairpin loop combined together by hydrogen-bonded stem sequences, with the loop part being complementary to the target DNA/RNA sequence. The 3' quencher suppresses the fluorescence of the 5' reporter when the molecular beacon is free in solution. However, when the hairpin loop hybridises with the target template, the fluorophore separates from the quencher, generating a quantifiable fluorescent signal, as shown in Figure 1.15 (Tyagi and Kramer 1996). Unlike TaqMan-based assays that rely on degradation, the detected fluorescent signal of molecular beacons is directly proportional to the amount of target

DNA in the reaction. The specificity of the assay can be improved through melting curve analysis. Molecular beacons are suitable for multiplex reactions and have been widely used in PCR, HDA, and NASBA amplification assays (Huang and Marti 2012). Molecular beacons were not used in the work.

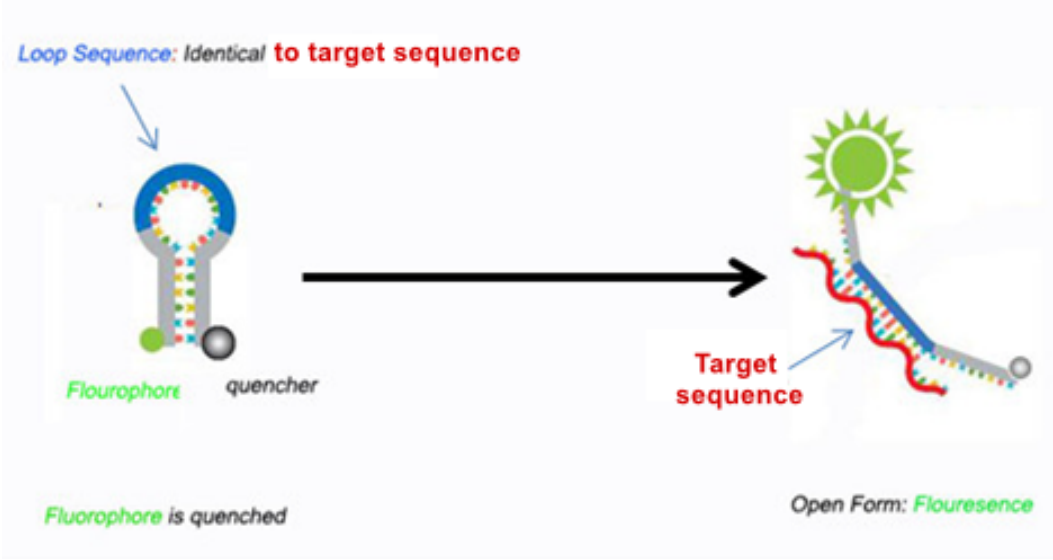

Figure 1.15 Mechanism of the molecular beacon.

1.17.5 RPA Probes

Real-time RPA-based detection traditionally uses two primers and one probe (Lobato and O'Sullivan 2018). Recently, TwistDx™ Ltd has commercialised a range of RPA detection probes, including the TwistAmp™ exo probe, TwistAmp® exo RT, TwistAmp™ fpg probe, and TwistAmp™ nfo probe for RPA lateral flow applications (TwistDx 2009). To enable RPA amplification, these probes are required to be incorporated with a primer pair usually consisting of sequences that are 30–35 bases long with a GC content ranging from 40% to 60%. In some cases, shorter PCR primers with lengths of 18–25 bases can be used in RPA reactions, although this may result in reduced reaction speed and sensitivity (TwistDx 2019).

Of these probes, exo-probe is a lengthy oligonucleotide consisting of 46-52 bases that are homologous to the target sequence. This probe incorporates unique modifications such as a fluorophore (e.g. FAM) and quencher (e.g. Black Hole Quencher 1 or 2) separated by a tetrahydrofuran residue. The probe also has a blocking group at the 3’ end, which encounters the synthesis of new DNA strands during the initial stages of the reaction, by preventing the polymerase from adding nucleotides. This blockage prevents any premature amplification until the probe specifically binds to its complementary target sequence. Once the exo probe recognises and binds to the target sequence, the blocking group is displaced and removed, allowing DNA synthesis by

polymerase which in turn will initiate the amplification process (Piepenburg and Armes 2018). After specific binding to the target sequence, the *E. coli* exonuclease III enzyme scans the exo-probe probe for a tetrahydrofuran abasic site, (THF) to digest it, revealing the 3'-OH end for polymerisation. This will lead to the separation of fluorophore from its quencher and produce a fluorescence signal that can be detected within 5-10 minutes during the RPA reaction, as demonstrated in Figure 1.16 (Hill-Cawthorne et al. 2014). The enzymatic cleavage of the RPA exo probe allows the DNA polymerases to extend and displace forward primer from the 3' ends, leading to an exponential increase in amplicons over time of reaction for downstream use as a template in another phase of amplification (Piepenburg et al. 2006). The enzymatic cleavage of the RPA exo probe triggers DNA polymerases to extend and displace the forward primer from the 3' ends of the target sequence. As a result, a rapid and exponential increase in the production of amplicons occurs as the reaction progresses. These amplicons serve as templates for subsequent phases of amplification, allowing for the generation of a large quantity of target DNA for fluorescence detection.

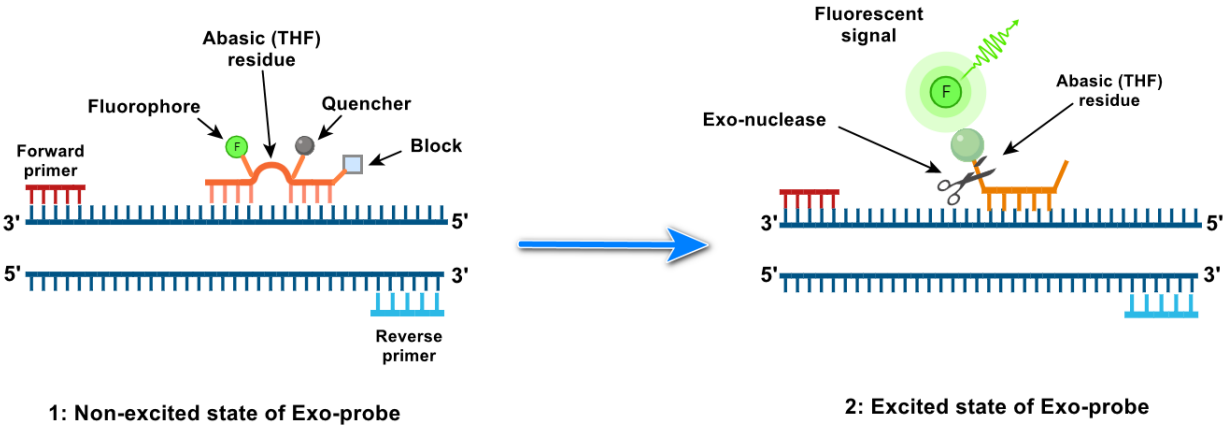

Figure 1.16 Mechanism of RPA exo-probe.

The fpg probe is also a long oligonucleotide like the exo probe, consisting of approximately 30-35 bases that specifically complement the target sequence. This probe is blocked at the 3' end to prevent immature elongation with a fluorophore and quencher separated by 4-5 nucleotides (with a maximum of 7). The fluorophore is attached to the ribose of an abasic nucleotide via a C-O-C linker, referred to as deoxyribose (dR)-fluorophore. Upon hybridisation between the target sequence and the fpg probe, the 8-oxo guanine DNA glycosylase enzyme digests the probe at the dR position, leading to the release of the fluorophore and the emission of the fluorescence signal (Piepenburg et al. 2011).

The nfo probe also contains a tetrahydrofuran residue that separates the quencher and the fluorophore. Here, the Endonuclease IV enzyme (Nfo) cleaves this probe at the abasic site

(tetrahydrofuran), creating a 3'-OH group for the polymerisation process. In cases of amplicon degradation during RPA reaction, incomplete cleavage may occur, yet this can still generate detectable signals, which can be suitable, especially in applications involving lateral flow strips (Kersting et al. 2014). Previous studies have indicated that exo probes can offer greater sensitivity in RPA-based detection compared to fpg and nfo probes (Boyle et al. 2013, Bhat et al. 2022, Chen and Xia 2022). The unique design and mechanism of the exo probe significantly improve the specificity and accuracy of the RPA assay.

1.17.6 Multiplexing Detection

Fluorescence technology has the potential for multiplexing genetic analysis, allowing the simultaneous detection and quantification of multiple targets in a single reaction while maintaining assay sensitivity and specificity. This is achieved by using multiple reporter dyes with distinct wavelengths to identify various targets within the same reaction pot (Hodzic et al. 2023). The complex composition of these assays can increase the likelihood of miss-priming and non-specific hybridisation among oligos and target sequences, particularly when there are differences in target concentrations, preventing sensitive detection (Jet et al. 2021). To overcome these limitations, bioinformatic analysis is required to evaluate the potential formation of secondary structures among oligos in the reaction. This analysis identifies the stable secondary structures, including self-dimers, hetero-dimers, and hairpin loop structures, which can inhibit the assay progress (Ahmad et al. 2004). Additionally, optimising the reaction conditions is important by involving iterative testing of assay on various samples to achieve the desired assay performance.

In some samples, different target sequences may be present in varying abundances. As a result, the abundant target will outcompete the other target sequences to consume amplification resources including reagents and enzymes of multiplex reaction, leading to reduced sensitivity for detecting low abundant targets (Elnifro et al. 2000). To address this constraint, primer and probe concentrations are required to be carefully optimised, ensuring that both high- and low-abundance targets can be sensitively and specifically detected (Sint et al. 2012). Alternatively, blocking primers can be introduced to high-concentration targets by selecting broad emission spectra of reporter fluorophores (Nikiforova et al. 2015). Multiplexing can also reduce time, reagent consumption and operating costs but requires a precise optical configuration including multiple filters and precise mechanical assemblies, increasing both cost and complexity. Different techniques like molecular beacons, hydrolysis probes and RPA exo probes demonstrated the adaptability for multiplex fluorescence detection (Besson and Kazanji 2009, Li et al. 2019b, Rajagopal et al. 2019). However,

a unique optical configuration is necessary for multiplexing detection that needs precise alignment and lensing, increasing both cost and complexity for desired detection system.

1.17.7 Optics configuration

The detection of amplified products in real-time is achieved by exciting the fluorophore to emit light at a specific wavelength, which in turn is collected and passed through an optical detection module (Fu et al. 2006). The standard configurations rely on the precise alignment of the light source with an optical detector, where the emission filter and fluorescence detector are positioned at a 90° angle relative to the position of the excitation source (Dandin et al. 2007). A schematic representation of fluorescence-based optical systems is depicted in Figure 1.17. Deploying these optical configurations in oceanic settings is impeded by various limitations, impacting the downstream molecular analysis. The sensitivity of these assays can be significantly reduced under high oceanic pressure conditions, changing the refractive index of the optical system, and decreasing the signal quality during molecular genetic testing (Mills and Fones 2012). A sturdy pressure housing for the optical detector can compromise the high pressures of deep seawater, accommodating pressure-tolerant molecular assays for environmental applications (Mowlem et al. 2011).

Moreover, the generation of air bubbles during the heating of reagents in molecular assays at high operating temperatures interferes with optical measurements, leading to gaps in the collected data (Lee et al. 2019b), and also observed in Chapter 6. The prolonged light exposure of molecular reagents bleaches the fluorophore, reducing the intensity of the optical signal. This can be avoided by lowering the exposure time, where the amplification microchamber should only be irradiated once every 1-30 seconds during the fluorescence measurement (Dimov et al. 2008).

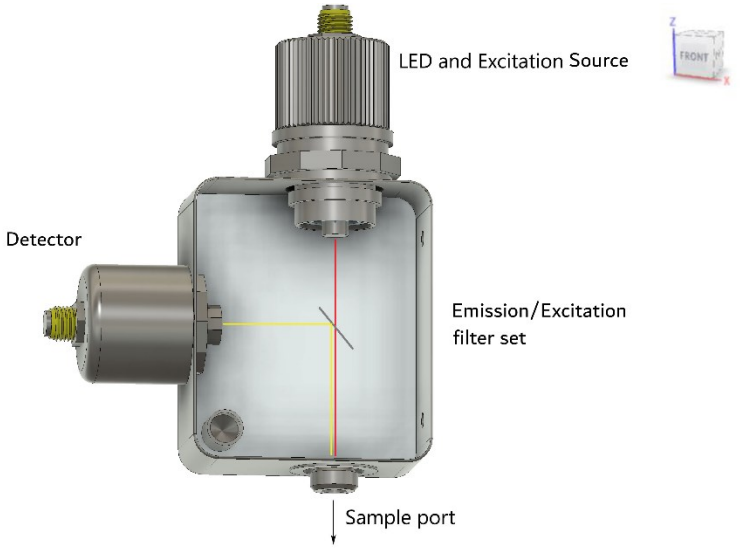

Figure 1.17 A schematic CAD diagram demonstrates the concept of fluorescence optical configuration.

There are additional challenges that limit the use of deployable optical systems. For example, optical sensitivity can be attenuated by the presence of background noise, originating from non-target particles present in assay reagents or processed samples (Homola 2003). Furthermore, commercially available optical detection systems are expensive making them financially prohibitive to obtain for many testing facilities (Gotz and Karst 2007). Alternatively, building a bespoke optical system demands extensive knowledge and hands-on expertise in optical detection as well as incorporating costly components (Prikryl and Foret 2014). Several studies demonstrated the adaptability of both off-the-shelf optical detection systems and customised optical setups within molecular detection platforms (Kuswandi et al. 2007). The use of readily available optical units offers a simple design and low-cost prototyping. This can lead to installing a simple, affordable instrument, by reducing both cost and complexity for manufacturers. Overcoming these challenges is important for ensuring the integrity and reliability of optical data and improving the accuracy and robustness of molecular analysis in oceanic environments.

1.18 State-of-the-Art

The molecular analysis presents a highly accurate, sensitive, and reliable quantification of harmful microorganisms compared to conventional regulatory methods (Theron and Cloete 2000). The integration of molecular-based methods with microfluidic technology can automate nucleic acid amplification, enabling a sample-to-answer workflow (Hazen et al. 2013). However, microfluidic-based integration is constrained by engineering challenges in accommodating various operations including fluid manipulation, sample processing, reagent preservation, precise temperature

management, and optical detection. Automating these functions mainly depends on specific designs, fabrication, and experimental characterization to enable the effective pumping, metering, and valving of fluids (Berlanda et al. 2021). These considerations introduce additional challenges in developing cost-effective, rapidly prototyped, and user-friendly instrumentation for environmental testing in low-resource settings.

This technological bottleneck poses a significant challenge to implement the desired high-throughput genetic analysis through integrated and on-site nucleic acid testing. Several integrated analytical systems are commercially available for automated molecular analysis such as Abbott's Afinion™ System, Qiagen's QIAxcel automatic DNA/RNA analyzer, and Siemens Healthcare's VERSANT® kPCR Molecular System. These systems are primarily designed as benchtop platforms and are larger in size compared to potential Lab-on-a-Chip (LOC) systems. Furthermore, these systems are expensive, and consume significant quantities of reagents, increasing operational expenses for running only a few tests per day. Additionally, these systems are non-reusable and require frequent maintenance, making them unsuitable for repeated usage between runs. The operation of these commercial systems demands intensive training, which greatly restricts their deployment for field testing, especially in resource-constrained environments and outbreak hotspots (Sin et al. 2011). These challenges have been addressed by customising several integrated LOC systems, allowing for the miniaturisation of molecular analysis processes. This has streamlined genetic detection procedures, resulting in substantial cost reductions for reagents, consumables, and equipment maintenance (Silva et al. 2022). This approach effectively addresses logistical challenges related to sample transportation and processing, eliminating the need for bulky desktop systems in centralised laboratories (Fiorini and Chiu 2005).

This thesis has led to the development of an innovative bench-top lab-on-chip sensor designed for on-site genomic sampling and quantification of the toxic diatom *P. multistriata*. This project involved multidisciplinary work to achieve an semi-automated on-chip DNA extraction protocol and LAMP amplification, ensuring the preservation of reaction components within an integrated system (as demonstrated in Chapter 6, page 78). This represents a key step towards the realisation of a fully portable, cost-effective, versatile, and readily deployable technology for on-site nucleic acid testing of microorganism targets in environmental settings.

1.19 Objectives and Structure of the Thesis

The primary objective of this work is to develop methodologies and technologies aimed at achieving rapid and sensitive genetic monitoring for the DA-producing marine diatom *Pseudo-nitzschia* spp.

The overarching vision is to contribute to the development of automated, decentralised nucleic acid testing technologies in the form of robust, miniaturised, user-friendly and deployable sensors and samplers. These innovations are intended to save time and expenses whilst increasing data quality and spatial coverage of environmental surveillance.

This work focuses on incorporating molecular assays with state-of-the-art microfluidic technologies to address a range of key research questions. These questions include identifying the current knowledge gaps related to the monitoring and detection of *Pseudo-nitzschia* diatoms. Additionally, the study aims to do the following:

1. Assess the precision of existing biological assays in providing accurate estimates of *Pseudo-nitzschia* cell concentrations. This includes the development of a molecular technique capable of providing specific and highly sensitive detection of *Pseudo-nitzschia*.
2. Leverage molecular analysis methods to quantify transcriptional activity as a reliable proxy for tracking *Pseudo-nitzschia* toxicity.
3. Investigate how gene expression changes in response to biological parameters, particularly nutrient fluctuations.
4. Determine the specific conditions or thresholds that serve as the 'tipping point' for triggering the production of DA by *Pseudo-nitzschia*.
5. Investigate the applicability of isothermal molecular analysis for quantifying the presence of the DA-encoding gene as an indicator of *Pseudo-nitzschia* toxicity in seawater samples from the environment.
6. Address the challenges of extending the stability and lifetime of reagents used in molecular analysis.
7. How to customise novel technologies to incorporate DNA purification, amplification, and detection to enable simple, cost-effective, and accurate quantification of *Pseudo-nitzschia*.
    a. Is it possible to provide an operational microfluidic instrument that is amenable to automation?
    b. Can a miniaturised lab-on-chip prototype for genetic analysis be produced?

To address these cutting-edge questions, interdisciplinary research activities emerged in the following chapters as outlined below.

Chapter 2: A novel assay for the quantification of *Pseudo-nitzschia* spp: In this chapter, a novel qPCR assay is developed to enable rapid, specific and sensitive quantification of *Pseudo-nitzschia spp*. The analytical performance of this assay is compared with other techniques,

including previously developed PCR assays, as well as statutory methods such as microscopy-based and immune-based detection methods.

Chapter 3: Induction of toxin biosynthesis by nutrient depletion and addition in *Pseudo-nitzschia multistriata*:

This chapter explores the response of nutrients-depleted *P. multistriata* to the addition of a phosphate (P), nitrate (N), and silicate (Si). Experimental treatments are conceptually similar to the naturally occurring stressors in the coastal systems, which are driven by increased inputs of nutrients. The experiment aims to estimate the 'tipping point for triggering DA production as a result of nutrient enrichment.

Chapter 4: Detection of *Pseudo-nitzschia spp*. using Isothermal DNA-Based Amplification.

Two amplification strategies under isothermal conditions are developed in this chapter: loop-mediated isothermal amplification (LAMP) and recombinase polymerase amplification (RPA). A comparative analysis of both techniques is conducted in terms of their analytical specificity and sensitivities, focusing on the quantification of the *dabD* toxin-encoding gene found in the marine diatom of *Pseudo-nitzschia* spp. Additionally, the applicability of both assays for integration into microfluidic platforms is assessed, taking into account factors such as analysis duration, reproducibility, cost of reagents, and adaptability to environmental samples. This comprehensive assessment aims to provide a clear understanding of the most effective and feasible method for detecting the target gene under isothermal conditions. The optimised LAMP assay is employed to enable the quantitative assessment of toxin-encoding gene levels in a number of environmental DNA samples. This assessment provides a profile dataset of gene abundances at a sampling location that experienced frequent peaks of long-lived *Pseudo-nitzschia* blooms.

Chapter 5: Pre-storage of vitrified reagents for simple, precise and rapid molecular detection

In this chapter, a preservation technique based on vitrification technology is developed and optimised to enable amplification detections using dried master mixtures with minimal assay preparation procedures. Custom-made formulations are tested to stabilise assay components in amplification assays at room temperature for long-term storage, for up to six months. To evaluate of reactivity of vitrified master mixes, linearity and sensitivity of quantification are analysed at various time points of storage. Additionally, quantification specificity is also validated via gel electrophoresis and melting curve analysis of amplified products. The

preservation procedures are optimised through this chapter to reduce the handling steps of reagents and improve the portability of molecular detection for end-users.

Chapter 6: LAMPTRON: a lab-on-a-chip system integrating DNA purification and loop-mediated isothermal amplified quantification of toxic diatom *Pseudo-nitzschia multistriata*.

This chapter focuses on developing a prototype of a microfluidic chip for DNA extraction using the dimethyl adipimidate (DMA) method from the *Pseudo-nitzschia* cells, to achieve non-chaotropic extraction and obtain high DNA recovery in a shorter time compared to the recovery resulting from a commercial purification kit. To confirm the DNA extraction performance of the DMA method, downstream analysis of extracted DNAs will be performed using a newly developed isothermal assay (LAMP). This technique is applied to quantify the processed *P. multistriata* cells using both preserved and wet reagents. This explores the efficiency of vitrification technology for preserving amplification reactions to extend the shelf-life of assay reagents, to promote the routine use of genetic monitoring of toxic *Pseudo-nitzschia* blooms.

Chapter 7: Conclusions and Future Work

This chapter provides a concise summary of the key thesis findings obtained and their implications. It incorporates the future aspects of development and the work that could maximise the potential of the biosensor prototype.

Chapter 2 A novel assay for the quantification of *Pseudo-nitzschia* spp.

2.1 Abstract

Outbreaks of domoic acid-producing species are frequent in certain regions but are typically only known after shellfish harvest, by detecting the toxin in shellfish flesh. A quantitative Polymerase Chain Reaction (qPCR) method was developed here to quantify *Pseudo-nitzschia* cells through the amplification of the genetic marker of the geranyl pyrophosphate synthase gene (GPP). The assay was specific for the GPP gene across 10 isolated strains of toxic *Pseudo-nitzschia* species, with no detection of 8 other phytoplankton strains. Reliable quantification of 10^4 cells l^{-1} and 10.4 gene copies per reaction represent increased sensitivities compared to current statutory limit (1.5×10^5 cells l^{-1}). Cell concentrations calculated using qPCR showed a log-linear relationship with microscopy counts (R^2 = 1.0). Copy numbers of the GPP gene were well correlated with toxin content in ten strains of toxic *Pseudo-nitzschia* species (R^2= 0.9, *P* = 0.00007). The assay enabled the detection of *Pseudo-nitzschia* 35 minutes after the addition of DNA template. The developed assay offers the potential for rapid, high-throughput surveillance of toxic blooms. This is of particular importance for routine monitoring of the marine environment by advancing a more scalable and rapid assessment of the potential risk of *Pseudo-nitzschia* blooms.

2.2 Introduction

Diatoms of the genus *Pseudo-nitzschia* are known to produce the neurotoxin domoic acid (DA), causing severe and lasting damage to marine industries and human and animal health. In 2015, a *Pseudo-nitzschia* bloom led to a prolonged and expansive closure of shellfisheries and finfisheries along the American northwest coast (McCabe et al. 2016, Anderson et al. 2021). The toxic effects of DA on wildlife are particularly striking, leading to the death or illness of fish, seabirds, sea otters, sea lions and whales (Lefebvre et al. 2002a, Bates and Trainer 2006a). The risk to humans is mostly associated with the consumption of filter-feeding shellfish, which are eaten before depuration (Mafra et al. 2010, Tasker 2016, Sauvey et al. 2021), leading to 'Amnesic Shellfish Poisoning' or ASP, damaging the brain, blood and liver cells (Gajski et al. 2020, Stuchal et al. 2020, Petroff et al. 2021), which could cause human fatalities (Bates et al. 1989). In addition to the detrimental effects related

to DA, *Pseudo-nitzschia* blooms can impact ecosystems through the sequestration of light, nutrients and oxygen (Trainer et al. 2020).

Microscopic identification of *Pseudo-nitzschia* cells may represent a challenge because the morphometric characteristics of cells can vary in response to environmental conditions and at times overlap among different strains of the same species (Cerino et al. 2005, Lundholm et al. 2006a, Amato et al. 2007, Hansen et al. 2011). Toxic cells can be detected by measuring the DA concentration by High-Performance Liquid Chromatography (HPLC), with a limit of detection of approximately 25 ng ml^{-1} (Lopez-Rivera et al. 2005). Enzyme-linked immunosorbent Assay can be also used to measure DA levels with respective limits of detection of 10 µg l^{-1} in water (Kleivdal et al. 2007a) and 0.003 µg g^{-1} in seafood (Kania and Hock 2002). For comparison, the suggested regulatory limit of DA in shellfish for human consumption is 20 µg g^{-1}, which is close to the statutory limit (O'Mahony 2018).

PCR-based detection has been reported for the detection of *Pseudo-nitzschia* species, targeting conserved regions of the ribosomal RNA (rRNA) encoding genes or the internal transcribed spacer 1 (ITS-1) and ITS-2 (McDonald et al. 2007, Trobajo et al. 2010, Penna and Galluzzi 2013b, Tan et al. 2015, Kim et al. 2017). Most existing PCR methods target conserved regions of the ribosomal RNA (rRNA) encoding genes or the internal transcribed spacer 1 (ITS-1) and ITS-2 (Lundholm et al. 2006b, Penna and Galluzzi 2008). Others have targeted sequences within mitochondrial genes (cytochrome c-oxidase subunit 1; COI), and chloroplast genes (ribulose-1,5-biphosphate carboxylase/oxygenase large subunit; *rbcL*) (Amato et al. 2007, Tan et al. 2015). Recently, *Pseudo-nitzschia* genome sequencing was used to identify a cluster of four genes, *dabA*, *dabB*, *dabC* and *dabD*, implicated in the biosynthesis of DA in toxigenic *Pseudo-nitzschia multiseries* (Brunson et al. 2018). DabA performs the catalytic conversion of L-glutamate to N-geranyl-L-glutamic acid through N-geranylation, using geranyl diphosphate/pyrophosphate synthase (GPP) as a prenyl donor (Brunson et al. 2018, Chekan et al. 2020). Geranyl pyrophosphate (GPP) is classified as an enzyme within the isoprenoid biosynthesis, polyprenyl synthetase, and prenyltransferase protein families (Savage et al. 2012, Athanasakoglou and Kampranis 2019b). GPP synthase activity was not detectable in the catalytic assays of prenyltransferases involved in DA biosynthesis (Badarou 2021). The undetectable activity was attributed to the presence of heterodimeric prenyltransferases which lack the essential catalytic residues for the GPP protein expression (Badarou 2021). Interestingly, different studies have reported GPP expression during DA production in strains of both *P. multiseries* and *P. seriata* (Brunson et al. 2018, Hardardottir et al. 2019, Chekan et al. 2020).

In this study, the development and evaluation of a method for the detection and quantification of GPP-containing *Pseudo-nitzschia* cells in an algal culture medium and natural seawater sample are described. A novel qPCR assay was developed to use the geranyl pyrophosphate (GPP) gene to provide specific quantification across 10 strains within the *Pseudo-nitzschia* genus.

2.3 Methods

2.3.1 Strains and culturing conditions

Pseudo-nitzschia strains (listed in Table A1, Appendix A) were grown in *f/2* growth medium, and cultures of non-*Pseudo-nitzschia* strains were maintained in L1 and BG11 growth media (Guillard 1983). Growth media was prepared with artificial seawater and cultures were maintained at a temperature of 18°C, with a 12-hour light:dark photoperiod. An exponentially dividing culture was enumerated using a Sedgwick–Rafter cell counting slide (PYSER-SGI) and a compound light microscope (Carl Zeiss, Oberkochen, Germany), and dilutions were prepared in a fresh batch of f/2 medium.

2.3.2 Genomic DNA extraction

Pseudo-nitzschia cells were harvested in 50mL polypropylene tubes, by centrifugation at 7,160 rpm for 10-12 minutes at 4°C, using a refrigerated centrifuge, to limit fluctuations in DA concentration over the growth phases for parallel domoic acid toxin analyses (see section 2.3.13 below) (Bates et al. 2018). The supernatant was removed carefully, without disturbing the cell pellet, which was washed twice in Phosphate Buffered Saline (PBS), and then stored at −80°C until further processing. DNA was extracted using the DNeasy Plant Mini Kit (Qiagen, Hilden Germany) following the manufacturer's recommended protocol. DNA concentration and purity were measured fluorometrically using a Qubit fluorometer (Thermo Fisher Scientific Inc., UK) and NanoDrop spectrophotometer (ND-1000, Thermo Fisher Scientific Inc., UK) and stored at −20°C until use.

2.3.3 Primer design for *Pseudo-nitzschia* species

Primer design included *Pseudo-nitzschia* prenyltransferase sequences obtained from multiple sequence data repositories, as shown in Table A2, Appendix A. The sequences were collected from multiple *Pseudo-nitzschia* genomes via the National Centre for Biotechnology Information (NCBI)

GenBank database (https://www.ncbi.nlm.nih.gov/) and the Marine Microbial Eukaryote Transcriptome Sequencing Project (MMETSP) through (https://www.imicrobe.us/) (Keeling et al. 2014), the SZN institute database (https://bioinfo.szn.it/), the Earlham institute's database (http://apollo.tgac.ac.uk/) (Basu et al. 2017), Ensembl portal (https://protists.ensembl.org/) and the Joint Genome Institute (JGI) (https://genome.jgi.doe.gov/portal/) (Boissonneault et al. 2013). Additional *Pseudo-nitzschia* sequences were obtained from previous publications including previous publications including (Lema et al. 2019), (Russo et al. 2018), (Di Dato et al. 2015), (Basu et al. 2017) and (Hardardottir et al. 2019). A total of 51 resulting sequences from multiple *Pseudo-nitzschia* species were aligned using a ClustalW multiple sequence alignment algorithm with the default settings including a cost matrix at 85% similarity, gap open penalty of 12, gap extension penalty of 3, and refinement iterations of 2. ClustalW version 2.1 and Geneious R11 Bioinformatics Software (Biomatters Ltd, Auckland, NZ) were used for sequence alignment to identify the consensus regions of the target gene as shown in (Figure 2.1) (Larkin et al. 2007).

PCR primers were designed to target the conserved region in the sequences from *Pseudo-nitzschia* species, using the 'Primer3' tool (Untergasser et al. 2012). The primers were designed to anneal within conserved regions of the target gene sequences, as determined by multiple sequence alignment. The primers were designed to meet the minimum design criteria as described by (Alvarez-Fernandez 2013). All primer sets were designed to amplify target gene fragments ranging from 100 to 300 bp in length. Primers were synthesised by Integrated DNA Technologies, Inc. (Germany).

2.3.4 Screening for *Pseudo-nitzschia*-specific primers

A SYBR-based PCR reaction was employed for an initial assessment of the newly designed primer pairs. 25µl PCR amplification reactions were carried out with 12.5 µL of IQ SYBR Supermix containing SYBR Green I DNA binding dye, 50 U ml^{-1} Taq DNA polymerase, 0.4 mM per each deoxynucleoside triphosphate (dNTPs; dATP, dCTP, dGTP and dTTP), 6 mM $MgCl_2$, and reaction buffer (Bio-Rad Laboratories, Inc.). Genomic DNA of *P. multiseries*, strain ML-59 was added to the reaction mixture to achieve < 10^6 copies of the target gene as a positive control. Negative controls containing nuclease-free water were used in triplicate. 0.4 µM concentration of primers was used for the initial evaluation of qPCR reactions. qPCR amplification was performed using a Light Cycler 2.0 real-time qPCR machine (Roche Molecular Systems, Germany) with an initial denaturation at 95 °C for 120 s, followed by 40 cycles of 95 °C for 15 s, 62.5°C for 20 s, finishing with a final extension

at 72°C for 60s. PCR products were evaluated using agarose gel electrophoresis and a melting dissociation curve (software v.3.0.1; Applied Biosystem, USA).

2.3.5 Sequencing of PCR products

Amplified products from the best-performing PCRs were purified using a QIAquick PCR purification kit (Qiagen GmbH, Hilden, Germany). 3 µl of purified PCR products were cloned into pGEM®-T Easy Vector (Promega, Wisconsin, USA) and used to transform OneShot TOP10 competent cells (Invitrogen, Carlsbad, CA, USA). 4 clones each, carrying the target sequence were picked and grown overnight at 37ºC in a shaking incubator. Plasmids containing the target genes were purified from cultured cells after overnight growth in 10 ml LB medium with 15 µg/ml Ampicillin using the QIAprep® Spin Miniprep Kit (Qiagen, Valencia, CA, USA) per the manufacturer's protocol. Purified and cloned PCR products were Sanger sequenced on ABI 3730XL (Applied Biosystems, Foster City, CA, USA) using the same primers for PCR products and the T7 sequencing primers for cloned products, according to the SmartSeq Kit manufacturer's instructions (Eurofins Genomics, Ebersberg, Germany). The sequencing data was compared against target gene alignments used for designing qPCR primer pairs for the detection of *Pseudo-nitzschia* species.

Both BLASTN and BLASTX analysis were conducted against the available *Pseudo-nitzschia* genomes in the non-redundant (nr/nt) databases of NCBI using the Basic Logical Alignment Search Tool (BLAST) (Altschul et al. 1990). To further examine the specificity, an additional BLASTN analysis was performed against the *Pseudo-nitzschia multistriata* genome available here http://protists.ensembl.org/Pseudonitzschia_multistriata/Tools/Blast. The BLAST analysis was performed using the following settings: E-value cutoff= 0.05-0.1, match/mismatch scores= 2-3, word size = 7-28, the gap costs of existence= 5, extension=2 and a threshold of 1–100 hits per query. The top hits of BLAST results are summarised in Table 2.2. The NCBI tool of the Conserved Domain Database (CDD) was used to identify the homologous protein domains (Marchler-Bauer et al. 2017). The web-based NCBI tool of iCn3D (I-see-in-3D) was employed to investigate the three-dimensional structure and function of protein molecules (Wang et al. 2020b).

2.3.6 Hydrolysis probe design

The consensus sequence derived from Sanger sequencing of the PCR and plasmid products for *Pseudo-nitzschia* species was used to design specific hydrolysis probes following standard design

criteria (Van der Velden et al. 2001). Up to 5 probe candidates were generated between two PCR primers. Putative secondary structures of potential probes were analysed using the 'Oligo Analyser' online tool (https://eu.idtdna.com/calc/analyzer). The Gibbs free energy (ΔG) of any self-dimers, hairpins, and heterodimers of ≤–9.0 kcal/mole was considered thermodynamically stable and therefore these candidates were discarded (Van Pelt-Verkuil et al. 2008a). The probes were also checked using the primer-BLAST tool to confirm the target specificity (Ye et al. 2012). The hydrolysis probes that met the design criteria were synthesised using a FAM reporter associated with an internal ZEN-Quencher and a Black Hole Quencher®-1 (BHQ) near the 3' end of the probe sequence to reduce any background signal and to increase probe intensity during amplification reaction (Integrated DNA Technologies, Inc., UK). Probe stock solutions were prepared at a concentration of 100 µM, working stocks at 10 µM (Invitrogen, Carlsbad, CA, USA) and then stored at -20°C.

2.3.7. Optimisation of hydrolysis probe-based qPCR reactions

Probe-based assays were performed in triplicate on a LightCycler 96 real-time PCR machine (Roche), using a TaqMan™ Fast Advanced Master Mix kit (Applied Biosystems™, Foster City, CA, USA). 150 nM and 250 nM concentrations of probes were tested with the optimised concentration of the forward and reverse primer at 1.5 µM and 1 µM, respectively. The cycling protocol consisted of 1 cycle at 95°C for 120 sec followed by 45-55 cycles at 95°C for 15 sec and 53°C-59°C for 60 sec. To ensure as high a reaction efficiency as possible, the annealing and elongation temperatures were combined into a single step to ensure that the probe remains bound to its target during primer extension (Langlois et al. 2021). The performance of reactions was assessed over a range of annealing/elongation temperatures from 53°C to 59°C for 60 sec. The optimal reaction conditions were selected by comparing C_t value, fluorescence rate and product specificity by running amplified sequences on 1.5-2% agarose-TAE gels. Contamination and primer/probe dimer formation were assessed by incorporating a triplicate of negative control reactions (No template control; NTC) in each qPCR run.

2.3.8. qPCR reaction conditions

Probe-based qPCR assays were performed in triplicate on a LightCycler 96 real-time PCR machine (Roche), using a TaqMan™ Fast Advanced Master Mix kit (Applied Biosystems™, Foster City, CA, USA). The qPCR reaction volumes were 25 µl and contained a 2 µl DNA template. 250 nM concentration of probe was used with the concentrations of the forward and reverse primer at 1.5

µM and 1 µM, respectively. The PCR conditions include 1 cycle at 95°C for 120 sec followed by 55 cycles at 95°C for 15 sec and 59°C for 60 sec. Contamination was assessed by incorporating a triplicate of negative control reactions (No template control; NTC) in each qPCR run.

2.3.9. Specificity testing

The specificity of the qPCR probe was evaluated experimentally against a panel of 10 *Pseudo-nitzschia* species and 8 non-target phytoplankton strains at equivalent cell concentrations of ~10^5 cells l^{-1}, listed in Table 2.3. The analytical specificity of the qPCR assay was estimated as a percentage of (true negatives)/(true negatives + false positives)×100 (Hashish et al. 2022).

2.3.10. Sensitivity optimisation

Assay sensitivity was evaluated based on the linear dynamic range of a dilution series spanning eight orders of magnitude, from amplicon standards were prepared as described (Stuken et al. 2011, Savela et al. 2016, Mendoza-Flores et al. 2018). A separate set of standards was generated from DNA extracted from *Pseudo-nitzschia*-spiked seawater. Natural seawater was collected from Station L4 (50˚15'N, 4˚13'W) in the Western Channel Observatory, Plymouth, UK and then spiked with quantified *P. multistriata* SZN-B955 cultured cells to obtain the spiked standard concentrations of 1.02x10^{10}, 2.1 x10^9, 1.6x10^8, 3.1x10^7, 1.1x10^6, 1.1x10^5, and 1.1x10^4 cells per litre. Each of the spiked seawater samples was vacuum filtered through a 0.2 µm pore size membrane (Fisher Scientific, UK) and transferred to a 2ml tube containing 700 µl of Lysis buffer AP1 (Qiagen, Hilden, Germany), then stored at -80°C. The filters were used to extract DNA with the DNeasy Plant Mini Kit (Qiagen, Hilden, Germany). Amplifications were performed on the triplicates of each concentration from amplicon copies and spiked seawater, to assess the linear regression between C_t values and standard concentrations using Origin software (OriginLab, Northampton, MA, USA).

2.3.11. Quantification of *Pseudo-nitzschia* species

The standard curve for geranyl pyrophosphate synthase (GPP) gene copies was created using a 10-fold dilution series of a known concentration of fresh PCR product, ranging from 1.0 x 10^8 to 1.0 x 10^0 amplicon copies. The fresh PCR product was purified using a QIAquick PCR purification kit (Qiagen), and then evaluated on a NanoDrop spectrophotometer (ND-1000, Thermo Fisher Scientific Inc., UK) and quantified using Qubit fluorometer (Thermo Fisher Scientific Inc., UK). GPP

gene copy numbers were calculated from the amplicon size and concentrations as in (Mendoza-Flores et al. 2018).

Three replicate qPCR reactions were performed as described above with fresh PCR standards to quantify GPP gene copy numbers from triplicate DNA templates extracted from *P. multistriata* SZN-B954, *P. multistriata* SZN-B955, *P. pungens* CCAP 1061/44, *P. multiseries* NWFSC 713, *P. multiseries* NWFSC 714, *P. multiseries* NWFSC 715, *P. multiseries* ML-54, *P. multiseries* ML-55, *P. multiseries* ML-56, *P. multiseries* ML-59, and non-target algal species that are listed in Table 2.3. These cultures were maintained in a laboratory incubator and sampled on random days and at different growth phases. The number of cells in each sample was quantified by direct microscopy. Finally, the number of GPP gene copies in the samples was divided by the total cell count in the qPCR template to obtain the number of GPP gene copies per cell (Stuken et al. 2011).

2.3.12. Statistical analysis

The mean values and standard deviations of biological replicates, as well as the linear regression between C_t values and standard concentrations were determined using Origin software (OriginLab, Northampton, MA, USA). SPSS statistics software version 28.0 (IBM Inc., Armonk, NY, USA) was used for investigating the correlation between GPP gene copy numbers, and toxin concentrations by Pearson's correlation test. All variables were tested for normality using the Shapiro–Wilk normality test. A p-value of 0.05 was chosen as the threshold of statistical significance.

2.3.13. Domoic acid measurements

All *Pseudo-nitzschia* species were screened for toxin production using an ELISA assay. Aliquots of each *Pseudo-nitzschia* culture were subject to sonication at 40W for 10 minutes within an ice bath (Ultrasonic processor, Sonics & Materials Inc., CT, USA). Cellular extracts were then filtered using a 0.2 µm pore size filtration membrane and clarified by centrifugation at 7,100 x g for 10 min at 4°C (Tatters et al. 2012b). Stored cell extracts were thawed and then diluted using 50% methanol (MeOH) prior to analysis. DA samples were quantified using a microplate reader (BMG FLUOstar OPTIMA reader, BMG LabTech, UK) following the manufacturer's instructions described in the Biosense Domoic Acid ELISA kit (Bergen, Norway). Total DA concentration was measured in the whole algal samples including intracellular DA plus extracellular DA in the growth medium. Toxin levels were normalised to cell counts at harvest (Fehling et al. 2004).

2.4 Results

2.4.1. Assay Design

Short reads and those containing gaps were eliminated from the sequencing alignment. After trimming, homology ranged from 75-86%. A total of 29 *Pseudo-nitzschia* sequences were aligned (Figure 2.1). The alignment had an overall identity of 86.3% over a 161 bp fragment, which revealed conserved regions for designing primers and hydrolysis probes. A panel of six candidate forward and reverse primers were considered for %GC content between 40%-50% and melting temperature (Tm) between 57°C-63°C, to amplify a relatively conserved region at a size between 120-200 bp from the target gene within *Pseudo-nitzschia* genus. The primer sets were evaluated experimentally by amplifying a DNA template extracted from *P. multiseries*, strain ML-59, with nuclease-free water as a negative control in the presence of an SYBR-green reporter dye, as described in the materials and methods. Amplified targets were evaluated using agarose gel electrophoresis and a melting dissociation curve. Of the three pairs of primers designed generated a single, specific PCR product, with the lowest C_t value was selected for further study; the primer sequences of Psn-fw and Psn-rv are given in Table 2.1.

To obtain the optimum assay performance, this primer set was tested over a variation of primer concentrations, annealing temperature and extension time until achieving the best results by gel electrophoresis and melting curve analysis (data not shown). Primer sequences not used for further study, but which efficiently amplified the target sequence, are given in Appendix A, Table A3. Figure 2.1 shows a truncated version of the multiple sequence alignment results, focusing on the region selected as the target for the qPCR assay design. The primers were designed to anneal within conserved regions of aligned sequences, by setting the standard parameters. None of the primers shared complete identity with all of the 29 *Pseudo-nitzschia* sequences due to the sequence diversity of the gene (84% identity). However, the forward and reverse primers were identical to 13/29 (~44%) and 24/29 (~82%) of the sequences, respectively, which were considered sufficiently inclusive for the assay to be useful for screening the presence of *Pseudo-nitzschia* spp..

To confirm amplification specificity, PCR amplicons of the chosen primers were sequenced as described in section 2.3.5. The sequencing data was incorporated into the multiple sequence alignment previously used in the primer design process to facilitate the subsequent design of a GPP-gene-specific hydrolysis probe. The probe annealing site is 100% identical to 18/29 (~62%) gene

sequences, without the incorporation of mixed (degenerate) bases, Figure 2.1. 150 nM and 250 nM concentrations of probes were tested with the optimised concentration of the forward and reverse primer at 1.5 µM and 1 µM, respectively. The inclusion of a hydrolysis probe could therefore reduce the overall inclusivity of the assay, however, the advantage in selectivity offered by using a gene probe in combination with specific primers was preferred. The binding region of the hydrolysis probe exploits additional nucleotide differences between *Pseudo-nitzschia* species and closely related marine algae, supporting the specificity of the qPCR assay for *Pseudo-nitzschia* species.

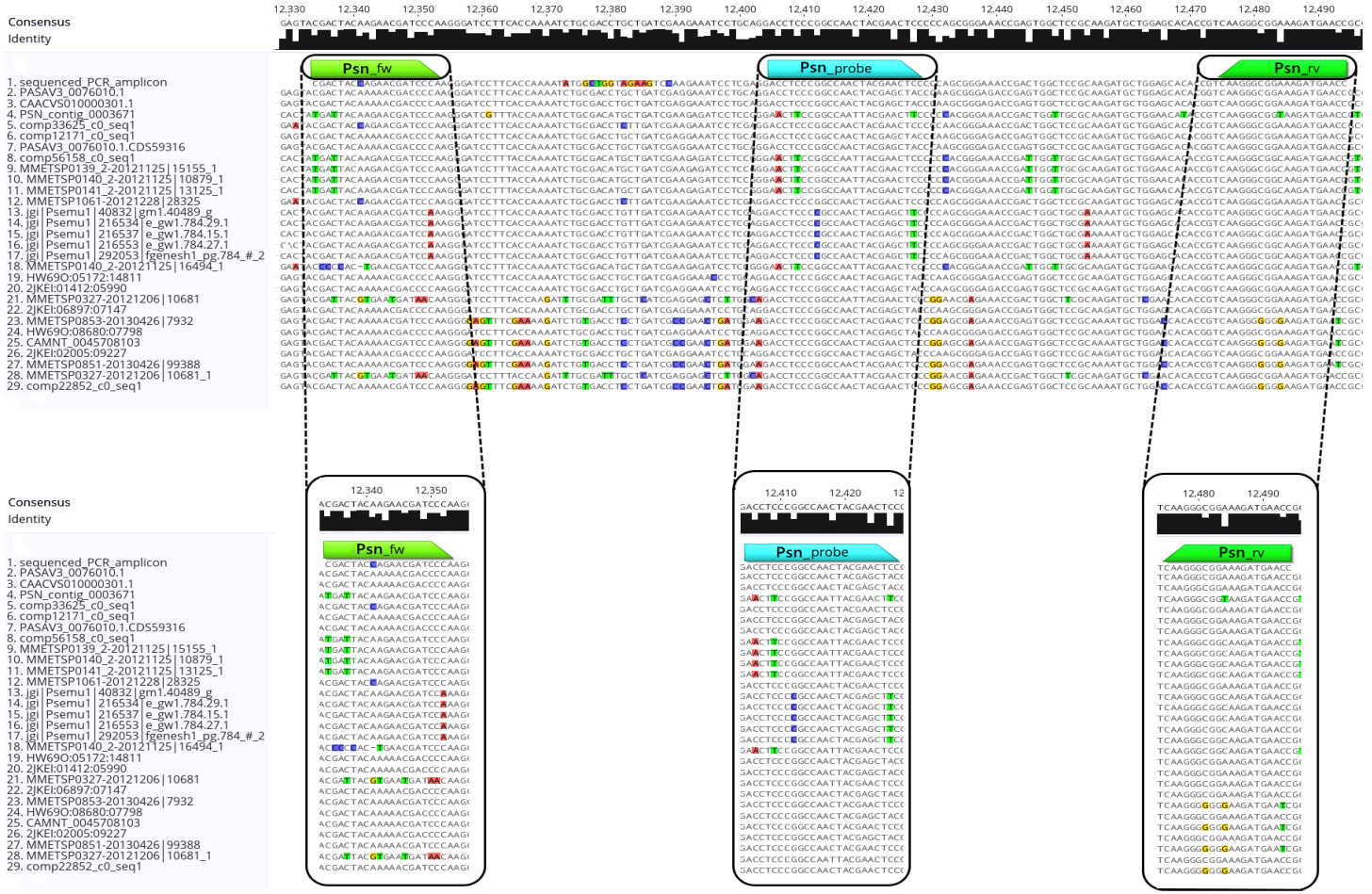

Figure 2.1 Multiple Sequence Alignment of Gene Sequence Fragments. Primer and probe binding sites are marked and detailed. The target region within the primer binding sites was 161 bp in length.

Table 2.1 Oligonucleotide Sequences

Name	Sequence (5' - 3')
Psn-fw	CGACTACCAGAACGATCCCA
Psn-rv	GGTTCATCTTTCCGCCCTTG
Psn_probe	(FAM)-ACCTCCCGGCCAACTACGAACTCC-(BHQ1)

FAM = Fluorescein; BHQ1 = Black Hole Quencher 1

The BLASTN analysis demonstrated a 100% similarity between the target sequence and the PSNMU_V1.4_AUG-EV-PASAV3_0076010 gene, which is categorized under the Isoprenoid Biosynthesis superfamily in *P. multistriata* (Table 2.2). The BLASTX analysis additionally revealed that the protein products originating from the 161 bp target sequence yielded homologous matches with proteins having accession numbers VEU40706.1 and VEU44695.1 in the ENSMBL Protist genome database of *P. multistriata* (Table 2.2). The results of the NCBI Search Tool (CCD) found that the conserved domains of VEU40706.1, and VEU44695.1 are associated with classes of Isoprenoid Biosynthesis and Terpene synthase 2, C-terminal metal binding, respectively.

Table 2.2 Top hits of BLAST analysis through *Pseudo-nitzschia* genomes.

			BLASTN			
Species	**Strain**	**Percent Identity**	**E- value**	**Query Cover**	**Accession Number**	**Source**
P. multistriata	119-C4	89.7%	6e-05	18%	MZ486440.1	NCBI[a]
P. multistriata	MS3	89.7%	6e-05	18%	MZ486439.1	NCBI[a]
P. multistriata	119-A4	89.7%	6e-05	18%	MZ486438.1	NCBI[a]
P. multistriata	MS2	89.7%	6e-05	18%	MZ486437.1	NCBI[a]
P. multiseries	15091C3	100%	0.003	18%	MH202990.1	NCBI[a]
P. multistriata	B856	100%	0.0004	100%	PASAV3_0076010	SZN[c]
			BLASTX			
P. multistriata	B856	81.1%	1.3e-25	85.3%	VEU40706	Ensembl[b]
P. multistriata	B856	56.5%	0.07	37.0%	VEU44695	Ensembl[b]

[a] NCBI; National Centre for Biotechnology Information GenBank, [b] Ensembl; Ensembl Genome Portal (Protists), [c]SZN; Genome database of the Stazione Zoologica Anton Dohrn.

The three-dimensional structure and catalytic sites of the VEU40706.1 protein were determined using iCn3D analysis, revealing residues of the substrate binding pocket, substrate-Mg2+ binding site, aspartate-rich region 1, and aspartate-rich region 2. These residues were found in a related *P. multiseries* prenyltransferase. Similarly, the VEU44695.1 has catalytic residues of Terpene_syn_C_2, a characteristic also observed in *P. multistriata* prenyltransferase. These observations agree with the gene alignments, where the majority of homologous sequences were specifically annotated as encoding prenyltransferase activities, including geranyl pyrophosphate/diphosphate synthase (GPP), Farnesyl pyrophosphate/diphosphate synthase (FPP), Prenyltransferases, Terpenoid cyclase, and Terpene synthase (Figure 2.1) (Savage et al. 2012, Athanasakoglou and Kampranis 2019a). Recent studies have highlighted the importance of these functional activities for the DA biosynthesis in *Pseudo-nitzschia* (Brunson et al. 2018, Hardardottir et al. 2019, Jiang 2019, Chekan et al. 2020, Badarou 2021).

However, it is important to note that the majority of these functions have been assigned according to homology-driven automated annotations, rather than being confirmed through biochemical activities or experimentation. Among the homologous sequences, PSN_contig_0003671 emerges as the closest relative (84% identity relative to this study's PCR amplicon) with experimentally validated transcription in a study of toxigenic *Pseudo-nitzschia seriata* under toxin-producing conditions (Hardardottir et al. 2019) (Figure 2.1). The PSN_contig_0003671 gene sequence from (Hardardottir et al. 2019) encodes geranylgeranyl pyrophosphate synthase (GPP), which is thought to serve as an intermediate in DA biosynthesis in *P. seriata*. The selectivity and significance of the GPP gene were investigated here as a genetic marker through qPCR analysis using DNA samples extracted from both *Pseudo-nitzschia* strains and closely related microalgal species.

2.4.2. Assay Selectivity

The results of the DA immuno-assay and the qPCR assay selectivity testing are summarised in Table 2.3. The GPP gene assay showed 100% analytical specificity for *Pseudo-nitzschia* species with no cross-amplification against other algal strains, as shown in Figure 2.2. Ten *Pseudo-nitzschia* species tested positive for DA based on the ELISA analysis, but with a wide range of concentrations from 3.8 to 172.3 µg L^{-1}, corresponding to 4.3 to 2.4pg DA $cell^{-1}$ (recorded for *P. pungens* and *P.*

multiseries ML-59, respectively). Neither DA nor the GPP gene could be detected in any of the non-*Pseudo-nitzschia* algal cultures. Table 2.3 shows variable GPP gene copies across *Pseudo-nitzschia* species, with the lowest copy cell^{-1} at 0.2 ± 0.2 in *P. pungens* cells and the highest copies cell^{-1} at 1.2 ± 0.3 in *P. multiseries* ML-59 cells and *P. pungens* cells, respectively, corresponding to the minimum and the maximum toxin amount at 0.1 ± 0.001 pg DA cell^{-1} and 4.3 ± 0.2 pg DA cell^{-1}.

Table 2.3 Domoic acid concentrations and GPP qPCR results for a panel of marine algal species.

Species	Isolate Accession	DA Concentration (pg DA cell^{-1})	GPP copies cell^{-1}	qPCR Amplification
Pseudo-nitzschia multistriata	SZN-B954	2.4 ± 0.01	0.6 ± 0.001	+
Pseudo-nitzschia multistriata	SZN-B955	4.1 ± 0.1	0.8 ± 0.1	+
Pseudo-nitzschia pungens	CCAP 1061/44	0.1 ± 0.001	0.2 ± 0.2	+
Pseudo-nitzschia multiseries	NWFSC 713	3.4 ± 0.1	0.7 ± 0.1	+
Pseudo-nitzschia multiseries	NWFSC 714	3.6 ± 0.1	0.8 ± 0.04	+
Pseudo-nitzschia multiseries	NWFSC 715	1.5 ± 0.01	0.4 ± 0.03	+
Pseudo-nitzschia multiseries	ML-54	1.8 ± 0.06	0.5 ± 0.01	+
Pseudo-nitzschia multiseries	ML-55	1.2 ± 0.01	0.3 ± 0.002	+
Pseudo-nitzschia multiseries	ML-56	1.4 ± 0.02	0.4 ± 0.01	+
Pseudo-nitzschia multiseries	ML-59	4.3 ± 0.2	1.2 ± 0.3	+
Karenia brevis	CCMP2228	nd	nd	-
Karenia mikimotoi	CCAP 1127/2	nd	nd	-
Alexandrium tamarense	CCAP 1119/25	nd	nd	-
Synechococcus sp	CCAP 1479/9	nd	nd	-
Prorcentrum lima	CCAP 1136/12	nd	nd	-
Alexandrium minutum	CCAP 1119/15	nd	nd	-
Lingulodinium polyedra	CCAP 1121/7	nd	nd	-
Prorcentrum cordatum	CCAP 1136/16	nd	nd	-

(+) positive amplification, (-) no amplification, nd = not detected.

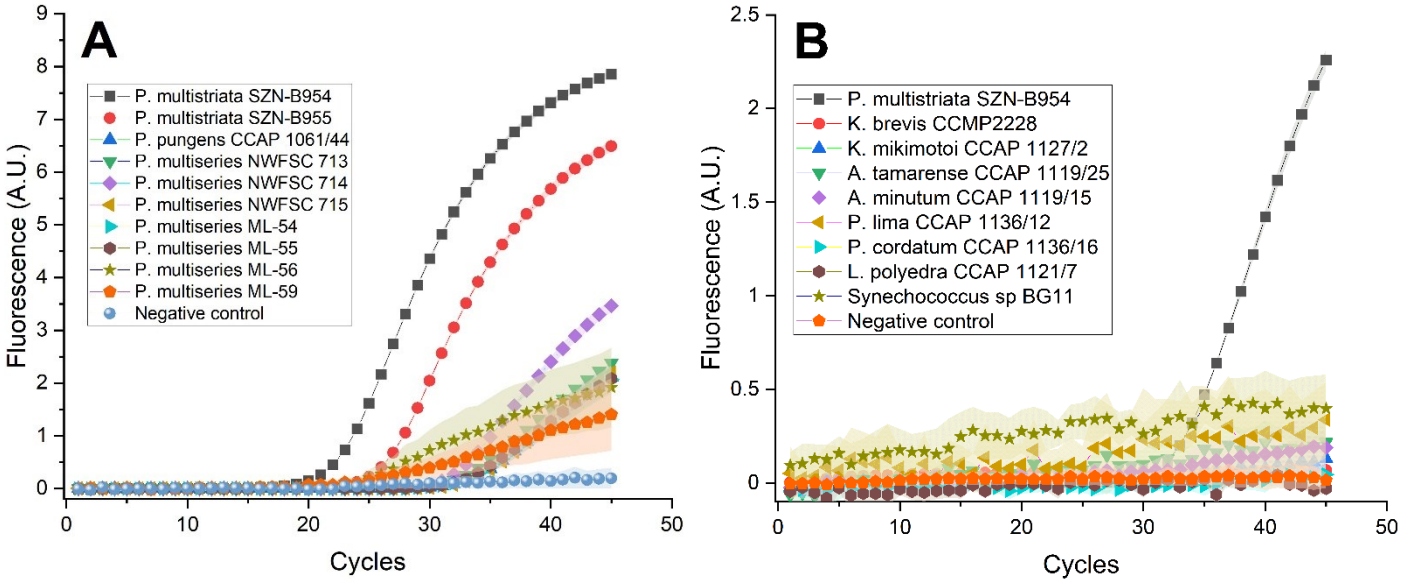

Figure 2.2 Specificity testing of GPP sequence amplification in *Pseudo-nitzschia* strains and other algal species. (A): Amplification plots of *P. multistriata* SZN-B954, *P. multistriata* SZN-B955, *P. pungens* CCAP 1061/44, *P. multiseries* NWFSC 71, *P. multiseries* NWFSC 714, *P. multiseries* NWFSC 715, *P. multiseries* ML-54, *P. multiseries* ML-55, *P. multiseries* ML-56, *P. multiseries* ML-59. (B) Amplification plot of *P. multistriata* SZN-B954 (Positive control), and confirms no reactions for *K. brevis* CCMP2228, *K. mikimotoi* CCAP 1127/2, *A. tamarense* CCAP 1119/25, *A. minutum* CCAP 1119/15, *P. lima* CCAP 1136/12, *P. cordatum* CCAP 1136/16, *L. polyedra* CCAP 1121/7, *Synechococcus sp* BG11. The results show the mean of triplicate reactions. The filled areas of amplification curves denote the standard error of the mean.

Table 2.4 Inclusivity results of qPCR amplification of marine algal species used in the study. The C_t values were generated from the amplification reactions presented in Figure 2.2.

Species	Isolate Accession	Amplification Plot	C_t value
Pseudo-nitzschia multistriata	SZN-B954	Fig. 2.2-A	18.2 ± 0.004
Pseudo-nitzschia multistriata	SZN-B955	Fig. 2.2-A	22.6 ± 0.04
Pseudo-nitzschia pungens	CCAP 1061/44	Fig. 2.2-A	31.2 ± 0.3
Pseudo-nitzschia multiseries	NWFSC 713	Fig. 2.2-A	30.1 ± 0.08
Pseudo-nitzschia multiseries	NWFSC 714	Fig. 2.2-A	29.4 ± 0.04
Pseudo-nitzschia multiseries	NWFSC 715	Fig. 2.2-A	31.5 ± 0.2
Pseudo-nitzschia multiseries	ML-54	Fig. 2.2-A	30.8 ± 0.4
Pseudo-nitzschia multiseries	ML-55	Fig. 2.2-A	30.7 ± 0.2

Pseudo-nitzschia multiseries	ML-56	Fig. 2.2-A	22.9 ± 2.3
Pseudo-nitzschia multiseries	ML-59	Fig. 2.2-A	20.7 ± 3.4
Pseudo-nitzschia multistriata	SZN-B954	Fig. 2.2-B	30.7 ± 0.02
Karenia brevis	CCMP2228	Fig. 2.2-B	nd
Karenia mikimotoi	CCAP 1127/2	Fig. 2.2-B	nd
Alexandrium tamarense	CCAP 1119/25	Fig. 2.2-B	nd
Synechococcus sp	CCAP 1479/9	Fig. 2.2-B	nd
Prorcentrum lima	CCAP 1136/12	Fig. 2.2-B	nd
Alexandrium minutum	CCAP 1119/15	Fig. 2.2-B	nd
Lingulodinium polyedra	CCAP 1121/7	Fig. 2.2-B	nd
Prorcentrum cordatum	CCAP 1136/16	Fig. 2.2-B	nd

nd = not detected.

2.4.3. Sensitivity, Linearity and Accuracy of Amplification for Predicting *Pseudo-nitzschia* Cell Number

The assay generated a PCR product from as few as an estimated 1.0 copies of the GPP sequence, and 10^4 *P. multistriata* cells, shown in Figure 2.3A, Figure 2.3C. The comparison of C_t values with the estimated GPP gene copy number generated a log-linear response relative to the copy number, when amplifying from between 1.0 x 10^0 and 1.0 x 10^8 estimated copies, as shown in Figure 2.3B, with a simple log-linear regression and R-squared of 1. The limit of detection (LOD) of the GPP gene assay was determined by the C_t value generated by the lowest number of target copies that can be amplified using triplicates of genomic DNA. The limit of Quantification LOQ was estimated from the lowest valid and consistently amplified C_t value from each amplification reaction of replicated standard dilutions (Kralik and Ricchi 2017). Accordingly, the LOQ and the LOD of the GPP gene qPCR assay were 10.4 copies.

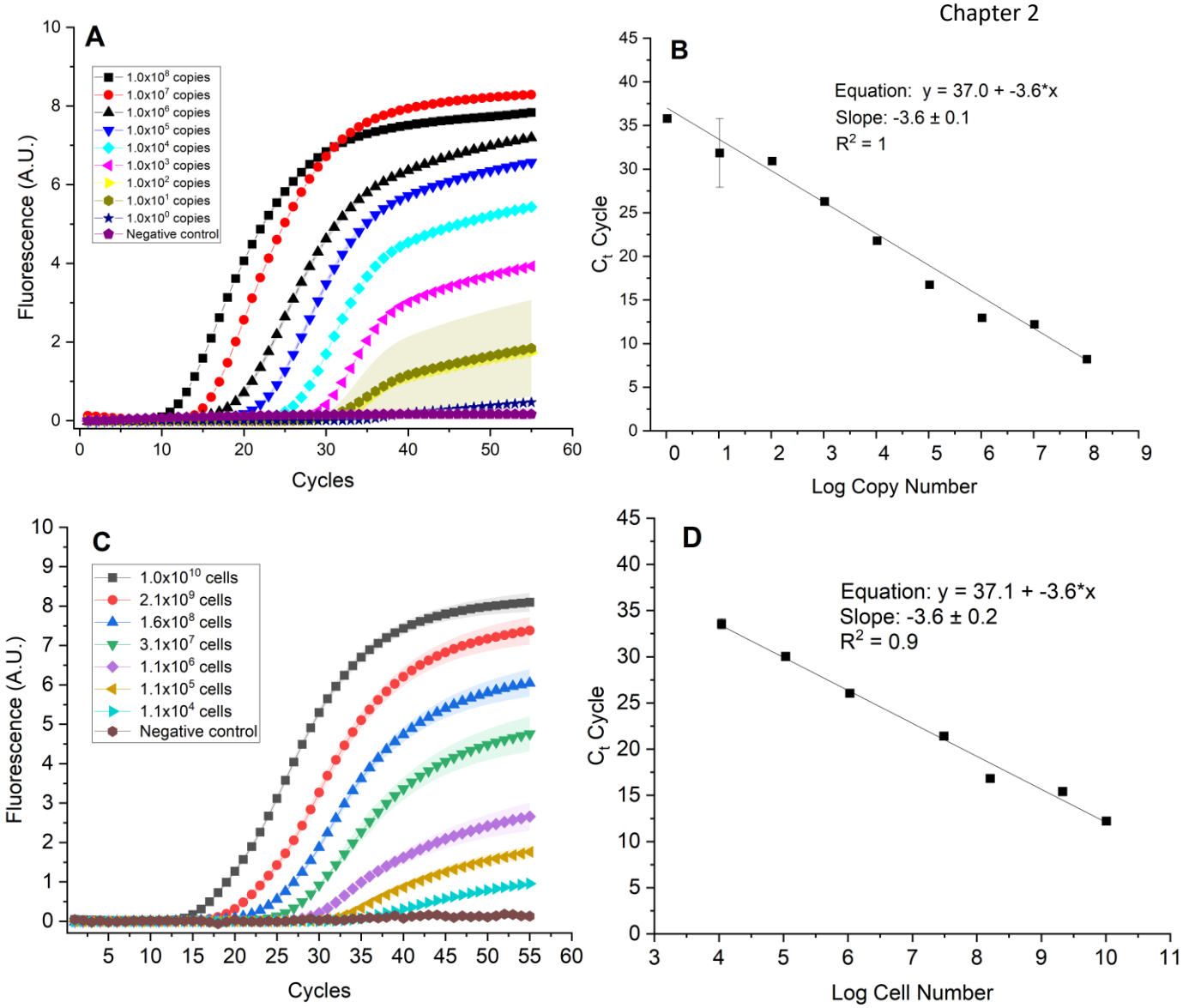

Figure 2.3 Sensitivity and Linearity of the GPP gene qPCR Assay. (A) qPCR amplification of GPP gene amplicon standards, diluted to contain $1.0x10^0$-$1.0x10^8$ number of copies. (B) A standard curve was generated using the data presented in panel A, by comparing C_t values with the estimated GPP gene copy number. (C) qPCR amplification from genomic DNA isolated from natural seawater spiked with between 10^7 to 10 cells of *P. multistriata*. (D) A standard curve was generated using the data presented in panel C, by comparing C_t values with cell concentrations. The filled areas of amplification curves and error bars of standard curves, where visible, are the standard deviations from triplicate qPCR reactions.

The efficiency of the qPCR primers was calculated from the slope of the linear regression for each standard curve (Figure 2.3B and Figure 2.3D) according to the equation: Efficiency (E) = $10^{(-1/\text{slope})}$ (Rebrikov and Trofimov 2006, Amagliani et al. 2010). The relationship between C_t and GPP gene copy number, or between C_t and cell number, generated amplification efficiencies of 90%, and 89% for the concentrations ranging from 10^4 to 10^{10} cells, and 1.0 $x10^0$ to 1.0 $x10^8$ copies, respectively.

2.4.4. Utility of Quantitative qPCR analysis

P. multistriata cells were enumerated from culture samples at random growth periods using direct microscopic counts. There was no consistent relationship between the GPP copy number per mL and cell concentration per mL in each culture and the number of GPP gene copies per cell varies across these strains (R^2=0.1, Figure 2.4A). The number of *GPP* gene copies per cell in *Pseudonitzschia* strains was used to calculate a GPP gene copy number per cell for each culture (Figure 2.3B, y-axis).

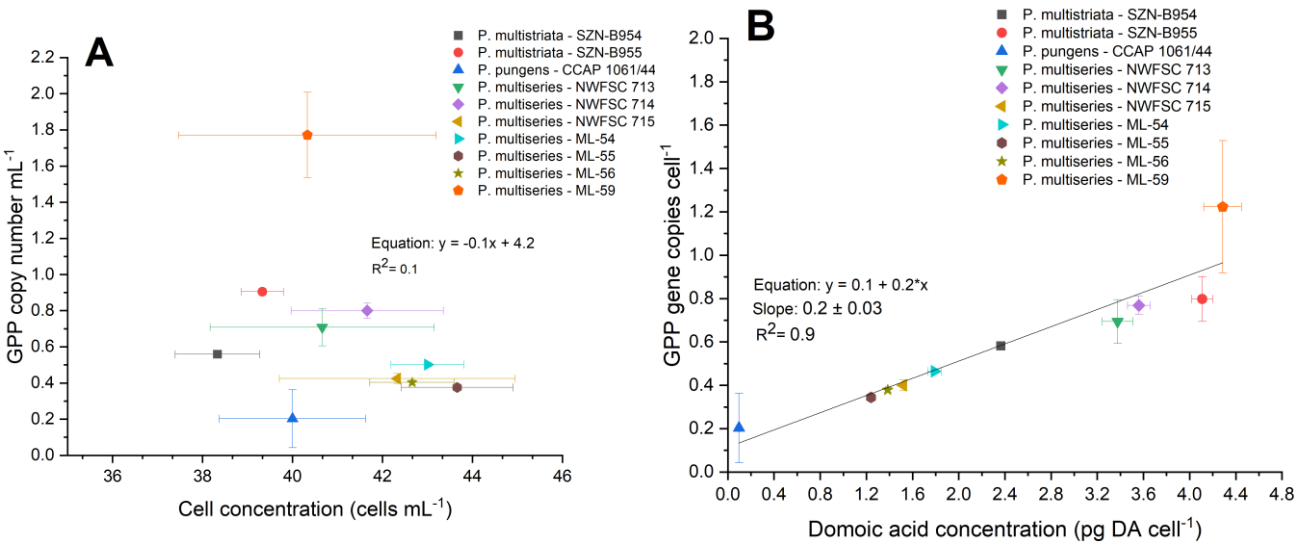

Figure 2.4 (A) the correlation between the number of the GPP gene copies $mL^{-1}$and the cell concentration in cells mL^{-1} measured for each culture. The copy number was divided by cell concentration to calculate copies per cell for each strain in Figure 2.4B. (B) GPP gene copies per cell vs. domoic acid concentrations (pg DA $cell^{-1}$) of *Pseudo-nitzschia* strains shows a positive relationship. The error bars where visible represent the standard deviation from replicate qPCR experiments performed on different days (n = 2).

Cellular DA concentrations (pg DA $cell^{-1}$) and GPP gene copy numbers per cell (R^2=0.9), (Figure 2.4B) were linearly correlated (Pearson correlation coefficient r = 0.9; n = 10; *P* = 0.00007). The significant relationship spanned 0.1±0.001 and 4.3±0.2 pg DA $cell^{-1}$ toxin concentration and 0.2±0.2 and 1.2±0.3 GPP gene copies $cell^{-1}$ for *P. pungens* CCAP 1061/44 at the lowest concentration and *P. multiseries* ML-59 cells at the highest concentration, respectively.

2.5. Discussion

A novel, real-time quantitative PCR (qPCR) assay was designed to target a fragment of the geranyl pyrophosphate synthase (GPP) gene sequence of *Pseudo-nitzschia* spp. The sensitivity of this PCR reaction was high, with a LOD of ~1.0x10^1 GPP gene copies per reaction (Figure 2.3). This high sensitivity of detection of a gene implicated in toxin production is the first to our knowledge and can be useful for monitoring toxic *Pseudo-nitzschia* blooms, though an equivalent sensitivity of ten copies per reaction was achieved previously for a *Pseudo-nitzschia* ribosomal DNA (rDNA) gene (Orsini et al. 2004, Penna et al. 2013). The calculation of qPCR-derived estimates of cell abundance is described in section 2.3.11. The log-linear trend was observed over the full range of cell concentrations tested, from 10^4 to 10^8 cells l^{-1}, confirmed using direct cell counts by microscopy. Further dilution of cell concentrations indicated that GPP genes could be detected by qPCR amplification of DNA extracted from an estimated 10^3 cells l^{-1} *P. multistriata* cells. However, amplification was not reliable in replicate qPCR reactions (data not shown), while reliable amplification was achieved for 10^4 cells l^{-1}. Therefore, the LOQ and LOD were found at 10^4 cells l^{-1}. This suggests that the qPCR is an accurate method for enumerating *P. multistriata* in culture.

A positive correlation was observed between GPP gene copy numbers and cellular toxin quota for ten *Pseudo-nitzschia* strains using the developed qPCR assay (R^2 = 0.9) (Figure 2.4B). More predictably, previous studies have shown that the GPP transcription of *Pseudo-nitzschia* strains was correlated with toxin concentrations (Brunson et al. 2018, Hardardottir et al. 2019, Lema et al. 2019). Under the culture conditions employed, it is suggested by the data that the number of gene copies per cell is correlated with the concentration of domoic acid across *Pseudonitzschia* spp. . While some variation does exist, the strong relationship suggests that the standard conditions under the maintained cultures for this analysis do not induce or supress DA biosynthesis in the species tested, with a consistent background DA biosynthesis level perhaps based on constitutive expression. P. multistriata SZN-B955 sample in Figure 2.4B showed an unprecedented production of up to 4.1 ± 0.1 pg DA $cell^{-1}$, corresponding to the reduced growth and lower cell concentration (39.3 ± 0.5 cells mL^{-1}). Further comprehensive studies are required to provide insights into the use

of the assay for species-specific testing for the biosynthetic potential to produce domoic acid in *Pseudo-nitzschia* strains.

Given that *Pseudo-nitzschia* blooms can exceed one million cells per litre within a few days following bloom initiation, reducing analysis time is critical (Du et al. 2016b). The bloom can occur when cell density ranges from 10^5 to 10^7 cells l^{-1} (Bates et al. 2018). UK HAB surveillance programmes set a threshold limit of 1.5×10^5 cells of *Pseudo-nitzschia* spp. per litre of seawater to enforce sampling and analysis of shellfish for algal bio-toxins (Downes-Tettmar et al. 2013). The qPCR assay generated in the current study can detect the target gene, shown here to relate to DA concentrations, from far lower abundances of *Pseudo-nitzschia* cells (approximately 10^2 cells per litre) in an hour and 35 minute assay (including the time needed for DNA extraction, PCR preparation and qPCR), in contrast to requirements for most *Pseudo-nitzschia* assays, including qPCR assays, which take 1.5 hours for the qPCR alone (Andree et al. 2011, Pugliese et al. 2017). The new qPCR assay presented here demonstrated a LOD of 10^4 cells l^{-1} *P. multistriata* cells, fifteen times below the UK threshold for monitoring, which could provide early warning of toxic bloom events. In previous work, the detection limit of *Pseudo-nitzschia* from cultures *via* RNA microarray was 1.2 x 10^3 to 5 x 10^4 cells of *Pseudo-nitzschia* spp., which is below the current study's limit of detection if cells are extracted from a litre of seawater (Medlin and Kegel 2014). Similarly, the amplification of a DNA sequence encoding the RuBisCO small subunit (*rbcS*) gene via PCR had a detection limit of 10^3 *P. multiseries* cells in a litre of seawater (Delaney et al. 2011). Later, (Kim et al. 2017) reported a qPCR assay with a LOD of less than one cell of *P. pungens*, targeting the internal transcribed spacer region (ITS).

(Fitzpatrick et al. 2010) reported single-cell sensitivity by amplifying a fragment of the 18S rDNA gene. However, the rDNA assay tended to overestimate cell abundance below the 100 cells l^{-1} threshold. Similarly, another rDNA assay overestimated cell concentrations during early bloom initiation (Andree et al., 2011). Overestimation by both assays may relate to the difference in rDNA copy number between the strain used for the standard curve and the environmental strains tested. In the current study, there was a strong correlation between calculated cell abundance (using GPP gene qPCR) and true cell number by microscopy, Figure A1, Appendix A. The method offers sensitive detection of *Pseudo-nitzschia*, thus providing a reliable tool for monitoring bloom development in

the early stages and presenting advantages in avoiding deleterious consequences for marine wildlife and seafood consumers.

2.6. Conclusion

A novel, real-time quantitative PCR (qPCR) assay was designed to target the genetic marker of the geranyl pyrophosphate (GPP) gene. This gene codes for geranyl pyrophosphate synthase, a putative precursor for DA production in *Pseudo-nitzschia* spp. (Brunson et al. 2018, Hardardottir et al. 2019, Chekan et al. 2020). The assay developed in this study can provide a quantitative proxy of *Pseudo-nitzschia* abundance, at pre- and early-bloom development. This is of particular importance for routine monitoring of the marine environment by advancing a more scalable and rapid assessment of the potential risk of *Pseudo-nitzschia* blooms.

Chapter 3 Induction of toxin biosynthesis by nutrient depletion and addition in *Pseudo-nitzschia multistriata*

3.1. Abstract

Anthropogenic nutrient loading in coastal waters supports the growth of phytoplankton, including harmful bloom-forming *Pseudo-nitzschia* species, which produce domoic acid (DA), a potent marine neurotoxin that causes amnesic shellfish poisoning (ASP). Nutrient enrichment can thereby indirectly exacerbate threats to public health, marine ecosystems, food production, and the economic well-being of coastal communities. At the same time, warming waters are more stratified and oligotrophic. It is important to understand the compounding effects of background nutrient stress with periodic increases in nutrients, on *Pseudo-nitzschia* toxicity. In this study, nutrient-depleted *P. multistriata* cultures were exposed to a 48-hour pulse addition of phosphate (P), nitrate (N), and silicate (Si) to simulate natural stressors caused by increased nutrient input in coastal systems. The relationships between differential transcription of the geranyl pyrophosphate synthase (GPP) gene, toxin concentration, cellular growth, and nutrient consumption were investigated in this chapter. . Significant induction of DA production was observed at 2 hours after Si-addition, 6 hours after N-addition, and 48 hours after P-addition. These inductions were accompanied by increases in GPP gene transcription, with fold changes of 3.9 after Si-addition, 4.0 after N-addition, and 14.7 after P-addition, compared to the baseline before nutrient addition (0 hours) in N-, P-, and Si-depleted cells. A strong correlation was found between GPP transcript abundance and DA content in P-depleted cells (r = 1.0, R^2 = 1.0, P = 0.0004), with a weaker but significant correlation in Si-depleted cells (r = 0.9, R^2 = 0.7, P= 0.03). The phosphate treatment resulted in the highest production of domoic acid compared to all other treatments, with a level of 0.6 ± 0.2 pg DA $cell^{-1}$ at t=48 h after the addition of phosphate. The novel assay was developed in Chapter 2 and provided sufficient sensitivity for early detection of toxic bloom development and detected all 10 toxigenic *Pseudo-nitzschia* strains tested, with potential environmental applications to avoid harmful effects of domoic acid in oligotrophic coastal regions on marine wildlife, seafood consumers and aquaculture industries.

3.2. Introduction

Global coastal ecosystems have experienced a rapid increase in nutrient loading in recent decades, with an input rate of approximately 48 × 10^9 kg N yr^{-1}, making them among the most rapidly changing regions on earth (Malone and Newton 2020). Certain species of the *Pseudo-nitzschia* genus have developed adaptive strategies that allow them to survive in a wide range of conditions (Trainer et al. 2012). *Pseudo-nitzschia* blooms can be stimulated by nutrient enrichment from various sources such as anthropogenic nutrient loads from agriculture and sewage, upwelling, and turbulence (Glibert 2020). While anthropogenic nutrient loading and eutrophication are major coastal sources of phosphate and nitrate (Trainer et al. 2012), the silicate input can originate from various sources, including coastal upwelling (Palma et al. 2010). *Pseudo-nitzschia* cells adjust toxin production in response to various abiotic and biotic environmental factors including changes in nutrient levels, pCO2, pH, salinity light, temperature, as well as interactions with bacteria and grazers. (Lelong et al. 2012, Bates et al. 2018). Though the function of domoic acid remains elusive, DA accumulation in marine organisms can result in mass mortalities of marine life and can potentially contaminate seafood consumed by humans, causing illness and in some cases fatalities (Bargu et al. 2002, Costa et al. 2005, Bates and Trainer 2006, Mafra et al. 2010).

Toxic occurrences of *Pseudo-nitzschia* blooms have been associated with increased nitrogen and phosphorus enrichment in some coastal regions (Bates 1998, Van Meerssche et al. 2018). Conversely, a negative relationship between domoic acid and nitrogen and phosphorus concentrations has been found both in cultures (Schnetzer et al. 2007) and in the environment in Narragansett Bay (Sterling et al. 2022). Higher domoic acid (DA) was measured in cultures of *Pseudo-nitzschia* species under phosphorus-deficient conditions (Hagstrom et al. 2011, Sun et al. 2011, Lema et al. 2017), while an increase was observed in *P. multiseries* cultures after addition of fresh f/2 + Si medium (however, it remains uncertain whether the increase was due to phosphorous supply or other factors in the medium (Lewis et al. 2018). Nitrate addition increased DA levels, and caused cells to reproduce rapidly (Bates et al. 1991). In other studies, the production of DA increased under nitrate-replete conditions (Ben Garali et al. 2016, Radan and Cochlan 2018, Kelly et al. 2021). Low DA content was observed in Si-depleted *P. seriata cultures* (Fehling et al. 2005) and in Si-depleted *P. multiseries* cells but only following silicate addition (Pan et al. 1996b). To fully

understand the variation in DA production due to different nutrients, it is now possible to decouple measures of the transcriptional response from DA production among *Pseudo-nitzschia* species under simulated eutrophication.

In the face of rapidly changing coastal regions, sensitive analysis of *Pseudo-nitzschia* toxic activity is now critical. However, conventional methods for *Pseudo-nitzschia* testing, such as light and electron microscopy, can be time-consuming and unreliable due to the morphometric variability of cells in response to environmental conditions and the overlap of characteristics between different strains of the same species (Cerino et al. 2005, Lundholm et al. 2006a, Amato et al. 2007, Hansen et al. 2011, Bates et al. 2018). To overcome these challenges, molecular methods such as qPCR and RT-qPCR have been widely adopted for specific and sensitive detection of *Pseudo-nitzschia* species (McDonald et al. 2007, Trobajo et al. 2010, Penna and Galluzzi 2013b, Tan et al. 2015, Kim et al. 2017). The rationale behind choosing the geranyl pyrophosphate synthase (GPP) target was based on several factors. Firstly, studies suggest that GPP is an essential precursor for the N-geranylation process, which is catalysed by DabA during the biosynthesis of DA (Tran and Savage 2017, Chekan et al. 2020). Additionally, previous studies have experimentally measured expression of GPP in toxigenic *Pseudo-nitzschia* strains under toxin-producing conditions (Brunson et al. 2018, Hardardottir et al. 2019, Jiang 2019). Importantly, GPP synthase catalysis was undetectable in DA biosynthesis in a biochemical study, but this was attributed to potential heterodimeric prenyltransferases lacking the required residues for GPP catalytic activity (Badarou 2021).

The impact of adding individual nutrients (nitrate, phosphate, or silicate, supplied approximating the Redfield-Brzezinski Ratio but at high concentrations to simulate eutrophication events) on domoic acid (DA) production in the *P. multistriata* SZN-B955 strain depleted of respective nutrients was investigated in this study. The main objective of the current study was to identify the differential effects of nutrients on GPP gene transcription and DA production in *P. multistriata*, in simulated coastal eutrophication events. Consequently, this experiment followed changes in activities following nutrient addition to nutrient-depleted cultures. Therefore, a sensitive and specific RT-qPCR assay was employed to quantify the expression of the GPP gene as a potential marker for the activation of toxin production in P. multistriata cells in response to nutrient variability.

3.3. Material and methods

3.3.1. Growth conditions

P. multistriata SZN-B955 was grown in three growth media with varying phosphate, nitrate, and silicate concentrations, in triplicate, with a total of 12 cultures. Cultures were maintained in 500 mL flasks (Corning Erlenmeyer, Germany) with ~260 mL of media, and an initial cell concentration of 500 cells mL^{-1}, at 18±1°C under a 12:12 light:dark photoperiod. The control culture was maintained in a standard f/2+Si medium (Guillard 1983), whereas experimental cultures were grown in f/2+Simedium with diluted nutrient concentrations. The cultures underwent a one-month acclimation period to adapt to the experimental nutrient conditions through direct transfer before being divided into triplicates for control and experimental treatments. The control medium had a Redfield-Brzezinski Ratio of Si:N:P = 15:16:1 (400 µM nitrate, 25 µM phosphate, 375 µM silicate) for steady-state growth of *Pseudo-nitzschia* culture (Redfield 1960, Brzezinski 1985). Experimental cultures were adapted to 50 µM nitrate, 4 µM phosphate, and 46 µM silicate in three different nutrient-depleted media for 22 days. The concentrations of nitrate and silicate in the depleted cultures were 8-fold lower compared to the nutrient-replete cultures. Similarly, the concentrations of phosphate in the depleted cultures were 6.25-fold lower than those in the nutrient-replete cultures. Then, 400 µM of nitrate, 25 µM of phosphate, and 400 µM silicate were added, and cells were sampled in the middle of the daylight period at -2, 0, 2, 24, and 48h for RNA isolation and domoic acid measurements from the three experimental media of N-depleted, P-depleted, and Si-depleted conditions (Figure 3.1). Enumeration of *P. multistriata* cells was performed every 2-3 days using a glass Sedgwick–Rafter cell counting slide (PYSER-SGI, Kent, England) and a light microscope (Carl Zeiss, Oberkochen, Germany) (Woelkerling et al. 1976). To ensure statistically reliable cell counts, a specific threshold of 50 to 200 cells per field was established for counting in each replicate sample, accommodating variations in cell density (Lund et al. 1958). Additionally, cell counts were repeated for each sample until the standard error of the mean reached below ten percent (Venrick 1978). Growth rates were calculated per day using linear regression of the natural log of cell concentration over time. The equation used is growth rate (µ): $\mu=(LnC_{t2}-LnC_{t1})/(t_2-t_1)$ where C is cell concentration at the time point of t_1 and t_2 (Lundholm et al. 2004).

Figure 3.1 Schematic illustration of the experimental treatments to which three replicates of *P. multistriata* cultures were subjected over a 48-h duration following the nutrient additions. A total of 72 DA and RNA samples were isolated in triplicates across all experimental treatments across the time from -2 to 48 h post-addition of nutrients to the growth-depleted cultures.

3.3.2. RNA extraction

Total RNA was harvested from each biological replicate. Cells were centrifuged at 7,800 rpm for 10 min at 4°C and the residual media were carefully removed. The resulting cell pellets were immediately immersed into liquid nitrogen to 'snap freeze' and then stored at -80°C. RNA extraction was performed using the RNeasy Mini kit (Qiagen, Hilden, Germany) with minor modifications to the manufacturer's recommended protocol. Improving RNA extraction efficiency was necessary to compromise any reduction in the number of cultured cells in response to the stress of depleted nutrient conditions. Optimisation procedures are described in detail in Appendix B, section B1. The protocol chosen for RNA extraction involved a 10-minute incubation of glass-beaded cells at 56°C with RNeasy lysis buffer, and these procedures were used to extract RNA samples from both control

and experimental treatments. The RNA isolation protocol is not 100 % effective at removing genomic DNA contamination, and therefore any residual DNA was removed using a DNase I digestion set (79254, Qiagen, Hilden, Germany) according to the manufacturer's instructions followed by purification using the RNeasy Mini Kit (Qiagen, Hilden, Germany).

The sampling was carried out at time points during the light phase to avoid any potential diurnal variability in gene expression (Depauw et al. 2012). Total RNA was harvested from each biological replicate prior to, and post-addition of nitrate, phosphate and silicate to respective depleted cultures as outlined in Figure 3.1. Triplicate samples are essential as some RNA samples can be difficult to recover after extraction procedures (Boissonneault et al. 2013, Lema et al. 2019). RNA yield was quantified spectrophotometrically using a NanoDrop 2000 (Thermo Fisher Scientific, Waltham, MA), 2100 bioanalyzer (Agilent, Santa Clara, CA, USA) and an Invitrogen Qubit 2.0 Fluorometer (Life Technologies, Carlsbad, CA, USA) using the Qubit® RNA HS kit (Q32852, Thermo Fisher Scientific) following the manufacturer's instructions. 50 µL of RNA was eluted in nuclease-free water and then stored in a -80°C freezer till used.

2.1. Reverse transcription of RNA samples

In total, 72 RNA samples were collected from both control and nutrient-depleted cultures at all experimental time points. RNA samples were reverse transcribed using a QuantiTect® Reverse Transcription Kit (Qiagen, Hilden, Germany) into a hybrid of single-stranded cDNA and RNA fragments. QuantiTect reverse transcriptase is a multifunctional enzyme with 3 distinct enzymatic activities: an RNA-dependent DNA polymerase, RNase H, and a DNA-dependent DNA polymerase (QuantiTect Reverse Transcription kit, Qiagen, Hilden, Germany). RNA-dependent DNA-polymerase activity (reverse transcription) transcribes the RNA template into a hybrid of single-stranded cDNA and RNA fragments. The RNase H activity of Quantiscript reverse transcriptase allows the degradation of RNA hybridised to cDNA, without effect on pure RNA. DNA-dependent DNA polymerase activity enables the formation of double-stranded cDNA templates for downstream real-time qPCR. A genomic DNA elimination step was performed using gDNA Wipeout Buffer at 42°C for 2 min before reverse transcription. 20 µL master mix contained 0.3 units μL^{-1} Quantiscript® Reverse Transcriptase, 4 µL Quantiscript RT Buffer, 5x, and 1 µL RT Primer Mix and 14 µL gDNA

elimination reaction. The reverse transcription master mix is incubated at 42°C for 30 min and is then inactivated at 95°C. The RT Primer Mix (Qiagen, Hilden, Germany) combines oligo-dT and random primers for a comprehensive binding of RNA fragments. This ensured unbiased amplification of the entire target gene's 5' and 3' regions during PCR (Tichopad et al. 2009). RNase-free water was used instead of reverse transcriptase (-RT control) as a negative control of the RT reaction to detect any genomic DNA contamination for the downstream PCR analysis.

3.3.3. Selection of the reference gene for RT-qPCR analysis

The tubulin gene (*tubA*) is widely used as a reference gene in qPCR analysis to normalise transcript quantification in *Pseudo-nitzschia* (Boissonneault et al. 2013, Adelfi et al. 2014, Basu et al. 2017). It encodes the tubulin α chain, a cytoskeleton component that was found to be stably expressed in most diatom cells (Siaut et al. 2007). The *tubA* gene was selected as the most stable reference gene for *P. multistriata* (Adelfi et al. 2014) and was used to normalise GPP gene transcription.

3.3.4. Quantitative real-time RT-qPCR

qPCR primers targeting GPP and *tubA* genes were designed using the 'Primer3' tool (Untergasser et al. 2012) and hydrolysis probes were designed following the standard design criteria (Van der Velden et al. 2001). qPCR assays were performed in triplicate on a LightCycler 96 real-time PCR machine (Roche), using a TaqMan™ Fast Advanced Master Mix kit (Applied Biosystems™, Foster City, CA, USA). The qPCR reaction volumes were 25 µl and comprised a 2 µl DNA template. 250 nM concentration of probe was used with the concentrations of the forward and reverse primer at 1.5 µM and 1 µM, respectively. The PCR conditions include 1 cycle at 95°C for 120 sec followed by 55 cycles at 95°C for 15 sec and 59°C for 60 sec. Contamination was assessed by incorporating a triplicate of negative control reactions (No template control; NTC) in each qPCR run. Optimized qPCR conditions are listed in Table 3.1.

Reliable quantification of targets was ensured by including serial dilutions of known concentrations of the linearised plasmids containing GPP and *tubA* genes. PCR-amplified products of the GPP target gene and *tubA* reference gene were purified using the MinElute PCR Purification Kit (Qiagen, Valencia, CA, USA), then ligated into pGEM®-T Easy Vector (Promega, Wisconsin, USA) and cloned

into One Shot™ TOP10 Chemically Competent *E. coli* cells (Invitrogen, Life Technologies, Carlsbad, CA).

To confirm successful cloning, a 'colony PCR screen' was conducted where a sample of the bacterial colony was subjected to PCR using primers flanking the multiple cloning site (MCS). The presence of the PCR product inserted into the MCS was verified through agarose gel electrophoresis (2% w/v) in 1× Tris-acetate-EDTA buffer, followed by ethidium bromide staining under a UV irradiation unit (Molecular Imager® Gel Doc™ XR System, Bio-Rad, Hercules, CA, USA). Bacterial colonies that were confirmed to contain the plasmid with the GPP and *tubA* gene sequences were cultured overnight in LB medium at 37 °C. The plasmids containing the expected target fragments were purified using the QIAprep® Spin Miniprep Kit according to the manufacturer's instructions (Qiagen, Valencia, CA, USA). These purified plasmids were then linearised by overnight restriction digestion using the NdeI restriction enzyme (ER0582, Thermo Fisher Scientific Baltics UAB, Vilnius, Lithuania) and the successful linearisation was confirmed by gel electrophoresis with a high mass ladder. The linearised plasmids of the desired target size were quantified using a NanoDrop spectrophotometer (ND-1000, NanoDrop Technologies, Wilmington, DE) as well as a Qubit fluorometer with a dsDNA HS Assay Kit (Invitrogen, Carlsbad, CA, USA).

To establish a standard curve for target quantification, the linear plasmid DNA was serially diluted to concentrations ranging from a minimum single copy to a maximum of 10^8 copies (Figure 3.5). The dilution series of linearised plasmids containing GPP and *tubA* genes were amplified in the same qPCR run with cDNA samples. Amplification of GPP and *tubA* genes was performed using a TaqMan™ Fast Advanced Master Mix kit (Applied Biosystems™, Foster City, CA, USA) and included triplicate negative control samples without the addition of the reverse transcriptase (-RT) to evaluate genomic DNA contamination. The efficiency of the qPCR primers was calculated from the slope of the linear regression for GPP and *tubA* gene standard curve according to the equation: Efficiency (E) = $10^{(-1/\text{slope})}$ (Rebrikov and Trofimov 2006, Amagliani et al. 2010).

Gene expression was analysed using the relative ratio by comparing ΔCq of the target gene GPP and reference gene *tubA* and adjusting for differences in PCR efficiencies (Pfaffl 2001). The Cq values were determined by averaging technical triplicates of controls and experimental samples.

The difference in Cq values (ΔCq) between the target and reference genes was calculated for each sample between control and treatment (Derveaux et al. 2010).

$$\text{ratio} = \frac{(E_{\text{target}})^{\Delta \text{CP}_{\text{target}}(control - sample)}}{(E_{\text{ref}})^{\Delta \text{CP}_{\text{ref}}(control - sample)}}$$ (Pfaffl 2001)

The relative transcription ratio of a target gene, where: E is the efficiency calculated for GPP*: tubA* genes, CP is the Crossing Point for each gene in the different conditions, E_{target} is the real-time PCR efficiency of the target gene (GPP), E_{ref} is the real-time PCR efficiency of a reference gene (*tubA*), ΔCP_{target} is the CP deviation of control - sample of the target gene transcript, and ΔCP_{ref} is the CP deviation of control - sample of reference gene transcript (Pfaffl 2001). Log2 transformation was applied to the mean expression ratios of GPP in response to nutrient additions from biological triplicates.

3.3.5. Nutrient analysis

15 mL of culture treatments were filtered using GF/F filters of 0.2 µm pore size (Whatman, UK) and stored at −80°C until analysis. To bring the concentration between the calibration range of the instrument, samples were diluted 10, 20 or 50 times. Concentrations of phosphate (PO_4), nitrate+nitrite ($NO_3 + NO_2$) and silicic acid ($Si(OH)_4$) were measured with a SEAL QuAAtro39 auto-analyzer following standard protocols (Becker et al. 2020) and certified reference materials were used (KANSO, Japan). Six working standards were prepared in Milli-Q water and the concentration ranged as follows; NO_3 1-60 µM, PO_4 0.5-6 µM and $Si(OH)_4$ 1-60 µM.

3.3.6. Domoic acid quantification

10 mL of culture were collected periodically at -2, 0, 2, 24, and 48 h post-nutrient addition. The domoic acid concentration was measured according to (Boissonneault et al. 2013). The method used for DA quantification in this study is ELISA (Enzyme-Linked Immunosorbent Assay). ELISA-based methods are relatively low-cost, and can be used to measure water and seafood DA levels with high specificity and sensitivity at limits of detection of 10 µg L^{-1} (Kleivdal et al. 2007a) and 0.003 µg g^{-1} (Kania and Hock 2002); for comparison, the suggested regulatory limit of DA in shellfish for

human consumption is 20 µg g^{-1} (O'Mahony 2018). The samples were sonicated at 50 % power on an ice bath for 2 min (Ultrasonic processor, Sonics & Materials Inc., CT, USA). The cell extracts were then gently filtered onto a 0.2 µm pore filter (S-PAK, Millipore, UK) via vacuum pressure. When preservation was necessary, the supernatant was stored at -80 °C until processing. In laboratory studies, measurable levels of domoic acid are only present during the stationary phase of cell growth, rather than during exponential growth (Bates 1998). DA samples were quantified using a microplate reader (BMG FLUOstar OPTIMA reader, BMG labTech, UK) following the manufacturer's instructions described in the Biosense Domoic Acid ELISA kit (Bergen, Norway). Final Domoic acid (DA) concentrations were calculated and normalised by subtracting the average background level. Then, The cell quota of domoic acid was determined by dividing the total DA concentration by cell counts at harvest (Fehling et al. 2004).

3.3.7. Statistical analysis

Data for growth rates, nutrient levels, DA quotas, and GPP transcript abundance were analysed for normal distribution (Shapiro–Wilk normality test, $p > 0.05$). Values of nutrient levels and growth rates were log-transformed to address the non-normal distribution of data. Paired sample test was used to assess statistical differences between pre- and post-experimental time points for the data of growth rates, DA content, nutrient concentrations, and relative fold change of GPP expression between pre- and post-experimental time points. Pearson's correlation test was performed to analyse linear relationships between relative GPP transcript levels and DA content. Statistical significance was determined at $p<0.05$ using SPSS statistics software version 28.0 (IBM Inc., Armonk, NY, USA).

3.4. Results

3.4.1. Growth at the experimental nutrient regimes

The exponential growth of nutrient-replete control culture was observed to continue for several weeks, reaching its maximum rate of 1.3 ± 0.05 day^{-1} and 0.4 ± 0.2 day^{-1} on day 4 and day 11, respectively and transitioning to the stationary phase at a growth rate of 0.04 ± 0.02 day^{-1} on day

22 (Figure 3.2, Appendix B, Table B3). In contrast, the stationary growth phase for nutrient-depleted cultures was observed between days 14 to 22, resulting in a decline in growth rates. At day 22, the growth rates were measured at 0.003 ± 0.006 day^{-1}, 0.08 ± 0.003 day^{-1}, and 0.002 ± 0.008 day^{-1} for the P-starved, N-starved, and S-starved treatments at day 22, respectively (Figure 3.2). The transition period between the exponential and stationary growth phases for the control treatment occurred between days 16-18, during which growth rates declined within the range of 0.2 ± 0.01 and 0.06 ± 0.02 day^{-1}. In contrast, the transition between the exponential and stationary growth phases occurred earlier for the P-depleted treatment (days 9-11) with a growth rate of 0.1 ± 0.002 - 0.3 ± 0.05 day^{-1}, for the N-depleted treatment (days 11-14) with a growth rate of 0.1 ± 0.001 - 0.3 ± 0.4 day^{-1}, and for the Si-depleted treatment (days 14-16) with a growth rate of 0.3 ± 0.1 - 0.02 ± 0.06 day^{-1}. The observed fluctuations in growth rate within the indicated time intervals can be attributed to various factors, such as temporal variations in nutrient availability, variations in metabolic activity, and the influence of cellular regulatory mechanisms such as sexual reproduction by *P. multistriata* cells (Annunziata et al. 2022). These fluctuations are commonly observed in *Pseudo-nitzschia* growth during the early stages of the stationary phase, where cells experience periodic bursts of growth followed by periods of reduced growth (Lelong et al. 2011). These findings suggest that the depletion of P, N, and Si led to an earlier onset of the stationary phase and decreased growth rates in *P. multistriata* cells. The P-depleted growth rate was 0.5-fold higher than the control cultures at the time of nutrient addition (day 22), while the N-depleted and Si-depleted growth rates were 5.4-fold and -0.9-fold lower, respectively. The growth rate decreased after 24 hours of nutrient addition for P-starved, N-starved, and S-starved cultures by -0.04 ± 0.005 d^{-1}, -0.04 ± 0.01 d^{-1}, and -0.01 ± 0.02 d^{-1}, respectively (Figure 3.2). The addition of fresh nutrients to these growth-depleted cultures led to a significant increase in growth rates at t=48h compared to t=0h, with 12.7-fold, 15.5-fold, and 0.6-fold increases for P-, N-, and S-depleted treatments, respectively. Growth rates were significantly different between the control cultures and nutrient-depleted treatments throughout the experiment ($P < 0.05$), except for the Si-deficient growth rates ($P = 0.2$).

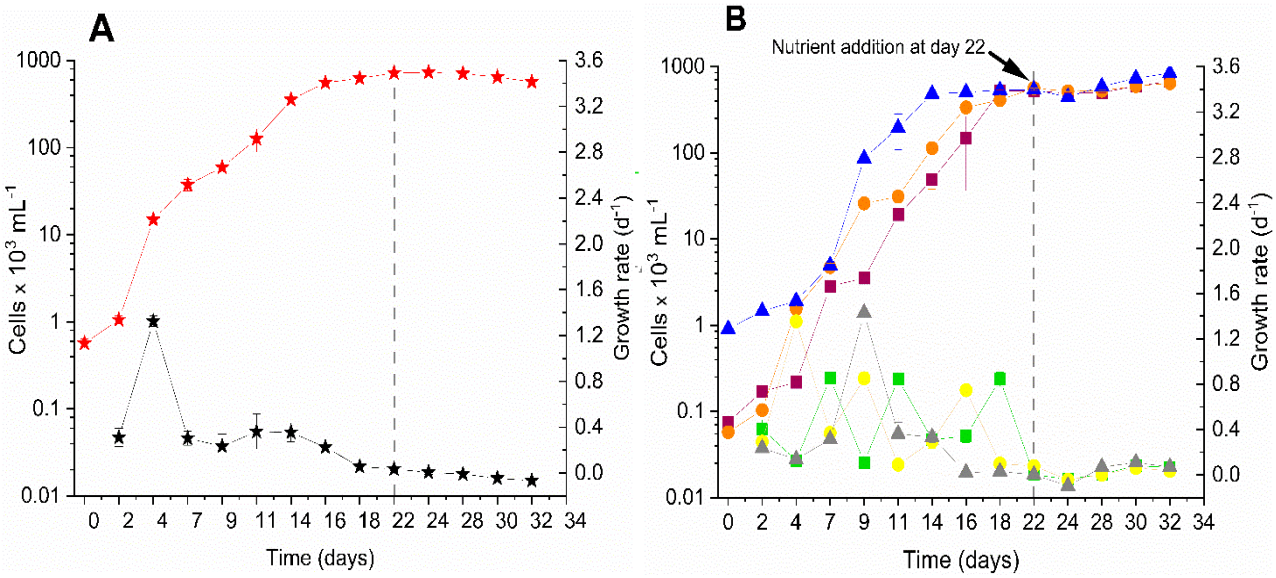

Figure 3.2 *P. multistriata* SZN-B955 growth in f/2 medium with varying nitrate, phosphate, and silicate concentrations in nutrient-replete (A; showing cell concentration (- ★ -), and growth rate (–★–) of control treatment) and the depleted conditions (B; showing cell concentration (–■–), and growth rate (–■–) of phosphate-depleted treatment, and cell concentration (–●–), and growth rate (–●–) of nitrate-depleted treatment, and cell concentration (–▲–), and growth rate (–▲–) of silicate-depleted treatment, with growth curves and growth rate (d^{-1}). The vertical line at (A & B) represents the time of nutrient addition. RNA and toxin analysis were performed at -2h, 0h, 2h, 24h, and 48h after nutrient addition. Error bars represent standard deviations of triplicate samples for each treatment.

3.4.2. Nutrient consumption

P. multistriata cells grew exponentially in *f/2* control media for 14-16 days due to high initial phosphate, nitrate, and silicate concentrations at 25 µM, 400 µM, and 375 µM respectively. In the nutrient-replete control, the levels of phosphate (P) remained stable between time points t=0h and t=48h, ranging from 6.6 ± 3.0 to 6.7 ± 3.2 µM. The level of nitrate (N) decreased from 199.7 ± 1.4 µM to 145.9 ± 54.6 µM, while the level of silicate (Si) decreased from 236.7 ± 36.4 µM to 231.5 ± 39.5 µM during the same period for the control treatment. These nutrient levels were observed to be relatively stable throughout the experiment (Figure 3.3A). The levels of phosphate, nitrate, and silicate decreased in P-stressed cells during the 48-hour study period (Figure 3.3B). Specifically, the level of phosphate declined from 72.1 ± 1.9 µM at t=0 h to 3.2 ± 0.4 µM at t=48 h. Similarly, the level of nitrate decreased from 161.7 ±15.9 µM at t=0 h to 17.6 ± 0.4 µM at t=48 h, while the level

of silicate decreased from 258.3 ± 24.7 µM at t=0 h to 9.1 ± 0.7 µM at t=48 h. Under N-depleted treatment conditions, the initial levels of phosphate, nitrate, and silicate were determined to be 145.3 ± 12.1 µM, 439.0 ± 36.8 µM, and 270.5 ± 19.2 µM, respectively, at (t= 0h). After 48 hours of exposure to added nitrate (t=48 h), the levels of phosphate, nitrate, and silicate decreased to 43.8 ± 30.6 µM, 62.6 ± 1.6 µM, and 11.7 ± 0.2 µM, respectively. In the Si-depleted treatment, the levels of phosphate, nitrate, and silicate were 3.5 ± 3.3 µM, 319.9 ± 38.0 µM, and 602.7 ± 51.3 µM, respectively, at t=0h. Following the addition of silicate, the phosphate level decreased to 0.7 ± 0.6 µM, the nitrate level decreased to 19.6 ± 5.2 µM, and the silicate level decreased to 11.2 ± 0.7 µM at (t=48 h). These results indicate that starved *P.multistriata* cultures consume the added nutrients quickly and reach a plateau at 24-48h, despite variations in initial nutrient concentrations.

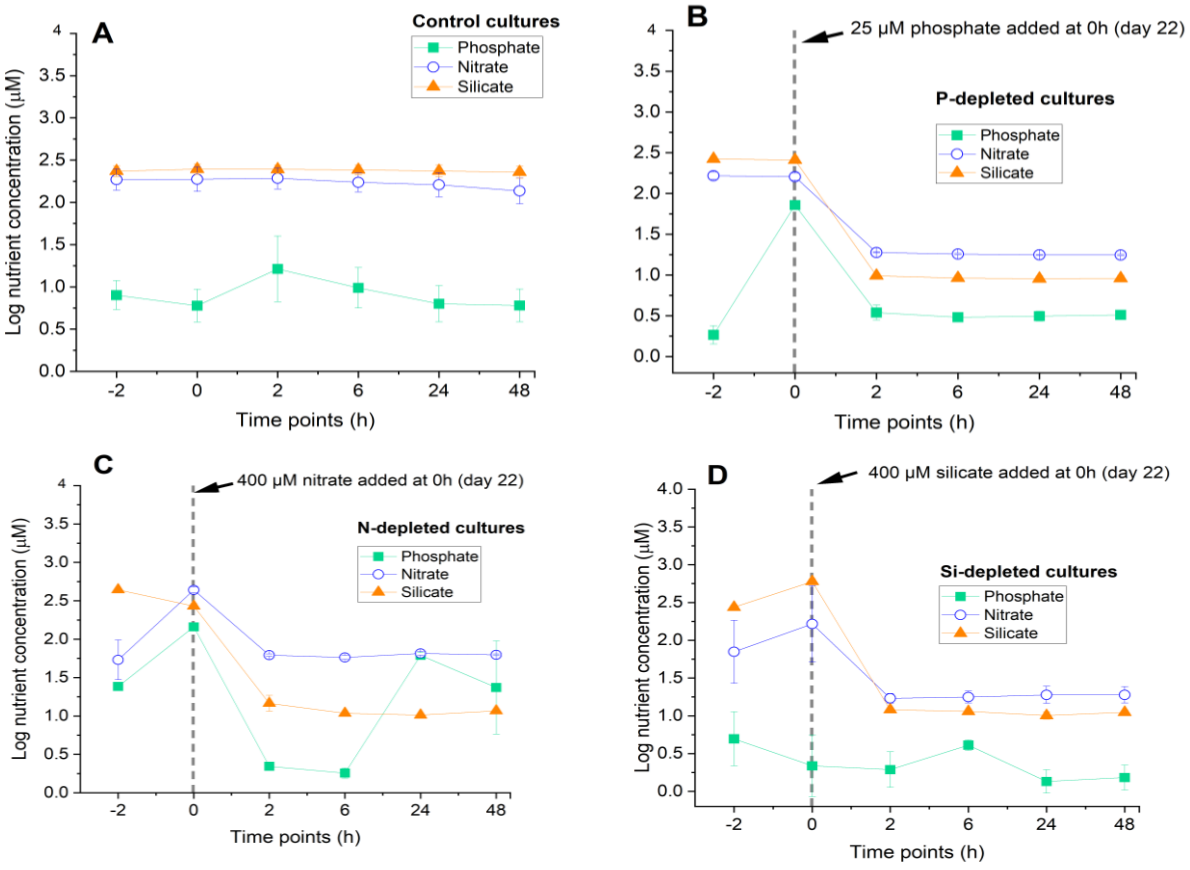

Figure 3.3 Changes in key dissolved macronutrients of phosphate (P), nitrate (N), and silicate (Si) across control and experimental treatments. Mean values were computed from triplicate samples and shown as phosphate (solid black squares), nitrate (open grey circles), and silicate (solid grey triangle). Logarithmic transformations were used to expand the scale for clarity of wide-range concentrations. Error bars denote the standard deviations of triplicate treatments.

3.4.3. Domoic acid levels

Domoic acid levels in nutrient-sufficient cells remained steady in control media, with a range of 0.1 ± 0.06 to 0.1 ± 0.06 pg DA $cell^{-1}$ over the course of the experiment. As nutrient consumption remained steady in control cultures, domoic acid levels decreased slightly by 0.02-fold between pre- and post-experimental nutrient addition. All experimental treatments showed peaks in domoic acid values at varying times following the nutrient addition (Figure 3.4). Phosphate-driven increases in toxin production were more prominent in cultures re-supplied with nitrate and silicate. The highest peak value for domoic acid was 0.6 ± 0.2 pg DA $cell^{-1}$, 3.7 times higher in P-depleted cultures than in nutrient-replete cells. Phosphate addition to low P-cultures induced a gradual increase of domoic acid by 1.3-fold during the experiment. The smallest increase was in N-depleted treatment at 0.3 ± 0.2 pg DA $cell^{-1}$, 0.5-fold higher than the control. Nitrate addition resulted in a decline in toxin production at 2h and 24h time points, with a slight increase at 48h. An intermediate increase was reported for Si-depleted cultures at 0.5 ± 0.4 pg DA $cell^{-1}$, 0.9-fold higher than the control. In the Si-depleted treatment, domoic acid reached its highest level at 0.5 ± 0.4 pg DA $cell^{-1}$ at 2h after Si-addition, then decreased to 0.2 ± 0.07 pg DA $cell^{-1}$ by the end of the experiment (t=48h). The P-depletion treatment showed a statistically significant difference in domoic acid values compared to the control value (P= 0.009), while N- and Si-starved treatments showed an insignificant difference (P= 0.1 and P= 0.1, respectively).

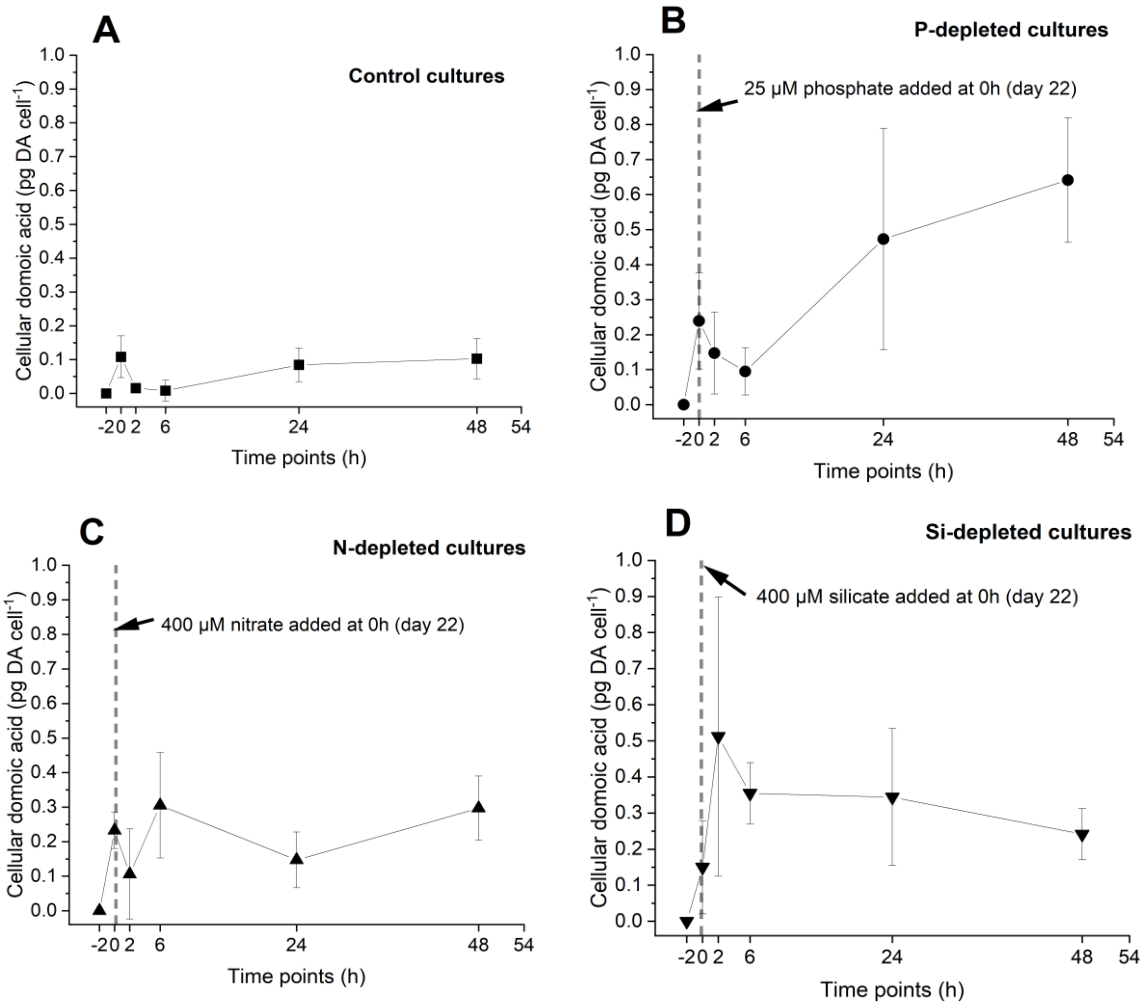

Figure 3.4 Domoic acid (pg DA cell^{-1}) levels were measured in *P. multistriata* SZN-B955 under control and nutrient-depleted conditions over two days (t=-2h: pre-experimental timepoint; t=0h: taken directly after nutrient addition; t = 48h: 48h after nutrient addition) for (A: nutrient-replete control, B: P-depleted treatment, C: N-depleted treatment, D: Si-depleted treatment). Error bars represent the standard deviation of triplicates for each treatment.

3.4.4. Sensitivity, and efficiency of primer pairs

The primer efficiency of the GPP qPCR assay was calculated at 102.5% when amplifying a 10-fold dilution series of GPP linearised plasmid standard, with a R^2 value of 1.0, as summarised in Table 3.1. However, efficiency decreased to 90% when amplifying standards of DNA extracted from seawater spiked with *P. multistriata* SZN-B955, as shown in Figure 2.3C & D, Chapter 2. These GPP assay standard types have Limits of Detection (LOD) of a single GPP gene copy and 10^4 cells L^{-1}, respectively. Another standard curve was constructed using linearised *tubA* plasmid of target *P. multistriata* SZN-B955, with a R^2 value of 1.0 and primer efficiency of 95.5%. Both GPP and *tubA*

gene assays were sensitive to a single copy per reaction and demonstrated good linearity over seven orders of magnitude for qPCR (Figure 3.5).

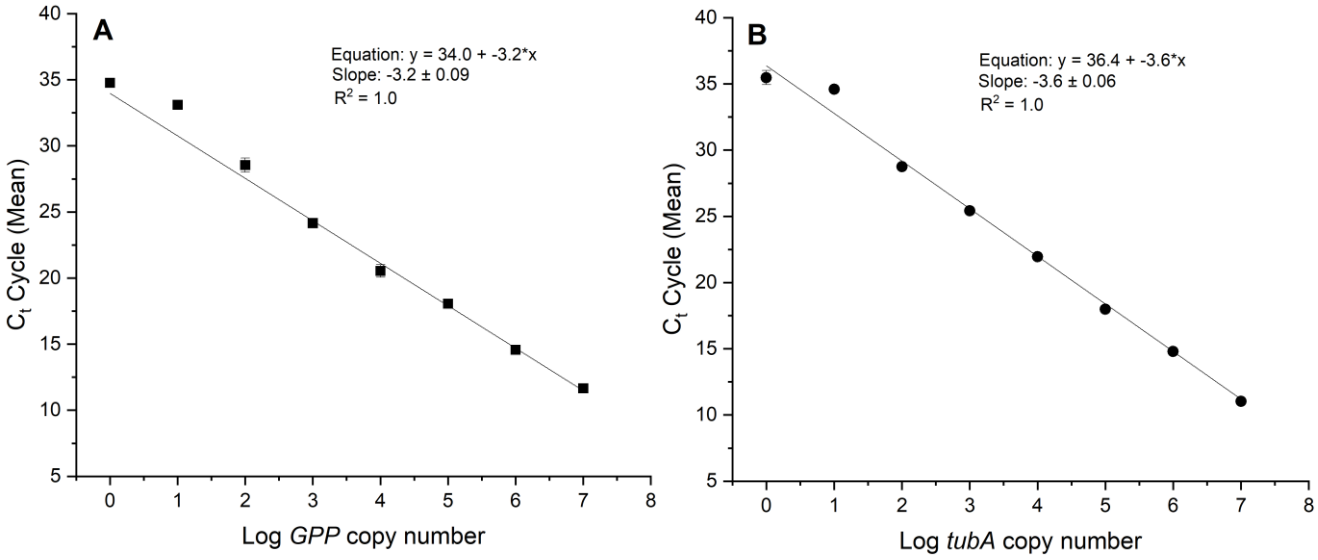

Figure 3.5 The sensitivity of both qPCR GPP and *tubA* gene novel assays is indicated using standard curves of GPP and *tubA* plasmids (A and B, respectively) were plotted with Ct values against the number of serially diluted copies. The standard dilution range was from a single copy to 10^7 copies. The error bars represent the standard deviation from triplicate qPCR reactions. Ct represents the threshold cycle or the cycle at which fluorescent signal first rises above the detection threshold.

Table 3.1 Details of each qPCR assay used in this study. "LightCycler" refers to the thermal cycler (LightCycler96, Roche Diagnostics, Germany) that was used in this study for qPCR and RT-qPCR analyses. "NTC" or no template control indicates negative controls containing nuclease-free water were used in triplicate in qPCR reactions.

		GPP gene	*tubA* gene
Primer & probes	Forward primer	5'-CGACTACCAGAACGATCCCA-3' (1500 nM)	5'-GTTGCCGAAATCACCAGCAC-3' (1000 nM)
	Reverse primer	5'-GGTTCATCTTTCCGCCCTTG-3' (1000 nM)	5'-GACGACATCTCCACGGTACA-3' (1000 nM)
	Probe	5'-(FAM)-ACCTCCCGGCCAACTACGAACTCC-(BHQ1)-3' (250 nM)	5'-HEX-TCGAGCCTACCAACATGATGACCAAGTGC-BHQ1-3' (250 nM)

	Annealing temperature	62.5 °C	59 °C
	Product size (bp)	161	111
	Assay reference	developed & optimised in this study	developed & optimised in this study
LightCycler results	NTC	No amplification	No amplification
	Slope	-3.2	-3.6
	Y-intercept	34.0	36.4
	qPCR efficiency	102.5%	95.5%
	R^2	1.0	1.0

3.4.4. RT-qPCR analysis

Normalised expression of GPP peaked at 2.7-, 3.5- and 3.2-fold within 2 hours of adding P, N, and Si, respectively. In the P-depleted cultures, a gradual increase in GPP gene expression was observed with a minor increase at 0 and 24 hours, culminating in the highest expression at 48 hours after P-addition (Figure 3.6B). N-depleted cultures showed strong down-regulation 0 and 24 hours post N-addition, increasing by 48 hours (Figure 3.6C). Si-addition led to moderate up-regulation, with a 4.1-fold increase over 48 hours (Figure 3.6D). Overall, GPP gene expression showed a maximum increase of 9.6-fold under P-depletion, 6.5-fold for N-depletion and 4.1-fold for Si-depletion over the 48-hour time course. The Pfaffl method was used to determine the fold change in the target gene relative to the reference gene and control sample (Pfaffl 2001). P and Si addition significantly affected GPP expression in *P. multistriata* (p= 0.03 and p= 0.01, respectively). However, no significant difference was observed in response to N addition (p=0.2).

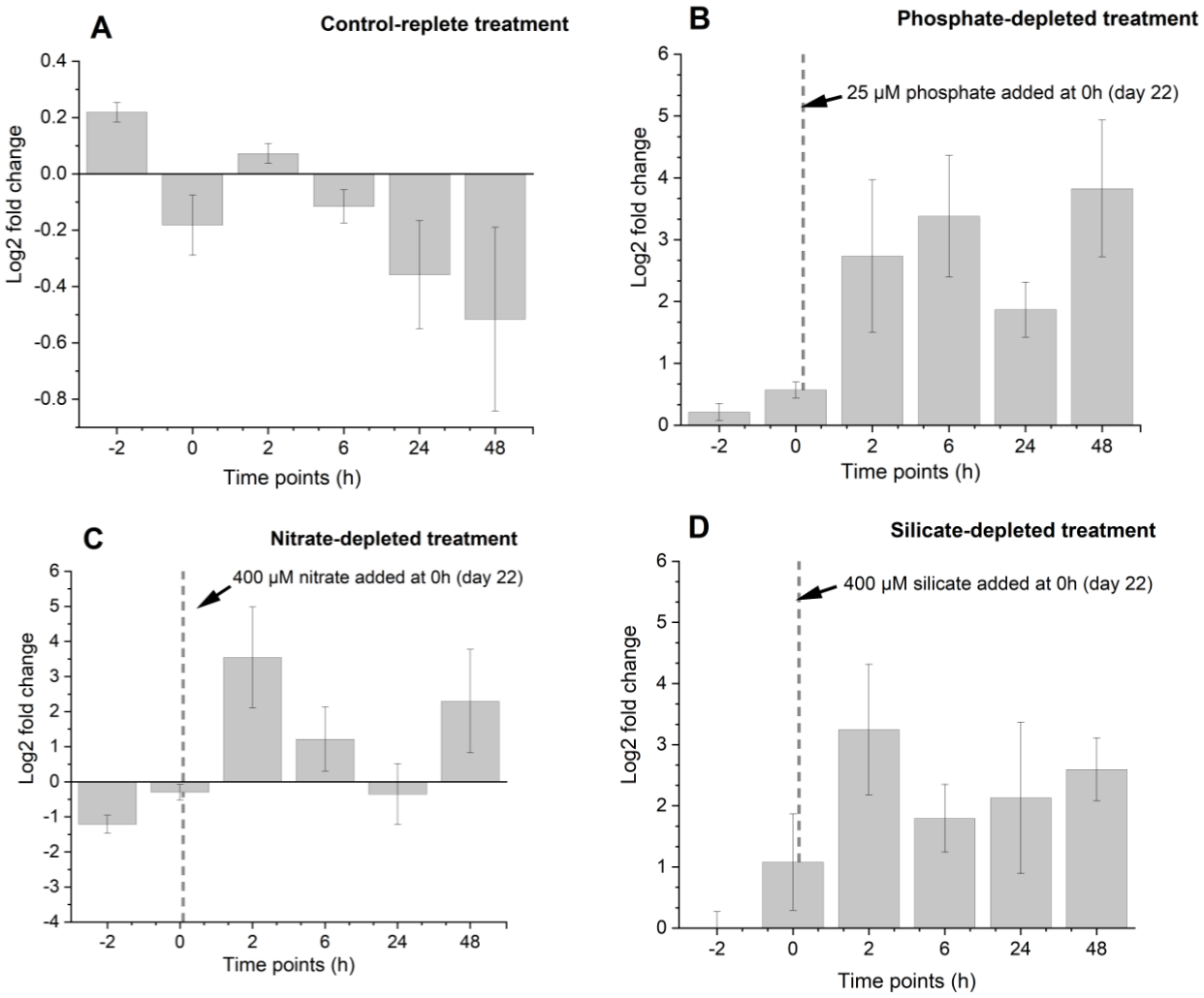

Figure 3.6 Expression of the GPP gene in *P. multistriata* was examined before and after nutrient addition. GPP transcript levels were normalized to reference gene *tubA*. The log2 values of GPP*/tubA* transcripts show the differential expression in response to phosphate, nitrate, and silicate addition (B, C, and D) vs. control treatment (A). Nutrients were added at time 0h. The cutoff threshold between down and up-regulation is indicated by the horizontal line in A, C, and D. Error bars denote the standard deviation associated with the mean of triplicate incubations.

3.4.5. Correlation analysis of GPP expression level with potential regulating factors

The correlation between normalised GPP transcript abundance and domoic acid concentrations (DA pg cell^{-1}) was evaluated using Pearson's correlation coefficient (Table 3.2). Analysis of both variables throughout the experiment was performed by determining the magnitude and direction of the correlation and the goodness of fit (R-Square value between 0-1). Pearson's analysis showed an inverse correlation between toxin concentrations and GPP transcript levels in nutrient-sufficient control cells (r = -0.8, P = 0.04, R^2 = 0.7) (Table 3.2). The strongest direct positive correlation was

observed in P-depleted cultures (r = 1.0, P = 0.0004, R^2 = 1.0), with a weaker positive correlation in Si-depleted cultures (r = 0.9, P = 0.03, R^2 = 0.7).

Table 3.2 Pearson's correlation test results between the relative expression ratio of GPP*: tubA* and the domoic acid concentrations (DA pg cell^{-1}) in response to the addition of phosphate (P), and nitrate (N) in *P. multistriata*. The correlation results are presented with significant values highlighted in bold (P<0.05).

Groups	Pearson correlation coefficient (r)	P-value	R^2
Control culture	**-0.8**	**0.04**	**0.7**
P-depleted culture	**1.0**	**0.0004**	**1.0**
N-depleted culture	0.3	0.5	0.1
Si-depleted culture	**0.9**	**0.03**	**0.7**

3.5. Discussion

This study investigated the effects of adding nutrients (phosphate, nitrate, and silicate) to nutrient-depleted cultures of *P. multistriata* by monitoring the changes in growth rates, domoic acid concentration, and the GPP gene expression during a 48-hour experiment. Previous studies have demonstrated that nutrient influx in coastal regions could support sporadic blooms of domoic acid-producing *Pseudo-nitzschia* for extended periods (Ryan et al. 2017, Van Meerssche et al. 2018, Kelchner et al. 2021). Anthropogenic nutrient loading, capable of causing blooms of *Pseudo-nitzschia* species in coastal waters (Mengelt and Prézelin Barbara 2005, Olesen et al. 2020), was simulated in this study by exposing nutrient-depleted cells of *P. multistriata* SZN-B955 to a pulse addition of 25 µM phosphate (P), 400 µM nitrate (N), and 400 µM silicate (Si), approximating the Redfield Ratio inclusive of Si for diatom cell walls. Prior to nutrient addition, *P. multistriata* experimental cells were subjected to nutrient starvation of phosphate, nitrate, and silicate. Although the levels of the nutrients added are uncommon in marine waters, they have been reported in areas with recurring blooms, such as the English Channel (France) and North Atlantic

waters off the coasts of Rhode Island and the Gulf of Maine (USA) (Lelong et al. 2012, Husson et al. 2016, Clark et al. 2019, Romero et al. 2022, Sterling et al. 2022). The physiological response to nutrient availability was studied, examining growth rates, nutrient consumption, and GPP transcription in toxic *P. multistriata* cells.

A comparative assessment of growth rates among replicate cultures of control, P-depleted, N-depleted, and Si-depleted groups indicates that growth rates showed a statistically significant change after nutrient addition for each nutrient treatment of P-, N-, and Si-depleted, as confirmed by paired t-tests (P= 0.001, P= 0.003, and P= 0.004, respectively). In contrast, the replicates of the control treatment did not demonstrate any significant difference in growth rates at this growth phase (P= 0.1).

The transition period between the exponential and stationary growth phases were earlier in the nutrient-depleted conditions than the control, consistent with previous studies (Bates et al. 1991, Bates 1998, Fehling et al. 2004, Tatters et al. 2012a, Lewis et al. 2018). On day 22, before nutrient addition (i.e. t=0), the N-depleted treatment exhibited a higher growth rate of 0.08 ± 0.003 day^{-1} compared to the P-depleted treatment at 0.003 ± 0.005 day^{-1} and the Si-depleted treatment at 0.002 ± 0.007 day^{-1}.

Table 3.3 Domoic acid levels (pg DA $cell^{-1}$) were measured in *P. multistriata* SZN-B955 under control and nutrient-depleted conditions.

Timepoints (h)	Control culture	Phosphate-depleted treatment	Nitrate-depleted treatment	Silicate-depleted treatment
-2	0	0	0	0
0	0.1 ± 0.06	0.2 ± 0.1	0.2 ± 0.05	0.1 ± 0.1
2	0.02 ± 0.01	0.1 ± 0.1	0.1 ± 0.1	0.5 ± 0.4
6	0.008 ± 0.03	0.1 ± 0.1	0.305 ± 0.2	0.4 ± 0.1
24	0.08 ± 0.05	0.5 ± 0.3	0.147 ± 0.1	0.3 ± 0.2
48	0.1 ± 0.06	0.6 ± 0.2	0.3 ± 0.1	0.2 ± 0.07

There was no significant difference in DA concentration between cultures at (t = 0 h) (Table 3.3). The addition of 25 µM phosphate to P-depleted cultures resulted in a significant increase in the domoic acid concentration, which peaked in the last time points, coinciding with lowest growth rates (Figure 3.4B, Table 3.3; 0.006 ± 0.01 and -0.04 ± 0.006 day^{-1}, respectively). This finding

supports previous results that indicate P-depleted cells prioritise domoic acid production over growth (Pan et al. 1998). Peak DA concentrations after 400 µM nitrate addition to N-depleted cultures were lower than P-depleted cultures (Table 3.3), and growth rates remained low. These findings are consistent with previous studies reporting reduced growth rates and toxin production under excess nitrate availability (Martin-Jezequel et al. 2015).

Following the addition of 400 µM silicate to Si-depleted cells, the toxin concentration was variable but was similar to the control after 48 h (Table 3.3), coinciding with an increased growth rate (Figure 3.2B). In contrast to N and P, Si is not required for domoic acid synthesis (La Barre et al. 2014, Brunson et al. 2018, Hardardottir et al. 2019) but it is critical for growth in diatoms (Martin-Jezequel et al. 2000, Sauvey et al. 2023). The findings of the current study found an inverse relationship between domoic acid levels and growth rates in the P- and N-treatments and nutrient-replete control. These results may elucidate the interplay between different nutrient sources in sustaining slow-growing *Pseudo-nitzschia* blooms in coastal waters relative to toxin production.

Nutrient levels were compared to the variations in total toxin per cell in both control and experimental treatments over a 48-hour period. The control cultures maintained steady-state nutrient concentrations throughout the experiment from t=0h to t=48h (Figure 3.3A). In replete control cultures of *P. multistriata*, nutrient concentrations gradually decreased during the exponential growth phase (Appendix B, Table B2). Nutrient concentrations remained relatively high at the later time point (48h), consistent with the decrease in nutrient consumption during growth arrest in replete *P. multistriata* cultures (Annunziata et al. 2022). Different nutrient utilisation strategies were observed in response to nitrogen and silicon depletions of *P. multistriata*, with N-starved cultures exhibiting a reduced demand for phosphate and higher phosphate concentrations, while Si-starved cultures demonstrated a higher demand for phosphate and lower phosphate concentrations.

When nitrate was added at time point t=0h, N-starved cultures accumulated phosphate to 145.3 ± 12.1 µM. *Pseudo-nitzschia* may prioritise the utilisation of nitrogen over phosphate when available nitrate can support growth and metabolic processes, resulting in higher phosphate concentration in N-starved cultures (Hagstrom et al. 2011). In contrast, the addition of silicate at the same time point (t=0h) in Si-starved cultures induced phosphate uptake, leading to lower phosphate

concentrations of 3.5 ± 3.3 µM. The uptake of phosphate in *Pseudo-nitzschia* is regulated by silicon metabolism, which plays a crucial role in cellular growth and the formation of cellular structures (Fuentes et al. 2014). These findings highlight the relationship between nutrient availability and the physiological responses of *P. multistriata* under nutrient-stressed conditions. No significant differences in nutrient levels were observed in the control treatment throughout the experiment ($P < 0.05$). This demonstrates the distinct and preferred nutrient utilisation strategies employed by *P. multistriata* in response to depletion of different nutrients.

Previous studies have shown high production of domoic acid linked to the excessive consumption of phosphate (Hagstrom et al. 2011, Wingert and Cochlan 2021a). This is consistent with results from the P-depleted cultures, which consumed 95% of the added phosphate within 48 hours, coinciding with a significant increase in domoic acid from t=0h t= 48 h after phosphate addition (Table 3.3). In contrast, no significant change in domoic acid concentrations was observed between time points (t=0h) and (t= 48 h), after N-depleted cells consumed 85% of resupplied nitrate at (t=48h) post nitrate addition (Table 3.3). It is possible that an extended period of nitrate depletion would result in further increases in DA concentrations, as reported previously when the DA concentration in *P. multiseries* cells reached 10 pg DA cell^{-1} 40 days after nitrate addition (Bates et al. 1991). Domoic acid levels remained steady between time points (t=0h) and (t=48h) when experimental Si-depleted cultures consumed 98% of the added silicate within 48h (Table 3.3). A previous study showed that extended silicate depletion in *P. multiseries* cells resulted in a modest increase in domoic acid production, reaching 0.1 pg DA cell^{-1} on day 35 (Pan et al. 1996b). Here, it is demonstrated that nutrient consumption was comparable in N and Si-depleted treatments, with no significant difference in N and Si concentrations across experimental time points in both treatments ($P > 0.05$). Conversely, a significant difference in phosphate concentration was observed from t=0h to t=48h in the P-depleted treatment ($P < 0.05$), resulting in the maximum concentration of domoic acid at 0.6 ± 0.2 pg DA cell^{-1} at 48 h across all experimental cultures of *P. multistriata* (Table 3.3). These results suggest that *Pseudo-nitzschia* cells invest excess nutrients towards DA production to reduce the high cost of photosynthesis and are unable to sustain optimal growth (Zabaglo et al. 2016).

In comparison, the toxin level in the control treatment remained relatively constant between time points t=0h and t=48h (Table 3.3). This constant level of toxicity in treatments with stable nutrient

levels is consistent with previous results (Trainer et al. 2012, Bates et al. 2018). In this experiment, the control cultures were grown to reach a higher cell concentration (720333 ± 64.9 cells mL^{-1}) under optimal growth conditions, resulting in a lower DA concentration (approximately 0.1 pg DA $cell^{-1}$). These findings highlight a correlation between low cell density and increased production of DA (Lewis et al. 2018).

The biosynthesis of domoic acid is dependent on the availability of phosphate and nitrogen substrates (Howard et al. 2007, Kudela et al. 2008, Thessen et al. 2009, Hardardottir et al. 2019, Lema et al. 2019). Geranyl pyrophosphate synthase (GPP) is a precursor for the N-geranylation process, a reaction catalysed by DabA during the biosynthesis of domoic acid (DA) (Brunson et al. 2018, Hardardottir et al. 2019). In this study, relative GPP expression was normalised to the reference gene *tubA* (Pfaffl 2001, Adelfi et al. 2014). P-depleted cells showed a rapid and high increase in GPP transcription within 2 hours of P addition, reaching a peak within 48 hours (Figure 3.6B). Pearson's analysis showed that domoic acid production was more responsive to P addition than to N or Si additions (Table 3.2). The association between normalised GPP transcription and domoic acid levels was non-significant in the nitrate treatment (r = 0.3, R^2 = 0.1, P = 0.5). Upregulation of GPP transcript peaked at 2 hours after N and Si addition (Figure 3.6C & Figure 3.6D). A positive correlation between domoic acid and GPP transcript levels (r = 0.9, R^2 = 0.7, P= 0.03) was also observed after silicate addition, with a peak value of DA at t=2h (Table 3.2). Following the addition of nitrate and silicate, low concentrations of DA were observed after 24 hours, as depicted in (Table 3.3). Previous studies have reported undetectable levels of DA shortly after nitrate and silicate additions to *Pseudo-nitzschia* cultures (Bates et al. 1991, Pan et al. 1996b), indicating that the biosynthesis of DA may not be initiated by nitrate or silicate addition (Chekan et al. 2020).

In the present study, a strong correlation was found between GPP transcript level and domoic acid production (r = 1.0, R^2 = 1.0, P = 0.0004) in the phosphate treatment, exhibiting the highest level of domoic acid among all other treatments, with a level of 0.6 ± 0.2 pg DA $cell^{-1}$ at t=48 h after phosphate addition. Phosphorous plays a significant role in domoic acid biosynthesis through the MEP pathway in plastids (Lichtenthaler 2010, Athanasakoglou and Kampranis 2019a). The role of phosphate was shown in modulating the toxin transcriptional profile through the MEP pathway (Hardardottir et al. 2019). *Pseudo-nitzschia* cells can store domoic acid intracellularly in the plastid reservoir and release it extracellularly under stress (Trainer et al. 2012, Quijano-Scheggia et al.

2020). Extracellular toxin secretion in P-depleted cells showed no significant change from t=0h to t=24, following P-addition (Table 3.3). However, variations in the timing of DA induction were observed among different nutrient additions (2 hours for Si, 6 hours for N, and 48 hours for P) which could be associated with the following factors: 1) Variations in the availability and concentration of the respective nutrients in the growth media may influence the metabolic pathways involved in DA production (Lema et al. 2017). 2) Differential uptake rates of specific nutrients by *P. multistriata* cells can affect the timing of DA production (Trainer et al. 2012). The observed variations of GPP transcription upregulation between different nutrient additions (Si vs N vs P) may be influenced by the following factors: 1) Differential gene regulation mechanisms specific to each nutrient, leading to variable expression levels (Boissonneault et al. 2013) and 2) Varied metabolic pathways related to the utilisation of Si, N, and P, which may indirectly affect the transcription (Lema et al. 2019), 3) The potential roles of post-transcriptional regulatory mechanisms are proposed and the extracellular release of domoic acid may account for the inconsistencies observed between the timing and magnitude of GPP expression and toxin levels across the experimental time points (Figure 3.4 & Figure 3.5) (Zabaglo et al. 2016, Cohen et al. 2018). These discrepancies warrant further investigations to reveal the underlying mechanism modulating the observed toxic activity in *Pseudo-nitzschia* cells in response to nutrient inputs occurring in coastal waters.

The analysis of GPP gene expression was performed using a RT-qPCR method which is specific to the *Pseudo-nitzschia* species as discussed in Chapter 2. The qPCR assay was coupled with a reverse transcription step to examine the impact of nutrient addition on the genetic control of toxin production using normalised GPP expression. This method can provide an important tool for predicting and potentially mitigating harmful blooms of DA-producing *Pseudo-nitzschia*, which can reach high cell densities at 10^5 to 10^7 cells L^{-1}, quickly during bloom initiation (Du et al. 2016a, Bates et al. 2018). UK HAB surveillance programs set a threshold of 1.5×10^5 cells per litre of seawater to trigger sampling and analysis of shellfish for algal toxins (Downes-Tettmar et al. 2013). The genetic marker for GPP in *Pseudo-nitzschia* is detected by our qPCR assay from low cell densities of 10^4 cells L^{-1} (i.e., times below the UK threshold for monitoring toxic blooms). Reducing analysis time is also crucial in detecting and monitoring *Pseudo-nitzschia*. This assay offers rapid detection, with the ability to identify a single copy of the target within 35 minutes of DNA template addition without post-analysis steps, in contrast to the majority of current *Pseudo-nitzschia* assays that need time-

consuming post-PCR analysis involving gel electrophoresis or melting analysis of amplicons (Andree et al. 2011, Pugliese et al. 2017).

These results provide insights into the use of assay for specific nucleic acid-based testing of *Pseudo-nitzschia* species. However, the proposed qPCR assay lacks the analytical capability to differentiate between toxigenic and non-toxigenic *Pseudo-nitzschia* strains. The PCR analysis of the GPP in non-toxic *Pseudo-nitzschia* species was not possible due to the limited availability of these algal cultures and their bioinformatic data. Thus, amplification of GPP using the qPCR assay can not necessarily serve as a proxy for the strain's DA biosynthesis potential. The GPP gene may be used in other biochemical pathways and the complete production of domoic acid necessitates the full activation of a gene cluster (Brunson et al. 2018, Chekan et al. 2020). Additional tests are required to establish the specificity and efficacy of GPP assay on non-toxigenic *Pseudo-nitzschia* strains for practical purposes. However, the GPP transcription approach shows promise in providing predictive capabilities regarding toxicity caused by anthropogenic nutrient enrichment.

3.6. Conclusions

This study provides a quantitative evaluation of growth, domoic acid production and the GPP transcription, in response to the addition of high concentrations of essential nutrients (phosphate, nitrate, and silicate) to nutrient-depleted *P. multistriata* cells. This study revealed that the addition of phosphate to P-depleted cultures resulted in a peak in both domoic acid concentration and GPP gene expression at 48 h. The regulation of nutrient consumption was observed to be governed by both cellular growth metabolism and toxin production in this chapter. . Notably, a novel assay has been successfully developed to study the regulation between nutrient availability and the physiology of *Pseudo-nitzschia* under nutrient-stressed conditions. The proposed method has the potential to enhance the routine monitoring of coastal waters by enabling a rapid and scalable assessment of the risk of *Pseudo-nitzschia* blooms in oligotrophic coastal areas. The current study has made a significant contribution towards improving our understanding of the environmental drivers resulting in the production of domoic acid (DA), thereby providing promising avenues for predictive capabilities, novel regulatory measures, and the deployment of early warning systems

for the optimum timing of aquaculture harvest. This innovative approach can effectively assist to safeguard public health while improving the sustainability and resilience of aquatic industries.

Chapter 4 Detection of *Pseudo-nitzschia spp.* using Isothermal DNA-Based Amplification

4.1 Abstract

Nucleic acid detection has proven useful in the field monitoring of Harmful Algal Blooms (HABs). The standard Polymerase Chain Reaction (PCR) technique offers precise and sensitive identification within centralised laboratories. However, PCR-based methods demand expensive laboratory equipment, advanced training and time-intensive protocols, making them unsuitable for on-site and decentralised HAB detection. The objective was to develop an isothermal assay that eliminates the need for thermal cycling, thereby simplifying the molecular analysis of HABs. This study focuses on providing simple, rapid, and precise identification of HABs that can be applied in environmental settings. Loop-mediated isothermal amplification (LAMP) and recombinase polymerase amplification (RPA) assays were developed to enable real-time, sensitive, and precise identification of *Pseudo-nitzschia* spp., microalgae responsible for producing the neurotoxin domoic acid.

The analytical specificity and sensitivities of LAMP and RPA assays were compared to detect the cytochrome CYP450 *dabD* toxin-encoding gene of the marine diatom of *Pseudo-nitzschia* spp. Both the LAMP and RPA assays successfully amplified DNA from 100% and 90% of the tested cultures of *Pseudo-nitzschia* strains, respectively. Both assays demonstrated no cross-detection when analysing genomic DNA samples of non-target algal species. The optimised LAMP assay achieved a limit of detection down to a single copy, whereas the optimised RPA assay demonstrated a limit of detection of 10^3 copies μl^{-1}. Of the two methods, the LAMP method showed high sensitivity, specificity, and performance. Therefore, LAMP analysis was used to quantify the *Pseudo-nitzschia* DNA target from environmental seawater samples. Environmental seawater samples were collected on an almost weekly basis over six months from three sites within known shellfish production areas located in a HAB hotspot, namely St Austell Bay in Cornwall, England. Among the 44 seawater samples, the LAMP assay positively detected 34 samples, resulting in a sensitivity rate of 77.3%. The LAMP measurements revealed an increase in the copy numbers of *dabD Pseudo-nitzschia* spp. during both the Autumn and Spring seasons. The findings were reported in the context of the prospective advantages and

constraints associated with isothermal amplification methods against conventional qPCR techniques, along with the promising applicability of LAMP in field-deployable systems for HAB surveillance.

4.2 Introduction

Harmful algal blooms (HABs) of the marine diatom *Pseudo-nitzschia* spp., are capable of producing the neurotoxin domoic acid (DA), posing a significant threat to both marine ecosystems and human health (Lelong et al. 2012). Exposure to domoic acid causes neurotoxic illness in both humans and marine organisms, known as amnesic shellfish poisoning (ASP), following the consumption of DA-contaminated fish or shellfish (Bates et al. 2018). Acute exposure to DA can trigger mass mortalities of marine life for example, at the razor clam harvesting site on the coast of Washington, USA, which resulted in economic losses estimated at approximately US$ 40 million (Ferriss et al. 2017). These DA incidents have led to the closures of fisheries, and aquaculture sites, and the shut-down of tourism activities, resulting in substantial economic losses and damages to the well-being of coastal communities dependent on these activities (Trainer et al. 2012).

The current assessment of human exposure to DA relies on the analysis of seawater or shellfish homogenates following the consumption of DA-contaminated seafood and after the sick individuals show neurotoxicity symptoms. However, enumerating *Pseudo-nitzschia* cells in seawater requires tedious and time-consuming sample preparation and taxonomic expertise for distinguishing morphometric characteristics of cells (Arapov et al. 2023). An alternative culture-based technique involves the use of competitive enzyme-linked immunosorbent assay (ELISA) and high-performance liquid chromatography (HPLC) to identify DA in shellfish homogenate samples (Kleivdal et al. 2007b, Quijano-Scheggia et al. 2008). However, the presence of DA analogues in the collected samples, which share structural similarities with DA, can result in non-specific and inaccurate detection (Smith and Kitts 1994). Those existing methodologies depend on a growth-based detection that permits quantification of cell number or DA level only at or above the management thresholds, limiting the prediction of DA-related risks in the future or near real-time scenarios. Thereby, current time-intensive methods can significantly delay analysis and results, preventing timely interventions to avoid shell fishery and aquaculture closures and alleviating the consumption of DA-contaminated seafood.

In contrast, nucleic acid-based analysis provides precise, highly sensitive, and reliable quantification of harmful microorganisms compared to conventional regulatory techniques. Nucleic acids (DNA/RNA) are of great importance for encoding, transmitting and expressing genetic information (Moore 1999). Sensing technologies that rely on the detection and quantification of nucleic acid sequences are increasingly common to provide low-cost, rapid detection of biological hazards from diverse environments and sample matrices (Holland and Kiechle 2005, Yager et al. 2006). These technologies often operate through nucleic acid sequence amplification to accurately identify genetic sequences (genes and their mutations) that are unique and inclusive to a target group and quantify their concentration to infer gene expression levels (Ivnitski et al. 2003, Lauri and Mariani 2009, Sperança et al. 2016). The applications for molecular analytics are centred around in vitro diagnostics (IVD) and environmental surveillance and monitoring, including advanced early warning of bio-hazards in food and water supplies (Celis et al. 2000). With human population expansion and the associated challenges in healthcare, food production and environmental management there is an increasing need for rapid, low cost, specific and sensitive methods to capture the early signs of any increase in risk.

Isothermal nucleic-acid-based amplification allows real-time detection at ambient or slightly elevated temperatures which eliminates the need for thermal profiling, and expensive and complex heating elements, resulting in simple, cost-effective and lower power consumption compared to conventional molecular techniques such as PCR (Chang et al. 2012). Isothermal methodologies can offer rapid, affordable, versatile tools for decentralised testing, tolerating inhibitors and crude samples collected from the environment (Li et al. 2019a). In contrast, PCR analysis requires highly purified DNA samples, and long comprehensive post-analysis procedures (Lefferts and Lefferts 2017). As a result, the PCR-based analysis can be only achieved after the extensive extraction procedures of DNA from the collected samples, and followed by validation tests after the contaminated shellfish have been harvested and consumed. This delay in obtaining detection results will prevent the timely implementation of measures aimed at mitigating the toxic risks of HABs. Still, both PCR and isothermal techniques demand careful validation and statistical interpretation to account for inter-assay variability and technical differences, resulting from different thermal cyclers and varying laboratory conditions (Ozsolak and Milos 2011, Fang et al. 2012). Additionally, the lack of a denaturation step in isothermal reactions increases the possibilities of non-specific and off-target amplification, affecting the reproducibility of the results (Toley et al. 2015). Therefore, careful design of an isothermal assay

is critical to ensure the accuracy, reliability, and reproducibility of detection (Tsai et al. 2012, Ye et al. 2019). Isothermal assays can offer versatile detection capabilities for both DNA and RNA targets at a constant temperature through diverse mechanisms, such as recombinase polymerase amplification (RPA) (Piepenburg et al. 2006), nucleic acid sequence-based amplification (NASBA) (Compton 1991), loop-mediated amplification (LAMP) (Notomi et al. 2000), helicase-dependent amplification (HDA) (Vincent et al. 2004), rolling circle amplification (RCA) (Lizardi et al. 1998), and strand displacement amplification (Walker et al. 1992, Shuler et al. 2012). The main mechanisms of RPA and LAMP processes are summarised in Chapter 1, sections 1.11.4.3.1 and 1.11.4.3.2, respectively.

Two novel isothermal LAMP and RPA assays were developed for the rapid, inclusive, and highly sensitive detection of the DA-encoding gene (cytochrome, *dabD*) specific to the marine diatom *Pseudo-nitzschia* spp. This study aimed to evaluate the amplification specificity of both assays across a panel of target *Pseudo-nitzschia* spp., and non-target microalgae species. The sensitivity of both amplification chemistries was subsequently evaluated using a serial dilution of known concentrations of the target sequence spanning seven orders of magnitude. The LAMP assay described herein enabled the DNA-based quantification of the *Pseudo-nitzschia* target obtained from environmental samples collected in St Austell Bay, a well-known hotspot for HABs in Cornwall, England.

4.3 Material and Methods

4.3.1 Identification of Target Region.

The gene of interest is the cytochrome P450 *DabD* gene, which plays a crucial role in the biosynthesis of domoic acid (DA) in *Pseudonitzschia* spp. (Brunson et al. 2018). In the term "Cytochrome P450" CYP stands for "Cytochrome", P for protein and 450 is a reference to the characteristic spectral absorption peak at 450 nanometers when the cytochrome is exposed to carbon monoxide. Cytochrome P450 enzymes are a superfamily of enzymes that are involved in the oxidative metabolism of a wide range of compounds, including drugs, xenobiotics, and endogenous substances such as fatty acids and steroids (McLean and Munro 2016). The genetic sequence of the cytochrome P450 *DabD* gene was recently characterised in DA-producing diatom *P. multiseries* (Brunson et al. 2018). BLAST analysis was performed using the following settings: E-value cutoff= 0.05-0.1, match/mismatch scores= 2-3,

word size = 7-28, the gap costs of existence= 5, extension=2 and a threshold of 1–100 hits per query (Altschul et al. 1990). This target sequence was then searched across available *P. multistriata* genomes in public databases such as the National Centre for Biotechnology Information (NCBI) GenBank database (https://www.ncbi.nlm.nih.gov/), the SZN institute database (https://bioinfo.szn.it/), the Earlham institute's database (http://apollo.tgac.ac.uk/), (Basu et al. 2017), (Di Dato et al. 2015) and the Ensembl database (https://protists.ensembl.org/). To identify conserved regions suitable for oligonucleotide binding, a set of 8 sequences was used from the highest-scored BLAST hits and then aligned using the ClustalW multiple sequence alignment tool, version 2.1 (Larkin et al. 2007). In order to validate the accuracy of amplifying the target sequence, additional verification measures were taken as follows; the consensus sequence was subjected to comparison with the reference protein sequences available in the GenBank database using BlastX (Camacho et al. 2009). Furthermore, protein domains were analysed to examine the translated protein sequence of the target conserved region (Marchler-Bauer et al. 2017). The bioinformatics analyses were conducted using either the NCBI website's toolkit or Geneious Prime® v2019.2.3 software (Biomatters Ltd, Auckland, NZ).

4.3.2 RPA Assay

The RPA primers were designed following the guidelines provided by TwistDx Ltd., UK (TwistDx 2009), to amplify the identified target region. The RPA primers and exo-probe were designed using Geneious Prime® v2019.2.3 software (Biomatters Ltd, Auckland, NZ) as no other specific software was reported for the design of RPA assays. Five candidates of RPA primers were identified and screened for their efficiency using the 5x5 primer candidate matrix approach (TwistDx 2019). The amplification was performed using the TwistAmp® Liquid Basic kit (Catalogue ID: TALQBAS01, TwistDx Ltd., UK), followed by amplified products purification using the MinElute PCR purification kit (Catalogue ID: 28006, Qiagen, Hilden Germany) and visualised via 2% agarose gel electrophoresis using ImageJ software. The combinations of RPA primers were categorised based on specificity, product yield, and product/noise ratio. The RPA exo-probe was designed to bind to the region between the optimal primers, incorporating unique modifications like the tetrahydrofuran spacer, fluorescent 6-FAM dye (FAM-dT), tetrahydrofuran residue (THF), and black hole quencher 1 (BHQ1-dT), along with a 3'-modification group of C3-spacer, as per TwistDx's instructions for RPA exo probes design (TwistDx 2009). To optimise the RPA assay with the exo-probe, different reaction temperatures ranging from 36°C to 40°C

were tested. All RPA reactions were performed in triplicates and included negative controls (no template control; NTC) and control reaction mixtures supplied with the RPA TwistAmp™ exo kit (Catalogue ID: INLQEXO, TwistDx Ltd., UK). The real-time RPA assay was conducted in a total volume of 25 µL, comprising 400 nM of RPA primers, 150 nM of RPA exo-probe, 400 nM of each dNTP, and 1X TwistAmp Reaction components obtained from the TwistAmp™ exo Kit (Catalogue ID: INLQEXO, TwistDx Ltd., UK). To initiate the RPA reaction, the RPA mastermix was combined with 14 mM magnesium acetate and 1 µL of DNA template into the lids of 0.2 mL microcentrifuge tubes. The lids were securely closed and centrifuged before 36°C incubation for 30 minutes in the LightCycler 96 real-time instrument.

4.3.3 LAMP Assay

The LAMP assay was designed using PrimerExplorer™ V5 software (Eiken Chemical Co., Ltd., Tokyo, Japan). The LAMP primers were synthesised by Integrated DNA Technologies Ltd and purified by HPLC, before being diluted to the appropriate concentrations using PCR-grade water. The sequences of LAMP primers are provided in Table 4.1. To prepare the LAMP reaction, 1X Warm Start LAMP master mix (New England Biolabs, Hitchin, Hertfordshire, UK), was mixed with 1X LAMP fluorescent intercalating dye (New England Biolabs, Hitchin, Hertfordshire, UK), and 2 µL of DNA template. Standard concentrations of 1.6 µM of forward inner primer and backward inner primer (i.e. FIP/BIP primers) and 0.2 µM of forward and backward (F3/B3) primers were used in all LAMP reactions. Different concentrations of loop primers ranging from 0.4, 0.8, and 1 µM were tested. To achieve a total volume of 25 µl, the reaction mixture was adjusted with nuclease-free water. The incubation was carried out at 65 °C for 1 hour. Real-time LAMP assays were performed using the LightCycler 96 real-time PCR instrument by measuring fluorescence signals from LAMP Fluorescein (FAM) at 30-second intervals to generate real-time amplification curves. To evaluate the accuracy of the primers in detecting cytochrome *P450 dabD* target among *Pseudo-nitzschia* strains, both 2% gel electrophoresis and high-resolution melting (HRM) curve analysis were conducted following the LAMP reaction. The melting temperature of LAMP amplified products was determined using the LightCycler 96 Software (Version 1.1.0.1320, Roche Diagnostics, Germany).

4.3.4 Control Strains

Control cultures of *Pseudo-nitzschia* species and non-target algal species were grown in sterile, filtered f/2, L1, and BG11 growth media prepared from artificial seawater, respectively (Guillard 1983, Keller et al. 1987). These cultures were maintained at a constant temperature of 18°C and subjected to a 12-hour light-dark photoperiod using a self-contained incubator (LEEC Ltd, PL3, Nottingham, UK). Domoic acid quantification was undertaken for all microalgal strains in the study using the ELISA method as described by (Boissonneault et al. 2013). Details of the algal strains, their respective origin, and corresponding domoic acid levels (pg DA $cell^{-1}$) can be found in Table 4.5. The cells were pelleted by centrifugation at 7,160 rpm for 10 minutes at 4°C, utilizing a refrigerated centrifuge. Following centrifugation, the supernatant was carefully removed, and the cell pellets were preserved at -80°C. Upon thawing, the cell pellets were homogenised with glass beads (0.5 mm diameter, catalogue number 110779105, Biospec Products, UK) and a vortex adapter (catalogue number 13000-V1-24, Qiagen, Germany) using a vortexer (Vortex-Genie 2, Mo Bio Laboratories, US). Subsequently, DNA extraction was carried out using the DNeasy Plant Mini Kit (Qiagen, Hilden, Germany) in accordance with the manufacturer's instructions. The DNA concentration was then quantified using the Qubit fluorometer (Thermo Fisher Scientific Inc., UK) and NanoDrop 1000 spectrometer (Thermo Scientific, Wilmington, DE). The extracted DNA samples were subsequently preserved at -80°C until use.

4.3.5 Specificity and Sensitivity Testing

For specificity evaluation of the developed assays, the same genomic DNA samples extracted from control cultures were amplified by both RPA and LAMP reactions. The analytical specificity of the LAMP and RPA assays was calculated as a percentage using the following formula: (true negatives) / (true negatives + false positives) × 100 (Hashish et al. 2022). Furthermore, the inclusivity of both assays was further confirmed through agarose gel electrophoresis analysis. The electrophoresis analysis was conducted using a 2% (w/v) agarose gel in 1X TAE buffer (AppliChem GmbH, Germany). The gel was stained with 5 µl of SYBR-Safe (10,000x in DMSO) (Invitrogen, Carlsbad, CA) and run at 86 V and room temperature. After electrophoresis, the DNA bands were visualized using a UV transilluminator, and their sizes were determined by comparing them to a 50 bp DNA ladder (New England Biolabs, Hertfordshire, UK). Additionally, the positive control, which was a DNA plasmid containing the target

insert, and the negative control, consisting of nuclease-free water, were also tested in the electrophoresis analysis. Furthermore, LAMP amplified products were analysed by melting dissociation curve (Wong et al. 2018). This technique involves a controlled temperature increase to denature the double-stranded amplified products, resulting in the determination of a distinct melting temperature specific to on-target products. The melting temperature is determined by the properties of the products, including product length and GC content (Ozay and McCalla 2021).

To assess the sensitivity of the designed assays, the genomic DNA sample of the *P. multistriata* SZN-B954 strain was used as a template in a PCR reaction. A 265 bp fragment truncated from the target sequence of the cytochrome P450 (CYP450, *dabD*) gene was amplified using RPA_fw and RPA_rv primers in a PCR amplification reaction. The PCR reaction mixture consisted of 2 µl DNA template, 0.05 units μl^{-1} One Taq DNA Polymerase (New England Biolabs, Hertfordshire, UK), 0.4 µM of each primer, 2 mM $MgCl_2$ (New England Biolabs, Hertfordshire, UK), 200 µM dNTPs mixture (New England Biolabs, Hertfordshire, UK), 1X One Taq Reaction Buffer (New England Biolabs, Hertfordshire, UK), 16.9 µl Nuclease-Free Water (Invitrogen), and 2 µl DNA template, resulting in a total reaction volume of 25 µl. PCR amplification was conducted under the following thermal cycling conditions: 1 cycle at 95°C for 120 sec followed by 45 cycles at 94°C for 15 sec, 61°C for 20 sec and 72°C for 30 sec. The PCR reactions were carried out on a LightCycler 96 real-time PCR machine (Roche).

The PCR product was purified using the QIAquick PCR purification kit (Qiagen GmbH, Hilden, Germany) and then employed directly for the cloning the target gene into a DNA plasmid using the pGEM®-T Easy Vector (Promega, Wisconsin, USA) following the manufacturer's protocol. Four recombinant plasmid clones were distinguished through blue-white colony selection. These identified specific colonies were subsequently introduced into *Escherichia coli* cells using OneShot TOP10 competent cells (Invitrogen, Carlsbad, CA, USA). The *E. coli* cells were cultivated in 10 ml LB medium supplemented with 15 µg ml^{-1} ampicillin and grown overnight at 37ºC.

Plasmids containing the target gene were extracted from cultured cells through the QIAprep® Spin Miniprep Kit (Qiagen, Valencia, CA, USA) following the manufacturer's protocol. These purified plasmids were then linearised by overnight restriction digestion using the NdeI restriction enzyme (ER0582, Thermo Fisher Scientific Baltics UAB, Vilnius, Lithuania) and the successful linearisation was confirmed through gel electrophoresis with a high mass ladder. The linearised plasmids were analysed

through electrophoresis using a 2% (w/v) agarose gel in 1X TAE buffer (AppliChem GmbH, Germany). The gel was stained with 5 µl of SYBR-Safe (10,000x in DMSO) (Invitrogen, Carlsbad, CA) and run at 86 V and room temperature. Following electrophoresis, the DNA bands were visualized using a UV transilluminator, and their sizes were determined by comparing them to a 1 kbp ladder (New England Biolabs, Hertfordshire, UK). After confirming the desired target size of linearised plasmid via PCR, quantification of plasmid was performed using both a NanoDrop spectrophotometer (ND-1000, NanoDrop Technologies, Wilmington, DE) and a Qubit fluorometer with a dsDNA BR Assay Kit (Invitrogen, Carlsbad, CA, USA). To construct a standard curve for precise target quantification, the linearised plasmid containing the target insert was subjected to serial dilution, generating concentrations spanning from a minimum of a single copy to a maximum of 10^7 copies. The copy numbers of the target sequence were calculated from the concentration of the recombinant DNA plasmid based on the equation previously described by (Hardinge et al. 2018). The same dilutes of linearised plasmids were amplified using both LAMP and RPA assays in triplicated reactions. The limit of detection (LOD) was determined based on the minimum detectable copy number of the target sequence in each amplification reaction of replicated genomic DNAs (Kralik and Ricchi 2017). The quantification accuracy of the isothermal assays was assessed by establishing a linear correlation between the copy number of the template sequence and the threshold time (T_t) values, using the goodness of fit (R-squared value) across seven orders of magnitude (Euler et al. 2012, Nguyen et al. 2020). The T_t value is defined by the time point at which the fluorescence signal exceeds the threshold fluorescence level during the amplification reaction (Diego et al. 2019).

4.3.6 Environmental Samples

Coastal seawater samples were collected via boat from three offshore points in St Austell Bay, Southern England, UK. The collection sites are located within shellfish production areas, namely Ropehaven Outer (grid reference SX05744972), Porthallow North (grid reference SW80212383), and South Mevagissey Bottom (grid reference SX05214698), along the Southwest coast of England, as depicted in Figure 4.1. The sampling started from September 13, 2021, to March 28, 2022, with a temporary suspension during December and early January due to low temperatures and reduced phytoplankton levels in the water. Not all sites were sampled weekly during the duration of the study.

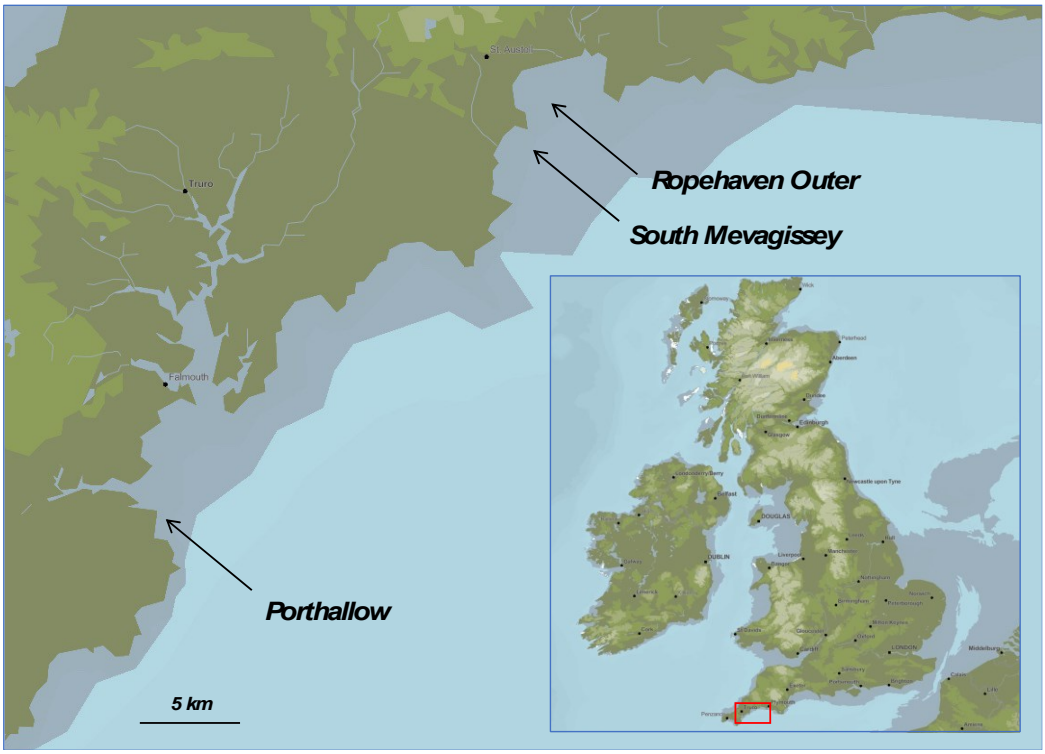

Figure 4.1 Samples collection from three shellfish production sites situated in St Austell Bay, Cornwall, UK, recognised as a hotspot for harmful algal blooms (HABs), during the period spanning September 2021 to March 2022.

A total of 44 filtered water samples were collected throughout the study for downstream molecular analysis. Water collection was carried out using a pole sampling technique (Suthers et al. 2009), followed by immediate filtration through a 0.2-micron pore size Sterivex filtration unit (Millipore, USA) (polyethersulfone membrane). A disposable 50 mL plastic syringe with a Luer lock was employed to filter seawater, followed by a brief air chase to facilitate membrane drying. The filtered units were securely sealed with parafilm tape (Sigma-Aldrich), cooled on dry ice, and transported back to the shore for storage at -80°C until subsequent processing.

DNA extraction from the Sterivex filter units was performed using the Power Water DNA Isolation Kit (Qiagen, Hilden, Germany) in accordance with the manufacturer's protocol. The elution step involved Tris-EDTA (pH 8.0), yielding a final eluant volume of 100 µl from each Sterivex unit. Prior to LAMP analysis, the extracted DNA from each sample was quantified using a Nanodrop spectrophotometer. If necessary, additional DNA purification was conducted using the QIAquick DNA Purification Kit

(Qiagen) following the manufacturer's recommended protocol. The DNA samples were stored at -20°C until their intended use.

The filter membranes were processed to extract DNA, which was subsequently analysed by LAMP amplification to estimate the CYP450/*dabD* copy numbers in the collected seawater. The LAMP method, which provided greater accuracy and linearity in comparison to the RPA assay when using DNA plasmid standards, was exclusively employed for the analysis of the collected seawater samples. The DNA plasmid standards synthesised in section 4.3.5 were employed to extrapolate the number of template sequence copies in each sample through simple linear regression analysis of line fitted to the standard curve data points. The averaged time threshold T_t values were obtained from triplicate independent LAMP reactions for each water sample. Full details of the sampling routine are provided in Table C1 in Appendix C.

4.4 Results and Discussion

Isothermal amplification methods have been widely used for the rapid and accurate detection of HAB species (Toldra et al. 2019). Among those isothermal techniques, the RPA method can amplify both DNA and RNA target sequences at a low and constant temperature of 37ºC, employing an enzyme mixture consisting of recombinase and exonuclease polymerase with two target-specific primers (Piepenburg et al. 2008). Real-time detection of RPA amplicons can be achieved by the incorporation of fluorogenic exo-probe in the reaction mixture (Lobato and O'Sullivan 2018). The RPA method has previously demonstrated high analytical performance for specifically amplifying low quantities of HAB target sequences from mixed genetic material. For example, the RPA technique has been used to detect toxic marine microalgae *Karlodinium veneficum, Karlodinium armiger, and Chattonella marina* (Toldra et al. 2018, Zhang et al. 2022a). While the real-time RPA method offers the advantage of highly sensitive and inclusive quantification of HABs' genetic targets, developing a real-time RPA assay demands substantial design expertise and time-consuming steps to incorporate complex nucleotide modifications into the oligonucleotide sequence of the exo-probe (Daher et al. 2016). Subsequently, the generation of a fluorometric exo-probe will involve costly and time-consuming synthesis procedures. Although the specific amplification chemistry of exo-probe offers a targeted detection of DNA sequences, the inherent binding and extension process could potentially delay the positive

amplification results, especially when amplifying low target copy numbers from complex samples containing diverse genetic pools (Lobato and O'Sullivan 2018). Therefore, the use of exo probes in RPA reactions necessitates extra time for optimisation and labour-intensive procedures to adjust the reaction conditions to ensure optimal performance.

Alternatively, the LAMP method offers a simpler and more rapid amplification process catalysed by a single polymerase enzyme responsible for both strand extension and displacement (Moehling et al. 2021). Several LAMP assays have been developed for quantifying HAB-forming microalgal species including *Karenia mikimotoi* (Wang et al. 2020c), *Karlodinium veneficum* (Huang et al. 2017a), *Alexandrium catenella* and *Alexandrium minutum* (Zhang et al. 2012), and *Prorocentrum minimum* (Zhang et al. 2014a). The specific LAMP amplification is supported by a set of six primers that are designed to anneal with six distinct fragments of the target sequence. As a result, the high specificity of LAMP primers enables their application in the detection of the target sequence from mixed and complex genetic samples. In contrast, some isothermal techniques lack such tolerance to complex DNA matrices in environmental samples. For instance, a NASBA assay was developed to amplify the rubisco small subunit (*rbsc*) mRNA transcript of viable cells from *Pseudo-nitzschia multiseries* (Delaney 2010). However, this method showed reduced specificity due to the relatively low reaction temperature (41°C), resulting in false-positive results when assayed the related *Pseudo-nitzschia* species (Delaney 2010). The loss of enzymatic activity of NASBA enzymes can be caused by inhibitors present in environmental samples of RNA transcripts (Delaney 2010). The inhibition of the NASBA reaction could be also associated with the secondary structure formations between primer and molecular beacon, leading to oligonucleotide depletion during the amplification reaction. The reverse transcription loop-mediated isothermal amplification (RT-LAMP) method has demonstrated the successful detection of RNA sequences extracted from *Prorocentrum donghaiense* microalgae (Chen et al. 2013). A limitation of the LAMP methodology is the potential inhibition of amplification due to the formation of secondary structures among the multiple LAMP primers (Huang et al. 2022). To obviate this constraint, careful design considerations should be given to avoid regions in the target sequence that contain a likelihood of dimer formation in LAMP primers (Shirshikov and Bespyatykh 2022). In addition, meticulous optimisation of LAMP conditions can ensure an efficient LAMP amplification.

Therefore, when designing RPA and LAMP assays, regions with excessive palindromic and extreme GC content sequences were avoided here to reduce the potential for secondary structure formation. Both RPA and LAMP assays were designed to target a sequence of minimal repeated stretches within the cytochrome P450 (CYP450, *dabD*) gene. The biosynthesis of domoic acid was recently described by (Brunson et al. 2018). This gene was selected as the target for the specific detection of *Pseudo-nitzschia* species. The *dabD* gene encodes the cytochrome P450 (CYP450) enzyme, which catalyses a key biosynthetic step to yield the domoic acid (DA) (Brunson et al. 2018). In addition to its essential role in DA synthesis, this target gene is unique to *Pseudo-nitzschia* and absent in other microalgal species (Steele et al. 2022). Assessing the activity or abundance of such target genes through isothermal assays can offer rapid and valuable insights into the ecological risk of this neurotoxin in the marine environment.

4.4.1 Development of RPA and LAMP Isothermal Assays for *Pseudo-nitzschia spp.* Detection

For the detection of *Pseudo-nitzschia* species, RPA and LAMP DNA-based amplification methods were developed. The RPA and LAMP oligonucleotides flanked a consensus region of a total of 269 base pairs with a pairwise identity of 76% (Figure 4.2). Table 4.2 contains the ID numbers and functional annotations corresponding to the *Pseudo-nitzschia* sp sequences that were employed to determine the consensus target sequence. The consensus sequence obtained from the alignment analysis was employed for the design of the LAMP assay. The designed oligonucleotides shared approximately 77.4% identity with all *P. multistriata cytochrome P450* sequences (Figure 4.2). Likewise, when comparing the *CYP450* (*dabD*) sequences of *Pseudo-nitzschia multiseries* isolate 15091C3 (NCBI Gene ID: MH202990) with those of *Pseudo-nitzschia multistriata* from (Brunson et al. 2018), a complete identity was not achieved, showing a pairwise identity of 83%. Nevertheless, both sequences from *P. multistriata* and *P. multiseries* were included to establish a local database for conducting alignment analysis. As a result, a consensus sequence was generated, covering the genetic diversity of the target cytochrome P450 (*dabD*) gene within the *Pseudo-nitzschia* genome, and served as a target for RPA and LAMP assay.

A novel RPA assay was developed on the consensus sequence obtained from the alignment analysis for the amplification of the *cytochrome P450 dabD* target, a toxin-encoding gene. Five sets of primers were designed for RPA assay using the 'Primer3' tool on Geneious R11 Bioinformatics Software (Biomatters Ltd, Auckland, NZ). During the screening of RPA primers, challenges were encountered related to the length of the primers (30-35bp), which increased the likelihood of hetero- and self-dimerisation. Out of the five primer sets initially designed, only three sets showed successful amplification. The primer sets designed for RPA amplification in this study can be found in Appendix C, Table C2. To avoid further dimerisation issues, an additional screening step was performed using the 'Oligo Analyser' (https://eu.idtdna.com/calc/analyzer) to design the exo-probe. The selection process involved identifying exo-probe candidates with low self-affinity under predicted reaction conditions, and the probe with the lowest folding score was chosen for optimising real-time RPA amplification assay.

LAMP primers were designed to target six distinct regions of the cytochrome P450 (*dabD*) gene in *P. multistriata* (Figure 4.2). Table 4.1 provides a list of the LAMP primers. BLASTN analysis was initially conducted against the *P. multistriata* genome available at http://protists.ensembl.org/Pseudonitzschia_multistriata/Tools/Blast. To validate the specificity of the target region used for LAMP primer design, all the available sequences of the cytochrome P450 (*dabD*) gene were downloaded and aligned with the sequences of the *dabD* gene of the *P. multiseries* isolate 15091C3 (GenBank: MH202990) to reveal conserved regions for the primer set's binding regions. The alignment analysis suggested percentage identities for the LAMP primer binding sites: 77.9% for LAMP-F3, 77.4% for LAMP-B3, 73% for LAMP-FIP, 77.8% for LAMP-BIP, 74.3% for LAMP-LF, and LAMP-LB demonstrated the highest percentage identity of 81.3% (Figure 4.2). A concentration of 0.8 µM of LP/LF loop primer pair was selected for further LAMP experiments based on gel electrophoresis analysis that yielded the correct product size and generated the highest fluorescence signals (Figure 4.5).

Table 4.1 LAMP and RPA oligonucleotides were designed and used in this study.

Primer name	Sequence (5' --- 3')
RPA_fw_primer	GCATGTATCCCCAGCCGCCCCTCTTGATTC
RPA_rv_primer	ATCTCGTTCGGGTACAGCATTTTTGACCACTTTAC

RPA_exoprobe	GCCTATTCACTTGATTCATAGACATCCTGA-[FAM-dT]C[THF]T[BHQ1-dT]-GGAAGGACCCCGAAG-[C3-spacer]
LAMP-F3_primer	CGGAAAACACCATGCCCAA
LAMP-B3_primer	TCTCGTTCGGGTACAGCA
LAMP-FIP_primer	GGCCAGAACCTTTCGTCTCTGTCAAGGGTGATTCGGGGAATG
LAMP-BIP_primer	AATCCCGACACTTTCGATCCCGTCGAAGCCCTTCCAGTCTG
LAMP-LB_primer	GGTTCACCCGACCCTACAAGA
LAMP-LF_primer	ATATTGTACAAGGGCAAAAAGATGT

FAM-dT, Fluorescein modified deoxythiamine; BHQ1-dT, Black Hole Quencher 1 modified deoxythiamine; THF, tetrahydrofuran; C3-spacer, phosphate group.

To evaluate potential secondary structures among LAMP primers, the Oligo Analyser folding tool (https://eu.idtdna.com/calc/analyzer) and PrimerExplorer™ V5 software (Eiken Chemical Co., Ltd., Tokyo, Japan) were employed. With a focus on the 3' end regions, as they are critical in promoting stable binding and elongation during the amplification process, achieving specific LAMP amplification (Shirshikov and Bespyatykh 2022). The selection of potential LAMP primer candidates was guided by a Gibbs free energy (ΔG) threshold of -7 kcal/mol. This criterion was employed to prevent mispriming among the six LAMP primers during the amplification process (Rychlik 1995). Therefore, primer pairs with lower ΔG values, which could result in thermodynamically stable heterodimers and non-specific LAMP products, were excluded. This strategy effectively prevented the formation of heterodimers, thus ensuring efficient and specific LAMP amplification (Figure 4.7).

-

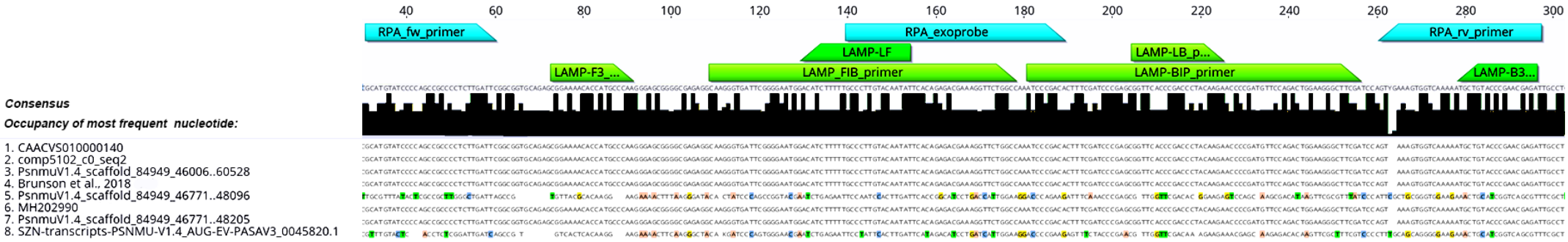

Figure 4.2 Multiple Sequence Alignment of the *P. multistriata Cytochrome CYP450 dabD* gene sequences, revealing binding sites for the oligonucleotides used in the isothermal assays of LAMP (green annotations) and RPA (blue annotations).

Table 4.2 List of *Cytochrome CYP450 dabD* gene sequences obtained from *Pseudo-nitzschia* genomes.

Species	Strain	Accession Number	Functional annotation	Source
P. multistriata	B856	CAACVS010000140	Cytochrome CYP450	Ensembl Protists [a]
P. multistriata	B857	PSNMU-V1.4_AUG-EV-PASAV3_0045820.1	Cytochrome CYP450	SZN [b]
P. multiseries	15091C3	MH202990	Cytochrome CYP450	SZN [b]
P. multistriata	N/A	Brunson et al., 2018	Cytochrome CYP450	(Brunson et al. 2018)
P. multistriata	B939	PsnmuV1.4_scaffold_84949_46006..60528	Cytochrome CYP450	(Basu et al. 2017)
P. multistriata	B936	PsnmuV1.4_scaffold_84949_46771..48096	Cytochrome CYP450	(Basu et al. 2017)
P. multistriata	B856	PsnmuV1.4_scaffold_84949_46771..48205	Cytochrome CYP450	EarlHam [d]
P. multistriata	B936	comp5102_c0_seq2	Cytochrome CYP450	(Di Dato et al. 2015)

[a] Ensembl Protists; European Nucleotide Archive for Protist Genomes, [b] SZN; Genome database of the Stazione Zoologica Anton Dohrn, [c] NCBI; National Centre for Biotechnology Information GenBank, [d] EarlHam; The genome portal of the Earlham institute, UK.

Table 4.3 The hits of BLAST analysis for consensus region spanning both RPA and LAMP amplicons.

				BLASTN		
Species	**Strain**	**Percent Identity**	**E- value**	**Score**	**Accession Number**	**Source**
P. multistriata	B856	100%	2.7e-145	259	PSNMU_V1.4_AUG-EV-PASAV3_0045820	Ensembl Protists [a]
				BLASTX		
P. multistriata	B856	100%	4.9e-60	86	VEU37775	Ensembl Protists [a]
P. multistriata	B856	53.8%	3.1e-20	52	VEU41686	Ensembl Protists [a]
P. multistriata	B856	43.3%	0.001	30	VEU45241	Ensembl Protists [a]
P. multistriata	B856	33.3%	0.02	39	VEU36549	Ensembl Protists [a]
P. multistriata	B856	36.1%	0.04	36	VEU36302	Ensembl Protists [a]
P. multistriata	B856	61.1%	3.1e-20	18	VEU41686	Ensembl Protists [a]
P. multistriata	B856	37.9%	0.06	29	VEU44693	Ensembl Protists [a]

[a] Ensembl Protists; European Nucleotide Archive for Protist Genomes.

Due to the limited availability of annotated *dabD* sequences specific to the *Pseudo-nitzschia multistriata* in the National Centre for Biotechnology Information (NCBI, release date: 25 July 2023), the target fragment was compared that spanned a 259 bp across LAMP and RPA amplicons against ENSMBL Protist genome repository using both BLASTN and BLASTX analysis following default settings(http://protists.ensembl.org/Pseudonitzschia_multistriata/Tools/Blast).The BLASTN results revealed significant homologous matches with the PSNMU_V1.4_AUG-EV-PASAV3_0045820 gene of the Cytochrome P450 in *Pseudo-nitzschia multistriata* (Table 4.3). Furthermore, BLASTX results showed that protein products derived from a 259 bp consensus sequence exhibited 100% similarity to the complete Cytochrome P450 protein in *P. multistriata* of *the* ENSMBL Protist genome database. Despite the limited genetic information available on the species-specific DabD protein in the *P. multistriata* SZN-B954 strain, a bioinformatic search was undertaken to identify the domain composition of the protein of isothermally amplified products of the LAMP and RPA assays using the NCBI tool of the Conserved Domain Database (CDD) (Marchler-Bauer et al. 2017). The results revealed that the 259 bp consensus sequence displayed an identical domain structure to the annotated Cytochrome P450 protein under NCBI accession number: cl41757. The Cytochrome P450 (*dabD*) gene was found to play a crucial role in the biosynthesis of domoic acid within the *P. multiseries* species (Brunson et al. 2018).

4.4.2 RPA Assay Optimisation

To identify optimal RPA primer combinations, 25 primer combinations from the RPA primers listed in Table C2 in Appendix C were tested for the amplification of the target gene in *Pseudo-nitzschia spp*. The RPA amplified products were detected using gel electrophoresis as shown in Figure 4.3.

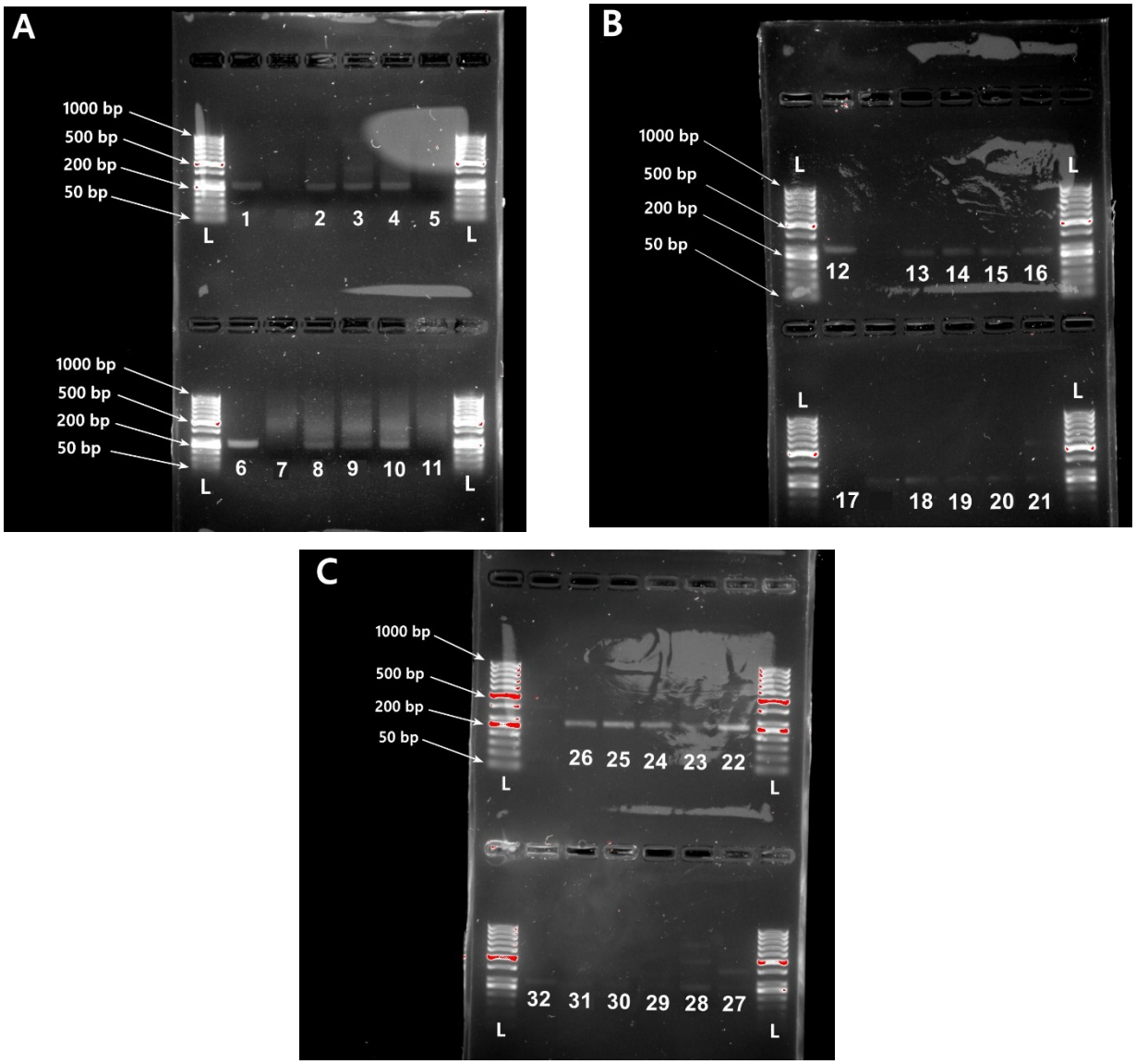

Figure 4.3 Gel Electrophoresis results of RPA primer screening experiment. The RPA-amplified products were purified prior to electrophoresis analysis. Panels A: C shows Lane L: 50 bp DNA ladder, Lane 1, Positive control; Lane 2, Primer Mix 1; Lane 3, Primer Mix 2; Lane 4, Primer Mix 3; Lane 5, Primer Mix 4; Lane 6, Positive control; Lane 7, Primer Mix 5; Lane 8, Primer Mix 6; Lane 9, Primer Mix 7; Lane 10, Primer Mix 8; Lane 11, Primer Mix 9; Lane 12, Positive control, Lane 13, Primer Mix 10; Lane 14, Primer Mix 11; Lane 15, Primer Mix 12; Lane 16, Primer Mix 13; Lane 17, Primer Mix 14; Lane 18, Primer Mix 15; Lane 19, Primer Mix 16; Lane 20, Primer Mix 17; Lane 21, Primer Mix 18; Lane 22, Positive control; Lane 23, Primer Mix 19; Lane 24, Primer Mix 20; Lane 25, Primer Mix 21; Lane 26, Primer Mix 22; Lane 27, Primer Mix 23; Lane 28, Primer Mix 24; Lane 29, Primer Mix 25; Lane 30-32, Negative control.

Only eleven primer combinations generated positive and specific RPA amplification as well as control reactions (Figure 4.3). None of the negative control reactions produced an amplicon using nuclease-free water. Based on gel band intensity and the concentrations (ng/µl) of the RPA amplified products, three combinations of forward and reverse primers (Primer Mix 3, Primer Mix 21, and Primer Mix 22) were chosen for the subsequent optimisation with the designed RPA exo-probe, which can be detected in real-time via fluorescence. The optimal RPA primers and exo-probe enabled the successful amplification of the target gene (Figure 4.4B). Further experiments to optimise conditions of real-time RPA reaction. Details of the optimal combination of RPA primers and probes can be found in Table 4.1. Among the various reaction temperatures tested varying from 36°C to 40°C, the highest amplification yield was obtained at 37°C , the shortest time of amplification onset, and the most significant change in fluorescence signals.

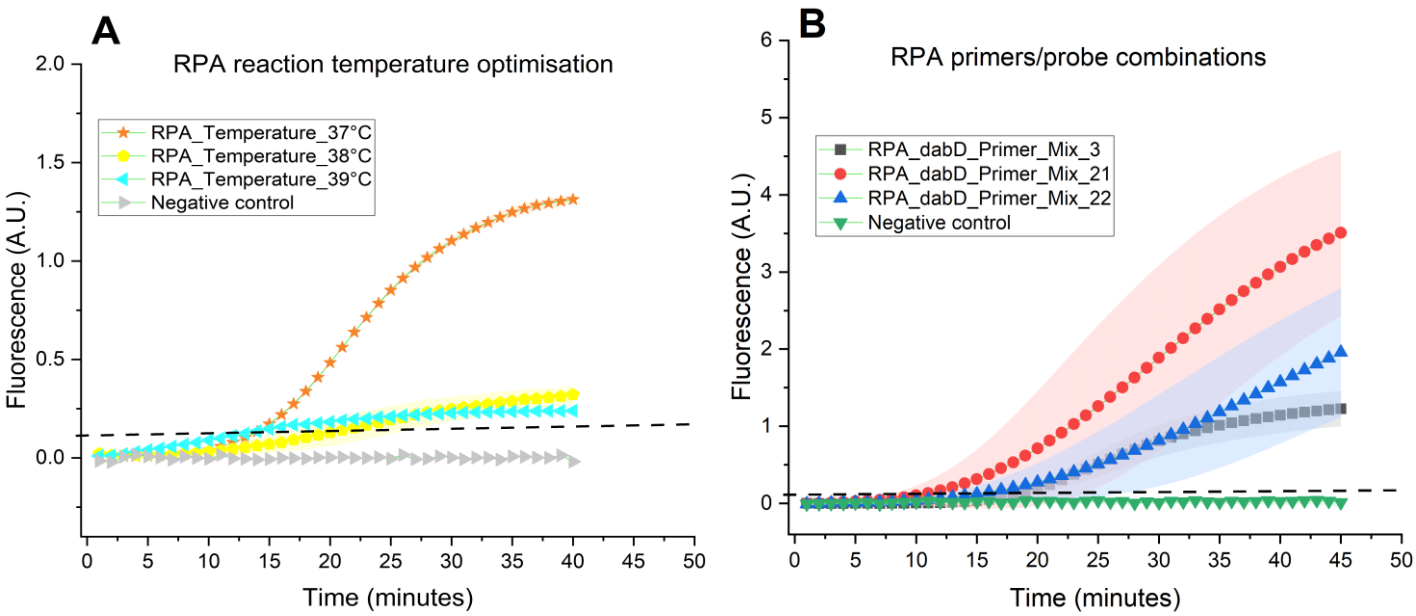

Figure 4.4 Optimisation of RPA amplification for the *cytochrome P450 (dabD)* gene. A) The RPA results were obtained from three different reaction temperatures. B) RPA results obtained with various primer combinations combined with the RPA exo probe. The threshold background level is represented by the dashed line.

A threshold level is set automatically by a thermocycler instrument (LightCycler 96, Roche), above the background fluorescence baseline to avoid premature amplifications occurring in the background fluorescence range. All the real-time RPA reactions were positive and exceeded the fluorescence detection threshold of the average background signal at 0.004 (Figure 4.4). An accurate threshold level is imperative for the reliable calculation of the time threshold value when the fluorescence of the RPA amplification reaction rises above the background threshold level (Lobato and O'Sullivan 2018). Using the time threshold value, the time taken for each primer/exo-

probe combination to reach the threshold fluorescence value was compared . Among the combinations, the RPA reaction mixture containing the second primer/exo-probe combination (Primer Mix 2) at the reaction temperature of 37°C yielded the lowest time threshold value, with detectable fluorescence signals achieved in 15.0 ± 1.6 minutes and saturated at 3.5 ± 1.1 (A.U.). This combination was selected for downstream analysis. Details of the optimal primer/exo-probe combinations for the RPA assay are presented in Table 4.1.

4.4.3 LAMP Assay Optimisation

All LAMP reactions were performed at a relatively high annealing temperature of 65ºC, to facilitate the denaturation of any potential secondary structures, hairpins, and self-dimers among LAMP primers. This approach significantly contributed to robust, accurate and efficient amplifications during subsequent optimisation efforts. Loop primers served as the “core” primers that directly govern the performance of amplification reaction, enabling highly efficient LAMP assays (Shirshikov and Bespyatykh 2022). Efficient annealing of loop primers with target sequence leads to the creation of single-stranded loop structures that act as substrates for initiating the first stage of the LAMP amplification process (Shirshikov and Bespyatykh 2022). Therefore, a concentration gradient of LAMP Loop primers varying from 0.4, 0.8, to 1 µM, was tested to determine the optimal reaction condition for LAMP amplification. These primer mixtures were formulated by incorporating the varied loop primer concentrations (Loop F & Loop B) with inner primers (FIP & BIP), and outer primers (F3 & B3) at concentrations of 1.6 µM and 0.2 µM, respectively. All primer combinations consistently generated positive results, successfully yielding specific amplification products (Figure 4.5). To assess the inhibitory effects of primer mixtures on the LAMP run, triplicate negative control reactions (No template control; NTC) were included. None of the reaction mixtures within the NTC replicates generated any amplification product.

To quantify the performance of each primer combination, the time to threshold (T_t) value was determined across all replicates of the reactions, and the results were presented as the mean ± standard deviation (SD) (Table 4.4). The T_t value is defined by the time at which the fluorescence signal crosses the threshold fluorescence level during the LAMP amplification (Diego et al. 2019). Among the tested primer combinations, primer mix 3 yielded the lowest T_t value at 14.3 ± 0.3, indicating the fastest LAMP amplification. This T_t value was accompanied by a high fluorescence signal observed at 14.9 ± 0.4 (A.U.) during the late phases of the LAMP reaction. The on-target amplification at the tested primer concentrations was further confirmed through gel electrophoresis analysis of all LAMP amplicons (Figure 4.5B).

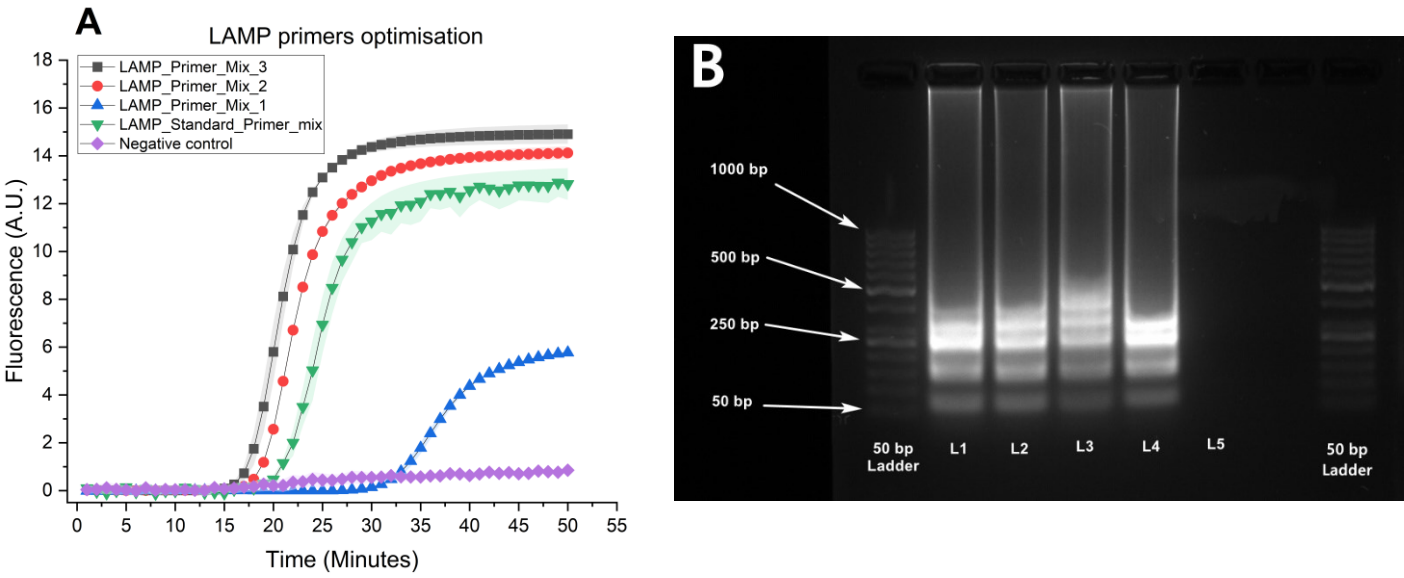

Figure 4.5 LAMP reaction optimisation A) Fluorescence results of amplification using varying LAMP primer concentrations. B) Gel electrophoresis results confirm the specificity of LAMP-amplified products through different primer concentration combinations. The gel includes a 50 bp DNA ladder, L1 lane: control or standard concentration of LAMP primers, L2 lane: primer mix 1, L3 lane: primer mix 2, L4 lane: primer mix 3, L5 lane: NTC.

Table 4.4 LAMP amplification results with varying primer concentrations.

	Standard Primer Mix	Primer Mix 1	Primer Mix 2	Primer Mix 3
T_t value	16.9 ± 0.7	28.4 ± 0.5	15.6 ± 0.2	14.3 ± 0.3
Fluorescence end-point	12.8 ± 0.7	5.8 ± 0.06	14.1± 0.3	14.9 ± 0.4

4.4.4 Specificity Testing of RPA and LAMP Assays

The inclusivity of the newly developed RPA and LAMP assays was evaluated by employing an inclusivity panel comprising 10 different *Pseudo-nitzschia* species, with an exclusivity panel consisting of 8 non-target microalgal strains, as detailed in Table 4.5. The LAMP reactions

consistently and accurately detected all tested *Pseudo-nitzschia* strains, demonstrating 100% analytical specificity without any cross-amplification against other algal strains (Figure 4.7). On the other hand, the RPA reaction demonstrated a 90% identification efficiency for *Pseudo-nitzschia*, with no amplification observed for the *P. pungens* strain and other microalgae (Figure 4.6B). The specificity of RPA products was confirmed through the assessment of the specific fluorescence signals from the exo-probe (Figure 4.6). Similarly, the verification of LAMP amplified products was accomplished using fluorescence measurements, as well as through 2% agarose gel electrophoresis analysis (Figure 4.7).

The melting curve analysis revealed specific LAMP products characterised by consistent melting temperature centred at Tm= 88 ± 0.08 °C (Figure 4.7C) and Tm= 87.9 ± 0.2 °C (Figure 4.7D). Additionally, specific bands at 222 bp were exclusively observed, confirming the 100% inclusivity of LAMP assay for testing *Pseudo-nitzschia* strains, while no bands were detected in other microalgal strains (Figure 4.7E & Figure 4.7F). Likewise, RPA fluorescence measurements indicated the absence of cross-amplification against other microalgal strains (Figure 4.6). Interestingly, all tested *Pseudo-nitzschia* strains have positive results for DA according to the ELISA analysis. However, the detected concentrations ranged widely from 3.8 to 172.3 µg L^{-1}, which corresponded to 4.3 to 2.4 pg DA $cell^{-1}$, observed for *P. pungens* and P. multiseries ML-59, respectively. In contrast, neither DA nor the *dabD* target was detected in any of the non-*Pseudo-nitzschia* algal cultures. The results of the DA immuno-assay and the selectivity evaluation of LAMP and RPA methods are presented in Table 4.5.

Table 4.5 LAMP and RPA results for a set of *Pseudo-nitzschia* target species and closely related microalgal species. The concentration of domoic acid (pg DA $cell^{-1}$) was measured through the ELISA method for all tested strains.

Species	Isolate Accession	DA Concentration (pg DA $cell^{-1}$)	LAMP Amplification	RPA Amplification
Pseudo-nitzschia multistriata	SZN-B954	2.4 ± 0.01	+	+
Pseudo-nitzschia multistriata	SZN-B955	4.1 ± 0.09	+	+
Pseudo-nitzschia pungens	CCAP 1061/44	0.1 ± 0.001	+	-
Pseudo-nitzschia multiseries	NWFSC 713	3.4 ± 0.1	+	+
Pseudo-nitzschia multiseries	NWFSC 714	3.6 ± 0.1	+	+
Pseudo-nitzschia multiseries	NWFSC 715	1.5 ± 0.01	+	+
Pseudo-nitzschia multiseries	ML-54	1.8 ± 0.06	+	+
Pseudo-nitzschia multiseries	ML-55	1.2 ± 0.01	+	+
Pseudo-nitzschia multiseries	ML-56	1.4 ± 0.02	+	+
Pseudo-nitzschia multiseries	ML-59	4.3 ± 0.2	+	+
Karenia brevis	CCMP2228	nd	-	-
Karenia mikimotoi	CCAP 1127/2	nd	-	-

Alexandrium tamarense	CCAP 1119/25	nd	-	-
Synechococcus sp	CCAP 1479/9	nd	-	-
Prorcentrum lima	CCAP 1136/12	nd	-	-
Alexandrium minutum	CCAP 1119/15	nd	-	-
Lingulodinium polyedra	CCAP 1121/7	nd	-	-
Prorcentrum cordatum	CCAP 1136/16	nd	-	-

(+) positive amplification, (-) no amplification, nd = not detected.

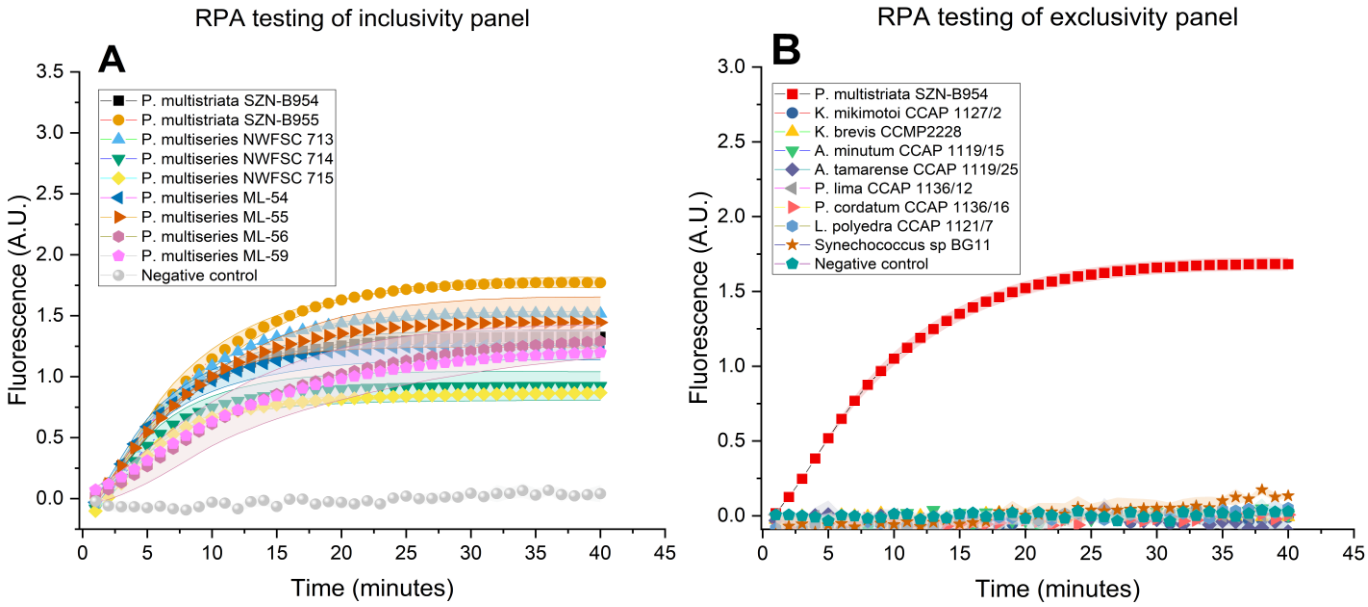

Figure 4.6 The specificity of real-time RPA amplification was evaluated through an inclusivity set of *Pseudo-nitzschia* strains (A) and the exclusivity set containing other algal species (B). The strains tested in each panel are outlined in Table 4.5. Each amplification curve represents the average of two independent measurements. The shaded regions within the amplification curves indicate the standard error of the averaged measurement.

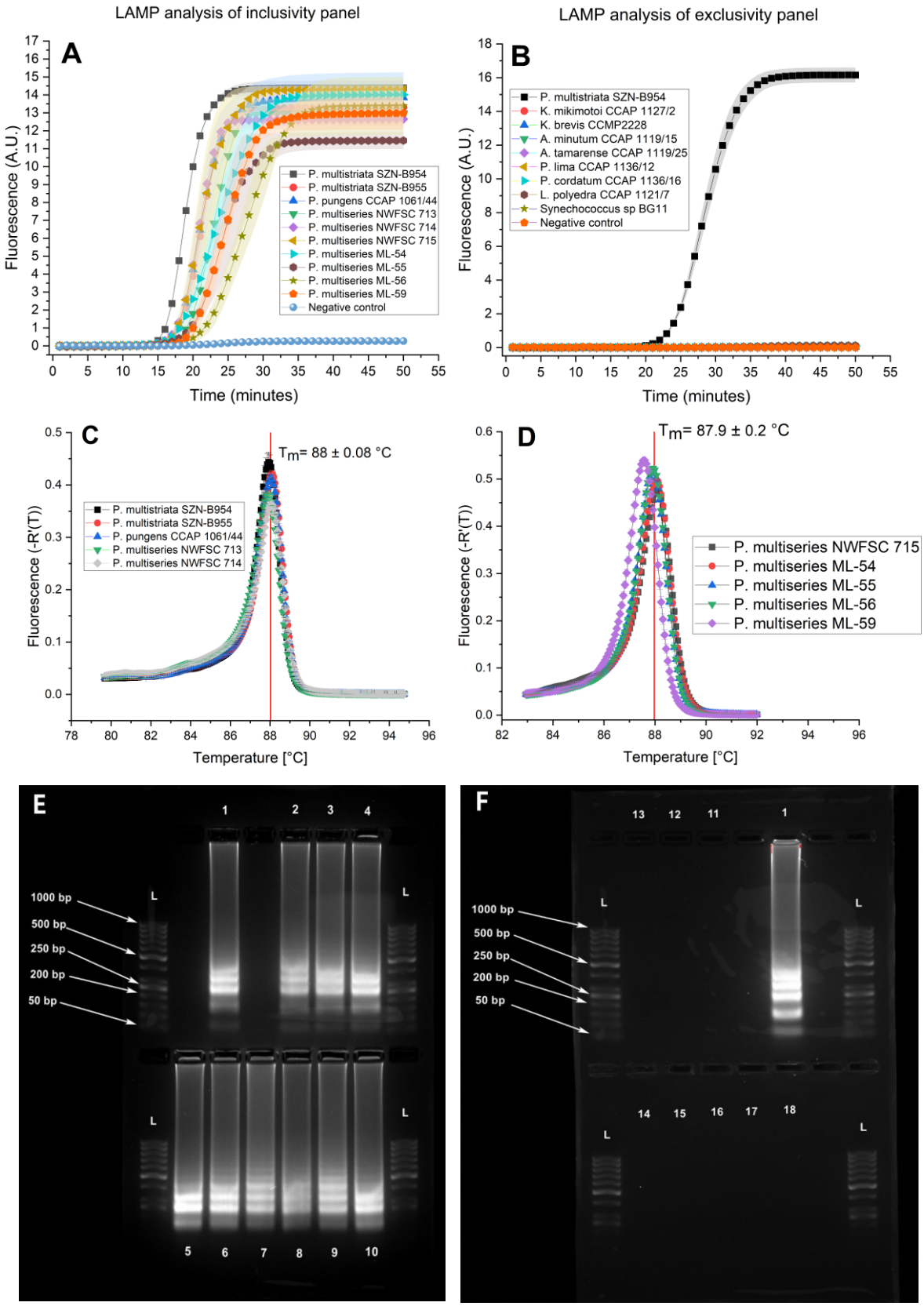

Figure 4.7 Evaluating the specificity of the LAMP assay. The LAMP reactions employed DNA samples isolated from *Pseudo-nitzschia* strains (Panel A) and closely related algal species (Panel B). The LAMP products obtained from the amplifications in Panels A and B were subjected to subsequent analyses using melting curve analysis (Panels C and D) and gel electrophoresis

(Panels E and F). Melting curve analysis was performed on the LAMP-amplified products from *Pseudo-nitzschia* strains (n=10) (Panels C and D). The vertical lines represent the mean specific melting temperature values derived from triplicate LAMP amplicons for each taxon. The melting curve error bars indicate the standard deviation (n=3). Gel electrophoresis of the LAMP amplicons (Panels E and F) confirms the on-target amplification, with Panel E, Lane 1, *P. multistriata* SZN-B955; Lane 2, *P. multistriata* SZN-B954; Lane 3, *P. pungens* CCAP 1061/44; Lane 4, *P. multiseries* NWFSC 713; Lane 5, *P. multiseries* NWFSC 714; Lane 6, *P. multiseries* NWFSC 715; Lane 7, *P. multiseries* ML-54; Lane 8, *P. multiseries* ML-55; Lane 9, *P. multiseries* ML-56; Lane 10, *P. multiseries* ML-59. Panel F shows gel results of Lane 11, *K. brevis* CCMP2228; Lane 12, *K. mikimotoi* CCAP 1127/2; Lane 13, *A. tamarense* CCAP 1119/25; Lane 14, *A. minutum* CCAP 1119/15; Lane 15, *P. lima* CCAP 1136/12; Lane 16, *P. cordatum* CCAP 1136/16; Lane 17, *L. polyedra* CCAP 1121/7; Lane 18, *Synechococcus sp* BG11; lane L, 50 bp DNA ladder.

4.4.5 Sensitivity and Rapidity Testing of RPA and LAMP Assays

The sensitivity of LAMP and RPA assays was evaluated by generating standard curves through the amplification of the same tenfold dilutions of linearised plasmids containing the target insert, spanning known concentrations from 1 to 10^7 copies μl^{-1}. The LAMP assay revealed a higher sensitivity in comparison to the RPA assay (Figure 4.8 & Figure 4.9). The efficiency of RPA and LAMP quantifications was revealed by exploring the linear relationship between the threshold time (T_t) values (analogous to the threshold cycle in real-time PCR) of the fluorescence amplification plots (Figure 4.8) and the logarithmic value of the target sequence concentration (Figure 4.9). The quantification of RPA standards resulted in R-squared value (R^2) of 0.8, reflecting a steep regression line with a slope of -1.9, leading to a weaker linear correlation and subsequently lower quantification efficiency. As a result, the detection limit increased to 10^3 copies μl^{-1} for RPA quantification. This could result from the variability in the enzyme kinetics of the three enzymes involved in the RPA reaction, which may compromise the sensitivity and robustness of RPA quantification (Li et al. 2019a).

In contrast, the LAMP reaction employs a single DNA polymerase for strand displacement, enabling DNA synthesis from both single- and double-strand DNA templates through the annealing of 6 primers at multiple sites (Shirshikov and Bespyatykh 2022). Therefore, the LAMP amplification relies on a single enzymatic activity, in combination with the optimal primer concentration and a constant reaction temperature. Consequently, LAMP demonstrated higher efficiency in terms of both detection time and sensitivity when compared to the RPA assay. The LAMP quantification of standards showed a stronger linear correlation (R^2 = 1.0), the limit of detection at a single copy level, improving its sensitivity to 100-fold higher than RPA quantification. LAMP detected 10^3 copies

μl^{-1} within 14.0 minutes, while RPA required 34.5 minutes to quantify the same target concentration.

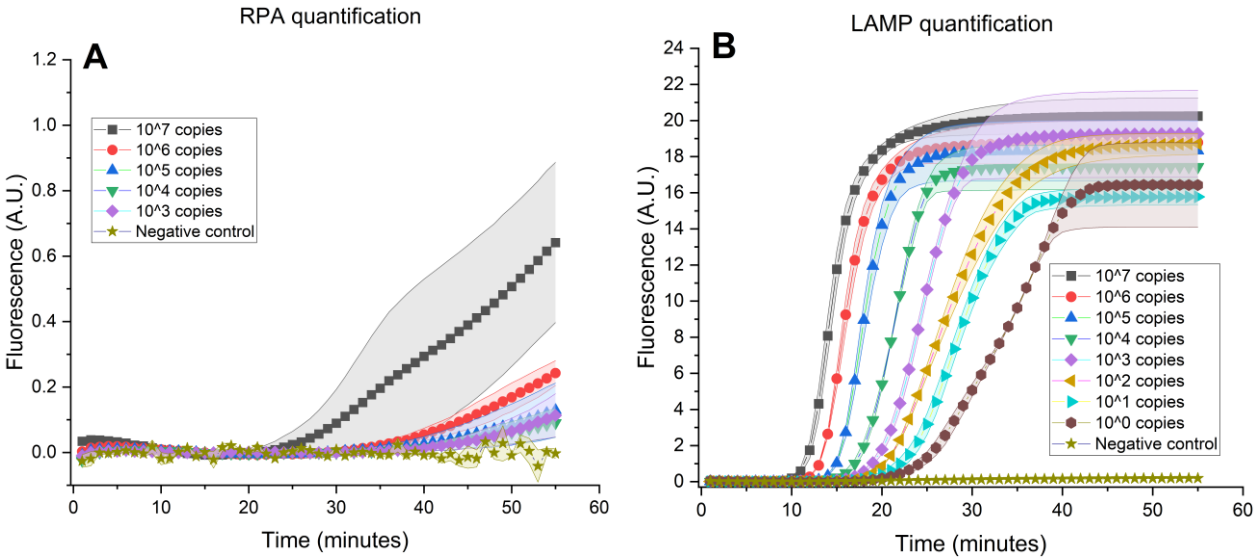

Figure 4.8 Amplification plot of RPA (A) and LAMP (B) using serial dilutions of CYP450 DNA standard plasmids, ranging from 1 to 10^7 copies μl^{-1}.

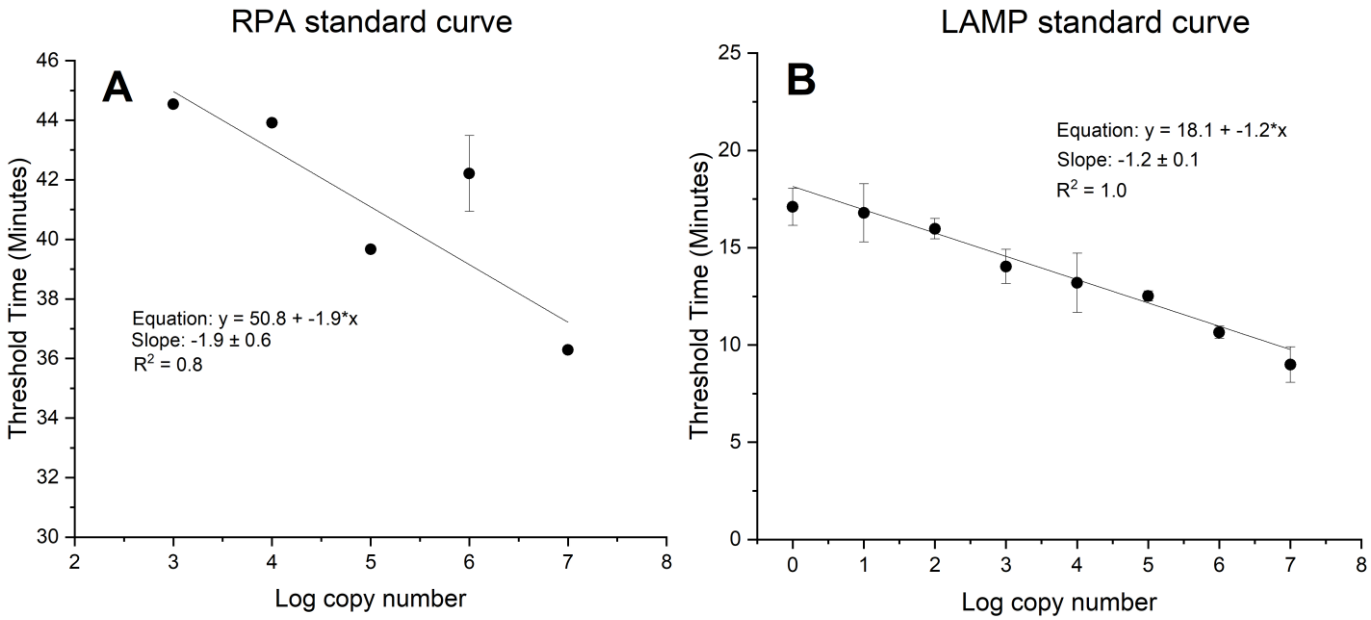

Figure 4.9 A comparison of RPA (A) and LAMP (B) quantification for CYP450 DNA standard plasmid dilutions, spanning from 1 to 10^7 copies μl^{-1} across three independent assays. The standard curves show the mean threshold time values versus the template copy number. The error bars indicate the standard error of the mean derived from triplicate reactions.

4.4.6 LAMP Analysis of Environmental Samples

Comparing the quantification performance through RPA and LAMP analyses suggested that LAMP provides a more precise method for determining DNA copy numbers. The fitting of a linear trendline to the logarithmic plot of the target copy number against the time threshold (T_t) value of the LAMP assay yielded R^2 values exceeding 1.0. In contrast, the linearity of the relationship within the RPA dataset decreased to 0. 8, indicating a reduction in the sensitivity and efficiency of the RPA assay. As a result, the LAMP method was adopted for quantifying the unknown copy numbers of the target gene from the processed seawater samples through a series of LAMP reactions.

For the first time, the LAMP technique was employed for a time-series measurement of *Pseudo-nitzschia* spp. within a field survey in this region. The LAMP assay was successfully tested in three coastal shellfish production areas, demonstrating its effectiveness in early detection of Harmful Algal Blooms (HABs). This capability is crucial for protecting public health and the shellfish industry. The LAMP-based quantification involved 44 seawater samples to estimate copy numbers per microlitre from September 2021 to March 2022 at three coastal sites in Southwest England (Figure 4.10).

Pseudo-nitzschia spp. has previously been identified in the studied region of Southwest England, even outside of bloom events (Downes-Tettmar et al. 2013). Among the 44 samples, the CYP450 LAMP assay yielded positive results in 34 samples (sensitivity = 77.3%). The estimated CYP450 copy numbers spanned a range, with the lowest value at 0.1 ± 1.1 copies/µl in samples collected between January and March, and the highest, around 5.1 ± 0 estimated copies/µl, recorded at the Porthallow site in mid-January. The levels of CYP450 copy numbers were highest in the early phase of the study, spanning from September to January. Towards the end of the study (late March), the LAMP tests revealed an increase in estimated copy numbers, ranging from 3.9 ± 0.2 to 4.9 ± 0 copies μl^{-1} across all sites.

Pseudo-nitzschia copy numbers followed a consistent pattern across all study sites, increasing during the beginning and end of the study, coinciding with elevated sea temperatures and sunlight intensity (Brown et al. 2022). An increase in estimated copy numbers was observed at all sites from late February, suggesting the onset of a potential 'spring' bloom. The only exception was the Outer

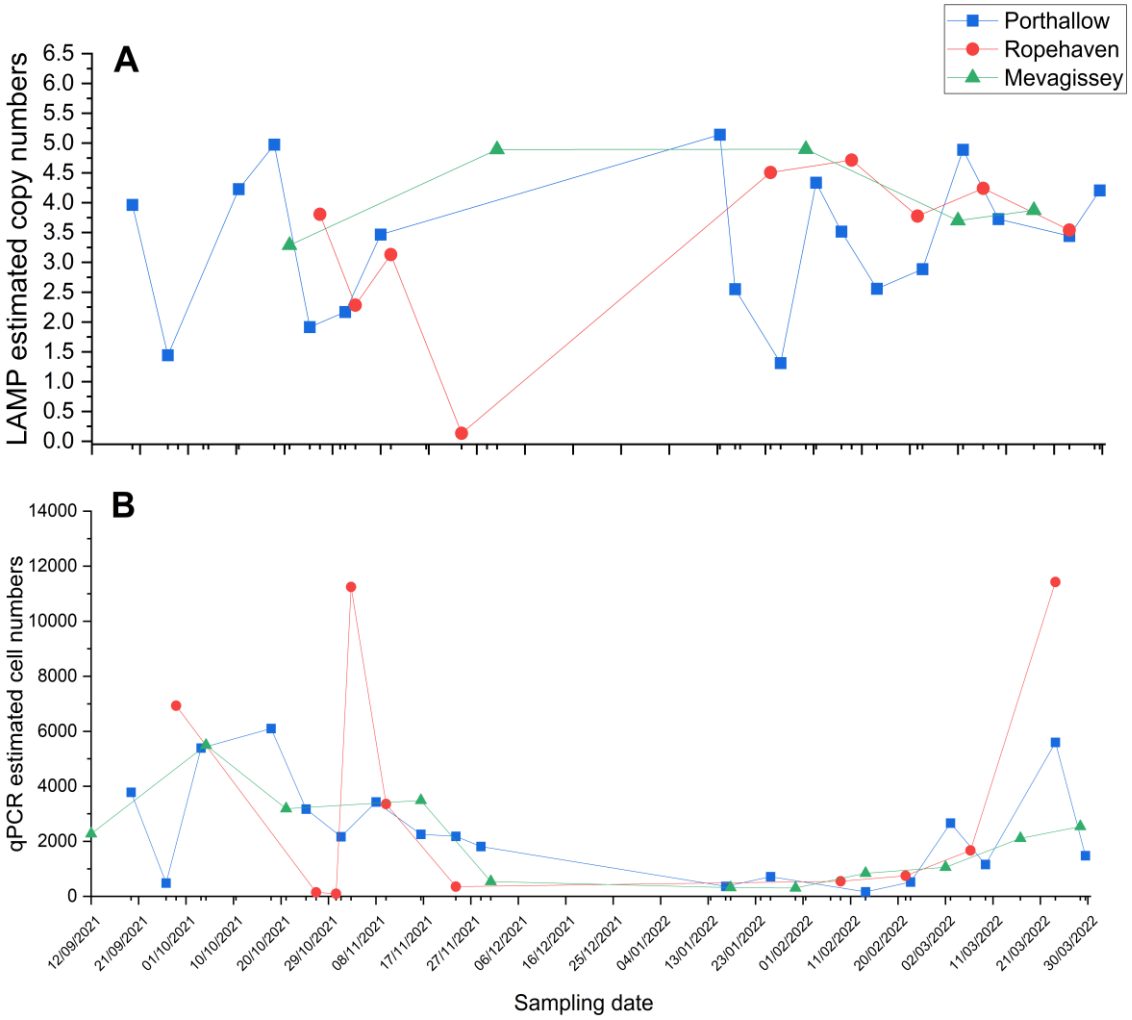

Figure 4.10 Collection of water samples from three shellfish production regions followed by filtration to capture cells. The recovered filter membranes were then transported to the laboratory for DNA isolation, purification, and downstream LAMP analysis (A) to determine the CYP450 copies of *Pseudo-nitzschia* spp at each study site throughout the study timeframe. (B) the concentrations of *Pseudo-nitzschia spp* cells in terms of cells per litre of filtered seawater were estimated using qPCR analysis.

Ropehaven site, where estimated copy numbers decreased below a single copy in November. The extremely low copy numbers observed at the Ropehaven site indicate the high sensitivity of the LAMP methodology for identifying the initial phases of the spring bloom. Thus, the proposed LAMP assay can offer an early-warning tool for tracking *Pseudo-nitzschia* trends across sampling locations and throughout monitoring time frames.

LAMP amplification of plasmid DNA standards revealed a detection limit (LoD) equivalent to a single copy per µl. However, when applied to DNA extracted from environmental samples, the LoD was determined as 0.1 ± 1.1 copies μl^{-1}. Therefore, careful interpretation of LAMP-based LoD calculations from environmental samples is warranted, given the need for extracted samples to provide a sufficient and representative abundance of genomic copies to meet environmentally relevant levels. This presented a challenge due to the lack of available microscopy cell count data throughout the study duration. However, blooms of toxic *Pseudo-nitzschia* have been previously documented in the study region (Downes-Tettmar et al. 2013, Brown et al. 2022). On the other hand, achieving absolute quantification for measuring target gene sequences through the LAMP assay presents challenges, demanding more information on the genetic structure and diversity of local populations within the study region. This genomic dataset could elaborate on the correlation between cell abundance and CYP450 gene copies.

Breaches in permissible levels of cells within St Austell Bay are common. Particularly, the Ropehaven site has experienced repeated HAB events since the site opened in 2010 (Ross Brown et al. 2022). Mean HAB frequencies in 2010-2017 (expressed as % of weeks throughout May-August, in which cell counts in surface water (2 m depth) exceeded advisory trigger levels) was 4% for *Pseudo-nitzschia spp*. The filter membranes were also processed to extract DNA, which was analysed by qPCR to estimate the levels of *Pseudo-nitzschia spp*. The results provided a comparison of the relative levels of *Pseudo-nitzschia spp.* in different samples. Then, the target gene copy number was estimated by extrapolating values from a standard curve to produce an estimate of the number of cells per litre of filtered water. Cell number was determined using cell number standards prepared from living cultures of *Pseudo-nitzschia multistriata*, as described in section C1, Appendix C. Figure 4.10B shows the results of qPCR-based quantification of *Pseudo-nitzschia spp* from September 2021 to March 2022 for the 3 sites, with the results expressed as estimated cells per litre.

The estimated levels of *Pseudo-nitzschia* spp. were generally far higher than for both other groups, never falling below ~1,000 cells/L, and reaching more than 100,000 estimated cells/L at the Outer Ropehaven site during March, a trigger level of 150,000 cells/L was never breached (McQuillan et al. 2023). The significance of these results is unclear because, for reasons that are discussed below, the use of qPCR data for the estimation of cell numbers is subject to a number of assumptions. Nonetheless, the measurement of the comparative levels of target DNA sequences in LAMP analysis between samples (e.g. the identification of an upward or downward trend in phytoplankton cell number) is not subject to these assumptions and can be interpreted with greater confidence.

Quantitative PCR analysis revealed a more variable yet consistent pattern of *Pseudo-nitzschia spp*. abundance across the sampling timepoints when compared to the trends observed using LAMP estimation of the target gene. While LAMP accurately quantified extremely low concentrations of the target gene, qPCR exhibited a wider dynamic range, allowing for the quantification of a broader range of DNA concentrations, especially at very low and very high levels. The LAMP assay used in this study targeted the cytochrome encoding gene sequence, which can vary considerably in copy number between species and under changing conditions, potentially contributing to some inaccuracies. Both methods showed potential for providing early warnings of *Pseudo-nitzschia* blooms due to their significantly faster analytical processes compared to other regulatory methods such as cell counting by microscopy. However, neither qPCR nor the LAMP method can unequivocally discriminate between DNA obtained from living and dead cells; all DNA collected on the filter membranes will have contributed to the PCR amplification.

Excluding extracellular DNA from qPCR and LAMP analysis can be achieved by treating samples to selectively degrade or digest nucleic acids not protected by an intact cell membrane (Nocker et al. 2006, Champlot et al. 2010). However, implementing this approach adds complexity, cost, and delays, and introduces additional sources of error to the monitoring workflow. To reduce the DNA overestimation bias, Reverse Transcription qPCR (RT-qPCR) or Reverse Transcription LAMP (RT-LAMP) can be used to quantify RNA, a labile analogue of DNA that is only synthesised by living and metabolically active cells and has a short environmental 'half-life' (Li et al. 2017). This is particularly relevant in scenarios where only the viable cell fraction is important, such as in the detection of infectious agents. However, as the RNA component of a cell can vary under changing conditions, interpreting quantitative results without a detailed understanding of how cellular RNA levels are regulated in the target group can be challenging. Therefore, both techniques, RT-qPCR and RT-LAMP, can be employed for a time-series measurement of *Pseudo-nitzschia spp*. in this region, depending on the specific objectives and constraints of the analysis.

LAMP results indicate sensitive quantification against potential inhibitors within environmental samples. LAMP amplification was found to be less susceptible to crude or complex samples compared to conventional molecular methods such as PCR (Poon et al. 2006, Inacio et al. 2008). While PCR methodology can provide higher sensitivity, its implementation demands costly thermal cyclers and involves time-consuming, labour-intensive procedures, and additional steps, such as agarose gel electrophoresis for amplification result confirmation (Yang and Rothman 2004). These challenges can significantly limit PCR practicality in field settings. In contrast, LAMP offers greater adaptability with minimal instrumentation, facilitating simple, real-world and affordable applications for HABs environmental surveillance (Wong et al. 2018, Huang et al. 2022).

4.5 Conclusions

Two novel isothermal DNA-based assays, LAMP and RPA, were developed for the species-specific quantification of *Pseudo-nitzschia spp*. Real-time LAMP-based quantification demonstrated greater accuracy compared to RPA-based quantification. The LAMP assay was optimised to enable highly sensitive target detection in environmental water samples. The LAMP assay demonstrated a 77.3% accuracy in identifying the early stages of the spring bloom. This suggests significant potential for improving regulatory monitoring through early warning systems, thereby protecting public health and the shellfish industry. The LAMP method presents a simple, sensitive, and specific tool suitable for decentralised environmental testing.

Chapter 5 Pre-storage of vitrified reagents for simple, precise and rapid molecular detection

5.1. Abstract

Vitrification technology increases the potential to satisfy the current demand for enabling quick and simple nucleic acid-based tests in field settings. Here, a new storage method was developed for PCR and LAMP amplification reaction mixtures at ambient temperature. The technique relies on air-drying all reagents of the amplification reaction for 45 minutes at 25ºC. The method was successfully applied to two different chemistries that perform real-time detection including PCR hydrolysis probes labelled with FAM and HEX fluorophores and LAMP intercalating dye. The storage stability of vitrified reagents was validated by measuring changes in limits of detection for tested molecular assays over a time span of six months. Both HEX-labelled qPCR and FAM-labelled LAMP vitrified assays yielded a limit of detection of a single copy after six months of storage at room temperature. However, the limit of detection of FAM-labelled qPCR vitrified assay decreased to 10^2 copies per reaction after a six-month period of storage. 18% and 7% increase in amplification efficiency resulted from six months of vitrified HEX-labelled and FAM-labelled qPCR mixtures, respectively, compared to freshly prepared reaction mixtures. Real-time stability of both qPCR and isothermal-based vitrified assays revealed the functional stability of the dry-reagent amplification reaction mix at room temperatures, with a shelf life of six months. These results offer a versatile method for stabilising various molecular detection techniques, facilitating the deployment of nucleic acid testing in field conditions and low-resource locations where reliable, simple-to-use and cost-effective monitoring tools are critically needed.

5.2. Introduction

Early detection of biological hazards (bio-hazards) is important to protect public health and alleviate the economic losses associated with public health incidents, including for example, the contamination of food products with toxigenic or infectious microorganisms. Nucleic acid testing is able to provide rapid, and sensitive detection of these microorganisms, but the methods are usually confined to centralised and highly resourced facilities. This increases costs and causes delays between sampling and results, and these facilities are seldom available in remote or undeveloped regions. Field deployment of nucleic acid tests (NATs) is therefore a logical step towards addressing these challenges. In the environmental sciences, the ability to conduct NATs outside of the

laboratory would provide a platform for the rapid early warning of biological hazards in, for example, natural water systems. It would also alleviate the risk of 'bottling artefacts' that arise if an unstable biological sample is stored for transit.

Developing fieldable nucleic acid testing faces two significant challenges: (i) the need to maintain test reagents at low temperatures and (ii) the requirement for precise formulation of reaction mixture immediately before use. In a laboratory setting, this process is typically accomplished by storing reagent stocks in a frozen state until needed, and then preparing reagent mixtures on ice using accurate 'micropipettors' with sterile, disposable plasticware. However, when working in the field, refrigeration is often unavailable, and performing prolonged procedures of reagent preparation outside controlled laboratory conditions becomes impractical. To overcome these challenges, a potential solution is to preformulate test reagents under controlled laboratory conditions and then preserve these mixtures until they are required. Thereby, pre-prepared aliquots can be transported to the sampling location at ambient temperatures and activated on-site, offering a more practical approach to field-based nucleic acid testing.

A range of reagent preparation and preservation strategies have emerged for this purpose. Of these, freeze-drying has been successful for the preservation of various NAT reagent mixtures including those for Polymerase Chain Reactions (PCR) (Arunrut et al. 2018, Xu et al. 2020) and isothermal loop-mediated isothermal amplification (LAMP) (Lim et al. 2021, Song et al. 2022b) and Recombinase Polymerase Amplification (RPA) (Davi et al. 2019, Khaliliazar et al. 2021). Freeze drying, also referred to as lyophilisation, involves the extraction of water from frozen mixtures by sublimation, utilising a vacuum and condenser (Ward and Matejtschuk 2021). Whilst freeze-drying can work well, there is a risk of damaging assay-critical enzymes and bio-components because the freezing process can lead to the formation of ice crystals, that may disrupt enzyme structure (Roy and Gupta 2004). This can be mitigated by the incorporation of cryoprotectants and lyoprotectants, which help to maintain the structural integrity of assay enzymes (Ward and Matejtschuk 2021). Another limitation of the technique is the requirement to pre-freeze the material prior to preservation as freezing protocols vary between laboratories and batches, leading to inconsistent outcomes (Patel et al. 2010). Freeze-drying can also be a time-consuming process, requiring overnight drying, and the need for costly vacuum and condenser equipment may be prohibitively expensive in resource-limited regions.

Alternatively, gelification is a promising preservation and storage option for NAT reagents (Rosado et al. 2011, Franco De Sarabia Rosado Pedro et al. 2016). 'Gelification' relies on a partial dehydration process to preserve reagents by employing stabilising agents to convert a liquid solution to a semi-

solid gelified state (Loukas et al. 2017). The 'gelled' condition was found to prevent enzyme denaturation due to an entrapping mechanism, with the reagents supported by a viscous matrix (Loukas et al. 2017). The stability of gelified reagents was previously demonstrated in trials involving nucleic acid sequence-based amplification (NASBA) and PCR. In these studies, gelified reagents have demonstrated a shelf life of up to eight months when stored under refrigerated conditions at 4°C (Sun et al. 2013, Tasoglu et al. 2013). However, limitations of the technique include the requirement for a vacuum drying instrument and, since gelification remains a proprietary protocol (owned by Biotools (Biotools A/S, Spain) (Høgberg et al. 2011)), it is not currently widely available for experimentation, development and applications without a high economic cost.

The limitations of the aforementioned storage techniques have driven the emergence of vitrification technology to fulfil the growing demand for a simple, reliable and rapid reagent stabilisation solution. Vitrification has been widely adopted for dry storage of qPCR (Rombach et al. 2014b, Yu et al. 2015), qRT-PCR (Hayashida et al. 2015), PSR (Liu et al. 2018) and isothermal amplification assays including RPA (Udugama et al. 2017), LAMP (Hayashida et al. 2015), RT-LAMP (Hayashida et al. 2019, Phillips et al. 2019), and SDA (Lafleur et al. 2016). Vitrifying protocols depend on a combination of stabilisers and a rapid air-drying process to immobilise the assay components at ambient temperature into a glass-like state. The vitrification method takes advantage of the glass transition temperature (Tg) of stabilisers such as trehalose, glycerol, and sucrose to solidify reagents (Grasmeijer et al. 2013, Liu et al. 2018), as discussed in Chapter 1, section 1.14.1.3. For example, trehalose has a Tg of 106°C (Roser 1991) that acts as a temperature threshold governing its physical state, including its viscosity. When the temperature falls below the Tg, trehalose with mixed reagents undergoes a significant increase in viscosity, limiting their molecular mobility within an inactive state. This step is crucial in preparing the reagent mixture for the downstream air-drying process which is conducted at room temperature to remove water molecules, allowing stabilisers like trehalose to create a solid, glassy vitrified matrix around the NAT components without undergoing crystalline transformation (Aksan and Toner 2004). This eliminates the need to freeze the mixtures, avoiding ice crystal formation (Mensink et al. 2017). Stabilisation of vitrified reagents has addressed key problems associated with 1) temperature shocks; protein active sites are greatly influenced by extreme temperatures (Nolting 1996) and 2) pressure stresses; mechanical compression of proteins may result in shrinkage and collapse of their native structure during freezing or gelification (Bhatnagar et al. 2007), 3) humidity interference; due to the low moisture content of freeze-dried reagents which subject them to interference due to ambient humidity (Wang et al. 2012), 4) protein adsorption; denaturation of proteins can led to adsorption to ice crystal surfaces (Hedoux et al. 2012), and 5) pH changes; the structure of proteins is susceptible to

changes in pH, which can be triggered by freezing (Sundaramurthi and Suryanarayanan 2010). Perhaps the most significant advantage of vitrification is its requirement for a very basic apparatus to undergo the drying process, which can be completed in a few hours or less, making it an affordable and universally accessible choice for a wide range of NAT applications.

In this study, a novel vitrification protocol was developed and tested for the dry storage of two PCR-based methods and a LAMP assay over a 6-month experiment. The vitrification included all of the necessary reagents in a single step. The pre-storage of both vitrified qPCR and LAMP reagents simplified the preparation of amplification master mixes, alleviating requirements for expensive instruments, and well-trained personnel. Reducing multiple pipetting steps lowers the possibilities of analytical variability among end-users and minimises cross-contamination from repeated freezing and thawing of reagents prior to use. A ready-to-use format of vitrified assays offers the advantages of an inexpensive, simple and rapid application for low-healthcare systems and field monitoring.

5.3. Materials and Methods

5.3.1. Preparation of DNA Templates

Plasmid DNA standards were prepared from amplified PCR products of target genes, as described in Appendix D, section D1. The resulting PCR product was then cleaned up with a QIAquick PCR purification kit (Qiagen, Hilden, Germany). 3 µl of purified PCR products were ligated into pGEM®-T Easy Vector (Promega, Wisconsin, USA) and cloned into One Shot™ TOP10 Chemically Competent *E. coli* cells (Invitrogen, Life Technologies, Carlsbad, CA). Plasmid colonies were cultured in Luria Broth with an antibiotic additive of 15 µg/ml Ampicillin at 37^{o}C. To confirm the presence of target sequences, plasmids were amplified following the cycling conditions as demonstrated in Supporting Information. The amplified plasmids were subjected to electrophoretic analysis using ethidium bromide-containing (2% w/v) agarose gel in a TAE buffer. Of bacterial colonies, the plasmids containing the expected target fragments were purified using the QIAprep® Spin Miniprep Kit according to the manufacturer's instructions (Qiagen, Hilden, Germany). The purified plasmids were linearised by overnight restriction digest, using 10 units/µL NdeI restriction enzyme (Thermo Fisher Scientific, Vilnius, Lithuania) as per the manufacturer's protocol. To explore a successful linearisation, both undigested and linearised plasmids were equivalently gel electrophoresed with a high mass ladder. The linearised plasmids of the desired target size were then quantified with a NanoDrop spectrophotometer (NanoDrop Technologies, Wilmington, USA). Quantification of

linearised plasmids was further verified using a Qubit fluorometer with a dsDNA HS Assay Kit (Invitrogen, Carlsbad, USA) to obtain accurate copy number estimates. A 10-fold serial dilution was executed in nucleases-free water to obtain a known concentration of copy number standards ranging from 10^0 copies to 10^7 copies and then stored at -80 ^oC. Finally, standard curves were created from a dilution series of linear DNA plasmid with gene inserts during the time course of the storage experiment.

5.3.2. Selection of Vitrifying Agent

A concoction of vitrifying excipients has been evaluated to facilitate the vitrification and drying process. To determine the optimal concentration of these vitrifying agents, different formulations were incorporated into a qPCR mixture which in turn stored at room temperature for two weeks. The stability of each formulation was tested by qPCR analysis against two experimental controls of freshly prepared vitrified reagents as well as freshly non-vitrified reagents, as described in Appendix D, section D2. Table 5.1 shows the concentration increments of vitrification-promoting substances used in five different formulations. The recovered amplicons from those reactions were compared based on the C_t values calculated by LightCycler 2.0 software (Roche Molecular Systems, Germany), and the intensity of gel bands and their expected size using Image Lab software (Version 6, Bio-Rad Laboratories, Inc.), following electrophoresis analysis using 2% agarose gel in TAE buffer stained by SYBR Safe (Invitrogen).

Table 5.1 Concentrations of vitrifying agents

	Concentration sets (%w/v)				
Constituents	1	2	3	4	5
Trehalose	1.0	1.5	1.6	2.0	2.5
Glycerol	0.05	0.25	0.25	0.5	1.0
Polyoxyethylene glycol	0.001	0.005	0.005	0.01	0.1
Bovine Serum Albumin	6.8	2	1.75	1.5	0.75

5.3.3. Vitrification of qPCR and LAMP Reaction Mixtures

Three replicates of the vitrified qPCR master mixture were prepared at a final volume of 50 µl containing, 2 mM each dNTPs (New England Biolabs, UK), 1X PCR buffer of 10 mM Tris-HCl and 50 mM KCl (New England Biolabs, UK), 2mM $MgCl_2$ (New England Biolabs, UK), 1 µM of each forward and reverse primer and 0.25 µM hydrolysis probe (Table 5.1), 2% (w/v) Trehalose, 0.5% (w/v)

Glycerol, 0.01% (w/v) Polyoxyethylene glycol (PEG), 1.5% (w/v) Bovine Serum Albumin, and 0.025 units/µL of One Taq DNA polymerase (New England Biolabs, UK).

50 µl vitrified LAMP assays consisted of 1.4 mM each dNTPs (New England Biolabs, UK), 1X isothermal buffer of 20 mM Tris-HCl, 10 mM $(NH_4)_2SO_4$, 50 mM KCl, 2 mM $MgSO_4$ and 0.1% Tween® 20 (New England Biolabs, UK), 6 mM of $MgSO_4$ (8 mM in total) (New England Biolabs, UK), 1X LAMP Fluorescent dye (New England Biolabs, UK), 2% (w/v) Trehalose, 0.5% (w/v) Glycerol, 0.01% (w/v) Polyoxyethylene glycol (PEG), 1.5% (w/v) Bovine Serum Albumin, and 0.025 units/µL of One Taq DNA polymerase (New England Biolabs, UK). A primer mixture of 1.6 µM of *dabD* FIB/BIP primers, 0.2 µM of *dabD* F3/B3 primers, and 0.8 µM of *dabD* Loop primers were added to the vitrified LAMP master mix (Table 5.1).

The prepared reaction mixture was placed in an air introduction box connected with an air pump (M361-C; Charles Austen Pumps LTD, Surrey, England, UK) in a sterile biosafety cabinet. The air-drying setting is depicted in Supporting Information. With lids of 0.2 ml tubes (LightCycler 8-tube strips, Roche Molecular Systems Inc.) opened, a continuous air flow at 0.45 m/s for 45 minutes at room temperature. The vitrified mixtures were stored at room temperature in Aluminium barrier film bags with MiniPax® Silica Gel Desiccant Sachet (Sigma-Aldrich, UK), until use.

Later, the vitrified reaction mixtures of both qPCRs and LAMP assays were activated by adding a rehydration mixture consisting of DNA copy number standard and 5 mM dNTPs (total volume 8 ul), with a brief spin using VWR Galaxy mini PCR strip micro-centrifuge (VWR international LTD, UK) for one minute to allow for the reconstitution of vitrified reagents. Then, all amplification reactions were performed using a Light Cycler 2.0 real-time PCR thermal cycler (Roche Molecular Systems Inc.). The PCR thermal cycling comprised of an initial denaturing step at 95°C for 120 sec followed by 55 cycles at 95°C for 15 sec and 59°C for 60 sec. The change in fluorescence of the PCR amplified products was measured by capillary electrophoresis using an Agilent 2100 Bioanalyzer and the DNA 1000 Kit (data not shown) (Agilent Technologies, UK). The LAMP mixture was incubated at 65^{o}C for 1 hour followed by a high-resolution melting (HRM) step. The melting analysis was used to determine the fluorescence intensity released by LAMP amplicons, ensuring the specificity of LAMP amplification. Later, the concentration of LAMP amplicons was also quantified using a Qubit fluorometer (Thermo Fisher Scientific Inc., UK).

5.3.4. Performance of Vitrified qPCR and LAMP reactions

The prepared DNA standards were amplified to create the standard curves using vitrified qPCRs and LAMP assays over the experimental timeline of dry storage. The standard curves were constructed

by plotting log 10 of the initial copy number of the target against the threshold cycle number (C_t). Wet reaction mixes of vitrified assays served as a reference control. Standard curves were also constructed from both fresh qPCRs and LAMP vitrified reagents. The efficiency of the qPCR and LAMP primers was calculated from the slope of the linear regression for each standard curve according to the Pfaffl equation: Efficiency (E) = $[10^{(-1/\text{slope})} -1] \times 100$, whereby the slope of the linear fit of standard curves of the log of the target concentration against the C_t threshold values (Pfaffl 2001, Nguyen et al. 2020). The efficiency of LAMP amplification was estimated using the equation of isothermal doubling times (IDT = - 0.301 x m), where: m = the slope of the graph of T_t value plotted against the copy number of target DNA and 0.301 corresponds on the base 10 logarithmic scale to twofold change in concentration at 2 (Nixon et al. 2014). The T_t value, analogous to the C_t value, is defined as the time point during the LAMP amplification reaction when the fluorescence signal exceeds the threshold fluorescence level (Diego et al. 2019). The fluorescence points used for linear fitting were within a linear exponential interval of the curve where amplification is more reproducible from sample to sample than at the endpoint (Kralik and Ricchi 2017). The endpoint fluorescence of vitrified qPCR and LAMP amplicons was measured over the timeline of the storage experiment across three classes of DNA standard concentration; high=10^7 copies; medium= 10^4 copies; low=10 copies.

5.4. Results and Discussion

In this chapter, a simple procedure was developed to demonstrate the effectiveness of vitrification in the long-term preservation of reaction mixtures, employing different detection chemistries such as qPCR and LAMP amplification methods. The procedure involved a novel vitrification formulation consisting of stabilising agents, protectants, and surfactants to facilitate the transformation of liquid amplification reagents into a solid, glass-like state. This was achieved by rapid air-drying of reaction mixtures using a simple and cost-effective technique. This technique has eliminated the requirements for bulky lyophilisation equipment and refrigeration processing (Appendix D, Figure D3).

A number of earlier studies have investigated the use of vitrification for the preservation of NAT reagents, however, to date no study has developed the method for the preservation of complete reaction mixtures (i.e., all reagents included in a single mixture) in a single step process. Others have described the vitrification of only a subset of reagents, adding the remaining essential reaction components immediately prior to use, or in some cases the components have been vitrified separately and then recombined. Nevertheless, previous studies have successfully achieved long-term preservation of NAT reagents using the vitrification technique (Hayashida et al. 2015, Liu et

al. 2018, Hayashida et al. 2019, Phillips et al. 2019). However, these studies did not involve the complete assembly of all the components of the amplification reaction with vitrifying stabilizing agents during the drying process. Typically, the mixture of amplification reaction consists of enzymes, reaction buffer, dNTPs mixture, primers, fluorometric probe or dye, and DNA/RNA template. In the studies conducted by (Hayashida et al. 2015, Hayashida et al. 2019), the LAMP components were not included in a single step: they initially air-dried the LAMP primers with some vitrifying components (such as Trehalose and glycerol) (step 1), followed by air-drying the LAMP enzyme and dNTPs with additional Trehalose (step 2). To re-activate their vitrified LAMP reaction, the dried primers and enzymes were rehydrated by adding DNA samples, LAMP buffer, and $MgSO_4$. Similarly, (Phillips et al. 2019), LAMP components were not vitrified simultaneously, and the procedure was conducted in two distinct steps. In Step 1, a mixture containing LAMP primers, glycerol, and Triton X-100 was air-dried. In Step 2, the LAMP enzyme, dNTPs, and sucrose were air-dried on top of the previously dried primers. To reactivate the LAMP reaction, the dried primers and enzyme were rehydrated by adding a DNA sample, LAMP buffer, and Betaine. (Rombach et al. 2014b) did not vitrify all the PCR components simultaneously. Instead, the PCR primers and probe were mixed with trehalose and xanthan, at final concentrations of 56 mM and 2.78 mM, respectively, before the air-drying process. Later, a mixture of PCR enzyme, buffer, and DNA sample was introduced to rehydrate the dried PCR primers and probe. In contrast, (Liu et al. 2018) focused on vitrifying reagents for the polymerase spiral reaction (PSR) by air-drying the enzyme, primers, and dNTPs in the PSR reaction tubes, sealed with paraffin wax. However, the detection dye specific to the PSR assay, cresol red-phenol red, was not included in the vitrifying mixture.

In contrast to previous methods, this study introduced a novel combination of ingredients that allowed for the vitrification of all components of the reaction mixture in a single step. This was enabled by conducting a simple vitrification protocol that facilitated a rapid stabilising process compared to conventional vitrification techniques. Furthermore, this vitrification technique significantly decreased the number of handling steps required to assemble the amplification reaction, reducing the risk of contamination. The result was a ready-to-use format for nucleic acid testing that can be user-friendly and accessible for individuals with limited expertise in the field.

To primarily test the effect of vitrification on enzyme activity, five formulations of vitrified agents of two weeks shelf-life were used against two controls of freshly-vitrified and freshly-made master mixes in qPCR reactions. Storage stability of vitrifying formulations was assessed in duplicate qPCR experiments against wet reaction mixes. All the vitrifying formulations generated positive qPCR amplifications and resulted in a specific amplicon size at 161 bp, Appendix D, Figure D2. The vitrifying agent 4 was found to generate the highest amplification rate with the lowest Ct value at

10.27±0.06, corresponding to the most intense gel band of vitrified amplicons upon agarose gel analysis, as shown in Appendix D, Figure D2, and Table D1. Based on these findings, vitrifying agent 4 was used for downstream stability analysis. Following the recipe of vitrifying agent 4, trehalose was included in the master mix at a final concentration of 2% (w/v). Trehalose is one of the most common thermostabilisers that can form multiple hydrogen bonds with the hydration sites of the peptide chains replacing the enzyme-surrounding water molecules, allowing maintenance of the native state of the amplification enzymes (Lins et al. 2004). A vitrifying agent of trehalose and xanthan preserved a qPCR mixture for up to one year at room temperature (Rombach et al. 2014b). 0.5% (w/v) glycerol was included in the vitrifying agent 4, to prevent freezing/crystalline formation due to its low glass transition temperature (T_g = −92°C) (Bell and Hageman, 1996). Similarly, 0.28% (w/v) glycerol was used to prevent freezing damage during the vitrification process (Phillips et al. 2019). Polyethene glycol (PEG) was used as a surfactant with a final concentration of 0.01% (w/v) to generate a mesh structure of high interfacial tension, preventing the denaturation of reagents. PEG has a long-chain structure that provides a rigid glassy matrix for vitrified reagents (Chang and Pikal 2009). The addition of bovine serum albumin was found to enhance the fluorescence signal of the vitrified PCR mixture by 90% (Yu et al. 2015). At an optimised concentration of 1.5% (w/v), BSA was therefore added as a fluorescent signal protectant and served as an additional bulking agent to preserve the tertiary structure of the amplification enzyme in a glass state. The optimum conditions for vitrification were determined as a supplement of 2% trehalose, 0.5% glycerol, 0.01% polyethene glycol and 1.5% bovine serum albumin were chosen (Table 5.1).

After reconstitution of the vitrified master mixes, the amplification reactions were performed in triplicates at 0 weeks, 2 weeks, 4 weeks, 6 weeks, 8 weeks, 4 months, 5 months and 6 months. Different detection chemistries of FAM and HEX hydrolysis probes and a LAMP assay labelled by FAM-intercalating dye were tested over the time course of the experiment. The HEX-labelled assay showed no loss in reactivity at any DNA concentration for 6 months (Figure 5.2) and with an increase of efficiency at 18% after 6 months of storage. The limit of detection for the HEX-labelled assay remained the same after six months at a single copy of the DNA target (Figure 5.2). However, the FAM-labelled qPCR master mix exhibited a significant decrease in activity at a lower range of 10^0-10^3 copies after 2-4 months of storage (Figure 5.1). The limit of detection (LOD) changed for FAM-labelled qPCR from a single copy of the target at a shelf-life of two weeks to 10^3 copies at a shelf-life of two months (Figure 5.1). The LOD estimates of FAM-labelled qPCR assay at two months were two orders of magnitudes higher than the threshold of detection of the fresh assay. It was found that the activity of the LAMP vitrified master mix remained after 6 months, without any drop in detection limit over target concentrations tested compared to fresh LAMP assay (Figure 5.3).

Therefore, the detection limit of the LAMP assay was found at a single copy after 6 months of storage (Figure 5.3). This is in concordance with the results of the vitrified LAMP assay employed for the detection of *M. tuberculosis* bacterium after 2 months of storage (Liu et al. 2018). Similarly, vitrifying agent 4 enabled high retention of enzymatic activity of HEX-labelled qPCR and FAM-labelled LAMP mixes after 6 months of dried storage at room temperature (Figure 5.1-Figure 5.3).

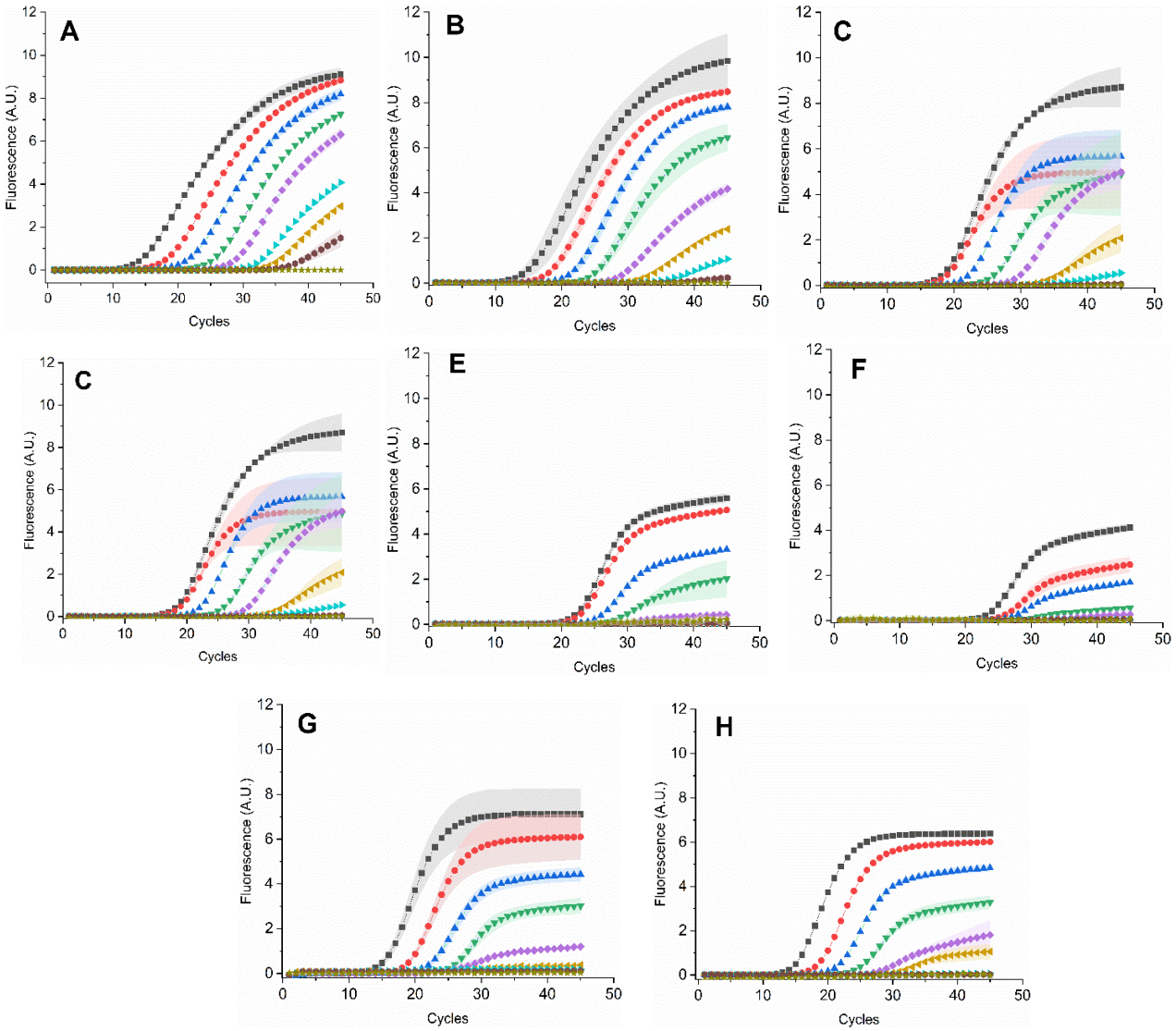

Figure 5.1 Real-time qPCR amplification plots of fully premixed FAM-labelled vitrified assays at different storage times. A set of standards containing 10^0-10^7 copies of DNA target were amplified using A) fresh FAM-labelled qPCR vitrified master mix (the reference), B) 2 weeks old vitrified FAM-labelled qPCR master mix, C) 4 weeks old vitrified FAM-labelled qPCR master mix, D) 6 weeks old vitrified FAM-labelled qPCR master mix, and E) 8 weeks old vitrified FAM-labelled qPCR master mix, F) 4 months old vitrified FAM-labelled qPCR master mix, G) 5 months old vitrified FAM-labelled qPCR master mix, and H) 6 months old vitrified FAM-labelled qPCR master mix. Each graph panel presents standard concentrations in a range, including 10^7 copies (—■—), 10^6 copies (—●—), 10^5 copies (—▲—), 10^4 copies (—▼—), 10^3 copies (—◆—), 10^2 copies (—◀—), 10^1 copies (—▶—),

10^0 copies ( ) and negative control ( ). Each data point represents the average of triplicate reactions and the coloured areas indicate standard deviation.

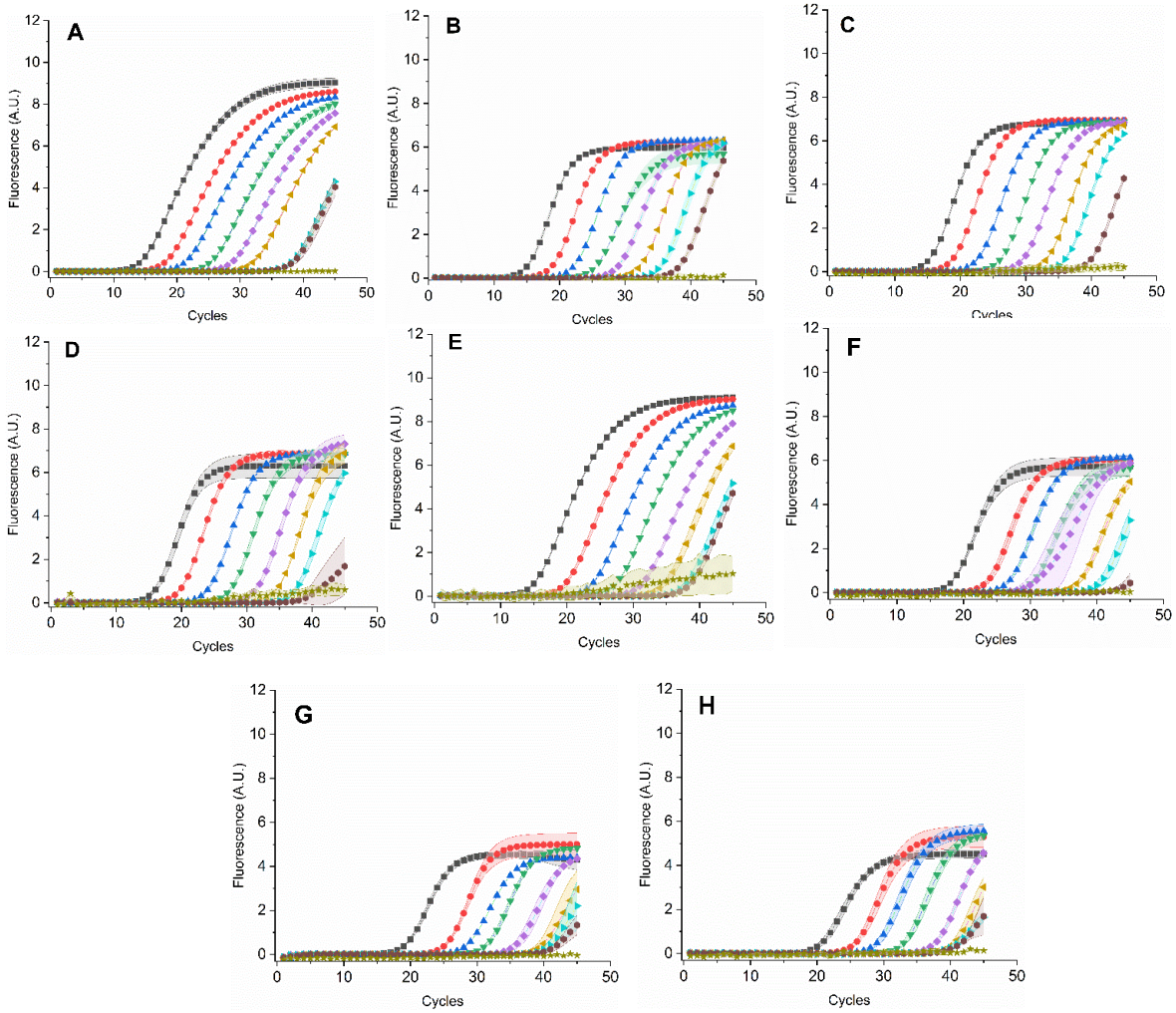

Figure 5.2 qPCR amplification data of fully pre-mixed HEX-labelled vitrified assay after storage at ambient temperatures. The fluorescence signals were measured upon amplifying a 10-fold dilution of standards containing 10^0-10^7 copies of DNA target using A) fresh HEX-labelled qPCR vitrified master mix (the reference), B) 2 weeks old vitrified HEX-labelled qPCR master mix, C) 4 weeks old vitrified HEX-labelled qPCR master mix, D) 6 weeks old vitrified HEX-labelled qPCR master mix, and E) 8 weeks old vitrified HEX-labelled qPCR master mix, F) 4 months old vitrified HEX-labelled qPCR master mix, G) 5 months old vitrified HEX-labelled qPCR master mix, and H) 6 months old vitrified HEX-labelled qPCR master mix. Each graph panel illustrates standard concentrations within a range, including 10^7 copies ( ), 10^6 copies ( ), 10^5 copies ( ), 10^4 copies ( ), 10^3 copies ( ), 10^2 copies ( ), 10^1 copies ( ), 10^0 copies ( ) and negative control ( ). Each data point represents the average of triplicate reactions and the filled areas indicate standard deviation.

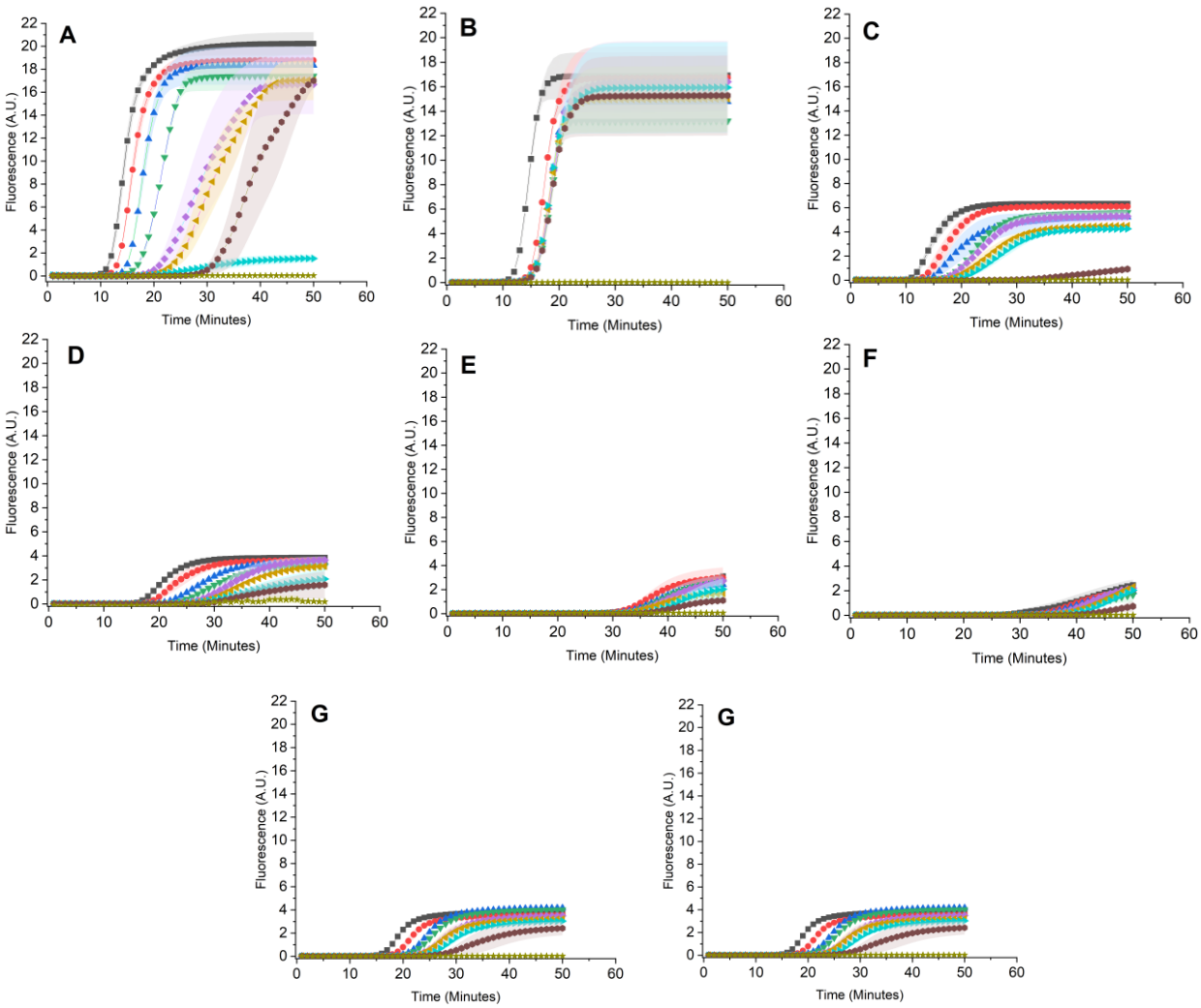

Figure 5.3 Results of real-time amplification of fully pre-mixed vitrified LAMP reagents stored for different durations. A serial dilution of DNA target containing 10^0-10^7 copies was amplified using A) Fresh vitrified LAMP reagents (the reference), B) 2 weeks vitrified LAMP reagents, C) 4 weeks vitrified LAMP reagents, D) 6 weeks vitrified LAMP reagents, E) 8 weeks vitrified LAMP reagents, F) 4 months vitrified LAMP reagents, G) 5 months vitrified LAMP reagents, and H) 6 months vitrified LAMP reagents. In each graph panel, the standard concentrations are demonstrated in a range of 10^7 copies ( ), 10^6 copies ( ), 10^5 copies ( ), 10^4 copies ( ), 10^3 copies ( ), 10^2 copies ( ), 10^1 copies ( ), 10^0 copies ( ) and negative control ( ). Each data point denotes the average of triplicate reactions and coloured areas represent the standard error of the mean for each set of replicates per dilution.

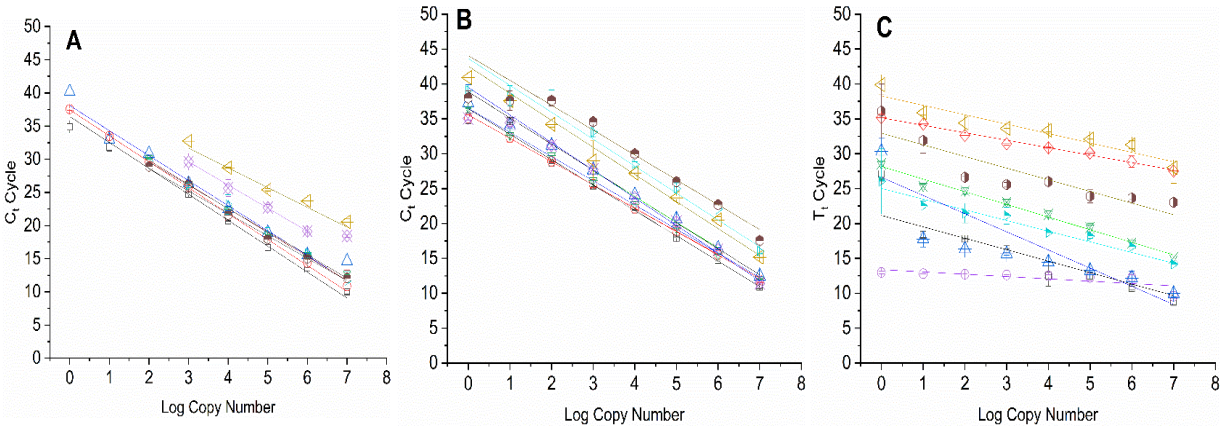

Figure 5.4 Effect of vitrification on the reaction kinetics of qPCRs and isothermal LAMP reactions. Standard curves were constructed from serial dilution of target concentrations ranging from 10^0 to 10^7 copies. A) FAM-labelled qPCR vitrified reagents, B) HEX-labelled qPCR vitrified reagents, and C) LAMP vitrified reagents. The quantification range of vitrified preserved assays was evaluated over a storage period ranging from 2 weeks ( ), 4 weeks ( ), 6 weeks ( ), 8 weeks ( ), 4 months ( ), 5 months ( ), 6 months ( ) in comparison to a freshly-prepared control assay ( ). Each data point shows the average of n = 3 reactions, with error bars representing standard deviation.

The sensitivity of the vitrified assays (relative to freshly prepared wet reagents) was tested using a standard curve obtained from 10-fold serial dilution of DNA plasmid target concentration ranging from 10^0 to 10^7 copies. After six months of storage, the HEX-labelled qPCR and FAM-labelled LAMP assays successfully detected their target sequence across the range of concentrations examined (10^0 -10^7) copy number (Figure 5.4B & Figure 5.4C). Although both assays showed a reduced amplification rate (Figure 5.2 & Figure 5.3), they retained the ability to quantify down to a single copy following six months of dry storage. However, the time speed for LAMP detection of the single copy number decreased gradually from the week 2 storage, corresponding to the decrease of T_t from 25 to 41 (Figure 5.4). The delayed detection by vitrified LAMP assay has been previously reported (Thapa et al. 2019). These findings reflect the robust stability of qPCR polymerases compared to isothermal polymerases after a long time of dry storage.

There was a significant loss in the activity of FAM-labelled PCR reagents after 6-8 weeks of storage and with only the DNA samples containing lower numbers of target sequence copies (10^3-10^0 per reaction) with null amplification as shown in (Figure 5.2). This observation raised some concerns about the possible contamination of the DNA template before addition to vitrified master mixes. DNA samples can be prone to degradation or carryover contamination due to repeating freeze-thaw steps (Aeschbach and Dion 2017). To mitigate contamination risks of PCR standards in the downstream experiments, the stock solution of standards was re-quantified and then re-diluted

based on fluorometric estimation in a range between 10^7 and 10^0 copies/µl. After re-calibration of DNA standards, the sensitivity of the vitrified assay improved enabling detection as low as 10^2 copy numbers after 6 months of storage. This result indicates that long-term freezing of DNA plasmid standards can introduce the risk of template degradation, which consequently skewed the actual detection limit of the reaction.

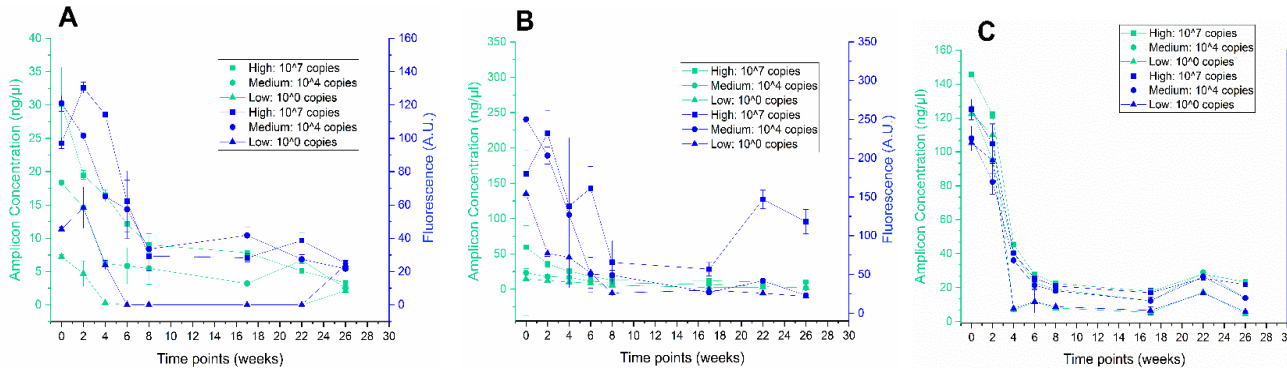

Figure 5.5 Stability assessment of qPCRs and LAMP amplified products using fully premixed vitrified reagents following long-term storage at ambient temperatures. The final fluorescent value (Arbitrary unit; A.U.) of vitrified amplicons over the time course of the storage experiment is plotted against the concentration of vitrified amplicons (ng/µl). Output measurements for vitrified amplicons using three final concentrations of DNA target at 10^7 copies (High), 10^4 copies (Medium), and a single copy (Low). A) FAM-labelled qPCR reagents, B) HEX-labelled qPCR reagents, and C) FAM-labelled LAMP reagents. Error bars denote the calculated standard deviations for the biological duplicates.

The changes in recovered fluorescence signals and concentration of vitrified amplicons upon 6 months of storage phase are compared to freshly-prepared wet assays in (Figure 5.5). The fluorescent signal of FAM-labelled qPCR amplicons dramatically decreased 6 months after drying, corresponding to the percentage signal recovered at 74%, 82% and 47% less than the fresh reagents from 10^7, 10^4 and 10^0 copies, respectively. The concentrations of FAM-labelled vitrified qPCR amplicons plateaued at 3.3 and 2.5 ng/µl after storage of six months for 10^7 and 10^4 copies number, respectively. Similarly, vitrification caused a reduction in the amount and the fluorescence signal of HEX-labelled qPCR amplified products (Figure 5.5B). A lower signal loss was observed at 34%, 30%, and 85% for HEX-vitrified reagents at concentrations of 10^7, 10^4 and 10^0 number of copies, respectively. Both HEX-amplicons of 10^4, 10^0 were 2 ng/µl, and 10^7 was 10 ng/µl after six months of storage. A similar trend was observed for 6-month stored LAMP assays compared with wet LAMP master mix at template concentrations of 10^7 10^4 and 10^0 copies with 23.3, 13.9 and 4.3 ng/µl, respectively. As shown in (Figure 5.5C), the fluorescence signal gradually decreased at a percent of 33%, 27% and 21% for 10^7 and 10^4 copies number, respectively. However, the detection limit of HEX and FAM fluorescently labelled qPCR and LAMP assays remains at a single copy. These findings

indicate that fluorescent signal reductions did not impair the quantitative detection of both PCR-based and isothermal vitrified assays after six months of dry storage.

Table 5.2 Evaluation of amplification performance as a function of storage time (weeks) using air-dried master mixes of vitrified qPCR and LAMP assays.

Storage time (weeks)	Primers efficiency % FAM-labelled qPCR assay (*n=3*)	Primers efficiency % HEX-labelled qPCR assay (*n=3*)	Isothermal Doubling Time (IDT) FAM-labelled LAMP assay (*n=3*)
0	87.84±3.1	88.7±1.2	62.3±8.7
2	83.1±7.3	99.6±2.4	6.7±1.9
4	96.5±7.4	90.7±5.3	55.5±15.6
6	94.4±2.4	94.0±0.3	54.1±3.8
8	123.4±13.2	93.3±1.3	31.0±3.4
17	133.5±14.9	91.5±1.9	41.4±2.1
22	85.2±18.8	91.5±9.1	42.7±5.9
26	94.6±3.6	104.9±5.3	33.5±3.2

Storage for up to six months enhanced the primer efficiency of FAM-labelled qPCR assay from 87.8±3.1 to 94.6±3.6, with a 7% increase (Table 5.2). In the case of the HEX-labelled qPCR assay, the primer efficiency was increased by more than 18% from 88.7±1.2 to 104.9±5.3 upon storage for six months (Table 5.2). In another study, storage of vitrified qPCR assay for one year had no impact on the efficiency of reactions labelled by HEX and FAM hydrolysis probe (Rombach et al. 2014b). 46% decrease in Isothermal Doubling Time (IDT) value was observed for 6-months preserved LAMP assay compared to wet LAMP assay from 62.3±8.7 to 33.5±3.2, without any impact on the viability of vitrified LAMP reaction mix to detect as few as a single copy of the target. These observations are consistent with minimal degradation of HEX fluorophore and FAM intercalating dye of LAMP assay during the storage phase as was previously shown in (Figure 5.2 & Figure 5.3). Where vitrification supported high retention of enzymatic activity after six months of dried storage at room temperature, the off-the-shelf vitrified assays can provide an accurate estimation of target sequences.

5.5. Conclusions

In this study, a simplified protocol was employed to dry the amplification reaction mixtures and store them at ambient temperature. By vitrifying the assay components, the reactivity of the reaction remained stable, with reduced fluorescence signals observed over six months. The results

suggest that the long-term stability of vitrified assays depended on the detection chemistry of each assay. By shortening the steps for assay assembly, the vitrification technique reduced the risks of onsite contamination during multiple pipetting steps. Rehydration of the vitrified assays required a single pipetting step that would enable a ready-to-use format of nucleic-acid testing, that increases the resilience of the supply chain and allows stockpiling of assays for future outbreaks. Vitrified assays can overcome some major analytical challenges associated with limited healthcare settings by providing fast, cost-effective and simplified detection methods for end users.

Chapter 6 LAMPTRON: a lab-on-a-chip system integrating DNA purification and loop-mediated isothermal amplified quantification of toxic diatom *Pseudo-nitzschia multistriata*

6.1 Abstract

Microfluidic technology has enhanced the way nucleic acid testing is performed, by transforming the functions of bulky laboratory instruments and labour-intensive measurements into easy-to-use, and inexpensive miniaturised systems that offer rapid and sensitive analysis. However, the benefits of microfluidic technology in nucleic acid testing are often constrained by the complicated and expensive DNA purification prerequisites for downstream diagnostic analysis. To address this challenge, a genetic lab-on-a-chip (LOC) platform was developed that integrates a dimethyl adipimidate (DMA)-based functionalised silica extraction method with a simple, rapid, and real-time loop-mediated isothermal amplification (LAMP) for quantitative DNA analysis and demonstrate its performance by detecting *Pseudo-nitzschia* cells. An optimised design of the extraction module enabled a maximum capture capacity of DNA at 61.7 ± 1.0 ng/µL on the functionalised available surface of silica beads, resulting in a DNA recovery efficiency of 75%, which is lower than the commercial extraction kit at 92%. While the DMA-based method reduced the cost per sample by 97% compared to a common commercial nucleic acid isolation kit. The subsequent on-chip LAMP process was capable of sensitively quantifying a target gene (the *dabD* gene, coding for a component of the domoic acid toxin production pathway in *Pseudo-nitzschia spp*), in the purified DNA sample, resulting in low limits-of-detection of 10 cells/mL. The detection chamber in the LAMPTRON system was preloaded with preserved air-dried LAMP reagents with a "shelf-life" of five months at ambient conditions, alleviating the need for multiple preparation steps for untrained users and allowing storage and transportation of the device without cold chains. There was no significant difference in assay performance between the preserved LAMP and freshly prepared LAMP mixtures using wet reagents. By integrating microfluidic extraction and amplification into the LAMPTRON system, the total analysis time for 10 cells/mL, from sample to answer, was achieved within one hour. The favourable long-term stability of assay reagents, , which are required for simple, fast, and robust genetic testing, is demonstrated in this chapter. Using cost-effective extraction methodologies, a compact fluorescence detection system and eliminating the

need for thermocycling, this system has the potential for a simple and economical application in environmental monitoring and public health, providing a quick and accurate tool for the detection of harmful microorganisms.

6.2 Introduction

Rapid and accurate genetic testing is critical for the timely diagnosis and treatment of infectious diseases, harmful algal blooms, and food and environmental contamination (Li et al. 2023). Nucleic acid amplification methods provide several advantages over traditional methods for microorganism detection, being both specific and sensitive (Oliveira et al. 2021). Nucleic acid testing (NAT) allows for the detection and quantification of genetic markers, providing insight into the severity of an outbreak (Gao et al. 2022). The polymerase chain reaction (PCR) is the gold standard method for the detection of microorganisms, and it has been validated for the toxigenic diatom *Pseudo-nitzschia* species (Kim et al. 2017, Pugliese et al. 2017). *Pseudo-nitzschia* cells produce the potent neurotoxin domoic acid, which can enter marine food webs and lead to mass mortalities in marine wildlife, posing a risk to human health (Bates et al. 2018). Recent research has identified the *dabD* gene, which encodes the cytochrome P450 protein performing specific oxidation reactions in the domoic acid biosynthetic pathway (Brunson et al. 2018). Harmful algal blooms (HAB) of *Pseudo-nitzschia* have resulted in significant economic losses due to the closure of fishing and tourism regions (Berdalet et al. 2016). Current methods for detecting *Pseudo-nitzschia*, including microscopic and PCR techniques, are typically performed in centralised laboratories after sample collection and transport. A portable solution to enable field detection for faster response would be especially impactful in remote coastlines, developing countries and outbreak regions (Lelong et al. 2012).

Microfluidic technology provides an alternative approach to simplify and miniaturise complex laboratory procedures for molecular detection, allowing an automated testing workflow with short turnaround times in a small, single-lab-bench footprint (Pattanayak et al. 2021). The microfluidic platform provides critical information for rapid response to HAB outbreaks and management of threats to aquaculture and human health. In addition, the use of isothermal amplification methods, such as loop-mediated amplification (LAMP) (Notomi et al. 2000), recombinase polymerase amplification (RPA) (Piepenburg et al. 2006), nucleic acid sequence-based amplification (NASBA) (Compton 1991), helicase-dependent amplification (HDA) (Vincent et al. 2004), rolling circle amplification (RCA) (Lizardi et al. 1998), and strand displacement amplification (Shuler et al. 2012); (Walker et al. 1992), allows for molecular detection without the requirement of thermal cycling.

The LAMP technique is a widely used and established isothermal amplification method that operates at a single temperature of 65°C, allowing for flexible amplification product detection strategies using various chemistries at the endpoint of the reaction (Soroka et al. 2021). This greater flexibility in detection strategies compared to other isothermal techniques makes it suitable for simpler microfluidic installations and minimises maintenance needs. LAMP has shown potential for fast, accurate, and reliable quantification of various pathogens such as harmful algal blooms (Zhang et al. 2012, Huang et al. 2017a), viruses (Nakauchi et al. 2014, Wang et al. 2016, Huang et al. 2020, Tang et al. 2022), and bacterial pathogens (Wu et al. 2018, Zhan et al. 2019). However, no previous microfluidic devices have been applied to the DNA extraction or LAMP detection of *Pseudo-nitzschia* cells.

Preserving molecular assays on 'lab-on-a-chip' (LOC) platforms is important to maintain the stability and applicability of genetic testing in limited-resource areas (Sun et al. 2013, Lafleur et al. 2016, Phillips et al. 2019). Vitrification technology enables low-cost, fast, and stable preservation of reagents for the detection of nucleic acids, which is a significant improvement compared to evaporative storage techniques such as lyophilisation and gelification (Hayashida et al. 2015, Loukas et al. 2017, Hayashida et al. 2019, Phillips et al. 2019). Vitrified assays address the problems associated with prolonged lyophilisation procedures, refrigeration, centralised vacuum instruments, and proprietary licensed stabilising additives, which can limit broad-scale nucleic acid testing (Rombach et al. 2014b, Yu et al. 2015, Liu et al. 2018, Chen et al. 2020).

In this study, a microfluidic system "LAMPTRON" was designed" which combines both DMA silica-based DNA extraction and real-time LAMP amplification for the sensitive detection of toxigenic *P. multistriata* across a concentration range of 10–10^5 cells/mL. The vitrification technique was employed to maintain the stability of LAMP assay components of *P. multistriata* for up to five months, allowing for the storage and transport of LAMP reagents at ambient temperatures. The sample-to-sample variability of the LAMPTRON system was also assessed on the quantification of *P. multistriata* cells using fresh and vitrified LAMP assays. The goal of simplifying the operation for end-users was pursued by conducting on-chip vitrified LAMP reactions in a single step, thereby eliminating the requirement for multiple preparation steps and expensive equipment.

6.3 Experimental

6.3.1 Principle of the LAMPTRON microfluidic system

DNA detection from seawater involves cell concentration (optional but often required), cell lysis, DNA purification, amplification and 'analysis,' most often optical detection of amplified gene targets. The LAMPTRON prototype employs a combination of chemical cell lysis, DMA-based extraction techniques to purify DNA, and isothermal nucleic acid amplification (LAMP) to detect the target gene from *P. multistriata* cells that were achieved within approximately 49 min (Figure 6.1A, right). Cells were suspended in a lysis buffer and DMA mixture for the subsequent purification procedures which involved using amine-functionalised silica beads with dimethyl adipimidate (DMA) for capturing DNA. The methodology of using functionalised silica substrates for DNA extraction has been previously described (Shin et al. 2015, Han et al. 2016, Jin et al. 2017, Yoon et al. 2018, Jang et al. 2019). Previous studies have shown that functionalised silica substrates are effective for DNA extraction by hydrolysing the H-bonded silanol groups of the silica surface using ozone treatment with APTES solution, resulting in a hydrophilic surface enriched with positive charged amine-reactive groups that bind to negatively charged DNA molecules (Shin et al. 2015, Jang et al. 2019). The DMA chemical structure contains bifunctional imidoester groups, which enable the capture of DNA by both electrostatic interaction and covalent bonding (Jin et al. 2017, Yoon et al. 2018). The amidine bonds between imidoester groups of the DMA and the amine group of DNA molecules are pH-dependent, making it possible to capture and release DNA by altering the pH. The optimum pH for binding DNA and RNA molecules occurs at a pH of approximately 8 while releasing molecules requires a high pH (>10) (Shin et al. 2015, Yoon et al. 2018). The DMA protocol was implemented on a microfluidic chip. Phosphate-buffered saline (PBS) was adjusted to a pH of approximately 8 and used to maintain the binding of DNA molecules and wash cellular debris, non-specific and unbound molecules (Jin et al. 2017, Yoon et al. 2018). 10 mM sodium bicarbonate (pH 10.6) was used as an elution buffer to release DNA by breaking the interaction between the DNA/DMA complex and the amine-functionalised silica surface in the system (Shin et al. 2015, Jang

et al. 2019). The eluted DNA from cells was used for genetic analysis using a real-time LAMP amplification reaction (Figure 6.1).

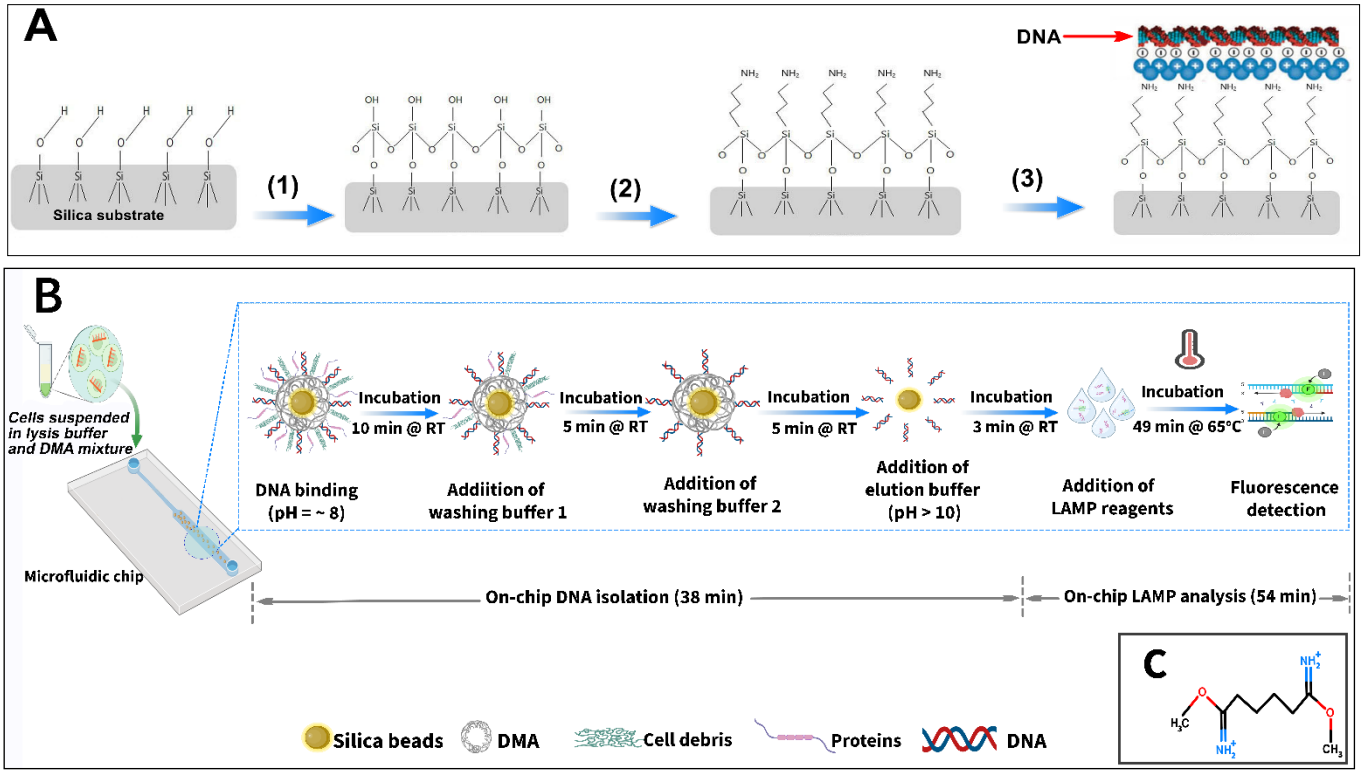

Figure 6.1 Schematic representation of the lab-on-a-chip system for rapid and simple DNA isolation using the DMA-based DNA extraction method on silica beads, followed by real-time LAMP analysis. (A) Surface treatment of silica beads with APTES: (1) substrate hydroxylation by UV ozone treatment for 10 min, (2) APTES solution hydrolyses the exposed silanol groups on silica substrate by liquid deposition at 65 °C for 1h, (3) Adsorption of the negatively charged DNA molecule on the positively charged amine-modified silica surface. (B) Schematic process of DMA-based extraction of DNA sample. The chemical lysis of cells was carried out off-chip, and the resulting cell lysate was injected onto a chip with DMA as a binding agent, where the DNA binds to the amine-modified silica beads. Non-specific molecules are removed by washing and elution. Amplification of DNA occurs on the chip with the LAMP reagents, while no amplification occurs on the chip with the negative controls. (C) Chemical structure of DMA.

6.3.2 Design and fabrication of the LAMPTRON system

The LAMPTRON system is comprised of two functional components. The first component is a DNA extraction module, which consists of a circular microfluidic chip (Ø = 119 mm) manufactured from two-layer dark polymethyl methacrylate (PMMA) with precision-milled microchannels using Datron Neo milling machine (DATRON Dynamics, Inc., Milford, England). A solvent bonding method was used to ensure the strong sealing of microchannels and minimal deformation of other microfluidic components (Ogilvie et al. 2010). The microfluidic chip was designed using AutoCAD™ and Fusion 360 (Autodesk, Inc., San Rafael, CA) to form a network of microfluidic channels (approximately 950

µm wide × 950 µm deep) and two reservoirs (approximately 246 µL volume for the extraction microchamber and approximately 65 µL volume for the detection microchamber). Fluid control is achieved using five micro-inert solenoid valves (LFNA1250325H, The Lee Company, Connecticut, U.S.A.) mounted directly onto the chip. A custom-designed syringe pump unit is employed for pumping, comprising four glass barrels: one each for sample/lysis buffer mixture, first washing buffer, second washing buffer, and elution buffer (Figure 6.2). The fluid flow to and from each barrel is controlled by two solenoid valves through an isolated fluidic circuit, enabling them to function as individually addressable pumps (Figure 6.2A). Perfluoro-elastomer moving seals (Polymax Ltd., UK) are fixed on the pump plungers on a stainless-steel shaft. All pump plungers are mechanically linked to operate simultaneously and are driven by a size 11 torque stepper motor (Haydon Kirk, U.S.A.). Magnetic field sensors “hall effect” are incorporated into the pumping system that provide the pump with positional feedback. Sample and reagent solutions are pumped into the system from 50 mL conical tubes (Falcon™) via tubing (poly(tetrafluoroethylene) (PTFE), 1.6 mm OD × 0.5 mm ID) mounted on the outside layer of the chip via 1/4 in.-28 fluidic fitting (LT-115X, IDEX Health and Science LLC, Washington, U.S.A.). A fluid storage bag (Flexboy, Sartorious) is hung behind the system to collect waste (Figure 6.2). Fluidic control is automated using a 32-bit microcontroller-based electronics package with 16-bit analogue-to-digital inputs, which can stream raw data (1 Hz) over USB and store it on an 8 GB flash memory card, as previously described (Beaton et al. 2012).

The second component of the LAMPTRON system was designed to conduct the LAMP amplification reaction and record resulting fluorescence measurements. To maintain the on-chip LAMP reaction temperature, a Peltier thermoelectric heater (ET-127-08-15, Adaptive JUNIOR Temperature Controller, European Thermodynamics LTD, Leicestershire, UK) was installed above the reaction microchamber. Temperature feedback control was achieved in real-time using a thermoelectric cooler controller (ADJ-48-450-UR, Adaptive JUNIOR Temperature Controller, European Thermodynamics LTD, Leicestershire, UK). A FluoSens integrated fluorescence detector (QIAGEN GmbH, Hilden, Germany) was mounted beneath the reaction chamber to measure fluorescence emission during the LAMP reaction. To improve the platform's optical performance and prevent external light from interfering with optical measurements, dark PMMA sheets were utilised to absorb stray light emitted by the light-emitting diodes (LEDs) (Floquet et al. 2011). The distance between the detector light output and reaction microchamber was optimised to 7 mm for all LAMP reactions. The fluorescence signals were sampled through an excitation wavelength of 465 nm and

a detection wavelength of 510 nm. The fluorescence data were streamed in real-time to a laptop connected via a USB interface (Figure 6.2).

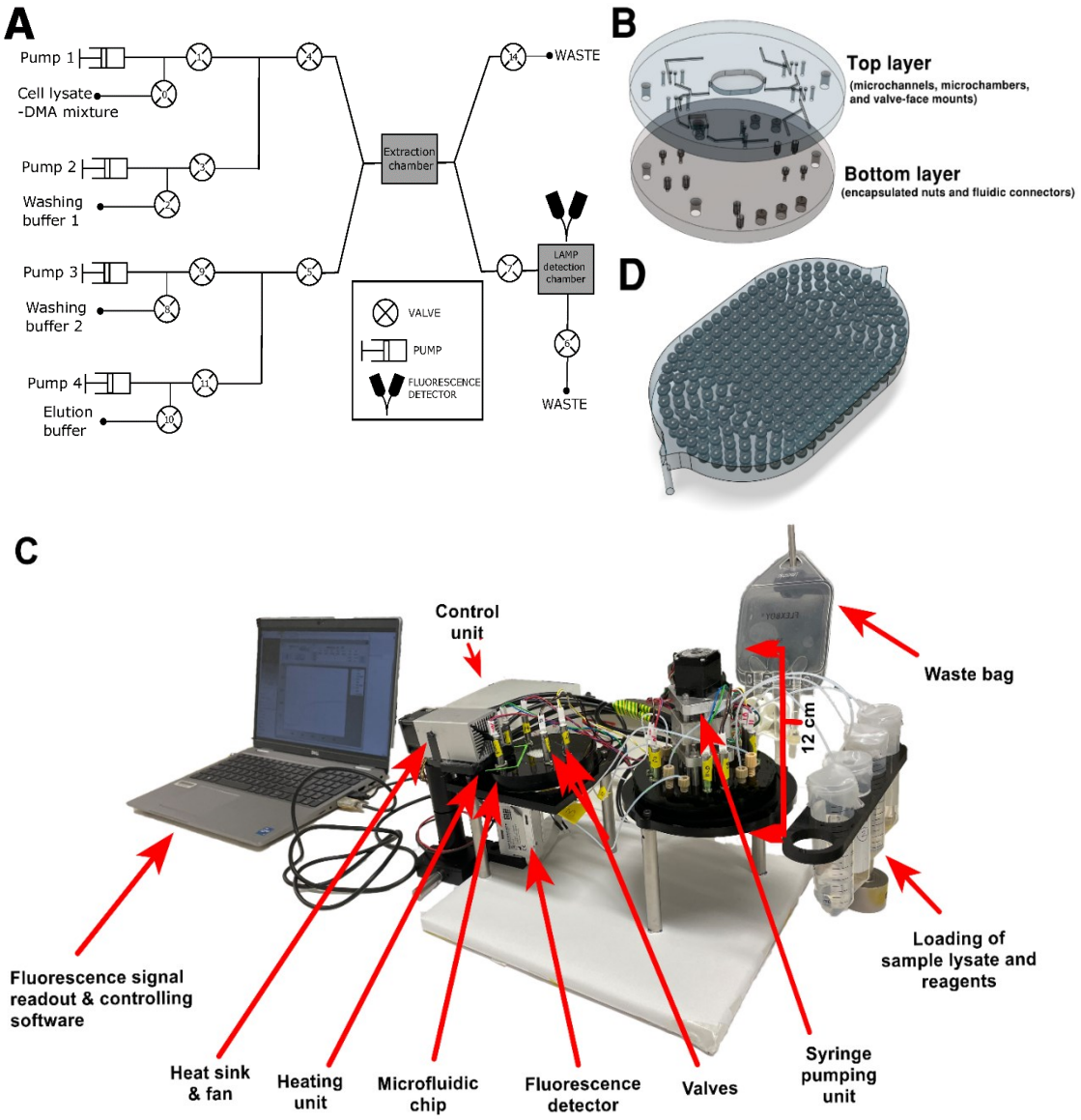

Figure 6.2 LAMPTRON system: A Lab-on-Chip analyser combines sample processing and LAMP-enabled analysis of extracted DNA samples. A) Fluidic diagram shows the components that control the microfluidic working flow. B) Exploded schematic of the microfluidic chip (119 mm in diameter) showing the PMMA layers of the system. C) Assembled LOC system that integrates microfluidic, mechanical, electronic, electronic, and optical components that support automated DNA isolation and result interpretation. D) Oblique view of the extraction microchamber (depth= 3 mm) packed with silica beads.

6.3.3 Preparation of amine-functionalised silica beads

Silica beads with a diameter of 710 µm were purchased from Sigma-Aldrich, UK and were autoclaved prior to use. To activate silanol groups on the surface of beads, the silica beads were

treated with oxygen plasma for 10 min under 70 sccm of O_2 flow rate using a plasma system (Diener electronic GmbH & Co. KG, Ebhausen, Germany). The beads were then immersed in a 2% H_2O solution of 3-aminopropyltriethoxysilane (APTES, Sigma-Aldrich) for 60 minutes at 65°C, followed by washing with deionised water and drying under a nitrogen stream. The APTES-treated beads were stored in safe-lock tubes (Eppendorf, UK) at room temperature until use. The treated silica beads were packed into the extraction chamber from the exposed top side of the chip, which was designed with 150-µm-diameter access microchannels etched from both sides of the extraction chamber to trap the silica beads. The extraction chamber was sealed with PCR-compatible sealing tape for stable packing of the beads, and to enable the beads' convenient replacement, thus allowing reuse of the LAMPTRON. Glass fibre membranes (GF/F grade, Whatman™ GE Healthcare Life Sciences, Leicestershire, UK) were cut to pattern the layout of the extraction chamber using a CO_2 based laser-cutting machine (Speedy 100 Laser Cutter, Trotec Laser GmbH, Boldon, UK), and then treated with ozone and APTES solution as described above.

A preliminary trial was conducted to investigate an alternative silica substrate for DNA capture. The treated glass fibre membranes were loaded into the extraction reservoir to compare their efficiency in DNA purification with the silica beads. The findings of this experiment are detailed and discussed in Appendix E, section E1.

6.3.4 Culture conditions and preparation of cell standards

Pseudo-nitzschia multistriata SZN-B954 was obtained from the culture collection at Stazione Zoologica Anton Dohrn institute (SZN), Italy. The strain was cultured in a sterile filtered f/2 growth medium at 18°C, under a 12-hour light: dark photoperiod (Guillard 1983). Enumeration of cells was carried out using a light microscope (Carl Zeiss, Oberkochen, Germany) and a Beckman Coulter with a glass Sedgwick-Rafter cell counting slide (PYSER-SGI, Kent, UK). To obtain triplicates of standard concentrations, *P. multistriata* cells were serially diluted to obtain the concentrations of $1.07x10^1$, $1.3x10^2$, $1.3x10^3$, $2.3x10^4$, $1.6x10^5$ cells/mL in 10 mL of sterile filtered f/2 medium. Known numbers of cells were harvested by centrifugation at 7,100 rpm for 3 minutes at 4°C to obtain cell pellets in approximately ~200 µl supernatant and stored at -80°C until further processing.

6.3.5 On-chip DNA isolation using DMA-based extraction on silica beads

The microfluidic chip-based DNA extraction process for the current study involves four main steps: sample mixing, DNA binding, washing, and elution, as illustrated in Figure 6.1. All solutions used for DNA extraction were prepared in ultrapure DEPC-treated water (Thermo Fisher Scientific, UK). Cells

were pelleted by centrifugation at 7,100 rpm for 3 min, and the culture medium was discarded. To initiate the on-chip DMA-based DNA extraction protocol, the cell pellets were thawed and mixed with an equivalent volume of DMA lysis buffer (1:1). The DMA lysis buffer contains 100 mM Tris-HCl (pH 8.0) (SERVA, Germany), 10 mM ethylenediaminetetraacetic acid (EDTA) (Invitrogen, UK), 1% sodium dodecyl sulfate (SDS) (Sigma-Aldrich, UK), and 10% Triton X-100 (Sigma-Aldrich, UK), 0.1 mg/mL Proteinase K enzyme (Qiagen, Germany), and 100 mg/mL dimethyl adipimidate (DMA) agent (Alfa Aesar, UK). The cell lysate in DMA solution was loaded into the microfluidic chip at a flow rate of 350 µL/min and then incubated for 5 min at room temperature in the extraction microchamber to increase the binding of released DNA to the silica beads. Silica beads were washed twice with 0.01 M PBS (Sigma-Aldrich) as washing buffer 1, and with 0.1M trisodium citrate (Alfa Aesar, UK) in a 10% ethanol solution as washing buffer 2 (Figure 6.2). The washing buffers were added to the extraction microchamber at a flow rate of 250 µL/min and incubated for 5 minutes. Finally, an elution buffer consisting of 10 mM sodium bicarbonate (pH 10.6) (Sigma-Aldrich, UK) was added at a flow rate of 150 µL/min through the silica beads, and the mixture was incubated for 3 min to recover the DNA sample. The DNA samples collected from the platform were evaluated for integrity by assessing their concentration and purity using a NanoDrop 2000 (Thermo Fisher Scientific, Waltham, MA) and Qubit 2.0 Fluorometer (Life Technologies, Carlsbad, CA, USA). A commercial kit (DNeasy Mini Kit, Qiagen) was used as a positive control, following the manufacturer's protocols, to extract DNA from the same cell sample.

To prevent any potential carryover of extraction between samples, a series of clean-up procedures were employed. These involved replacing the silica beads with freshly treated ones before each extraction, ensuring the removal of any bound debris, proteins, or other potential LAMP inhibitors. Subsequently, 80% ethanol (v/v) solution, DNA away solution (Thermo Fisher Scientific, UK), and 1% w/v bovine serum albumin (BSA) (Sigma Aldrich, UK) in ultrapure nuclease-free water (Invitrogen, UK) were loaded into the chip using a 10 mL Luer slip syringe (BD Plastipak, UK). To completely dry the cleaned chip, it was dried in a convection oven (Heraeus, Thermo fisher scientific, UK) at 45°C for 1 h.

Several modification steps to the DMA-based DNA purification protocol were assessed using a microfluidic device and APTES-treated silica beads. The following modifications were made: (i) optimisation of the volume of cells and DMA lysis buffer with input ratios of 1:1 and 1:2; (ii) testing of two washing buffers, 0.1 M trisodium citrate in 10% ethanol and 0.01 M PBS buffer; and (iii) evaluation of the impact of elution step detention times of 3 and 10 min on DNA yield and quality. Across these modifications, the methods described above were optimised for a DMA-based DNA

purification procedure employing the APTES-treated silica beads on the microfluidic LAMPTRON system.

6.3.6 LAMP assay operation

The LAMP primers utilised in this study were designed using PrimerExplorer™ V5 software (Eiken Chemical Co., Ltd., Tokyo, Japan), with additional support from Geneious R11 Bioinformatics Software (Biomatters Ltd, Auckland, NZ). The LAMP assay targeted a 222 bp region of the cytochrome P450 *dabD* gene, which is involved in the biosynthesis of the neurotoxin domoic acid in *Pseudo-nitzschia* species (Brunson et al. 2018, Hardardottir et al. 2019). The development of the LAMP assay is described in the Chapter 4, section 4.3.3. The LAMP amplification primers were synthesised by Integrated DNA technologies (IDT, Leuven, Belgium) and are listed in Table 6.1.

Table 6.1 Sequences of LAMP primers.

Primer name	Sequence (5' --- 3')
LAMP-F3	CGGAAAACACCATGCCCAA
LAMP-B3	TCTCGTTCGGGTACAGCA
LAMP-FIP	GGCCAGAACCTTTCGTCTCTGTCAAGGGTGATTCGGGGAATG
LAMP-BIP	AATCCCGACACTTTCGATCCCGTCGAAGCCCTTCCAGTCTG
LAMP-LB	GGTTCACCCGACCCTACAAGA
LAMP-LF	ATATTGTACAAGGGCAAAAAGATGT

The fresh LAMP reaction was prepared using 1X Warm Start LAMP master mix (New England Biolabs, Hitchin, Hertfordshire, UK), 1X LAMP fluorescent intercalating dye (New England Biolabs, Hitchin, Hertfordshire, UK), 1.6 µM of FIB/BIP primers, 0.2 µM of F3/B3 primers, 0.8 µM of Loop primers LP/LF, 6 µL DNA template, and nuclease-free water (Invitrogen) to make a 50 µL reaction mixture. The vitrified LAMP mixture was prepared in a similar way to the fresh reaction, but the nuclease-free water was substituted with a solution containing 2% (w/v) Trehalose (Acros Organics, Belgium), 0.5% (w/v) Glycerol (Sigma-Aldrich, UK), 0.01% (w/v) Polyoxyethylene glycol (PEG) (Sigma-Aldrich, UK), and 1.5% (w/v) Bovine Serum Albumin (Thermo Fisher Scientific, UK).

To prepare vitrified LAMP reaction mixtures, an air pump (M361-C; Charles Austen Pumps LTD, Surrey, England, UK) was used to air dry the reaction mixture with a continuous airflow of 0. 5 m/s for 45 minutes in a sterile biosafety cabinet. Fresh and preserved LAMP reaction replicates were both prepared off-chip in clean 0.2 mL non-transparent tube strips (Roche Molecular Systems Inc, UK). The freshly prepared LAMP reactions were used on the same day, whereas the tubes

containing vitrified LAMP reagents were stored at room temperature for up to five months in Aluminium film bags filled with MiniPax® Silica Gel Desiccant Sachet (Sigma-Aldrich, UK) before use. Vitrified preserved LAMP reagents were reconstituted by adding 5 mM dNTPs (New England Biolabs, Hitchin, Hertfordshire, UK) before being mix-pipetted with DNA sample extracted on-chip using the DMA-based method, resulting in a final reaction volume of approximately 50 µl. The reaction microchamber was then sealed with sealing tape (Applied biosystems, UK) and the mixture was subsequently incubated for 49 min at 65 °C using the heating element fixed above the amplification chamber. Negative controls were triplicated throughout the on-chip DMA protocol and then analysed by both fresh and pre-stored LAMP reactions (negative control is no template control where the DNA template is replaced by nuclease-free water). A compact detector (FluoSens integrated, QIAGEN GmbH, Hilden, Germany) was employed to measure the real-time LAMP fluorescence signals for amplified DNAs from triplicates of each cell standard concentration extracted using an on-chip DMA-based method. In total, 21 runs were performed on the LAMPTRON platform to evaluate the reproducibility of DNA analysis extracted from a tenfold serial dilution of *P. multistriata* cells ranging from 10 –10^5 cells/mL in tandem with the negative controls. DNA templates from triplicate samples of known cell concentrations were analysed by LAMP, and repeated in triplicates using both fresh and preserved vitrified LAMP reagents. Raw fluorescence intensities were extracted from time points over 49 min of all LAMP reactions and normalised by the average baseline fluorescence of the first ten cycles for each amplification reaction (Hardinge and Murray 2019). The Time to threshold (T_t) value of the LAMP reaction was determined as the time at which the fluorescence signal crosses the threshold fluorescence value (Diego et al. 2019). The LAMPTRON chip was cleaned between runs as described in the above section 6.3.5 to eliminate any potential effect from sample-to-sample carryover.

6.4 Results and discussion

6.4.1 Working process of the LAMPTRON LOC system

The LAMPTRON system merged two fundamental functions: (1) DNA extraction and (2) real-time LAMP amplification. The sample-to-answer workflow of this LAMP detection device was enabled by the microfluidic flow that was driven by a custom electronics package equipped with eight 16-bit ADC controller, a stepper motor driver for the syringe pump, hold circuits for the valve solenoids, a heater, a temperature sensor, and a real-time fluorescence detector (Figure 6.2). First, *P. multistriata* cells were processed off-chip by centrifugation to remove the liquid medium and mixed with a lysis buffer containing DMA reagent. The premixed solution of the sample and DMA was then

introduced onto the LAMPTRON platform, which was preloaded with silica beads that were pre-activated with amine-reactive groups on their surface to electrostatically capture DNA-DMA reagent complexes. DMA reagent has previously been used as an amino-reactive cross-linking agent (Shin et al. 2015, Jang et al. 2019). The homobifunctional imidoesters (HIs) such as dimethyl adipimidate (DMA) provide a dual binding mechanism via (1) the bi-functional imidoester groups of DMA that directly bind with negatively charged DNA by electrostatic capture, and (2) DMA reagent forms with the amine groups of treated silica substrate that generates more positively charged amidine bonds that extensively attract negatively charged DNA (Shin et al. 2015). In this study, the DMA reagent was coupled with silica beads to increase the surface area available for amine functionalisation to enrich the amidine bonds between DMA and DNA molecules. Relatively large beads were also incorporated (diameter 710 µm) to avoid handling-related issues related to trapping and controlling the movement of smaller microbeads. The use of nano and microbeads can pose significant handling challenges in DNA microfluidic extraction systems, which can eventually affect extraction performance (Wen et al. 2008). DNA was captured on bead-treated silica surfaces at pH 8, while the lysate solution flowed into the extraction microchamber and incubated for 10 min at room temperature. Cell debris such as proteins, lipids, and polysaccharides were removed via sequential washing for 10 min. Subsequently, increasing pH to (>pH 10) reverses the crosslinking bonds in 3 min and allows the release of DNA eluted with sodium bicarbonate buffer.

In order to optimise the functionality of the LAMPTRON chip, various channel dimensions and microchamber geometries were evaluated to ensure laminar fluid flow. To do this, COMSOL Multiphysics 5.5 software was employed to simulate fluid flow in a 3D geometrical model of an extraction microchamber packed with silica beads. Initially, The potential challenge of bead slurry aggregation in microchannels, which could block fluid flow and delay reagent flushing during the extraction process, was investigated (Zhong et al. 2007). Simulation results demonstrated that the beads-packed reservoir remained structurally stable, and steady laminar flow was observed under current microchannel dimensions and operating conditions, as summarised in sections 6.3.1 and 6.3.5 (Figure 6.3). The resulting Reynolds number (Re) was below the threshold of 2300, allowing for steady laminar flow through the beads-packed microchamber (Benz et al. 2001). Another functional limitation was the resistance to the fluid flow caused by packed glass beads into microchannels, which could resist the fluid flow and lead to backpressure, as demonstrated in similar beads-based systems (Oleschuk et al. 2000, Wolfe et al. 2002). This backflow could lead to a carryover of extraction reagents, inhibiting amplification reactions and impeding the automated DNA extraction process (Reinholt and Baeumner 2014). Figure 6.3. demonstrated a steady velocity

field that maintained the concentration profile through beads immobilised on the bed of the extraction chamber to ensure high DNA binding. Fluid retention was also sustained using a pair of solenoid valves mounted at the entry and exit port of the detection microchamber to stop any backflow that could contaminate and inhibit the LAMP reaction. By switching the flow via these valves, the eluted DNA was titrated to rehydrate the vitrified LAMP reagents that were manually loaded into the detection chamber. LAMP products were detected via a small and compact fluorescence unit aligned directly beneath the reaction microchamber. The use of a miniaturised and compact fluorescence unit provided the advantages of less complexity, cost savings, and quick assembly in an orderly manner at the functional interface of the LAMPTRON prototype. As a result, the on-chip DNA extraction protocol and LAMP detection can be adapted into a semi-automated workflow.

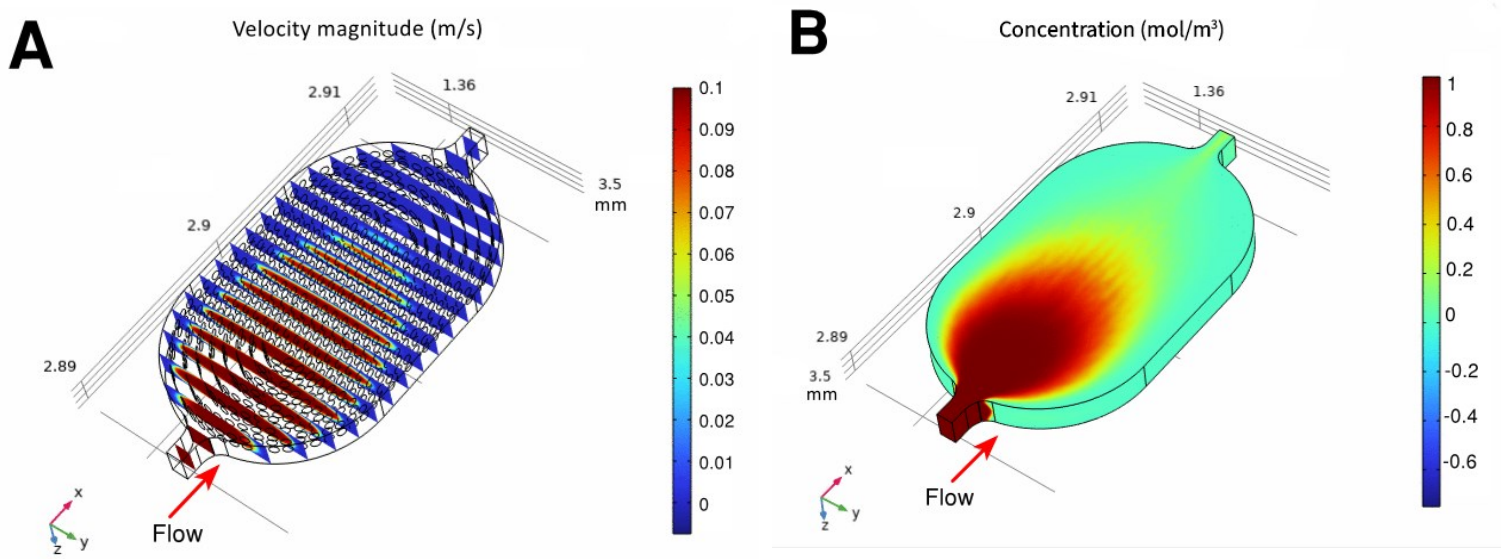

Figure 6.3 Simulation results of velocity and concentration distribution show the transport of fluid at an average flow velocity of 0.03 m s^{-1} through the y-z slices (A) and the x-y plane concentration surface (B) of the microfluidic extraction chamber packed with silica beads.

6.4.2 Optimisation of the LAMPTRON DNA purification module

Five variations of the DMA-based extraction method were quantified using replicates harvested from the same *P. multistriata* cell number at 32,080 ± 240.5 cells/mL against a reference control labelled as DMA: Sample (2:1) (Figure 6.4). The modified protocol using a 1:1 DMA: Sample input ratio resulted in the highest extraction efficiency, with a DNA yield of 43.7 ± 0.7 ng/µL and an absorption ratio of 260/280 of 1.5 ± 0.02 (Figure 6.4A). DNA samples are prone to contamination during handling, which can lead to decreased yield and a reduced 230/280 ratio below 2 (Wang 2012). To prevent sample carryover contamination, washing was employed using 0.1 M trisodium citrate and 0.01 M PBS. Multiple washing steps using 0.1 M trisodium citrate allowed for higher

DNA recovery, with a concentration of 38.5 ± 1.4 ng/µL and a 230/280 ratio of 1.6 ± 0.1, compared to 0.01 M PBS washing buffer, which yielded a DNA concentration of 31.1 ± 0.1 ng/µL and a 230/280 ratio of 1.2 ± 0.06 (Figure 6.4). The duration of the elution process can have a substantial effect on the yield of DNA extracted (Ali et al. 2017b). Therefore, the impact of elution times ranging from 3 to 10 minutes on DNA recovery was examined. A 3-minute detention time with 10 mM sodium bicarbonate (pH 10.6) elution buffer resulted in a DNA yield of 35.8 ± 0.4 ng/µL with a purity ratio of 1.7 ± 0.03. In contrast, a 10-minute detention time did not improve the quality of the eluted DNA samples, resulting in a concentration of 28.6 ± 0.5 ng/µL and a purity ratio of 1.3 ± 0.04 (230/280). Based on these results, a combination of three protocol modifications that improved DNA recovery was selected for further experiments using the on-chip DNA extraction module.

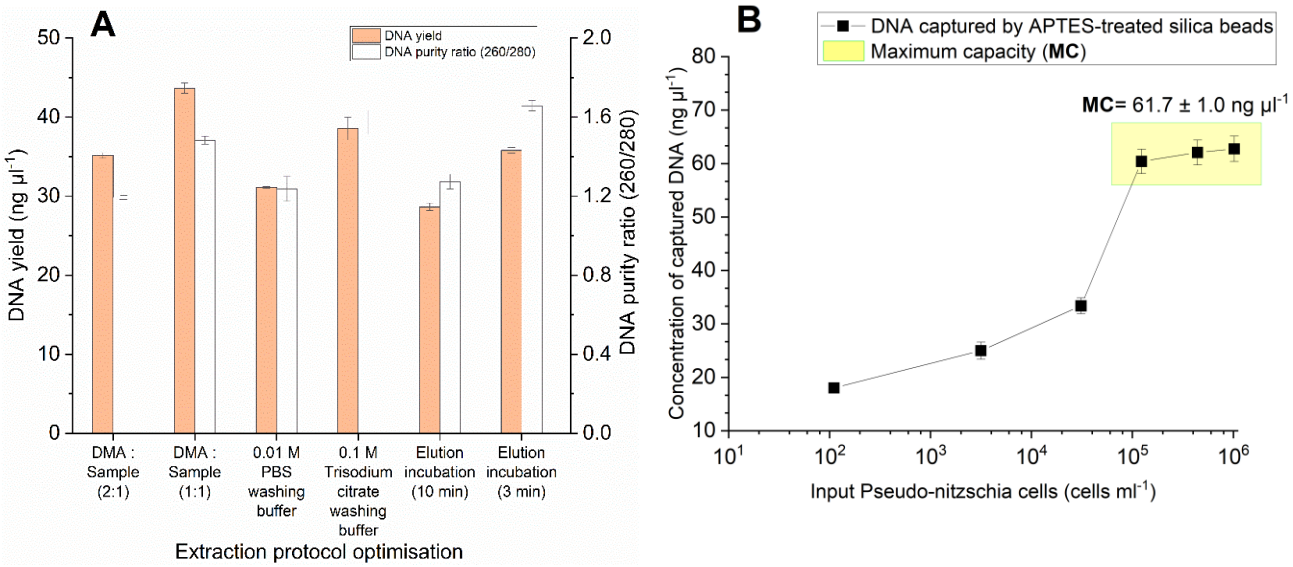

Figure 6.4 Assessment of DNA integrity resulting from experimental extraction protocols as determined by DNA concentration and absorbance ratios of 260/280 (A), and capacity for DNA purification at different sample concentrations, revealing the DNA-beads binding capacity at 61.7 ± 1.0 ng/µL (yellow). (B). Error bars denote the standard deviation of mean values between triplicate samples of the same *P. multistriata* culture.

To assess the performance of an optimised protocol, the LAMPTRON extraction module was utilised to process *P. multistriata* samples with cell concentrations ranging from 1.0 x 10^6 to 1.1 x10^2 cells/mL, following the extraction protocol described in section 6.3.5. The DNA yield for the lowest cell concentration was 18.0 ± 0.8 ng/µL. Results showed that DNA yield was no longer significantly increased when processing 4.4 x10^5 and 1.0 x 10^6 cells/mL. Previous studies have suggested that DNA efficiency is dependent on beads capacity and cell loading to the extraction microfluidic system (Price et al. 2009). The maximum DNA binding capacity of LAMPTRON was experimentally measured at an average of 61.7 ± 1.0 ng/µL when extracting DNA from cells at concentrations ranging from 1.0 x 10^6 to 1.2 x10^5 cells/mL. Results suggested that the available space on the surface

of APTES-treated beads was saturated with cell numbers above the range of 4.4 x10^5 to 1.0 x 10^6 cells/mL, limiting any additional DNA binding above the threshold of 61.7 ± 1.0 ng/µL. The DNA capture efficiency between silica beads and glass fiber membrane was compared , which both received the same APTES treatment. The results indicated that silica beads led to higher DNA extraction efficiency than silica membranes, regardless of the sample source (Appendix E, Figure E1). As a result, I proposed that increasing the size of the extraction microchamber may enhance the loading capacity of silica beads and eventually improve DNA recovery beyond the current capacity of the LAMPTRON system. Alternatively, enhancement of DNA binding can be achieved by decreasing the size of silica beads and therefore increasing the surface area to volume ratio (Price et al. 2009). However, technical limitations have been reported upon the incorporation of nano-micro silica beads into a microfluidic system (Kebede et al. 2022).

To confirm the functionality of the LAMPTRON, the DNA eluents were quantified of *Pseudo-nitzschia* and *Alexandrium* cells using a silica-based extraction method with real-time PCR downstream analysis (Appendix E, section E2). Downstream qPCR analysis revealed no significant amplification inhibition from LAMPTRON DNA samples compared to the standard on-column commercial method (Qiagen), as shown by the comparison of cycle threshold (C_t) values in Figure E3, Appendix E). Based on the above data, an optimal DMA-based DNA purification protocol was identified and performed in subsequent experiments involving the APTES-treated silica beads, 1:1 DMA and sample input ratio, 0.1M trisodium citrate washing buffer, and 3-min elution step as described in section 6.3.5.

6.4.3 Evaluation of quantitative LAMP detection on the LOC system

The performance of the LAMPTRON system in detecting and quantifying *P. multistriata* cells was assessed using on-chip DMA-based extractions for DNA templates that underwent LAMP analysis. Based on DNA binding capacity results (Figure 6.4), LAMPTRON was loaded with known cell numbers of the *P. multistriata* SZN-B954 strain ranging in concentration from 10^5 to 10^1 cells/mL. The LAMP results suggested that the reuse of the extraction module of LAMPTRON produced DNA of sufficient yield and quality across independent LAMPTRON runs, suggesting minimum run-to-run variability, as shown in (Figure 6.5 (fresh reagents) and Figure 6.6 (preserved and stored reagents)).

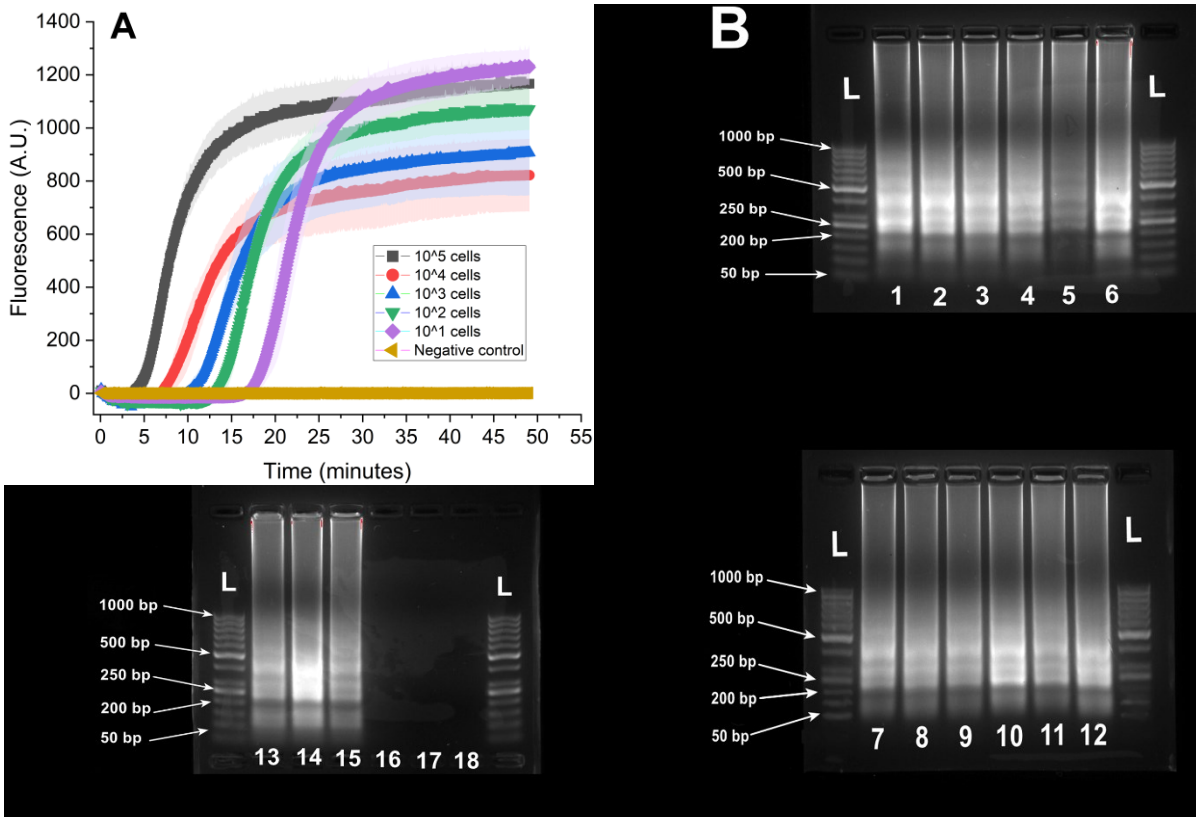

Figure 6.5 Fluorescence real-time detection of *P. multistriata* cell standards using freshly prepared LAMP reagents (A). Samples were analysed on the LAMPTRON system in triplicates for each concentration as represented by coloured datapoints; (black; $1.6x10^5$ cells/mL, red; $2.3x10^4$ cells/mL, blue; $1.3x10^3$ cells; green; $1.3x10^2$, purple; $1.1x10^1$ cells/mL; brown; non-template control (NTC). The LAMP reaction achieved a detection threshold of $1.1x10^1$ cells/mL (n=3). Error bars are represented as coloured filled area mean ± SD (n = 3 independent experiments). B) Gel electrophoresis data of the fluorescent LAMP products produced from the reactions in panel A, confirming the size of the LAMP amplicon at 222 bp. Lane L: DNA ladder (50 bp), lanes 1, 2, and 3 are replicates of $1.6x10^5$ cells/mL amplicons, lanes 4, 5, and 6 are replicates of $2.3x10^4$ cells/mL amplicons, lanes 7, 8, and 9 are replicates of $1.3x10^3$ cells/mL amplicons, lanes 10, 11, and 12 are replicates of $1.3x10^2$ cells/mL amplicons, lanes 13, 14, and 15 are replicates of $1.1x10^1$ cells/mL amplicons, lanes 16, 17, and 18 are replicates of non-template control (NTC).

A stepwise decrease in T_t value was observed when increasing cell number from 10^5 to 10 cells/mL, likely due to the relatively high abundance of nucleic acid recovered from high cell number compared to the lower cell number (Figure 6.5 & Figure 6.6). In accordance with these results, an improvement in DNA recovery was observed with increased input of cells into the DMA-based extraction module (Figure 6.4B). The high yield of isolated DNA in the system enables reliable quantitative LAMP analysis of *P. multistriata* cells. LAMP standard curves were used to show the T_t value as a function of cell number in each reaction in log scale (Figure 6.7), which demonstrated a good linear relationship between T_t and known cell numbers in both fresh and preserved LAMP

methods, indicating diagnostic abilities of the current LOC system for detection and quantification of *Pseudo-nitzschia* cells. Target-specific amplification was successfully demonstrated by the device, as shown in the gel electrophoresis results (Figure 6.5B & Figure 6.6B). Furthermore, the efficiency of LAMP amplification was calculated based on standard curves and the equation of isothermal doubling times (IDT = - 0.301 x m), where m represents the slope of the graph of T_t value plotted against the amount of target DNA/cells and 0.301 corresponds to a twofold change in concentration at 2 (Nixon et al. 2014). Repetitive experiments of fresh and vitrified LAMP reactions resulted in primer efficiencies with an average value of 94.0 ± 7.4 and 129.3 ± 16.6, respectively. Equations and coefficient of determination (R^2) values were derived from log-transformed copies number of cells and the mean values of T_t of LAMP reactions plotted on a linear scale (Figure 6.7). The fresh and preserved LAMP assays achieved strong correlation coefficients of 1.0 and 1.0, respectively, indicating suitable quantitative detection of *P. multistriata* cells under optimal conditions using the LAMPTRON system.

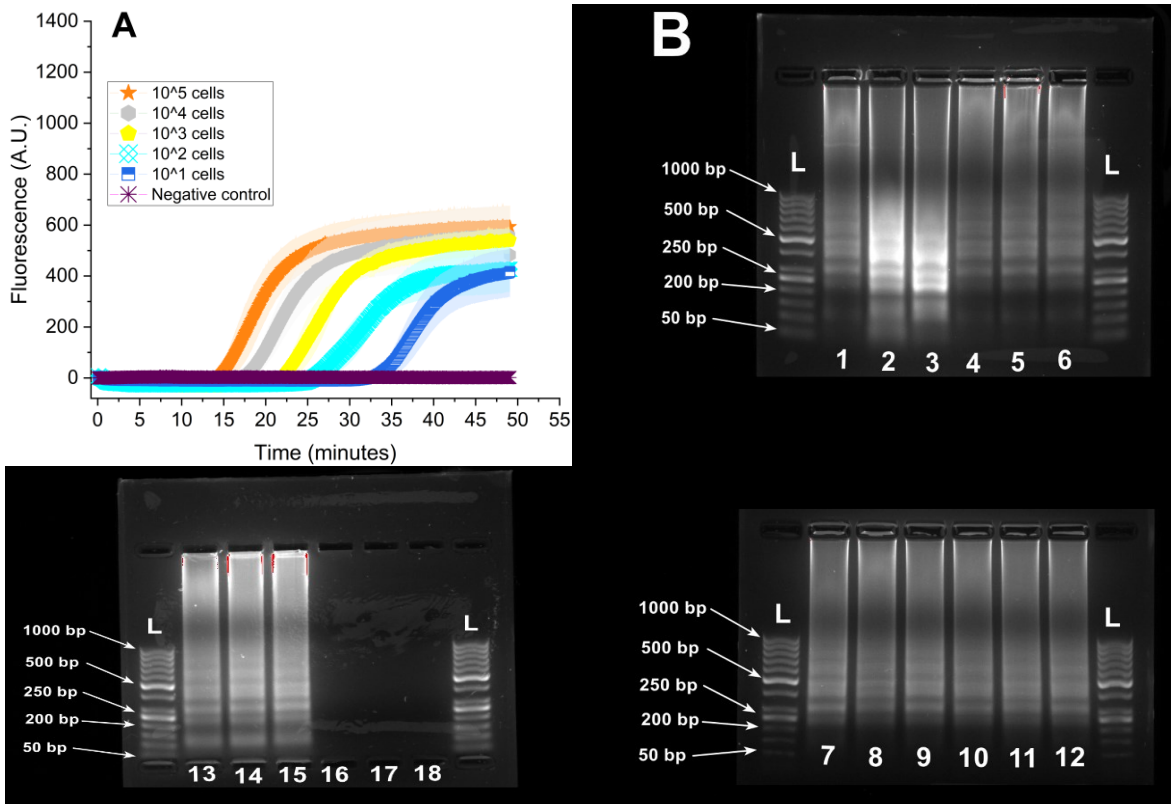

Figure 6.6 Performance of pre-stored LAMP reaction of five months shelf-life. A) Amplification curves of amplified *P. multistriata* cell standards were represented by (orange; $1.6x10^5$ cells/mL, grey; $2.3x10^4$ cells/mL, yellow; $1.3x10^3$ cells; cyan; $1.3x10^2$, dark blue; $1.1x10^1$ cells/mL; purple; non-template control (NTC). Each data point represents the average of independent triplicate reactions, and the coloured areas indicate standard deviation. A limit of detection was determined at approx. $1.1x10^1$ cells/mL using vitrified LAMP reaction on LAMPTRON system (n=3). B) Gel electrophoresis results of the vitrified LAMP products produced from the reactions in panel A. The lanes of electrophoretic agarose gel confirmed the specificity of LAMP amplicon at a size of 222 bp. Lane L

represents DNA ladder (50 bp), lanes 1, 2, and 3 represent replicates of $1.6x10^5$ cells/mL amplicons, lanes 4, 5, and 6 represent replicates of $2.3x10^4$ cells/mL amplicons, lanes 7, 8, and 9 represent replicates of $1.3x10^3$ cells/mL amplicons, lanes 10, 11, and 12 represent replicates of $1.3x10^2$ cells/mL amplicons, lanes 13, 14, and 15 represent replicates of $1.1x10^1$ cells/mL amplicons, lanes 16, 17, and 18 represent replicates of non-template control (NTC).

The long-term stability and robustness of LAMPTRON analysis were tested by preserving LAMP assays using an off-chip vitrification method for five months at room temperature prior to use on the LAMPTRON system. The existing vitrification methods for preserving LAMP reagents entailed adding enzymes and primers at the rehydration step (Hayashida et al. 2015, Hayashida et al. 2019, Phillips et al. 2019). In contrast, A new approach was employed in which all LAMP reaction components, including enzyme, primers, and reaction buffer, were preserved at room temperature for up to five months (Figure 6.6). This protocol simplified the operating of LAMPTRON by eliminating the need for additional pipetting steps, reducing the risk of contamination, and making the operating procedure more user-friendly for non-specialists. To reconstitute the vitrified LAMP assays, DNA templates were added, as described in section 6.3.6. However, preserving LAMP reagents can lead to variability in diagnostic performance compared to freshly prepared assays, due to the decrease in enzyme reactivity of the reaction reactivity (Diego et al. 2019, Mohan et al. 2021). As demonstrated in the LAMP amplification curves (Figure 6.5A & Figure 6.6A), there was a performance variability when the fluorescence signals of fresh LAMP amplicons reached saturation level at an earlier T_t value than vitrified LAMP amplicons. Specifically, the detection of DNA templates extracted from the same sample (10^5 cells/mL) was delayed by approximately 10 min when vitrified LAMP reagents were used. Similarly, the time required for both fresh and vitrified LAMP reactions to amplify the lowest cell number varied between 20.2 ± 1.1 and 36.3 ± 1.6 min. Such discrepancies in T_t values have been previously reported for both fresh and preserved LAMP reagents (Hayashida et al. 2015, Diego et al. 2019, Mohan et al. 2021, Toppings et al. 2021).

The robustness of the LAMPTRON analysis was tested by preserving LAMP assays for an extended period. The results revealed that LAMPTRON exhibited relatively stable performance with minimal variability in T_t values among replicates of the same preserved LAMP reaction, indicating low inhibitory effects from sample-to-sample carryover (Appendix E, Figure E4). The coefficient of variation (CV) of LAMP T_t values for triplicate measurements of 1.1×10^1 and 1.6×10^5 cells input using freshly prepared LAMP reagents were 0.05 and 0.05, respectively. Similarly, the CV of LAMP T_t values for triplicate measurements of 1.1×10^1 and 1.6×10^5 cells input using preserved LAMP reagents with a shelf life of five months were 0.04 and 0.06, respectively. The detection of 1.1×10^1

cells/mL *P. multistriata* cells took less than 36.3±1.6 minutes (i.e., T_t value) following a sample processing time of approximately 25 minutes, resulting in a total analysis time of less than one hour. This is three times faster compared to conventional detection methods such as PCR, which takes about 1 hour excluding post-amplification analysis, and two hours for standard DNA extraction. LAMP assay also provided more sensitive detection of *Pseudo-nitzschia* cells compared to conventional detection methods. For instance, while PCR measurements have quantified *Pseudo-nitzschia* cells at 10^3 per mL (Fitzpatrick et al. 2010), 1.2–8.9 $\times 10^7$ cells/mL (Penna et al. 2013), 33 cells/mL (McDonald et al. 2007), most of these measurements rely on post-amplification processing, which can prolong the time for an answer and result in complications in interpreting data. In contrast, LAMP analysis provided faster detection time, greater simplicity, and sensitivity by detecting the amplification of DNA template from 10 cells/mL of *P. multistriata* only in a 20-minute assay (Figure 6.5A). The use of LAMP alleviates post-amplification processing, thereby providing faster detection time, greater simplicity, and sensitivity.

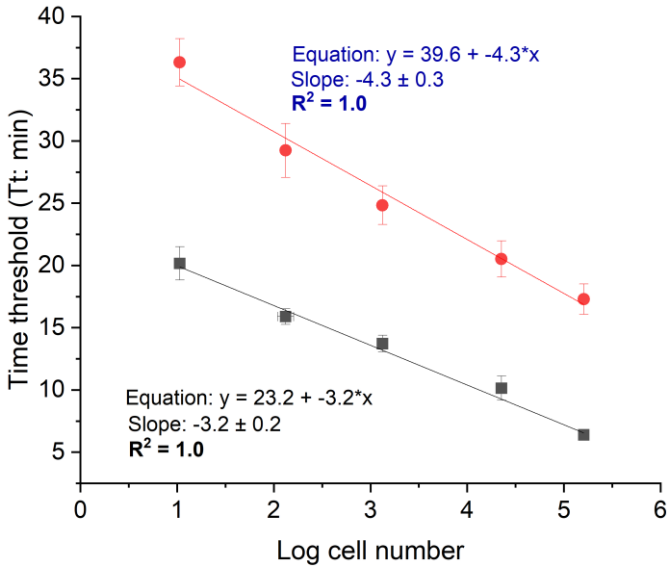

Figure 6.7 Quantification curve of LAMPTRON system for quantifying *P. multistriata* cells in concentrations ranging from $1.6x10^5$ to $1.1x10^1$ cells/mL, as obtained using real-time fresh LAMP (black square) and vitrified preserved LAMP (red circle) methods. The data are expressed as the mean ± SM (standard error of the mean) of at least 3 independent samples for each standard concentration. The insets show slopes, intercepts, and correlation coefficients (R^2) of linear regression of data for fresh LAMP (represented by the black text below the graph) and vitrified preserved reagents (represented by the blue text above the graph).

The precision of LAMPTRON was evaluated by generating standard curves from LAMP T_t values of known cell numbers (Figure 6.7). The limit of quantification (LoQ) was determined using the lowest concentration on the standard curve that resulted in positive amplification over multiple LAMP amplifications, whereas the limit of detection (LoD) was estimated from the last concentration that

produced positive amplification in all replicates (Seo and Yoo 2020). The establishment of the LoD was based on a set of real-time LAMP amplification curves (Figure 6.5A & Figure 6.6A), and the last positive concentration from the standard curve over repeated LAMP amplification was used to estimate the LoQ (Figure 6.7). LAMPTRON was found to have LoD and LoQ below 1.1x10 cells/mL, using both fresh and vitrified preserved reactions. Fresh LAMP exhibited the best overall performance, detecting 1.1x10 cells/mL (LoD & LOQ) in less than 6 minutes. By increasing the reaction time of LAMP over 49 minutes, The limit of detection (LoD) of the on-chip LAMP assay was improved to detect low cell numbers at 1.1x10 cells/mL, as previously proposed in (Kaur et al. 2019). The quality of the DNA template is critical for determining LAMP reaction kinetics and may adversely affect the LoD and delay detection time (Mohan et al. 2021). The LAMPTRON chip was cleaned through multiple cleaning steps to remove sample-to-sample inhibitors/cross-contamination by lipids, protein, DNA and reagents that may affect the LoD. The LAMPTRON platform provided a sensitivity that was nearly fifteen times greater than the statutory limit of 150 cells/mL established by UK guidelines for conducting emergency statutory testing of seawater and shellfish to avoid human health risks (Downes-Tettmar et al. 2013). The quality of the DNA template was shown to be critical for determining LAMP reaction kinetics and could adversely affect the LoQ and LoD and delay detection time.

The LAMPTRON system presents a simplified and cost-effective method for DNA purification compared to commercially available kits. The on-chip DMA purification method in LAMPTRON requires only three steps, including lysis-binding reaction, washing, and elution, which takes only 25 min before LAMP analysis of DNA extracts from *Pseudo-nitzschia* cells. In contrast, the DNeasy Plant Mini kit (Catalogue number: 69104, Qiagen) requires 27 steps in approximately 2 hours to extract DNA from the same *Pseudo-nitzschia* cells. Moreover, the DNeasy Plant Mini method (Qiagen) involves an additional grinding step using TissueLyser (Qiagen) and a heating block for cell lysis that are not provided with the kit, increasing the time, cost, and complexity of the extraction protocol. Reagent costs per sample are estimated to decrease by 97.3% with the DMA-based extraction protocol, as summarised in Table E1, in Appendix E, providing a rapid and cost-effective alternative for DNA purification. Hence, the DMA-based technique is not only cost-effective but also demands minimal hands-on time for executing the streamlined analysis on LAMPTRON.

6.5 Conclusions

A microfluidic system that allows flexible customization for lab-on-chip DNA extraction and real-time quantification was developed. The DNA extraction process leverages the high surface-to-

volume ratios of silica beads, using a dimethyl adipimidate (DMA) method to achieve high-efficiency DNA capture. By automating the repetitive liquid handling operations during the DNA extraction process, high DNA yield was achieved using small reagent volumes, which reduces cost and minimises sample-to-sample cross-contamination. LAMPTRON prototype also achieved reproducible on-chip-based LAMP analysis of the *Pseudo-nitzschia* toxin-encoding target within 49 min. The LAMP quantification method offers faster analysis than traditional methods that require costly reagents, sophisticated equipment and a centralised laboratory. The streamlined on-chip operations for automated DNA extraction and LAMP testing for detecting as low as 10 cells/mL were completed within less than one hour. Such early-stage detection of *Pseudo-nitzschia* blooms can mitigate human health risks and economic costs (Trainer et al. 2012). Additionally, the preserved LAMP assay allows for flexible testing workflows in decentralised settings with minimal user intervention, avoiding potential sources of contamination or human-introduced error. The reusable chip, fluorescence detector, thermal profiling unit, and electronics minimise the cost, waste, and consequently the environmental footprint of LAMPTRON. The study demonstrated the simplicity of performing quantification using dried LAMP and the versatility of the DNA capture method from a range of microbial cells, which make LAMPTRON potentially applicable in a variety of environmentally relevant settings. Future work will focus on engineering a multiplexable autonomous system that multiplies a number of simultaneous DNA extractions coupled with nucleic acid amplification testing which will be amenable for field-use settings to bypass sample transportation and lab processing.

Chapter 7 Conclusions and future work

7.1 Conclusions

The goal of this work was to develop nucleic acid-based amplification methodologies for the detection of the harmful microalgae species known as *Pseudo-nitzschia*. This particular diatom species poses a significant threat to both human health and aquatic organisms due to its production of a potent neurotoxin responsible for causing the life-threatening condition known as amnesic shellfish poisoning (ASP) (Trainer et al. 2012). The proposed molecular analysis was aimed to be integrated with a microfluidic device towards regular monitoring for rapid and accurate genetic analysis of *Pseudo-nitzschia*. The overarching aim was to demonstrate proof-of-concept for a genetic sensor, adaptable for on-site nucleic acid-based analysis of harmful algal blooms (HABs) caused by *Pseudo-nitzschia* with a focus on achieving high sensitivity. Although the autonomous use of a developed lab-on-a-chip device has yet to be fully realised, operational procedures were successfully optimised for semi-automated, fast, and miniaturised genetic analysis, offering the potential for future development steps towards a fully autonomous deployable genetic sampler.

This thesis reports on (1) the development of a novel qPCR assay for quantifying the microalgae species *Pseudo-nitzschia*. The efficiency of this assay was evaluated by comparing its estimates of cell abundance with conventional microscopy cell counting. (2) The utilisation of a newly developed qPCR assay to investigate toxin production and transcriptomic responses of nutrient-depleted *Pseudo-nitzschia* treatment following exposure to the addition of phosphate (P), nitrate (N), and silicate (Si). (3) Developing and optimising novel isothermal amplification methods for rapid, simple, and sensitive detection of *Pseudo-nitzschia* spp. (4) the use of fully pre-prepared and preserved reaction mixtures to represent field-based assays, along with evaluating the long-term stability of various amplification chemistries at ambient conditions. (5) Developing a lab-on-a-chip system designed to automate DNA analysis of *Pseudo-nitzschia spp* via integrating processes of nucleic acid purification and real-time isothermal detection. These interconnected research avenues collectively contribute to a comprehensive exploration of molecular methodologies for monitoring the *Pseudo-nitzschia* microalgae.

Nucleic acid amplification-based methodologies have been widely applied in food and water biosecurity, public health protection, and environmental monitoring (Nikiforova et al. 2015). These techniques can be automated and performed using portable or deployable instrumentation, thereby extending the reach of high-quality analytical capabilities to remote regions with limited

resources. However, the gold standard molecular method, PCR, has certain limitations due to its energy demands and the technical challenges of heating reagents to high temperatures. In contrast, isothermal reaction chemistries present promising alternatives, offering convenient operation of genetic analysis at constant and low temperatures, making them amenable for deployment on portable Lab-on-a-Chip (LOC) platforms.

An isothermal technology (known as 'LAMP') was successfully applied here for the detection of *Pseudo-nitzschia* diatoms. Furthermore, a vitrification-based preservation protocol has been developed for the long-term stability of LAMP components, eliminating the need for cold-chain reagent delivery and storage. This approach can mitigate the potential errors associated with multiple reagent preparation steps, particularly when conducted by untrained users. As a result, the workflow has led to a reduction in handling time and a simplified analysis protocol. The development of integrated sensor technology has significantly progressed through thesis work by merging 'front-end' processes of sampling and preservation, and 'back-end' procedures of nucleic acid amplification and detection to provide *in situ* genetic analysis capability. Easy-to-use testing could be valuable for emergency and outbreak response, by facilitating the automated genetic analysis for end-users situated outside of centralised laboratory facilities.

7.1.1 PCR-Based Early Detection of Harmful *Pseudo-nitzschia* Blooms for Enhanced Environmental Protection

In Chapter 2, a PCR-based detection technique was developed for *Pseudo-nitzschia* detection. This method involved multiple denaturing, annealing and extension-based amplification cycles to provide specific and sensitive identification of *Pseudo-nitzschia* spp. The novel qPCR assay was inclusive to toxic *Pseudo-nitzschia* strains, without cross-amplification with non-target microalgal species. This assay was sensitive to quantify 10^4 cells l^{-1}, providing a quantification of *Pseudo-nitzschia* levels lower than the regulatory thresholds of 1.5×10^5 cells l^{-1}. The qPCR was used for quantifying cell numbers from spiked natural seawater, resulting in a good agreement between qPCR-based cell enumeration and microscopic cell counts. This quantitative performance of the developed qPCR assay offers the potential for early detection of *Pseudo-nitzschia* blooms at low cell abundance, allowing for timely intervention before regulatory thresholds are breached. The amount of Domoic Acid present in the *Pseudo-nitzschia* cultures was proportionally correlated with the target copy numbers of the geranyl pyrophosphate synthase (GPP) gene (R^2= 0.9, P = 0.00007). Thereby, the application of this assay could facilitate risk management of harmful bloom of *Pseudo-nitzschia*, protecting public health, marine wildlife, and aquatic industries. However, PCR-based amplification relies on cycling through different temperatures posing a barrier for on-site, simple

and fast molecular analysis of *Pseudo-nitzschia* blooms. Therefore, further work in the subsequent chapter 4 was conducted to investigate alternative amplification strategies that can be performed under simpler conditions for the *Pseudo-nitzschia* detection.

7.1.2 RNA-Based Monitoring of Nutrient-Induced Domoic Acid Responses

In Chapter 3, the capability of the newly developed quantitative PCR (qPCR) assay was extended by incorporating a reverse transcription step, enabling real-time RNA quantification to analyse metabolically viable cells. The separate reverse transcription step effectively maintained the labile nature of the RNA template for subsequent qPCR amplification reactions. RNA-based quantification by qPCR was employed to assess the gene expression of the geranyl pyrophosphate synthase (GPP) gene in *P. multistriata*, aiming to explore correlations between the accumulation of domoic acid (DA) and transcript abundance. To simulate natural stressors caused by increased nutrient input in coastal systems, The nutrient-depleted *P. multistriata* treatments were exposed to a 48-hour pulse addition of phosphate (P), nitrate (N), and silicate (Si). This study aimed to evaluate the response of stressed *P. multistriata* to variations in nutrient levels, cellular growth, and gene expression with regard to DA production. The RT-qPCR method was employed to genetically track the differential transcription of the geranyl pyrophosphate synthase (GPP) gene under different nutrient treatments between the pre-and post-experimental period. DA production was significantly induced at 2 hours after Si-addition, 6 hours after N-addition, and 48 hours after P-addition. These inductions were accompanied by increases in target gene transcription, with fold changes of 3.9 after Si-addition, 4.0 after N-addition, and 14.7 after P-addition, compared to the baseline before nutrient addition (0 hours) in N-, P-, and Si-depleted cells. The phosphate treatment yielded the highest production of domoic acid compared to other treatments, reaching a level of 0.6 ± 0.2 pg DA $cell^{-1}$ at t=48 h following the addition of phosphate. A strong correlation was found between transcript abundance and DA content in P-depleted cells (r = 1.0, R^2 = 1.0, P = 0.0004), with a weaker but significant correlation in Si-depleted cells (r = 0.9, R^2 = 0.7, P= 0.03). These findings suggest that the nutrient enrichment in coastal waters would induce domoic acid episodes, exacerbating intoxication threats to marine organisms within marine food chains towards humans. As a result, the RNA-based molecular technique offers an advantage as an indicator for tracking changes in toxin production in response to nutrient variability. However, several questions have still not been completely elucidated through this experimental study, including the environmental role of DA, and the impact of DA production on the whole marine ecosystem. Addressing these questions requires large-scale monitoring of *Pseudo-nitzschia* response to environmental fluctuations, enabling the reliable management of anticipated outbreaks in coastal regions. Despite the precise quantification

offered by the new RT-qPCR method, it presents multiple challenges due to the requirement for repeated and power-hungry thermocycling, affecting the integrity of short-lived RNA samples being analysed in a single amplification reaction. This also may require complex and expensive instrumentation for operating large-scale genetic monitoring.

7.1.3 Isothermal Amplification for *Pseudo-nitzschia* Detection

Chapter 4 focused on the development of isothermal amplification assays for DNA-based detection of the marine diatom of *Pseudo-nitzschia* spp. Two novel assays, loop-mediated isothermal amplification assay (LAMP) and recombinase polymerase amplification (RPA) assay were designed for *Pseudo-nitzschia* detection. LAMP and RPA assays amplified the cytochrome P450, *dabD* gene which plays a significant role in the DA biosynthetic route. These amplification strategies involve repetitive cleavage of nucleic acid template catalysed by thermal-labile enzymes such as DNA polymerase, nucleases, and exonuclease (Yan et al. 2014).

Both the optimised LAMP and RPA assays demonstrated on-target amplification without off-target amplification when assaying the DNA samples of non-target algal species. To compare their sensitivities, a set of known concentrations of the target sequence was synthesised within DNA plasmids, subjecting them to LAMP and RPA amplification. The LAMP and RPA results were analysed by evaluating the time threshold (T_t) value, representing the time point at which the fluorescence signal crosses the threshold fluorescence level during the amplification reaction (Diego et al. 2019). A decrease in T_t value was observed when amplifying higher genetic target concentrations, in contrast to higher T_t values obtained when amplifying samples with lower genetic target concentrations. The linear relationship between the concentration of the target sequence and the Tt values allows for quantitative assessment of both isothermal assays (Euler et al. 2012, Nguyen et al. 2020). LAMP assay demonstrated superior quantitative linearity, yielded R^2 values at 1.0 which is higher than the R^2 value of 0.8 for the RPA assay. The LAMP reaction demonstrated greater sensitivity by detecting a single copy per µl of the target gene, compared to the RPA reaction which detected approximately 10^3 copies μl^{-1}. This difference could be explained by enzymatic-assisted amplifications in the LAMP reaction provided by a single enzyme, the DNA polymerase, in the LAMP amplification reaction, in contrast to the variable kinetics among RPA enzymes involved in the RPA amplification reaction (Piepenburg et al. 2006, Li et al. 2019a).

Given the superior performance of the LAMP assay, the LAMP-based amplification was further validated by quantifying unknown copy numbers of the target gene in real-world seawater samples. These environmental seawater samples were collected on an almost weekly basis over six months

from September 13, 2021, to March 28, 2022, from three sites in the known harmful algal bloom hotspot of St Austell Bay in Cornwall, England, where toxic *Pseudo-nitzschia* species had been previously reported (Downes-Tettmar et al. 2013, Brown et al. 2022). Among the 44 DNA samples extracted from seawater, the LAMP assay was positive for only 34 samples, achieving a sensitivity rate of 77.3%. Whilst LAMP assay showed a tolerance with potential inhibitors in environmental samples, LAMP-based quantification yielded environmentally irrelevant levels of the target sequence in one sample. Therefore, careful attention is needed to ensure environmentally representative and accurate genetic results, when quantifying targets from complex extracts. The LAMP analysis revealed an increase in the *Pseudo-nitzschia* target gene during both the Autumn and Spring seasons. With the high sensitivity of LAMP assay in environmental testing, it can offer an advantage for identifying the onset of blooms through time-series analysis of natural seawater. Additionally, rapid LAMP testing can be useful to avoid serious implications of *Pseudo-nitzschia* bloom for human health, the environment and industries, particularly before DA toxin levels breach safe regulatory levels.

7.1.4 Vitrification for Long-Term Preservation of Nucleic Acid Amplification Mixtures

Chapter 5 introduced an optimised procedure for preserving nucleic acid-based amplification mixtures. This preservation technique relies on vitrification technology that transitions the liquid status of molecular reagents into a viscous, coiled, and inactive status (Liu et al. 2018). This vitrified status was achieved by drying the wet reagents of the amplification reaction in a mixture of stabilisers such as trehalose, glycerol and Polyoxyethylene glycol. Various combinations of vitrifying components at different concentrations were evaluated to optimise the preservation protocol. Additionally, two different rehydration methods were assessed to re-activate the dried amplification master mixes at ambient conditions.

The vitrification technology was effective in maintaining the reactivity of nucleic acid-based amplification reactions as demonstrated in this chapter. The standard amplification reaction mixture consists of key components: containing reaction buffer, primers, fluorescent reporter dye, nucleotides, and DNA sample. The commonly used vitrification method in the literature involves a separate drying of a single component of the reaction mixture (e.g., enzyme or primers or both) with a vitrifying agent, followed by an air-drying step and subsequent rehydration with the remaining components of the amplification reaction (Rombach et al. 2014b, Hayashida et al. 2015, Yu et al. 2015, Hayashida et al. 2019, Phillips et al. 2019). In contrast, the presented preservation

protocol here assembles all the reaction mixture components into a single sticky matrix which was rehydrated later with the addition of the DNA sample of the *Pseudo-nitzschia*.

The optimised preservation technique was further evaluated using two different amplification chemistries of real-time detection including PCR hydrolysis probes labelled with the FAM and HEX fluorophores as well as LAMP fluorogenic dye. To evaluate the reduction in enzymatic activity of each amplification strategy, plasmid DNA standards were amplified using all vitrified reactions in comparison with freshly prepared reaction mixtures. The change in rapidity, sensitivity and performance of vitrified-based detections was monitored over a duration of six months.

LAMP and Hex-labelled vitrified master mixes demonstrated stable sensitivity at a single copy of target DNA after 6 months of storage. In comparison, the FAM-labelled vitrified master mix showed lower sensitivity, detecting 10^3 copies per reaction after the same storage duration. LAMP vitrified reactions with a 6-month shelf life demonstrated faster and greater sensitive analysis compared to vitrified qPCR reactions with the same shelf life. However, a reduction in fluorescence signal and amplicon was observed in the vitrified reactions compared to wet reactions, suggesting a loss of reactivity of enzymes due to harsh vitrification storage at ambient conditions. Therefore, the functional reactivity of vitrified enzymes could be enhanced upon refrigeration storage at lower temperatures rather than ambient conditions. The refrigeration storage of PCR amplification reaction would also enable more rapid analysis of low abundant targets compared to vitrified reactions at ambient temperatures (Sun et al. 2013). In summary, long-term stabilisation of the full LAMP reaction mixture was achieved under ambient conditions for a minimum of six months without refrigeration. The vitrified reactions were activated upon the addition of an aqueous DNA sample. This procedure can be useful for ready-to-use amplification reactions, offering minimal preparation steps, alleviating risks of contamination due to frequent freeze-thawing of refrigerated reaction components and preventing potential human pipetting errors from non-trained personnel. Preserved assays can also enable simple, low-cost and fast molecular analysis in limited-resource areas and during bloom outbreaks, where sustainable cold-chain transportation of molecular reagents may not be logistically feasible.

7.1.5 LAMPTRON: A Miniaturized Genetic Sensor for Rapid *Pseudo-nitzschia* Detection and Analysis

Chapter 6 demonstrated the successful development of the lab-on-chip device, known as "LAMPTRON." This chapter presents the developmental process involved in creating this innovative genetic sensor, "LAMPTRON", which was designed to enable rapid and precise quantification of the

harmful microorganism *Pseudo-nitzschia*. The LAMPTRON prototype incorporates a state-of-the-art Lab-on-a-Chip technology with isothermal nucleic acid detection using the Loop-mediated isothermal Amplification (LAMP) method. The initial prototype of LAMPTRON enabled a miniaturised LAMP-based detection by amplifying the DNA target in a single step. To operate real-time measurement of the fluorescence signal at the reaction endpoint, a newly developed fluorescence detector was incorporated. The fluorescence signal is directly proportional to the quantity of DNA product generated during the LAMP reaction. A key innovation in LAMPTRON is the use of a prestored LAMP master mix at ambient temperatures, alleviating the need for multiple preparation steps and expensive instrumentation for reagent preservation. To initiate LAMP amplification, the DNA sample was used to reconstitute the vitrified reaction mixture. The 'shelf-life' of the preserved LAMP reagents was extended up to 2 months, with no significant differences in assay performance compared to freshly prepared LAMP mixtures that relied on cold-chain-dependent, wet reagents. To simplify the operation for end-users, real-time LAMP detection was achieved within 45 minutes using pre-stored reagents on a disposable, and reusable PMMA cartridge. The prototype of LAMPTRON was presented at the Marine Autonomy and Technology Conference in 2022 (available at https://techoceans.eu/resources/). This prototype serves as a proof-of-concept of an *in-situ* and reusable genetic analyser that could satisfy the requirements for simple, and fast environmental monitoring.

The development of the second prototype aimed to interface with the existing autonomous single-step LAMP analysis with a miniaturised nucleic acid extraction and purification method. To achieve this, a novel microfluidic system was designed to integrate two key components: the module responsible for DNA extraction, and the amplification-detection module. Each of these modules was independently optimised before being combined into a self-contained analyser, resulting in the LAMPTRON second prototype. The on-chip DNA purification protocol involved the utilisation of amine-functionalised silica beads and dimethyl adipimidate (DMA) to ensure efficient DNA capture. Firstly, the sample preparation step was initiated by pelleting the algal cells toward DMA-mediated DNA purification. DMA maximises the DNA capture through a dual binding mechanism when 1) the amino groups of DMA directly bind with negatively charged DNA by electrostatic capture, and 2) DMA reagent forms covalent bonds with functionalised silica substrate to generate extra positively charged amidine bonds that extensively attract negatively charged DNA (Shin et al. 2015, Jin et al. 2017, Yoon et al. 2018). In addition, the DMA extraction method was coupled with small, functionalised silica beads to increase the available surface area for DNA capture. Subsequently, the purified DNA is amplified using downstream single-step LAMP analysis directly on the microfluidic chip.

LAMPTRON demonstrated a reproducible on-chip-based DNA extraction and LAMP analysis, with the capability to detect as low as 10 cells/mL within one hour. In addition, the sample-to-sample variability of the LAMPTRON system was evaluated by quantifying cell replicates using both fresh and vitrified LAMP assays. The analytical capacity of the LAMPTRON system was evaluated in analysing *Pseudo-nitzschia* samples ranging in concentration from 1.1 $x10^2$ to 1.0 x 10^6 cells/mL. Results indicated that the maximum DNA binding capacity of LAMPTRON was approximately 61.7 ± 1.0 ng/µL when extracting DNA from cells in the concentration range from 1.0 x 10^6 to 1.2 $x10^5$ cells/mL. The LAMPTRON demonstrated a limit of detection of *Pseudo-nitzschia* 10 cells/mL, representing the minimum number of cells enough for successful on-chip subsequent LAMP amplification. The OTE research group has a pipeline of next-generation hardware for enabling a wide range of Lab-on-a-Chip (LOC) applications. Continuous fluid actuation was effectively managed through an electronic rig, offering automated control of pumps, valves, and heaters via a custom user interface. The fluorescence measurements were recorded in the real-time during LAMP amplification of DNA using a compact detector.

The vitrification technique was used to preserve the stability of LAMP assay components for up to five months, allowing storage of LAMP reagents at ambient temperatures. The LAMP amplification reactions were conducted at a constant temperature of 65ºC, which could increase the risk of bubble generation. The vitrified status of LAMP reaction mixtures was proven to reduce this risk by maintaining a gelifed matrix which was trapped in the reaction chamber during the amplification reaction, due to incomplete wetting. Consequently, the vitrification of the LAMP mixture effectively reduced the generation of bubbles and avoided a loss in reaction volume albeit under the challenging conditions of a 65ºC incubation during the LAMP amplification reaction. The preloading of the LAMP reaction mixture on a microfluidic system has also proven to be highly advantageous for expediting nucleic acid testing.

The LAMPTRON system merged two fundamental functions: (1) DNA extraction and (2) real-time LAMP amplification, replacing the need for bulky and expensive laboratory instruments with an easy-to-use and affordable miniaturised system. LAMPTRON offers a significantly economical and simplified approach to molecular analysis in comparison to the commercial competitors, which rely on large, expensive instruments and consume excessive amounts of reagents and power such as the Afinion™ System (Abbott), the QIAxcel automatic DNA/RNA analyser (Qiagen), and the VERSANT® kPCR Molecular System (Siemens Healthcare). In contrast, LAMPTRON operated only three steps of DNA extraction, taking just 25 minutes before initiating LAMP analysis, reducing the cost of reagents per sample to £0.15. This represents 97.3% lower than a commercial DNA extraction kit which requires a labour-intensive 27 steps and takes approximately 2 hours to extract

a DNA sample. LAMPTRON also offers advantages of minimal instrumentation with low manufacturing and operating expenditures. The preloading of assay reagents onto the microfluidic chip of LAMPTRON eliminated the multiple preparation steps of the DNA extraction step and LAMP assay, decreased contamination risks, and eliminated the need for laboratory equipment. In summary, LAMPTRON has the potential to allow cost-effective and simple molecular detection and eventually portable genetic analysis.

7.2 Future work:

There are a number of suggestions for further improving this research as outlined in the following sections:

7.2.1 Discriminating Toxigenic from Non-Toxigenic *Pseudo-nitzschia* species in the Domoic Acid Biosynthesis Pathway

Despite significant research progress in understanding the genes and transcripts involved in the domoic acid (DA) biosynthesis pathway, challenges persist in discriminating between toxigenic and non-toxigenic *Pseudo-nitzschia* species using genetic molecular techniques. The limited genetic information available for the DA transcriptome library in non-toxigenic *Pseudo-nitzschia* species hinders the ability to determine the presence or absence of DA-biosynthetic genes in these strains. Additionally, non-toxigenic strains lack data on protein expression or enzymatic activity related to DA biosynthesis. To address this, further investigations employing sequencing analysis of DA-encoding genes or their homologs in non-toxigenic strains are necessary. Moreover, experimental studies are required to assess the metabolic capabilities of non-toxigenic strains, including their potential to produce DA analogues or the final DA product. These comprehensive studies can lead to characterising and identifying a robust genetic marker for distinguishing between toxigenic and non-toxigenic *Pseudo-nitzschia species*, enabling the development of a highly discriminatory molecular assay. The development of a molecular tool capable of providing a simple "yes" or "no" answer regarding the genetic capability of a tested *Pseudo-nitzschia* strain to produce DA, would enhance the ability to rapidly and accurately assess the risk of harmful algal blooms and their potential impact on aquatic environments, industries and public health. This molecular tool has the potential to revolutionize the current environmental monitoring towards scalable point-of-sampling testing, offering efficient, rapid and reliable information about the presence of DA-producing strains. Such information can facilitate timely interventions when required, enabling the efficient protection of ecosystems, shellfish industries, and public well-being.

7.2.2 Ecological Role of Domoic Acid

Further research is needed to address the existing gaps in our understanding of the regulation and function of DA in the environment. Previous studies proposed a range of potential functions for DA, including its possible role either as microbial signalling function, metal chelator, allelopathic toxicity, osmoprotectant, antagonist to nutrient loading, bacterial antibiotic, pheromone or waste product (La Barre et al. 2014). Multi-omics studies would be useful in providing valuable insights to confirm the function of DA by incorporating genetic sequencing (genomics), mRNA (transcriptomics), metabolites (metabolomics) and proteins (proteomics) (Bates et al. 2018). Whilst next-generation methods can provide high-throughput characterization of genome functions in *Pseudo-nitzschia* species, they may be limited due to their high-cost, complex protocols and time-consuming analysis. Alternatively, molecular assays offer an effective and affordable solution for point-of-harvest testing, enabling a cost-effective option for HABS monitoring.

7.2.3 Complexity of Domoic Acid Production

While significant research advances in elucidating the molecular pathways underlying DA production, several knowledge gaps remain. Previous studies identified various key genes associated with DA biosynthesis (Boissonneault et al. 2013, Brunson et al. 2018, Hardardottir et al. 2019, Jiang 2019). However, the activation of DA-encoding genes depends on the intraspecific diversity of *Pseudo-nitzschia* and various parameters including biological and non-biological conditions (Hardardottir et al. 2019, Lema et al. 2019). This necessitates the testing of multiple strains of a species to comprehensively study DA production under diverse environmental conditions including pH, light, nutrients, temperature and the presence of zooplankton. Yet, it remains uncertain whether the genomes of non-toxigenic *Pseudo-nitzschia* species possess the encoding genes for DA production (Bates et al. 2018, Bates et al. 2019). In addition, another challenge was raised due to the presence of certain DA-encoding genes in non-*Pseudo-nitzschia* species (Chekan et al. 2020, Steele et al. 2022). Therefore, developing a highly discriminatory molecular method targeting DA-encoding genes could assist monitoring efforts by differentiating between non-toxigenic and toxigenic *Pseudo-nitzschia* species. The key challenge is to select an appropriate genetic marker for toxicity identification, as an excessively variable genetic marker could potentially lead to an overestimation of genetic diversity.

7.2.4 Isothermal mRNA-Based Analysis of Domoic Acid-Producing *Pseudo-nitzschia*

Isothermal mRNA-based amplification assays can be further explored to enable the analysis of transcriptome activity within viable *Pseudo-nitzschia* samples. The analysis of RNA offers the advantage of quantifying viable and transcriptionally active cells compared to DNA which can be present in inactive or dead cells. Multiplex isothermal RNA-based detection can further enable the quantification of multiple DA-encoding genes in a single reaction, This approach can be used to provide gene expression levels of these genes in response to various toxin production conditions. Quantifying the transcriptomic responses of toxic cells can unveil patterns of DA-linked transcription of environmental samples, allowing high-resolution time-series data. Through lab-on-a-chip (LOC) testing of RNA extracted from *Pseudo-nitzschia* field samples, more immediate data will be available to understand the seasonal dynamic and diel transcriptional changes of the DA biosynthetic machinery. By relying on genetic quantitative data rather than pure arbitrary observations such as satellite images of HABS, A dependable and fit-for-purpose model capable of predicting the toxic capability of blooms to protect public health and the environment can be developed..

7.2.5 Enhancing Stability and Sensitivity of Vitrified Assays for *Pseudo-nitzschia* Molecular Analysis

While vitrification proved effective for molecular analysis of *Pseudo-nitzschia* in Chapter 4, there were instances of reduced sensitivity in certain amplification chemistries. To address this the stability of vitrified reagents can be improved through an optimised preservation protocol. This improvement involves exploring the use of different stabilizers and optimising the performance of vitrified assays across a range of ambient temperatures. Alternatively, investigating the refrigeration of vitrified reagents could extend their stability beyond the current six-month shelf-life. Furthermore, it may be beneficial to compare vitrification with other pre-storage methods, such as freeze-drying, to determine the most effective preservation technique.

7.2.6 Enhancing LAMPTRON for *in-Situ* Genetic Analysis in Environmental Monitoring

While the LAMPTRON system featured in Chapter 6 demonstrated the integration of genetic extraction and LAMP isothermal testing into a simple, low-cost system, it currently lacks ideal capabilities for full *in-situ* deployment. The sample preparation module currently involves collecting and pelleting *Pseudo-nitzschia* cells off-device using centrifugation. This would significantly limit the

LAMPTRON's real-world applicability for environmental testing. The cell lysate was subsequently suspended in a DMA solution and loaded into a microfluidic chip for miniaturised DNA extraction. Further optimisation of this process could lead to a simpler, flexible, and automated protocol towards on-chip sample preparation and detection for untrained end-users without specialized training. Automation of the sampling program in the LAMPTRON system would allow the validation of a fully automated extraction module on real-world samples but also enable routine measurements in remote and challenging environments.

7.2.7 Autonomous LAMPTRON System

Enabling full autonomy in the operation of the LAMPTRON system would facilitate the continuous streaming of genetic data during field deployments outside centralised laboratories in the natural environment. Deploying LAMPTRON in natural waters would also serve to evaluate its robustness and performance in real-world applications. The integration of lab-on-chip molecular detection technologies with an autonomous sampler could be fully automated through the precise actuation of reagent dispensing using components such as pumps, valves, and mixers. Furthermore, this user-friendly *in-situ* genetic sensor can be interfaced with water-ongoing platforms including moorings, remote-operated observatories and autonomous underwater vehicles. The resulting system has the potential to provide high temporal resolution in monitoring harmful algal blooms through field deployments at hotspot sites. By combining nucleic acid analysis with measurements of environmental parameters such as salinity, temperature, and nutrient concentration, the vulnerability of environmental sites to initiate harmful blooms can be comprehensively assessed. By developing a time-resolved genetic analysis using a deployable automated sensor, a paradigm shift can be introduced in the way we monitor the ubiquitous blooming of harmful algae in the environment.

7.2.8 Enhancing LAMPTRON for Affordable Algal Bloom Detection and Environmental Monitoring

Several modifications to the LAMPTRON hardware can be done to address the current complex design and to reduce the long time for fabrication and assembly. Simplifying the instrumentation of LAMPTRON could decrease fabrication costs by creating truly disposable devices, offering the ease of automation for untrained personnel. The flexible microfluidic platform is a feasible option to seemingly conduct molecular detection via manipulating amplification reagents through channels and voids between layers of adhesive and non-adhesive tape. These flexible fluidic

structures provide several advantages including low-cost materials, bioassays compatible materials, minimal manufacturing waste, and a reduced environmental footprint of sensors. This also facilitates the rapid prototyping for mass production. As a result, the fabrication of the LAMPTRON prototype in the future can be scaled up into large numbers. The simplicity and cost-effective fabrication process offers an opportunity to establish a network of sensors deployed across a broad spatial scale. The resulting quantitative genetic data can be used in a sensor-driven model to analyse the dynamics of algal blooms, providing a predictive tool for identifying new HABS hotspots. Implementing an intelligent monitoring network can enhance our understanding of ecological changes in high-risk areas, protecting public health, and enabling improved environmental management and regulations.

In the application of molecular methods to cultured samples, both advantages and limitations emerged. Cultured samples afford controlled conditions, enhancing reproducibility, facilitating result verification, and ensuring the reliability of findings. Using cultured samples also allows the in-depth analysis of specific biological processes, permitting precise manipulation of variables and providing metrics that may be challenging to observe in natural environments. However, drawbacks include the potential deviation of results from real-world scenarios while employing cultured samples with molecular methods. The controlled culture might not fully replicate the complexity of natural conditions, potentially limiting the validation of experimental results. Artificial conditions in cultured samples may induce responses differing from those in natural environments, challenging the broader applicability of these findings. As a result, the findings obtained from cultured samples may not be directly applicable to understanding the interactions in the natural environment, thus limiting the ecological relevance of the findings, and introducing uncertainties when translating laboratory results to real-world applications.

Although, the integration of cultured samples with novel molecular techniques has the potential to significantly enhance sensitivity and specificity in detecting targets. Cultured samples facilitate quantitative data on specific sequence abundance, offering precise measurements crucial for understanding gene expression variations, as demonstrated in Chapter 3. Using complex and natural samples albeit the cultured samples in this study would pose challenges for molecular assays due to the risk of cross-contamination, which could potentially yield false-positive results, thereby impacting the accuracy of the obtained results. Nonetheless, the implementation of qPCR and isothermal amplification methods may require specialised equipment and ultra-clean reagent dispensing, increasing costs of molecular assay deployment, and thus limiting their accessibility in certain environmental settings. Addressing these considerations requires additional resources such as time, skilled labour, and equipment to ensure the practicality of molecular methodologies.

Furthermore, integrating data obtained through novel molecular techniques, such as qPCR and isothermal amplification methods, with established methods for detecting *Pseudo-nitzschia* spp. in the environment enhances the reliability and scalability of environmental assessments. Effective intercalibration between both methods involves applying them to independent sample sets, such as synthetic DNA sequences, to assess performance. This intercalibration requires stringent quality control measures for both methods, monitoring and addressing potential bias or variability in sampling protocols, DNA extraction methods, and data analysis pipelines. Identifying workflow discrepancies between novel molecular techniques, including qPCR or isothermal techniques, and established methods, such as microscopy morphological detection, and biotoxin quantification, would minimise the variations in sample processing, analysis, and downstream data. For instance, conducting cross-validation studies between microscopy cell count, and qPCR-based cell enumeration can ensure the validity of *Pseudo-nitzschia* quantification, as demonstrated in Chapter 2 and (McQuillan et al. 2023). By addressing standardisation issues, intercalibrated data obtained through novel molecular techniques with established methods can provide a comprehensive assessment with higher temporal and spatial resolution of the presence and abundance of *Pseudo-nitzschia* spp. in the real-world environment. Integrating these datasets allows for more detailed monitoring of the bloom dynamics over time and across different environmental locations. In navigating the use of cultured or environmental samples with molecular techniques, a balanced consideration of advantages, challenges, and intercalibration is essential for chosen methodologies.

7.2.9 Sample processing for Field-Ready Genetic Analysis

The LAMPTRON system features an innovative approach involving the continuous flow of liquid through functionalised silica beads, allowing the processing of large-volume samples. To facilitate this, the incorporation of a Sterivex filter capsule can be connected to the sample inlet to prevent particle clogging associated with large volumes of processed crude water samples. This approach could enable the concentration of hundreds of millilitres of seawater onto the microfluidic chip, enabling highly efficient capture of DNA targets from natural water. There is a potential to develop the current LAMPTRON into a multiplexable autonomous system capable of simultaneously performing multiple DNA extractions in parallel, coupled with existing LAMP amplification testing. This can be a step towards accommodating multiplexing extraction technology for field-use settings that bypass sample transportation and laboratory processing. The multiplexing function of LAMPTRON promises real-world applicability for different targets, delivering new-to-business capabilities from commercialisation and environmental monitoring perspectives.

7.2.10 Paper-Based Microfluidics for Discriminating Toxigenic and Non-Toxigenic *Pseudo-nitzschia* Species

Paper-based microfluidic devices offer a range of advantages, including the detection of various analytes such as genetic markers and antibodies/antigens, employing both colourimetric and fluorometric detection chemistries. These platforms offer several benefits not typically found in traditional testing platforms, including rapid prototyping, low-cost, flexible material usage, amenable layouts, and the ability to perform multiple assays in a single device. By adapting the LAMP technique to target genetic markers associated with toxin production in *Pseudo-nitzschia*, the efficiency of current environmental monitoring can be enhanced. Furthermore, performing LAMP and ELISA testing in parallel on the same device opens up promising avenues for distinguishing between toxigenic and non-toxigenic *Pseudo-nitzschia* species using both genetic and metabolic techniques. Both LAMP and ELISA are known for their sensitivity and specificity, enabling the quantification of specific proteins or genes linked to domoic acid biosynthesis. Assay parallelization may enable the rapid, accurate, and cost-effective assessment of harmful algal bloom risks, offering a field-applicable tool for routine monitoring on a broader scale.

Appendix A

Table A1. List of *Pseudo-nitzschia* species and various algal isolates used to evaluate the specificity of primers and probes designed in the present study, including strain, geographic origin, and references.

Species	Strains	Origin	Source/Reference
Pseudo-nitzschia multistriata	SZN-B954	Gulf of Naples, Italy	(Ruggiero et al. 2018)
Pseudo-nitzschia multistriata	SZN-B955	Gulf of Naples, Italy	(Ruggiero et al. 2018)
Pseudo-nitzschia pungens	CCAP 1061/44	Argyll, Scotland, UK	CCAP [a]
Pseudo-nitzschia multiseries	NWFSC 713	NWFSC, NOAA, USA	NWFSC, NOAA [d]
Pseudo-nitzschia multiseries	NWFSC 714	NWFSC, NOAA, USA	NWFSC, NOAA [d]
Pseudo-nitzschia multiseries	NWFSC 715	NWFSC, NOAA, USA	NWFSC, NOAA [d]
Pseudo-nitzschia multiseries	ML-54	Monterey Bay, USA	(Bowers et al. 2018)
Pseudo-nitzschia multiseries	ML-55	Monterey Bay, USA	(Bowers et al. 2018)
Pseudo-nitzschia multiseries	ML-56	Monterey Bay, USA	(Bowers et al. 2018)
Pseudo-nitzschia multiseries	ML-59	Monterey Bay, USA	(Bowers et al. 2018)
Karenia brevis	CCMP2228	Sarasota, USA	CCMP [c]
Karenia mikimotoi	CCAP 1127/2	N/A [b]	
Alexandrium tamarense	CCAP 1119/25	Scallowy ,Scotland, UK	CCAP [a]
Synechococcus sp	CCAP 1479/9	Cumbria, England, UK	CCAP [a]
Prorcentrum lima	CCAP 1136/12	Lincolnshire, England, UK	CCAP [a]
Alexandrium minutum	CCAP 1119/15	Orkney, Scotland, UK	CCAP [a]
Lingulodinium polyedra	CCAP 1121/7	La Jolla Pier, USA	CCAP [a]
Prorcentrum cordatum	CCAP 1136/16	Loch Etive, Argyll, UK	CCAP [a]

[a] CCAP; Culture Collection of Algae and Protozoa, [b] N/A; not determined, [c] CCMP; Provasoli-Guillard National Center for Marine Algae and Microbiota (NCMA), [d] NWFSC & NOAA; Northwest Fisheries Science Center & National Oceanographic and Atmospheric Administration.

Table A2. List of sequences from *Pseudo-nitzschia* spp.

Species	Strain	Accession Number	Functional annotation	Source
P. multistriata	SZN-B955	sequenced_PCR_amplicon	Polyprenyl synthetase family/ Geranyl pyrophosphate synthase	This study
P. multistriata	B857	PASAV3_0076010.1	Geranyl pyrophosphate synthase	SZN [d], EarlHam [e]
P. multistriata	B856	CAACVS010000301.1	Isoprenoid Biosynthesis enzyme	Ensembl [b]
P. australis	Pa2	comp56158_c0_seq1	Isoprenoid Biosynthesis enzyme	(Lema et al. 2019)
P. multistriata	B857	PASAV3_0076010.1.CDS59316	Farnesyl pyrophosphate synthase	SZN [d]
P. multistriata	B857	comp12171_c0_seq1	Polyprenyl synthetase family	(Di Dato et al. 2015)
P. pungens	Pp1	comp33625_c0_seq1	Terpene synthase	(Lema et al. 2019)
P. australis	10249_10_AB	MMETSP0139_2-20121125|15155	Terpenoid synthase	MMETSP [b]
P. seriata	Disko 8	PSN_contig_0003671	Geranylgeranyl_pyrophosphate synthase	(Hardardottir et al. 2019)
P. multiseries	CLN-47	jgi|Psemu1|216553|e_gw1.784.27.1	Isoprenoid biosynthesis enzyme	JGI [c], (Boissonneault et al. 2013)
P. multiseries	CLN-47	jgi|Psemu1|292053|fgenesh1_pg.784_2	Isoprenoid biosynthesis enzyme	JGI [c], (Boissonneault et al. 2013)
P. australis	10249_10_AB	MMETSP0140_2-20121125|10879	Terpenoid synthase	MMETSP [b]
P. pungens	cf._pungens	MMETSP1061-20121228|28325	Terpenoid synthases	MMETSP [b]
P. multiseries	CLN-47	jgi|Psemu1|40832|gm1.40489_g	Isoprenoid biosynthesis enzyme	JGI [c], (Boissonneault et al. 2013)
P. australis	10249_10_AB	MMETSP0140_2-20121125|16494	Terpenoid synthase	MMETSP [b]
P. multiseries	CLN-47	jgi|Psemu1|216537|e_gw1.784.15.1	Isoprenoid biosynthesis enzyme	JGI [c], (Boissonneault et al. 2013)
P. australis	10249_10_AB	MMETSP0141-20121125|13125	Terpenoid synthase	MMETSP [b]
P. multiseries	CLN-47	jgi|Psemu1|216534|e_gw1.784.29.1	Isoprenoid biosynthesis enzyme	JGI [c], (Boissonneault et al. 2013)
P. delicatissima	UNC1205	MMETSP0327-20121206|10681_1	Terpenoid synthase	MMETSP [b]
P. multistriata	LV136_2_1	JKEI: 01412:05990	Prenyltransferase	(Russo et al. 2018)
P. fraudulenta	WWA7	CAMNT_0045708103	Terpenoid cyclase/protein prenyltransferase	MMETSP [b]
P. multistriata	LV136_2_1	HW69O: 08680:07798	Geranyl pyrophosphate synthase	(Russo et al. 2018)
P. multistriata	LV136_2_2	2JKEI:06897:07147	Geranyl pyrophosphate synthase	(Russo et al. 2018)
P. multistriata	LV136_1_2	HW69O: 05172:14811	Isoprenoid biosynthesis enzyme	(Russo et al. 2018)
P. delicatissima	B596	MMETSP0327-20121206|10681_1	Terpenoid synthase	MMETSP [b]
P. multistriata	LV136T3_1_1	JKEI: 02005:09227	Geranyl pyrophosphate synthase	(Russo et al. 2018)
P. fraudulenta	WWA7	MMETSP0853-20130426|7932	Terpenoid synthase	MMETSP [b]
P. fraudulenta	Pf2	comp22852_c0_seq1	Geranyl pyrophosphate synthase	(Lema et al. 2019)
P. fraudulenta	WWA7	MMETSP0851-20130426|99388	Farnesyl diphosphate synthase	MMETSP [b]

[a] NCBI; National Centre for Biotechnology Information GenBank, [b] MMETSP; Marine Microbial Eukaryote Transcriptome Sequencing Project database, [c] JGI; The genome portal of the Department of Energy Joint Genome Institute, [d] SZN; Genome database of the Stazione Zoologica Anton Dohrn.

Table A3. Additional primers for *Pseudo-nitzschia spp*.

Primer name	Target	Sequence (5'----> 3')
Psn-fw1	GPP	CAAGGGCGGAAAGATGAACC
Psn-rv1	GPP	AGGAGTCCATGATGTCGTCG
Psn-fw2	GPP	TCACCAAAATCTGCGACCTC
Psn-rv2	GPP	ATGCTGTCCTCGCCAATGAT

Table A4. Cell concentration (cells mL^{-1}) of *Pseudo-nitzschia* and non-target algal species.

Species	Isolate Accession	Cell Concentration (cells/ml)
Pseudo-nitzschia multistriata	SZN-B954	38.3 ± 0.9
Pseudo-nitzschia multistriata	SZN-B955	39.3 ± 0.5
Pseudo-nitzschia pungens	CCAP 1061/44	40.0 ± 1.6
Pseudo-nitzschia multiseries	NWFSC 713	40.7 ± 2.5
Pseudo-nitzschia multiseries	NWFSC 714	41.7 ± 1.7
Pseudo-nitzschia multiseries	NWFSC 715	42.3 ± 2.6
Pseudo-nitzschia multiseries	ML-54	43.0 ± 0.8
Pseudo-nitzschia multiseries	ML-55	43.7 ± 1.2
Pseudo-nitzschia multiseries	ML-56	42.7 ± 0.9
Pseudo-nitzschia multiseries	ML-59	40.3 ± 2.9
Karenia brevis	CCMP2228	137.3 ± 1.2
Karenia mikimotoi	CCAP 1127/2	128.7 ± 2.6
Alexandrium tamarense	CCAP 1119/25	324.7 ± 3.3
Synechococcus sp	CCAP 1479/9	1058.7 ± 21.3
Prorcentrum lima	CCAP 1136/12	531.0 ± 5.1
Alexandrium minutum	CCAP 1119/15	410.0 ± 3.7
Lingulodinium polyedra	CCAP 1121/7	218.7 ± 3.1
Prorcentrum cordatum	CCAP 1136/16	338.0 ± 4.5

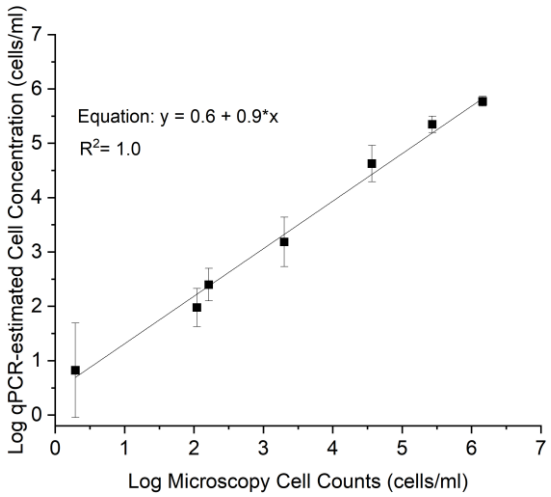

Figure A1. The relationship between estimated *P. multistriata* cell abundances was calculated using the qPCR assay vs. direct cell counts by microscopy.

Appendix B

Section B1: Optimization of RNA extraction protocol

Due to nutrient stress conditions, the cell numbers in the treated cultures decreased, resulting in a significant reduction in RNA recovery at post-experimental time points. Therefore, the RNA extraction protocol was optimised to ensure the effective and reproducible collection of high-quality RNA samples during the experiment.

To optimise RNA extraction protocol, modifications were made to the standard RNeasy Plant Mini Kit (Qiagen) as follows: 1) Frozen cell pellets were dissolved in three different lysis buffers, either in RNeasy lysis buffer which contains 10 µL β-Mercaptoethanol (β-ME) added to 1 mL Buffer RLT, or TriReagent (Sigma-Aldrich, Burlington, MA, USA) or TRIzol (Invitrogen, Carlsbad, CA, USA), prior to extraction with RNeasy protocol. 2) Incubation of RNA lysate with RNeasy lysis buffer at 56°C for 10 min, then homogenised by disruption with 0.5 mm diameter glass beads for 7 min prior to standard extraction steps. 3) Addition of an RNA clean-up step using RNA Clean & Concentrator™-25 kit (Zymo Research, Irvine, CA, USA), intended to remove any residual phenol carryover from the RNA lysis step. Each RNA extraction protocol was performed in duplicate of the same cell density of approximately 552,000 cells ml^{-1} *P. multistriata* SZN-B955.

The first protocol utilized the glass beads and RNeasy lysis buffer at 56°C for 10 min, resulting in the highest extraction efficiency based on the Qubit RNA concentration, Nanodrop absorption ratios of 260/280 and 230/280 and using the RNA Integrity Number (RIN) estimated by the Agilent Bioanalyzer as depicted in (Table B1). The bead-beating, TriReagent and TRIzol protocols improved the absorbance ratio 230/280 of the standard RNA method towards, 0.2 % and -0.2 %, 1.1 % and 0.3 %, respectively (Figure B1). The resulting RNA concentration of bead-beating and 56°C incubation increased up to 5.2-fold compared to the standard extraction protocol (P= 0.01, n=2).

Table B1. Quantification of duplicate RNA samples using five variations of the RNeasy extraction method.

Protocol	Sample ID	Concentration [ng μl^{-1}]	Abs ratio 260/280	Abs ratio 230/280	RIN value
Standard RNeasy Plant Mini Kit	1	7.9	2.00	0.7	7.4
	2	4.6	2.1	1.2	8
TriReagent	3	20.9	1.6	0.5	6.6
	4	3.9	1.7	1.6	7.1
TRIzol	5	28.3	1.5	0.8	6.8
	6	54.0	1.6	0.5	N/A
Bead-beating & 56°C incubation	7	45.1	2.1	1.8	9
	8	12.6	2	1.4	8.1
Additional RNA clean-up (Zymo)	9	10.6	5.4	1.0	7.2
	10	3.2	2.1	1.3	6.9

The RNA samples with potential ethanol and phenol contamination are known to reduce the 230/280 ratio below 2 (Wang 2012). Therefore, the protocol employed for the additional clean-up was tested. The RNA Clean & Concentrator™-25 kit (Zymo Research) was included post the DNase digestion and yielded the lowest RNA recovery. Thereby, a customised protocol was developed to extract a total of 72 RNA samples from control and experimental cultures as follows: cells were pelleted from 250 mL of culture by centrifugation at 7,800 rpm for 20 min at 4°C and were flash-frozen in liquid nitrogen until further use. Glass bead-beating was then performed on the thawed cell pellets in a mixture of 10 µL β-mercaptoethanol (β-ME) and 1 mL Buffer RLT at 56°C for 10 min. RNA was then purified using RNeasy Plant Minikit (Qiagen) with RNAase-free DNAase digestion step (Qiagen). 50 µL of RNA was eluted in nuclease-free water and then stored in a -80°C freezer till used.

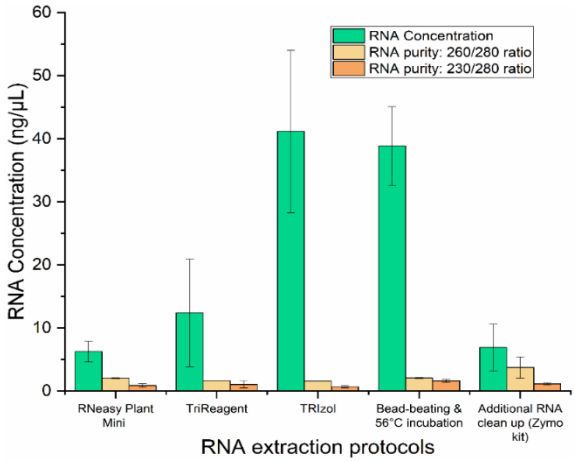

Figure B1. Assessment of RNA integrity resulting from extraction protocols as determined by RNA concentration and absorbance ratios of 260/280 and 230/280. Error bars denote the standard deviation of mean values between duplicate samples of *P. multistriata*.

Table B2. Concentration of nutrients (µM) including phosphate (P), nitrate (N), and silicate (Si) across control and experimental treatments.

Time points (h)	Control culture			Phosphate-depleted treatment			Nitrate-depleted treatment			Silicate-depleted treatment		
	Phosphate (µM)	Nitrate (µM)	Silicate (µM)	Phosphate (µM)	Nitrate (µM)	Silicate (µM)	Phosphate (µM)	Nitrate (µM)	Silicate (µM)	Phosphate (µM)	Nitrate (µM)	Silicate (µM)
-2	8.7 ± 3.5	194.1 ± 58.5	236.7 ± 36.4	1.1 ± 0.5	165.5 ± 17.2	265.8 ± 20.2	24.3 ± 1.4	114.2 ± 39.4	440.3 ± 6.3	7.0 ± 5.752	114.3 ± 110.0	274.1 ± 21.9
0	6.6 ± 3.0	199.7 ± 71.4	250.2 ± 35.6	72.2 ± 1.9	161.7 ± 15.9	258.3 ± 24.7	145.3 ± 12.1	439.0 ± 36.8	270.5 ± 19.2	3.5 ± 3.3	319.9 ± 338.0	602.7 ± 51.3
2	24.7 ± 22.1	201.2 ± 22.1	247.7 ± 27.9	3.5 ± 0.7	18.9 ± 0.2	9.8 ± 0.2	0.3 ± 0.04	62.0 ± 2.3	15.1 ± 3.8	2.3 ± 1.3	17.3 ± 2.7	12.0 ± 0.6
6	11.4 ± 6.7	178.6 ± 47.0	244.9 ± 32.9	3.1 ± 0.4	18.1 ± 0.3	9.2 ± 0.8	0.3 ± 0.1	57.9 ± 3.5	10.9 ± 0.3	4.1 ± 0.7	18.1 ± 3.5	11.4 ± 0.7
24	7.2 ± 3.8	170.7 ± 59.2	238.5 ± 40.5	3.2 ± 0.4	17.7 ± 0.2	9.0 ± 0.8	61.8 ± 4.8	65.4 ± 3.6	10.3 ± 0.3	0.7 ± 0.5	19.6 ± 5.4	10.1 ± 1.2
48	6.7 ± 3.2	145.9 ± 54.6	231.5 ± 39.5	3.3 ± 0.4	17.6 ± 0.4	9.1 ± 0.7	43.8 ± 30.6	62.6 ± 1.6	11.7 ± 0.2	0.7 ± 0.6	19.7 ± 5.2	11.2 ± 0.7

Table B3. Changes of growth rates (d^{-1}) in *P. multistriata* under different nutrient treatments between pre- and post-experimental time. The time of nutrient addition is highlighted in bold.

Time (days)	Control culture	Phosphate-depleted treatment	Nitrate-depleted treatment	Silicate-depleted treatment
2	0.3 ± 0.08	0.4 ± 0.08	0.3 ± 0.02	0.2 ± 0.02
4	1.3 ± 0.05	0.1 ± 0.04	1.4 ± 0.01	0.1 ± 0.02
7	0.3 ± 0.04	0.9 ± 0.003	0.4 ± 0.04	0.6 ± 0.4
9	0.2 ± 0.1	0.1 ± 0.002	0.9 ± 0.05	1.0 ± 0.5
11	0.4 ± 0.6	0.8 ± 0.05	0.09 ± 0.002	0.4 ± 0.2
14	0.4 ± 0.08	0.3 ± 0.05	0.3 ± 0.4	0.3 ± 0.2
16	0.2 ± 0.02	0.3 ± 0.6	0.08 ± 0.5	0.02 ± 0.005
18	0.06 ± 0.02	0.8 ± 0.6	0.5 ± 0.7	0.03 ± 0.02
22	**0.04 ± 0.02**	**0.003 ± 0.005**	**0.08 ± 0.003**	**0.002 ± 0.007**
24	0.006 ± 0.02	-0.04 ± 0.007	-0.04 ± 0.01	-0.1 ± 0.02
28	-0.008 ± 0.004	0.005 ± 0.009	0.004 ± 0.009	0.07 ± 0.005
30	-0.04 ± 0.01	0.07 ± 0.02	0.06 ± 0.006	0.1 ± 0.006
32	-0.07 ± 0.007	0.06 ± 0.02	0.04 ± 0.007	0.07± 0.01

Appendix C

Section C1: qPCR Estimation of Toxigenic *Pseudo-nitzschia spp* Abundance

Genomic DNA samples recovered from seawater samples were also analyzed using a qPCR assay targeting the 5.8S rRNA gene sequence of *Pseudo-nitzschia* spp. The qPCR was conducted following the protocols originally described by (Fitzpatrick et al. 2010), employing the forward primer 5'-CTGTGTAGTGCTTCTTAGAGG-3' and the reverse primer 5'-AGGTAGAACTCGTTGAATGC-3'. qPCR reaction was prepared in a dedicated PCR workstation with air filtration and Ultraviolet decontamination, using nuclease-free and DNA-free plastic consumables and reagents. Reactions were prepared on ice, using micro-pipettors with aerosol barrier tips. Each qPCR reaction was set-up to contain 12.5µL of Sso Fast EvaGreen Supermix (Biorad Ltd, UK), 1 µL of each primer, and 9 µL of PCR-grade water; template DNA (1 µL) was added to a total reaction volume of 25 µL. The qPCR reactions were carried out using a LightCycler 96 real-time PCR instrument (Roche) according to the manufacturer's recommended protocol. Each reaction was run for 40 cycles, followed by a high-resolution dissociation (melting) analysis. The thermal cycling parameters were as follows. The thermal cycling conditions of the assay were: 95^{o}C for 5 min, then 95^{o}C for 30 sec, 61^{o}C for 30 sec and 72^{o}C for 30 sec per cycle. Each reaction was prepared in triplicate, and the average threshold cycle (C_t) value for each replicate was used for analysis and quantification. Cell number was calculated as cells per 100mL of sampled water after considering the amount of DNA sample added to each reaction, and the quantity of water passed through the Sterivex filter unit when the sample was collected.

Quantification estimation for the *Pseudo-nitzschia* spp. was achieved using the cell number standard. This was prepared using a 10-fold dilution series of *Pseudo-nitzschia multistriata* (SZN-B954, originally recovered from the Gulf of Naples, Italy), maintained at conditions as described in section 4.3.4. An exponentially dividing culture was enumerated using a Sedgwick–Rafter cell counting slide (PYSER-SGI) and a compound light microscope (Carl-Zeiss), and dilutions were prepared in f/2 medium. DNA was extracted using the DNeasy Power Water kit and the DNA samples were used as templates for a series of qPCR reactions. The mean C_t value obtained from triplicate qPCR reactions for each standard and dilution was used to plot standard curves, from which the number of template sequence copies in each analysis was extrapolated using a simple linear regression line of best fit of the standard curve data points. An estimated number of target sequence copies in the genome was factored in to estimate the number of cells in each sample.

qPCR estimation of *Pseudo-nitzschia spp*. cell number did not assume a gene copy number, rather a cell count was determined from a standard curve produced from cultured *Pseudo-nitzschia sp.* cells (*P. multistriata*). This approach could improve the accuracy of cell counts if the cell standards contain the same genomic composition as the environmental populations, but this was unclear in this case. Altogether, the issue of absolute quantification for HAB assays that measure ribosomal gene sequences requires more information on the genetic composition and variability of populations within the study area, which could be achieved with the preparation of genome sequencing datasets to assess the relationship between cell number and rDNA gene copies.

Table C1: Sampling Plan

Week	1	2	3	4	5	6	7	8	9	10	11	12	13	14	15	16	17	18
Date	13/09/2021	20/09/2021	27/09/2021	04/10/2021	11/10/2021	18/10/2021	25/10/2021	01/11/2021	08/11/2021	15/11/2021	22/11/2021	29/11/2021	No Sampling					
Locations	PA and RH	PA and MS	PA and RH	PA and MS	PA and RH	PA and MS	PA and RH	PA and MS	PA and RH	PA and MS	PA and RH	PA and MS						
Week	**19**	**20**	**21**	**22**	**23**	**24**	**25**	**26**	**27**	**28**	**29**	**Total**						
Date	17/01/2022	24/01/2022	31/01/2022	07/02/2022	14/02/2022	21/02/2022	28/02/2022	07/03/2022	14/03/2022	21/03/2022	28/03/2022							
Locations	PA and MS	PA and RH	PA and MS	PA and RH	PA and MS	PA and RH	PA and MS	PA, RH and MS	PA, RH and MS	PA, RH and MS	PA, RH and MS	100						
PA = Porthallow																		
MS = Mevagissey South																		
RH = Ropehaven																		

Table C2. RPA primers were designed and tested in this study.

Primer name	Sequence (5’ --- 3’)
RPA_fw1	CATGTATCCCCAGCCGCCCCTCTTGATTCG
RPA_fw2	CGCATGTATCCCCAGCCGCCCCTCTTGATT
RPA_fw3	CGCATGTATCCCCAGCCGCCCCTCTTGATTC
RPA_fw4	GCATGTATCCCCAGCCGCCCCTCTTGATTCG
RPA_fw5	GCATGTATCCCCAGCCGCCCCTCTTGATTC
RPA_rv1	AGGCAATCTCGTTCGGGTACAGCATTTTTGACC
RPA_rv2	GGCAATCTCGTTCGGGTACAGCATTTTTGACCACT
RPA_rv3	AGGCAATCTCGTTCGGGTACAGCATTTTTGACCAC
RPA_rv4	CAATCTCGTTCGGGTACAGCATTTTTGACCACTTT
RPA_rv5	ATCTCGTTCGGGTACAGCATTTTTGACCACTTTAC

Appendix D

Section D1: Production of PCR amplicons for Standards Preparation

The genomic DNA template was isolated from the *Pseudo-nitzschia multistriata* SZN-B954 strain using the DNeasy Plant Mini Kit (Qiagen, Hilden, Germany) following the manufacturer's instructions. Genomic DNA samples were used to amplify genes of *dabD*, GPP and *tubA,* PCR reactions were carried out separately in 25 µl volumes containing 0.25 ng/µl DNA template, 200 µM dNTPs (New England Biolabs, UK), 1X Standard Taq (Mg-Free) reaction buffer (New England Biolabs, UK), 2mM $MgCl_2$ (New England Biolabs, UK), 0.4 µM of each forward and reverse primer (Appendix D, Table D2), and 0.025 units/µL of One Taq DNA polymerase (New England Biolabs, UK). The thermal cycle profile of PCR began with an initial denaturation at 95 °C for 120 s, followed by 40 cycles of 95 °C for 15 s, 62.5°C for 20 s, finishing with a final extension at 72°C for the 60s. The specificity of PCR products was assessed by electrophoresis using SYBR safe-containing (2% w/v) agarose gel in a TAE buffer.

Section D2: PCR Analysis for Selection of the Vitrifying Agent

To prepare vitrified qPCR mixtures, a final volume of 50 µl reactions contained 2 mM each dNTPs (New England Biolabs, UK), 1X PCR buffer of 10 mM Tris-HCl and 50 mM KCl (New England Biolabs, UK), 2mM $MgCl_2$ (New England Biolabs, UK), 1 µM of each forward and reverse primer and 0.25 µM hydrolysis probe (Table D2, Appendix D). A subsample of genomic DNA was extracted as previously described and then added to vitrified master mixes. The pre-set cycling conditions consisted of an initial denaturation step at 95°C for 120 sec followed by 45 cycles (denaturation: 95°C for 15 sec and final annealing-extension step at 59°C for 60 sec). Two different rehydration mixtures were tested by comprising a range volume of DNA template with 2, 4, 6, and 8 µl and 0, 2, 3, and 5 mM each dNTPs (New England Biolabs, UK) to reconstitute the vitrified PCR mixtures.

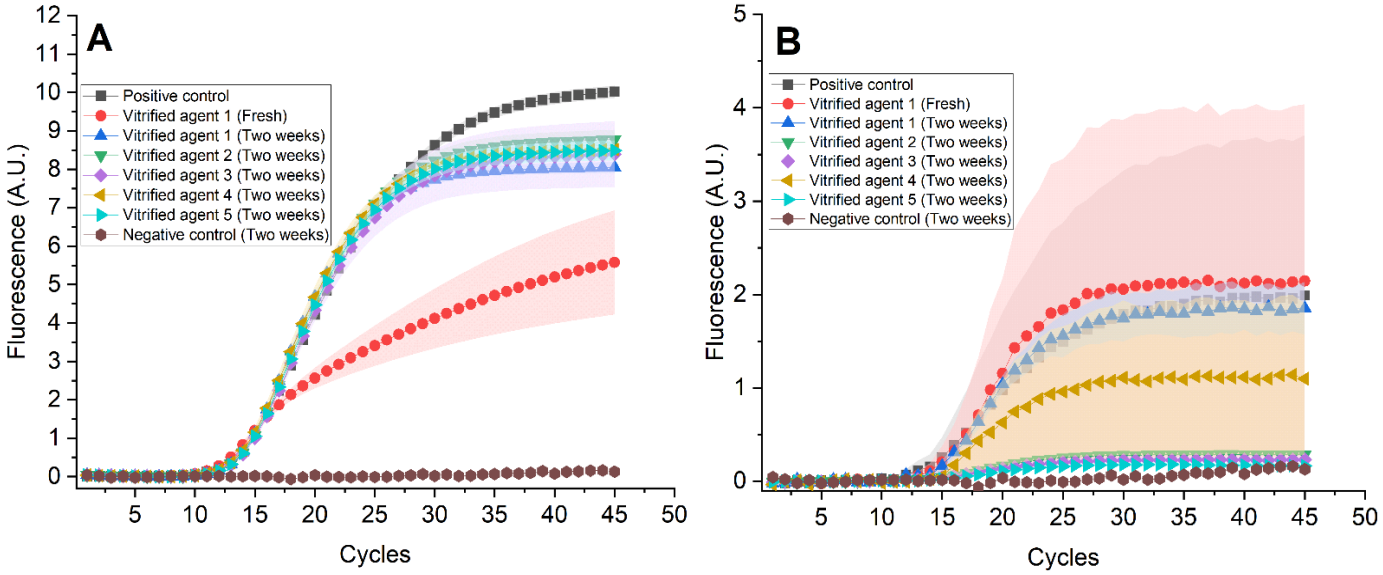

Figure D1. qPCR amplification following two weeks of shelf-lived vitrified master mixes with two freshly prepared experimental positive controls and negative control. A) qPCR amplification plots of vitrified agents (1-5) using rehydration mixture 1. B) qPCR amplification plots of vitrified agents (1-5) using rehydration mixture 2. Positive controls in Panels A & B were freshly prepared using a conventional qPCR master mix as described above in Supporting Information. Freshly prepared qPCR master mixes using vitrified agent 1 were either rehydrated by mixture 1 (Panel A) or mixture 2 (Panel B). Nuclease-free water was included as a template in negative control reactions of two weeks of vitrified agent 1 following the addition of rehydration mixture 1 (Panel A) and using rehydration mixture 2 (Panel B). Filled areas of each amplification curve show the standard deviations.

Table. D1. Comparison of C_t values measured for the vitrified qPCR master mixes by using vitrified agents 1-5 which were rehydrated by reconstitution mixture 1 and 2. The C_t values were extrapolated from the qPCR amplification curves that are plotted in Figure D1.

		Positive Control	Fresh Vitrified agent 1	Vitrified agent 1	Vitrified agent 2	Vitrified agent 3	Vitrified agent 4	Vitrified agent 5
Rehydration mixture 1	C_t value (Average, *n=2*)	9.4±0.02	10.7±0.2	10.5±0.2	10.3±0	10.4±0	**10.3±0.06***	10.5±0
Rehydration mixture 2	C_t value (Average, *n=2*)	10.6±0	12.0±0	13.0±0.7	ND	ND	14.5±0	ND

The vitrified agent 4 resulted in the lowest C_t value and therefore was selected for the subsequent vitrification analysis (in **bold). The positive control is prepared from a regular qPCR master mix as previously described without adding any vitrifying substances. ND: Not detected by PCR thermocycler Software (LightCycler 96, v1.1, Roche Diagnostics International Ltd).*

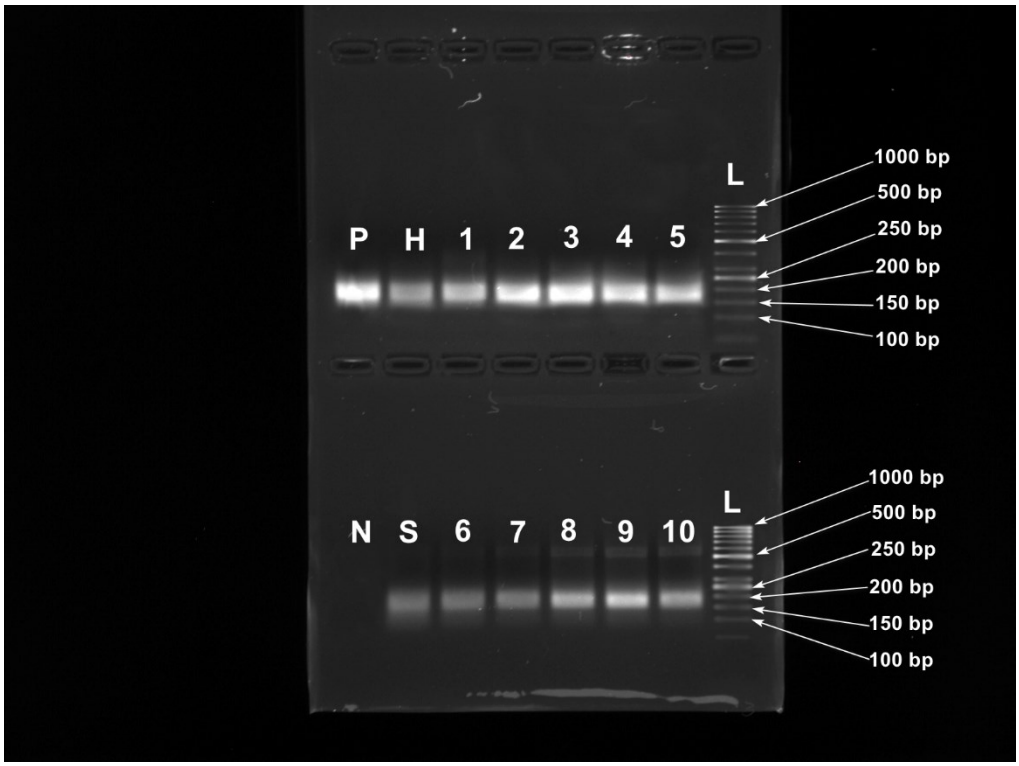

Figure D2. Gel Electrophoresis Data of qPCR vitrified master mixes of two weeks shelf-life against two freshly prepared experimental positive controls and negative control. The size of the amplicon is 161 bp. Lane L: DNA ladder (50 bp), Lane P: positive control of freshly non-vitrified reagents (i.e. using the regular qPCR master mix as described above in Appendix D, section D1). Lane H: freshly prepared vitrified qPCR master mix using vitrified agent 1 following the addition of rehydration mixture 1. Lanes 1-5: vitrified qPCR master mixes of two weeks shelf-life using rehydration mixture 1. Lane 1: Vitrified agent 1 with rehydration mixture 1, Lane 2: Vitrified agent 2 with rehydration mixture 1, Lane 3: Vitrified agent 3 with rehydration mixture 1, Lane 4: Vitrified agent 4 with rehydration mixture 1, Lane 5: Vitrified agent 5 with rehydration mixture 1, Lanes 6-10: vitrified qPCR master mixes of two weeks shelf-life using rehydration mixture 2. Lane S: freshly prepared vitrified qPCR master mix using vitrified agent 1 following the addition of rehydration mixture 2. Lane 6: Vitrified agent 1 with rehydration mixture 2, Lane 7: Vitrified agent 2 with rehydration mixture 2, Lane 8: Vitrified agent 3 with rehydration mixture 2, Lane 9: Vitrified agent 4 with rehydration mixture 2, Lane 10: Vitrified agent 5 with rehydration mixture 2, Lane N: Negative control of two weeks vitrified agent 1 following the addition of rehydration mixture 1 and using nuclease-free water as a template.

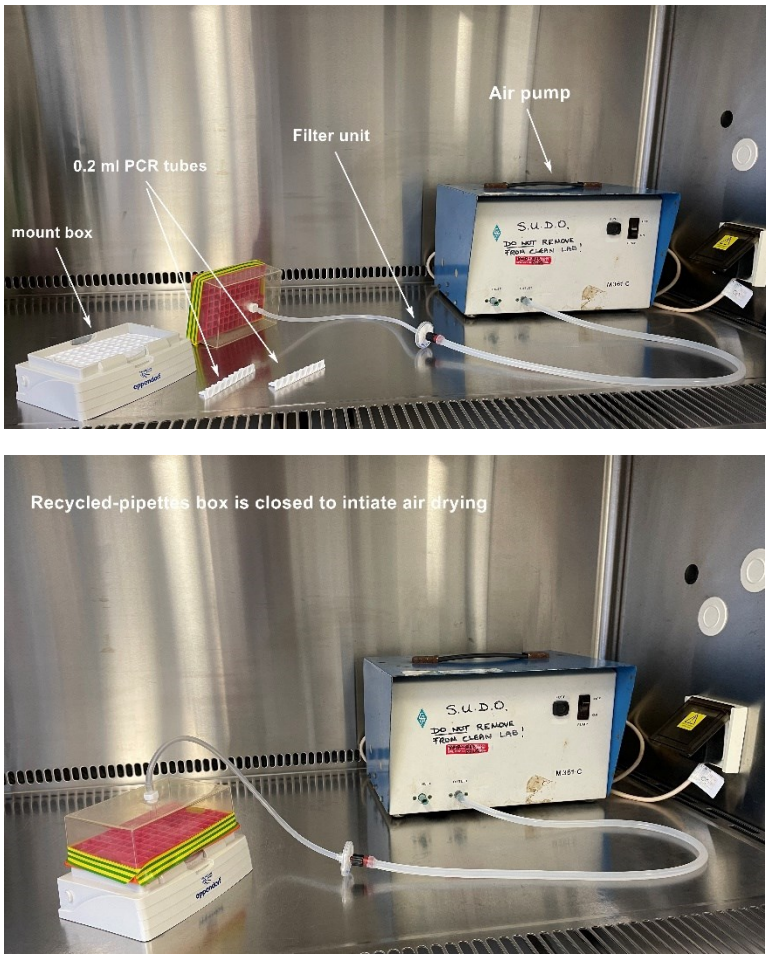

Figure D3. Stabilisation steps of qPCR and LAMP master mixtures for dried format and real-time assays. Vitrified master mixes were air-dried in a sterile Class2 cabinet using an air pump (M361-C; Charles Austen Pumps LTD, Surrey, England, UK) directed to 0.2 ml tubes (LightCycler 8-tube strips, Roche Molecular Systems Inc.). Clean air was pumped at 0.5 m/s through a 0.2 µm filter unit (Millipore, UK) for 45 minutes at room temperature. The vitrified mixtures were then stored at room temperature in Aluminium barrier film bags with MiniPax® Silica Gel Desiccant Sachet (Sigma-Aldrich, UK) at ambient temperature.

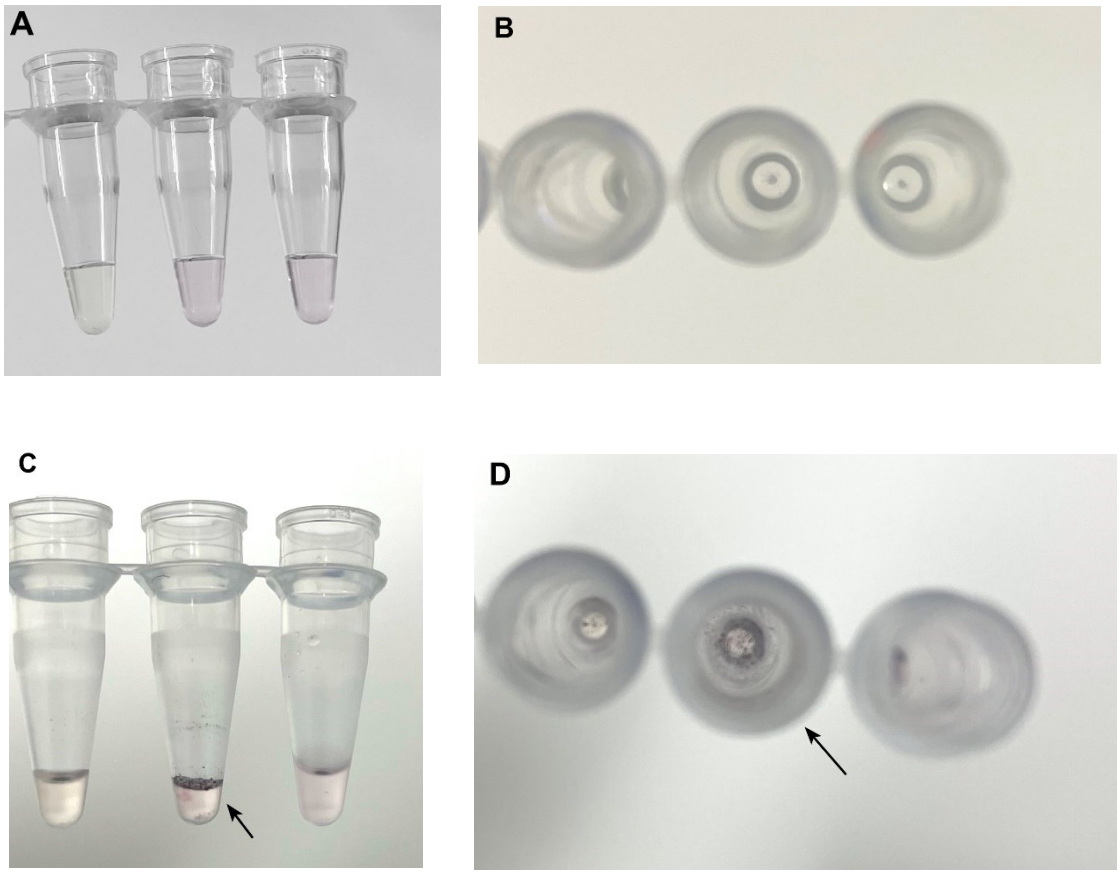

Figure D4. The transformation of qPCR and LAMP amplification reaction mixtures before (A & B) and after the vitrification process (C & D). All components of the amplification reactions were placed within DNase-free microtubes. (A) Depicts a side view of the tube, illustrating the fresh, liquid phase of the master mixtures, while (B) shows a top view of these tube wells. (C) demonstrates the transformation into a glass-like phase after drying, while (D) depicts a close-up top view of the vitrified mixtures. The variations in the appearance of vitrified mixtures are a result of optimising different formulations of vitrifying agents in microtubes (C & D), along with varying drying times involving a controlled flow of clean air on each microtube.

Table D2. Oligonucleotide sequences

Name	Target	Sequence (5'----> 3')
Psn-fw	GPP	CGACTACCAGAACGATCCCA
Psn-rv	GPP	GGTTCATCTTTCCGCCCTTG
Psn_probe	GPP	(FAM)-ACCTCCCGGCCAACTACGAACTCC-(BHQ1)
Psn-fw_2	*tubA*	GTTGCCGAAATCACCAGCAC
Psn-rv_2	*tubA*	GACGACATCTCCACGGTACA
Psn_probe_2	*tubA*	(HEX)-TCGAGCCTACCAACATGATGACCAAGTGC-(BHQ1)
LAMP-F3	*dabD*	CGGAAAACACCATGCCCAA
LAMP-B3	*dabD*	TCTCGTTCGGGTACAGCA
LAMP-FIP	*dabD*	GGCCAGAACCTTTCGTCTCTGTCAAGGGTGATTCGGGGAATG
LAMP-BIP	*dabD*	AATCCCGACACTTTCGATCCCGTCGAAGCCCTTCCAGTCTG
LAMP-LB	*dabD*	GGTTCACCCGACCCTACAAGA
LAMP-LF	*dabD*	ATATTGTACAAGGGCAAAAAGATGT

FAM = Fluorescein; HEX = Hexachloro-fluorescein; BHQ1 = Black Hole Quencher 1

Appendix E

Section E1: Quality verification of DMA-based extraction techniques across a variety of sample sources

The DMA extraction protocol was evaluated for the extraction of DNA from a variety of sources, including (Eukaryotic cells: *Pseudo-nitzschia* diatom, Bacteria: *Escherichia coli* and Dinoflagellates: *Alexandrium minutum*). The *Pseudo-nitzschia* cells were grown as previously described in section 6.3.4. *A. minutum* CCAP 1119/15 was grown in L1 medium (Keller et al. 1987). *A. minutum* cells were enumerated and grown at the same incubation condition as *Pseudo-nitzschia* as previously described in section 6.3.4. The bacterial strain used in this study was *Escherichia coli* NCTC9001 type strain (*E. coli*) that was obtained from the UK National Collection of Type Cultures (NCTC). *E. coli* cells were counted as described by (Newton et al. 2016, Walker et al. 2019). Then, the cells were harvested by centrifugation at 7,100 rpm for 5 minutes at 4°C and stored later at −80°C until further processing. Each cell replicate was processed into a microfluidic chip prototype to perform the same DMA extraction protocol as described previously in section 6.3.5. Commercial kits were used per the manufacturer's protocols as a standard control to evaluate two proposed DMA-based techniques upon employing the same input volume of crude samples. DNeasy Mini Kit (Qiagen), DNeasy Plant Pro Kit (Qiagen), and GenElute Bacterial Genomic DNA Kit (Sigma-Aldrich) were used as standard methods to extract DNA from *Pseudo-nitzschia*, *A. minutum, E. coli* cells, respectively. The extraction capabilities of two different silica substrates were evaluated, incorporating beads and glass fibre membrane in the extraction microchamber against the commercial extraction kits. The efficiency of DNA recovery was determined using various types of samples following the method described in (Bruijns et al. 2018).

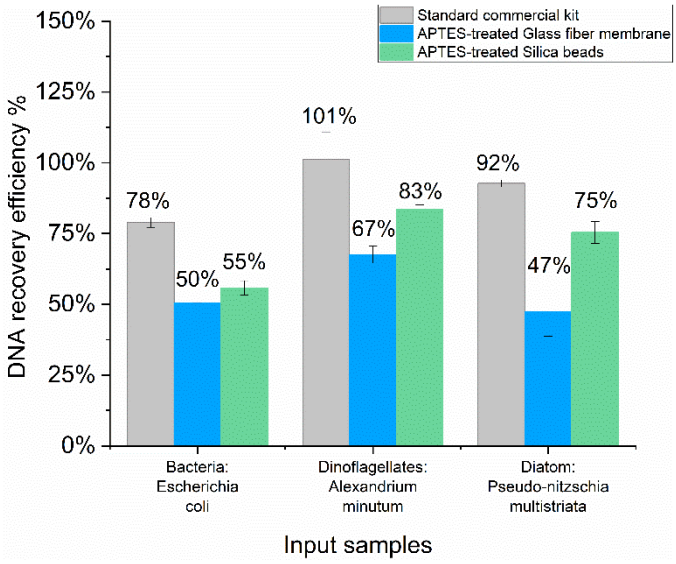

Figure E1. Performance assessment of DMA-based method for DNA extraction from various samples. The DNA capture efficiency was evaluated by comparing the proposed DMA microfluidic method using silica beads and glass fibre paper with the reference extraction by widely used kits processing the same volume of sample.

The APTES-treated silica beads yielded higher DNA recovery than the APTES-treated glass membrane with recovery at 55%, 83%, and 75% for *E. coli*, *A. minutum*, and *P. multistriata*, respectively. The result indicated that the purification performance was improved by amine-functionalised silica beads rather than glass fibre membrane, irrespective of the sample type (Figure E1). The capture of *P. multistriata* DNA on silica beads was approx. 75% which is lower than the value yielded by the commercial kit (92%), compared to another cell type such as *A. minutum* commercial DNA capture at 101% against silica beads DNA capture value (83%), and DNA capture of *E. coli* DNA using the commercial standard kit at 78% with DNA capture value by silica beads (55%). In contrast to bacterial cells (i.e. *E. coli*) and dinoflagellates (i.e. *A. minutum*), the cell wall formation is in diatoms (i.e. *P. multistriata*) forming a thick silicate structure that is armoured with hard features of the frustules, serving as predation defence, but impeding the release of DNA from the diatom cells (Hildebrand et al. 2018). It was observed that the quality and quantity of the DNA extracted using the DMA-based method depend on the number of cells (section 6.4.2, Figure 6.4). A high cell concentration of *E. coli* at 8 x 10^7 (colony formation unit) CFU/mL that was used in the DMA extractions using both functionalised silica beads and silica membrane was linked to the low efficiency of DNA capture. Overall, the DMA-based method provides a low-cost extraction technique (approx. > £1 per sample) compared to commercially available kits which cost hundreds of pounds per sample. This is of great interest for implementing DNA purification methods in field-based analysis in low-resource areas.

Section E2: Evaluation of the DMA-based nucleic acid extraction performance by the qPCR analysis

To further evaluate the use of extracted DNA using the DMA method employing the amine-functionalised silica beads in downstream analysis, the *sxtG* and GPP genes were amplified in PCR assays to assess the presence of potential inhibitors (Figure E2). The PCR conditions include 1 cycle at 95°C for 120 sec followed by 55 cycles at 95°C for 15 sec and 59°C for 60 sec. Contamination was assessed by spiking the extracted DNA pool with non-target or background DNA versus both non-spiked DNA samples and negative control reactions (No template control; NTC). Contaminated DNA will result in a higher C_t value than a clean DNA sample (van Pelt-Verkuil 2008). The qPCR conditions include initial denaturation of 1 cycle at 95°C for 120 sec followed by 40 cycles of 95 °C for 15 s, an annealing step of 59°C for 20 s, finishing with a final extension at 72°C for the 60s. 2 µL of DNA was used in a total volume of 25 µL containing 1X of IQ SYBR Supermix (Bio-Rad Laboratories, Inc.), 0.4 µM concentration of each primer and deionised water. The forward primers (5'-ACGTGCGGGACCCCTTCATCATGCT-3') and reverse primer (5'- ACGGGAACGGCTACAACGGGAGGAT-3') were used to amplify the *stxG* gene (Wilson 2020). The forward and reverse primers for amplifying the GPP gene were (5'-CGACTACCAGAACGATCCCA-3') and (5'-GGTTCATCTTTCCGCCCTTG-3'), respectively.

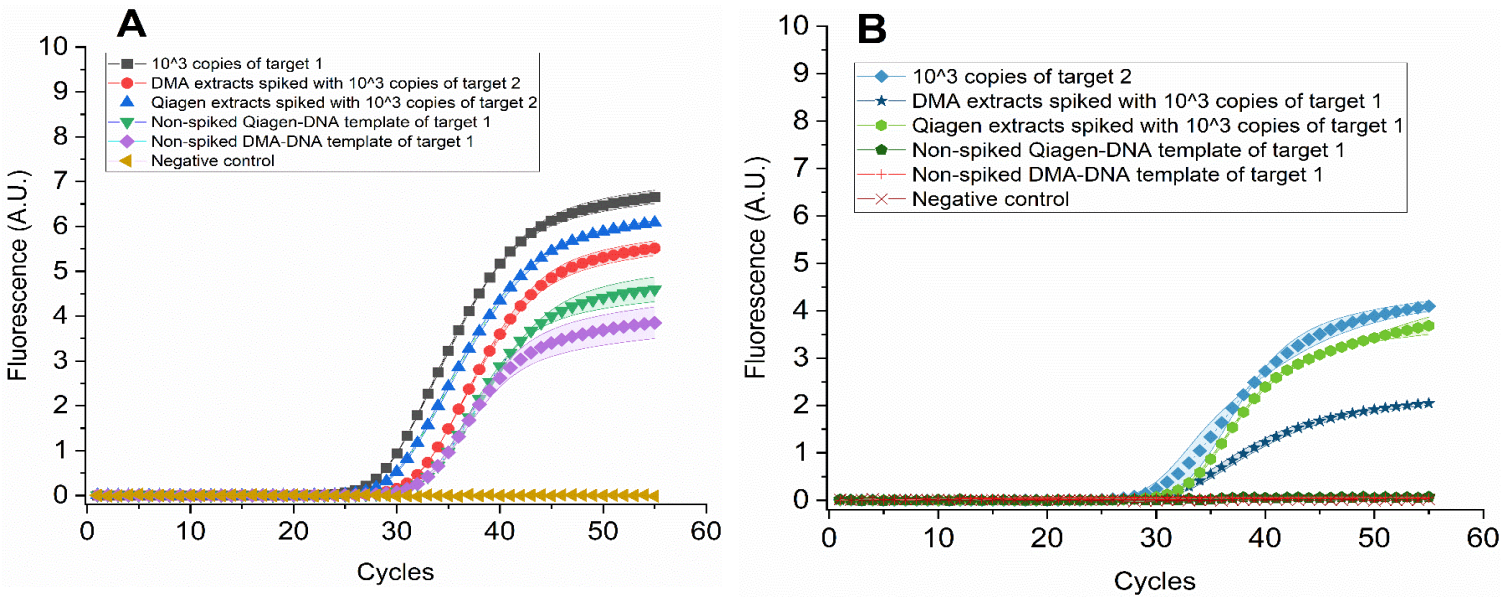

Figure E2. Real-time quantitative PCR of eluted DNA using the microfluidic DNA isolation chip using APTES-treated silica beads and on-column standard method. Targets 1 and 2 refer to the target genes of GPP and *sxtG*, respectively. A) Amplification plots are for 10^3 GPP plasmid standard (black) with C_t= 24.6 ± 0.2, Qiagen kit extracts spiked DNA template (blue) with C_t=25.9 ± 0.1, and DMA extracts spiked with 10^3 copies (red) with C_t=28.1 ± 0.2, Qiagen DNA template (non-spiked) (green) with C_t=26.8 ± 0.4 and DMA DNA template (Non-spiked) (purple) with C_t=28.9 ± 0.1. B) Amplification plots for ~10^3 *sxtG* copies DNA template of *Alexandrium* (black) at C_t= 29.2 ± 0.3, Qiagen kit *P.*

multistriata DNA spiked with 10^3 *sxtG* copies from *Alexandrium* DNA template (blue) with C_t=29.9 ± 0.2, and DMA extracts spiked with 10^3 *sxtG* copies from *Alexandrium* DNA template (red) at C_t=29.5 ± 0.6.

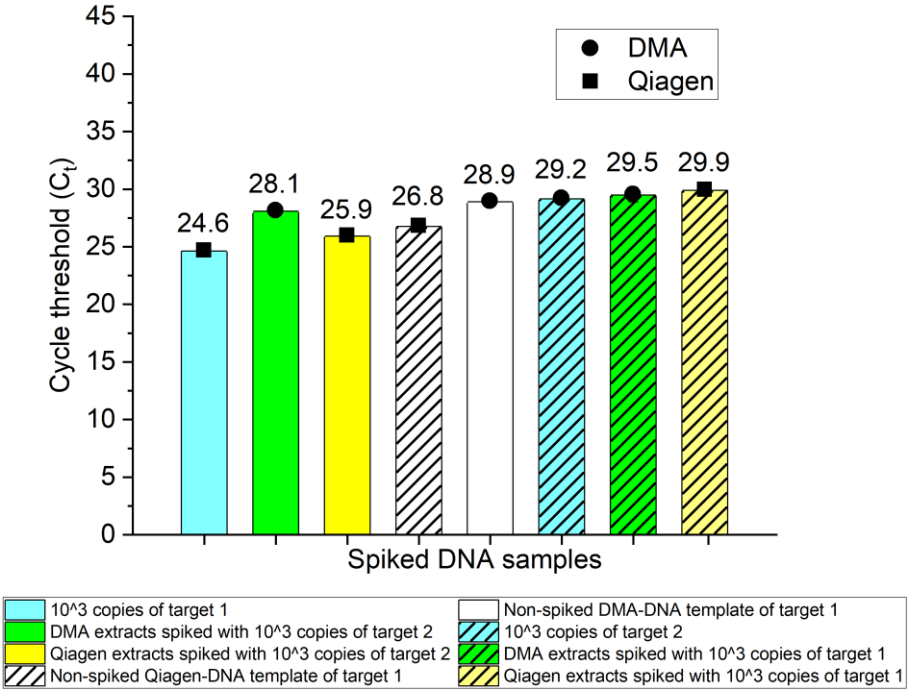

Figure E3. Comparison of threshold cycles (C_t) between the proposed DNA isolation using APTES-functionalised silica beads (DMA) and on-column reference method (Qiagen). The C_t values were extrapolated from the qPCR amplification data in Appendix E, Figure E2.A & Figure E2.B). The genes of GPP and *sxtG* are labelled as target 1 and target 2, respectively.

qPCR reactions were performed in triplicates to investigate the inhibition of extraction carryover from the DMA-based method and Qiagen standard on-column method. Contamination was further assessed by incorporating a triplicate of negative control reactions (No template control; NTC, Nuclease-free water (Invitrogen) in each qPCR run. Positive controls were the DNA samples that were extracted from *A. minimum* and *P. multistriata* cultures using the Qiagen reference method. The same culture pool was used to extract DNA samples using the DMA and functionalised silica beads. The DNA samples of both cultures extracted by the DMA method were split into two groups. The first group involves pure and non-spiked DNA samples of *P. multistriata* and *A. minimum*. The second group serves as inhibition control which includes *A. minimum* DNA was spiked with DNA plasmid standard containing ~ 10^3 copies of the GPP *Pseudo-nitzschia* non-target gene, and *P. multistriata* DNA sample that was spiked with DNA plasmid standard containing ~ 10^3 copies of the *sxtG Alexandrium* non-target gene. All the qPCR reactions contained equivalent template volumes at 2 µL of triplicate DNA samples extracted using both the Qiagen kit and DMA method, along with the positive and inhibition controls. The cycle threshold (C_t) of qPCR was used as an indicator of the

quality of DNA samples where low C_t values indicate high DNA quality and vice versa (Demeke and Jenkins 2010). Figures E2 & E3 demonstrate the dependence of the cycle threshold (C_t value) of amplified DNA extracted from the DMA method compared with that obtained from the commercial Qiagen kit. The Ct value of the spiked DMA DNA template of *P. multistriata* cells was 28.1 ± 0.2, compared to the Ct value = 25.9 ± 0.08 of Qiagen spiked DNA samples. Whilst the Ct values of spiked *A. minutum* DNA samples from Qiagen extraction and DMA-based extraction were 29. 9 ± 0.2 and 29.5 ± 0.6, respectively, as shown in Figure E3. These results indicate a small shift in C_t of spiked DMA DNA samples of targets 1 and 2, compared to spiked Qiagen DNA samples, due to the reduced inhibition in DNA samples extracted by the DMA-based method of the amplification reaction.

Section E3: Reproducibility of LAMPTRON analyser

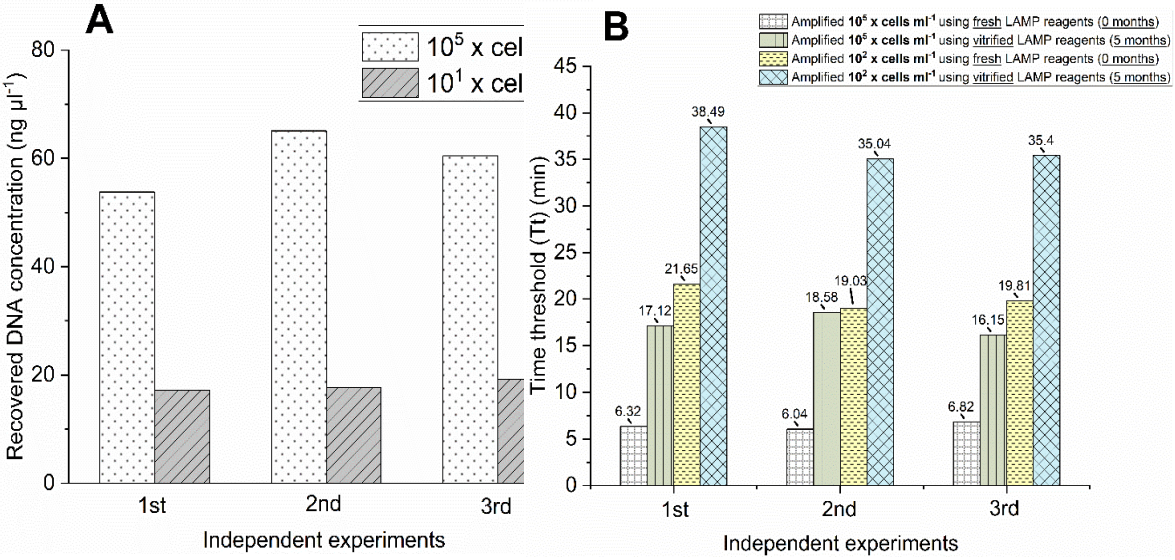

Figure E4. Reproducibility of DNA purification and fluorescence measurements by LAMPTRON analyser. A) Comparison of the quantity of the DNA isolated from $1.6x10^5$ and $1.1x10^1$ *P. multistriata* cells per mL from three independent experiments. B) The changes of Tt values of both *P. multistriata* cell numbers using both freshly prepared and pre-stored vitrified LAMP assays (5-month shelf-life) that were obtained by three independent experiments on the LAMPTRON system.

Section E4: Autonomous pumping system

The incorporation of the pumping system represents a step towards demonstrating the autonomous operation capability of the LAMPTRON system. This pump system has previously proved its utility in conducting *in-situ* chemical analyses at depths of up to 6,000 meters, as deployed in multiple oceanic locations by the Ocean Technology and Engineering Group (OTE) at the National Oceanography Centre (Mowlem et al. 2021, Beaton et al. 2022). For the first time, this system has been adapted to process biological samples, offering the potential for *in-situ* biological analyses in a wide array of environmental settings.

To enable autonomous operation, a revised version of the OTE pumping system was developed, accommodating a configuration with four bespoke syringe pumps each equipped with solenoid valves (LFNA1250125H, Lee Co., United States), and ¼-28 outlets, as illustrated in Figure E5. This design allows for transitions between various pumping speeds within a single pumping cycle. The term "pumping cycle" here refers to the sequence of steps involved in moving fluids through microchannels when the valve changes from a closed to an open state (Woias 2005). Most importantly, this design supports a pumping sequence that involves the individual loading of each DNA extraction reagent its respective container, followed by transportation into channels, mixing with different fluids or components such as microbeads, or disposal into a waste container. This flexible pumping system enables the free exchange among extraction reagents, facilitating an automated on-chip DNA extraction process.

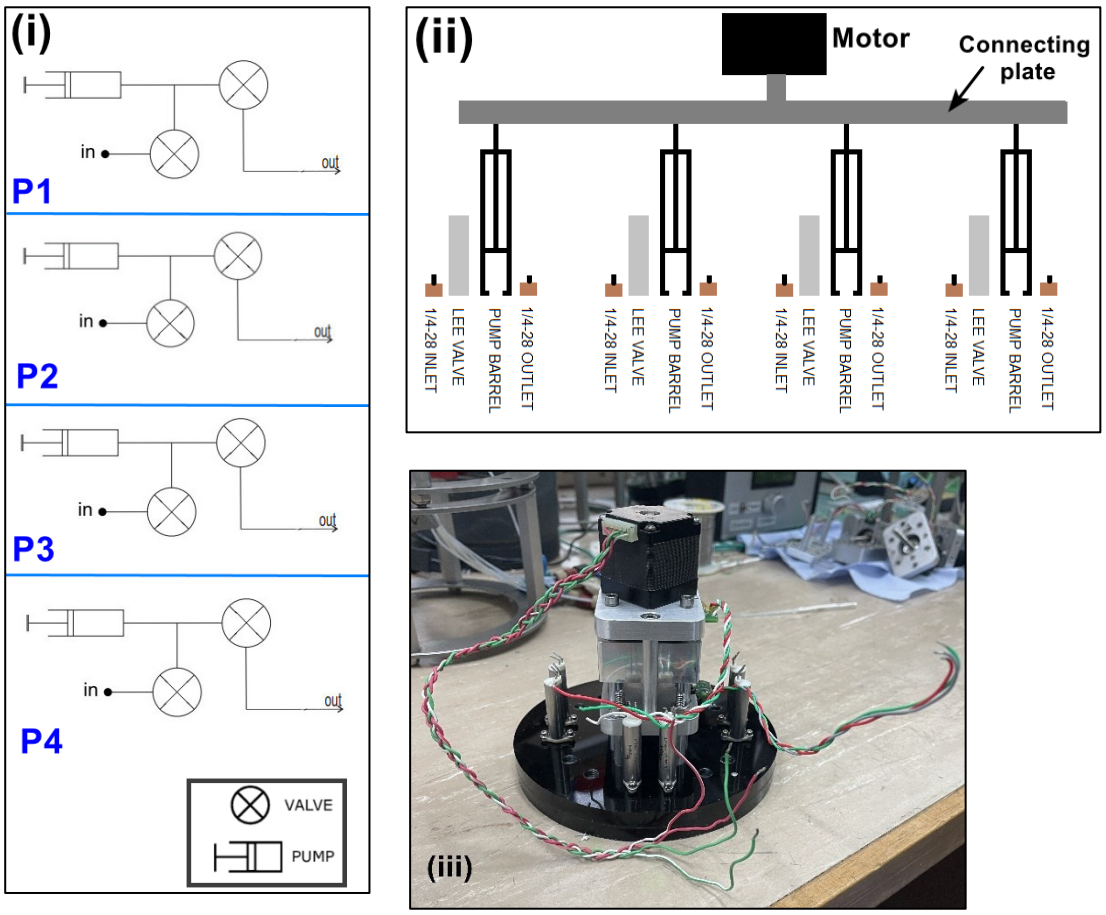

Figure E5. Autonomous Microfluidic pump system. i) A generic chip schematic demonstrating multiple individual fluidic routes, each connected to one of the four parallel syringe pumps (P1, P2, P3, and P4). ii) A schematic diagram shows the custom-made pumping system, which includes four syringe pumps, valves, and ¼-28 outlets for each pump, all actuated by a Haydon Kerk Size 11 stepper motor linear actuator. iii) An image shows the setup of the individually addressable pumping system.

Section E5: Oxygen plasma treatment of glass beads

Figure E6. Glass beads underwent oxygen plasma treatment to activate the surface silanol groups, employing a plasma activation system (Diener Electronic, Ebhausen, Germany). The effectiveness of the plasma treatment was assessed by observing the behaviour of water droplets on the beads. Resistance to wetting by beads indicated successful plasma treatment (Subeshan et al. 2020).

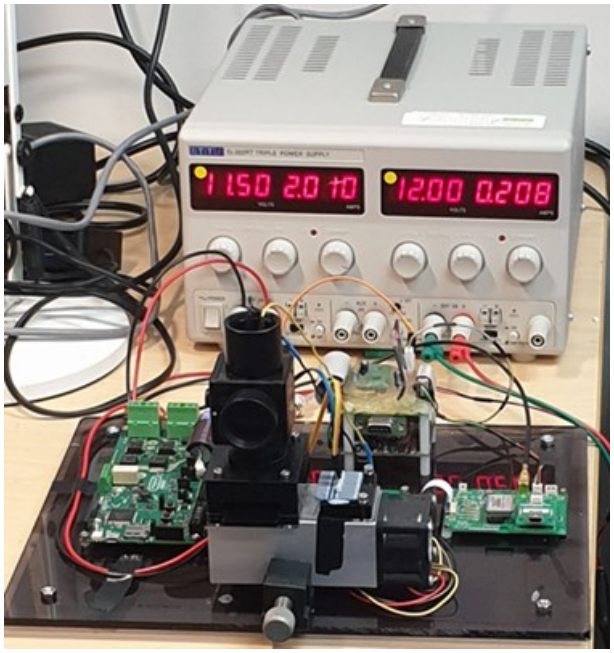

Figure E7. The first prototype of LAMPTRON incorporated an Arduino circuit for electronic control of the heater, temperature sensor and data capture.

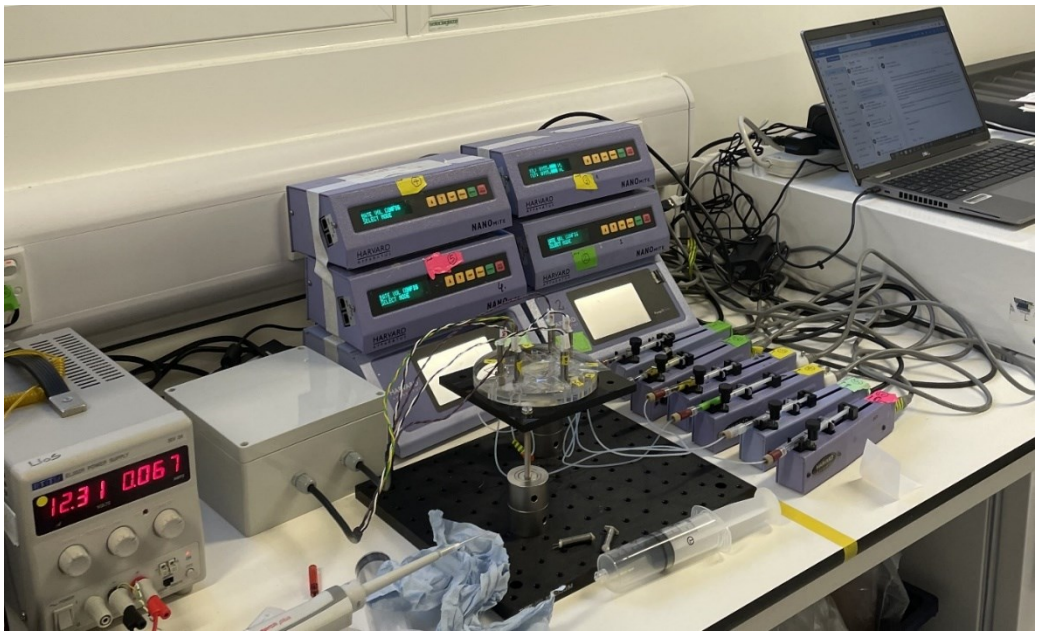

Figure E8. Optimisation of the DNA extraction module in LAMPTRON was conducted using a new transparent PMMA-built chip. Parameters such as reagent volumes, flow rates, and diffusion times were optimised within this experimental setup. Solenoid-operated valves were fixed on the test chip which was connected to syringe pumps for controlled injection of samples and reagents, controlled via a Windows-based software.

Table E1. Cost comparison for consumables and reagents between LAMPTRON extraction and Qiagen commercial methods.

Items Description	Component	Cost (£), inc. VAT per sample	Manufacturer	Product Number
Current extraction DMA-based method:	2% APTES (aminopropyl triethoxysilane)	0.006	Sigma-Aldrich	741442-100ML
	95% Ethanol	0.005	Sigma-Aldrich	652261
	0.1 M Tris-HCl (pH 8.0)	0.002	SERVA	39792.01
	10 mM EDTA	0.009	Invitrogen	15575-038
	1% sodium dodecyl sulfate (SDS)	0.005	Sigma-Aldrich	L4390-100G
	10% Triton X-100	0.003	Sigma-Aldrich	93443-500ML
	0.1 mg/mL Proteinase K	0.00001	Qiagen	56304
	100 mg/mL Dimethyl adipimidate (DMA)	0.07	Alfa Aesar	L10515.09
	0.01 M Phosphate-buffered saline (PBS)	0.0004	Sigma-Aldrich	P4417-100TAB
	0.1 M Trisodium citrate		Alfa Aesar	45558
	10 mM sodium bicarbonate	0.0008	Sigma-Aldrich	S7277-250G
	Glass beads	0.008	Sigma-Aldrich	G1152-100G
	DEPC-treated water	0.005	Thermo Fischer	R0601
Total cost per sample	£0.1			
Qiagen extraction method	DNeasy Plant Mini kit	4.2	Qiagen	69104
Total cost per sample	£4.2			

List of References

Abbasi, U., P. Chowdhury, S. Subramaniam, P. Jain, N. Muthe, F. Sheikh, S. Banerjee, and V. Kumaran. 2019. A cartridge based Point-of-Care device for complete blood count. Scientific Reports **9**.

Abrahams, A., R. W. Schlegel, and A. J. Smit. 2021. Variation and Change of Upwelling Dynamics Detected in the World's Eastern Boundary Upwelling Systems. Frontiers in Marine Science **8**.

Accoroni, S., S. Giulietti, T. Romagnoli, M. Siracusa, S. Bacchiocchi, and C. Totti. 2020. Morphological Variability of Pseudo-nitzschia pungens Clade I (Bacillariophyceae) in the Northwestern Adriatic Sea. Plants-Basel **9**.

Adelfi, M. G., M. Borra, R. Sanges, M. Montresor, A. Fontana, and M. I. Ferrante. 2014. Selection and validation of reference genes for qPCR analysis in the pennate diatoms Pseudo-nitzschia multistriata and P. arenysensis. Journal of Experimental Marine Biology and Ecology **451**:74-81.

Aeschbach, L., and V. Dion. 2017. Minimizing carry-over PCR contamination in expanded CAG/CTG repeat instability applications. Scientific Reports **7**.

Ahlford, A., B. Kjeldsen, J. Reimers, A. Lundmark, M. Romani, A. Wolff, A. C. Syvanen, and M. Brivio. 2010. Dried reagents for multiplex genotyping by tag-array minisequencing to be used in microfluidic devices. Analyst **135**:2377-2385.

Ahmad, S., M. M. Gromiha, and A. Sarai. 2004. Analysis and prediction of DNA-binding proteins and their binding residues based on composition, sequence and structural information. Bioinformatics **20**:477-486.

Ahmed, A., H. van der Linden, and R. A. Hartskeerl. 2014. Development of a Recombinase Polymerase Amplification Assay for the Detection of Pathogenic Leptospira. International Journal of Environmental Research and Public Health **11**:4953-4964.

Ahrberg, C. D., A. Manz, and B. G. Chung. 2016. Polymerase chain reaction in microfluidic devices. Lab on a Chip **16**:3866-3884.

Ajani, P. A., A. Verma, J. H. Kim, S. Woodcock, T. Nishimura, H. Farrell, A. Zammit, S. Brett, and S. A. Murray. 2021. Using qPCR and high-resolution sensor data to model a multi-species Pseudo-nitzschia (Bacillariophyceae) bloom in southeastern Australia. Harmful Algae **108**.

Ajani, P. A., A. Verma, M. Lassudrie, M. A. Doblin, and S. A. Murray. 2018. A new diatom species P. hallegraeffii sp nov belonging to the toxic genus Pseudo-nitzschia (Bacillariophyceae) from the East Australian Current. Plos One **13**.

Aksan, A., and M. Toner. 2004. Isothermal desiccation and vitrification kinetics of trehalose-dextran solutions. Langmuir **20**:5521-5529.

Al-Robaiy, S., S. Rupf, and K. Eschrich. 2001. Rapid competitive PCR using melting curve analysis for DNA quantification. Biotechniques **31**:1382-1388.

Ali, N., R. D. P. Rampazzo, A. D. T. Costa, and M. A. Krieger. 2017a. Current Nucleic Acid Extraction Methods and Their Implications to Point-of-Care Diagnostics. Biomed Research International **2017**.

Ali, N., R. D. P. Rampazzo, A. D. T. Costa, and M. A. Krieger. 2017b. Current Nucleic Acid Extraction Methods and Their Implications to Point-of-Care Diagnostics. Biomed Research International.

Altschul, S. F., W. Gish, W. Miller, E. W. Myers, and D. J. Lipman. 1990. Basic local alignment search tool. Journal of Molecular Biology **215**:403-410.

Alvarez-Fernandez, R. 2013. Explanatory Chapter: PCR Primer Design. Laboratory Methods in Enzymology: DNA **529**:1-21.

Alves, R. N., M. Rambla-Alegre, A. C. Braga, A. L. Mauhrault, V. Barbosa, M. Campas, L. Reverte, C. Flores, J. Caixach, J. Kilcoyne, P. R. Costa, J. Diogene, and A. Marque. 2019. Bioaccessibility

of lipophilic and hydrophilic marine biotoxins in seafood: An in vitro digestion approach. Food and Chemical Toxicology **129**:153-161.

Amagliani, G., E. Omiccioli, G. Brandi, I. J. Bruce, and M. Magnani. 2010. A multiplex magnetic capture hybridisation and multiplex Real-Time PCR protocol for pathogen detection in seafood. Food Microbiology **27**:580-585.

Amasia, M., M. Cozzens, and M. J. Madou. 2012. Centrifugal microfluidic platform for rapid PCR amplification using integrated thermoelectric heating and ice-valving. Sensors and Actuators B-Chemical **161**:1191-1197.

Amato, A., W. H. C. F. Kooistra, J. H. L. Ghiron, D. G. Mann, T. Proschold, and M. Montresor. 2007. Reproductive isolation among sympatric cryptic species in marine diatoms. Protist **158**:193-207.

Amato, A., A. Ludeking, and W. H. C. F. Kooistra. 2010. Intracellular domoic acid production in Pseudo-nitzschia multistriata isolated from the Gulf of Naples (Tyrrhenian Sea, Italy). Toxicon **55**:157-161.

Andersen, C. B., A. Holst-Jensen, K. G. Berdal, T. Thorstensen, and T. Tengs. 2006. Equal performance of TaqMan, MGB, molecular beacon, and SYBR green-based detection assays in detection and quantification of roundup ready soybean. Journal of Agricultural and Food Chemistry **54**:9658-9663.

Anderson, D. M., A. D. Cembella, and G. M. Hallegraeff. 2012. Progress in Understanding Harmful Algal Blooms: Paradigm Shifts and New Technologies for Research, Monitoring, and Management. Annual Review of Marine Science, Vol 4 **4**:143-176.

Anderson, D. M., E. Fachon, K. Hubbard, K. A. Lefebvre, P. Lin, R. Pickart, M. Richlen, G. Sheffield, and C. Van Hemert. 2022. Harmful Algal Blooms in the Alaskan Arctic an Emerging Threat as the Ocean Warms. Oceanography **35**.

Anderson, D. M., E. Fensin, C. J. Gobler, A. E. Hoeglund, K. A. Hubbard, D. M. Kulis, J. H. Landsberg, K. A. Lefebvre, P. Provoost, M. L. Richlen, J. L. Smith, A. R. Solow, and V. L. Trainer. 2021. Marine harmful algal blooms (HABs) in the United States: History, current status and future trends. Harmful Algae **102**:101975.

Anderson, R. C., X. Su, G. J. Bogdan, and J. Fenton. 2000. A miniature integrated device for automated multistep genetic assays. Nucleic Acids Research **28**.

Andree, K. B., M. Fernandez-Tejedor, L. M. Elandaloussi, S. Quijano-Scheggia, N. Sampedro, E. Garces, J. Camp, and J. Diogene. 2011. Quantitative PCR Coupled with Melt Curve Analysis for Detection of Selected Pseudo-nitzschia spp. (Bacillariophyceae) from the Northwestern Mediterranean Sea. Applied and Environmental Microbiology **77**:1651-1659.

Annunziata, R., B. H. Mele, P. Marotta, M. Volpe, L. Entrambasaguas, S. Mager, K. Stec, M. R. d'Alcala, R. Sanges, G. Finazzi, D. Iudicone, M. Montresor, and M. I. Ferrante. 2022. Trade-off between sex and growth in diatoms: Molecular mechanisms and demographic implications. Science Advances **8**.

Aoki, M. N., B. D. Coelho, L. G. B. Goes, P. Minoprio, E. L. Durigon, L. G. Morello, F. K. Marchini, I. N. Riediger, M. D. Debur, H. I. Nakaya, and L. Blanes. 2021. Colorimetric RT-LAMP SARS-CoV-2 diagnostic sensitivity relies on color interpretation and viral load. Scientific Reports **11**.

Arapov, J., M. Buzancic, S. Skejic, J. Mandic, A. Bakrac, M. Straka, and Z. N. Gladan. 2020. Phytoplankton Dynamics in the Middle Adriatic Estuary, with a Focus on the Potentially Toxic Genus Pseudo-nitzschia. Journal of Marine Science and Engineering **8**.

Arapov, J., S. Skejic, M. Buzancic, A. Bakrac, O. Vidjak, N. Bojanic, I. Ujevic, and Z. N. Gladan. 2017. Taxonomical diversity of Pseudo-nitzschia from the Central Adriatic Sea. Phycological Research **65**:280-290.

Arapov, J., T. Tomasevic, T. Bonacic, M. Pejkovic, M. Buzancic, I. Buselic, I. L. Pleic, S. Casabianca, A. Penna, S. Skejic, and Z. N. Gladan. 2023. A New Insight into the Taxonomy of Pseudo-

nitzschia Genus from the Adriatic Sea: Description of P. brasiliana, P. galaxiae, P. hasleana, and P. linea. Journal of Marine Science and Engineering **11**.

Ardyna, M., C. J. Mundy, N. Mayot, L. C. Matthes, L. Oziel, C. Horvat, E. Leu, P. Assmy, V. Hill, P. A. Matrai, M. Gale, I. A. Melnikov, and K. R. Arrigo. 2020. Under-Ice Phytoplankton Blooms: Shedding Light on the "Invisible" Part of Arctic Primary Production. Frontiers in Marine Science **7**.

Armbrust, E. V. 2009. The life of diatoms in the world's oceans. Nature **459**:185.

Arunrut, N., W. Kiatpathomchai, and C. Ananchaipattana. 2018. Multiplex PCR assay and lyophilization for detection of Salmonella spp., Staphylococcus aureus and Bacillus cereus in pork products. Food Science and Biotechnology **27**:867-875.

Asiello, P. J., and A. J. Baeumner. 2011. Miniaturized isothermal nucleic acid amplification, a review. Lab on a Chip **11**:1420-1430.

Athanasakoglou, A., and S. C. Kampranis. 2019a. Diatom isoprenoids: Advances and biotechnological potential. Biotechnology Advances **37**:107417.

Athanasakoglou, A., and S. C. Kampranis. 2019b. Diatom isoprenoids: Advances and biotechnological potential. Biotechnology Advances **37**.

Auro, M. E., and W. P. Cochlan. 2013. Nitrogen Utilization and Toxin Production by Two Diatoms of the Pseudo-nitzschia pseudodelicatissima Complex: P. cuspidata and P. fryxelliana. Journal of Phycology **49**:156-169.

Auroux, P. A., Y. Koc, A. deMello, A. Manz, and P. J. R. Day. 2004. Miniaturised nucleic acid analysis. Lab on a Chip **4**:534-546.

Avtar, R., A. A. Komolafe, A. Kouser, D. Singh, A. P. Yunus, J. Dou, P. Kumar, R. Das Gupta, B. A. Johnson, H. V. T. Minh, A. K. Aggarwal, and T. A. Kurniawan. 2020. Assessing sustainable development prospects through remote sensing: A review. Remote Sensing Applications-Society and Environment **20**.

Ayache, N., N. Lundholm, F. Gai, F. Herve, Z. Amzil, and A. Caruana. 2021. Impacts of ocean acidification on growth and toxin content of the marine diatoms Pseudo-nitzschia australis and P. fraudulenta. Marine Environmental Research **169**.

Badarou, A. A. 2021. Identifying the enzyme that catalyzes the synthesis of geranyl diphosphate, a precursor to domoic Acid in Pseudo-nitzchia.

Bahi, M. M., M. N. Tsaloglou, M. Mowlem, and H. Morgan. 2011. Electroporation and lysis of marine microalga Karenia brevis for RNA extraction and amplification. Journal of the Royal Society Interface **8**:601-608.

Bajarias, F. F. A., Y. Kotaki, J. R. R. Jr., M. L. J. Romero, E. F. Furio, L. Nina, K. Koike, Y. Fukuyo, and M. Kodama. 2006. Screening of diatoms producing domoic acid and its derivatives in the Philippines.

Bandala, E. R., L. Brito, and M. Pelaez. 2009. Degradation of domoic acid toxin by UV-promoted Fenton-like processes in seawater. Desalination **245**:135-145.

Bargu, S., C. L. Powell, S. L. Coale, M. Busman, G. J. Doucette, and M. W. Silver. 2002. Krill: a potential vector for domoic acid in marine food webs. Marine Ecology Progress Series **237**:209-216.

Basu, S., S. Patil, D. Mapleson, M. T. Russo, L. Vitale, C. Fevola, F. Maumus, R. Casotti, T. Mock, M. Caccamo, M. Montresor, R. Sanges, and M. I. Ferrante. 2017. Finding a partner in the ocean: molecular and evolutionary bases of the response to sexual cues in a planktonic diatom. New Phytologist **215**:140-156.

Bates, S., D. Garrison, and R. Horner. 1998. Bloom Dynamics and Physiology of Domoic-Acid-Producing Pseudo-nitzschia Species. Pages 267–292 *in* D. M. Anderson, A. D. Cembella, and G. M. Hallegraeff, editors. Physiological Ecology of Harmful Algal Blooms. Springer, Verlag, Heidelberg, Germany.

Bates, S., M. F. Hiltz, and C. Léger. 1999. Domoic acid toxicity of large new cells of Pseudo-nitzschia multiseries resulting from sexual reproduction. Proceedings of the Sixth Canadian Workshop on Harmful Marine Algae **2261**:21-26.

Bates, S., and V. Trainer. 2006a. The ecology of harmful diatoms. Pages 81-93 Ecology of harmful algae. Springer.

Bates, S. S. 1998. Ecophysiology and metabolism of ASP toxin production. NATO ASI series G ecological sciences **41**:405-426.

Bates, S. S., C. J. Bird, A. S. W. Defreitas, R. Foxall, M. Gilgan, L. A. Hanic, G. R. Johnson, A. W. Mcculloch, P. Odense, R. Pocklington, M. A. Quilliam, P. G. Sim, J. C. Smith, D. V. S. Rao, E. C. D. Todd, J. A. Walter, and J. L. C. Wright. 1989. Pennate Diatom Nitzschia-Pungens as the Primary Source of Domoic Acid, a Toxin in Shellfish from Eastern Prince Edward Island, Canada. Canadian Journal of Fisheries and Aquatic Sciences **46**:1203-1215.

Bates, S. S., A. S. W. Defreitas, J. E. Milley, R. Pocklington, M. A. Quilliam, J. C. Smith, and J. Worms. 1991. Controls on Domoic Acid Production by the Diatom Nitzschia-Pungens F Multseries in Culture - Nutrients and Irradiance. Canadian Journal of Fisheries and Aquatic Sciences **48**:1136-1144.

Bates, S. S., K. A. Hubbard, N. Lundholm, M. Montresor, and C. P. Leaw. 2018. Pseudo-nitzschia, Nitzschia, and domoic acid: New research since 2011. Harmful Algae **79**:3-43.

Bates, S. S., C. Léger, M. L. Wells, and K. Hardy. 2003. Photodegradation of domoic acid. Can. Tech. Rep. Fish. Aquat. Sci./Rapp. Tech. Can. Sci. Halieut. Aquat.:30-35.

Bates, S. S., N. Lundholm, K. A. Hubbard, M. Montresor, and C. P. Leaw. 2019. Toxic and Harmful Marine Diatoms. Diatoms: Fundamentals and Applications:389-434.

Bates, S. S., and V. L. Trainer. 2006b. The Ecology of Harmful Diatoms. Pages 81-93 *in* E. Granéli and J. T. Turner, editors. Ecology of Harmful Algae. Springer Berlin Heidelberg, Berlin, Heidelberg.

Bates, S. S., J. Worms, and J. C. Smith. 1993. Effects of Ammonium and Nitrate on Growth and Domoic Acid Production by Nitzschia-Pungens in Batch Culture. Canadian Journal of Fisheries and Aquatic Sciences **50**:1248-1254.

Bayareh, M., M. N. Ashani, and A. Usefian. 2020. Active and passive micromixers: A comprehensive review. Chemical Engineering and Processing-Process Intensification **147**.

Beaton, A. D., C. L. Cardwell, R. S. Thomas, V. J. Sieben, F. E. Legiret, E. M. Waugh, P. J. Statham, M. C. Mowlem, and H. Morgan. 2012. Lab-on-Chip Measurement of Nitrate and Nitrite for In Situ Analysis of Natural Waters. Environmental Science & Technology **46**:9548-9556.

Beaton, A. D., A. M. Schaap, R. Pascal, R. Hanz, U. Martincic, C. L. Cardwell, A. Morris, G. Clinton-Bailey, K. Saw, S. E. Hartman, and M. C. Mowlem. 2022. Lab-on-Chip for In Situ Analysis of Nutrients in the Deep Sea. Acs Sensors **7**:89-98.

Becherer, L., N. Borst, M. Bakheit, S. Frischmann, R. Zengerle, and F. von Stetten. 2020. Loop-mediated isothermal amplification (LAMP) - review and classification of methods for sequence-specific detection. Analytical Methods **12**:717-746.

Becker, H., and C. Gartner. 2000. Polymer microfabrication methods for microfluidic analytical applications. Electrophoresis **21**:12-26.

Becker, S., M. Aoyama, E. M. S. Woodward, K. Bakker, S. Coverly, C. Mahaffey, and T. Tanhua. 2020. GO-SHIP Repeat Hydrography Nutrient Manual: The Precise and Accurate Determination of Dissolved Inorganic Nutrients in Seawater, Using Continuous Flow Analysis Methods. Frontiers in Marine Science **7**.

Beebe, D. J., G. A. Mensing, and G. M. Walker. 2002. Physics and applications of microfluidics in biology. Annual Review of Biomedical Engineering **4**:261-286.

Bej, A. K., M. H. Mahbubani, and R. M. Atlas. 1991. Amplification of Nucleic-Acids by Polymerase Chain-Reaction (Pcr) and Other Methods and Their Applications. Critical Reviews in Biochemistry and Molecular Biology **26**:301-334.

Belgrader, P., W. Benett, D. Hadley, G. Long, R. Mariella, F. Milanovich, S. Nasarabadi, W. Nelson, J. Richards, and P. Stratton. 1998. Rapid pathogen detection using a microchip PCR array Instrument. Clinical Chemistry **44**:2191-2194.

Belgrader, P., W. Benett, D. Hadley, J. Richards, P. Stratton, R. Mariella, and F. Milanovich. 1999. Infectious disease - PCR detection of bacteria in seven minutes. Science **284**:449-450.

Bell, L. N., and M. J. Hageman. 1996. Glass transition explanation for the effect of polyhydroxy compounds on protein denaturation in dehydrated solids. Journal of Food Science **61**:372-+.

Ben Garali, S. M., I. Sahraoui, P. de la Iglesia, M. Chalghaf, J. Diogene, J. Ksouri, and A. S. Hlaili. 2016. Effects of nitrogen supply on Pseudo-nitzschia calliantha and Pseudo-nitzschia cf. seriata: field and laboratory experiments. Ecotoxicology **25**:1211-1225.

Bengtsson, K., J. Christoffersson, C. F. Mandenius, and N. D. Robinson. 2018. A clip-on electroosmotic pump for oscillating flow in microfluidic cell culture devices. Microfluidics and Nanofluidics **22**.

Benoiston, A. S., F. M. Ibarbalz, L. Bittner, L. Guidi, O. Jahn, S. Dutkiewicz, and C. Bowler. 2017. The evolution of diatoms and their biogeochemical functions. Philosophical Transactions of the Royal Society B-Biological Sciences **372**.

Benz, K., K. P. Jackel, K. J. Regenauer, J. Schiewe, K. Drese, W. Ehrfeld, V. Hessel, and H. Lowe. 2001. Utilization of micromixers for extraction processes. Chemical Engineering & Technology **24**:11-17.

Berdalet, E., L. E. Fleming, R. Gowen, K. Davidson, P. Hess, L. C. Backer, S. K. Moore, P. Hoagland, and H. Enevoldsen. 2016. Marine harmful algal blooms, human health and wellbeing: challenges and opportunities in the 21st century. Journal of the Marine Biological Association of the United Kingdom **96**:61-91.

Berensmeier, S. 2006. Magnetic particles for the separation and purification of nucleic acids. Applied Microbiology and Biotechnology **73**:495-504.

Berlanda, S. F., M. Breitfeld, C. L. Dietsche, and P. S. Dittrich. 2021. Recent Advances in Microfluidic Technology for Bioanalysis and Diagnostics. Analytical Chemistry **93**:311-331.

Berman, F. W., and T. F. Murray. 1997. Domoic acid neurotoxicity in cultured cerebellar granule neurons is mediated predominantly by NMDA receptors that are activated as a consequence of excitatory amino acid release. Journal of Neurochemistry **69**:693-703.

Besson, G., and M. Kazanji. 2009. One-Step, Multiplex, Real-Time PCR Assay with Molecular Beacon Probes for Simultaneous Detection, Differentiation, and Quantification of Human T-Cell Leukemia Virus Types 1, 2, and 3. Journal of Clinical Microbiology **47**:1129-1135.

Bhadra, S., T. E. Riedel, S. Lakhotia, N. D. Tran, and A. D. Ellington. 2021. High-Surety Isothermal Amplification and Detection of SARS-CoV-2. Msphere **6**.

Bhagat, A. A. S., E. T. K. Peterson, and I. Papautsky. 2007. A passive planar micromixer with obstructions for mixing at low Reynolds numbers. Journal of Micromechanics and Microengineering **17**:1017-1024.

Bhat, A. I., R. Aman, and M. Mahfouz. 2022. Onsite detection of plant viruses using isothermal amplification assays. Plant Biotechnology Journal **20**:1859-1873.

Bhat, I. A., M. Mashooq, D. Kumar, R. Varshney, and R. Rathore. 2019. Development of probe-based real-time loop-mediated isothermal amplification for detection of Brucella. Journal of Applied Microbiology **126**:1332-1339.

Bhatnagar, B. S., R. H. Bogner, and M. J. Pikal. 2007. Protein stability during freezing: Separation of stresses and mechanisms of protein stabilization. Pharmaceutical Development and Technology **12**:505-523.

Bhattacharya, S., A. Datta, J. M. Berg, and S. Gangopadhyay. 2005. Studies on surface wettability of poly(dimethyl) siloxane (PDMS) and glass under oxygen-plasma treatment and correlation with bond strength. Journal of Microelectromechanical Systems **14**:590-597.

Blanco, J., C. Marino, H. Martin, G. Alvarez, and A. E. Rossignoli. 2021. Characterization of the Domoic Acid Uptake Mechanism of the Mussel (Mytilus galloprovincialis) Digestive Gland. Toxins **13**.

Boissonneault, K. R., B. M. Henningsen, S. S. Bates, D. L. Robertson, S. Milton, J. Pelletier, D. A. Hogan, and D. E. Housman. 2013. Gene expression studies for the analysis of domoic acid production in the marine diatom Pseudo-nitzschia multiseries. Bmc Molecular Biology **14**.

Boom, R., C. J. A. Sol, M. M. M. Salimans, C. L. Jansen, P. M. E. Wertheimvandillen, and J. Vandernoordaa. 1990. Rapid and Simple Method for Purification of Nucleic-Acids. Journal of Clinical Microbiology **28**:495-503.

Bouillon, R. C., R. J. Kieber, S. A. Skrabal, and J. L. C. Wright. 2008. Photochemistry and identification of photodegradation products of the marine toxin domoic acid. Marine Chemistry **110**:18-27.

Bouillon, R. C., T. L. Knierim, R. J. Kieber, S. A. Skrabal, and J. L. C. Wright. 2006. Photodegradation of the algal toxin domoic acid in natural water matrices. Limnology and Oceanography **51**:321-330.

Bowers, H. A., J. P. Ryan, K. Hayashi, A. L. Woods, R. Marin, G. J. Smith, K. A. Hubbard, G. J. Doucette, C. M. Mikulski, A. G. Gellene, Y. W. Zhang, R. M. Kudela, D. A. Caron, J. M. Birch, and C. A. Scholin. 2018. Diversity and toxicity of Pseudo-nitzschia species in Monterey Bay: Perspectives from targeted and adaptive sampling. Harmful Algae **78**:129-141.

Boyd, P. W., T. Jickells, C. S. Law, S. Blain, E. A. Boyle, K. O. Buesseler, K. H. Coale, J. J. Cullen, H. J. W. de Baar, M. Follows, M. Harvey, C. Lancelot, M. Levasseur, N. P. J. Owens, R. Pollard, R. B. Rivkin, J. Sarmiento, V. Schoemann, V. Smetacek, S. Takeda, A. Tsuda, S. Turner, and A. J. Watson. 2007. Mesoscale iron enrichment experiments 1993-2005: Synthesis and future directions. Science **315**:612-617.

Boyle, D. S., D. A. Lehman, L. Lillis, D. Peterson, M. Singhal, N. Armes, M. Parker, O. Piepenburg, and J. Overbaugh. 2013. Rapid detection of HIV-1 proviral DNA for early infant diagnosis using recombinase polymerase amplification. MBio **4**:e00135-00113.

Briggs, L. R., C. O. Miles, J. M. Fitzgerald, K. M. Ross, I. Garthwaite, and N. R. Towers. 2004. Enzyme-linked immunosorbent assay for the detection of yessotoxin and its analogues. Journal of Agricultural and Food Chemistry **52**:5836-5842.

Brown, A. R., M. K. S. Lilley, J. Shutler, C. Widdicombe, P. Rooks, A. McEvoy, R. Torres, Y. Artioli, G. Rawle, J. Homyard, C. R. Tyler, and C. Lowe. 2022. Harmful Algal Blooms and their impacts on shellfish mariculture follow regionally distinct patterns of water circulation in the western English Channel during the 2018 heatwave. Harmful Algae **111**.

Brown, E. G. 2016. Office of the Governor to the US Department of Commerce.

Brown, R. B., and J. Audet. 2008. Current techniques for single-cell lysis. Journal of the Royal Society Interface **5**:S131-S138.

Bruijns, B. B., R. M. Tiggelaar, and H. Gardeniers. 2018. The Extraction and Recovery Efficiency of Pure DNA for Different Types of Swabs. Journal of Forensic Sciences **63**:1492-1499.

Brunet, C., R. Chandrasekaran, L. Barra, V. Giovagnetti, F. Corato, and A. V. Ruban. 2014. Spectral Radiation Dependent Photoprotective Mechanism in the Diatom Pseudo-nitzschia multistriata. Plos One **9**.

Brunson, J. K., S. M. K. McKinnie, J. R. Chekan, J. P. McCrow, Z. D. Miles, E. M. Bertrand, V. A. Bielinski, H. Luhavaya, M. Obornik, G. J. Smith, D. A. Hutchins, A. E. Allen, and B. S. Moore. 2018. Biosynthesis of the neurotoxin domoic acid in a bloom-forming diatom. Science **361**:1356-+.

Brzezinski, M. A. 1985. The Si-C-N Ratio of Marine Diatoms - Interspecific Variability and the Effect of Some Environmental Variables. Journal of Phycology **21**:347-357.

Burns, J. M., and J. L. Ferry. 2007. Adsorption of domoic acid to marine sediments and clays. Journal of Environmental Monitoring **9**:1373-1377.

Bustin, S. A., and R. Mueller. 2005. Real-time reverse transcription PCR (qRT-PCR) and its potential use in clinical diagnosis. Clinical Science **109**:365-379.

Byrnes, S. A., J. D. Bishop, L. Lafleur, J. R. Buser, B. Lutz, and P. Yager. 2015. One-step purification and concentration of DNA in porous membranes for point-of-care applications. Lab on a Chip **15**:2647-2659.

Camacho, C., G. Coulouris, V. Avagyan, N. Ma, J. Papadopoulos, K. Bealer, and T. L. Madden. 2009. BLAST plus : architecture and applications. Bmc Bioinformatics **10**.

Campas, M., P. de la Iglesia, M. Le Berre, M. Kane, J. Diogene, and J. L. Marty. 2008. Enzymatic recycling-based amperometric immunosensor for the ultrasensitive detection of okadaic acid in shellfish. Biosensors & Bioelectronics **24**:716-722.

Campbell, K. 2014. Surface Plasmon Resonance Biosensor Technology for Marine Toxin Analysis. Seafood and Freshwater Toxins: Pharmacology, Physiology, and Detection:347.

Campbell, K., T. McGrath, S. Sjolander, T. Hanson, M. Tidare, O. Jansson, A. Moberg, M. Mooney, C. Elliott, and J. Buijs. 2011. Use of a novel micro-fluidic device to create arrays for multiplex analysis of large and small molecular weight compounds by surface plasmon resonance. Biosensors & Bioelectronics **26**:3029-3036.

Cardona, S., C. Schebor, M. P. Buera, M. Karel, and J. Chirife. 1997. Thermal stability of invertase in reduced-moisture amorphous matrices in relation to glassy state and trehalose crystallization. Journal of Food Science **62**:105-112.

Caron, D. A., M. E. Garneau, E. Seubert, M. D. A. Howard, L. Darjany, A. Schnetzer, I. Cetinic, G. Filteau, P. Lauri, B. Jones, and S. Trussell. 2010. Harmful algae and their potential impacts on desalination operations off southern California. Water Research **44**:385-416.

Celis, J. E., M. Kruhoffer, I. Gromova, C. Frederiksen, M. Ostergaard, T. Thykjaer, P. Gromov, J. S. Yu, H. Palsdottir, N. Magnusson, and T. F. Orntoft. 2000. Gene expression profiling: monitoring transcription and translation products using DNA microarrays and proteomics. Febs Letters **480**:2-16.

Cenciarini-Borde, C., S. Courtois, and B. La Scola. 2009. Nucleic acids as viability markers for bacteria detection using molecular tools. Future Microbiology **4**:45-64.

Cerino, F., L. Orsini, D. Sarno, C. Dell'Aversano, L. Tartaglione, and A. Zingone. 2005. The alternation of different morphotypes in the seasonal cycle of the toxic diatom Pseudo-nitzschia galaxiae. Harmful Algae **4**:33-48.

Cha, R. S., and W. G. Thilly. 1993. Specificity, efficiency, and fidelity of PCR. PCR Methods Appl **3**:18-29.

Chadha, U., P. Bhardwaj, R. Agarwal, P. Rawat, R. Agarwal, I. Gupta, M. Panjwani, S. Singh, C. Ahuja, S. K. Selvaraj, M. Banavoth, P. Sonar, B. Badoni, and A. Chakravorty. 2022. Recent progress and growth in biosensors technology: A critical review. Journal of Industrial and Engineering Chemistry **109**:21-51.

Champagne, C. P., F. Mondou, Y. Raymond, and D. Roy. 1996. Effect of polymers and storage temperature on the stability of freeze-dried lactic acid bacteria. Food Research International **29**:555-562.

Champlot, S., C. Berthelot, M. Pruvost, E. A. Bennett, T. Grange, and E. M. Geigl. 2010. An Efficient Multistrategy DNA Decontamination Procedure of PCR Reagents for Hypersensitive PCR Applications. Plos One **5**.

Chan, W. S., A. C. M. Kwok, and J. T. Y. Wong. 2019. Knockdown of Dinoflagellate Cellulose Synthase CesA1 Resulted in Malformed Intracellular Cellulosic Thecal Plates and Severely Impeded Cyst-to-Swarmer Transition. Frontiers in Microbiology **10**.

Chang, C. C., C. C. Chen, S. C. Wei, H. H. Lu, Y. H. Liang, and C. W. Lin. 2012. Diagnostic Devices for Isothermal Nucleic Acid Amplification. Sensors **12**:8319-8337.

Chang, C. M., W. H. Chang, C. H. Wang, J. H. Wang, J. D. Mai, and G. B. Lee. 2013. Nucleic acid amplification using microfluidic systems. Lab on a Chip **13**:1225-1242.

Chang, L. Q., and M. J. Pikal. 2009. Mechanisms of Protein Stabilization in the Solid State. Journal of Pharmaceutical Sciences **98**:2886-2908.

Chao, C. C., T. Belinskaya, Z. W. Zhang, and W. M. Ching. 2015. Development of Recombinase Polymerase Amplification Assays for Detection of Orientia tsutsugamushi or Rickettsia typhi. Plos Neglected Tropical Diseases **9**.

Chekan, O. R., S. M. K. McKinnie, J. P. Noel, and B. S. Moore. 2020. Algal neurotoxin biosynthesis repurposes the terpene cyclase structural fold into an N-prenyltransferase. Proceedings of the National Academy of Sciences of the United States of America **117**:12799-12805.

Chen, G. F., C. S. Ma, C. Y. Zhang, J. Zhou, Y. Y. Wang, G. C. Wang, B. Y. Zhang, Z. Xu, and D. D. Lu. 2013. A rapid and sensitive method for field detection of Prorocentrum donghaiense using reverse transcription-coupled loop-mediated isothermal amplification. Harmful Algae **29**:31-39.

Chen, J. Y., X. M. Xu, Z. M. Huang, Y. Luo, L. J. Tang, and J. H. Jiang. 2018. BEAMing LAMP: single-molecule capture and on-bead isothermal amplification for digital detection of hepatitis C virus in plasma. Chemical Communications **54**:291-294.

Chen, L., A. Manz, and P. J. R. Day. 2007a. Total nucleic acid analysis integrated on microfluidic devices. Lab on a Chip **7**:1413-1423.

Chen, T. Y., J. L. Xin, S. J. Chang, C. J. Chen, and J. T. Liu. 2023. Surface Plasmon Resonance (SPR) Combined Technology: A Powerful Tool for Investigating Interface Phenomena. Advanced Materials Interfaces **10**.

Chen, X., D. F. Cui, C. C. Liu, H. Li, and J. Chen. 2007b. Continuous flow microfluidic device for cell separation, cell lysis and DNA purification. Analytica Chimica Acta **584**:237-243.

Chen, X., and S. M. Xia. 2022. Sensitive methods for detection of SARS-CoV-2 RNA. Covid-19 **50**:1-26.

Chen, X. Y., and J. N. Shen. 2017. Design and Simulation of a Chaotic Micromixer with Diamond-Like Micropillar Based on Artificial Neural Network. International Journal of Chemical Reactor Engineering **15**.

Chen, Y., Y. X. Mei, X. H. Zhao, and X. Y. Jiang. 2020. Reagents-Loaded, Automated Assay that Integrates Recombinase-Aided Amplification and Cas12a Nucleic Acid Detection for a Point-of-Care Test. Analytical Chemistry **92**:14846-14852.

Chin, C. D., V. Linder, and S. K. Sia. 2007. Lab-on-a-chip devices for global health: Past studies and future opportunities. Lab on a Chip **7**:41-57.

Chiu, M. L., W. Lawi, S. T. Snyder, P. K. Wong, J. C. Liao, and V. Gau. 2010. Matrix Effects-A Challenge Toward Automation of Molecular Analysis. Jala **15**:233-242.

Choi, G., T. J. Moehling, and R. J. Meagher. 2023. Advances in RT-LAMP for COVID-19 testing and diagnosis. Expert Review of Molecular Diagnostics.

Chon, C. H., and D. Li. 2008. Temperature Control in Microfluidic Systems. Pages 1976-1980 *in* D. Li, editor. Encyclopedia of Microfluidics and Nanofluidics. Springer US, Boston, MA.

Cicerone, M. T., and C. L. Soles. 2004. Fast dynamics and stabilization of proteins: Binary glasses of trehalose and glycerol. Biophysical Journal **86**:3836-3845.

Clark, S., K. A. Hubbard, D. M. Anderson, D. J. McGillicuddy, D. K. Ralston, and D. W. Townsend. 2019. Pseudo-nitzschia bloom dynamics in the Gulf of Maine: 2012-2016. Harmful Algae **88**.

Clark, S., K. A. Hubbard, D. K. Ralston, D. J. McGillicuddy, C. Stock, M. A. Alexander, and E. Curchitser. 2022. Projected effects of climate change on Pseudo-nitzschia bloom dynamics in the Gulf of Maine. Journal of Marine Systems **230**.

Clarke, K. R., and M. Ainsworth. 1993. A Method of Linking Multivariate Community Structure to Environmental Variables. Marine Ecology Progress Series **92**:205-219.

Cochlan, W. P., J. Herndon, and R. M. Kudela. 2008. Inorganic and organic nitrogen uptake by the toxigenic diatom Pseudo-nitzschia australis (Bacillariophyceae). Harmful Algae **8**:111-118.

Cohen, N. R., W. D. Gong, D. M. Moran, M. R. McIlvin, M. A. Saito, and A. Marchetti. 2018. Transcriptomic and proteomic responses of the oceanic diatom Pseudo-nitzschia granii to iron limitation. Environmental Microbiology **20**:3109-3126.

Colaco, C., S. Sen, M. Thangavelu, S. Pinder, and B. Roser. 1992. Extraordinary Stability of Enzymes Dried in Trehalose - Simplified Molecular-Biology. Bio-Technology **10**:1007-1011.

Compton, J. 1991. Nucleic-Acid Sequence-Based Amplification. Nature **350**:91-92.

Cook, K. B., J. P. Lacaze, M. Machairopoulou, and E. Bresnan. 2022. Investigations into the relationship between domoic acid and copepods in Scottish waters. Ices Journal of Marine Science **79**:963-973.

Coskun, O. 2016. Separation techniques: Chromatography. Northern Clinics of Istanbul **3**:156-160.

Costa, L. D. F., M. S. De Souza, C. C. Werlane, L. A. S. Madureira, S. C. Weigert, J. L. Colett, M. P. de Pinho, and J. S. Yunes. 2019. Domoic acid in the tropical South Atlantic Ocean - An environment case study. Toxicon **167**:101-105.

Costa, L. G., G. Giordano, and E. M. Faustman. 2010. Domoic acid as a developmental neurotoxin. Neurotoxicology **31**:409-423.

Costa, P. R., K. A. Baugh, B. Wright, R. RaLonde, S. L. Nance, N. Tatarenkova, S. M. Etheridge, and K. A. Lefebvre. 2009. Comparative determination of paralytic shellfish toxins (PSTs) using five different toxin detection methods in shellfish species collected in the Aleutian Islands, Alaska. Toxicon **54**:313-320.

Costa, P. R., S. M. Rodrigues, M. J. Botelho, and M. A. D. Sampayo. 2003. A potential vector of domoic acid: the swimming crab Polybius henslowii Leach (Decapoda-brachyura). Toxicon **42**:135-141.

Costa, P. R., R. Rosab, A. Duarte-Silva, V. Brotas, and M. A. M. Sampayo. 2005. Accumulation, transformation and tissue distribution of domoic acid, the amnesic shellfish poisoning toxin, in the common cuttlefish, Sepia officinalis. Aquatic Toxicology **74**:82-91.

Crannell, Z., A. Castellanos-Gonzalez, G. Nair, R. Mejia, A. C. White, and R. Richards-Kortum. 2016. Multiplexed Recombinase Polymerase Amplification Assay To Detect Intestinal Protozoa. Analytical Chemistry **88**:1610-1616.

Craw, P., and W. Balachandran. 2012. Isothermal nucleic acid amplification technologies for point-of-care diagnostics: a critical review. Lab on a Chip **12**:2469-2486.

Crego-Vicente, B., P. Fernandez-Soto, J. G. B. Diego, B. Febrer-Sendra, and A. Muro. 2023. Development of a Duplex LAMP Assay with Probe-Based Readout for Simultaneous Real-Time Detection of Schistosoma mansoni and Strongyloides spp. -A Laboratory Approach to Point-Of-Care. International Journal of Molecular Sciences **24**.

Crowe, J. H., J. F. Carpenter, and L. M. Crowe. 1998. The role of vitrification in anhydrobiosis. Annual Review of Physiology **60**:73-103.

Cusack, C. K., S. S. Bates, M. A. Quilliam, J. W. Patching, and R. Raine. 2002. Confirmation of domoic acid production by Pseudo-nitzschia australis (Bacillariophyceae) isolated from Irish waters. Journal of Phycology **38**:1106-1112.

Daher, R. K., G. Stewart, M. Boissinot, and M. G. Bergeron. 2016. Recombinase Polymerase Amplification for Diagnostic Applications. Clinical Chemistry **62**:947-958.

Dandin, M., P. Abshire, and E. Smela. 2007. Optical filtering technologies for integrated fluorescence sensors. Lab on a Chip **7**:955-977.

Dao, T. N. T., E. Y. Lee, B. Koo, C. E. Jin, T. Y. Lee, and Y. Shin. 2018. A microfluidic enrichment platform with a recombinase polymerase amplification sensor for pathogen diagnosis. Analytical Biochemistry **544**:87-92.

Davi, S. D., J. Kissenkotter, M. Faye, S. Bohlken-Fascher, C. Stahl-Hennig, O. Faye, O. Faye, A. A. Sall, M. Weidmann, O. G. Ademowo, F. T. Hufert, C. P. Czerny, and A. Abd El Wahed. 2019. Recombinase polymerase amplification assay for rapid detection of Monkeypox virus. Diagnostic Microbiology and Infectious Disease **95**:41-45.

de Baar, H. J. W., P. W. Boyd, K. H. Coale, M. R. Landry, A. Tsuda, P. Assmy, D. C. E. Bakker, Y. Bozec, R. T. Barber, M. A. Brzezinski, K. O. Buesseler, M. Boye, P. L. Croot, F. Gervais, M. Y. Gorbunov, P. J. Harrison, W. T. Hiscock, P. Laan, C. Lancelot, C. S. Law, M. Levasseur, A. Marchetti, F. J. Millero, J. Nishioka, Y. Nojiri, T. van Oijen, U. Riebesell, M. J. A. Rijkenberg, H. Saito, S. Takeda, K. R. Timmermans, M. J. W. Veldhuis, A. M. Waite, and C. S. Wong. 2005. Synthesis of iron fertilization experiments: From the iron age in the age of enlightenment. Journal of Geophysical Research-Oceans **110**.

de Baar, H. J. W., L. J. A. Gerringa, P. Laan, and K. R. Timmermans. 2008. Efficiency of carbon removal per added iron in ocean iron fertilization. Marine Ecology Progress Series **364**:269-282.

de La Iglesia, P., G. Gimenez, and J. Diogene. 2008. Determination of dissolved domoic acid in seawater with reversed-phase extraction disks and rapid resolution liquid

chromatography tandem mass spectrometry with head-column trapping. Journal of Chromatography A **1215**:116-124.

DeGrasse, S. L., J. A. DeGrasse, and K. Reuter. 2011. Solid core column technology applied to HPLC-FD of paralytic shellfish toxins. Toxicon **57**:179-182.

del Rio, J. S., T. Steylaerts, O. Y. F. Henry, P. Bienstman, T. Stakenborg, W. Van Roy, and C. K. O'Sullivan. 2015. Real-time and label-free ring-resonator monitoring of solid-phase recombinase polymerase amplification. Biosensors & Bioelectronics **73**:130-137.

Delaney, J. A. 2010. Molecular Detection of the Toxic Marine Diatom Pseudo-nitzschiamultiseries. University of South Florida, Graduate Theses and Dissertations.

Delaney, J. A., R. M. Ulrich, and J. H. Paul. 2011. Detection of the toxic marine diatom Pseudo-nitzschia multiseries using the RuBisCO small subunit (rbcS) gene in two real-time RNA amplification formats. Harmful Algae **11**:54-64.

Demeke, T., and G. R. Jenkins. 2010. Influence of DNA extraction methods, PCR inhibitors and quantification methods on real-time PCR assay of biotechnology-derived traits. Analytical and Bioanalytical Chemistry **396**:1977-1990.

Demirci, U., and G. Montesano. 2007. Cell encapsulating droplet vitrification. Lab on a Chip **7**:1428-1433.

Depauw, F. A., A. Rogato, M. Ribera d'Alcala, and A. Falciatore. 2012. Exploring the molecular basis of responses to light in marine diatoms. J Exp Bot **63**:1575-1591.

Dermastia, T. T., S. Dall'Ara, J. Dolenc, and P. Mozetic. 2022. Toxicity of the Diatom Genus Pseudo-nitzschia (Bacillariophyceae): Insights from Toxicity Tests and Genetic Screening in the Northern Adriatic Sea. Toxins **14**.

Derveaux, S., J. Vandesompele, and J. Hellemans. 2010. How to do successful gene expression analysis using real-time PCR. Methods **50**:227-230.

DeYoung, R. W., and R. L. Honeycutt. 2005. The molecular toolbox: Genetic techniques in wildlife ecology and management. Journal of Wildlife Management **69**:1362-1384.

Di Dato, V., F. Musacchia, G. Petrosino, S. Patil, M. Montresor, R. Sanges, and M. I. Ferrante. 2015. Transcriptome sequencing of three Pseudo-nitzschia species reveals comparable gene sets and the presence of Nitric Oxide Synthase genes in diatoms. Scientific Reports **5**.

Diego, J. G. B., P. Fernandez-Soto, B. Crego-Vicente, S. Alonso-Castrillejo, B. Febrer-Sendra, A. Gomez-Sanchez, B. Vicente, J. Lopez-Aban, and A. Muro. 2019. Progress in loop-mediated isothermal amplification assay for detection of Schistosoma mansoni DNA: towards a ready-to-use test. Scientific Reports **9**.

Dillon, M. J., and K. Campbell. 2023. Chapter Five - Hyphenating paper-based biosensors with smartphones. Pages 109-141 *in* J. L. D. Nelis and A. S. Tsagkaris, editors. Comprehensive Analytical Chemistry. Elsevier.

Dimov, I. K., J. L. Garcia-Cordero, J. O'Grady, C. R. Poulsen, C. Viguier, L. Kent, P. Daly, B. Lincoln, M. Maher, R. O'Kennedy, T. J. Smith, A. J. Ricco, and L. P. Lee. 2008. Integrated microfluidic tmRNA purification and real-time NASBA device for molecular diagnostics. Lab on a Chip **8**:2071-2078.

Dittami, S. M., V. Hostyeva, E. S. Egge, J. U. Kegel, W. Eikrem, and B. Edvardsen. 2013. Seasonal dynamics of harmful algae in outer Oslofjorden monitored by microarray, qPCR, and microscopy. Environmental Science and Pollution Research **20**:6719-6732.

Dittrich, P. S., K. Tachikawa, and A. Manz. 2006. Micro total analysis systems. Latest advancements and trends. Analytical Chemistry **78**:3887-3907.

Djaoueda, Y., M. Thibodeau, J. Robichaud, S. Balaji, S. Priya, N. Tchoukanova, and S. S. Bates. 2008. Photocatalytic degradation of domoic acid using nanocrystalline TiO2 thin films. Journal of Photochemistry and Photobiology a-Chemistry **193**:271-283.

Dos-Reis-Delgado, A. A., A. Carmona-Dominguez, G. Sosa-Avalos, I. H. Jimenez-Saaib, K. E. Villegas-Cantu, R. C. Gallo-Villanueva, and V. H. Perez-Gonzalez. 2023. Recent advances and challenges in temperature monitoring and control in microfluidic devices. Electrophoresis **44**:268-297.

Doucette, G. J., C. M. Mikulski, K. L. Jones, K. L. King, D. I. Greenfield, R. Marin, S. Jensen, B. Roman, C. T. Elliott, and C. A. Scholin. 2009. Remote, subsurface detection of the algal toxin domoic acid onboard the Environmental Sample Processor: Assay development and field trials. Harmful Algae **8**:880-888.

Douglas, A., and B. Atchison. 1993. Degradation of DNA during the denaturation step of PCR. Genome Research **3**:133-134.

Downes-Tettmar, N., S. Rowland, C. Widdicombe, M. Woodward, and C. Llewellyn. 2013. Seasonal variation in Pseudo-nitzschia spp. and domoic acid in the Western English Channel. Continental Shelf Research **53**:40-49.

Dragan, A., R. Pavlovic, J. McGivney, J. Casas-Finet, E. Bishop, R. Strouse, M. Schenerman, and C. Geddes. 2012a. SYBR Green I: fluorescence properties and interaction with DNA. Journal of fluorescence **22**:1189-1199.

Dragan, A. I., R. Pavlovic, J. B. McGivney, J. R. Casas-Finet, E. S. Bishop, R. J. Strouse, M. A. Schenerman, and C. D. Geddes. 2012b. SYBR Green I: Fluorescence Properties and Interaction with DNA. Journal of fluorescence **22**:1189-1199.

Druml, B., and M. Cichna-Markl. 2014. High resolution melting (HRM) analysis of DNA - Its role and potential in food analysis. Food Chemistry **158**:245-254.

Du, L., Y. Xia, Y. Y. He, Q. Q. Pu, R. Y. Hua, and W. Y. Wu. 2016a. Development and evaluation of enzyme-linked immunosorbent assay of nucleic acid sequence-based amplification for diagnosis of invasive aspergillosis. Amb Express **6**.

Du, X. N., W. Peterson, J. Fisher, M. Hunter, and J. Peterson. 2016b. Initiation and Development of a Toxic and Persistent Pseudo-nitzschia Bloom off the Oregon Coast in Spring/Summer2015. Plos One **11**.

Dubois, M., L. Demoulin, C. Charlier, G. Singh, S. B. Godefroy, K. Campbell, C. T. Elliott, and P. Delahaut. 2010. Development of ELISAs for detecting domoic acid, okadaic acid, and saxitoxin and their applicability for the detection of marine toxins in samples collected in Belgium. Food Additives and Contaminants Part a-Chemistry Analysis Control Exposure & Risk Assessment **27**:859-868.

Dyhrman, S. T., S. T. Haley, J. A. Borchert, B. Lona, N. Kollars, and D. L. Erdner. 2010. Parallel analyses of Alexandrium catenella cell concentrations and shellfish toxicity in the Puget Sound. Appl Environ Microbiol **76**:4647-4654.

Dzhembekova, N., S. Moncheva, N. Slabakova, I. Zlateva, S. Nagai, S. Wietkamp, M. Wellkamp, U. Tillmann, and B. Krock. 2022. New Knowledge on Distribution and Abundance of Toxic Microalgal Species and Related Toxins in the Northwestern Black Sea. Toxins **14**.

Easley, C. J., J. M. Karlinsey, J. M. Bienvenue, L. A. Legendre, M. G. Roper, S. H. Feldman, M. A. Hughes, E. L. Hewlett, T. J. Merkel, J. P. Ferrance, and J. P. Landers. 2006. A fully integrated microfluidic genetic analysis system with sample-in-answer-out capability. Proceedings of the National Academy of Sciences of the United States of America **103**:19272-19277.

Ebrahimi, N., C. H. Bi, D. J. Cappelleri, G. Ciuti, A. T. Conn, D. Faivre, N. Habibi, A. Hosovsky, V. Iacovacci, I. S. M. Khalil, V. Magdanz, S. Misra, C. Pawashe, R. Rashidifar, P. E. D. Soto-Rodriguez, Z. Fekete, and A. Jafari. 2021. Magnetic Actuation Methods in Bio/Soft Robotics. Advanced Functional Materials **31**.

Eckford-Soper, L. K., and N. Daugbjerg. 2015. Development of a multiplex real-time qPCR assay for simultaneous enumeration of up to four marine toxic bloom-forming microalgal species. Harmful Algae **48**:37-43.

Ehrmeyer, S. S., and R. H. Laessig. 2007. Point-of-care testing, medical error, and patient safety: a 2007 assessment. Clinical Chemistry and Laboratory Medicine **45**:766-773.

Eiken. 2023. PrimerExplorer V5.

Elnifro, E. M., A. M. Ashshi, R. J. Cooper, and P. E. Klapper. 2000. Multiplex PCR: Optimization and application in diagnostic virology. Clinical Microbiology Reviews **13**:559-+.

Emami, F., A. Vatanara, E. J. Park, and D. H. Na. 2018. Drying Technologies for the Stability and Bioavailability of Biopharmaceuticals. Pharmaceutics **10**.

Ereku, L. T., R. E. Mackay, P. Craw, A. Naveenathayalan, T. Stead, M. Branavan, and W. Balachandran. 2018. RPA using a multiplexed cartridge for low cost point of care diagnostics in the field. Analytical Biochemistry **547**:84-88.

Esser, K.-H., W. H. Marx, and T. Lisowsky. 2006. maxXbond: first regeneration system for DNA binding silica matrices. Nature Methods **3**:i-ii.

Etheridge, S. M. 2010. Paralytic shellfish poisoning: Seafood safety and human health perspectives. Toxicon **56**:108-122.

Euler, M., Y. J. Wang, O. Nentwich, O. Piepenburg, F. T. Hufert, and M. Weidmann. 2012. Recombinase polymerase amplification assay for rapid detection of Rift Valley fever virus. Journal of Clinical Virology **54**:308-312.

Fahy, G. M., and B. Wowk. 2015. Principles of Cryopreservation by Vitrification. Pages 21-82 *in* W. F. Wolkers and H. Oldenhof, editors. Cryopreservation and Freeze-Drying Protocols. Springer New York, New York, NY.

Fang, Z. D., J. Martin, and Z. Wang. 2012. Statistical methods for identifying differentially expressed genes in RNA-Seq exeriments. Cell and Bioscience **2**.

Farrar, J. S., G. H. Reed, and C. T. Wittwer. 2010. High-Resolution Melting Curve Analysis for Molecular Diagnostics. Molecular Diagnostics, 2nd Edition:229-245.

Farré, M., L. Kantiani, and D. Barceló. 2012. Chapter 7 - Microfluidic Devices: Biosensors. Pages 177-217 *in* Y. Picó, editor. Chemical Analysis of Food: Techniques and Applications. Academic Press, Boston.

Fehling, J., K. Davidson, and S. S. Bates. 2005. Growth dynamics of non-toxic Pseudo-nitzschia delicatissima and toxic P. seriata (Bacillariophyceae) under simulated spring and summer photoperiods. Harmful Algae **4**:763-769.

Fehling, J., K. Davidson, C. J. Bolch, and S. S. Bates. 2004. Growth and domoic acid production by Pseudo-nitzschia seriata (Bacillariophyceae) under phosphate and silicate limitation. Journal of Phycology **40**:674-683.

Feklistov, A. 2013. RNA polymerase: in search of promoters. Blavatnik Awards for Young Scientists 2012 **1293**:25-32.

Ferriss, B. E., D. J. Marcinek, D. Ayres, J. Borchert, and K. A. Lefebvre. 2017. Acute and chronic dietary exposure to domoic acid in recreational harvesters: A survey of shellfish consumption behavior. Environment International **101**:70-79.

Fiorini, G. S., and D. T. Chiu. 2005. Disposable microfluidic devices: fabrication, function, and application. Biotechniques **38**:429-446.

Fitzpatrick, E., D. A. Caron, and A. Schnetzer. 2010. Development and environmental application of a genus-specific quantitative PCR approach for Pseudo-nitzschia species. Marine Biology **157**:1161-1169.

Floquet, C. F. A., V. J. Sieben, A. Milani, E. P. Joly, I. R. G. Ogilvie, H. Morgan, and M. C. Mowlem. 2011. Nanomolar detection with high sensitivity microfluidic absorption cells manufactured in tinted PMMA for chemical analysis. Talanta **84**:235-239.

Foudeh, A. M., T. F. Didar, T. Veres, and M. Tabrizian. 2012. Microfluidic designs and techniques using lab-on-a-chip devices for pathogen detection for point-of-care diagnostics. Lab on a Chip **12**:3249-3266.

Fox, K. C. 1995. Biopreservation - Putting Proteins under Glass. Science **267**:1922-1923.

Franco De Sarabia Rosado Pedro, M., G. Limones Lopez, A. Madejon Seiz, and D. Marin Alberdi Maria. 2016. Method For Preparing Stabilised Reaction Mixtures, Which Are Totally Or Partially Dried, Comprising At Least One Enzyme, Reaction Mixtures And Kits Containing Said Mixtures. BIOTOOLS BIOTECHNOLOGICAL & MEDICAL LABORATORIES S A, EP.

Fritz, L., M. A. Quilliam, J. L. C. Wright, A. M. Beale, and T. M. Work. 1992. AN OUTBREAK OF DOMOIC ACID POISONING ATTRIBUTED TO THE PENNATE DIATOM PSEUDONITZSCHIA AUSTRALIS1. Journal of Phycology **28**:439-442.

Fu, J. L., Q. Fang, T. Zhang, X. H. Jin, and Z. L. Fang. 2006. Laser-induced fluorescence detection system for microfluidic chips based on an orthogonal optical arrangement. Analytical Chemistry **78**:3827-3834.

Fuentes, S., G. H. Wikfors, and S. Meseck. 2014. Silicon Deficiency Induces Alkaline Phosphatase Enzyme Activity in Cultures of Four Marine Diatoms. Estuaries and Coasts **37**:312-324.

Fujiyoshi, S., K. Yarimizu, Y. Miyashita, J. Rilling, J. J. Acuna, S. Ueki, G. Gajardo, O. Espinoza-Gonzalez, L. Guzman, M. A. Jorquera, S. Nagai, and F. Maruyama. 2021. Suitcase Lab: new, portable, and deployable equipment for rapid detection of specific harmful algae in Chilean coastal waters. Environmental Science and Pollution Research **28**:14144-14155.

Fukuba, T., A. Miyaji, T. Okamoto, T. Yamamoto, S. Kaneda, and T. Fujii. 2011. Integrated in situ genetic analyzer for microbiology in extreme environments. RSC Advances **1**:1567-1573.

Funk, J. A., M. G. Janech, J. C. Dillon, J. J. Bissler, B. J. Siroky, and P. D. Bell. 2014. Characterization of Renal Toxicity in Mice Administered the Marine Biotoxin Domoic Acid. Journal of the American Society of Nephrology **25**:1187-1197.

Gadkar, V. J., D. M. Goldfarb, S. Gantt, and P. A. G. Tilley. 2018. Real-time Detection and Monitoring of Loop Mediated Amplification (LAMP) Reaction Using Self-quenching and Dequenching Fluorogenic Probes. Scientific Reports **8**.

Gagez, A. L., A. Bonnet, P. Pineau, and M. Graber. 2017. Identification and quantification of domoic acid by UHPLC/QTOF tandem mass spectrometry, with simultaneous identification of non-target photodegradation products. International Journal of Environmental Analytical Chemistry **97**:1192-1205.

Gajski, G., M. Geric, A. M. Domijan, I. Golubovic, and B. Zegura. 2020. Marine toxin domoic acid induces in vitro genomic alterations in human peripheral blood cells. Toxicon **187**:93-100.

Gan, W. P., Y. Gu, J. P. Han, C. X. Li, J. Sun, and P. Liu. 2017. Chitosan-Modified Filter Paper for Nucleic Acid Extraction and '' in Situ PCR '' on a Thermoplastic Microchip. Analytical Chemistry **89**:3568-3575.

Gao, D. L., X. D. Guo, Y. Yang, H. Shi, R. Z. Hao, S. Q. Wang, Z. J. Li, R. T. Zhao, and H. B. Song. 2022. Microfluidic chip and isothermal amplification technologies for the detection of pathogenic nucleic acid. Journal of Biological Engineering **16**.

Garcia, E., J. R. Kirkham, A. V. Hatch, K. R. Hawkins, and P. Yager. 2004. Controlled microfluidic reconstitution of functional protein from an anhydrous storage depot. Lab on a Chip **4**:78-82.

Gervais, L., N. de Rooij, and E. Delamarche. 2011. Microfluidic Chips for Point-of-Care Immunodiagnostics. Advanced Materials **23**:H151-H176.

Gibson, U., C. A. Heid, and P. M. Williams. 1996. A novel method for real time quantitative RT-PCR. Genome Research **6**:995-1001.

Glibert, P. M. 2020. Harmful algae at the complex nexus of eutrophication and climate change. Harmful Algae **91**.

Gotz, S., and U. Karst. 2007. Recent developments in optical detection methods for microchip separations. Analytical and Bioanalytical Chemistry **387**:183-192.

Grasmeijer, N., M. Stankovic, H. de Waard, H. W. Frijlink, and W. L. J. Hinrichs. 2013. Unraveling protein stabilization mechanisms: Vitrification and water replacement in a glass transition temperature controlled system. Biochimica Et Biophysica Acta-Proteins and Proteomics **1834**:763-769.

Green, J. L., and C. A. Angell. 1989. Phase-Relations and Vitrification in Saccharide-Water Solutions and the Trehalose Anomaly. Journal of Physical Chemistry **93**:2880-2882.

Green, S. J., R. Venkatramanan, and A. Naqib. 2015. Deconstructing the polymerase chain reaction: understanding and correcting bias associated with primer degeneracies and primer-template mismatches. Plos One **10**:e0128122.

Gross, M. S., E. E. Woodward, and M. L. Hladik. 2022. Evaluation of ELISA for the analysis of imidacloprid in biological matrices: Cross-reactivities, matrix interferences, and comparison to LC-MS/MS. Chemosphere **286**.

Groussman, R. D., M. S. Parker, and E. V. Armbrust. 2015. Diversity and Evolutionary History of Iron Metabolism Genes in Diatoms. Plos One **10**.

Guell, C., M. Ferrando, A. Trentin, and K. Schroen. 2017. Apparent Interfacial Tension Effects in Protein Stabilized Emulsions Prepared with Microstructured Systems. Membranes **7**.

Gueroult, M., D. Picot, J. Abi-Ghanem, B. Hartmann, and M. Baaden. 2010. How Cations Can Assist DNase I in DNA Binding and Hydrolysis. Plos Computational Biology **6**.

Guillard, R. R. L. 1983. Culture of phytoplankton for feeding marine invertebrates. Pages 108–132 *in* M. Landau, editor. Culture of Marine-Invertebrates - Selected-Readings - Berg,Cj, Ross,H. Hutchinson Ross Publishing Co, Stroudsberg, PA.

Gunther, A., M. Jhunjhunwala, M. Thalmann, M. A. Schmidt, and K. F. Jensen. 2005. Micromixing of miscible liquids in segmented gas-liquid flow. Langmuir **21**:1547-1555.

Guo, L. L., Z. H. Sui, S. Zhang, Y. Y. Ren, and Y. Liu. 2015. Comparison of potential diatom 'barcode' genes (the 18S rRNA gene and ITS, COI, rbcL) and their effectiveness in discriminating and determining species taxonomy in the Bacillariophyta. International Journal of Systematic and Evolutionary Microbiology **65**:1369-1380.

Haeberle, S., and R. Zengerle. 2007. Microfluidic platforms for lab-on-a-chip applications. Lab on a Chip **7**:1094-1110.

Hagan, K. A., W. L. Meier, J. P. Ferrance, and J. P. Landers. 2009. Chitosan-Coated Silica as a Solid Phase for RNA Purification in a Microfluidic Device. Analytical Chemistry **81**:5249-5256.

Hagstrom, J. A., E. Graneli, I. Maneiro, A. Barreiro, A. Petermann, and C. Svensen. 2007. Release and degradation of amnesic shellfish poison from decaying Pseudo-nitzschia multiseries in presence of bacteria and organic matter. Harmful Algae **6**:175-188.

Hagstrom, J. A., E. Graneli, M. O. P. Moreira, and C. Odebrecht. 2011. Domoic acid production and elemental composition of two Pseudo-nitzschia multiseries strains, from the NW and SW Atlantic Ocean, growing in phosphorus- or nitrogen-limited chemostat cultures. Journal of Plankton Research **33**:297-308.

Hampson, D. R., X. P. Huang, J. W. Wells, J. A. Walter, and J. L. C. Wright. 1992. Interaction of Domoic Acid and Several Derivatives with Kainic Acid and Ampa Binding-Sites in Rat-Brain. European Journal of Pharmacology **218**:1-8.

Han, K., Y. J. Yoon, Y. Shin, and M. K. Park. 2016. Self-powered switch-controlled nucleic acid extraction system. Lab on a Chip **16**:132-141.

Han, S. I., K. H. Han, A. B. Frazier, J. P. Ferrance, and J. P. Landers. 2009. An automated micro-solid phase extraction device involving integrated \high-pressure microvalves for genetic sample preparation. Biomedical Microdevices **11**:935-942.

Hansen, L. R., S. I. Soylu, Y. Kotaki, O. Moestrup, and N. Lundholm. 2011. Toxin production and temperature-induced morphological variation of the diatom Pseudo-nitzschia seriata from the Arctic. Harmful Algae **10**:689-696.

Hardardottir, S., S. Wohlrab, D. M. Hjort, B. Krock, T. G. Nielsen, U. John, and N. Lundholm. 2019. Transcriptomic responses to grazing reveal the metabolic pathway leading to the biosynthesis of domoic acid and highlight different defense strategies in diatoms. Bmc Molecular Biology **20**.

Hardinge, P., G. Kiddle, L. Tisi, and J. A. H. Murray. 2018. Optimised LAMP allows single copy detection of 35Sp and NOSt in transgenic maize using Bioluminescent Assay in Real Time (BART). Scientific Reports **8**.

Hardinge, P., and J. A. H. Murray. 2019. Reduced False Positives and Improved Reporting of Loop-Mediated Isothermal Amplification using Quenched Fluorescent Primers. Scientific Reports **9**.

Harnett, C. K., J. Templeton, K. A. Dunphy-Guzman, Y. M. Senousy, and M. P. Kanouff. 2008. Model based design of a microfluidic mixer driven by induced charge electroosmosis. Lab on a Chip **8**:565-572.

Haroardottir, S., M. Pancic, A. Tammilehto, B. Krock, E. F. Moller, T. G. Nielsen, and N. Lundholm. 2015. Dangerous Relations in the Arctic Marine Food Web: Interactions between Toxin

Producing Pseudo-nitzschia Diatoms and Calanus Copepodites. Marine Drugs **13**:3809-3835.

Harris, L. D., and J. Griffith. 1987. Visualization of the Homologous Pairing of DNA Catalyzed by the Bacteriophage-T4 Uvsx Protein. Journal of Biological Chemistry **262**:9285-9292.

Harris, L. D., and J. D. Griffith. 1989. Uvsy Protein of Bacteriophage-T4 Is an Accessory Protein for Invitro Catalysis of Strand Exchange. Journal of Molecular Biology **206**:19-27.

Hashish, A., A. Sinha, Y. Sato, N. R. Macedo, and M. El-Gazzar. 2022. Development and Validation of a New TaqMan Real-Time PCR for the Detection of Ornithobacterium rhinotracheale (vol 10, 341, 2022). Microorganisms **10**.

Hasle G, R. 1978. The inverted microscope method. Phytoplankton manual.

Hatfield, C. L., E. J. J. Gauglitz, H. J. Barnett, J. A. K. Lund, J. C. Wekell, and M. Eklund. 1995. The fate of domoic acid in Dungeness crab (Cancer magister) as a function of processing. J. Shellfish Res. **14**:359-363.

Hayashida, K., K. Kajino, L. Hachaambwa, B. Namangala, and C. Sugimoto. 2015. Direct Blood Dry LAMP: A Rapid, Stable, and Easy Diagnostic Tool for Human African Trypanosomiasis. Plos Neglected Tropical Diseases **9**.

Hayashida, K., Y. Orba, P. C. Sequeira, C. Sugimoto, W. W. Hall, Y. Eshita, Y. Suzuki, L. Runtuwene, P. Brasil, G. Calvet, C. D. S. Rodrigues, C. C. dos Santos, M. A. M. Mares-Guia, J. Yamagishi, A. M. B. de Filippis, and H. Sawa. 2019. Field diagnosis and genotyping of chikungunya virus using a dried reverse transcription loop-mediated isothermal amplification (LAMP) assay and MinION sequencing. Plos Neglected Tropical Diseases **13**.

Hazen, T. C., A. M. Rocha, and S. M. Techtmann. 2013. Advances in monitoring environmental microbes. Current Opinion in Biotechnology **24**:526-533.

Hedoux, A., L. Paccou, S. Achir, and Y. Guinet. 2012. In Situ Monitoring of Proteins During Lyophilization Using Micro-Raman Spectroscopy: A Description of Structural Changes Induced by Dehydration. Journal of Pharmaceutical Sciences **101**:2316-2326.

Heeroma, A. J., and C. Gwenin. 2020. Development of Solid-Phase RPA on a Lateral Flow Device for the Detection of Pathogens Related to Sepsis. Sensors **20**.

Hessel, V., H. Lowe, and F. Schonfeld. 2005. Micromixers - a review on passive and active mixing principles. Chemical Engineering Science **60**:2479-2501.

Hildebrand, M., S. J. L. Lerch, and R. P. Shrestha. 2018. Understanding Diatom Cell Wall Silicification - Moving Forward. Frontiers in Marine Science **5**.

Hill-Cawthorne, G. A., L. O. Hudson, M. F. A. El Ghany, O. Piepenburg, M. Nair, A. Dodgson, M. S. Forrest, T. G. Clark, and A. Pain. 2014. Recombinations in Staphylococcal Cassette Chromosome mec Elements Compromise the Molecular Detection of Methicillin Resistance in Staphylococcus aureus. Plos One **9**.

Hodzic, E., A. Glavinic, and C. Wademan. 2023. A novel approach for simultaneous detection of the most common food-borne pathogens by multiplex qPCR. Biomolecules and Biomedicine **23**:640-648.

Hoffmeyer, M. S., M. S. Dutto, A. A. Berasategui, M. D. Garcia, R. E. Pettigrosso, G. O. Almandoz, V. D'Agostino, T. M. Garcia, E. Fabro, F. E. Paparazzo, M. Solis, G. Williams, J. L. Esteves, and B. Krock. 2020. DOMOIC acid, Pseudo-nitzschia spp and potential vectors at the base of the pelagic food web over the northern Patagonian coast, Southwestern Atlantic. Journal of Marine Systems **212**.

Høgberg, J., T. Christine, C. Cao, L. Florian, M. Agirregabiria, L. G. Monsalve, A. Goiriena, S. Rodriguez, A. Wolff, D. D. Bang, and J. Ruano-López. 2011. Gelification - A simple and efficient method for on-chip storage of reagents: Towards lab-on-a-chip systems for point-of-care diagnostics. 15th International Conference on Miniaturized Systems for Chemistry and Life Sciences 2011, MicroTAS 2011 **3**:1864-1866.

Holland, C. A., and F. L. Kiechle. 2005. Point-of-care molecular diagnostic systems - past, present and future. Current Opinion in Microbiology **8**:504-509.

Holtermann, K. E., S. S. Bates, V. L. Trainer, A. Odell, and E. V. Armbrust. 2010. Mass Sexual Reproduction in the Toxigenic Diatoms Pseudo-Nitzschia Australis and P-Pungens (Bacillariophyceae) on the Washington Coast, USA. Journal of Phycology **46**:41-52.

Homola, J. 2003. Present and future of surface plasmon resonance biosensors. Analytical and Bioanalytical Chemistry **377**:528-539.

Howard, M. D. A., W. P. Cochlan, N. Ladizinsky, and R. M. Kudela. 2007. Nitrogenous preference of toxigenic Pseudo-nitzschia australis (Bacillariophyceae) from field and laboratory experiments. Harmful Algae **6**:206-217.

Huang, C. X., H. C. Dong, N. Lundholm, S. T. Teng, G. C. Zheng, Z. J. Tan, P. T. Lim, and Y. Li. 2019. Species composition and toxicity of the genus Pseudo-nitzschia in Taiwan Strait, including P. chiniana sp. nov. and P. qiana sp. nov. Harmful Algae **84**:195-209.

Huang, H. L., P. Zhu, C. X. Zhou, S. He, and X. J. Yan. 2017a. The development of loop-mediated isothermal amplification combined with lateral flow dipstick for detection of Karlodinium veneficum. Harmful Algae **62**:20-29.

Huang, K. W., and A. A. Marti. 2012. Recent trends in molecular beacon design and applications. Analytical and Bioanalytical Chemistry **402**:3091-3102.

Huang, W., H. Zhang, J. S. Xu, S. Wang, X. J. Kong, W. Ding, J. Xu, and J. Feng. 2017b. Loop-Mediated Isothermal Amplification Method for the Rapid Detection of Ralstonia solanacearum Phylotype I Mulberry Strains in China (vol 8, 76, 2017). Frontiers in Plant Science **8**.

Huang, W. E., B. Lim, C. C. Hsu, D. Xiong, W. Wu, Y. J. Yu, H. D. Jia, Y. Wang, Y. D. Zeng, M. M. Ji, H. Chang, X. M. Zhang, H. Wang, and Z. F. Cui. 2020. RT-LAMP for rapid diagnosis of coronavirus SARS-CoV-2. Microbial Biotechnology **13**:950-961.

Huang, X., G. Y. Tang, N. Ismail, and X. W. Wang. 2022. Developing RT-LAMP assays for rapid diagnosis of SARS-CoV-2 in saliva. Ebiomedicine **75**.

Hui, M. P., P. L. Foley, and J. G. Belasco. 2014. Messenger RNA Degradation in Bacterial Cells. Annual Review of Genetics, Vol 48 **48**:537-559.

Husson, B., T. Hernandez-Farinas, R. Le Gendre, M. Schapira, and A. Chapelle. 2016. Two decades of Pseudo-nitzschia spp. blooms and king scallop (Pecten maximus) contamination by domoic acid along the French Atlantic and English Channel coasts: Seasonal dynamics, spatial heterogeneity and interannual variability. Harmful Algae **51**:26-39.

Ibrahim, J., M. Al Masri, I. Verrier, T. Kampfe, C. Veillas, F. Celle, S. Cioulachtjian, F. Lefevre, and Y. Jourlin. 2019. Surface Plasmon Resonance Based Temperature Sensors in Liquid Environment. Sensors **19**.

Inacio, J., O. Flores, and I. Spencer-Martins. 2008. Efficient identification of clinically relevant Candida yeast species by use of an assay combining panfungal loop-mediated isothermal DNA amplification with hybridization to species-specific oligonucleotide probes. Journal of Clinical Microbiology **46**:713-720.

Ivnitski, D., D. J. O'Neil, A. Gattuso, R. Schlicht, M. Calidonna, and R. Fisher. 2003. Nucleic acid approaches for detection and identification of biological warfare and infectious disease agents. Biotechniques **35**:862-869.

Jang, Y. O., C. E. Jin, E. H. Choi, J. H. Shin, J. Kweon, B. Koo, S. B. Lim, S. W. Lee, and Y. Shin. 2019. A homobifunctional imidoester-based microfluidic system for simultaneous DNA and protein isolation from solid or liquid biopsy samples. Lab on a Chip **19**:2256-2264.

Jawaid, W., J. Meneely, K. Campbell, M. Hooper, K. Melville, S. Holmes, J. Rice, and C. Elliott. 2013. Development and validation of the first high performance-lateral flow immunoassay (HP-LFIA) for the rapid screening of domoic acid from shellfish extracts. Talanta **116**:663-669.

Jeroish, Z. E., K. S. Bhuvaneshwari, F. Samsuri, and V. Narayanamurthy. 2021. Microheater: material, design, fabrication, temperature control, and applications—a role in COVID-19. Biomedical Microdevices **24**:3.

Jet, T., G. Gines, Y. Rondelez, and V. Taly. 2021. Advances in multiplexed techniques for the detection and quantification of microRNAs. Chemical Society Reviews **50**:4141-4161.

Jia, H. N., Z. Y. Chen, H. P. Wu, H. Ye, B. J. Zou, Q. X. Song, and G. H. Zhou. 2016. Pyrosequencing Templates Generated by Asymmetric Nucleic Acid Sequence-Based Amplification (Asymmetric-NASBA). Advances and Clinical Practice in Pyrosequencing:41-49.

Jiang, B. 2019. Analysis of prenyltransferase gene expression in Pseudo-nitzschia multiseries.

Jiang, H., Y. Li, X. F. Lv, Y. L. Deng, and X. Q. Li. 2023. Recent advances in cascade isothermal amplification techniques for ultra-sensitive nucleic acid detection. Talanta **260**.

Jin, C. E., T. Y. Lee, B. Koo, K. C. Cho, S. Chang, S. Y. Park, J. Y. Kim, S. H. Kim, and Y. Shin. 2017. Use of Dimethyl Pimelimidate with Microfluidic System for Nucleic Acids Extraction without Electricity. Analytical Chemistry **89**:7502-7510.

Johnson, D. S., and A. Loehr. 2015. Method for correction of bias in multiplexed amplification. Google Patents.

Johnson, S., K. Harrison, and A. D. Turner. 2016. Application of rapid test kits for the determination of Amnesic Shellfish Poisoning in bivalve molluscs from Great Britain. Toxicon **117**:76-83.

Joyce, S. 2000. The dead zones: Oxygen-starved coastal waters. Environmental Health Perspectives **108**:A120-A125.

Kaczmarska, I., M. M. LeGresley, J. L. Martin, and J. Ehrman. 2005. Diversity of the diatom genus Pseudo-nitzschia Peragallo in the Quoddy Region of the Bay of Fundy, Canada. Harmful Algae **4**:1-19.

Kainz, P. 2000. The PCR plateau phase–towards an understanding of its limitations. Biochimica et Biophysica Acta (BBA)-Gene Structure and Expression **1494**:23-27.

Kaiser, M. W., N. Lyamicheva, W. P. Ma, C. Miller, B. Neri, L. Fors, and V. I. Lyamichev. 1999. A comparison of eubacterial and archaeal structure-specific 5 '-exonucleases. Journal of Biological Chemistry **274**:21387-21394.

Kalinina, O., I. Lebedeva, J. Brown, and J. Silver. 1997. Nanoliter scale PCR with TaqMan detection. Nucleic Acids Research **25**:1999-2004.

Kamra, E., N. Singh, A. Khan, J. Singh, M. Chauhan, H. Kamal, and P. K. Mehta. 2022. Diagnosis of genitourinary tuberculosis by loop-mediated isothermal amplification based on SYBR Green I dye reaction. Biotechniques **73**.

Kanagawa, T. 2003. Bias and artifacts in multitemplate polymerase chain reactions (PCR). Journal of Bioscience and Bioengineering **96**:317-323.

Kang, J. S. 2012. Principles and Applications of LC-MS/MS for the Quantitative Bioanalysis of Analytes in Various Biological Samples. Tandem Mass Spectroscopy - Applications and Principles:441-492.

Kania, M., and B. Hock. 2002. Development of monoclonal antibodies to domoic acid for the detection of domoic acid in blue mussel (mytilus edulis) tissue by ELISA. Analytical Letters **35**:855-868.

Karban, R. 2011. The ecology and evolution of induced resistance against herbivores. Functional Ecology **25**:339-347.

Karlsson, M. A., M. Langton, F. Innings, B. Malmgren, A. Hojer, M. Wikstrom, and A. Lundh. 2019. Changes in stability and shelf-life of ultra-high temperature treated milk during long term storage at different temperatures. Heliyon **5**.

Kasper, J. C., G. Winter, and W. Friess. 2013. Recent advances and further challenges in lyophilization. European Journal of Pharmaceutics and Biopharmaceutics **85**:162-169.

Katevatis, C., A. Fan, and C. M. Klapperich. 2017. Low concentration DNA extraction and recovery using a silica solid phase. Plos One **12**.

Kaur, N., J. S. Michael, and B. J. Toley. 2019. A modular paper-and-plastic device for tuberculosis nucleic acid amplification testing in limited-resource settings. Scientific Reports **9**.

Kazmi, S. S. U., N. Yapa, S. C. Karunarathna, and N. Suwannarach. 2022. Perceived Intensification in Harmful Algal Blooms Is a Wave of Cumulative Threat to the Aquatic Ecosystems. Biology-Basel **11**.

Kebede, T. G., S. S. Nety, S. Dube, and M. M. Nindi. 2022. Chapter 5 - The miniaturization of liquid-phase extraction techniques. Pages 63-93 *in* T. Dalu and N. T. Tavengwa, editors. Emerging Freshwater Pollutants. Elsevier.

Keeling, P. J., F. Burki, H. M. Wilcox, B. Allam, E. E. Allen, L. A. Amaral-Zettler, E. V. Armbrust, J. M. Archibald, A. K. Bharti, C. J. Bell, B. Beszteri, K. D. Bidle, C. T. Cameron, L. Campbell, D. A. Caron, R. A. Cattolico, J. L. Collier, K. Coyne, S. K. Davy, P. Deschamps, S. T. Dyhrman, B. Edvardsen, R. D. Gates, C. J. Gobler, S. J. Greenwood, S. M. Guida, J. L. Jacobi, K. S. Jakobsen, E. R. James, B. Jenkins, U. John, M. D. Johnson, A. R. Juhl, A. Kamp, L. A. Katz, R. Kiene, A. Kudryavtsev, B. S. Leander, S. Lin, C. Lovejoy, D. Lynn, A. Marchetti, G. McManus, A. M. Nedelcu, S. Menden-Deuer, C. Miceli, T. Mock, M. Montresor, M. A. Moran, S. Murray, G. Nadathur, S. Nagai, P. B. Ngam, B. Palenik, J. Pawlowski, G. Petroni, G. Piganeau, M. C. Posewitz, K. Rengefors, G. Romano, M. E. Rumpho, T. Rynearson, K. B. Schilling, D. C. Schroeder, A. G. B. Simpson, C. H. Slamovits, D. R. Smith, G. J. Smith, S. R. Smith, H. M. Sosik, P. Stief, E. Theriot, S. Twary, P. E. Umale, D. Vaulot, B. Wawrik, G. L. Wheeler, W. H. Wilson, Y. Xu, A. Zingone, and A. Z. Worden. 2014. The Marine Microbial Eukaryote Transcriptome Sequencing Project (MMETSP): Illuminating the Functional Diversity of Eukaryotic Life in the Oceans through Transcriptome Sequencing. Plos Biology **12**.

Kelchner, H., K. E. Reeve-Arnold, K. M. Schreiner, S. Bargu, K. G. Roques, and R. M. Errera. 2021. Domoic Acid and Pseudo-nitzschia spp. Connected to Coastal Upwelling along Coastal Inhambane Province, Mozambique: A New Area of Concern. Toxins **13**.

Keller, M. D., R. C. Selvin, W. Claus, and R. R. L. Guillard. 1987. Media for the Culture of Oceanic Ultraphytoplankton. Journal of Phycology **23**:633-638.

Kelly, K. J., F. X. Fu, X. W. Jiang, H. Li, D. Xu, N. N. Yang, M. A. DeMers, J. D. Kling, K. S. Gao, N. I. H. Ye, and D. A. Hutchins. 2021. Interactions Between Ultraviolet B Radiation, Warming, and Changing Nitrogen Source May Reduce the Accumulation of Toxic Pseudo-nitzschia multiseries Biomass in Future Coastal Oceans. Frontiers in Marine Science **8**.

Kersting, S., V. Rausch, F. F. Bier, and M. von Nickisch-Rosenegk. 2014. Rapid detection of Plasmodium falciparum with isothermal recombinase polymerase amplification and lateral flow analysis. Malaria Journal **13**.

Khaliliazar, S., A. Toldra, G. Chondrogiannis, and M. M. Hamedi. 2021. Electroanalytical Paper-Based Nucleic Acid Amplification Biosensors with Integrated Thread Electrodes. Analytical Chemistry **93**:14187-14195.

Khan, Z., K. Poetter, and D. J. Park. 2008. Enhanced solid phase PCR: mechanisms to increase priming by solid support primers. Analytical Biochemistry **375**:391-393.

Kim, J., D. Byun, M. G. Mauk, and H. H. Bau. 2009. A disposable, self-contained PCR chip. Lab on a Chip **9**:606-612.

Kim, J. H., J. H. Kim, B. S. Park, P. B. Wang, S. K. Patidar, and M. S. Han. 2017. Development of a qPCR assay for tracking the ecological niches of genetic sub-populations within Pseudo-nitzschia pungens (Bacillariophyceae). Harmful Algae **63**:68-78.

Kim, J. Y., S. I. Kang, J. J. Lee, K. Lee, S. R. Sung, J. Erdenebaataar, B. Vanaabaatar, S. C. Jung, Y. H. Park, H. S. Yoo, and M. Her. 2016. Differential diagnosis of Brucella abortus by real-time PCR based on a single-nucleotide polymorphisms. Journal of Veterinary Medical Science **78**:557-562.

Kim, J. Y., and J. L. Lee. 2017. Development of a multiplex real-time recombinase polymerase amplification (RPA) assay for rapid quantitative detection of Campylobacter coli and jejuni from eggs and chicken products. Food Control **73**:1247-1255.

Kleivdal, H., S. I. Kristiansen, M. V. Nilsen, and L. Briggs. 2007a. Single-laboratory validation of the biosense direct competitive enzyme-linked immunosorbent assay (ELISA) for determination of domoic acid toxins in shellfish. Journal of Aoac International **90**:1000-1010.

Kleivdal, H., S. I. Kristiansen, M. V. Nilsen, A. Goksoyr, L. Briggs, P. Holland, and P. McNabb. 2007b. Determination of domoic acid toxins in shellfish by Biosense ASP ELISA - A direct competitive enzyme-linked immunosorbent assay: Collaborative study. Journal of Aoac International **90**:1011-1027.

Koivunen, M. E., and R. L. Krogsrud. 2006. Principles of immunochemical techniques used in clinical laboratories. Labmedicine **37**:490-497.

Kotaki, Y., E. F. Furio, M. Satake, N. Lundholm, T. Katayama, K. Koike, V. P. Fulgueras, F. A. Bajarias, Y. Takata, K. Kobayashi, S. Sato, Y. Fukuyo, and M. Kodama. 2005. Production of isodomoic acids A and B as major toxin components of a pennate diatom Nitzschia navis-varingica. Toxicon **46**:946-953.

Kotaki, Y., N. Lundholm, T. Katayama, E. Furio, m. l. Romero, J. R. Relox, T. Yasumoto, H. Naoki, M. Y. Hirose, T. Thanh, C. Thuoc, N. T. M. Huyen, P. Thu, Y. Takata, M. Kodama, and Y. Fukuyo. 2008. ASP toxins of pennate diatoms and bacterial effects on the variation in toxin composition.

Kouakou, C. R. C., and T. G. Poder. 2019. Economic impact of harmful algal blooms on human health: a systematic review. Journal of Water and Health **17**:499-516.

Kovacevic, N. 2016. Magnetic Beads Based Nucleic Acid Purification for Molecular Biology Applications. Sample Preparation Techniques for Soil, Plant, and Animal Samples:53-67.

Kozak, M. 2005. Regulation of translation via mRNA structure in prokaryotes and eukaryotes. Gene **361**:13-37.

Kralik, P., and M. Ricchi. 2017. A Basic Guide to Real Time PCR in Microbial Diagnostics: Definitions, Parameters, and Everything. Frontiers in Microbiology **8**.

Kudela, R. M., J. Q. Lane, and W. P. Cochlan. 2008. The potential role of anthropogenically derived nitrogen in the growth of harmful algae in California, USA. Harmful Algae **8**:103-110.

Kumar, K. P., S. P. Kumar, and G. A. Nair. 2009. Risk assessment of the amnesic shellfish poison, domoic acid, on animals and humans. Journal of Environmental Biology **30**:319-325.

Kuswandi, B., Nuriman, J. Huskens, and W. Verboom. 2007. Optical sensing systems for microfluidic devices: A review. Analytica Chimica Acta **601**:141-155.

Kvitek, R. G., J. D. Goldberg, G. J. Smith, G. J. Doucette, and M. W. Silver. 2008. Domoic acid contamination within eight representative species from the benthic food web of Monterey Bay, California, USA. Marine Ecology Progress Series **367**:35-47.

Kwon, E. Y., M. G. Sreeush, A. Timmermann, D. M. Karl, M. J. Church, S. S. Lee, and R. Yamaguchi. 2022. Nutrient uptake plasticity in phytoplankton sustains future ocean net primary production. Science Advances **8**.

La Barre, S., S. S. Bates, and M. A. Quilliam. 2014. Domoic Acid. Pages 189-216 Outstanding Marine Molecules.

Lafleur, L. K., J. D. Bishop, E. K. Heiniger, R. P. Gallagher, M. D. Wheeler, P. Kauffman, X. H. Zhang, E. C. Kline, J. R. Buser, S. Kumar, S. A. Byrnes, N. M. J. Vermeulen, N. K. Scarr, Y. Belousov, W. Mahoney, B. J. Toley, P. D. Ladd, B. R. Lutz, and P. Yager. 2016. A rapid, instrument-free, sample-to-result nucleic acid amplification test. Lab on a Chip **16**:3777-3787.

Lai, M. Y., C. H. Ooi, and Y. L. Lau. 2021. Validation of SYBR green I based closed-tube loop-mediated isothermal amplification (LAMP) assay for diagnosis of knowlesi malaria. Malaria Journal **20**.

Land, K. J., D. I. Boeras, X. S. Chen, A. R. Ramsay, and R. W. Peeling. 2019. REASSURED diagnostics to inform disease control strategies, strengthen health systems and improve patient outcomes. Nature Microbiology **4**:46-54.

Langlois, V. S., M. J. Allison, L. C. Bergman, T. A. To, and C. C. Helbing. 2021. The need for robust qPCR-based eDNA detection assays in environmental monitoring and species inventories. Environmental DNA **3**:519-527.

Larkin, M. A., G. Blackshields, N. P. Brown, R. Chenna, P. A. McGettigan, H. McWilliam, F. Valentin, I. M. Wallace, A. Wilm, R. Lopez, J. D. Thompson, T. J. Gibson, and D. G. Higgins. 2007. Clustal W and clustal X version 2.0. Bioinformatics **23**:2947-2948.

Lau, H. Y., Y. L. Wang, E. J. H. Wee, J. R. Botella, and M. Trau. 2016. Field Demonstration of a Multiplexed Point-of-Care Diagnostic Platform for Plant Pathogens. Analytical Chemistry **88**:8074-8081.

Lauri, A., and P. O. Mariani. 2009. Potentials and limitations of molecular diagnostic methods in food safety. Genes and Nutrition **4**:1-12.

Laursen, B. S., H. P. Sorensen, K. K. Mortensen, and H. U. Sperling-Petersen. 2005. Initiation of protein synthesis in bacteria. Microbiology and Molecular Biology Reviews **69**:101-+.

Leandro, L. F., G. J. Teegarden, P. B. Roth, Z. H. Wang, and G. J. Doucette. 2010. The copepod Calanus finmarchicus: A potential vector for trophic transfer of the marine algal biotoxin, domoic acid. Journal of Experimental Marine Biology and Ecology **382**:88-95.

Lee, D., O. Kwon, K.-H. Lee, J. Yun, C. kim, J. Seo, J. Koo, and G. M. Kim. 2019a. Automated Platform for Rapid and Reproducible Sample Preparations in Point-of-Care(POC) Molecular Diagnostics. Biochip Journal.

Lee, K., and A. Tripathi. 2022. An investigation into simplifying total RNA extraction with minimal equipment using a low volume, electrokinetically driven microfluidic protocol. Biomicrofluidics **16**.

Lee, L. G., C. R. Connell, and W. Bloch. 1993. Allelic discrimination by nick-translation PCR with fluorgenic probes. Nucleic Acids Research **21**:3761-3766.

Lee, S. H., Y. H. Baek, Y. H. Kim, Y. K. Choi, M. S. Song, and J. Y. Ahn. 2017. One-Pot Reverse Transcriptional Loop-Mediated Isothermal Amplification (RT-LAMP) for Detecting MERS-CoV. Frontiers in Microbiology **7**.

Lee, S. H., J. Song, B. Cho, S. Hong, O. Hoxha, T. Kang, D. Kim, and L. P. Lee. 2019b. Bubble-free rapid microfluidic PCR. Biosensors & Bioelectronics **126**:725-733.

Lefebvre, K. A., S. Bargu, T. Kieckhefer, and M. W. Silver. 2002a. From sanddabs to blue whales: the pervasiveness of domoic acid. Toxicon **40**:971-977.

Lefebvre, K. A., C. L. Powell, M. Busman, C. J. Doucette, P. D. R. Moeller, J. B. Sliver, P. E. Miller, M. P. Hughes, S. Singaram, M. W. Silver, and R. S. Tjeerdema. 1999. Detection of domoic acid in northern anchovies and California sea lions associated with an unusual mortality event. Natural Toxins **7**:85-92.

Lefebvre, K. A., L. Quakenbush, E. Frame, K. B. Huntington, G. Sheffield, R. Stimmelmayr, A. Bryan, P. Kendrick, H. Ziel, T. Goldstein, J. A. Snyder, T. Gelatt, F. Gulland, B. Dickerson, and V. Gill. 2016. Prevalence of algal toxins in Alaskan marine mammals foraging in a changing arctic and subarctic environment. Harmful Algae **55**:13-24.

Lefebvre, K. A., M. W. Silver, S. L. Coale, and R. S. Tjeerdema. 2002b. Domoic acid in planktivorous fish in relation to toxic Pseudo-nitzschia cell densities. Marine Biology **140**:625-631.

Lefferts, C. L., and J. A. Lefferts. 2017. Essential Concepts and Techniques in Molecular Biology. Pages 25-42 *in* W. B. Coleman and G. J. Tsongalis, editors. The Molecular Basis of Human Cancer. Springer New York, New York, NY.

Leira, F. J., J. M. Vieites, L. M. Botana, and M. R. Vyeites. 1998. Domoic acid levels of naturally contaminated scallops as affected by canning. Journal of Food Science **63**:1081-1083.

Lelong, A., E. Bucciarelli, H. Hegaret, and P. Soudant. 2013. Iron and copper limitations differently affect growth rates and photosynthetic and physiological parameters of the marine diatom Pseudo-nitzschia delicatissima. Limnology and Oceanography **58**:613-623.

Lelong, A., H. Hegaret, and P. Soudant. 2011. Cell-based measurements to assess physiological status of Pseudo-nitzschia multiseries, a toxic diatom. Research in Microbiology **162**:969-981.

Lelong, A., H. Hegaret, P. Soudant, and S. S. Bates. 2012. Pseudo-nitzschia (Bacillariophyceae) species, domoic acid and amnesic shellfish poisoning: revisiting previous paradigms. Phycologia **51**:168-216.

Lema, K. A., M. Latimier, E. Nezan, J. Fauchot, and M. Le Gac. 2017. Inter and intra-specific growth and domoic acid production in relation to nutrient ratios and concentrations in Pseudo-nitzschia: phosphate an important factor. Harmful Algae **64**:11-19.

Lema, K. A., G. Metegnier, J. Quere, M. Latimier, A. Youenou, C. Lambert, J. Fauchot, and M. Le Gac. 2019. Inter- and Intra-Specific Transcriptional and Phenotypic Responses of Pseudo-nitzschia under Different Nutrient Conditions. Genome Biology and Evolution **11**:731-747.

Less, R., K. L. M. Boylan, A. P. N. Skubitz, and A. Aksan. 2013. Isothermal vitrification methodology development for non-cryogenic storage of archival human sera. Cryobiology **66**:176-185.

Lewis, N. I., S. S. Bates, J. L. Mclachlan, and J. C. Smith. 1993. Temperature Effects on Growth, Domoic Acid Production, and Morphology of the Diatom Nitzschia-Pungens F-Multiseries. Toxic Phytoplankton Blooms in the Sea **3**:601-606.

Lewis, N. I., S. S. Bates, and M. A. Quilliam. 2018. Production of domoic acid from large-scale cultures of Pseudo-nitzschia multiseries: A feasibility study. Harmful Algae **79**:58-63.

Li, J., J. Macdonald, and F. von Stetten. 2019a. Review: a comprehensive summary of a decade development of the recombinase polymerase amplification. Analyst **144**:31-67.

Li, J., and K. M. Persson. 2021. Quick detection method for paralytic shellfish toxins (PSTs) monitoring in freshwater - A review. Chemosphere **265**.

Li, J., N. M. Pollak, and J. Macdonald. 2019b. Multiplex Detection of Nucleic Acids Using Recombinase Polymerase Amplification and a Molecular Colorimetric 7-Segment Display. Acs Omega **4**:11388-11396.

Li, R., H. M. Tun, M. Jahan, Z. Zhang, A. Kumar, W. G. Dilantha Fernando, A. Farenhorst, and E. Khafipour. 2017. Comparison of DNA-, PMA-, and RNA-based 16S rRNA Illumina sequencing for detection of live bacteria in water. Scientific Reports **7**:5752.

Li, X., Z. Y. Li, J. H. Chen, Q. Shi, R. T. Zhang, S. Wang, and X. R. Wang. 2014. Detection, occurrence and monthly variations of typical lipophilic marine toxins associated with diarrhetic shellfish poisoning in the coastal seawater of Qingdao City, China. Chemosphere **111**:560-567.

Li, Z., X. J. Xu, D. Wang, and X. Y. Jiang. 2023. Recent advancements in nucleic acid detection with microfluidic chip for molecular diagnostics. Trac-Trends in Analytical Chemistry **158**.

Liang, F. P., Y. Qiao, M. Q. Duan, A. Ju, N. Lu, J. J. Li, J. Tu, and Z. H. Lu. 2018. Fabrication of a microfluidic chip based on the pure polypropylene material. RSC Advances **8**:8732-8738.

Lichtenthaler, H. K. 2010. Chapter 7 The Non-mevalonate DOXP/MEP (Deoxyxylulose 5-Phosphate/Methylerythritol 4-Phosphate) Pathway of Chloroplast Isoprenoid and Pigment Biosynthesis. Pages 95-118 *in* C. A. Rebeiz, C. Benning, H. J. Bohnert, H. Daniell, J. K. Hoober, H. K. Lichtenthaler, A. R. Portis, and B. C. Tripathy, editors. The Chloroplast: Basics and Applications. Springer Netherlands, Dordrecht.

Lillis, L., D. Lehman, M. C. Singhal, J. Cantera, J. Singleton, P. Labarre, A. Toyama, O. Piepenburg, M. Parker, R. Wood, J. Overbaugh, and D. S. Boyle. 2014. Non-Instrumented Incubation of a Recombinase Polymerase Amplification Assay for the Rapid and Sensitive Detection of Proviral HIV-1 DNA. Plos One **9**.

Lim, B., J. Ratcliff, D. A. Nawrot, Y. J. Yu, H. R. Sanghani, C. C. Hsu, L. Peto, S. Evans, S. H. Hodgson, A. Skeva, M. Adam, M. Panopoulou, C. E. Zois, K. Poncin, S. R. Vasudevan, S. Q. Dai, S. Ren, H. Chang, Z. F. Cui, P. Simmonds, W. E. Huang, and M. I. Andersson. 2021. Clinical validation of optimised RT-LAMP for the diagnosis of SARS-CoV-2 infection. Scientific Reports **11**.

Lim, H., A. T. Jafry, and J. Lee. 2019. Fabrication, Flow Control, and Applications of Microfluidic Paper-Based Analytical Devices. Molecules **24**.

Lim, H. C., C. P. Leaw, S. N. P. Su, S. T. Teng, G. Usup, N. Mohammad-Noor, N. Lundholm, Y. Kotaki, and P. T. Lim. 2012. Morphology and Molecular Characterization of Pseudo-Nitzschia (Bacillariophyceae) from Malaysian Borneo, Including the New Species Pseudo-Nitzschia Circumpora Sp Nov. Journal of Phycology **48**:1232-1247.

Lin, Z. Z., S. Y. Chen, L. Li, A. H. Peng, and Z. Y. Huang. 2020. Rapid extraction of domoic acid by a magnetic molecularly imprinted silica before HPLC measurement. Heliyon **6**.

Lins, R. D., C. S. Pereira, and P. H. Hunenberger. 2004. Trehalose-protein interaction in aqueous solution. Proteins-Structure Function and Bioinformatics **55**:177-186.

Liu, B. Y., Z. W. Li, J. F. Du, W. Zhang, X. Z. Che, Z. R. Zhang, P. Chen, Y. Z. Wang, Y. Li, S. L. Wang, and X. H. Ding. 2022. Loop-Mediated Isothermal Amplification (LAMP) for the Rapid and Sensitive Detection of Alternaria alternata (Fr.) Keissl in Apple Alternaria Blotch Disease with Aapg-1 Encoding the Endopolygalacturonase. Pathogens **11**.

Liu, C. C., M. G. Mauk, R. Hart, X. B. Qiu, and H. H. Bau. 2011. A self-heating cartridge for molecular diagnostics. Lab on a Chip **11**:2686-2692.

Liu, D., P. Wang, G. R. Wei, W. B. Dong, and F. Hui. 2013. Removal of algal blooms from freshwater by the coagulation-magnetic separation method. Environmental Science and Pollution Research **20**:60-65.

Liu, H. B., X. J. Du, Y. X. Zang, P. Li, and S. Wang. 2017. SERS-Based Lateral Flow Strip Biosensor for Simultaneous Detection of Listeria monocytogenes and Salmonella enterica Serotype Enteritidis. Journal of Agricultural and Food Chemistry **65**:10290-10299.

Liu, R. H., J. N. Yang, M. Z. Pindera, M. Athavale, and P. Grodzinski. 2002. Bubble-induced acoustic micromixing. Lab on a Chip **2**:151-157.

Liu, W., D. Y. Zou, X. M. He, D. Ao, Y. X. Su, Z. Yang, S. M. Huang, Q. H. Zhao, Y. Tang, W. Ma, Y. F. Lu, J. Wang, X. J. Wang, and L. Y. Huang. 2018. Development and application of a rapid Mycobacterium tuberculosis detection technique using polymerase spiral reaction. Scientific Reports **8**.

Liu, Y. B., T. Lei, Z. Y. Liu, Y. B. Kuang, J. X. Lyu, and Q. Wang. 2016. A Novel Technique to Detect EGFR Mutations in Lung Cancer. International Journal of Molecular Sciences **17**.

Livak, K. J., S. Flood, J. Marmaro, W. Giusti, and K. Deetz. 1995. Oligonucleotides with fluorescent dyes at opposite ends provide a quenched probe system useful for detecting PCR product and nucleic acid hybridization. Genome Research **4**:357-362.

Lizardi, P. M., X. H. Huang, Z. R. Zhu, P. Bray-Ward, D. C. Thomas, and D. C. Ward. 1998. Mutation detection and single-molecule counting using isothermal rolling-circle amplification. Nature Genetics **19**:225-232.

Lobato, I. M., and C. K. O'Sullivan. 2018. Recombinase polymerase amplification: Basics, applications and recent advances. Trac-Trends in Analytical Chemistry **98**:19-35.

Lockhart, D. J., and E. A. Winzeler. 2000. Genomics, gene expression and DNA arrays. Nature **405**:827-836.

Lopez-Rivera, A., B. A. Suarez-Isla, P. O. Eilers, C. G. Beaudry, S. Hall, M. F. Amandi, A. Furey, and K. J. James. 2005. Improved high-performance liquid chromatographic method for the determination of domoic acid and analogues in shellfish: effect of pH. Analytical and Bioanalytical Chemistry **381**:1540-1545.

Loukas, C. M., J. S. McQuillan, F. Laouenan, M. N. Tsaloglou, J. M. Ruano-Lopez, and M. C. Mowlem. 2017. Detection and quantification of the toxic microalgae Karenia brevis using lab on a chip mRNA sequence-based amplification. Journal of Microbiological Methods **139**:189-195.

Lund, J. W. G., C. Kipling, and E. D. Le Cren. 1958. The inverted microscope method of estimating algal numbers and the statistical basis of estimations by counting. Hydrobiologia **11**:143-170.

Lundholm, N., P. J. Hansen, and Y. Kotaki. 2004. Effect of pH on growth and domoic acid production by potentially toxic diatoms of the genera Pseudo-nitzschia and Nitzschia. Marine Ecology Progress Series **273**:1-15.

Lundholm, N., G. R. Hasle, G. A. Fryxell, and P. E. Hargraves. 2002. Morphology, phylogeny and taxonomy of species within the Pseudo-nitzschia americana complex (Bacillariophyceae) with descriptions of two new species, Pseudo-nitzschia brasiliana and Pseudo-nitzschia linea. Phycologia **41**:480-497.

Lundholm, N., B. Krock, U. John, J. Skov, J. F. Cheng, M. Pancic, S. Wohlrab, K. Rigby, T. G. Nielsen, E. Selander, and S. Hardardottir. 2018. Induction of domoic acid production in diatoms-Types of grazers and diatoms are important. Harmful Algae **79**:64-73.

Lundholm, N., O. Moestrup, Y. Kotaki, K. Hoef-Emden, C. Scholin, and P. Miller. 2006a. Inter- and intraspecific variation of the Pseudo-nitzschia delicatissima complex (Bacillariophyceae) illustrated by rRNA probes, morphological data and phylogenetic analyses. Journal of Phycology **42**:464-481.

Lundholm, N., Ø. Moestrup, Y. Kotaki, K. Hoef-Emden, C. Scholin, and P. Miller. 2006b. INTER- AND INTRASPECIFIC VARIATION OF THE PSEUDO-NITZSCHIA DELICATISSIMA COMPLEX (BACILLARIOPHYCEAE) ILLUSTRATED BY RRNA PROBES, MORPHOLOGICAL DATA AND PHYLOGENETIC ANALYSES1. Journal of Phycology **42**:464-481.

Lundholm, N., J. Skov, R. Pocklington, and O. Moestrup. 1994. Domoic Acid, the Toxic Amino-Acid Responsible for Amnesic Shellfish Poisoning, Now in Pseudonitzschia-Seriata (Bacillariophyceae) in Europe. Phycologia **33**:475-478.

Lunn, M.-L., P. Mouritzen, K. Faber, and N. Jacobsen. 2008. MicroRNA quantitation from a single cell by PCR using SYBR® Green detection and LNA-based primers. Nature Methods **5**:iii-iv.

Lutz, S., P. Weber, M. Focke, B. Faltin, J. Hoffmann, C. Muller, D. Mark, G. Roth, P. Munday, N. Armes, O. Piepenburg, R. Zengerle, and F. von Stetten. 2010. Microfluidic lab-on-a-foil for nucleic acid analysis based on isothermal recombinase polymerase amplification (RPA). Lab on a Chip **10**:887-893.

Mackay, I. M. 2004. Real-time PCR in the microbiology laboratory. Clinical Microbiology and Infection **10**:190-212.

Maeda, M., T. Kodama, T. Tanaka, H. Yoshizumi, T. Takemoto, K. Nomoto, and T. Fujita. 1986. Structures of Isodomoic Acid-a, Acid-B and Acid-C, Novel Insecticidal Amino-Acids from the Red Alga Chondria-Armata. Chemical & Pharmaceutical Bulletin **34**:4892-4895.

Mafra, L. L., V. M. Bricelj, C. Ouellette, and S. S. Bates. 2010. Feeding mechanics as the basis for differential uptake of the neurotoxin domoic acid by oysters, Crassostrea virginica, and mussels, Mytilus edulis. Aquatic Toxicology **97**:160-171.

Magnani, M., L. Galluzzi, and I. J. Bruce. 2006. The use of magnetic nanoparticles in the development of new molecular detection systems. Journal of Nanoscience and Nanotechnology **6**:2302-2311.

Mahalanabis, M., H. Al-Muayad, M. D. Kulinski, D. Altman, and C. M. Klapperich. 2009. Cell lysis and DNA extraction of gram-positive and gram-negative bacteria from whole blood in a disposable microfluidic chip. Lab on a Chip **9**:2811-2817.

Maldonado, M. T., M. P. Hughes, E. L. Rue, and M. L. Wells. 2002. The effect of Fe and Cu on growth and domoic acid production by Pseudo-nitzschia multiseries and Pseudo-nitzschia australis. Limnology and Oceanography **47**:515-526.

Malik, N., O. Gouseti, and S. Bakalis. 2017. Effect of freezing with temperature fluctuations on microstructure and dissolution behavior of freeze-dried high solid systems. Proceedings of 1st International Conference on Sustainable Energy and Resource Use in Food Chains (Icfes 2017), Including Symposium on Heat Recovery and Efficient Conversion and Utilisation of Waste Heat **123**:2-9.

Malone, T. C., and A. Newton. 2020. The Globalization of Cultural Eutrophication in the Coastal Ocean: Causes and Consequences. Frontiers in Marine Science **7**.

Malpartida-Cardenas, K., L. Miglietta, T. Peng, A. Moniri, A. Holmes, P. Georgiou, and J. Rodriguez-Manzano. 2022. Single-channel digital LAMP multiplexing using amplification curve analysis. Sensors & Diagnostics **1**:465-468.

Mao, X. W., P. H. Myavagh, S. Lotfikatouli, B. J. S. Hsiao, and H. W. Walker. 2020. Membrane Bioreactors for Nitrogen Removal from Wastewater: A Review. Journal of Environmental Engineering **146**.

Marchetti, A., D. Catlett, B. M. Hopkinson, K. Ellis, and N. Cassar. 2015. Marine diatom proteorhodopsins and their potential role in coping with low iron availability. Isme Journal **9**:2745-2748.

Marchetti, A., C. M. Moreno, N. R. Cohen, I. Oleinikov, K. deLong, B. S. Twining, E. V. Armbrust, and R. H. Lampe. 2017. Development of a Molecular-Based Index for Assessing Iron Status in Bloom-Forming Pennate Diatoms. Journal of Phycology **53**:820-832.

Marchetti, A., M. S. Parker, L. P. Moccia, E. O. Lin, A. L. Arrieta, F. Ribalet, M. E. P. Murphy, M. T. Maldonado, and E. V. Armbrust. 2009. Ferritin is used for iron storage in bloom-forming marine pennate diatoms. Nature **457**:467-470.

Marchler-Bauer, A., Y. Bo, L. Y. Han, J. E. He, C. J. Lanczycki, S. N. Lu, F. Chitsaz, M. K. Derbyshire, R. C. Geer, N. R. Gonzales, M. Gwadz, D. I. Hurwitz, F. Lu, G. H. Marchler, J. S. Song, N. Thanki, Z. X. Wang, R. A. Yamashita, D. C. Zhang, C. J. Zheng, L. Y. Geer, and S. H. Bryant. 2017. CDD/SPARCLE: functional classification of proteins via subfamily domain architectures. Nucleic Acids Research **45**:D200-D203.

Marras, S. A. E., F. R. Kramer, and S. Tyagi. 2002. Efficiencies of fluorescence resonance energy transfer and contact-mediated quenching in oligonucleotide probes. Nucleic Acids Research **30**.

Marshall, L. A., L. L. Wu, S. Babikian, M. Bachman, and J. G. Santiago. 2012. Integrated Printed Circuit Board Device for Cell Lysis and Nucleic Acid Extraction. Analytical Chemistry **84**:9640-9645.

Martin-Jezequel, V., G. Calu, L. Candela, Z. Amzil, T. Jauffrais, V. Sechet, and P. Weigel. 2015. Effects of Organic and Inorganic Nitrogen on the Growth and Production of Domoic Acid by Pseudo-nitzschia multiseries and P. australis (Bacillariophyceae) in Culture. Marine Drugs **13**:7067-7086.

Martin-Jezequel, V., M. Hildebrand, and M. A. Brzezinski. 2000. Silicon metabolism in diatoms: Implications for growth. Journal of Phycology **36**:821-840.

Martin, J. H., and S. E. Fitzwater. 1988. Iron-Deficiency Limits Phytoplankton Growth in the Northeast Pacific Subarctic. Nature **331**:341-343.

Martinez-Perinan, E., C. Gutierrez-Sanchez, T. Garcia-Mendiola, and E. Lorenzo. 2020. Electrochemiluminescence Biosensors Using Screen-Printed Electrodes. Biosensors-Basel **10**.

McCabe, R. M., B. M. Hickey, R. M. Kudela, K. A. Lefebvre, N. G. Adams, B. D. Bill, F. M. D. Gulland, R. E. Thomson, W. P. Cochlan, and V. L. Trainer. 2016. An unprecedented coastwide toxic algal bloom linked to anomalous ocean conditions. Geophysical Research Letters **43**:10366-10376.

McCarron, P., and P. Hess. 2006. Tissue distribution and effects of heat treatments on the content of domoic acid in blue mussels, Mytilus edulis. Toxicon **47**:473-479.

McDonald, S. M., D. Sarno, and A. Zingone. 2007. Identifying Pseudo-nitzschia species in natural samples using genus-specific PCR primers and clone libraries. Harmful Algae **6**:849-860.

McKiernan, H. E., and P. B. Danielson. 2017. Chapter 21 - Molecular Diagnostic Applications in Forensic Science. Pages 371-394 *in* G. P. Patrinos, editor. Molecular Diagnostics (Third Edition). Academic Press.

McLean, K. J., and A. W. Munro. 2016. Cytochrome P450 (cyp). Pages 1-18 *in* S. Choi, editor. Encyclopedia of Signaling Molecules. Springer New York, New York, NY.

McNamee, S. E., C. T. Elliott, P. Delahaut, and K. Campbell. 2013. Multiplex biotoxin surface plasmon resonance method for marine biotoxins in algal and seawater samples. Environmental Science and Pollution Research **20**:6794-6807.

McQuillan, J. S., A. Alrefaey, A. D. Turner, N. Morrell, O. Stoner, R. Brown, S. Kay, S. Cooke, and T. Bage. 2023. Quantitative Polymerase Chain Reaction for the estimation of toxigenic microalgae abundance in shellfish production waters. Harmful Algae **128**:102497.

McQuillan, J. S., and J. C. Robidart. 2017. Molecular-biological sensing in aquatic environments: recent developments and emerging capabilities. Current Opinion in Biotechnology **45**:43-50.

Medlin, L. K., and J. U. Kegel. 2014. Validation of the detection of Pseudo-nitzschia spp. using specific RNA probes tested in a microarray format: Calibration of signal based on variability of RNA content with environmental conditions. Harmful Algae **37**:183-193.

Medlin, L. K., and J. Orozco. 2017. Molecular Techniques for the Detection of Organisms in Aquatic Environments, with Emphasis on Harmful Algal Bloom Species. Sensors **17**.

Mendoza-Flores, A., I. Leyva-Valencia, C. J. Band-Schmidt, C. E. Galindo-Sanchez, and J. J. Bustillos-Guzman. 2018. Identification of the Gene sxtA (Domains sxtA1 and sxtA4) in Mexican Strains of Gymnodinium catenatum (Dinophyceae) and Their Evolution. Frontiers in Marine Science **5**.

Mengelt, C., and B. Prézelin Barbara. 2005. A Potential Novel Link Between Organic Nitrogen Loading and Pseudo-nitzschia spp. Blooms. California and the World Ocean '02:882-896.

Mengelt, C. a. P., Barbara B. 2002. Dark survival and subsequent light recovery for Pseudo-nitzschia multiseries. Pages 388-390. Florida Fish and Wildlife Conservation Commission, Florida Institute of ….

Mensink, M. A., H. W. Frijlink, K. V. Maarschalk, and W. L. J. Hinrichs. 2017. How sugars protect proteins in the solid state and during drying (review): Mechanisms of stabilization in relation to stress conditions. European Journal of Pharmaceutics and Biopharmaceutics **114**:288-295.

Miao, X. Y., Z. Q. Zhu, H. S. Jia, C. C. Lu, X. H. Liu, D. S. Mao, and G. F. Chen. 2020. Colorimetric detection of cancer biomarker based on enzyme enrichment and pH sensing. Sensors and Actuators B-Chemical **320**.

Miesner, A. K., N. Lundholm, B. Krock, and T. G. Nielsen. 2016. The effect of Pseudo-nitzschia seriata on grazing and fecundity of Calanus finmarchicus and Calanus glacialis. Journal of Plankton Research **38**:564-574.

Miller, P. E., and C. A. Scholin. 1998. Identification and enumeration of cultured and wild Pseudo-nitzschia (Bacillariophyceae) using species-specific LSU rRNA-targeted fluorescent probes and filter-based whole cell hybridization. Journal of Phycology **34**:371-382.

Mills, C., and K. Campbell. 2022. A new chapter for anti-idiotypes in low molecular weight compound immunoassays. Trends in Biotechnology **40**:1102-1120.

Mills, C., M. J. Dillon, P. K. Kulabhusan, D. Senovilla-Herrero, and K. Campbell. 2022. Multiplex Lateral Flow Assay and the Sample Preparation Method for the Simultaneous Detection of Three Marine Toxins. Environmental Science & Technology **56**:12210-12217.

Mills, G., and G. Fones. 2012. A review of in situ methods and sensors for monitoring the marine environment. Sensor Review **32**:17-28.

Miralles, V., A. Huerre, F. Malloggi, and M.-C. Jullien. 2013. A Review of Heating and Temperature Control in Microfluidic Systems: Techniques and Applications. Pages 33-67 Diagnostics.

Mirasoli, M., F. Bonvicini, N. Lovecchio, G. Petrucci, M. Zangheri, D. Calabria, F. Costantini, A. Roda, G. Gallinella, D. Caputo, G. de Cesare, and A. Nascetti. 2018. On-chip LAMP-BART reaction for viral DNA real-time bioluminescence detection. Sensors and Actuators B-Chemical **262**:1024-1033.

Miserere, S., G. Mottet, V. Taniga, S. Descroix, J. L. Viovy, and L. Malaquin. 2012. Fabrication of thermoplastics chips through lamination based techniques. Lab on a Chip **12**:1849-1856.

Moehling, T. J., G. Choi, L. C. Dugan, M. Salit, and R. J. Meagher. 2021. LAMP Diagnostics at the Point-of-Care: Emerging Trends and Perspectives for the Developer Community. Expert Review of Molecular Diagnostics **21**:43-61.

Mohan, S., A. Pascual-Garrigos, H. Brouwer, D. Pillai, J. Koziol, A. Ault, J. Schoonmaker, T. Johnson, and M. S. Verma. 2021. Loop-Mediated Isothermal Amplification for the Detection of Pasteurella multocida, Mannheimia haemolytica, and Histophilus somni in Bovine Nasal Samples. Acs Agricultural Science & Technology **1**:100-108.

Monosik, R., M. Stred'ansky, and E. Sturdik. 2012. Application of Electrochemical Biosensors in Clinical Diagnosis. Journal of Clinical Laboratory Analysis **26**:22-34.

Moore, D., and D. Dowhan. 2002. Purification and Concentration of DNA from Aqueous Solutions. Current Protocols in Molecular Biology **59**:2.1.1-2.1.10.

Moore, M. D., and L. A. Jaykus. 2017. Recombinase polymerase amplification: a promising point-of-care detection method for enteric viruses. Future Virology **12**:421-429.

Moore, P. B. 1999. Structural motifs in RNA. Annual Review of Biochemistry **68**:287-300.

Moore, S. K., S. J. Dreyer, J. A. Ekstrom, K. Moore, K. Norman, T. Klinger, E. H. Allison, and S. L. Jardine. 2020. Harmful algal blooms and coastal communities: Socioeconomic impacts and actions taken to cope with the 2015 US West Coast domoic acid event. Harmful Algae **96**.

Moore, S. K., J. B. Mickett, G. J. Doucette, N. G. Adams, C. M. Mikulski, J. M. Birch, B. Roman, N. Michel-Hart, and J. A. Newton. 2021. An Autonomous Platform for Near Real-Time Surveillance of Harmful Algae and Their Toxins in Dynamic Coastal Shelf Environments. Journal of Marine Science and Engineering **9**.

Moreno, A. R., C. Anderson, R. M. Kudela, M. Sutula, C. Edwards, and D. Bianchi. 2022. Development, calibration, and evaluation of a model of Pseudo-nitzschia and domoic acid production for regional ocean modeling studies. Harmful Algae **118**.

Morrison, C., and F. Gannon. 1994. The impact of the PCR plateau phase on quantitative PCR. Biochimica et Biophysica Acta (BBA)-Gene Structure and Expression **1219**:493-498.

Mos, L. 2001. Domoic acid: a fascinating marine toxin. Environmental Toxicology and Pharmacology **9**:79-85.

Moschandreou, K. K., A. D. Baxevanis, P. Katikou, D. Papaefthimiou, G. Nikolaidis, and T. J. Abatzopoulos. 2012. Inter- and intra-specific diversity of Pseudo-nitzschia (Bacillariophyceae) in the northeastern Mediterranean. European Journal of Phycology **47**:321-339.

Mowlem, M., A. Beaton, R. Pascal, A. Schaap, S. Loucaides, S. Monk, A. Morris, C. L. Cardwell, S. E. Fowell, M. D. Patey, and P. Lopez-Garcia. 2021. Industry Partnership: Lab on Chip Chemical Sensor Technology for Ocean Observing. Frontiers in Marine Science **8**.

Mowlem, M. C., M. N. Tsaloglou, E. M. Waugh, C. F. A. Floquet, K. Saw, L. Fowler, R. Brown, D. Pearce, J. B. Wyatt, A. D. Beaton, M. P. Brito, D. A. Hodgson, G. Griffiths, M. Bentley, D. Blake, L. Capper, R. Clarke, C. Cockell, H. Corr, W. Harris, C. Hill, R. Hindmarsh, E. King, H. Lamb, B. Maher, K. Makinson, J. Parnell, J. Priscu, A. Rivera, N. Ross, M. J. Siegert, A. Smith, A. Tait, M. Tranter, J. Wadham, B. Whalley, and J. Woodward. 2011. Probe Technology for the Direct Measurement and Sampling of Ellsworth Subglacial Lake. Antartic Subglacial Aquatic Environments **192**:159-186.

Munday, R., P. T. Holland, P. McNabb, A. I. Selwood, and L. L. Rhodes. 2008. Comparative toxicity to mice of domoic acid and isodomoic acids A, B and C. Toxicon **52**:954-956.

Myers, F. B., and L. P. Lee. 2008. Innovations in optical microfluidic technologies for point-of-care diagnostics. Lab on a Chip **8**:2015-2031.

Nagy, A., E. Vitaskova, L. Cernikova, V. Krivda, H. Jirincova, K. Sedlak, J. Hornickova, and M. Havlickova. 2017. Evaluation of TaqMan qPCR System Integrating Two Identically Labelled Hydrolysis Probes in Single Assay. Scientific Reports **7**.

Nakauchi, M., I. Takayama, H. Takahashi, M. Tashiro, and T. Kageyama. 2014. Development of a reverse transcription loop-mediated isothermal amplification assay for the rapid diagnosis of avian influenza A (H7N9) virus infection. Journal of Virological Methods **204**:101-104.

Narayanamurthy, V., Z. E. Jeroish, K. S. Bhuvaneshwari, P. Bayat, R. Premkumar, F. Samsuri, and M. M. Yusoff. 2020. Advances in passively driven microfluidics and lab-on-chip devices: a comprehensive literature review and patent analysis. RSC Advances **10**:11652-11680.

Navarro, E., G. Serrano-Heras, M. J. Castano, and J. Solera. 2015. Real-time PCR detection chemistry. Clinica Chimica Acta **439**:231-250.

Neuzil, P., J. Pipper, and T. M. Hsieh. 2006. Disposable real-time microPCR device: lab-on-a-chip at a low cost. Molecular Biosystems **2**:292-298.

Newton, J. M., D. Schofield, J. Vlahopoulou, and Y. H. Zhou. 2016. Detecting cell lysis using viscosity monitoring in E-coli fermentation to prevent product loss. Biotechnology Progress **32**:1069-1076.

Ng, B. Y. C., E. J. H. Wee, N. P. West, and M. Trau. 2015. Rapid DNA detection of Mycobacterium tuberculosis-towards single cell sensitivity in point-of-care diagnosis. Scientific Reports **5**.

Nguyen, H. H., J. Park, S. Kang, and M. Kim. 2015. Surface Plasmon Resonance: A Versatile Technique for Biosensor Applications. Sensors **15**:10481-10510.

Nguyen, H. Q., V. D. Nguyen, H. V. Nguyen, and T. S. Seo. 2020. Quantification of colorimetric isothermal amplification on the smartphone and its open-source app for point-of-care pathogen detection. Scientific Reports **10**.

Nguyen, N. T., and Z. G. Wu. 2005. Micromixers - a review. Journal of Micromechanics and Microengineering **15**:R1-R16.

Nguyen, T. N. T., M. C. Kim, J. S. Park, and N. E. Lee. 2008. An effective passive microfluidic mixer utilizing chaotic advection. Sensors and Actuators B-Chemical **132**:172-181.

Nicolas, B. A., B. Daniel, T. Deborah, M. Raquel, and G. Leticia. 2017. Titratable Acidity at pH = 7 Estimated fro the pH of a Soil:Buffer Mixture. Agrociencia-Uruguay **21**:105-108.

Niemz, A., T. M. Ferguson, and D. S. Boyle. 2011. Point-of-care nucleic acid testing for infectious diseases. Trends in Biotechnology **29**:240-250.

Nikiforova, M. N., W. A. LaFramboise, and Y. E. Nikiforov. 2015. Chapter 4 - Amplification-Based Methods. Pages 57-67 *in* S. Kulkarni and J. Pfeifer, editors. Clinical Genomics. Academic Press, Boston.

Nixon, G. J., H. F. Svenstrup, C. E. Donald, C. Carder, J. M. Stephenson, S. Morris-Jones, J. F. Huggett, and C. A. Foy. 2014. A novel approach for evaluating the performance of real time quantitative loop-mediated isothermal amplification-based methods. Biomol Detect Quantif **2**:4-10.

Njage, P. M. K., and E. Buys. 2020. A High Resolution DNA Melting Curve Analysis for the Rapid and Efficient Molecular Diagnostics of Extended Spectrum beta-Lactamase Determinants from Foodborne Escherichia coli. Microorganisms **8**.

Nocker, A., C.-Y. Cheung, and A. K. Camper. 2006. Comparison of propidium monoazide with ethidium monoazide for differentiation of live vs. dead bacteria by selective removal of DNA from dead cells. Journal of Microbiological Methods **67**:310-320.

Nolting, B. 1996. Temperature-jump induced fast refolding of cold-unfolded protein. Biochemical and Biophysical Research Communications **227**:903-908.

Norris, V., and B. Manners. 1993. Deformations in the Cytoplasmic Membrane of Escherichia-Coli Direct the Synthesis of Peptidoglycan - the Hernia Model. Biophysical Journal **64**:1691-1700.

Northrup, M. A., L. A. Christel, W. A. McMillan, K. Petersen, F. Pourahmadi, L. Western, and S. Young. 1999. 8 - A new generation of PCR instruments and nucleic acid concentration systems. Pages 105-125 *in* M. A. Innis, D. H. Gelfand, and J. J. Sninsky, editors. PCR Applications. Academic Press, San Diego.

Notomi, T., H. Okayama, H. Masubuchi, T. Yonekawa, K. Watanabe, N. Amino, and T. Hase. 2000. Loop-mediated isothermal amplification of DNA. Nucleic Acids Research **28**.

O'Mahony, M. 2018. EU Regulatory Risk Management of Marine Biotoxins in the Marine Bivalve Mollusc Food-Chain. Toxins **10**.

Ochman, H., F. J. Ayala, and D. L. Hartl. 1993. Use of Polymerase Chain-Reaction to Amplify Segments Outside Boundaries of Known Sequences. Methods in Enzymology **218**:309-321.

Oddone, I., A. Arsiccio, C. Duru, K. Malik, J. Ferguson, R. Pisano, and P. Matejtschuk. 2020. Vacuum-Induced Surface Freezing for the Freeze-Drying of the Human Growth Hormone: How Does Nucleation Control Affect Protein Stability? Journal of Pharmaceutical Sciences **109**:254-263.

Ogilvie, I. R. G., V. J. Sieben, C. F. A. Floquet, R. Zmijan, M. C. Mowlem, and H. Morgan. 2010. Reduction of surface roughness for optical quality microfluidic devices in PMMA and COC. Journal of Micromechanics and Microengineering **20**.

Ohtake, S., and Y. J. Wang. 2011. Trehalose: Current Use and Future Applications. Journal of Pharmaceutical Sciences **100**:2020-2053.

Okino, S. T., M. Kong, and Y. T. Wang. 2015. Evaluation of bias associated with high-multiplex, target-specific pre-amplification. Cancer Research **75**.

Oleschuk, R. D., L. L. Shultz-Lockyear, Y. B. Ning, and D. J. Harrison. 2000. Trapping of bead-based reagents within microfluidic systems: On-chip solid-phase extraction and electrochromatography. Analytical Chemistry **72**:585-590.

Olesen, A. J., S. Hardardottir, N. Daugbjerg, P. Andersen, M. Lyngsgaard, B. Krock, and N. Lundholm. 2020. The impact of urea on toxic diatoms - Potential effects of fertilizer silo breakdown on a Pseudo-nitzschia bloom. Harmful Algae **95**.

Oliveira, B. B., B. Veigas, and P. V. Baptista. 2021. Isothermal Amplification of Nucleic Acids: The Race for the Next “Gold Standard”. Frontiers in Sensors **2**.

Oliver, D. M., M. van Niekerk, D. Kay, A. L. Heathwaite, J. Porter, L. E. Fleming, J. L. Kinzelman, E. Connolly, A. Cummins, C. McPhail, A. Rahman, T. Thairs, A. M. D. Husman, N. D. Hanley, I. Dunhill, L. Globevnik, V. J. Harwood, C. J. Hodgson, D. N. Lees, G. L. Nichols, A. Nocker, C. Schets, and R. S. Quilliam. 2014. Opportunities and limitations of molecular methods for quantifying microbial compliance parameters in EU bathing waters. Environment International **64**:124-128.

Olson, M. B., E. J. Lessard, C. H. J. Wong, and M. J. Bernhardt. 2006. Copepod feeding selectivity on microplankton, including the toxigenic diatoms Pseudo-nitzschia spp., in the coastal Pacific Northwest. Marine Ecology Progress Series **326**:207-220.

Orlova, T. Y., and O. Shevchenko. 2002. The first finding of Pseudo-nitzschia americana (Bacillariophyta) in Russian Seas. Russian Journal of Marine Biology **28**:336-339.

Orsini, L., G. Procaccini, D. Sarno, and M. Montresor. 2004. Multiple rDNA ITS-types within the diatom Pseudo-nitzschia delicatissima (Bacillariophyceae) and their relative abundances across a spring bloom in the Gulf of Naples. Marine Ecology Progress Series **271**:87-98.

Oscorbin, I. P., G. Y. Shevelev, K. A. Pronyaeva, A. A. Stepanov, D. V. Shamovskaya, O. V. Mishukova, D. V. Pyshnyi, and M. L. Filipenko. 2021. Detection of SARS-CoV-2 RNA by a Multiplex Reverse-Transcription Loop-Mediated Isothermal Amplification Coupled with Melting Curves Analysis. International Journal of Molecular Sciences **22**.

Oyinloye, T. M., and W. B. Yoon. 2020. Effect of Freeze-Drying on Quality and Grinding Process of Food Produce: A Review. Processes **8**.

Ozay, B., and S. E. McCalla. 2021. A review of reaction enhancement strategies for isothermal nucleic acid amplification reactions. Sensors and Actuators Reports **3**.

Ozsolak, F., and P. M. Milos. 2011. RNA sequencing: advances, challenges and opportunities. Nature Reviews Genetics **12**:87-98.

Padovan-Merhar, O., and A. Raj. 2013. Using variability in gene expression as a tool for studying gene regulation. Wiley Interdisciplinary Reviews-Systems Biology and Medicine **5**:751-759.

Palenzuela, J. M. T., L. G. Vilas, F. M. Bellas, E. Garet, A. Gonzalez-Fernandez, and E. Spyrakos. 2019. Pseudo-nitzschia Blooms in a Coastal Upwelling System: Remote Sensing Detection, Toxicity and Environmental Variables. Water **11**.

Palma, S., H. Mourino, A. Silva, M. I. Barao, and M. T. Moita. 2010. Can Pseudo-nitzschia blooms be modeled by coastal upwelling in Lisbon Bay? Harmful Algae **9**:294-303.

Pan, Y., S. S. Bates, and A. D. Cembella. 1998. Environmental stress and domoic acid production by Pseudo-nitzschia: a physiological perspective. Natural Toxins **6**:127-135.

Pan, Y. L., D. V. S. Rao, and K. H. Mann. 1996a. Changes in domoic acid production and cellular chemical composition of the toxigenic diatom Pseudo-nitzschia multiseries under phosphate limitation. Journal of Phycology **32**:371-381.

Pan, Y. L., D. V. S. Rao, K. H. Mann, R. G. Brown, and R. Pocklington. 1996b. Effects of silicate limitation on production of domoic acid, a neurotoxin, by the diatom Pseudo-nitzschia multiseries .1. Batch culture studies. Marine Ecology Progress Series **131**:225-233.

Pan, Y. L., D. V. S. Rao, K. H. Mann, W. K. W. Li, and W. G. Harrison. 1996c. Effects of silicate limitation on production of domoic acid, a neurotoxin, by the diatom Pseudo-nitzschia multiseries .2. Continuous culture studies. Marine Ecology Progress Series **131**:235-243.

Panlilio, J. M., K. M. Hammar, N. Aluru, and M. E. Hahn. 2023. Developmental exposure to domoic acid targets reticulospinal neurons and leads to aberrant myelination in the spinal cord. Scientific Reports **13**:2587.

Panova, M., H. Aronsson, R. A. Cameron, P. Dahl, A. Godhe, U. Lind, O. Ortega-Martinez, R. Pereyra, S. V. M. Tesson, A. L. Wrange, A. Blomberg, and K. Johannesson. 2016. DNA Extraction Protocols for Whole-Genome Sequencing in Marine Organisms. Marine Genomics: Methods and Protocols **1452**:13-44.

Papadakis, G., A. K. Pantazis, N. Fikas, S. Chatziioannidou, V. Tsiakalou, K. Michaelidou, V. Pogka, M. Megariti, M. Vardaki, K. Giarentis, J. Heaney, E. Nastouli, T. Karamitros, A. Mentis, A. Zafiropoulos, G. Sourvinos, S. Agelaki, and E. Gizeli. 2022. Portable real-time colorimetric LAMP-device for rapid quantitative detection of nucleic acids in crude samples. Scientific Reports **12**.

Park, J. H., Y. W. Cho, and T. H. Kim. 2022. Recent Advances in Surface Plasmon Resonance Sensors for Sensitive Optical Detection of Pathogens. Biosensors-Basel **12**.

Patel, S. M., T. Doen, and M. J. Pikal. 2010. Determination of End Point of Primary Drying in Freeze-Drying Process Control. Aaps Pharmscitech **11**:73-84.

Pattanayak, P., S. K. Singh, M. Gulati, S. Vishwas, B. Kapoor, D. K. Chellappan, K. Anand, G. Gupta, N. K. Jha, P. K. Gupta, P. Prasher, K. Dua, H. Dureja, D. Kumar, and V. Kumar. 2021. Microfluidic chips: recent advances, critical strategies in design, applications and future perspectives. Microfluidics and Nanofluidics **25**.

Pearson, L. A., P. M. D'Agostino, and B. A. Neilan. 2021. Recent developments in quantitative PCR for monitoring harmful marine microalgae. Harmful Algae **108**:102096.

Penna, A., E. Bertozzini, C. Battocchi, L. Galluzzi, M. G. Giacobbe, M. Vila, E. Garces, A. Luglie, and M. Magnani. 2007. Monitoring of HAB species in the Mediterranean Sea through molecular methods. Journal of Plankton Research **29**:19-38.

Penna, A., S. Casabianca, F. Perini, M. Bastianini, E. Riccardi, S. Pigozzi, and M. Scardi. 2013. Toxic Pseudo-nitzschia spp. in the northwestern Adriatic Sea: characterization of species composition by genetic and molecular quantitative analyses. Journal of Plankton Research **35**:352-366.

Penna, A., and L. Galluzzi. 2008. PCR techniques as diagnostic tools for the identification and enumeration of toxic marine phytoplankton species. Algal Toxins: Nature, Occurrence, Effect and Detection:261-283.

Penna, A., and L. Galluzzi. 2013a. The quantitative real-time PCR applications in the monitoring of marine harmful algal bloom (HAB) species. Environ Sci Pollut Res Int **20**:6851-6862.

Penna, A., and L. Galluzzi. 2013b. The quantitative real-time PCR applications in the monitoring of marine harmful algal bloom (HAB) species (vol 20, pg 6851, 2013). Environmental Science and Pollution Research **20**:6903-6903.

Perl, T. M., L. Bedard, T. Kosatsky, J. C. Hockin, E. C. D. Todd, and R. S. Remis. 1990. An Outbreak of Toxic Encephalopathy Caused by Eating Mussels Contaminated with Domoic Acid. New England Journal of Medicine **322**:1775-1780.

Petroff, R., A. Hendrix, S. Shum, K. S. Grant, K. A. Lefebvre, and T. M. Burbacher. 2021. Public health risks associated with chronic, low-level domoic acid exposure: A review of the evidence. Pharmacology & Therapeutics **227**.

Petroff, R., T. Richards, B. Crouthamel, N. McKain, C. Stanley, K. S. Grant, S. Shum, J. Jing, N. Isoherranen, and T. M. Burbacher. 2019. Chronic, low-level oral exposure to marine toxin,

domoic acid, alters whole brain morphometry in nonhuman primates. Neurotoxicology **72**:114-124.

Pezzi, H. M., D. J. Niles, J. L. Schehr, D. J. Beebe, and J. M. Lang. 2018. Integration of Magnetic Bead-Based Cell Selection into Complex Isolations. Acs Omega **3**:3908-3917.

Pfaffen, S., R. Abdulqadir, N. E. Le Brun, and M. E. P. Murphy. 2013. Mechanism of Ferrous Iron Binding and Oxidation by Ferritin from a Pennate Diatom. Journal of Biological Chemistry **288**:14917-14925.

Pfaffl, M. W. 2001. A new mathematical model for relative quantification in real-time RT-PCR. Nucleic Acids Research **29**.

Phillips, E. A., T. J. Moehling, K. F. K. Ejendal, O. S. Hoilett, K. M. Byers, L. A. Basing, L. A. Jankowski, J. B. Bennett, L. K. Lin, L. A. Stanciu, and J. C. Linnes. 2019. Microfluidic rapid and autonomous analytical device (microRAAD) to detect HIV from whole blood samples. Lab on a Chip **19**:3375-3386.

Piepenburg, O., and N. A. Armes. 2018. DNA glycosylase/lyase and AP endonuclease substrates. Google Patents.

Piepenburg, O., C. H. Williams, and N. A. Armes. 2008. Methods for multiplexing recombinase polymerase amplification. Google Patents.

Piepenburg, O., C. H. Williams, and N. A. Armes. 2011. Methods for multiplexing recombinase polymerase amplification. Google Patents.

Piepenburg, O., C. H. Williams, D. L. Stemple, and N. A. Armes. 2006. DNA detection using recombination proteins. Plos Biology **4**:1115-1121.

Pierce, R. W., and J. T. Turner. 1992. Ecology of Planktonic Ciliates in Marine Food Webs. Reviews in Aquatic Sciences **6**:139-181.

Pinto, A., M. J. Botelho, C. Churro, J. Asselman, P. Pereira, and J. L. Pereira. 2023. A review on aquatic toxins - Do we really know it all regarding the environmental risk posed by phytoplankton neurotoxins? Journal of Environmental Management **345**:118769.

Pistocchi, R., F. Guerrini, L. Pezzolesi, M. Riccardi, S. Vanucci, P. Ciminiello, C. Dell'Aversano, M. Forino, E. Fattorusso, L. Tartaglione, A. Milandri, M. Pompei, M. Cangini, S. Pigozzi, and E. Riccardi. 2012. Toxin Levels and Profiles in Microalgae from the North-Western Adriatic Sea-15 Years of Studies on Cultured Species. Marine Drugs **10**:140-162.

Plouffe, B. D., S. K. Murthy, and L. H. Lewis. 2015. Fundamentals and application of magnetic particles in cell isolation and enrichment: a review. Reports on Progress in Physics **78**.

Politza, A. J., T. Y. Liu, and W. H. Guan. 2023. Programmable magnetic robot (ProMagBot) for automated nucleic acid extraction at the point of need. Lab on a Chip **23**:3882-3892.

Polz, M. F., and C. M. Cavanaugh. 1998. Bias in template-to-product ratios in multitemplate PCR. Applied and Environmental Microbiology **64**:3724-3730.

Poon, L. L. M., B. W. Y. Wong, E. H. T. Ma, K. H. Chan, L. M. C. Chow, W. Abeyewickreme, N. Tangpukdee, K. Y. Yuen, Y. Guan, S. Looareesuwan, and J. S. M. Peiris. 2006. Sensitive and inexpensive molecular test for falciparum malaria: Detecting Plasmodium falciparum DNA directly from heat-treated blood by loop-mediated isothermal amplification. Clinical Chemistry **52**:303-306.

Price, C. W., D. C. Leslie, and J. P. Landers. 2009. Nucleic acid extraction techniques and application to the microchip. Lab on a Chip **9**:2484-2494.

Prikryl, J., and F. Foret. 2014. Fluorescence Detector for Capillary Separations Fabricated by 3D Printing. Analytical Chemistry **86**:11951-11956.

Primiceri, E., M. S. Chiriaco, F. M. Notarangelo, A. Crocamo, D. Ardissino, M. Cereda, A. P. Bramanti, M. A. Bianchessi, G. Giannelli, and G. Maruccio. 2018. Key Enabling Technologies for Point-of-Care Diagnostics. Sensors **18**.

Prince, E. K., F. Irmer, and G. Pohnert. 2013. Domoic Acid Improves the Competitive Ability of Pseudo-nitzschia delicatissima against the Diatom Skeletonema marinoi. Marine Drugs **11**:2398-2412.

Pugliese, L., S. Casabianca, F. Perini, F. Andreoni, and A. Penna. 2017. A high resolution melting method for the molecular identification of the potentially toxic diatom Pseudo-nitzschia spp. in the Mediterranean Sea. Scientific Reports **7**.

Pulido, O. M. 2008. Domoic acid toxicologic pathology: A review. Marine Drugs **6**:180-219.

Pulido, O. M. 2014. Domoic acid: biological effects and health implications. Toxins and Biologically Active Compounds from Microalgae, Volume 2: Biological Effects and Risk Management **2**:219.

Quijano-Scheggia, S., E. Garces, K. B. Andree, P. de la Iglesia, J. Diogene, J. M. Fortuno, and J. Camp. 2010. Pseudo-nitzschia species on the Catalan coast: characterization and contribution to the current knowledge of the distribution of this genus in the Mediterranean Sea. Scientia Marina **74**:395-410.

Quijano-Scheggia, S., E. Garces, N. Sampedro, K. van Lenning, E. Flo, K. Andree, J. M. Fortuno, and J. Camp. 2008. Identification and characterisation of the dominant Pseudo-nitzschia species (Bacillariophyceae) along the NE Spanish coast (Catalonia, NW Mediterranean). Scientia Marina **72**:343-359.

Quijano-Scheggia, S. I., A. Olivos-Ortiz, E. Garcia-Mendoza, Y. Sanchez-Bravo, R. Sosa-Avalos, N. S. Marias, and H. C. Lim. 2020. Phylogenetic relationships of Pseudo-nitzschia subpacifica (Bacillariophyceae) from the Mexican Pacific, and its production of domoic acid in culture. Plos One **15**.

Quilliam, M. 2003. Chemical methods for lipophilic shellfish toxins. Manual on harmful marine microalgae:211-245.

Quilliam, M. A., P. G. Sim, A. W. Mcculloch, and A. G. Mcinnes. 1989. High-Performance Liquid-Chromatography of Domoic Acid, a Marine Neurotoxin, with Application to Shellfish and Plankton. International Journal of Environmental Analytical Chemistry **36**:139-154.

Quilliam, M. A., and J. L. C. Wright. 1989. The Amnesic Shellfish Poisoning Mystery. Analytical Chemistry **61**:A1053-+.

R. Harwood, C., and A. Wipat. 2002. 15 - Bacterial Protein Synthesis. Pages 321-III *in* M. Sussman, editor. Molecular Medical Microbiology. Academic Press, London.

Radan, R. L., and W. P. Cochlan. 2018. Differential toxin response of Pseudo-nitzschia multiseries as a function of nitrogen speciation in batch and continuous cultures, and during a natural assemblage experiment. Harmful Algae **73**:12-29.

Rajagopal, A., D. Yurk, C. Shin, K. Menge, L. Jacky, S. Fraser, T. A. Tombrello, and G. J. Tsongalis. 2019. Significant Expansion of Real-Time PCR Multiplexing with Traditional Chemistries using Amplitude Modulation. Scientific Reports **9**.

Ramirez, F. J., V. A. Guinder, C. Ferronato, and B. Krock. 2022. Increase in records of toxic phytoplankton and associated toxins in water samples in the Patagonian Shelf (Argentina) over 40 years of field surveys. Harmful Algae **118**.

Ramirez, R. 2023. Hundreds of dolphins and sea lions have washed up dead or sick in California amid toxic algae outbreak. CNN.

Ramsdell, J. S. 2007. The Molecular and Integrative Basis to Domoic Acid Toxicity. Phycotoxins: Chemistry and Biochemistry:223-250.

Rebrikov, D. V., and D. Trofimov. 2006. [Real-time PCR: approaches to data analysis (a review)]. Prikl Biokhim Mikrobiol **42**:520-528.

Redfield, A. C. 1960. The biological control of chemical factors in the environment. Sci Prog **11**:150-170.

Reedy, C. R., J. M. Bienvenue, L. Coletta, B. C. Strachan, N. Bhatri, S. Greenspoon, and J. P. Landers. 2010. Volume reduction solid phase extraction of DNA from dilute, large-volume biological samples. Forensic Science International-Genetics **4**:206-212.

Reinholt, S. J., and A. J. Baeumner. 2014. Microfluidic Isolation of Nucleic Acids. Angewandte Chemie-International Edition **53**:13988-14001.

Rezadoost, M. H., M. Kordrostami, and H. H. Kumleh. 2016. An efficient protocol for isolation of inhibitor-free nucleic acids even from recalcitrant plants. 3 Biotech **6**.

Rhodes, L., P. Holland, J. Adamson, P. McNabb, and A. Selwood. 2003. Production of a new isomer of domoic acid by New Zealand isolates of the diatom Pseudo-nitzschia australis.

Ribeiro, J. A., M. G. F. Sales, and C. M. Pereira. 2022. Electrochemistry combined-surface plasmon resonance biosensors: A review. Trac-Trends in Analytical Chemistry **157**.

Rida, A., and M. A. M. Gijs. 2004. Manipulation of self-assembled structures of magnetic beads for microfluidic mixing and assaying. Analytical Chemistry **76**:6239-6246.

Robertson, P. K. J., J. M. C. Robertson, and D. W. Bahnemann. 2012. Removal of microorganisms and their chemical metabolites from water using semiconductor photocatalysis. Journal of Hazardous Materials **211**:161-171.

Roche, K. M., A. R. Sterling, T. A. Rynearson, M. J. Bertin, and B. D. Jenkins. 2022. A Decade of Time Series Sampling Reveals Thermal Variation and Shifts in Pseudo-nitzschia Species Composition That Contribute to Harmful Algal Blooms in an Eastern US Estuary. Frontiers in Marine Science **9**.

Rohrman, B., and R. Richards-Kortum. 2015. Inhibition of Recombinase Polymerase Amplification by Background DNA: A Lateral Flow-Based Method for Enriching Target DNA. Analytical Chemistry **87**:1963-1967.

Rolando, J. C., E. Jue, J. T. Barlow, and R. F. Ismagilov. 2020. Real-time kinetics and high-resolution melt curves in single-molecule digital LAMP to differentiate and study specific and non-specific amplification. Nucleic Acids Research **48**.

Rombach, M., D. Kosse, B. Faltin, S. Wadle, G. Roth, R. Zengerle, and F. von Stetten. 2014a. Real-time stability testing of air-dried primers and fluorogenic hydrolysis probes stabilized by trehalose and xanthan. Biotechniques **57**:151-155.

Rombach, M., D. Kosse, B. Faltin, S. Wadle, G. Roth, R. Zengerle, and F. von Stetten. 2014b. Real-time stability testing of air-dried primers and fluorogenic hydrolysis probes stabilized by trehalose and xanthan (vol 57, pg 151, 2014). Biotechniques **57**:213-213.

Romero, E., J. Garnier, G. Billen, A. Ramarson, P. Riou, and R. Le Gendre. 2022. Assessing the water quality of the Seine land-to-sea continuum for three agro-food system scenarios. Frontiers in Marine Science **9**.

Romero, M. L. J., Y. Kotaki, N. Lundholm, H. Thoha, H. Ogawa, J. R. Relox, R. Terada, S. Takeda, Y. Takata, K. Haraguchi, T. Endo, P. T. Lim, M. Kodama, and Y. Fukuyo. 2011. Unique amnesic shellfish toxin composition found in the South East Asian diatom Nitzschia navis-varingica. Harmful Algae **10**:456-462.

Roos, Y. H., and M. Karel. 1991. Plasticizing Effect of Water on Thermal-Behavior and Crystallization of Amorphous Food Models. Journal of Food Science **56**:38-43.

Rosado, P. M. F. D. S., G. L. Lopez, A. M. Seiz, and M. D. M. Alberdi. 2011. Process for preparing stabilized reaction mixtures which are partially dried, comprising at least one enzyme, reaction mixtures and kits containing said mixtures. Google Patents.

Roser, B. 1991. Trehalose, a new approach to premium dried foods. Trends in Food Science & Technology **2**:166-169.

Ross Brown, A., M. K. S. Lilley, J. Shutler, C. Widdicombe, P. Rooks, A. McEvoy, R. Torres, Y. Artioli, G. Rawle, J. Homyard, C. R. Tyler, and C. Lowe. 2022. Harmful Algal Blooms and their impacts on shellfish mariculture follow regionally distinct patterns of water circulation in the western English Channel during the 2018 heatwave. Harmful Algae **111**:102166.

Rossi, S., M. P. Buera, S. Moreno, and J. Chirife. 1997. Stabilization of the Restriction Enzyme EcoRI Dried with Trehalose and Other Selected Glass-Forming Solutes. Biotechnology Progress **13**:609-616.

Rotting, O., W. Ropke, H. Becker, and C. Gartner. 2002. Polymer microfabrication technologies. Microsystem Technologies-Micro-and Nanosystems-Information Storage and Processing Systems **8**:32-36.

Roumani, F., S. Gomez, C. Rodrigues, J. Barros-Velazquez, A. Garrido-Maestu, and M. Prado. 2022. Development and evaluation of a real-time fluorescence, and naked-eye colorimetric,

loop-mediated isothermal amplification-based method for the rapid detection of spoilage fungi in fruit preparations. Food Control **135**.

Roy, I., and M. N. Gupta. 2004. Freeze-drying of proteins: some emerging concerns. Biotechnology and Applied Biochemistry **39**:165-177.

Roy, S., I. Abd Rahman, and M. U. Ahmed. 2016. Paper-based rapid detection of pork and chicken using LAMP-magnetic bead aggregates. Analytical Methods **8**:2391-2399.

Ruggiero, M. V., D. D'Alelio, M. I. Ferrante, M. Santoro, L. Vitale, G. Procaccini, and M. Montresor. 2018. Clonal expansion behind a marine diatom bloom. Isme Journal **12**:463-472.

Russo, M. T., L. Vitale, L. Entrambasaguas, K. Anestis, N. Fattorini, F. Romano, C. Minucci, P. De Luca, E. Biffali, W. Vyverman, R. Sanges, M. Montresor, and M. I. Ferrante. 2018. MRP3 is a sex determining gene in the diatom Pseudo-nitzschia multistriata. Nature Communications **9**.

Ryan, J. P., R. M. Kudela, J. M. Birch, M. Blum, H. A. Bowers, F. P. Chavez, G. J. Doucette, K. Hayashi, R. Marin, C. M. Mikulski, J. T. Pennington, C. A. Scholin, G. J. Smith, A. Woods, and Y. Zhang. 2017. Causality of an extreme harmful algal bloom in Monterey Bay, California, during the 2014-2016 northeast Pacific warm anomaly. Geophysical Research Letters **44**:5571-5579.

Rychlik, W. 1995. Priming Efficiency in Pcr. Biotechniques **18**:84-&.

Ryu, W.-S. 2017. Chapter 4 - Diagnosis and Methods. Pages 47-62 *in* W.-S. Ryu, editor. Molecular Virology of Human Pathogenic Viruses. Academic Press, Boston.

Saeed, A. F., S. A. Awan, S. M. Ling, R. Z. Wang, and S. Wang. 2017a. Domoic acid: Attributes, exposure risks, innovative detection techniques and therapeutics. Algal Research-Biomass Biofuels and Bioproducts **24**:97-110.

Saeed, A. F. U. H., S. M. Ling, J. Yuan, and S. H. Wang. 2017b. The Preparation and Identification of a Monoclonal Antibody against Domoic Acid and Establishment of Detection by Indirect Competitive ELISA. Toxins **9**.

Sahraoui, I., A. S. Hlaili, H. H. Mabrouk, C. Leger, and S. S. Bates. 2009. Blooms of the Diatom Genus Pseudo-Nitzschia H. Peragallo in Bizerte Lagoon (Tunisia, Sw Mediterranean). Diatom Research **24**:175-190.

Salamin, O., T. Kuuranne, M. Saugy, and N. Leuenberger. 2017. Loop-mediated isothermal amplification (LAMP) as an alternative to PCR: A rapid on-site detection of gene doping. Drug Testing and Analysis **9**:1731-1737.

Salvi, G., P. De los Rios, and M. Vendruscolo. 2005. Effective interactions between chaotropic agents and proteins. Proteins-Structure Function and Bioinformatics **61**:492-499.

Sandoval-Belmar, M., J. Smith, A. R. Moreno, C. Anderson, R. M. Kudela, M. Sutula, F. Kessouri, D. A. Caron, F. P. Chavez, and D. Bianchi. 2023. A cross-regional examination of patterns and environmental drivers of Pseudo-nitzschia harmful algal blooms along the California coast. Harmful Algae **126**.

Santana-Viera, S., and P. A. Lara-Martin. 2023. Analysis of paralytic shellfish toxins in seafood by liquid chromatography: A critical review of the methodologies developed. Trends in Environmental Analytical Chemistry **37**.

Santiago-Felipe, S., L. A. Tortajada-Genaro, S. Morais, R. Puchades, and A. Maquieira. 2015. Isothermal DNA amplification strategies for duplex microorganism detection. Food Chemistry **174**:509-515.

Santiago-Felipe, S., L. A. Tortajada-Genaro, R. Puchades, and A. Maquieira. 2016. Parallel solid-phase isothermal amplification and detection of multiple DNA targets in microliter-sized wells of a digital versatile disc. Microchimica Acta **183**:1195-1202.

Sauvey, A., P. Claquin, B. Le Roy, O. Jolly, and J. Fauchot. 2023. Physiological conditions favorable to domoic acid production by three Pseudo-nitzschia species. Journal of Experimental Marine Biology and Ecology **559**.

Sauvey, A., F. Denis, H. Hégaret, B. Le Roy, C. Lelong, O. Jolly, M. Pavie, and J. Fauchot. 2021. Interactions between Filter-Feeding Bivalves and Toxic Diatoms: Influence on the Feeding

Behavior of Crassostrea gigas and Pecten maximus and on Toxin Production by Pseudo-nitzschia. Toxins **13**.

Savage, T. J., G. J. Smith, A. T. Clark, and P. N. Saucedo. 2012. Condensation of the isoprenoid and amino precursors in the biosynthesis of domoic acid. Toxicon **59**:25-33.

Savela, H., K. Harju, L. Spoof, E. Lindehoff, J. Meriluoto, M. Vehniainen, and A. Kremp. 2016. Quantity of the dinoflagellate sxtA4 gene and cell density correlates with paralytic shellfish toxin production in Alexandrium ostenfeldii blooms. Harmful Algae **52**:1-10.

Schaikhaev, G. O. 2005. Dry amplification reagent mixture for polymerase chain reaction and the technique of pcr analysis.*in* W. I. P. Organizantion, editor.

Schebor, C., M. del Pilar Buera, and J. Chirife. 1996. Glassy state in relation to the thermal inactivation of the enzyme invertase in amorphous dried matrices of trehalose, maltodextrin and PVP. Journal of Food Engineering **30**:269-282.

Schlappi, T. S., S. E. McCalla, N. G. Schoepp, and R. F. Ismagilov. 2016. Flow-through Capture and in Situ Amplification Can Enable Rapid Detection of a Few Single Molecules of Nucleic Acids from Several Milliliters of Solution. Analytical Chemistry **88**:7647-7653.

Schnetzer, A., P. E. Miller, R. A. Schaffner, B. A. Stauffer, B. H. Jones, S. B. Weisberg, P. M. DiGiacomo, W. M. Berelson, and D. A. Caron. 2007. Blooms of Pseudo-nitzschia and domoic acid in the San Pedro Channel and Los Angeles harbor areas of the Southern California Bight, 2003-2004. Harmful Algae **6**:372-387.

Schoffman, H., H. Lis, Y. Shaked, and N. Keren. 2016. Iron-Nutrient Interactions within Phytoplankton. Frontiers in Plant Science **7**.

Scholin, C. A., R. Marin, P. E. Miller, G. J. Doucette, C. L. Powell, P. Haydock, J. Howard, and J. Ray. 1999. DNA probes and a receptor-binding assay for detection of Pseudo-nitzschia (Bacillariophyceae) species and domoic acid activity in cultured and natural samples. Journal of Phycology **35**:1356-1367.

Sekula-Wood, E., A. Schnetzer, C. R. Benitez-Nelson, C. Anderson, W. M. Berelson, M. A. Brzezinski, J. M. Burns, D. A. Caron, I. Cetinic, J. L. Ferry, E. Fitzpatrick, B. H. Jones, P. E. Miller, S. L. Morton, R. A. Schaffner, D. A. Siegel, and R. Thunell. 2009. Rapid downward transport of the neurotoxin domoic acid in coastal waters. Nature Geoscience **2**:272-275.

Selander, E., E. C. Berglund, P. Engstrom, F. Berggren, J. Eklund, S. Hardardottir, N. Lundholm, W. Grebner, and M. X. Andersson. 2019. Copepods drive large-scale trait-mediated effects in marine plankton. Science Advances **5**.

Seo, M. J., and J. C. Yoo. 2020. Fully Automated Lab-On-A-Disc Platform for Loop-Mediated Isothermal Amplification Using Micro-Carbon-Activated Cell Lysis. Sensors **20**.

Shanbhag, M. M., G. Manasa, R. J. Mascarenhas, K. Mondal, and N. P. Shetti. 2023. Fundamentals of bio-electrochemical sensing. Chemical Engineering Journal Advances **16**.

Shen, J. N., J. Y. Ye, M. X. Lao, C. Q. Wang, D. H. Wu, X. Y. Chen, L. H. Lin, W. Y. Geng, and X. G. Guo. 2022. Evaluation of the real-time fluorescence loop-mediated isothermal amplification assay for the detection of Ureaplasma urealyticum. Amb Express **12**.

Shen, L., H. P. Xu, and X. L. Guo. 2012. Satellite Remote Sensing of Harmful Algal Blooms (HABs) and a Potential Synthesized Framework. Sensors **12**:7778-7803.

Shin, Y., S. Y. Lim, T. Y. Lee, and M. K. Park. 2015. Dimethyl adipimidate/Thin film Sample processing (DTS); A simple, low-cost, and versatile nucleic acid extraction assay for downstream analysis. Scientific Reports **5**.

Shin, Y., A. P. Perera, K. W. Kim, and M. K. Park. 2013. Real-time, label-free isothermal solid-phase amplification/detection (ISAD) device for rapid detection of genetic alteration in cancers. Lab on a Chip **13**:2106-2114.

Shin, Y., A. P. Perera, C. C. Wong, and M. K. Park. 2014. Solid phase nucleic acid extraction technique in a microfluidic chip using a novel non-chaotropic agent: dimethyl adipimidate. Lab on a Chip **14**:359-368.

Shirshikov, F. V., and J. A. Bespyatykh. 2022. Loop-Mediated Isothermal Amplification: From Theory to Practice. Russian Journal of Bioorganic Chemistry **48**:1159-1174.

Shuler, A. J., J. Paternoster, M. Brim, K. Nowocin, T. Tisdale, K. Neller, J. A. Cahill, T. A. Leighfield, S. Fire, Z. H. Wang, and S. Morton. 2012. Spatial and temporal trends of the toxic diatom Pseudo-nitzschia in the Southeastern Atlantic United States. Harmful Algae **17**:6-13.

Sia, S. K., and G. M. Whitesides. 2003. Microfluidic devices fabricated in poly(dimethylsiloxane) for biological studies. Electrophoresis **24**:3563-3576.

Siaut, M., M. Heijde, M. Mangogna, A. Montsant, S. Coesel, A. Allen, A. Manfredonia, A. Falciatore, and C. Bowler. 2007. Molecular toolbox for studying diatom biology in Phaeodactylum tricornutum. Gene **406**:23-35.

Silva, G., M. Bomer, C. Nkere, P. L. Kumar, and S. E. Seal. 2015. Rapid and specific detection of Yam mosaic virus by reverse-transcription recombinase polymerase amplification. Journal of Virological Methods **222**:138-144.

Silva, T. C., M. Eppink, and M. Ottens. 2022. Automation and miniaturization: enabling tools for fast, high-throughput process development in integrated continuous biomanufacturing. Journal of Chemical Technology and Biotechnology **97**:2365-2375.

Silver, M. W., S. Bargu, S. L. Coale, C. R. Benitez-Nelson, A. C. Garcia, K. J. Roberts, E. Sekula-Wood, K. W. Bruland, and K. H. Coale. 2010. Toxic diatoms and domoic acid in natural and iron enriched waters of the oceanic Pacific. Proceedings of the National Academy of Sciences of the United States of America **107**:20762-20767.

Sin, M. L. Y., J. Gao, J. C. Liao, and P. K. Wong. 2011. System Integration - A Major Step toward Lab on a Chip. Journal of Biological Engineering **5**.

Sint, D., L. Raso, and M. Traugott. 2012. Advances in multiplex PCR: balancing primer efficiencies and improving detection success. Methods in Ecology and Evolution **3**:898-905.

Smith, C. J., R. D. Delaune, and W. H. Patrick. 1983. Carbon-Dioxide Emission and Carbon Accumulation in Coastal Wetlands. Estuarine Coastal and Shelf Science **17**:21-29.

Smith, D. S., and D. D. Kitts. 1994. A Competitive Enzyme-Linked Immunoassay for Domoic Acid Determination in Human-Body Fluids. Food and Chemical Toxicology **32**:1147-1154.

Smith, J., P. Connell, R. H. Evans, A. G. Gellene, M. D. A. Howard, B. H. Jones, S. Kaveggia, L. Palmer, A. Schnetzer, B. N. Seegers, E. L. Seubert, A. O. Tatters, and D. A. Caron. 2018. A decade and a half of Pseudo-nitzschia spp. and domoic acid along the coast of southern California. Harmful Algae **79**:87-104.

Smith, M. C., L. Bodrossy, and P. Craw. 2022. Chapter 6 - Advances in in situ molecular systems for phytoplankton research and monitoring. Pages 191-215 *in* L. A. Clementson, R. S. Eriksen, and A. Willis, editors. Advances in Phytoplankton Ecology. Elsevier.

Sobrinho, B. F., L. M. de Camargo, L. Sandrini-Neto, C. R. Kleemann, E. D. Machado, and L. L. Mafra. 2017. Growth, Toxin Production and Allelopathic Effects of Pseudo-nitzschia multiseries under Iron-Enriched Conditions. Marine Drugs **15**.

Song, J., B. Cha, J. Moon, H. Jang, S. Kim, J. Jang, D. Yong, H. J. Kwon, I. C. Lee, E. K. Lim, J. Jung, H. G. Park, and T. Kang. 2022a. Smartphone-Based SARS-CoV-2 and Variants Detection System using Colorimetric DNAzyme Reaction Triggered by Loop-Mediated Isothermal Amplification (LAMP) with Clustered Regularly Interspaced Short Palindromic Repeats (CRISPR). Acs Nano.

Song, J. Z., C. C. Liu, M. G. Mauk, S. C. Rankin, J. B. Lok, R. M. Greenberg, and H. H. Bau. 2017. Two-Stage Isothermal Enzymatic Amplification for Concurrent Multiplex Molecular Detection. Clinical Chemistry **63**:714-722.

Song, X., F. J. Coulter, M. Yang, J. L. Smith, F. G. Tafesse, W. B. Messer, and J. H. Reif. 2022b. A lyophilized colorimetric RT-LAMP test kit for rapid, low-cost, at-home molecular testing of SARS-CoV-2 and other pathogens. Scientific Reports **12**.

Sontag, E. D. 2005. Molecular systems biology and control: A qualitative-quantitative approach. 2005 44th Ieee Conference on Decision and Control & European Control Conference, Vols 1-8:2314-2319.

Soroka, M., B. Wasowicz, and A. Rymaszewska. 2021. Loop-Mediated Isothermal Amplification (LAMP): The Better Sibling of PCR? Cells **10**.

Sperança, M. A., R. B. Suzuki, A. D. Cabral, and A. M. dos Santos Carmo. 2016. Nucleic Acid-based Diagnosis and Epidemiology of Infectious Diseases. Nucleic Acids-From Basic Aspects to Laboratory Tools:59.

Steele, T. S., J. K. Brunson, Y. Maeno, R. Terada, A. E. Allen, M. Yotsu-Yamashita, J. R. Chekan, and B. S. Moore. 2022. Domoic acid biosynthesis in the red alga Chondria armata suggests a complex evolutionary history for toxin production. Proceedings of the National Academy of Sciences of the United States of America **119**.

Sterling, A. R., R. D. Kirk, M. J. Bertin, T. A. Rynearson, D. G. Borkman, M. C. Caponi, J. Carney, K. A. Hubbard, M. A. King, L. Maranda, E. J. McDermith, N. R. Santos, J. P. Strock, E. M. Tully, S. B. Vaverka, P. D. Wilson, and B. D. Jenkins. 2022. Emerging harmful algal blooms caused by distinct seasonal assemblages of a toxic diatom. Limnology and Oceanography **67**:2341-2359.

Stevens, D. Y., C. R. Petri, J. L. Osborn, P. Spicar-Mihalic, K. G. McKenzie, and P. Yager. 2008. Enabling a microfluidic immunoassay for the developing world by integration of on-card dry reagent storage. Lab on a Chip **8**:2038-2045.

Stone, H. A., A. D. Stroock, and A. Ajdari. 2004. Engineering flows in small devices: Microfluidics toward a lab-on-a-chip. Annual Review of Fluid Mechanics **36**:381-411.

Stonik, I. V., T. Y. Orlova, I. V. Chikalovets, N. A. Aizdaicher, A. I. Aleksanin, V. A. Kachur, and T. V. Morozova. 2019. Pseudo-nitzschia species (Bacillariophyceae) and the domoic acid concentration in Pseudo-nitzschia cultures and bivalves from the northwestern Sea of Japan, Russia. Nova Hedwigia **108**:73-93.

Stuchal, L. D., L. M. Grattan, K. M. Portier, K. A. Kilmon, L. M. Manahan, S. M. Roberts, and J. G. Morris. 2020. Dose-response assessment for impaired memory from chronic exposure to domoic acid among native American consumers of razor clams. Regulatory Toxicology and Pharmacology **117**.

Stuken, A., R. J. S. Orr, R. Kellmann, S. A. Murray, B. A. Neilan, and K. S. Jakobsen. 2011. Discovery of Nuclear-Encoded Genes for the Neurotoxin Saxitoxin in Dinoflagellates. Plos One **6**.

Su, L., W. Jia, C. Hou, and Y. Lei. 2011. Microbial biosensors: A review. Biosensors and Bioelectronics **26**:1788-1799.

Subbotin, S. A. 2019. Recombinase polymerase amplification assay for rapid detection of the root-knot nematode Meloidogyne enterolobii. Nematology **21**:243-251.

Subeshan, B., A. Usta, and R. Asmatulu. 2020. Deicing and self-cleaning of plasma-treated superhydrophobic coatings on the surface of aluminum alloy sheets. Surfaces and Interfaces **18**.

Sun, J., D. A. Hutchins, Y. Y. Feng, E. L. Seubert, D. A. Caron, and F. X. Fu. 2011. Effects of changing pCO(2) and phosphate availability on domoic acid production and physiology of the marine harmful bloom diatom Pseudo-nitzschia multiseries. Limnology and Oceanography **56**:829-840.

Sun, R., P. F. Sun, J. H. Zhang, S. Esquivel-Elizondo, and Y. H. Wu. 2018. Microorganisms-based methods for harmful algal blooms control: A review. Bioresource Technology **248**:12-20.

Sun, W. Q., and A. C. Leopold. 1994. Glassy State and Seed Storage Stability - a Viability Equation Analysis. Annals of Botany **74**:601-604.

Sun, Y., J. Hogberg, T. Christine, L. Florian, L. G. Monsalve, S. Rodriguez, C. Cao, A. Wolff, J. M. Ruano-Lopez, and D. D. Bang. 2013. Pre-storage of gelified reagents in a lab-on-a-foil system for rapid nucleic acid analysis. Lab on a Chip **13**:1509-1514.

Sundaramurthi, P., and R. Suryanarayanan. 2010. Trehalose Crystallization During Freeze-Drying: Implications On Lyoprotection. Journal of Physical Chemistry Letters **1**:510-514.

Suthers, I., L. Bowling, T. Kobayashi, and D. Rissik. 2009. Sampling methods for plankton. Plankton: A Guide to Their Ecology and Monitoring for Water Quality:73-114.

Suurmond, J., and B. Diamond. 2015. Autoantibodies in systemic autoimmune diseases: specificity and pathogenicity. Journal of Clinical Investigation **125**:2194-2202.

Suzuki, C. A. M., and S. L. Hierlihy. 1993. Renal Clearance of Domoic Acid in the Rat. Food and Chemical Toxicology **31**:701-706.

Tammilehto, A., T. G. Nielsen, B. Krock, E. F. Moller, and N. Lundholm. 2015. Induction of domoic acid production in the toxic diatom Pseudo-nitzschia seriata by calanoid copepods. Aquatic Toxicology **159**:52-61.

Tan, S. C., and B. C. Yiap. 2009. DNA, RNA, and Protein Extraction: The Past and The Present. Journal of Biomedicine and Biotechnology.

Tan, S. H., N. T. Nguyen, Y. C. Chua, and T. G. Kang. 2010. Oxygen plasma treatment for reducing hydrophobicity of a sealed polydimethylsiloxane microchannel. Biomicrofluidics **4**.

Tan, S. N., H. C. Lim, S. T. Teng, P. T. Lim, and C. P. Leaw. 2015. Pseudo-nitzschia species (Bacillariophyceae) identification and delineation using mitochondrial cox1 gene sequences as compared to LSU rDNA. Fisheries science **81**:831-838.

Tang, R. H., H. Yang, J. R. Choi, Y. Gong, S. S. Feng, B. Pingguan-Murphy, Q. S. Huang, J. L. Shi, Q. B. Mei, and F. Xu. 2017. Advances in paper-based sample pretreatment for point-of-care testing. Critical Reviews in Biotechnology **37**:411-428.

Tang, Y. C., and A. Amon. 2013. Gene Copy-Number Alterations: A Cost-Benefit Analysis. Cell **152**:394-405.

Tang, Z. F., R. Nouri, M. Dong, J. B. Yang, W. Greene, Y. S. Zhu, M. Yon, M. S. Nair, S. V. Kuchipudi, and W. H. Guan. 2022. Rapid detection of novel coronavirus SARS-CoV-2 by RT-LAMP coupled solid-state nanopores. Biosensors & Bioelectronics **197**.

Tankovic, M. S., A. Baricevic, M. Geric, A. M. Domijan, D. M. Pfannkuchen, N. Kuzat, I. Ujevic, M. Kuralic, M. Rozman, K. Matkovic, M. Novak, B. Zegura, M. Pfannkuchen, and G. Gajski. 2022. Characterisation and toxicological activity of three different Pseudo-nitzschia species from the northern Adriatic Sea (Croatia). Environmental Research **214**.

Tanner, N. A., Y. H. Zhang, and T. C. Evans. 2015. Visual detection of isothermal nucleic acid amplification using pH-sensitive dyes. Biotechniques **58**:59-68.

Tasker, R. A. 2016. Domoic Acid and Other Amnesic Toxins: Toxicological Profile. Marine and Freshwater Toxins:93-112.

Tasoglu, S., U. A. Gurkan, S. Q. Wang, and U. Demirci. 2013. Manipulating biological agents and cells in micro-scale volumes for applications in medicine. Chemical Society Reviews **42**:5788-5808.

Tatters, A. O., F. X. Fu, and D. A. Hutchins. 2012a. High CO2 and silicate limitation synergistically increase the toxicity of Pseudo-nitzschia fraudulenta. Plos One **7**:e32116.

Tatters, A. O., F. X. Fu, and D. A. Hutchins. 2012b. High CO2 and Silicate Limitation Synergistically Increase the Toxicity of Pseudo-nitzshia fraudulenta. Plos One **7**.

Teitelbaum, J., S. Carpenter, and N. R. Cashman. 1990. Neurologic Sequelae after Ingestion of Mussels Contaminated with Domoic Acid. New England Journal of Medicine **323**:1632-1633.

Temiz, Y., R. D. Lovchik, G. V. Kaigala, and E. Delamarche. 2015. Lab-on-a-chip devices: How to close and plug the lab? Microelectronic Engineering **132**:156-175.

Terray, A., J. Oakey, and D. W. M. Marr. 2002. Microfluidic control using colloidal devices. Science **296**:1841-1844.

Tester, P. A., Y. Pan, G. J. Doucette, and C. Scholin. 2000. Accumulation of domoic acid activity in copepods. Harmful algal blooms:418-420.

Thapa, J., B. Maharjan, M. Malla, Y. Fukushima, A. Poudel, B. D. Pandey, K. Hyashida, S. V. Gordon, C. Nakajima, and Y. Suzuki. 2019. Direct detection of Mycobacterium tuberculosis in clinical samples by a dry methyl green loop-mediated isothermal amplification (LAMP) method. Tuberculosis **117**:1-6.

Thebaud, O., G. Veron, and S. Fifas. 2005. Incidences des épisodes d'efflorescences de micro algues toxiques sur les écosystèmes et sur les pêcheries de coquillages en baie de Douarnenez.

Theron, J., and T. E. Cloete. 2000. Molecular techniques for determining microbial diversity and community structure in natural environments. Critical Reviews in Microbiology **26**:37-57.

Thessen, A. E., H. A. Bowers, and D. K. Stoecker. 2009. Intra- and interspecies differences in growth and toxicity of Pseudo-nitzschia while using different nitrogen sources. Harmful Algae **8**:792-810.

Thomas, K., M. Tremblay, J. Walter, and M. Quilliam. 2008. NRC CRM-DA-f, a certified calibration solution reference material for domoic acid. CRMP Technical Report CRM-DA-f-20071205, June 2008.

Thorel, M., P. Claquin, M. Schapira, R. Le Gendre, P. Riou, D. Goux, B. Le Roy, V. Raimbault, A. F. Deton-Cabanillas, P. Bazin, V. Kientz-Bouchart, and J. Fauchot. 2017. Nutrient ratios influence variability in Pseudo-nitzschia species diversity and particulate domoic acid production in the Bay of Seine (France). Harmful Algae **68**:192-205.

Thorel, M., J. Fauchot, J. Morelle, V. Raimbault, B. Le Roy, C. Miossec, V. Kientz-Bouchart, and P. Claquin. 2014. Interactive effects of irradiance and temperature on growth and domoic acid production of the toxic diatom Pseudo-nitzschia australis (Bacillariophyceae). Harmful Algae **39**:232-241.

Tian, C. J., Z. X. Lin, X. M. He, Q. Luo, C. B. Luo, H. Q. Yu, R. Chen, X. W. Wu, D. Z. Zhu, Z. J. Ren, Y. Z. Bi, and J. Ji. 2012. Development of a fluorescent-intercalating-dye-based reverse transcription loop-mediated isothermal amplification assay for rapid detection of seasonal Japanese B encephalitis outbreaks in pigs. Archives of Virology **157**:1481-1488.

Tichopad, A., R. Kitchen, I. Riedmaier, C. Becker, A. Stahlberg, and M. Kubista. 2009. Design and Optimization of Reverse-Transcription Quantitative PCR Experiments. Clinical Chemistry **55**:1816-1823.

Toldra, A., M. Jauset-Rubio, K. B. Andree, M. Fernandez-Tejedor, J. Diogene, I. Katakis, C. K. O'Sullivan, and M. Campas. 2018. Detection and quantification of the toxic marine microalgae Karlodinium veneficum and Karlodinium armiger using recombinase polymerase amplification and enzyme-linked oligonucleotide assay. Analytica Chimica Acta **1039**:140-148.

Toldra, A., C. K. O'Sullivan, and M. Campas. 2019. Detecting Harmful Algal Blooms with Isothermal Molecular Strategies. Trends in Biotechnology **37**:1278-1281.

Toley, B. J., I. Covelli, Y. Belousov, S. Ramachandran, E. Kline, N. Scarr, N. Vermeulen, W. Mahoney, B. R. Lutza, and P. Yagera. 2015. Isothermal strand displacement amplification (iSDA): a rapid and sensitive method of nucleic acid amplification for point-of-carediagnosis. Analyst **140**:7540-7549.

Toppings, N. B., A. N. Mohon, Y. Lee, H. Kumar, D. Lee, R. Kapoor, G. Singh, L. Oberding, O. Abdullah, K. Kim, B. M. Berenger, and D. R. Pillai. 2021. A rapid near-patient detection system for SARS-CoV-2 using saliva. Scientific Reports **11**.

Trainer, V. L., S. S. Bates, N. Lundholm, A. E. Thessen, W. P. Cochlan, N. G. Adams, and C. G. Trick. 2012. Pseudo-nitzschia physiological ecology, phylogeny, toxicity, monitoring and impacts on ecosystem health. Harmful Algae **14**:271-300.

Trainer, V. L., B. M. Hickey, E. J. Lessard, W. P. Cochlan, C. G. Trick, M. L. Wells, A. MacFadyen, and S. K. Moore. 2009. Variability of Pseudo-nitzschia and domoic acid in the Juan de Fuca eddy region and its adjacent shelves. Limnology and Oceanography **54**:289-308.

Trainer, V. L., R. M. Kudela, M. V. Hunter, N. G. Adams, and R. M. McCabe. 2020. Climate Extreme Seeds a New Domoic Acid Hotspot on the US West Coast. Frontiers in Climate **2**.

Tran, H., and T. Savage. 2017. Identifying the Metal That Activates the Prenyltransferase That Catalyzes Formation of Geranyl Diphosphate in the Diatom Pseudo-nitzschia multiseries. Faseb Journal **31**.

Trauba, J. M., and C. T. Wittwer. 2017. Microfluidic extreme PCR:< 1 minute DNA amplification in a thin film disposable. J Biomed Sci Eng **10**:219-231.

Trick, C. G., B. D. Bill, W. P. Cochlan, M. L. Wells, V. L. Trainer, and L. D. Pickell. 2010. Iron enrichment stimulates toxic diatom production in high-nitrate, low-chlorophyll areas.

Proceedings of the National Academy of Sciences of the United States of America **107**:5887-5892.

Trimborn, S., N. Lundholm, S. Thoms, K. U. Richter, B. Krock, P. J. Hansen, and B. Rost. 2008. Inorganic carbon acquisition in potentially toxic and non-toxic diatoms: the effect of pH-induced changes in seawater carbonate chemistry. Physiologia Plantarum **133**:92-105.

Trobajo, R., D. G. Mann, E. Clavero, K. M. Evans, P. Vanormelingen, and R. C. McGregor. 2010. The use of partial cox 1, rbc L and LSU rDNA sequences for phylogenetics and species identification within the Nitzschia palea species complex (Bacillariophyceae). European Journal of Phycology **45**:413-425.

Tsai, Y. L., H. T. T. Wang, H. F. G. Chang, C. F. Tsai, C. K. Lin, P. H. Teng, C. Su, C. C. Jeng, and P. Y. Lee. 2012. Development of TaqMan Probe-Based Insulated Isothermal PCR (iiPCR) for Sensitive and Specific On-Site Pathogen Detection. Plos One **7**.

Tsaloglou, M. N., M. M. Bahi, E. M. Waugh, H. Morgan, and M. Mowlem. 2011. On-chip real-time nucleic acid sequence-based amplification for RNA detection and amplification. Analytical Methods **3**:2127-2133.

Tsaloglou, M. N., F. Laouenan, C. M. Loukas, L. G. Monsalve, C. Thanner, H. Morgan, J. M. Ruano-Lopez, and M. C. Mowlem. 2013. Real-time isothermal RNA amplification of toxic marine microalgae using preserved reagents on an integrated microfluidic platform. Analyst **138**:593-602.

Tsao, Z. J., Y. C. Liao, B. H. Liu, C. C. Su, and F. Y. Yu. 2007. Development of a monoclonal antibody against domoic acid and its application in enzyme-linked immunosorbent assay and colloidal gold immunostrip. Journal of Agricultural and Food Chemistry **55**:4921-4927.

Tseng, H. Y., V. Adamik, J. Parsons, S. S. Lan, S. Malfesi, J. Lum, L. Shannon, and B. Gray. 2014. Development of an electrochemical biosensor array for quantitative polymerase chain reaction utilizing three-metal printed circuit board technology. Sensors and Actuators B-Chemical **204**:459-466.

Turner, A. D., R. G. Hatfield, B. H. Maskrey, M. Algoet, and J. F. Lawrence. 2019. Evaluation of the new European Union reference method for paralytic shellfish toxins in shellfish: A review of twelve years regulatory monitoring using pre-column oxidation LC-FLD. TrAC Trends in Analytical Chemistry **113**:124-139.

Turner, S. A., R. Abou Shaar, and Z. B. Yang. 2023. The basics of commonly used molecular techniques for diagnosis, and application of molecular testing in cytology. Diagnostic Cytopathology **51**:83-94.

Turrell, E., E. Bresnan, C. Collins, L. Brown, J. Graham, and A. Grieve. 2008. Detection of Pseudo-nitzschia (Bacillariophyceae) species and amnesic shellfish toxins in Scottish coastal waters using oligonucleotide probes and the Jellet Rapid Test (TM). Harmful Algae **7**:443-458.

TwistDx. 2009. Appendix to the Twist Amp TM reaction kit manuals. TwistDx Cambridge, UK.

TwistDx, I. 2019. RPA Assay Design.

Tyagi, S., and F. R. Kramer. 1996. Molecular beacons: Probes that fluoresce upon hybridization. Nature Biotechnology **14**:303-308.

Udugama, B., P. Kadhiresan, A. Samarakoon, and W. C. W. Chan. 2017. Simplifying Assays by Tableting Reagents. Journal of the American Chemical Society **139**:17341-17349.

Unger, M. A., H. P. Chou, T. Thorsen, A. Scherer, and S. R. Quake. 2000. Monolithic microfabricated valves and pumps by multilayer soft lithography. Science **288**:113-116.

Untergasser, A., I. Cutcutache, T. Koressaar, J. Ye, B. C. Faircloth, M. Remm, and S. G. Rozen. 2012. Primer3-new capabilities and interfaces. Nucleic Acids Research **40**.

Van der Velden, V. H. J., T. Szczepański, and J. J. M. van Dongen. 2001. Polymerase Chain Reaction, Real-Time Quantitative. Pages 1503-1506 *in* S. Brenner and J. H. Miller, editors. Encyclopedia of Genetics. Academic Press, New York.

Van Dolah, F. M. 2000. Marine algal toxins: Origins, health effects, and their increased occurrence. Environmental Health Perspectives **108**:133-141.

Van Meerssche, E., D. I. Greenfield, and J. L. Pinckney. 2018. Coastal eutrophication and freshening: Impacts on Pseudo-nitzschia abundance and domoic acid allelopathy. Estuarine Coastal and Shelf Science **209**:70-79.

Van Meerssche, E., and J. L. Pinckney. 2017. The influence of salinity in the domoic acid' effect on estuarine phytoplankton communities. Harmful Algae **69**:65-74.

van Pelt-Verkuil, E. 2008. The PCR in Practice. Pages 17-23 *in* E. van Pelt-Verkuil, A. van Belkum, and J. P. Hays, editors. Principles and Technical Aspects of PCR Amplification. Springer Netherlands, Dordrecht.

Van Pelt-Verkuil, E., v. B. Alex, and P. H. John. 2008a. Chapter 5: PCR Primers. Pages 63-90 *in* E. van Pelt-Verkuil, A. van Belkum, and J. P. Hays, editors. Principles and Technical Aspects of PCR Amplification. Springer Netherlands, Dordrecht.

van Pelt-Verkuil, E., v. B. Alex, and P. H. John. 2008b. PCR Primers. Pages 63-90 *in* E. van Pelt-Verkuil, A. van Belkum, and J. P. Hays, editors. Principles and Technical Aspects of PCR Amplification. Springer Netherlands, Dordrecht.

Varona, M., and J. L. Anderson. 2021. Advances in Mutation Detection Using Loop-Mediated Isothermal Amplification. Acs Omega **6**:3463-3469.

Venrick, E. 1978. How many cells to count. Phytoplankton Manual. Monographs on oceanographic methodology **6**:167-180.

Verpoorte, E. 2002. Microfluidic chips for clinical and forensic analysis. Electrophoresis **23**:677-712.

Vestad, T., D. W. M. Marr, and J. Oakey. 2004. Flow control for capillary-pumped microfluidic systems. Journal of Micromechanics and Microengineering **14**:1503-1506.

Vilarino, N., M. C. Louzao, M. R. Vieytes, and L. M. Botana. 2010. Biological methods for marine toxin detection. Analytical and Bioanalytical Chemistry **397**:1673-1681.

Vincent, M., Y. Xu, and H. Kong. 2004. Helicase-dependent isothermal DNA amplification. EMBO reports **5**:795-800.

Von Lode, P., A. Syrjala, V. Hagren, H. Kojola, T. Soukka, T. Lovgren, and J. Nurmi. 2007. Fully automated, homogeneous nucleic acid detection technology based on dry-reagent assay chemistry and time-resolved fluorometry. Clinical Chemistry **53**:2014-2017.

Wachiralurpan, S., T. Sriyapai, S. Areekit, P. Sriyapai, D. Thongphueak, S. Santiwatanakul, and K. Chansiri. 2017. A one-step rapid screening test of Listeria monocytogenes in food samples using a real-time loop-mediated isothermal amplification turbidity assay. Analytical Methods **9**:6403-6410.

Walker, D. I., J. McQuillan, M. Taiwo, R. Parks, C. A. Stenton, H. Morgan, M. C. Mowlem, and D. N. Lees. 2019. A highly specific Escherichia coli qPCR and its comparison with existing methods for environmental waters (vol 126, pg 101, 2017). Water Research **161**:652-652.

Walker, G. T., M. S. Fraiser, J. L. Schram, M. C. Little, J. G. Nadeau, and D. P. Malinowski. 1992. Strand displacement amplification—an isothermal, in vitro DNA amplification technique. Nucleic Acids Research **20**:1691-1696.

Walter, J. A., D. M. Leek, and M. Falk. 1992. Nmr-Study of the Protonation of Domoic Acid. Canadian Journal of Chemistry-Revue Canadienne De Chimie **70**:1156-1161.

Wan, J. J., J. P. Guo, Z. X. Lu, X. M. Bie, F. X. Lv, and H. Z. Zhao. 2020. Development of a test kit for visual loop-mediated isothermal amplification of Salmonella in spiked ready-to-eat fruits and vegetables. Journal of Microbiological Methods **169**.

Wang, H., X. H. Tong, Y. Yuan, X. H. Peng, Q. Z. Zhang, S. Zhang, C. Y. Xie, X. Y. Zhang, S. Z. Yan, J. W. Xu, L. Z. Jiang, B. K. Qi, and Y. Li. 2020a. Effect of Spray-Drying and Freeze-Drying on the Properties of Soybean Hydrolysates. Journal of Chemistry **2020**.

Wang, J. 2002. Electrochemical nucleic acid biosensors. Analytica Chimica Acta **469**:63-71.

Wang, J. 2012. DNA/RNA Isolation and Quantitation. Pages 11-22 *in* P. Hu, M. Hegde, and P. A. Lennon, editors. Modern Clinical Molecular Techniques. Springer New York, New York, NY.

Wang, J., H. Jiang, L. Pan, X. Gu, C. Xiao, P. Liu, Y. Tang, J. Fang, X. Li, and C. Lu. 2023. Rapid on-site nucleic acid testing: On-chip sample preparation, amplification, and detection, and their integration into all-in-one systems. Frontiers in Bioengineering and Biotechnology **11**.

Wang, J. Y., P. Youkharibache, D. C. Zhang, C. J. Lanczycki, R. C. Geer, T. Madej, L. Phan, M. Ward, S. N. Lu, G. H. Marchler, Y. L. Wang, S. H. Bryant, L. Y. Geer, and A. Marchler-Bauer. 2020b. iCn3D, a web-based 3D viewer for sharing 1D/2D/3D representations of biomolecular structures. Bioinformatics **36**:131-135.

Wang, L., C. Zhang, G. Chen, Y. Wang, and M. Fu. 2020c. Development of a rapid screening test for Karenia mikimotoi by using loop-mediated isothermal amplification and lateral flow dipstick. Journal of Applied Phycology **32**:3143-3155.

Wang, S. Y., N. Liu, L. Y. Zheng, G. Z. Cai, and J. H. Lin. 2020d. A lab-on-chip device for the sample-in-result-out detection of viable Salmonella using loop-mediated isothermal amplification and real-time turbidity monitoring. Lab on a Chip **20**:2296-2305.

Wang, W., M. Chen, and G. H. Chen. 2012. Issues in Freeze Drying of Aqueous Solutions. Chinese Journal of Chemical Engineering **20**:551-559.

Wang, X., F. G. Yin, Y. H. Bi, G. Cheng, J. Li, L. D. Hou, Y. L. Li, B. Z. Yang, W. J. Liu, and L. M. Yang. 2016. Rapid and sensitive detection of Zika virus by reverse transcription loop-mediated isothermal amplification. Journal of Virological Methods **238**:86-93.

Wang, X. F., Z. F. Fu, X. Y. Chen, C. Peng, X. L. Xu, W. Wei, F. W. Li, and J. F. Xu. 2017. Use of a novel metal indicator to judge loop-mediated isothermal amplification for detecting the 35S promoter. Analytical and Bioanalytical Chemistry **409**:881-889.

Ward, K. R., and P. Matejtschuk. 2021. The Principles of Freeze-Drying and Application of Analytical Technologies. Pages 99-127 *in* W. F. Wolkers and H. Oldenhof, editors. Cryopreservation and Freeze-Drying Protocols. Springer US, New York, NY.

Warmt, C., C. Yaslanmaz, and J. Henkel. 2022. Investigation and validation of labelling loop mediated isothermal amplification (LAMP) products with different nucleotide modifications for various downstream analysis. Scientific Reports **12**.

Wei, L., Q. T. Wang, Y. Xin, Y. D. Lu, and J. Xu. 2017. Enhancing photosynthetic biomass productivity of industrial oleaginous microalgae by overexpression of RuBisCO activase. Algal Research-Biomass Biofuels and Bioproducts **27**:366-375.

Wekell, J. C., J. Hurst, and K. A. Lefebvre. 2004. The origin of the regulatory limits for PSP and ASP toxins in shellfish. Journal of Shellfish Research **23**:927-930.

Wen, J., L. A. Legendre, J. M. Bienvenue, and J. P. Landers. 2008. Purification of nucleic acids in microfluidic devices. Analytical Chemistry **80**:6472-6479.

Whitesides, G. M. 2006. The origins and the future of microfluidics. Nature **442**:368-373.

Wild, D. 2013. The immunoassay handbook: theory and applications of ligand binding, ELISA and related techniques. Newnes.

Wilding, P., M. A. Shoffner, and L. J. Kricka. 1994. Pcr in a Silicon Microstructure. Clinical Chemistry **40**:1815-1818.

Wilson, M. W. 2020. Development of Automated Nucleic Acid Technologies for Marine Point of Sample Diagnostics. University of Southampton.

Wingert, C. J., and W. P. Cochlan. 2021a. Effects of ocean acidification on the growth, photosynthetic performance, and domoic acid production of the diatom Pseudo-nitzschia australis from the California Current System. Harmful Algae **107**:102030.

Wingert, C. J., and W. P. Cochlan. 2021b. Effects of ocean acidification on the growth, photosynthetic performance, and domoic acid production of the diatom Pseudo-nitzschia australis from the California Current System. Harmful Algae **107**.

Woelkerling, W. J., R. R. Kowal, and S. B. Gough. 1976. Sedgwick-rafter cell counts: a procedural analysis. Hydrobiologia **48**:95-107.

Wohlrab, S., U. John, K. Klemm, T. Eberlein, A. M. F. Grivogiannis, B. Krock, S. Frickenhaus, L. T. Bach, B. Rost, U. Riebesell, and D. B. Van de Waal. 2020. Ocean acidification increases

domoic acid contents during a spring to summer succession of coastal phytoplankton. Harmful Algae **92**.

Woias, P. 2005. Micropumps - past, progress and future prospects. Sensors and Actuators B-Chemical **105**:28-38.

Wolfe, K. A., M. C. Breadmore, J. P. Ferrance, M. E. Power, J. F. Conroy, P. M. Norris, and J. P. Landers. 2002. Toward a microchip-based solid-phase extraction method for isolation of nucleic acids. Electrophoresis **23**:727-733.

Wong, Y. P., S. Othman, Y. L. Lau, S. Radu, and H. Y. Chee. 2018. Loop-mediated isothermal amplification (LAMP): a versatile technique for detection of micro-organisms. Journal of Applied Microbiology **124**:626-643.

Work, T. M., B. Barr, A. M. Beale, L. Fritz, M. A. Quilliam, and J. L. C. Wright. 1993. Epidemiology of Domoic Acid Poisoning in Brown Pelicans (Pelecanus occidentalis) and Brandt's Cormorants (Phalacrocorax penicillatus) in California. Journal of Zoo and Wildlife Medicine **24**:54-62.

Wright, J., C. Bird, D. Hampson, J. McDonald, and M. Quilliam. 1990. Chemistry, biology, and toxicology of domoic acid and its isomers. Canada diseases weekly report= Rapport hebdomadaire des maladies au Canada **16**:21-26.

Wright, J. L. C., R. K. Boyd, A. S. W. Defreitas, M. Falk, R. A. Foxall, W. D. Jamieson, M. V. Laycock, A. W. Mcculloch, A. G. Mcinnes, P. Odense, V. P. Pathak, M. A. Quilliam, M. A. Ragan, P. G. Sim, P. Thibault, J. A. Walter, M. Gilgan, D. J. A. Richard, and D. Dewar. 1989. Identification of Domoic Acid, a Neuroexcitatory Amino-Acid, in Toxic Mussels from Eastern Prince-Edward-Island. Canadian Journal of Chemistry-Revue Canadienne De Chimie **67**:481-490.

Wu, D. D., J. W. Kang, B. S. Li, and D. X. Sun. 2018. Evaluation of the RT-LAMP and LAMP methods for detection of Mycobacterium tuberculosis. Journal of Clinical Laboratory Analysis **32**.

Xu, J. S., J. Wang, Z. C. Zhong, X. S. Su, K. Y. Yang, Z. F. Chen, D. X. Zhang, T. D. Li, Y. B. Wang, S. Y. Zhang, S. X. Ge, J. Zhang, and N. S. Xia. 2020. Room-temperature-storable PCR mixes for SARS-CoV-2 detection. Clinical Biochemistry **84**:73-78.

Yager, P., T. Edwards, E. Fu, K. Helton, K. Nelson, M. R. Tam, and B. H. Weigl. 2006. Microfluidic diagnostic technologies for global public health. Nature **442**:412-418.

Yakes, B. J., J. Buijs, C. T. Elliott, and K. Campbell. 2016. Surface plasmon resonance biosensing: Approaches for screening and characterising antibodies for food diagnostics. Talanta **156**:55-63.

Yamanaka, E. S., L. A. Tortajada-Genaro, and A. Maquieira. 2017. Low-cost genotyping method based on allele-specific recombinase polymerase amplification and colorimetric microarray detection. Microchimica Acta **184**:1453-1462.

Yan, L., J. Zhou, Y. Zheng, A. S. Gamson, B. T. Roembke, S. Nakayama, and H. O. Sintim. 2014. Isothermal amplified detection of DNA and RNA. Molecular Biosystems **10**:970-1003.

Yang, S., and R. E. Rothman. 2004. PCR-based diagnostics for infectious diseases: uses, limitations, and future applications in acute-care settings. Lancet Infectious Diseases **4**:337-348.

Yang, S. Y., and W. J. Wen. 2021. Lyophilized Ready-to-Use Mix for the Real-Time Polymerase Chain Reaction Diagnosis. Acs Applied Bio Materials **4**:4354-4360.

Yang, Y., X. D. Qin, Y. J. Sun, T. Chen, and Z. D. Zhang. 2016. Rapid detection of highly pathogenic porcine reproductive and respiratory syndrome virus by a fluorescent probe-based isothermal recombinase polymerase amplification assay. Virus Genes **52**:883-886.

Yarimizu, K., S. Sildever, Y. Hamamoto, S. Tazawa, H. Oikawa, H. Yamaguchi, L. Basti, J. I. Mardones, J. Paredes-Mella, and S. Nagai. 2021. Development of an absolute quantification method for ribosomal RNA gene copy numbers per eukaryotic single cell by digital PCR. Harmful Algae **103**.

Ye, J., G. Coulouris, I. Zaretskaya, I. Cutcutache, S. Rozen, and T. L. Madden. 2012. Primer-BLAST: A tool to design target-specific primers for polymerase chain reaction. Bmc Bioinformatics **13**.

Ye, X., X. E. Fang, Y. Li, L. J. Wang, X. X. Li, and J. L. Kong. 2019. Sequence-Specific Probe-Mediated Isothermal Amplification for the Single-Copy Sensitive Detection of Nucleic Acid. Analytical Chemistry **91**:6738-6745.

Ye, X., J. Xu, L. J. Lu, X. X. Li, X. E. Fang, and J. L. Kong. 2018. Equipment-free nucleic acid extraction and amplification on a simple paper disc for point-of-care diagnosis of rotavirus A. Analytica Chimica Acta **1018**:78-85.

Yin, J. X., Y. J. Suo, Z. Y. Zou, J. J. Sun, S. Zhang, B. Wang, Y. W. Xu, D. Darland, J. X. Zhao, and Y. Mu. 2019. Integrated microfluidic systems with sample preparation and nucleic acid amplification. Lab on a Chip **19**:2769-2785.

Yonesaki, T., and T. Minagawa. 1985. T4 Phage Gene Uvsx Product Catalyzes Homologous DNA Pairing. Embo Journal **4**:3321-3327.

Yoon, J., Y. J. Yoon, T. Y. Lee, M. K. Park, J. Chung, and Y. Shin. 2018. A disposable lab-on-a-chip platform for highly efficient RNA isolation. Sensors and Actuators B-Chemical **255**:1491-1499.

Young, N., C. Robin, R. Kwiatkowska, C. Beck, D. Mellon, P. Edwards, J. Turner, P. Nicholls, G. Fearby, D. Lewis, D. Hallett, T. Bishop, T. Smith, R. Hyndford, L. Coates, and A. Turner. 2019. Outbreak of diarrhetic shellfish poisoning associated with consumption of mussels, United Kingdom, May to June 2019. Eurosurveillance **24**:2-6.

Yu, C. Y., G. Y. Ang, K. G. Chan, K. K. B. Singh, and Y. Y. Chan. 2015. Enzymatic electrochemical detection of epidemic-causing Vibrio cholerae with a disposable oligonucleotide-modified screen-printed bi-sensor coupled to a dry-reagent-based nucleic acid amplification assay. Biosensors & Bioelectronics **70**:282-288.

Yu, F. Y., B. H. Liu, T. S. Wu, T. F. Chi, and M. C. Su. 2004. Development of a sensitive enzyme-linked immunosorbent assay for the determination of domoic acid in shellfish. Journal of Agricultural and Food Chemistry **52**:5334-5339.

Yu, Y. J., J. X. Y. Zhou, B. B. Li, M. M. Ji, Y. Wang, E. Carnaby, M. I. Andersson, W. E. Huang, and Z. F. Cui. 2022. A quantitative RT-qLAMP for the detection of SARS-CoV-2 and human gene in clinical application. Microbial Biotechnology **15**:2619-2630.

Yuan, L., M. F. Wang, X. T. Zhang, and Z. X. Wang. 2017. Effects of protease and non-starch polysaccharide enzyme on performance, digestive function, activity and gene expression of endogenous enzyme of broilers. Plos One **12**.

Yuan, Y. L., S. Q. Wei, G. P. Liu, S. B. Xie, Y. Q. Chai, and R. Yuan. 2014. Ultrasensitive electrochemiluminescent aptasensor for ochratoxin A detection with the loop-mediated isothermal amplification. Analytica Chimica Acta **811**:70-75.

Zabaglo, K., E. Chrapusta, B. Bober, A. Kaminski, M. Adamski, and J. Bialczyk. 2016. Environmental roles and biological activity of domoic acid: A review. Algal Research-Biomass Biofuels and Bioproducts **13**:94-101.

Zadeh, A. H. M., A. R. Najafabadi, A. Vatanara, H. Faghihi, and K. Gilani. 2017. Effect of molecular weight and ratio of poly ethylene glycols' derivatives in combination with trehalose on stability of freeze-dried IgG. Drug Development and Industrial Pharmacy **43**:1945-1951.

Zaghloul, H., and M. El-shahat. 2014. Recombinase polymerase amplification as a promising tool in hepatitis C virus diagnosis. World journal of hepatology **6**:916.

Zanoli, L., and G. Spoto. 2013. Isothermal amplification methods for the detection of nucleic acids in microfluidic devices. Biosensors **3**:18-43.

Zapata, M., F. Rodríguez, S. Fraga, L. Barra, and M. V. Ruggiero. 2011. Chlorophyll c pigment patterns in 18 species (51 strains) of the genus pseudo-nitzschia (bacillariophyceae) 1. Journal of Phycology **47**:1274-1280.

Zhan, L. Z., D. F. Song, Q. Gu, T. T. Yan, and C. C. Ma. 2019. Reverse transcription - loop-mediated isothermal amplification assay for the rapid detection of pathogenic Listeria monocytogenes in meat products. Canadian Journal of Microbiology **65**:913-921.

Zhang, C. Y., Y. C. Yang, F. G. Liu, Y. Y. Wang, and G. F. Chen. 2022a. Recombinase polymerase amplification combined with lateral flow dipstick for the rapid detection of Chattonella marina. Journal of Applied Phycology **34**:1607-1620.

Zhang, F. Y., Y. H. Shi, K. J. Jiang, W. Song, C. Y. Ma, Z. L. Xu, and L. B. Ma. 2014a. Rapid detection and quantification of Prorocentrum minimum by loop-mediated isothermal amplification and real-time fluorescence quantitative PCR. Journal of Applied Phycology **26**:1379-1388.

Zhang, F. Y., Y. H. Shi, K. J. Jiang, Z. L. Xu, and L. B. Ma. 2012. Sensitive and rapid detection of two toxic microalgae Alexandrium by loop-mediated isothermal amplification. Acta Oceanologica Sinica **31**:139-146.

Zhang, J., Q. Hou, W. M. Ma, D. N. Chen, W. B. Zhang, A. K. Wubshet, Y. Z. Ding, M. M. Li, Q. Li, J. Chen, J. F. Dai, G. H. Wu, Z. T. Zhang, A. D. Zaberezhny, Z. Pejsak, K. Tarasiuk, M. U. Z. Khan, Y. Wang, J. J. He, and Y. S. Liu. 2022b. A Naked-Eye Visual Reverse Transcription Loop-Mediated Isothermal Amplification with Sharp Color Changes for Potential Pen-Side Test of Foot-and-Mouth Disease Virus. Viruses-Basel **14**.

Zhang, J. Z., X. S. Su, J. S. Xu, J. Wang, J. T. Zeng, C. Y. Li, W. D. Chen, T. D. Li, X. P. Min, D. X. Zhang, S. Y. Zhang, S. X. Ge, J. Zhang, and N. S. Xia. 2019. A point of care platform based on microfluidic chip for nucleic acid extraction in less than 1minute. Biomicrofluidics **13**.

Zhang, L., Y. Zhang, C. Y. Wang, Q. A. Feng, F. Fan, G. J. Zhang, X. X. Kang, X. Z. Qin, J. S. Sun, Y. G. Li, and X. Jiang. 2014b. Integrated Microcapillary for Sample-to-Answer Nucleic Acid Pretreatment, Amplification, and Detection. Analytical Chemistry **86**:10461-10466.

Zhao, Y. X., F. Chen, Q. Li, L. H. Wang, and C. H. Fan. 2015. Isothermal Amplification of Nucleic Acids. Chemical Reviews **115**:12491-12545.

Zheng, G. C., H. Y. Wu, H. Y. Che, X. K. Li, Z. H. Zhang, J. X. Peng, M. M. Guo, and Z. J. Tan. 2022. Residue Analysis and Assessment of the Risk of Dietary Exposure to Domoic Acid in Shellfish from the Coastal Areas of China. Toxins **14**.

Zhong, L. L., Q. Zhou, C. Y. Tan, A. P. Roberts, M. A. E. Ahmed, G. P. Chen, M. Dai, F. Yang, Y. Xia, K. Liao, Y. J. Liang, Y. Q. Yang, S. Y. Feng, X. B. Zheng, and G. B. Tian. 2019. Multiplex loop-mediated isothermal amplification (multi-LAMP) assay for rapid detection of mcr-I to mcr-5 in colistin-resistant bacteria. Infection and Drug Resistance **12**:1877-1887.

Zhong, R., D. Liu, L. Yu, N. Ye, Z. Dai, J. Qin, and B. Lin. 2007. Fabrication of two-weir structure-based packed columns for on-chip solid-phase extraction of DNA. Electrophoresis **28**:2920-2926.

Zhong, R. T., X. Y. Pan, L. Jiang, Z. P. Dai, J. H. Qin, and B. C. Lin. 2009. Simply and reliably integrating micro heaters/sensors in a monolithic PCR-CE microfluidic genetic analysis system. Electrophoresis **30**:1297-1305.

Zhu, Z., P. P. Qu, F. X. Fu, N. Tennenbaum, A. O. Tatters, and D. A. Hutchins. 2017. Understanding the blob bloom: Warming increases toxicity and abundance of the harmful bloom diatom Pseudo-nitzschia in California coastal waters. Harmful Algae **67**:36-43.

Zirath, H., J. R. Peham, G. Schnetz, A. Coll, L. Brandhoff, A. Spittler, M. J. Vellekoop, and H. Redl. 2016. A compact and integrated immunoassay with on-chip dispensing and magnetic particle handling. Biomedical Microdevices **18**.

Zou, Y. P., M. G. Mason, and J. R. Botella. 2020. Evaluation and improvement of isothermal amplification methods for point-of-need plant disease diagnostics. Plos One **15**.